Australian Government
Geoscience Australia

Proceedings of the 2011 Australian Geothermal Energy Conference

Anthony R Budd

Record
2011/43
GeoCat # 73026

Proceedings of the 2011 Australian Geothermal Energy Conference

GEOSCIENCE AUSTRALIA
RECORD 2011/43

Edited by

Anthony Budd
Geoscience Australia

Department of Resources, Energy and Tourism
Minister for Resources and Energy: The Hon. Martin Ferguson, AM MP
Secretary: Mr Drew Clarke

Geoscience Australia
Chief Executive Officer: Dr Chris Pigram

ISSN 1448-2177
ISBN 978-1-921954-56-6

GeoCat # 73026

Recommended bibliographic reference: Budd, A.R. (editor), 2011. Proceedings of the 2011 Australian Geothermal Energy Conference, 16-18 November, Melbourne, Geoscience Australia, Record 2011/43.

Recommended bibliographic citation: Gurgenci, H. (2011), What will make EGS geothermal energy a viable Australian renewable energy option? in: Budd, A.R. (editor), 2011. Proceedings of the 2011 Australian Geothermal Energy Conference, 16-18 November, Melbourne, Geoscience Australia, Record 2011/43, 81-84.

The Convenors would like to thank the following sponsors for their kind support:

Gold sponsors

Silver sponsors

Bronze sponsors

Dinner sponsors

Introduction

This volume is a compilation of Extended Abstracts presented at the 2011 Australian Geothermal Energy Conference, 16-18 November 2011, Sebel Albert Park, Melbourne, organised by the Australian Geothermal Energy Association and the Australian Geothermal Energy Group.

As editor of these proceedings, I first would like to thank the Technical Committee who have been very generous with their time to review the submissions and to work with the authors of the accepted submissions to improve the quality of the Abstracts and the presentations.

I also thank the Conference Chair Mark Miller, Vicki Cleveland and the rest of the Organising Committee who were brave enough to take on the job organising this fourth event on behalf of the Australian Geothermal Energy Association and the Australian Geothermal Energy Group.

Rob Bulfield and Sapro Conference Management have done an excellent job in assisting the organisation.

I also thank again the sponsoring companies for their generous support.

I thank Geoscience Australia for publishing the proceedings.

Finally, thanks to all delegates without whose participation none of this is worthwhile.

Anthony Budd

Organising Committee

Mark Miller – Chair	Greenearth Energy
Susan Jeanes	Chief Executive, AGEA
Graeme Beardsmore	Hot Dry Rocks Pty Ltd
Betina Bendall	PIRSA
Anthony Budd	Geoscience Australia
Vicki Cleveland	Administration Manager, AGEA
Barry Goldstein	PIRSA
Hal Gurgenci	University of Queensland
Donald Payne	Direct Energy
Justin McFarlane	
Rob Bulfield	conference secretariat, Sapro conference management

Technical Committee

Anthony Budd – Chair	Geoscience Australia
Betina Bendall	PIRSA
Cameron Huddlestone-Holmes	CSIRO
Doone Wyborn	Geodynamics
Hal Gurgenci	University of Queensland

Contents

Smart Nanosensors for *In-Situ* Temperature Measurement in Fractured Geothermal Reservoirs

Mohammed Alaskar[1], Morgan Ames[1], Chong Liu[2], Steve Connor[2], Roland Horne[1], Kewen Li[1], Yi Cui[2]

askar@stanford.edu; mames@stanford.edu; chong813@stanford.edu; horne@stanford.edu; stconnor@stanford.edu,kewenli@stanford.edu; yicui@stanford.edu

[1]Department of Energy Resources Engineering, Stanford University
367 Panama Street, Stanford, CA 94305-2220, USA
[2]Department of Materials Science and Engineering, Stanford University
496 Lomita Mall, Stanford, CA 94305-4034, USA

Temperature measurements are important for the optimum development and energy extraction of enhanced and conventional geothermal resources. Currently, temperature is only measured in the wellbore, as no technology exists to provide information far into the formation. The development of temperature-sensitive nanotracers could allow for such measurements virtually anywhere in the formation.

This paper describes the synthesis and characterisation of two types of temperature-sensitive particles: tin-bismuth alloy nanoparticles and silica nanoparticles with covalently linked dye. Three experiments were performed with the tin-bismuth nanoparticles: a heating test, a slim-tube injection, and a Berea sandstone core injection. Both the heated sample and the effluent samples were characterised using Scanning Electron Microscopy (SEM) and Dynamic Light Scattering (DLS). A heating experiment was also performed with the dye-linked silica particles, and the heated sample was characterised using SEM imaging and fluorimetry.

The feasibility of using nanomaterials as tracers to measure reservoir temperature in-situ and estimate the geolocation of these measurements is addressed.

Keywords: in-situ temperature measurement, nanoparticles.

1. Introduction

There is currently no practical way to measure the reservoir temperature and pressure beyond the wellbore region. The overall goal of this research is to develop nanomaterials capable of measuring reservoir temperature and pressure and correlating such information to fracture connectivity and geometry. This idea is based on the fact that certain types of nanomaterials have the property of undergoing observable changes as a function of temperature and pressure, and that nanoparticles are of the appropriate size to fit through the reservoir pore spaces. Temperature-sensitive nanotracers could be used to assess reservoir performance by measuring temperature far from the wells, thereby providing thermal breakthrough information. Temperature-sensitive nanomaterials have already been developed and used in the biomedical industry for drug delivery. Thus, synthesising temperature-sensitive nanomaterials for geothermal applications is a feasible goal.

Making functional nanomaterials for reservoir sensing involves novel material syntheses to fabricate them and new reservoir engineering approaches to infer reservoir parameters based on the study of their transport properties. Several pressure- and temperature-sensitive nanoparticle concepts have been explored, but are subject to further evaluation from material and reservoir engineering standpoints. Each candidate chosen for investigation will be evaluated according to the following criteria: mobility in reservoir rock, temperature sensitivity, ease of recovery and detection, accuracy of sensing and ease of corresponding analyses, cost, and toxicity.

In order to accomplish the objectives of this study, syntheses of temperature-sensitive nanoparticles were explored for proof of concept and ultimate development. Preliminary heating experiments were conducted to investigate temperature sensitivity, and flow experiments were conducted to investigate the feasibility of transporting these nanoparticles through porous and fractured rocks. An initial investigation of the feasibility of estimating the geolocation of temperature measurements was also performed. The overall objective was to identify and understand the processes involved in the development and use of tailored nanosensors.

2. Tin-bismuth Alloy Nanoparticles

Tin-bismuth alloy nanoparticles were chosen for our first investigation of temperature-sensitive nanoparticles. This alloy has a melting temperature that is tunable between 139°C and 271°C by adjusting its composition, as shown in the phase diagram in Figure 1. A simple sensing scheme of melting and subsequent particle growth was conceived. The growth of native gold nanoparticles upon melting in geologic Arsenian pyrite has been observed by Reich et al. (2006) using transmission electron microscopy during in situ heating to 650°C. It was shown that when the gold nanopar-

ticles melted, they became unstable, leading to diffusion-driven Ostwald ripening and ultimately resulting in the coarsening of the size distribution. We hypothesised that upon melting, the size distribution of tin-bismuth alloy nanoparticles would also coarsen.

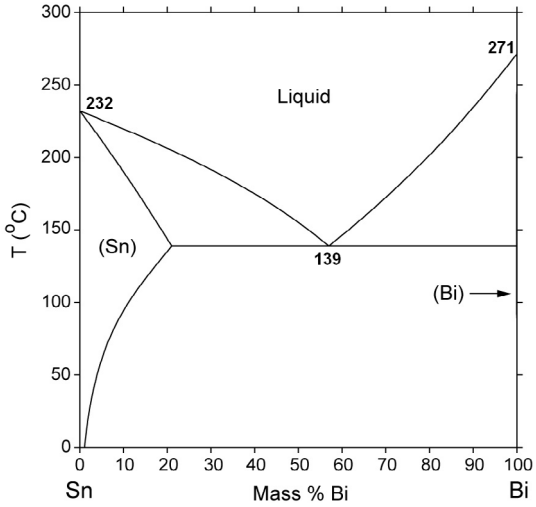

Figure 1: Phase diagram of tin-bismuth (NIST).

Tin-bismuth alloy nanoparticles of eutectic composition were synthesised via ultrasonic processing. These particles were characterised using DLS and SEM imaging. A bench heating experiment was also performed to study the thermal sensitivity of these nanoparticles. The sample was characterised again with DLS and SEM imaging after heating. Injection experiments were performed in a slim-tube packed with glass beads and a Berea sandstone core, and effluent samples were analysed with DLS and SEM imaging.

2.1 Synthesis of tin-bismuth alloy nanoparticles

To perform the synthesis, Sn and Bi were melted together at the eutectic composition (~60 wt % Bi and ~40 wt % Sn). After the alloy was cooled to room temperature, 100 mg was sonicated in 10 ml of mineral oil, a slight variation of the sonochemical method suggested by Chen (2005). The VC-505 ultrasonic processor manufactured by Sonics & Materials, Inc. with a 0.75 in. diameter high gain solid probe was used. The sonicator was operated at 200 W (~95% amplitude) with a pulse setting of 20 s on, 10 s off. The mixture was cooled to room temperature. The alloy particles were washed and centrifuged several times with a 1:1 mixture of hexane and acetone, rinsed in a solution of 0.1 M polyvinyl pyrrolidone (PVP) in ethanol, and finally suspended in ethanol. The centrifuge setting was 6000 rpm for 15 minutes each time.

2.2 Characterisation of tin-bismuth alloy nanoparticles

The tin-bismuth alloy nanoparticles were characterised in terms of size and shape using DLS and SEM imaging.

It was determined from three consecutive DLS measurements that there was a wide distribution of the particle hydrodynamic diameter, as shown in Figure 2.

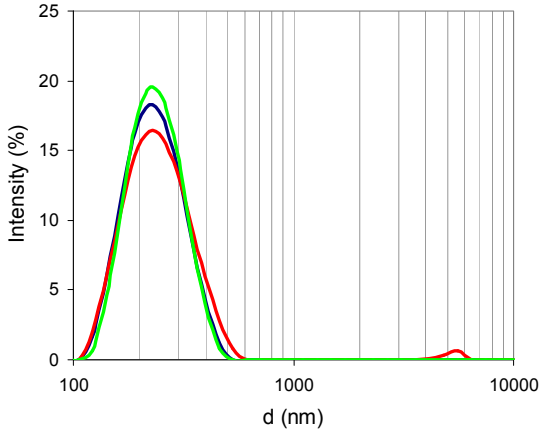

Figure 2: Logarithmic particle size distribution based on hydrodynamic diameter for original tin-bismuth nanoparticle sample.

The three measurements are in reasonable agreement, with an average modal value of 235 nm. The hydrodynamic diameter ranged from ~100 nm to ~600 nm, with Run 2 showing a small peak at ~5500 nm. This indicates that there may have been large particles in the sample, either due to aggregation or from the original synthesis.

The SEM images of the sample show good agreement with the DLS measurements, as shown in Figures 3 – 5.

It is apparent from Figures 3 – 5 that the tin-bismuth nanoparticles range from 50 nm to less than 600 nm. Furthermore, although many of the nanoparticles seem to be spherical as expected, the presence of nonspherical crystalline structures indicates that the sonochemical synthesis did not reach completion. Aggregation on the substrate is observed in both figures, but it is unclear whether this aggregation occurs in solution or upon drying on the substrate. The DLS results suggest that the latter may be the case.

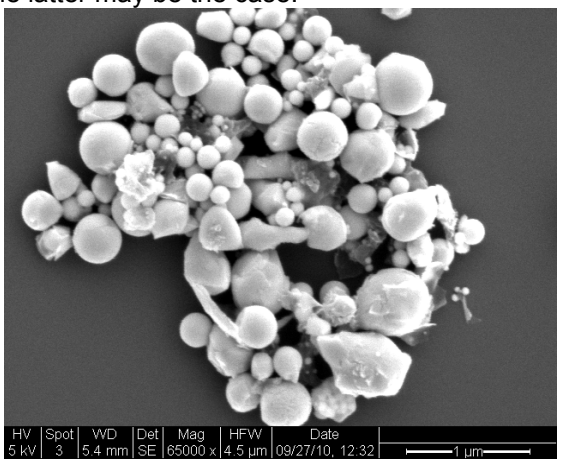

Figure 3: SEM image showing the wide range of tin-bismuth nanoparticle sizes.

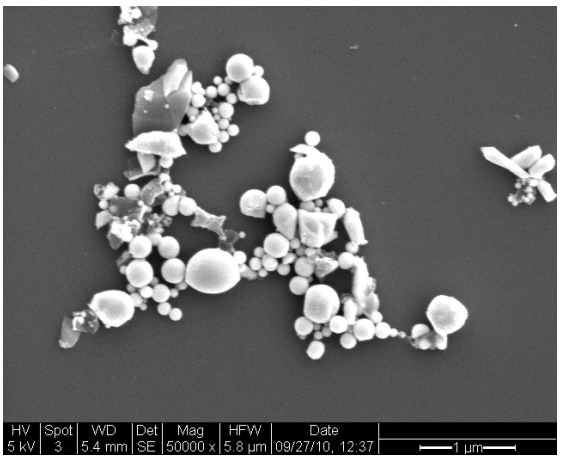

Figure 4: SEM image showing the wide range of tin-bismuth nanoparticle sizes.

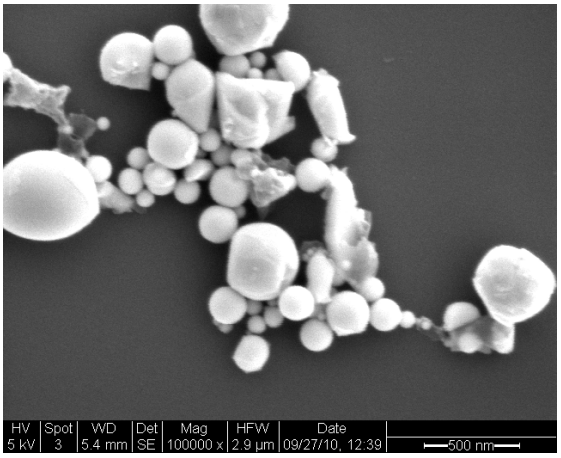

Figure 5: SEM image of tin-bismuth nanoparticles at higher magnification.

2.3 Tin-bismuth nanoparticle heating experiment

To begin investigating the melting behavior of tin-bismuth nanoparticles within the temperature range of interest, a sample of the nanofluid (tin-bismuth in mineral oil) was subjected to a preliminary heating experiment. Although ultimately we are interested in the melting behavior of the tin-bismuth nanoparticles in water, the heating experiments were performed in oil due to the complications associated with the boiling of water at experimental conditions. As shown in the phase diagram Figure 1, at the eutectic composition, the tin-bismuth alloy melts at 139°C. In fact, the nanoparticles likely melt at a slightly lower temperature than this due to melting point depression due to their size.

2.4 Experimental methods used in heating

The sample was heated using a heating mantle connected to a temperature controller with a feedback thermometer, as shown in Figure 6.

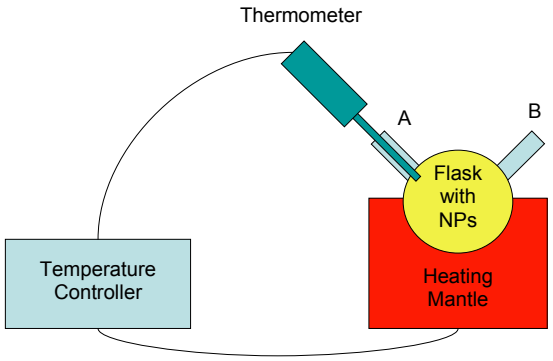

Figure 6: Experimental apparatus for tin-bismuth heating experiment

The flask containing the tin-bismuth nanoparticles in oil was placed in the heating mantle, which was connected to the temperature controller. The temperature controller was also connected to a thermometer, the feedback from which affected whether the mantle was heated, cooled, or maintained and the rate at which this was done. The thermometer was positioned in port A.

The sample was heated in steps to the expected melting point of 139°C. The sample was monitored for a color change near the expected melting point, and when none occurred, the sample was heated in steps to 210°C. No color change ever occurred, but the heating was stopped to prevent the mineral oil from burning. Also, it is likely that melting occurred regardless of the absence of color change. Finally, when the apparatus was at room temperature, the sample was removed from the flask.

The sample was then washed and centrifuged several times with a 1:1 mixture of hexane and acetone, rinsed in a solution of 0.1 M PVP in ethanol, and finally suspended in ethanol. The centrifuge setting was 6000 rpm for 15 minutes each time. This sample was characterised using DLS and SEM imaging.

2.5 Heating experiment results

The DLS results of the sample subjected to heating are shown in Figure 7.

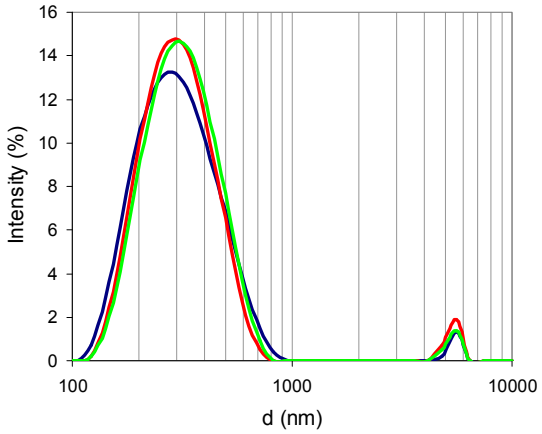

Figure 7: Logarithmic particle size distribution based on hydrodynamic diameter for heated tin-bismuth nanoparticle sample.

The three measurements are in relatively close agreement, with an average modal value of 321 nm. The hydrodynamic diameter ranged from ~100 nm to ~1000 nm. Appreciable secondary peaks in the range of ~4100 nm to ~6400 nm were observed for all runs. This indicates that there are large particles in the sample, most likely due to aggregation and fusion of the particles. Selected particle size distribution curves for comparison of the original and heated samples are shown in Figure 8.

As shown in the figure, the particle size distribution peak shifted noticeably to a larger size. Also, the secondary peak in the micron scale is noticeably larger, indicating that there are more large aggregates. SEM images of the heated sample are shown in Figures 9 and 10.

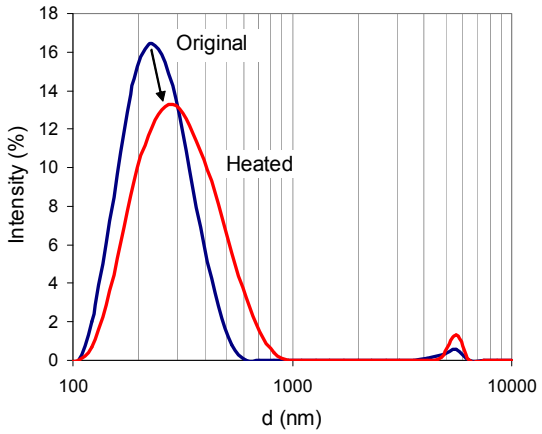

Figure 8: Comparison of logarithmic particle size distribution based on hydrodynamic diameter for original and heated tin-bismuth nanoparticle samples.

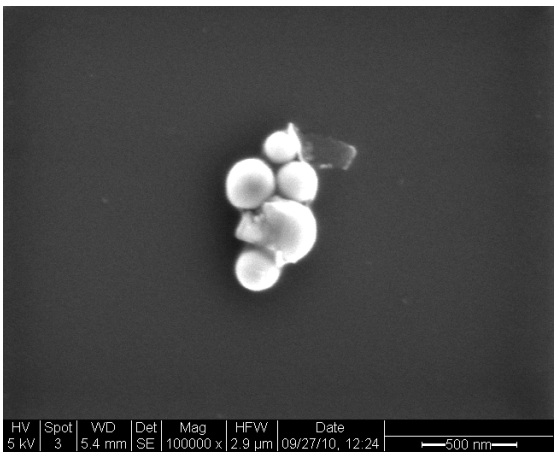

Figure 9: SEM image showing heated tin-bismuth nanoparticles.

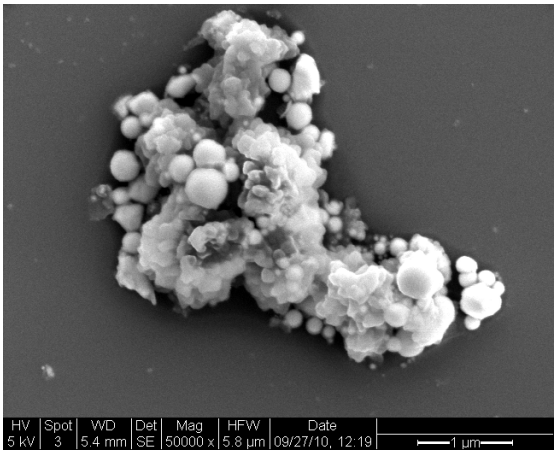

Figure 10: SEM image showing large aggregate of heated tin-bismuth nanoparticles.

Fusion of melted particles can be observed in both figures, and the sizes of both particles and large aggregates are within the range suggested by DLS results. While the fusion of melted particles could account for the shift in particle size distribution, it is difficult to reach any definite conclusions from the SEM results due to the very wide particle size distributions of both the heated and unheated samples. To avoid this ambiguity, the synthesis will be repeated with adjusted parameters in order to achieve a more uniform particle size distribution. Additionally, heating experiments will be repeated directly on a silicon substrate, and a small region of this substrate will be marked for unambiguous SEM analysis.

2.6 Tin-bismuth nanofluid injection experiments

Because of the temperature sensitivity of the tin-bismuth alloy nanoparticles and their potential to be used as a geothermal resource temperature sensor, transport of these particles through porous media was investigated. The nanoparticle suspensions were injected into a slim tube packed with glass beads and into a Berea sandstone core.

2.7 Berea sandstone and slim tube characterisation

The porosity of the core sample was measured by resaturation with pure water and found to be around 17.5% with pore volume in the order of 10 cm^3.

The liquid permeability was measured by introducing pure water at different flow rates ranging from 1 to 5 cm^3/min. The average permeability was found to be approximately 125.4 *md*. By mercury intrusion, it was found that the sandstone core has pore sizes in the range from 0.01 to 20 *μm.*

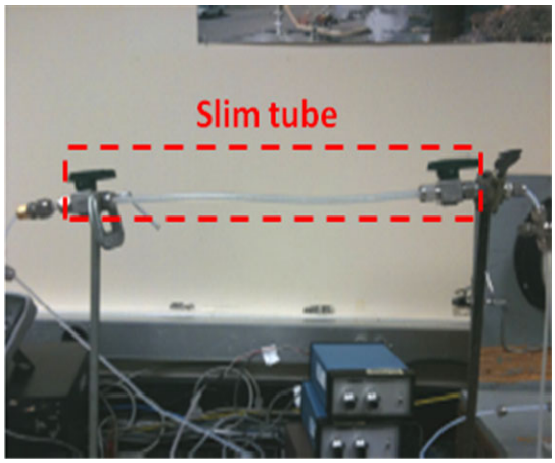

Figure 11: Polypropylene slim tube packed with glass beads.

To investigate the mobility of nanoparticles in the absence of rock materials (such as clays), the nanoparticles were injected into a slim tube packed with glass beads. A 30 *cm* long polypropylene slim tube was constructed. The tube was packed with glass beads (Glasperlen 0.1 *cm* in diameter from B. Braun Biotech International) and fitted with screens and valves at each end. This polypropylene slim tube is pictured in Figure 11. The permeability and pore volume of the slim tube packed with glass beads were found to be approximately 18.1 *md* and 2.6 cm^3, respectively.

2.8 Experimental methods used in injection

Tin-bismuth nanoparticle injections were conducted to investigate their flow mechanism through the pores of Berea sandstone. The apparatus used is depicted in Figure 12. Nanofluid solution was contained in a pressure vessel downstream of the water pump. The nanoparticles were injected with the aid of nitrogen gas.

Initially, the core was preflushed with several pore volumes of pure water to displace rock fines and debris. About 30% (3 cm^3 of nanofluid) of the pore volume was then injected. Subsequent to the injection of the nanofluid, a post injection of 13 pore volumes of pure water was introduced. In addition, the core was backflushed with 5 pore volumes in attempt to mobilise nanoparticles that might be trapped at the inlet of the core. The injection was at the rate of 1 cm^3/min. A total of 40 effluent samples were collected at the rate of 2 cm^3 per sample. The effluent sample volume was increased to 6 cm^3 for the last six pore volumes. During the backflushing of the core, the flow rate was varied between 1 to 5 cm^3/min. The higher flow rates were used to investigate their effect on the mobility of the nanoparticles. SEM imaging was used to analyse the selected effluent samples.

2.9 Injection experiment results

Tin-bismuth nanoparticles were identified in a few effluent samples in very low concentrations. It was observed that only nanoparticles with diameters 200 *nm* and smaller were transported within the pore spaces of the rock, as shown in the SEM image in Figure 13A. Note that the influent sample (Figure 3) contained nanoparticles as large as 600 *nm*. It was speculated that larger particles (greater than 200 *nm*) were trapped at the inlet of the core. In fact, SEM imaging of the backflushing effluents showed that there was entrapment of various nanoparticle sizes, including the sizes greater than 200 *nm* (Figure 13B). The rock filtered the nanofluid injected allowing only a certain particle sizes to flow across it. It should be noted that this is a qualitative analysis in which the determination of the relative numbers of particles recovered was not possible.

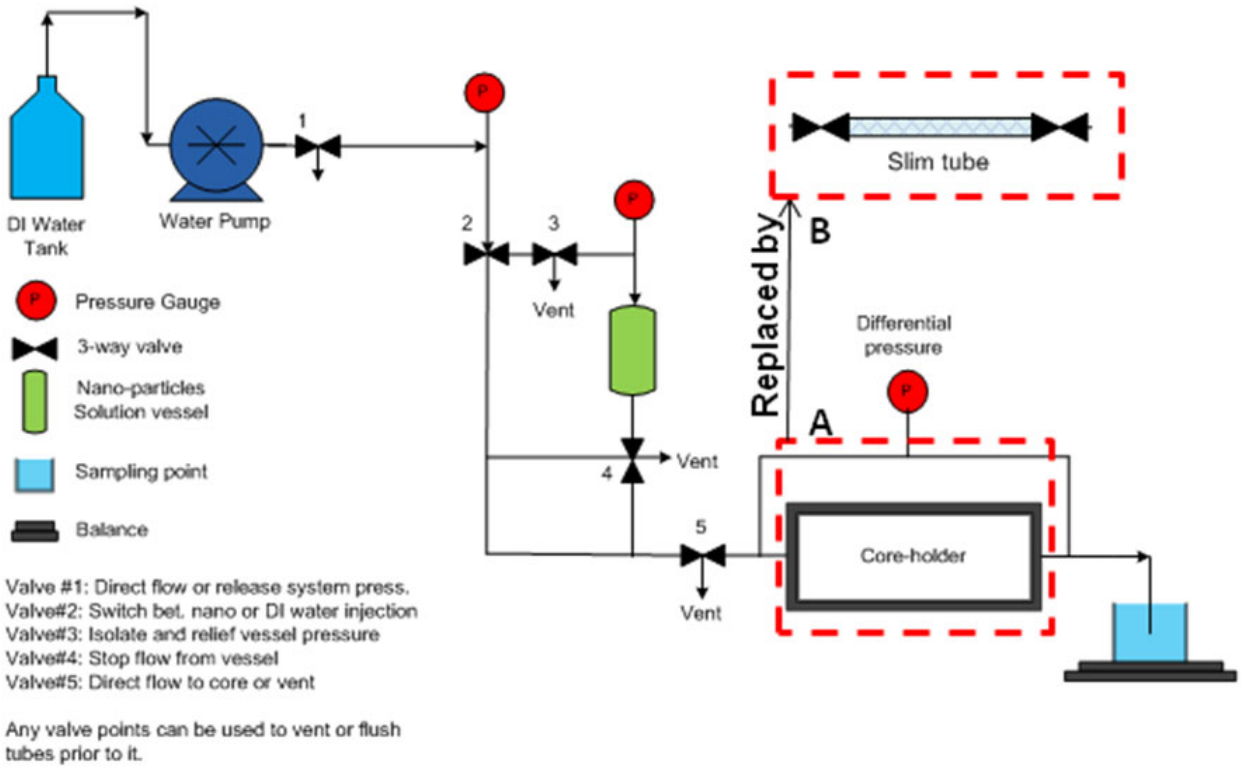

Figure 12: Schematic of the flow experiment apparatus used for injections into (A) core plug and (B) slim tube packed with glass beads.

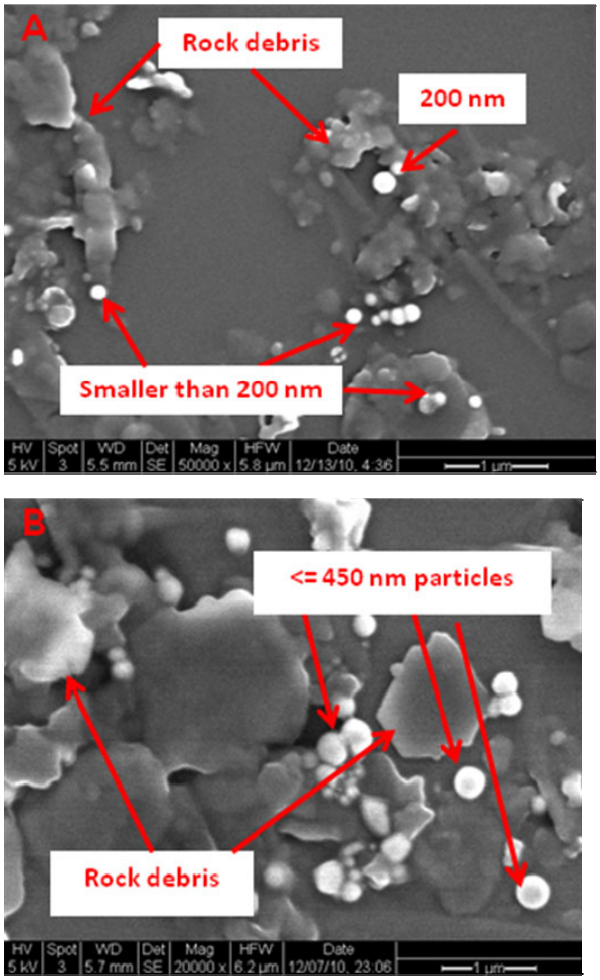

Figure 13 (left): SEM imaging showing the tin-bismuth nanoparticles at the effluent during (A) injection and (B) backflushing of the Berea sandstone. Only particles smaller than 200 nm transported through pore spaces while larger particles trapped at the inlet of the core and mobilised during backflushing.

The permeability measurements during the injection agree with this finding. The permeability as a function of the injected volume is depicted in Figure 14. There was a sudden drop in permeability to about 56% of the original value, after which the permeability remained at that level during the first post injected pore volume, indicating the partial plugging of the pores. Then, permeability started to increase until reached a plateau at approximately 82% of its value prior to the nanofluid injection. At this time, only nanoparticles of 200 *nm* and smaller were observed in the effluent, using SEM (Figure 13A). As mentioned earlier, the backflushing of the core mobilised some particles and as a result the permeability of the rock improved slightly by 8% (i.e. back to 90% of its original value).

However, permeability improvement (from 56% to 90% of original value) does not imply a good recovery of the injected nanoparticles. If the injected nanofluid has a visible color, it is possible to observe the nanoparticles in the effluent visually. In the case of the tin-bismuth injection, the influent had a dark gray color that was characterised by being highly concentrated with nanoparticles. All effluent samples appeared transparent, so it was hypothesised that many of these nanoparticles were trapped within the rock pores, most likely at

the inlet of the core. Examining the pore spaces of the rock itself confirmed that considerable numbers of the tin-bismuth nanoparticles were trapped (Figures 15 and 16).

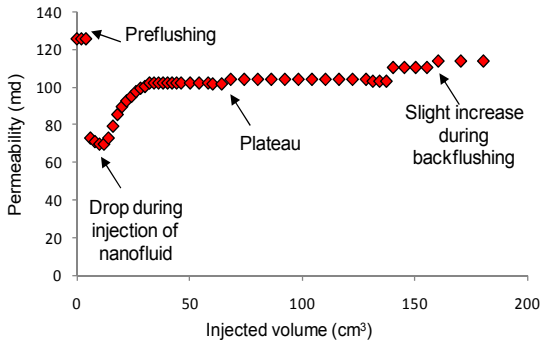

Figure 14: Permeability measurements during the injection of the tin-bismuth nanoparticles.

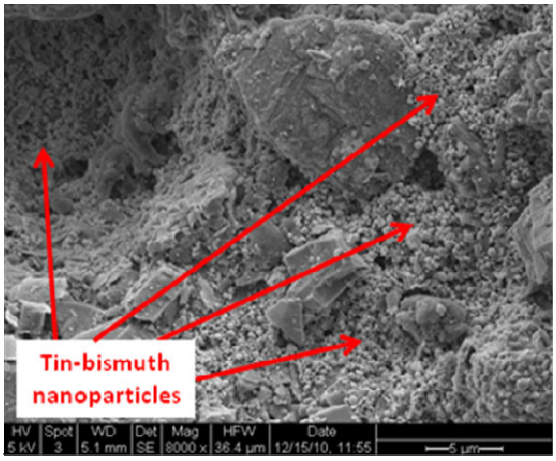

Figure 15: SEM image of the pore space at the inlet of Berea sandstone used during the tin-bismuth injection. Nanoparticle entrapment is apparent.

Further evaluation using SEM imaging (Figure 16) of the rock pore spaces demonstrates the bridging and plugging of the tin-bismuth nanoparticles in the pore throat entry. Kanj et al. (2009) explained that small particles of high concentrations might bridge across the pore throat. The authors also added that larger particles could result in direct plugging of the pore entry. Both phenomena would impact the rock permeability negatively. Particles shown in Figure 16 could not be mobilised either by increasing the injection flow rate or by backflushing and were probably responsible for the permanent reduction in the rock permeability.

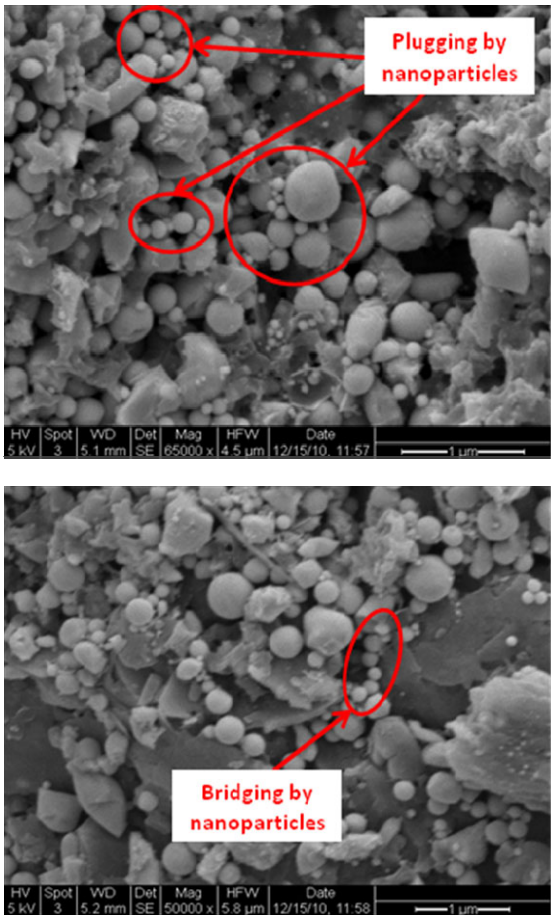

Figure 16: SEM images from within the pore spaces of the Berea sandstone. They demonstrate the bridging and plugging phenomena.

The SEM analysis did not provide conclusive evidence of the mechanism of particle entrapment. Alaskar et al. (2010) reported that the nanoparticles' shape and surface characteristics play a major role in their transport through a porous medium. They also reported that the spherical silicon dioxide (SiO_2) nanoparticles with narrow size distribution and surface charge compatible to that of the rock were transported successfully through the pore spaces of Berea sandstone. SiO_2 nanoparticles were not trapped in the pore spaces by hydraulic, chemical or electrostatic effects. The tin-bismuth nanoparticles exhibit similar properties in terms of shape and surface charge (negatively charged), except that the tin-bismuth nanoparticles had a wide distribution of sizes between 50 to 600 *nm* (Figure 2 and 3). Thus, particle shape and surface charge should not impose flow constraints. The optimised testing program suggested by Kanj et al. (2009) emphasises particle size, influent concentration and affinity of particles to rock matrix.

In the case of tin-bismuth injection, although the influent sample had wide distribution of particle sizes, they were all within the size of the pore network. Therefore, it was concluded that the tin-bismuth nanoparticles affinity and/or concentration may have caused their entrapment.

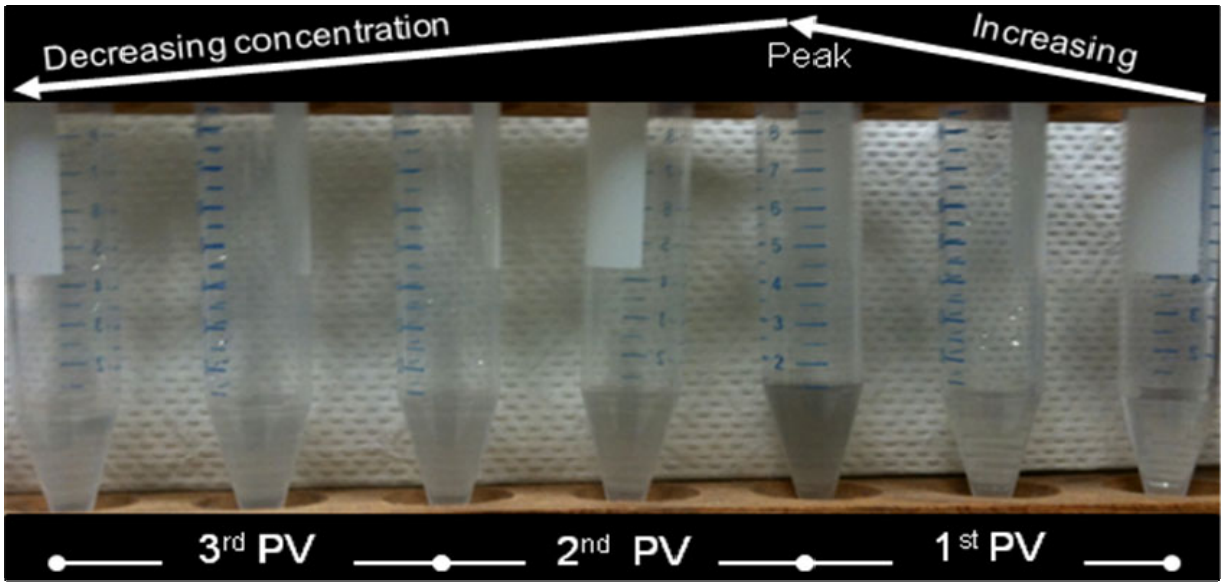

Figure 17: Visual characterisation of effluent samples for their tin-bismuth nanoparticles content based on colour.

Further investigation of particle affinity to Berea sandstone was carried out by injecting the same influent sample with identical concentration to a slim tube packed with glass beads. This allowed testing the transport of the tin-bismuth nanoparticles in the absence of the core material. One pore volume of the nanofluid was injected at the rate of 0.5 cm^3/min followed by continuous injection of pure water at the same rate. Several effluent samples were collected and analysed by SEM imaging.

It was found that the tin-bismuth nanoparticles of all sizes flowed through the slim tube. The increasing concentration of the nanoparticles was observed visually through the injection of the first post-injected pore volume as illustrated in Figure 17. SEM imaging confirmed this finding as depicted in Figure 18.

Thus, it has been demonstrated that the spherically shaped tin-bismuth nanoparticles can be recovered following their injection into tube packed with glass beads without being trapped within the flow conduits, but not through the pore network of the rock (which has much smaller pores). This might be attributed to an affinity of these nanoparticles to the sandstone rock matrix or high nanoparticle concentration imposing constraints to their flow. The complexity of the rock pore network compared the large pores in the glass beads was not taken into consideration during this analysis.

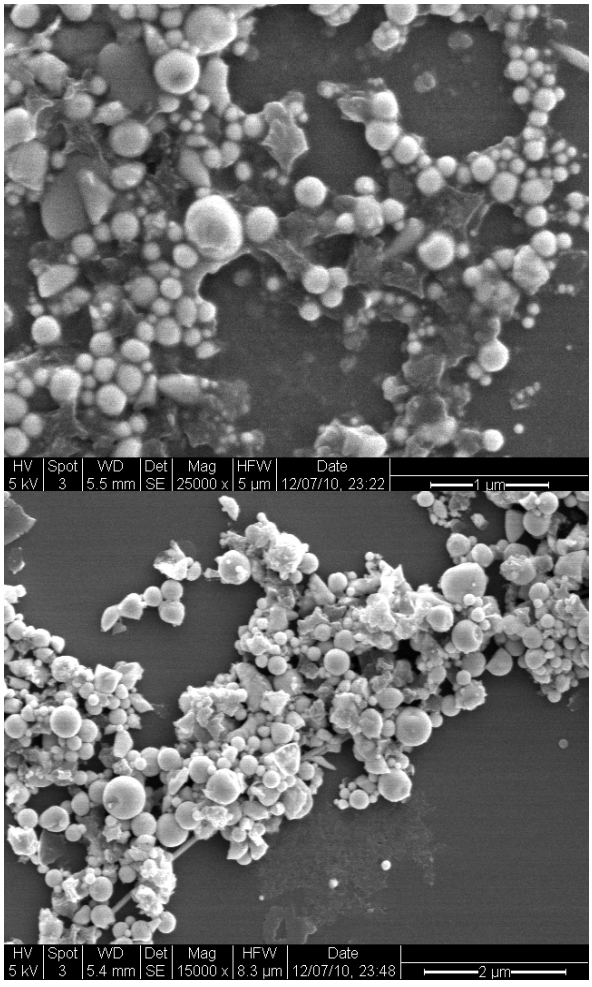

Figure 18: SEM images of the effluent collected during the injection of tin-bismuth nanoparticles into the slim tube packed with glass beads.

3. Silica nanoparticles with covalently-attached fluorescent dye

As silica particles have been proved to have transported through sandstone core successfully, we further changed their surface properties to explore their temperature response. According to the report by Wu et al. (2008), when free fluorescent dye molecule was attached to silica nanoparticles' surface, through energy transfer, the fluorescent properties of these molecules were changed. Therefore, when the covalent bond between fluorescent dye molecule and surface modified silica nanoparticle is broken under high temperature; the difference of fluorescent behavior before and after heating experiment would be detected.

3.1 Synthesis of fluorescent dye-attached silica nanoparticles

First, silica nanoparticles (Nanogiant, LLC) were prepared by surface modification. In a typical reaction, 0.5ml of 3-Aminopropyltriethoxysilane (APTS) was added to 100mg silica nanoparticle suspended in 25 ml of toluene under nitrogen and heating to ~95 °C for 4 hours. The resulting particles were washed by centrifugation in ethanol and acetone (10min at 4,400 rpm). Then the particles were dried at ~95°C overnight.

After that, we attached dye molecules (Oregon 488, Invitrogen) to the surface of the modified silica nanoparticles. A suspension of 1.0 mg of the amino-modified Silica nanoparticles in a mixture of 1ml of ethanol and 15 μl of a 10mmol/L phosphate buffer (pH 7.3) was reacted with 12.7 μl of dye molecule solution (1mg/ml water solution) in dark for 3 hours at room temperature. The resulting particles were washed by centrifugation (10min at 4,400 rpm) in ethanol and acetone.

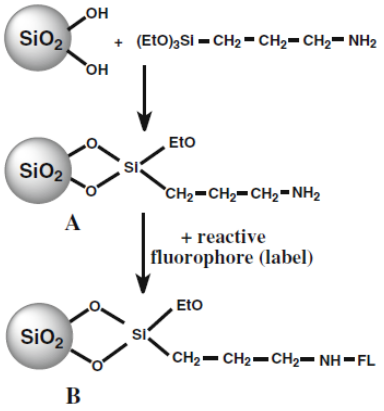

Figure 19: Schematic representation of silica nanoparticle surface modification and dye attachment by Saleh, et al. (2010).

We also performed surface modification and dye attachment reaction on a monolayer of silica nanoparticles on quartz substrate using the same experiment parameters.

3.2 Characterisation of silica nanoparticles

We used Fluorescent Microscopy, SEM and Fluorescent Spectrum to characterise the dye-attached silica nanoparticles.

Fluorescent microscopy characterisation as shown in Figure 20 was done using the substrate base dye-attached silica nanoparticle sample. We can see clearly that the dye molecules were attached successfully to the surface of silica nanoparticles. The whole substrate was fluorescent although not uniformly (some spots were brighter with more fluorescent molecules attached).

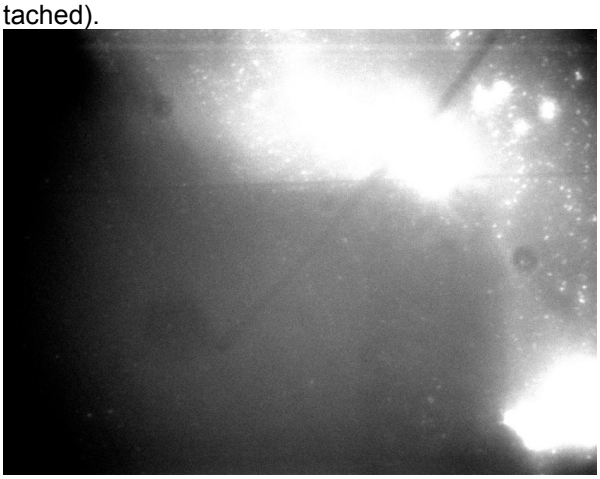

Figure 20: Fluorescent microscopy image of dye-attached silica nanoparticles on quartz substrate.

SEM was also used for characterisation.

We also measured the fluorescence spectra of free dye molecule solution, silica nanoparticle suspension, dye-attached silica nanoparticles both on substrate and in solution.

We used 400nm as the excitation wave length. We could see from the fluorescence spectrum of Oregon 488 solution that its emission peak is at ~530nm, shown in Figure 21.

As control, we measured the fluorescence spectrum of silica nanoparticles in water without dye attachment. We also measured the fluorescence spectra of dye-attached silica nanoparticles in water and on substrate. We used 400nm as excitation wavelength, shown in Figure 22. The results showed that, without dye attachment, there was no fluorescence response of the silica nanoparticles and after dye attachment, two peaks at ~425nm and ~530nm were observed in the spectrum.

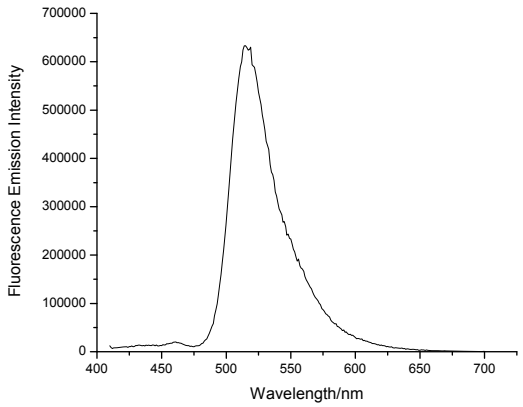

Figure 21: Fluorescence spectrum of Oregon 488 dye molecule solution (excitation wavelength 400nm).

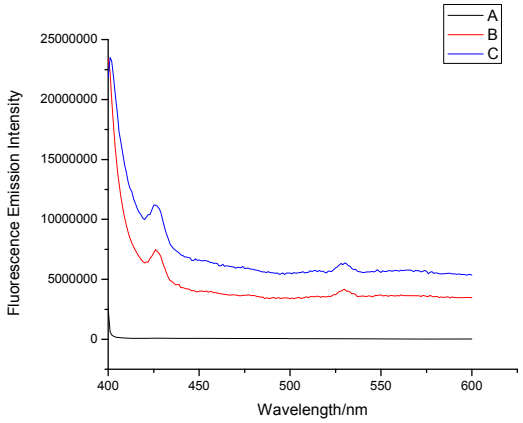

Figure 22: Fluorescence spectrum (excitation wavelength 400nm): (A) Silica nanoparticle without dye attachment as control; (B) Dye-attached silica nanoparticles in water; (C) Dye-attached silica nanoparticles on quartz substrate.

3.4 Heating experiment of dye-attached silica nanoparticle

A heating experiment was conducted using the sample of dye-attached silica nanoparticles on quartz substrate. We heated the substrate on a hot plate at 200°C for 15min. Then we soaked the substrate in ethanol and acetone respectively and washed the substrate both with ethanol and acetone. The substrate was dried in air. We used Fluorescence Spectrum to characterise this sample.

Fluorescence spectrum was measured after heating test, shown in Figure 23. We used an excitation wavelength of ~360nm. We can observe a wide peak at ~425nm of the heated sample which was obviously different from the sample before heating. Besides that, we observed at ~380nm and ~475nm there were two shoulder peaks and at ~575nm there was a small peak in both spectra.

Hence, a clearly identifiable property change (fluorescence) is available as a temperature indicator using this kind of nanoparticle.

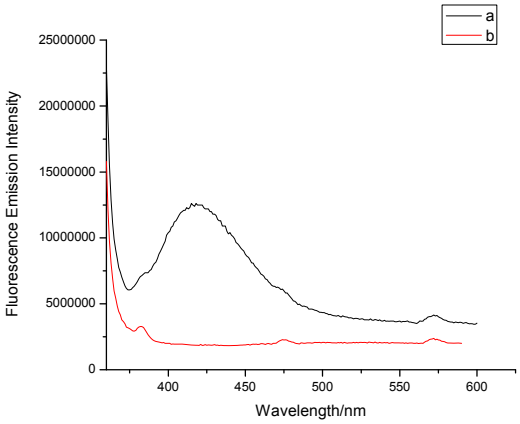

Figure 23: Fluorescence spectrum (excitation wavelength 360nm): (a) Dye-attached silica nanoparticle after heating experiment at 200°C for 15min; (b) Dye-attached silica nanoparticle without heating experiment.

4. Estimating the location of temperature measurements using dye-release nanosensors

We have demonstrated the potential capability of dye-attached silica nanoparticles to measure temperature in geothermal reservoirs. However, simply knowing that some region of the reservoir has a certain temperature without knowing the geolocation of the measurement is of limited use to reservoir engineers. If this geolocation could be estimated accurately, the reservoir temperature distribution could be mapped. This could make it possible to predict thermal breakthrough in a reservoir and would allow reservoir engineers to make more informed decisions. Here we discuss the potential capability of a nanosensor with a dye-release sensing mechanism (e.g. dye-attached silica nanoparticles) to measure reservoir temperature and estimate the geolocation of this measurement via analysis of the return curve of the released dye.

A thought experiment was performed consisting of two hypothetical tracer tests: one with a conservative solute tracer and one with dye-releasing nanosensors. Synthetic tracer return curves for these hypothetical tests were generated using an analytical solution to the advection-dispersion equation, which is often used to describe subsurface tracer flow. Juliusson and Horne (2011) expressed the one-dimensional form of this equation as:

$$R\frac{\partial C}{\partial t} = \alpha u \frac{\partial^2 C}{\partial x^2} - u\frac{\partial C}{\partial x} \qquad (1)$$

where C is tracer concentration, x is the spatial coordinate, t is time, u is the flux velocity, and α is

the dispersion length, and R is the tracer retardation factor, which accounts for the retardation of tracer transport caused by the reversible adsorption of tracer to rock interfaces. For this initial investigation, the simple case with a constant flux velocity v (i.e. constant flow rate) was considered, and it was assumed that R is constant with respect to t, x, and C for both the solute tracer and the nanosensors. The authors acknowledge that it might be more realistic to assume that R varies spatially, as is suggested by Chrysikopoulos (1993), and that nanoparticle flow likely requires even more complex treatment. With these caveats in mind, it was decided to first examine the simplest possible case.

Kreft and Zuber (1978) provided a solution to the advection-dispersion equation with flux injection and detection boundary conditions, and Juliusson and Horne (2011) rewrote this solution to include the retardation factor R:

$$C = \frac{mV_x}{qt\sqrt{4\pi V_\alpha qt}} \exp\left(-\frac{\left(qt - V_x\right)^2}{4V_\alpha qt}\right) \quad (2)$$

$$V_x = RA\phi x \quad (3)$$

$$V_\alpha = RA\phi\alpha \quad (4)$$

where m is the mass injected, q is the volumetric flowrate, t is time, V_x is the pore volume modified by the retardation factor R, V_α is the dispersion volume modified by R, A is cross-sectional area, φ is porosity, and α is the dispersion length.

Consider a geothermal reservoir that consists of a single fracture with length L, cross-sectional area A, and porosity φ. Before exploitation, the reservoir had a uniform temperature distribution with a temperature of T_1. Some years after the onset of exploitation, the thermal front has advanced to the position x_f, and the portion of the reservoir behind the front has cooled to temperature T_2, as shown in Figure 24. Suppose a nanosensor has been designed to release a fluorescent dye at the threshold temperature T_1, and assume that this release occurs instantaneously upon exposure to this threshold.

Two tracer tests are performed. In one test, a mass m_c of a conservative tracer with a retardation factor R_c is injected into the reservoir. The tracer is sampled at the production well (i.e. $x = L$), and the return curve can be described by Equations 5 – 7:

$$C_c = \frac{m_c V_{x,c}}{qt\sqrt{4\pi V_{\alpha,c} qt}} \exp\left(-\frac{\left(qt - V_{x,c}\right)^2}{4V_{\alpha,c} qt}\right) \quad (5)$$

$$V_{x,c} = R_c A\phi L \quad (6)$$

$$V_{\alpha,c} = R_c A\phi\alpha \quad (7)$$

where the subscript c denotes the conservative tracer.

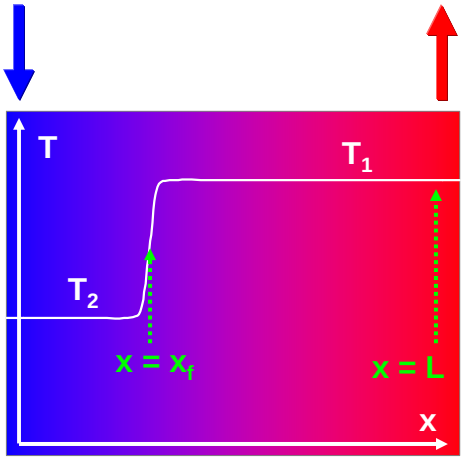

Figure 24: Cartoon of temperature distribution in a geothermal reservoir with a thermal front at position x_f .

In the second test, a slug of the dye-releasing nanosensors with retardation factor R_n is injected into the reservoir. Upon reaching exposure to the threshold temperature T_2 at position x_f, the nanosensors release a mass m_r of the attached dye, which itself behaves like the conservative solute tracer in the previous tracer test, and has a retardation factor R_c. The released dye is sampled at the production well. The return curve of the released dye is influenced by both R_n and R_c, because it travels with the nanosensor retardation factor R_n from $x = 0$ to $x = x_f$ and the retardation factor R_c from $x = x_f$ to $x = L$. Thus, the return curve of the released dye can be described by Equations 8 – 11:

$$C_r = \int_0^t \frac{m_r V_{x,n}}{qt\sqrt{4\pi V_{\alpha,n} q(t-\tau)}} \exp\left(-\frac{\left(q(t-\tau) - V_{x,n}\right)^2}{4V_{\alpha,n} q(t-\tau)}\right) \bullet \frac{qV_{x,r}}{qt\sqrt{4\pi V_{\alpha,c} q\tau}}$$

(8)

$$V_{x,n} = R_n A\phi x_f \quad (9)$$

$$V_{\alpha,n} = R_n A\phi\alpha \quad (10)$$

$$V_{x,r} = R_c A\phi\left(L - x_f\right) \quad (11)$$

where the subscript n denotes the nanosensors and the subscript r denotes the released dye. Note that $V_{x,r}$ can be rewritten as:

$$V_{x,r} = V_{x,c} - \frac{V_{\alpha,c}}{V_{\alpha,n}} V_{x,n} \quad (12)$$

Thus, the return curves for the conservative tracer can be fit to Equation 5 by adjusting the values of unknowns $V_{x,c}$ and $V_{\alpha,c}$ (i.e. minimising the norm of the differences between the return curve data and the model with the unknowns as decision

variables). Subsequently, the return curves for the released dye can be fit to Equation 8 by adjusting the values unknowns $V_{x,n}$ and $V_{\alpha,n}$. Note that $V_{x,r}$ is not explicitly adjusted here because it can be expressed in terms of the other unknowns. Once the values of the unknowns have been determined, one can calculate the geolocation of the thermal front using Equation 13:

$$x_{f,d} = \frac{x_f}{L} = \frac{V_{x,c} - V_{x,r}}{V_{x,c}} \qquad (13)$$

where $x_{f,d}$ is the dimensionless position of the thermal front.

This analysis was demonstrated successfully in an example problem with the parameter values shown in Table 1.

Table 1: Parameter Values Used In Return Curve Analysis Demonstration Problem

Parameter	Value
R_c	2
R_n	1
A	200 m^2
φ	0.10
L	1000 m
α	25 m
Pe = L / α	40

These values were chosen somewhat arbitrarily for the purposes of this demonstration. However, values of R_c and R_n were used such that the nanosensors experience no retardation and the solute tracer does experience retardation. This is based on studies of colloid transport in fractures which showed that colloids exhibit breakthrough more rapidly than solute tracers because they tend to stay in fluid streamlines and do not experience matrix diffusion (Reimus 1995).

Synthetic return curve data for the conservative tracer and the nanosensors were generated for various values of x_f using Equations 5 and 8, and Gaussian noise was added for the sake of realism. An optimisation solver was then used to find the best fit to Equations 5 and 8 by adjusting the unknowns. The results are tabulated in Table 2, and select return curves are plotted in Figure 25.

Reasonably good estimates of the geolocation of the thermal front were obtained for all scenarios except for x_f = 0.05. This is physically intuitive, because the return curves for the conservative tracer and the released dye are almost identical when the thermal front is still close to the injection well, making it difficult to estimate the front geolocation quantitatively. The poor fit of the return curve of the released dye can be attributed mathematically to the problematic nature of the optimisation surface for this scenario, which is shown in Figures 26 and 27.

Table 2: Parameter Values Used In Return Curve Analysis Demonstration Problem

$x_{f,d}$	$x_{f,d}$ estimate	Error
0.05	0.037	26%
0.15	0.155	3.2%
0.25	0.248	0.8%
0.35	0.382	9.1%
0.45	0.431	4.3%
0.55	0.517	5.9%
0.65	0.632	2.7%
0.75	0.746	0.6%
0.85	0.852	0.2%
0.95	0.925	2.7%

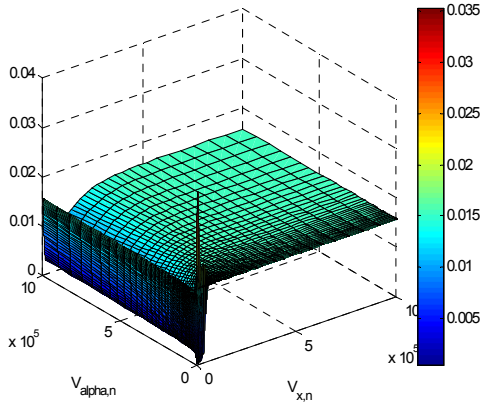

Figure 26: Objective function surface for fitting the return curve of the reactive tracer when x_f = 50 m.

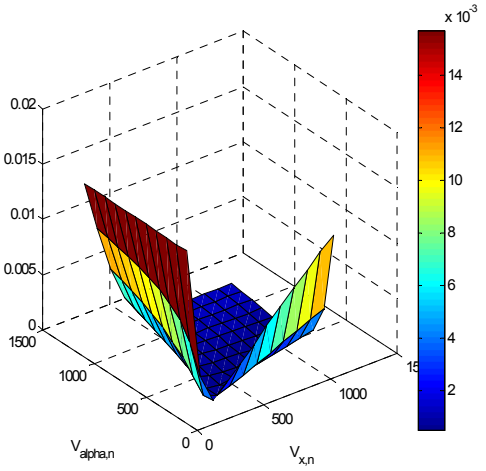

Figure 27: Objective function surface for fitting the return curve of the reactive tracer when x_f = 50 m, zoomed in near the minimum of ($V_{x,n}$ = 1000 m^3, $V_{\alpha,n}$ = 500 m^3). Note that the point chosen by the solver was ($V_{x,n}$ = 268.3 m^3, $V_{\alpha,n}$ = 180.8 m^3).

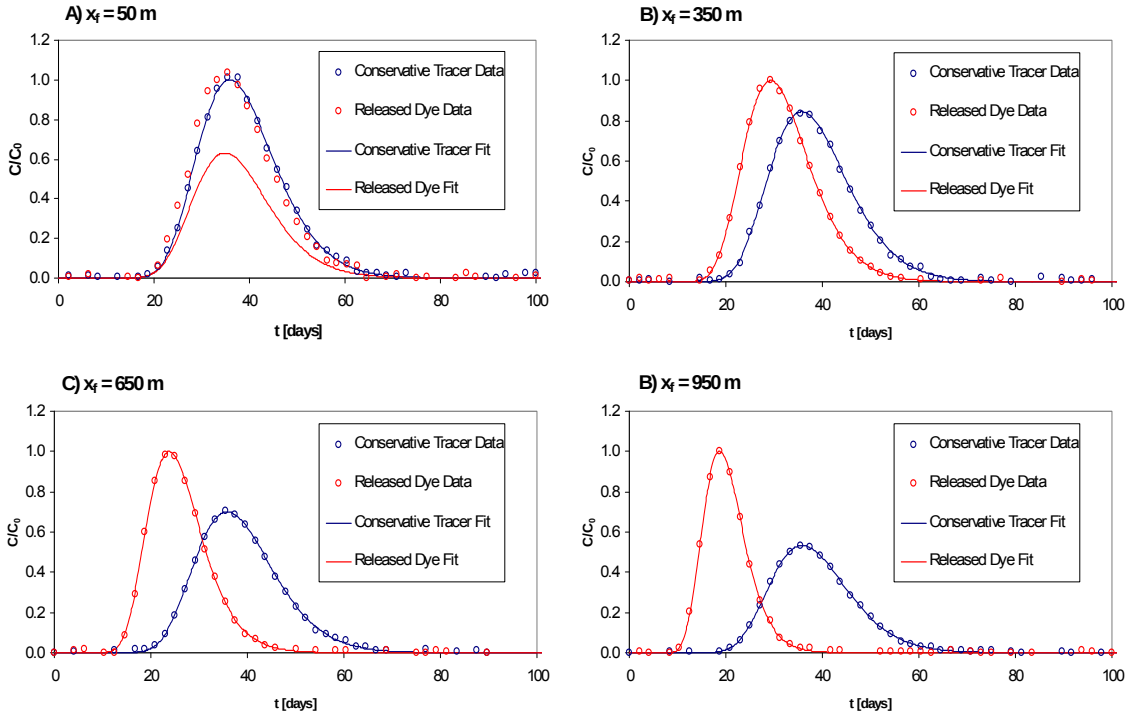

Figure 25: Return curve data and fits for A) x_f = 50 m, B) x_f = 350 m, C) x_f = 650 m, and D) x_f = 950 m. Note that released dye experiences breakthrough first because it is carried a distance x_f by the nanosensor, which has a retardation factor of 1, while the conservative tracer has a retardation factor of 2.

The large trough along the $V_{\alpha,n}$ axis in Figure 26 indicates that for large initial guesses of $V_{\alpha,n}$, the solver might get stuck far from the minimum (since change in the objective function is the termination criteria). Moreover, the values of the objective function vary very little near the minimum, as shown in Figure 27. This explains why the solver terminated at the point ($V_{x,n}$ = 268.3 m^3, $V_{\alpha,n}$ = 180.8 m^3) and resulted in a poor fit.

5. Conclusions

We have synthesised two types of temperature-sensitive nanoparticles and demonstrated their sensitivity in the geothermal temperature range. The two types are melting tin-bismuth alloy nanoparticles and silica nanoparticles with dyes incorporated using a temperature-sensitive covalent linkage. We performed an initial investigation of the feasibility of estimating the geolocation of temperature measurements using return curve analysis for a dye-releasing nanosensor.

Tin-bismuth alloy nanoparticles were synthesised using a sonochemical method. A heating experiment was performed using these nanoparticles, and particle growth was observed, which was indicative of melting. The flow characteristics of the tin-bismuth nanoparticles were also investigated. Tin-bismuth nanoparticles of all sizes were transported successfully through the slim-tube. However, when nanoparticles were injected into a Berea sandstone core, only particles with diameters of 200 *nm* and smaller were detected at very low concentrations in the effluent. Nanoparticle plugging and bridging was detected at the core inlet. As measurements of the particle size and surface charge did not indicate any flow constraints, entrapment was attributed either to an affinity of the tin-bismuth to the sandstone rock matrix or an excessively high nanoparticle concentration at the inlet, or both.

Moreover, dye-attached silica nanoparticles were synthesised through surface modification and fluorescent reaction. We demonstrated the successful synthesis by SEM and fluorescence spectrum characterisation. A heating experiment was also conducted using a sample of silica nanoparticles on substrate. The results showed that the fluorescence spectra of dye-attached silica nanoparticles in water and on quartz substrate are the same. After heating, the fluorescence spectrum showed an obvious difference at a wavelength of 425nm. Although the mechanism of this phenomenon is not fully understood yet, we did discover the excellent potential of dye-attached silica nanoparticles as temperature sensors for geothermal applications.

To emphasise the potential usefulness of a nanosensor with a dye-release mechanism (such as dye-attached silica nanoparticles), an initial study was performed to evaluate the feasibility of estimating the geolocation of temperature measurements by analysing the return curve of the released dye. Accurate estimation of measurement

geolocations would allow one to map the temperature distribution in a geothermal reservoir and provide information about thermal breakthrough. A simplified example problem was examined in which an analytical solution of the one-dimensional advection-dispersion equation was used to generate synthetic return curve data for two tracer tests: one with a conservative tracer and one with dye-releasing nanosensors. Gaussian noise was added to the synthetic data. Finally, return curves were fit to the data by adjusting the values of four unknowns (two unknowns for each return curve). Reasonably accurate estimates of the measurement geolocation were achieved for various scenarios, with the exception of a poor estimate when the thermal front had not advanced very far into the reservoir. This could possibly be remedied by using a more sophisticated optimisation algorithm.

6. Acknowledgements

The authors wish to thank Robert Jones, Sirion SEM Laboratory Manager, for his support during this project. The authors also acknowledge the continued support of the Department of Energy (under contract number DE-FG36-08GO18192).

7. References

Alaskar, M., Ames, M., Horne, R.N., Li, K., Connor, S. and Cui, Y.: "In-situ Multifuction Nanosensors for Fractured Reservoir Characterisation," GRC Annual Meeting, Sacramento, USA, vol. 34 (2010).

Botterhuis, N., Sun, Q., Magusin, P., Santen, R. and Sommerdijk, N.: "Hollow Silica Spheres with an Ordered Pore Structure and Their Application in Controlled Release Studies," *Chem. Eur. J.* 2006, **12**, 1448-56.

Chen, H., Li, Z., Wu, Z. and Zhang, Z.: "A novel route to prepare and characterize Sn-Bi nanoparticles," *Journal of Alloys and Compounds*. 2005, **394**, 282-285.

Digital image. Phase Diagrams & Computational Thermodynamics. The National Institute of Standards and Technology. Web. 7 July 2010. <http://www.metallurgy.nist.gov/phase/solder/bisn.html>.

Juliusson, E., and Horne, R.N.: "Analyzing Tracer Tests During Variable Flow Rate Injection and Production," Proc. of Thirty-Sixth Workshop on Geothermal Reservoir Engineering, Stanford University, Stanford, CA. 2011.

Kanj, M., Funk, J., and Al-Yousif, Z.: "Nanofluid Coreflood Experiments in the Arab-D," SPE paper 126161, presented at the 2009 SPE Saudi Arabia Technical Symposium and Exhibition held in Saudi Arabia, Alkhobar, May 09-11.

Kreft, A. and Zuber, A..: "On the physical meaning of the dispersion equation and its solutions for different initial and boundary conditions," *Chemical Engineering Science*. 1978, **33**(11), 1471–1480.

Reich, M., Utsunomiya, S., Kesler, S.E., Wang, L., Ewing, R.C., and Becker, U.: "Thermal behavior of metal nanoparticles in geologic materials," Geol. Soc. Am. **34**(2006).

Saleh, S.M., Muller, R., Mader, H.S., Duerkop, A., Wolfbeis, O.S.: "Novel multicolor fluorescently labeled silica nanoparticles for interface fluorescence resonance energy transfer to and from labeled avidin," *Anal Bioanal Chem* (2010) 398:1615-1623.

Sing, C., Kunzelman, J., and Weder, C.: "Time-temperature indicators for high temperature applications," *J. Mater. Chem.* **19** (2009).

Wu, E.C., Park, J.H., Park, J., Segal, E., Cunin, F., and Sailor, M.J.: Oxidation-triggered release of fluorescent molecules or drugs form mesoporous Si Microparticles," *ACS Nano* (2008), Vol.2 No.11:2401-2409.

A general framework for fracture intersection analysis: algorithms and practical applications

Younes Fadakar Alghalandis[1*], Chaoshui Xu[2] and Peter A. Dowd[3]
younes.fadakar@gmail.com
[1, 2] School of Civil, Environmental and Mining Engineering, The University of Adelaide.
[3] Faculty of Engineering, Computer and Mathematical Sciences, The University of Adelaide.

The modelling and simulation of fracture networks is a critical component of the assessment of hot dry rock (HDR) geothermal resources and of the design and creation of enhanced geothermal systems (EGS). The production of geothermal energy from an EGS depends on fluid pathways through the HDR and thus connectivity of fractures is essential. One way of assessing and modelling fracture connectivity is by intersection analysis. There is a notable lack of research in this area reported in the published literature probably because of the extreme complexity of three-dimensional fractures in HDR especially with respect to their geometrical characteristics i.e., shapes and orientations and spatial inter-relationships in the fracture network.

In this paper we present a framework for three-dimensional intersection analysis of fracture networks. The framework includes several robust algorithms for three-dimensional geometrical operations on various data structure configurations. We present two case studies to demonstrate the framework.

The first case study is a stochastic fracture network model generated by Monte Carlo sampling of marked point processes that incorporate the most significant fracture characteristics: location, orientation and shape. The second case study is a database of real measurements of fracture parameters. The proposed framework demonstrates the potential to accommodate any amount of complexity e.g., complicated intersections in a fracture network such as varying intensity, varying geometry and numbers of fractures. The resulting fracture intersection databases can be used for further applications such as statistical and spatial analysis of intersections and connectivity analysis.

Keywords: HDR, fracture intersection, rock fracture modelling, rock fracture connectivity

Introduction

Geothermal energy is expected to make up a substantial portion of the world renewable energy market. The renewed interest in geothermal energy over the past decade has stimulated research and development in areas including reservoir modelling, flow and heat transfer simulations, new equipment and new operational techniques (see MIT-led 2011).

Effective heat production from an EGS requires a fracture network in the rock mass so the heat can be efficiently transferred by means of a carrier (water or CO_2) when it passes through the system from the injection to the production well. Where there is a lack of fluid conducting natural fractures a stimulation operation is applied to extend the existing fractures or to create new fractures so as to enhance the performance of geothermal system. A non-productive fracture system (i.e., isolated fracture clusters) or an ill-connected fracture network could be improved by the stimulation process. One of the major challenges, however, is to obtain a realistic connectivity model between the wells. Such a model is critical to the assessment of the response of the system when it is subjected to fluid flow. The design process for a geothermal system is also affected considerably by the characteristics of the fracture system. In EGS, the host rock is, in general, crystalline and the only effective way to transfer fluid between the wells is through fractures. In other words, the production of geothermal energy from an EGS essentially depends on fluid pathways which are fractures and thus connectivity of fractures is a key factor. The connectivity of fractures in a fracture network is controlled by intersections between fractures and also between fractures and injection and production wells.

Due to the significant depth of the EGS (up to 5km below the surface) and the fact that only a few wells are drilled in an area of a few square kilometres, the direct observation and measurement of fractures is very limited if it not impossible. Thus, in practice, the whole fracture system is not observable on any meaningful scale and the only realistic approach is via a stochastic model conditioned by the available data – either directly (downhole logging) or indirectly (seismic events monitored during fracture stimulation process) (Xu et al, 2010). The use of marked point processes (MPP) has proved to be an effective means of developing stochastic fracture models (Mardia et al, 2007; Dowd et al, 2007; Xu and Dowd, 2010). As more conditioning data are used, the resulting network becomes more realistic. The interactions of fractures within the network (i.e., their intersections) define pathways for the transportation of fluid, which is the key factor in assessing the performance of geothermal systems. A simple but robust and practical framework is proposed in this paper to provide a

useful tool for effective and efficient fracture intersection analyses.

Fracture Network Modelling

Fracture locations are represented by points – the centre of 2D shapes or the centroid of 3D shapes. The assessment of dispersion patterns, the density and other characteristics can be obtained by analysing a real fracture data set or a simulated fracture network. For example, the traces of fractures on an outcrop can be used to estimate the size distribution of fractures. Fracture traces on outcrops or borehole imaging can be used to help estimate fracture density.

Stochastic modelling of fractures is based on a discrete fracture network concept in which fractures are generated in a stochastic manner according to a specified underlying process. In combination with marked point processes fractures are generated as follows:

a) Fracture locations are generated based on either a Poisson (homogeneous) point process or an inhomogeneous point process.

b) Fracture orientations are derived by means of Fisher or Von-Misses distribution functions.

c) Fracture shapes (lines in 2D) are defined and fracture sizes (lengths in 2D) are drawn from its distributions, either exponential or lognormal.

d) Other features can be added as required such as aperture, transmissivity and surface roughness.

Two examples of stochastic fracture networks are shown in Figure 1 for 2D and 3D cases.

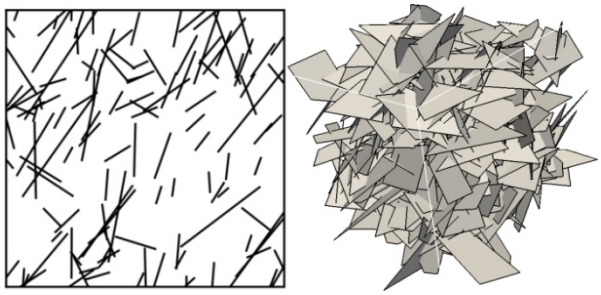

Figure 1: 2D and 3D Fracture Network Simulations via Stochastic Marked Point Processes

Other alternatives to represent fracture shapes in three-dimensional cases are ellipses (disks) or rectangles. However, polygon representation is the most general and realistic and this representation is used in our intersection analysis. We consider all fractures in this research as arbitrary shapes with varying number of nodes (vertices) and with the conditions that polygons are planar and convex. Note that every concave polygon can be reconstructed by an ensemble of convex polygons. In addition, any curved polygon (non-planar) can be divided into a set of planar polygons. Thus the framework described here (Figure 2) covers any amount of complexity of fracture shapes.

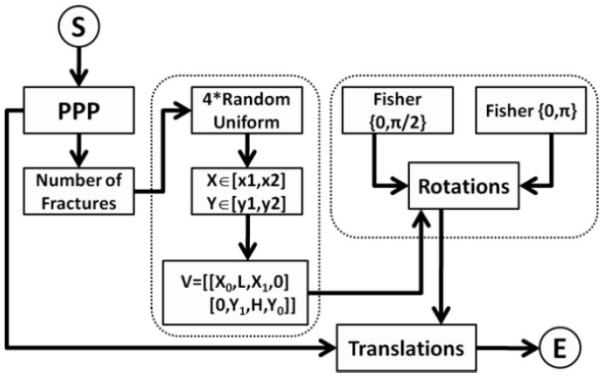

Figure 2: Framework to generate realistic fracture network by means of marked point process

Locations from Poisson point processes

An iterative process is used to generate a random number from a Poisson distribution with an intensity of λ. A uniformly distributed sequence of independent random variables is generated in the range of [0,1], $\{V_i, i=1,\ldots,n\}$. The process is stopped when one of the following conditions is satisfied (Ross 2007):

$$\prod_{i=1}^{n} V_i < e^{-\lambda} \quad \text{or} \quad \sum_{i=1}^{n} \log(V_i) < -\lambda$$

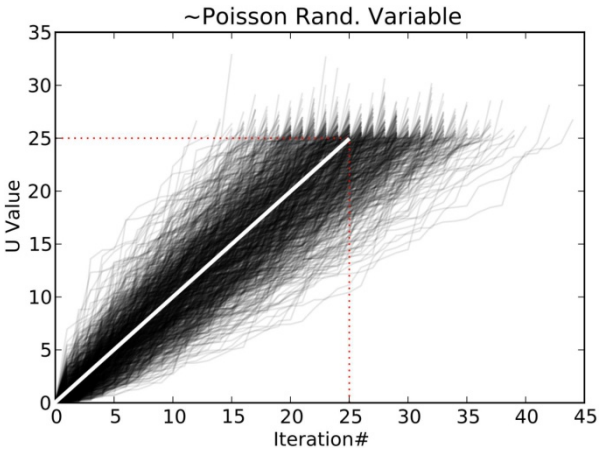

Figure 3: Demonstration of iteration number (n) for generating 1000 random number with Poisson distribution of density 25

The process is very efficient as can be seen in Figure 3 where the average number of iterations required for each random number is the density parameter (i.e., 25). Once n is determined within a region, the points are uniformly distributed within the region such as:

$$X_i\left\{(x_i,y_i,z) \in \mathbb{R}, \quad \begin{matrix} x_1 < x < x_2 \\ y_1 < y < y_2 \\ z_1 < z < z_2 \end{matrix}\right\}$$

Orientations from Fisher distribution

The orientation of a fracture plane can be described by its normal. In rock engineering, for a

fracture set, the deviation angle θ of the normal of a fracture plane from the mean normal of the set is commonly described by a Fisher distribution with parameter κ (Xu and Dowd, 2010)(Figure 4):

$$f(\theta,\kappa)=\frac{e^{\kappa\cos(\theta)}}{2\pi I_0(\kappa)},\qquad \kappa,\theta\in\mathbb{R}$$

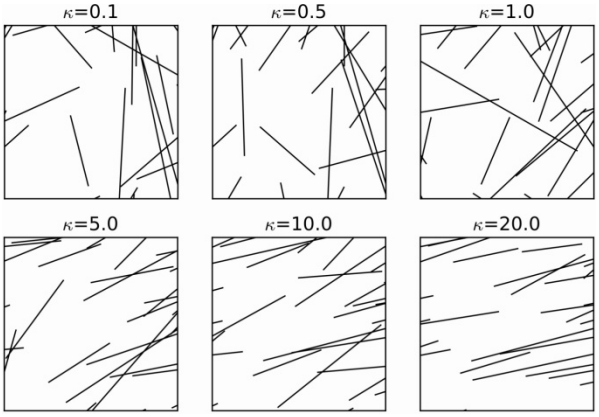

Figure 4: Demonstration of the effect of the variation of κ on Fisher function in the application for orientation angles of fractures

Any three-dimensional plane can also be described by two angles, dip and dip-direction (or azimuth), α and β:

$$\theta:\left\{\alpha,\beta\in\mathbb{R},\quad \begin{matrix}0<\alpha<2\pi\\ 0<\beta<\frac{\pi}{2}\end{matrix}\right\}$$

1- Sizes from exponential distributions

Any polygon can be bounded inside a rectangle regardless of its complexity. Therefore, to simulate the size of a fracture polygon, we first generate a rectangular shape using two numbers drawn from an exponential distribution. Then the following procedure is applied to achieve the desired polygonal shape.

Let l_1 and l_2 be two random numbers drawn from an exponential distribution defining the rectangle. Generate four points independently and randomly on the four sides of the rectangle from a uniform distribution. These four points are then connected (clockwise or counter-clockwise) to produce the final polygonal shape of the fracture. The fracture generated in this way is always convex and planar (Figure 5). Different values of l_1 and l_2 are used if anisotropy is required.

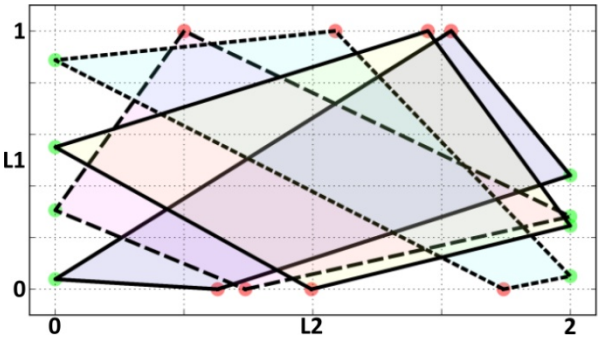

Figure 5: A robust algorithm to generate polygonal shapes for fractures

2- Rotation matrices

Based on the above definition, the transformation matrix to the local coordinate system can be written as (Vince, 2005):

$$\begin{bmatrix} cy*cz & a*cz+cx*sz & -b*cz+sx*sz\\ -cy*sz & -a*sz+cx*cz & b*sz+sx*cz\\ sy & -sx*cy & cx*cy\end{bmatrix}$$

$$cx=\cos(\phi),\qquad sx=\sin(\phi)$$
$$cy=\cos(\omega),\qquad sy=\sin(\omega)$$
$$cz=\cos(\psi),\qquad sz=\sin(\psi)$$
$$a=sx*sy,\qquad b=cx*sy$$

Where ϕ is the rotation angle around the X axis, ω is the rotation angle around the Y axis, and ψ is the rotation angle around the Z axis. Note that in practice only two rotation angles are needed so, for example, ψ can be set to zero. The rotation against the X axis in our defined coordinate system is the dip angle β (which is in the range [0, π/2]) while the rotation against the Y axis is the dip direction α and is in the range [0, 2π].

Translating the resulting polygons

To create the final fracture model, fracture polygons are first generated in the local coordinate system. The axes are then rotated so that the fractures are correctly orientated. The transformed fractures are then translated to their designated locations simulated by a point process.

Intersection Analysis (in 3D)

For the polygonal representations of fractures and the generated fracture network, there are nine possible types of intersection between any two fractures (see Figure 6).

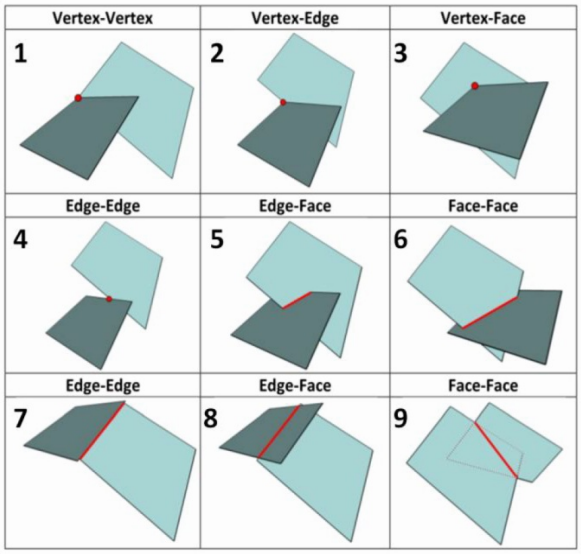

Figure 6: Possible intersection situations between two polygonal fractures in realistic fracture networks

The first four involve a vertex and the last one (Face-Face) can be seen as a special case of Edge-Edge intersection (No.7, Figure 6). The remaining four cases are of particular interest for assessing fracture intersections in a fracture network.

We propose a computationally efficient framework to analyse all intersections between fractures in a fracture network. Efficiency in this type of analysis is an important issue for large fracture networks, which is generally the case for HDR EGS. The complete framework is summarised in Figure 7.

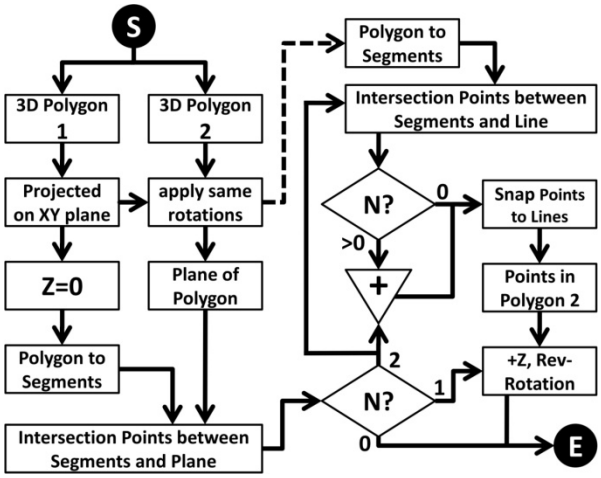

Figure 7: A full robust framework for fracture-fracture intersection analysis

Two core processes in the intersection analysis between fractures (as shown in Figure 7) are *SegXPln* (segment and plane intersection) and *SegXSeg* (segment and segment intersection). A sample pseudo-code for SegXPln is presented on Figure 8.

```
DEF SegXPln(seg, pln):
      n = pln unit normal
      u = (dx,dy,dz)[seg]
      b = (dx,dy,dz)[seg₀,pln₀]
      IF iszero(n.u) THEN
            IF iszero(n.b) THEN
                  RETURN segment is on plane
            ELSE
                  RETURN no intersection
            ENDIF
      ENDIF
      s = (n.-b)/(n.u)
      IF 0<=s<=1 THEN
            RETURN seg₀+s*u  #intersections
      ELSE
            RETURN no intersection
      ENDIF
ENDDEF
```

Figure 8: Pseudo-code for Segment-Plane intersection

The following statistics can be derived from the proposed intersection analysis.

1 - Intersection Density

One definition of fracture density in a fracture network is the density of the point process used. The density model can be parametric or non-parametric and model parameters can be estimated from sample data (Xu et al, 2003). We propose a similar definition here for fracture intersection density where points (2D applications) or lines (3D applications) of intersections are used to calculate the density value. The two are obviously related but the relationship is non-linear and complex as fracture model parameters all play a part in determining the relationship. Fracture intersections define fluid pathways and therefore are of great importance in the connectivity analysis of a fracture network model. We propose to use the density of intersection as a direct measurement of the effectiveness of the fracture network to provide pathways for fluid flow.

A 2D application example is given in Figures 9 and 10. Figure 9 shows a sample fracture network (left) and the locations of fracture centres (right: green dots) and the locations of intersection points (right: red dots). In Figure 10 it can be seen that the resulting models are different. In some areas, despite a high fracture density, the fracture intersections are limited and therefore the intersection density value is low. This part of the fracture network is expected to be less conducive for fluid flow.

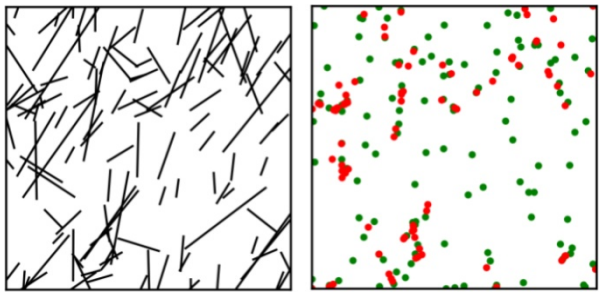

Figure 9: (left) Fracture Network HPPP; (right) Trace locations (green) and intersection points (red)

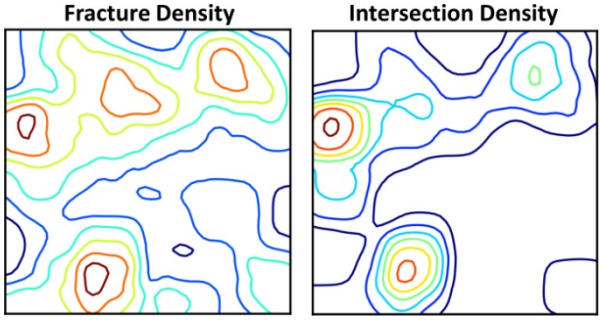

Figure 10: Density map of locations (left) and intersection points (right)

2 – Lengths of Intersection Lines

Fifteen simulations were generated to investigate the distribution of lengths of intersection lines in a three-dimensional fracture network. A homogenous marked Poisson point process was used for each realization. The histogram of the intersection lengths is shown in Figure 11 (fifteen

simulations on the same graph) with a smoothed curve fitted. It can be seen in this case that an exponential distribution satisfactorily models the distribution of lengths of intersection lines.

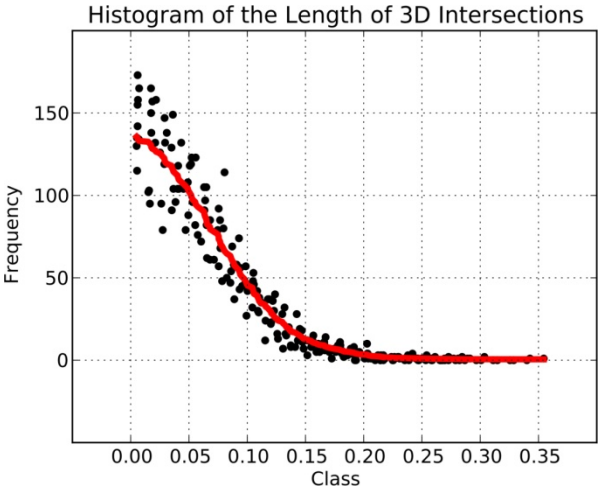

Figure 11: Distribution of the length of intersection lines in three-dimensional fracture network (class=length categories)

It is clear that long intersection lines are rare. The majority of intersection lines are of small length which demonstrates the importance of shorter intersection lines (not necessarily all from small fractures) in determining the connectivity of the fracture network.

3 - Effects of Fracture Length on Percolation State

It is interesting to investigate the relationship between percolation state and the fracture lengths of a 2D application. Fracture length is an important factor in the intersection between fractures in a fracture network and it affects the connectivity between any two points within the region.

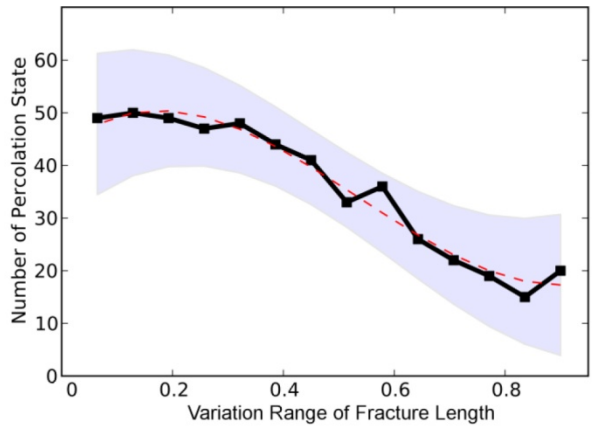

min	max	range	#state	min	max	range	#state
0.050	0.950	0.900	20	0.250	0.700	0.450	41
0.079	0.914	0.836	15	0.279	0.664	0.386	44
0.107	0.879	0.771	19	0.307	0.629	0.321	48
0.136	0.843	0.707	22	0.336	0.593	0.257	47
0.164	0.807	0.643	26	0.364	0.557	0.193	49
0.193	0.771	0.579	36	0.393	0.521	0.129	50
0.221	0.736	0.514	33	0.421	0.486	0.064	49

Figure 12: Relationship between percolation sate reached and the variation in the range of length of fractures

Figure 12 shows that larger range of variation of fracture lengths produces few number of percolation clusters for the cases investigated. In other words the homogeneity of the fracture length in the fracture network affects directly the percolation of the network. It was shown that the relationship is non-linear in this case. The simulation consists of 14 different ranges of length variations. For each variation, 50 realizations were generated. Clearly for the related analysis of connectivity evaluation of a fracture network (Xu et al, 2006) the fracture length will be a very important variable. Further study in this topic will be conducted.

Case Study - Leeds Fracture Data Set

In this section some of analyses are applied to a real fracture data set: the Leeds Fracture Data Set (Dowd et al, 2009), which was established by slicing a block of granite (Figure 13). Fractures in the data set are represented by quadratic polygons. 387 fractures are used for this study.

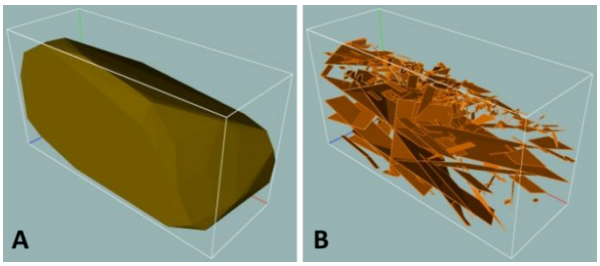

Figure 13: A 3D convex hull showing the block (left) and 387 fractures (right)

An intersection analysis of the fracture network of this block was conducted (see Figure 14) and the following results were obtained.

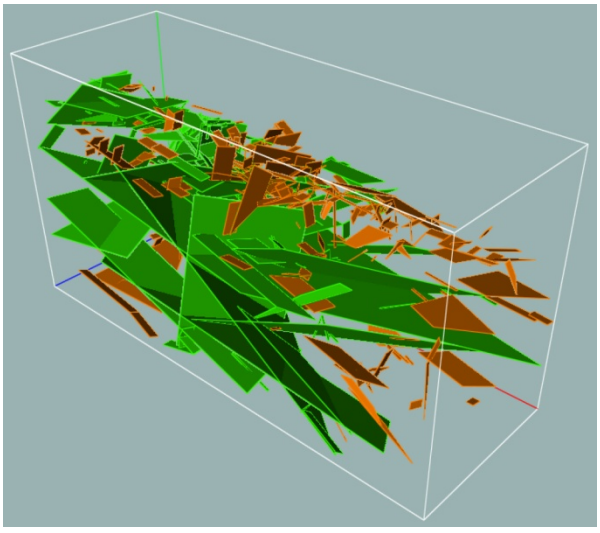

Figure 14: the result of intersection analysis which demonstrates the largest cluster of connected fractures (green)

The largest cluster (group of intersected fractures) in Figure 14 is shown in green. It can easily be seen that this cluster accounts for the percolations state of this block.

The histogram of the lengths of intersection lines for this block (Figure 15) is compatible with the results extracted from simulations (compare with Figure 11): the intersection lines have an exponential distribution.

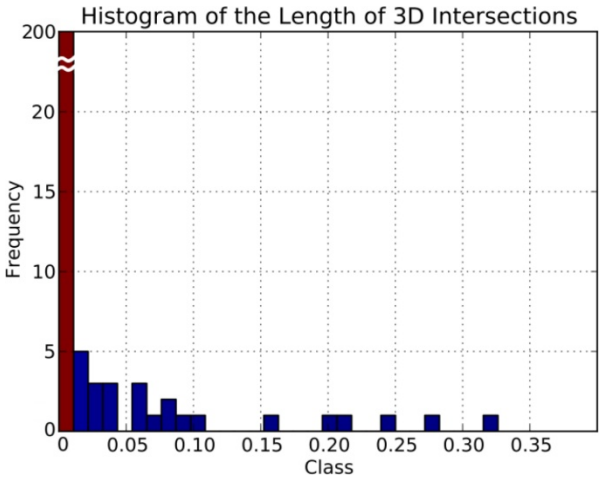

Figure 15: Distribution of the length of intersection lines in three-dimensional fracture network: Leeds Fracture Data Set (class=length categories)

The analysis of intersection density in 3D for this block is shown in Figure 16 in which subplot A is a 3D contour of the density of fracture centroid points while subplot B is the density of centres of intersection lines. It can be clearly seen that even for the same section the resulting density is different for fracture centroid points and intersection line centre points.

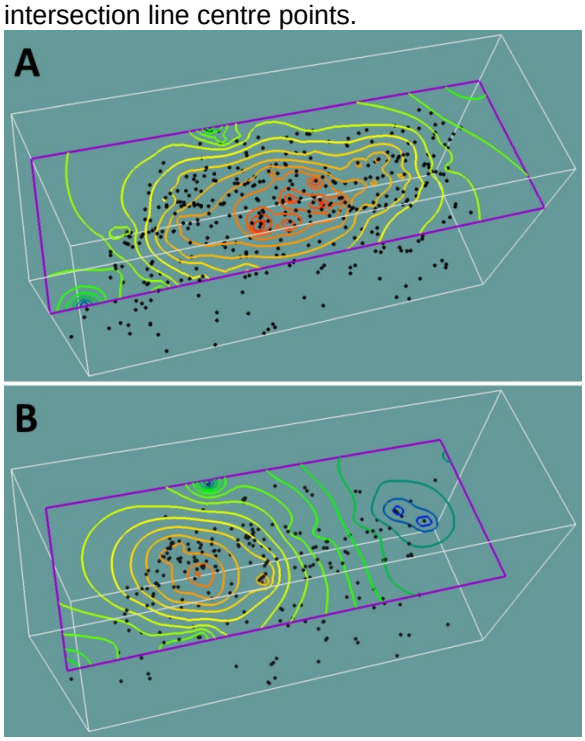

Figure 16: Density map of locations (A) and intersection points (B) of 3D fracture network, Leeds Fracture Data Set

As a result the right hand side of the block (Figure 16) has considerably less conductivity despite having a high density of fractures.

Conclusions

In this research we have developed robust algorithms/frameworks for the intersection analysis of fracture networks of any degree of complexity. Three novel analyses were conducted in this study including a) intersection density as an effective and realistic representation of the conductivity within a fracture network, b) distribution of the length of fracture intersection lines in a fracture network which is shown to be exponential, and c) the effect of length of fractures on the percolation state of a 2D fracture network. We have shown that the number of percolation clusters has a non-linear relationship to the range of variations in the fracture length. In other words, fracture size and its variability are both important variables in percolation analysis and connectivity index evaluation, which in turn are important measures for the quantification of fluid flow characteristics of fracture networks.

References

Dowd P.A, Martin J.A, Xu C, Fowell R.J, Mardia K.V, 2009, A three-dimensional fracture network data set for a block of granite, International Journal of Rock Mechanics & Mining Sciences, 46:811-818.

Dowd P.A, Xu C, Mardia K.V, Fowell R.J, 2007, A comparison of methods for the stochastic simulation of rock fractures, Mathematical Geology, 39:697-714.

Mardia K.V, Nyirongo V.B, Walder A.N, Xu C, Dowd P.A, Fowell R.J, Kent J.T, 2007, Markov Chain Monte Carlo Implementation of Rock Fracture Modelling, Mathematical Geology, 39:355-381.

MIT-led, 2010, The Future of Geothermal Energy, Technical Report, U.S. Government, http://geothermal.inel.gov, pp372.

Ross S.M, 2007, Introduction to Probability Models, Academic Press-Elsevier, USA, pp801.

Vince J, 2005, Geometry for Computer Graphics, Springer, London, p359.

Xu, C., Dowd, P. A., Mardia, K. V. and Fowell, R. J., 2006, A connectivity index for discrete fracture networks, Mathematical Geology, 38, pp. 611 – 634.

Xu C, Dowd P.A, 2010, A new computer code for discrete fracture network modelling, Computer & Geosciences, 36:292-301.

Xu C, Dowd P.A, Mardia K.V, Fowell R.J, 2003, Parametric point intensity estimation for stochastic fracture modelling, Leeds University Mining Association Journal, 16:85-93.

Xu C, Dowd P.A, Wyborn D, 2010, Optimised fracture network model for Habanero reservoir, Proceeding of Australian Geothermal Conference 2010, Australia, pp6.

Direct Geothermal Energy from Geostructures

Bouazza, A.[1*], Adam, D.[2], Rao Singh, M.[1], Ranjith, PG.[1]
malek.bouazza@monash.edu
[1] Monash University,
Department of Civil Engineering, Bldg. 60, Melbourne, Vic. 3800
[2] Vienna University of Technology
Institute of Geotechnics, Karlsplatz 13, A-1040, Vienna, Austria

Incorporation of heat exchangers into ground embedded structures (Geostructures) such as shallow foundations, pile foundations, diaphragm walls, tunnel cut-and-cover walls, tunnel linings and anchors, is a relatively novel sustainable technology for the intermittent storage of energy in the ground with a view of utilizing it for heating and cooling by means of suitable systems integrated into the geostructures. This innovative technology can provide not only substantial long-term cost savings in relation to conventional energy systems but also can make an important contribution to environmental protection by reducing fossil energy use and minimizing the carbon footprint of built structures.

Keywords: Direct geothermal energy, Geostructures, Heating, Cooling, Heat pumps, Pile foundations, Tunnels, Diaphragm walls.

Introduction

The adverse effects of greenhouse gas emissions and rapidly depleting natural energy resources has prompted governments across the world to identify ways of reducing carbon footprints and increasing the utilisation of alternative, renewable energy sources.

To facilitate this approach, legislations across the globe, internationally recognised and locally introduced, are being passed through governments to ensure that carbon reductions can be achieved in the near future.

With new technologies in the field of the alternative energy sources being continually developed and the recognition of its important contribution earned by government organizations and the general public, implementation has recently become more feasible. It is not surprising that the demand for renewable forms of energy such as geothermal energy is steadily increasing and is receiving at the same time a considerable amount of interest.

Traditional geothermal energy systems require interaction with kilometre-deep strata of rock, where thermal energy is much greater and can produce hot fluids to drive turbines for electricity (Preene and Powrie, 2009). Its use is however weighed down by cost and practicality, a technology that is more suited for larger scale applications. More recently, encouraging developments are being achieved in the field of shallow geothermal energy systems (i.e direct geothermal energy systems) using geostructures such as pile foundations, diaphragm walls, shallow foundations, tunnel cut-and-cover walls, tunnel linings and anchors. The geostructures utilise the required ground-concrete contact element to transfer the construction loads to the ground as well as acting as a heat exchanger unit. These systems show great potential, comparative to the traditional systems, in terms of long-term sustainability, access, flexibility and economics. Direct geothermal energy is based on the principle that the subsoil can be employed as a thermal energy source by using its natural potential and thermal storage capabilities.

Two different operation schemes for the use of geothermal energy from geostructures are possible: exclusive geothermal energy extraction or energy input; and alternating seasonal operation with heating and cooling storage.

For exclusive geothermal energy extraction, the energy flow takes place in one direction only, for example for heating purposes during winter. However, the seasonal operation uses the thermodynamic inertia of the soil in order to store thermal energy in the ground for later operation with reversed energy flow. Consequently, the seasonal operation can produce energy equilibrium in the ground over a complete heating/cooling period of a year. A geothermal cooling system extracts heat energy from a built structure via either an air-cooling system or a water-based cooling system, which can be integrated in ceilings and walls. The cooling system acts like a ‘reverse’ heat pump, and the thermal energy can be stored in the ground. Geothermal energy applications that need a very low service temperature can also be operated in ‘free heating’ or ‘free cooling’ mode. The necessary energy input then is limited to the electricity required to operate a circulation pump, because no heat pump is needed to raise the temperature level. For buildings, these technologies can now be considered as state-of-the-art.

Applications

Austria, Switzerland and Germany can be regarded as the pioneering countries that have investigated the use of geostructures for decades.

Extensive use of ground-source heat exchangers have been featured in Austria. Two notable examples are lot LT24 of the Lainzer tunnel and Uniqa Tower in the centre of Vienna. Lot LT24 was the first application in the world where heat exchanger technology, was applied to bored piles of a cut-and-cover tunnel. The lot comprised 59 'energy piles' with a diameter of 1.2 m and an average pile length of 17.1 m. The piles were equipped with absorber pipes connected to a service room. The absorber pipes were connected to collection pipes, which led to six heat pump units providing heat to an adjacent school building.

The Uniqa Tower, located in the centre of Vienna, is founded on diaphragm walls that reach down to 35 m below surface. At this depth, a high groundwater table and surrounding ground are ideal conditions for geothermal energy utilisation, where 7800 m^2 of diaphragm walls are used to absorb energy from the ground to produce a heating capacity of 420 kW and a cooling capacity of 240 kW. The annual heating output reaches up to 818 MWh and the annual cooling output up to 646 MWh (Adam and Markiewicz, 2009). Simulations of this energy system result in a minimum brine entry (into the diaphragm walls) temperature of -2.8 ^oC in January and a maximum entry temperature of 31.8 ^oC in August. The geothermal energy is used in combination with low-temperature heating systems such as wall and floor heating, and free cooling is used to support a conventional cooling system.

In Germany, energy piles have been used in the 200 m high Frankfurt Main tower. This building is founded on a 30 x 50 m^2 base supported by 213 piles, 112 of which are energy piles of 30 m in length (Ebnöther, 2008, Laloui et al., 2006). Berlin's International Solar Centre employs 200 energy piles to meet 20 % of heating and 100 % of cooling demands through seasonal heat storage (Fisch and Himmler, 2005). Germany has been quite receptive towards this new technology with the federal government offering incentives in an effort to promote the ground-source heat pump market. It has however been recommended that for this alternative energy source to be economically viable, both heating and cooling operations should be considered (Sanner et al., 1996).

Switzerland has had several decades of experience with ground-source heat pumps. Two notable examples of projects, which have employed the use of energy piles are at the Swiss Federal Institute of Technology in Lausanne and Dock Midfield Terminal Airport at Zurich Airport. The Lausanne project has also been part of an extensive performance monitoring program, in particular the investigation of the thermo-hydro-mechanical behaviour of surrounding soil (Boennec, 2008, Laloui et al., 2006). Over the past five years, the installation of geothermal pile foundations has grown exponentially in the UK. There were approximately ten times more geothermal pile foundations installed in 2008 than in 2005. The reason for this rise in production is mainly driven by the code for sustainable buildings that requires the construction of zero-carbon buildings by 2019 (Bourne-Webb *et al.* 2009).

Future Prospects and Feasibility in Australia

As a hot and dry country, climate change poses a substantial threat to Australia's economy and the way of life. For the past thirteen years, Australia has experienced eleven of the hottest years since records began and temperatures are projected to continue to rise over the next century. Global and local communities need to focus on reducing greenhouse gases, because even though the effects of global warming can no longer be avoided, people can make efforts to help minimize it.

Benefits of utilising Geothermal Geostructures in Australia

Although there are a significant amount of advantages to implementing direct geothermal energy geostructures, the environmental benefits are likely to be considered the most attractive. The Australian Government had recognised the potential impacts of climate change and have put in place certain legislation and policies focused on reducing carbon pollution. The White Paper (Australian Government, 2008) specifies goals to cut carbon emissions, by the year 2050, to 60% of the levels emitted in 2000. Furthermore, by the year 2020, the Australian government has committed this country to reduce its carbon pollution by up to 15% below 2000 levels via the Kyoto Protocol. Geothermal energy geostructures are one solution that has great potential in helping Australia to reduce carbon emissions and meet this commitment. This is confirmed as the Energy Efficiency Action plan states that energy use in households for the purpose of heating and cooling during the year 2005 contributed, on average, to 26% of the total greenhouse gas emissions in Australia. Governments, such as the state of Victoria, already have in place specific goals to implement alternative energy sources, the Victorian Environmental Sustainability Framework (2005) states that the Victorian Government aims to increase the share of Victoria's electricity consumption from renewable energy source from the 4% (in the year 2005) to 19% by the year 2010 (DSE, 2005).

For example, the inclusion of piles for structural integrity is already commonly identified in many commercial and industrial buildings in Australia. One example of an area where piles are

commonly used because of foundation limitations is Melbourne where Coode Island Silt is found along the urban area of Southbank. As a result, the adaptation of structural piles to include the geothermal energy pile systems is a very feasible and economically viable option.

The Australian Environment

The main cities in Australia exhibit significantly different types of foundations for their built structures. Some cities are predominantly founded on sandstones such as Hallett Cove sandstone in Adelaide and Hawkesbury sandstone in Sydney. This may result in increased costs of implementing geothermal geostructures as larger area of absorbers might be needed. The area of Melbourne is of particular focus due to the already large use of piles for structural purposes. Based on geological maps from the Victorian Geological Survey, the outer Eastern to North-Eastern areas of Melbourne consist mainly of mudstone, sandstone and siltstone whereas is the outer Northern and Western areas the geology consists predominantly of new volcanic materials such as basalt and scoria. Closer to Melbourne itself, the foundations consist of a variety of clay, silt, sand, gravel and peat (Peck et al., 1992). The main implications of this geological information are that each of these types of soils will affect the performance of the systems differently due to the varying thermal conductivities and geothermal gradients. This information also illustrates the need for detailed geotechnical investigations to be carried out in order to accurately determine the subsurface that will be in contact with the ground heat exchangers

Research Challenges

An issue that may arise with implementing this system in Australia is the imbalance between the heating and cooling needs of the user and this needs to be explored further. As a result of the warm climate conditions within Australia, there is likely to be more demand for cooling or otherwise known as heat rejection into the ground. The importance of achieving a balance between heat rejection and extraction has resulted in the requirement for building occupants to inform environmental authorities each year of the respective volume of energy abstraction and rejection. This ensures that individual systems do not short-circuit, that the natural recovery process can still occur long term and prevents possible impacts on other nearby installations (Dickinson et al., 2009). The thermal imbalance has been identified as a problem for some systems in other countries with similar climate conditions and a solution has already been proposed by Fan et al. (2008). Currently, a large research programme is being carried out at Monash University on direct geothermal energy piles. The research programme consists of detailed laboratory investigations and field study of geothermal pile foundations. The laboratory study investigates the impact of heating and cooling on surrounding soil at small scale. The geothermal pile at laboratory scale is being imitated by a temperature controlled heater. The field study includes static load test of a fully instrumented large scale pile connected to a heat pump. The field study aims at measuring stress, deformation, temperature and thermal properties of the fully instrumented geothermal pile and surrounding soils. The study at Monash will shed more light on the field performance of geothermal energy piles under local conditions

References

Adam, D. and Markiewicz, R., 2009. Energy from earth-coupled structures, foundations, tunnels and sewers. Géotechnique, 59**,** No3, 229-236.

Australian Government, 2008. Carbon Pollution Reduction Scheme, Australia's Low Pollution Future (White Paper). IN CHANGE, D. O. C. (Ed.). Canberra, Australian Government.

Boennec, O., 2008. Shallow ground energy systems. Proceedings of the Institution of Civil Engineers, Energy 161, EN2**,** 57-61

Bourne-Webb, P.J., Amatya, B., Soga, K., Amis, T., Davidson. C. and Payne, P., 2009, Energy pile test at Lambeth College, London: geotechnical and thermodynamic aspects of pile response to heat cycles, Geotechnique, 59, No. 3, 237-248.

Dickinson, J., Buik, N., Matthews, M.C. and Snijders, A. 2009. Aquifer thermal energy storage: theoretical and operational analysis. Géotechnique, 59, No3, 249-260.

DSE, 2005. Our Environment, Our Future, Victoria's Environmental Sustainability Framework. IN ENVIRONMENT, D. O. S. A. (Ed.). Melbourne, Department of Sustainability and Environment.

Ebnother, A., 2008. Energy Piles, The European Experience. GeoDrilling 2008. Haka Gerodur.

Fan, R., Jiang, Y.,Yao, Y. and Ma, Z., 2008. Theoretical study on the performance of an integrated ground-source heat pump system in a whole year. Energy, 33, 1671-1679.

FischI, M. N. and Himmler, R., 2005. International Solar Center Berlin - A comprehensive energy design. Building performance congress. Frankfurt Am Main, Germany, Messe Frankfurt GmbH.

Laloui, L., Nuth, M. and Vulliet, L., 2006 Experimental and numerical investigations of the behaviour of a heat exchanger pile. International Journal for Numerical and Analytical Methods in Geomechanics, 30, 763-781.

Peck, W. A., Meilson, J. L., Olds, R. J. And Seddon, K.D, 1992. Engineering geology of Melbourne.A.A.Balkema. Rotterdam, Netherlands.

Preene, M. and Powrie, W., 2009. Ground energy systems: from analysis to geotechnical design. Géotechnique, 59, 261-271.

Sanner, B., Hopkirk, R. J., Kabus, F., Ritter, W. and Rybach, L., 1996. Practical experiences in Europe of the combination of geothermal energy and heat pumps. Proc 5th IEA Conference on Heat Pumping Technologies, Toronto, 1:11 1–25

Curing Lost Circulation Issues and Strengthening Weak Formations with a Sealing Fluid for Improved Zonal Isolation of Wellbores

Brandl, A., Bray, W.S., Molaei, F.
Andreas.Brandl@BakerHughes.com
Baker Hughes
11211 FM 2920, Tomball, TX 77375, USA

An innovative fluid system was successfully applied to seal lost circulation zones and to strengthen the wellbore wall for improved cement slurry placement in highly permeable, fragile, and unconsolidated wells with low frac gradients. The fluid system, which contains a nano-engineered sealing material, has several operational and technical advantages (e.g. user friendliness, effectiveness up to 204 °C, no damage to producing formations) as compared with other common lost circulation systems. Lab test results, a model of the working mechanism, and case histories are presented to outline the performance and benefits of the sealing fluid in geothermal wells.

Keywords: Drilling, lost circulation, zonal isolation

Introduction

Geothermal wells typically have highly saline and corrosive environments with high temperature and pressure variations. Lost circulation is a common problem during drilling and cementing of geothermal wells due to fractures, fragile, unconsolidated, and highly permeable (>>1 D) formations with low fracture gradients. Conventional methods to reduce losses are pills with common lost circulation materials (LCMs) such as nut shells, granular materials, fibers, flakes, gunk, or cement plugs placed across the critical zones. All these options have disadvantages like inconsistent results, damage to producing zones, or temperature limitations, which result in failures, additional efforts, or complications that lead to delays and increased costs.

Low- and ultralow-density cementing systems are usually required in geothermal wells to prevent breakdown of weak formations. Failures of zonal isolation in geothermal wells have been directly attributed to corrosion of the cement sheath (Berra *et al.* 1988). Cement corrosion can be accelerated by poor cement bonds, cement sheath failures, and highly permeable cements, typically related to higher water content or lower density, respectively (Brandl *et al.* 2011).

The sealing fluid presented in this study addresses all these challenges - lost circulation control, strengthening the wellbore wall, and improving cement bond - to provide an operationally simple, all-in-one solution supporting zonal isolation. The fluid is usually pumped as a cement spacer to improve cement slurry placement where narrow equivalent circulation density (ECD) margins or low fracture gradients limit the density and constrain designs of cementing systems.

Fluid design and operational simplicity

The base fluid consists of a hydrophobically modified polysaccharide suspended in aqueous solutions with a concentration of 42 g/L. Rheologies are adjusted in the sealing fluid by varying the concentration of the polymer. Barite or any other common weighting material is used to modify the fluid density from 1.0 to 2.4 g/cm^3. Adding an organic bridging material in the range of 71 to 114 g/L improves the effectiveness of the base fluid to stop severe losses (e.g. due to fractures).

The materials can be stored as a dry blend in 60-lb sacks on the rig site and then mixed with any type of water (fresh, sea, or salt-saturated water) within 10 minutes. No special quality control is necessary, and the fluid system is tolerant of contamination.

The sealing fluid can be applied as a pill or designed as a spacer for proper mud removal before cement placement. The recommended spacer volume is 305 linear meters in the annulus or minimum of 10 minutes of contact time in the annulus (typically 40 to 50 bbl of spacer fluid). Flushing with clear water behind the sealing fluid will remove the seal. All components of the system are environmentally compliant (Pose Little or No Risk “PLONOR” certified) and can be disposed anywhere in the field.

Lab test results

The following performance tests for the sealing fluid system demonstrate its suitability for geothermal wells.

Fluid stability at HTHP

Fluid stability (solid support with minimal settling) at high temperatures is critical if pumping processes are temporarily stopped (for example, due to unforeseen operational issues). Settling can result in inconsistent fluid properties, increases in viscosity which can lead to pressure spikes when pumping is resumed. This can increase ECD pressures potentially leading to lost circulation.

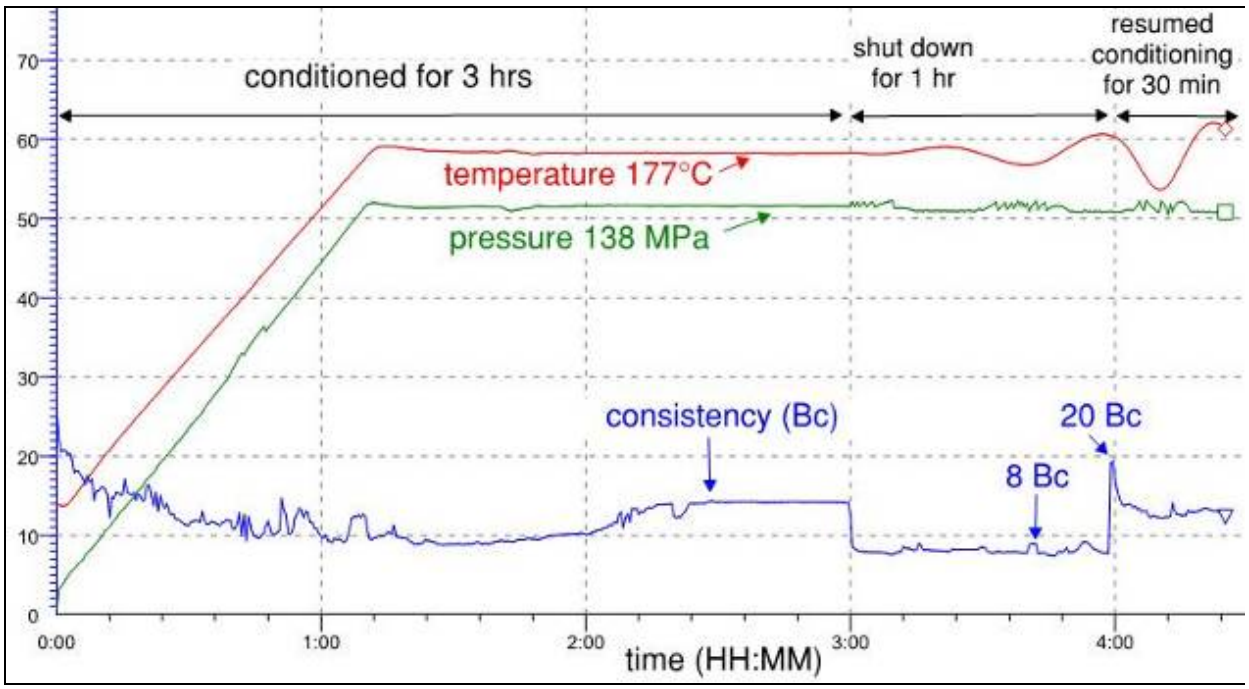

Figure 1: HTHP consistometer chart. Sealing fluid weighted with barite to 2.33 g/cm^3, conditioned at 177°C, static for 1 h, and resumed conditioning without a huge spike in consistency indicates no settling and so fluid stability.

Fluid stability and solids support of the base fluid system weighted up to 2.33 g/cm^3 with barite was tested in a high-temperature, high-pressure (HTHP) consistometer (Figure 1). The fluid shows a relatively consistent viscosity (10 to 20 Bearden units of consistency) during the increase to 177 °C at a pressure of 138 MPa. After 3 hours conditioning the circulation of the fluid was stopped ("shut down") for one hour. When the circulation of the fluid was resumed the consistency did not spike, but remained stable. This indicates that no settling of barite occurred during the shut-down period. After cooling, the visual evaluation confirmed a homogeneous fluid with no settling. The sealing fluid is stable at the tested temperature of 177°C.

Sealing efficiency at HTHP

The sealing efficiency of the innovative fluid was tested in an HTHP filter cell against (1) a bottom cap with a 2-mm-diameter port, (2) 20/40 frac sand with 200-D water permeability, and (3) a coarse gravel pack with 3,000-D water permeability. A thorough testing program for various design features at different conditions revealed that the sealing fluid system works if mixed with fresh water, sea water, or salt-saturated brines and up to temperatures of 204 °C at differential pressures of 6.9 MPa (Brandl *et al.* 2011):

The sealing spacer instantly stops losses when pressed against the simulated highly permeable formations (Figure 2A), whereas a typical spacer fluid completely blows through the same frac sand within seconds (Figure 2B).

In another test, the sealing fluid (with added organic bridging material) was pressed against the coarse gravel pack and effectively stopped losses. After the test, the sealing fluid above the coarse gravel pack was poured out of the cell. A neat cement slurry (dyed red to track penetration depths, Figure 2C) with a density of 1.89 g/cm^3 was placed on top of the treated coarse gravel pack. This simulated the displacement of the sealing spacer by a cement slurry pumped along a porous formation in the wellbore. Less than 1 cm cement filtrate invasion into the treated coarse gravel pack (3,000 D water permeability) was observed after 1 hour static at maximum differential pressure. The rapid stop of losses with low cement filtrate penetration confirmed the high efficiency of the sealing fluid and its ability to minimise damage effects to formations.

Return permeability tests

A permanent seal or plugging from any lost circulation material is undesirable along potential production zones. The damage to production zones would result in reduced production rates (such as for steam in geothermal wells).

In a previous study, 100% return permeability to oil was found after the sealing fluid was applied against *Berea* sandstones (water permeabilities of 9 and 0.3 D) at a differential pressure of 4.8 MPa in a *Hassler*-style core holder (Brandl *et al.* 2011). Further lab tests revealed that the seal generated by the innovative fluid against 20/40 frac sand at high differential pressure could be completely removed by flushing with fresh water. In particular, as soon as a water flow from the

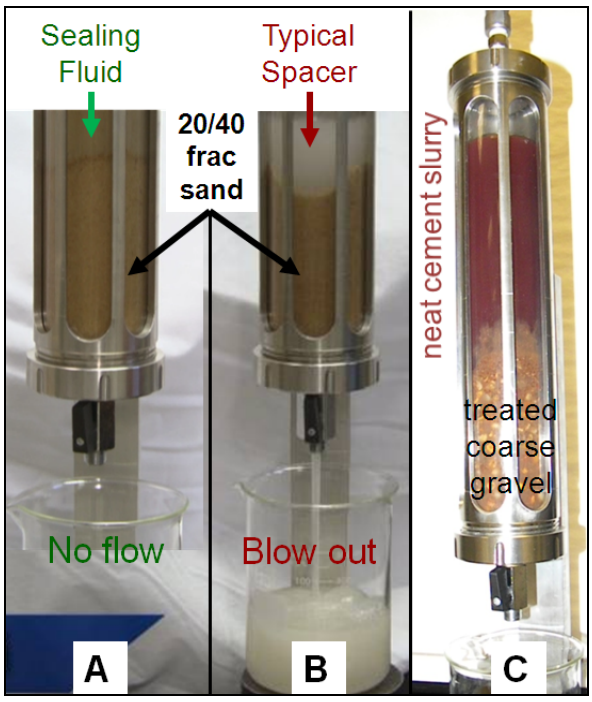

Figure 2: (A) Sealing fluid stops losses against 20/40 frac sand (200 D water permeability) at high differential pressure whereas a typical spacer (B) blows out. (C) Cement slurry on top of a coarse gravel pack (3,000 D water permeability) treated with the sealing fluid, shows minimal filtrate invasion at maximum differential pressure after 1 h.

opposite direction occurs, the seal is removed and the initial permeability is fully restored.

Reversible sealing mechanism

A simplified model, on a molecular level, describes the effective and reversible sealing mechanism of the nano-engineered fluid when applied against permeable formations or fractures in the wellbore. At a minimum concentration (critical micelle concentration (CMC) = 40 g/L) in aqueous solutions, the hydrophobically modified polysaccharides form micelles (Figure 3).

When the sealing fluid is pumped into the wellbore, a dynamic equilibrium exists between the adsorption of the micelles at the solid interface of the formation and their dispersion in the aqueous fluid. When contacting a permeable formation or a fracture at high differential pressures, an increasing number of these micelles adsorb and fill the pores in the formation / fracture (Figure 4).

With increasing differential pressure, the micelles break off and realign along the pores / fractures, forming a sealing film. The intermolecular forces among the hydrophobically modified polysaccharides of the sealing film are greater than the differential pressure applied to the fluid and therefore stop its penetration into the formation / fracture (Figure 5).

When the differential pressure is released or a flow from the opposite direction of the formation occurs (e.g., producing from the reservoir) the

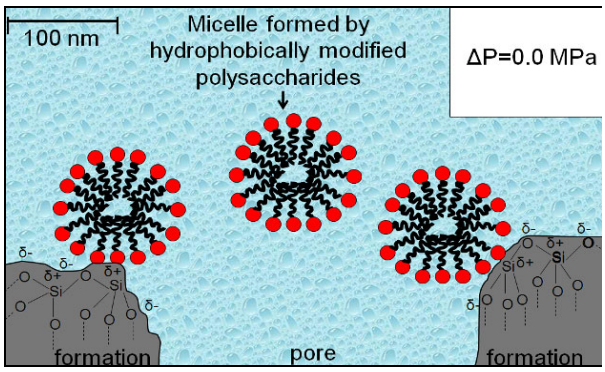

Figure 3: The hydrophobically modified polysaccharides within the aqueous sealing fluid form micelles. A dynamic equilibrium exists between adsorption at the formation and dispersion in the aqueous media.

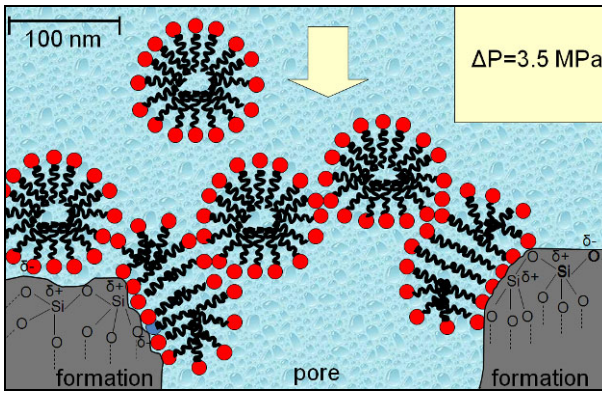

Figure 4: With increasing differential pressure, an increasing number of micelles adsorb and realign along the porous formation.

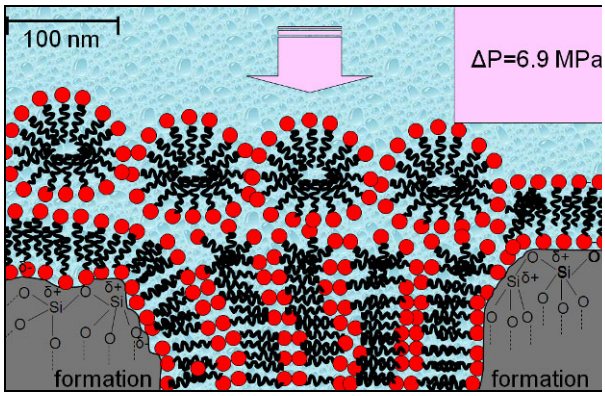

Figure 5: At maximum differential pressure, the adsorbed micelles have turned into a film, completely sealing the pore.

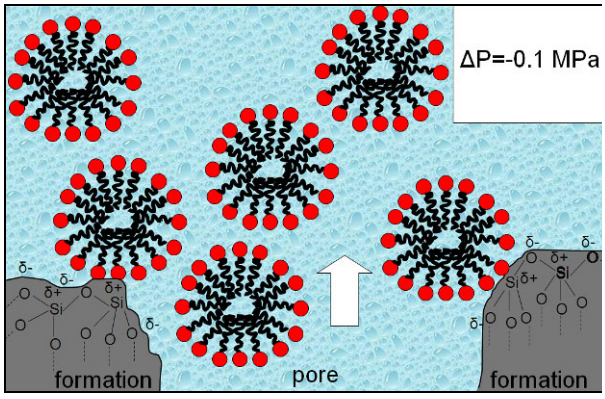

Figure 6: A flow from the opposite direction (e.g. producing from the reservoir) easily returns the micelles into solution.

sealing film turns back into micelles, dispersing in the aqueous solution, as demonstrated by the 100% return permeability test results (Figure 6).

The reversible sealing mechanism is based on differential pressure controlling the thermodynamic equilibrium of the micelles - either forming a film or being dispersed in aqueous solution. Neither cross linking nor any chemical reaction with the formation is taking place to seal the formation and to stop the losses.

Performance in the field

Two case histories demonstrate the benefits of the sealing fluid, first used as a pill to cure total losses and second used as a spacer to strengthen the wellbore wall prior cementing. Case histories showing that the sealing fluid used as a spacer improved cement bond logs were recently published by Metcalf *et al.* 2011.

Curing total losses

An operator in Texas experienced complete circulation losses of drilling fluids in several wells at around 2,000 m measured depth. Various pills and sweeps with different types of LCMs were pumped with no success in restoring circulation. Finally, 50-bbl pills of the sealing fluid containing 84 g/L of the hydrophobically modified polysaccharide and having a fluid density of 1.05 g/cm^3 were pumped down the drill string at 2 bbl/min, followed by drilling fluid. Within 12 to 18 hrs, a minimum of 60% returns had been established and most wells saw 100% returns within 18 to 24 hours.

Strengthening the wellbore wall

Strengthening the formation can be advantageous in situations where the predicted ECD to achieve good cement placement or top of cement to a certain point is greater than the maximum allowable ECD to prevent losses. Increasing ECDs during placement of the cement slurries can cause breakdowns of weak formations and lead to induced losses, contributing to a poor quality cement job. By strengthening the wellbore, losses can be prevented or minimized even at the higher ECDs encountered during the cement job.

Recent cementing operations in Spain were conducted using a stage tool because ECDs to bring the cement top to the desired height would have exceeded the maximum allowable ECD of 1.31 g/cm^3 based on a formation integrity test at the shoe. After successive operations in which the stage tool did not close properly, the operating company chose to cement the section in a single stage, hoping it could achieve sufficient height even with losses. To aid in this goal, 88-bbl of the sealing fluid spacer were pumped at the end of a spacer train preceding the cement. The final ECD at the shoe was calculated to be 1.44 g/cm^3. No losses were encountered during the job for the planned 1,000 m high cement column, and the top of cement was found by logging to be within 30 m of the desired top.

Using the sealing spacer allowed an increase to the ECD of 0.13 g/cm^3 without losses. In this case, the ability of the spacer to strengthen the wellbore and enable effective cementing in a single stage reduced rig time and simplified the job, reducing costs and improving quality.

Conclusions

The innovative sealing fluid offers several benefits:

1. Reduces lost circulation issues at temperatures up to 204 °C
2. Strengthens the wellbore & allows higher ECDs during cementing without cement top fallback.
3. Does not damage producing formations (minimum fluid invasion and 100% return permeability)

The favorable properties of the sealing fluid in combination with its operational simplicity have drawn interest among operators to solve potential lost circulation issues and to improve the quality of the cementing job. Test results demonstrate the sealing fluid is applicable at geothermal conditions. Since its introduction in February 2007, over 63,000 bbl of the sealing fluid have been pumped in more than 1,500 operations.

References

Berra, M., Fabbri, F., Facoetti, M., Noris, A., Pezzuoli, M., Ricciardulli, R., Romano, G. & Tarquini, B., 1988, Behaviour of a cementing hydraulic binder under severe geothermal conditions, Geothermics, no. 17 (5/6), p. 785-813.

Brandl, A., Cutler, J., Seholm, A., Sansil, M., and Braun, G. 2011. Cementing solutions for corrosive well environments. *SPE Drill & Compl*, no. 26 (2), p. 208-219. SPE-132228-PA.

Brandl, A., Bray, W.S., Magelky, C., Lant, K., Martin, R., St.-Clergy, J. 2011, An innovative cement spacer with biodegradable components sealing effectively severe lost circulation zones, presented at the 10th Offshore Mediterranean Conference and Exhibition in Ravenna, Italy, 23-25 March 2011.

Metcalf, A.S., Nix, K., Martinez-Guedry, J., 2011, Case histories: Overcoming lost circulation during drilling and primary cementing operations using an environmentally preferred system, presented at the SPE Production and Operations Symposium held in Oklahoma City, Oklahoma, USA, 27-29 March 2011. SPE-140723-MS-P.

Global Geothermal Deployment – the IEA Roadmap for the Future

Chris Bromley* and Milou Beerepoot
c.bromley@gns.cri.nz
GNS Science
Wairakei Research Centre, Bag 2000, Taupo, New Zealand

Geothermal energy deployment is progressing rapidly in many countries around the world. In order to assist decision makers with future policy development and investment decisions, a Technology Roadmap for Geothermal Heat and Power, with deployment projections out to 2050, has recently been published by the IEA (2011). This publication was assisted by collaborating parties within the IEA-GIA (Geothermal Implementing Agreement) along with many other geothermal specialists, including members of the IGA, the IPGT, and lead authors of the geothermal chapter of the recently published IPCC special report on renewable energy (SRREN, Goldstein et al., 2011). The outcome of the deployment projections was that by 2050, geothermal would potentially contribute 3.4% of the global electricity (1400 TWh/yr) and 3.9% of the global heat demand (5.8 EJ/yr), thereby displacing significant equivalent CO_2 emissions from fossil fuel energy sources.

Keywords: IEA roadmap, IEA-GIA, renewable energy, geothermal deployment

Introduction

A geothermal roadmap was instigated by the IEA in response to requests from government leaders for more detailed analysis of the growth pathway for geothermal energy, and its potential to help mitigate global climate change effects through CO_2 emissions reduction. The purpose was to provide deployment projections and describe approaches and tasks regarding RD&D, financing mechanisms, legal and regulatory frameworks, public engagement and international collaboration. The roadmap evolved from several related and concurrent activities (e.g. IPCC-SRREN report) and was strongly supported by members of the IEA-GIA. It was also financially supported by the governments of Japan, the Netherlands, Switzerland, USA, and the IEA-GIA. Three workshops were convened (in Europe, USA and Indonesia) to provide as broad an input to the report as possible. In addition, numerous geothermal experts, from a wide range of companies and research organisations, willingly provided information and reviews. These individuals are acknowledged in the report.

Resource Types

Different types of geothermal resources have been identified as having potential for energy utilisation around the world. These include the conventional high temperature resources which make up the bulk of the 11 GW_e (~70 TWh/yr) of existing global geothermal power generation, and 15 GW_{th} (~223 PJ/yr) of non-GSHP direct-use applications.

Deep aquifer systems in porous and permeable formations are an under-utilised source of intermediate temperature fluids for heating and/or power production. Globally they consist mostly of hot saline brines in sedimentary basins, and constitute a widespread resource type of significant potential. Local energy demand, drilling cost, pumping cost, and flow-rates, are the parameters that mostly determine viability.

The future global technical potential for geothermal energy, from a theoretical perspective, is vast; some estimates suggest as much as 45 EJ/yr of power (12.5 PWh_e) and 1040 EJ/yr (289 PWh_{th}) of heat could be tapped within the terrestrial part of the upper 10 km of the earth's crust. This estimate excludes, however, advanced geothermal technologies that potentially could tap into additional off-shore hydrothermal systems, super-critical fluids, magmatic and geopressured resources. Any one of these could become a significant energy resource by the turn of the next century. Therefore, the limitations to accelerated global deployment are economic, rather than theoretical or technical potential.

Economics

Economics is the key driver behind regional geothermal deployment rates and investment. In some settings, for example in New Zealand, deployment is expected to increase rapidly over the next decade, potentially doubling local generation capacity, because the levelised cost of energy (LCOE ~US$50/MWh) for geothermal development is significantly lower than all alternative new generation options, despite relatively high capital costs (typically US$2-4M/$MW_e$), moderate operating costs (~2.5% of capital per annum), and the absence of subsidies (except for a carbon emissions trading scheme). In other settings, including Australia and most of Europe, additional economic incentives such as direct investment subsidies, feed-in tariffs, renewable portfolio standards, drilling risk insurance, grid access, or other policy instruments, are required to reduce exploration risks and accelerate early investment in geothermal. In addition, it is anticipated that the learning curve, a benefit of applied research, will gradually bring down the cost in real terms.

Important Findings

The roadmap document shows that future base-load power and heat can be provided by a variety of renewable geothermal energy resources. These include hydrothermal resources and deep aquifer systems at a wide range of temperatures, and hot rock resources which are fractured or stimulated for energy extraction using fluids. The roadmap envisages deployment of geothermal heat and power by several different means.

In the period to 2030, rapid expansion of geothermal electricity and heat production will be dominated by accelerated deployment of conventional high-temperature hydrothermal resources, driven by relatively attractive economics in areas where such resources are available. Deployment of low- and medium-temperature hydrothermal resources in deep aquifers will also grow quickly, reflecting wider availability and increasing interest in their use for both heat and power.

By 2050, geothermal electricity generation could reach 1400 TWh per year, that is, about *3.5%* of global electricity production. Geothermal heat (not including ground source heat pumps) could contribute 5.8 EJ (1600 TWh thermal energy) per year by 2050, about 3.9% of global heat demand.

About *5*0% of the projected increase by 2050 comes from hot rock resources developed as enhanced geothermal systems (EGS). Greater research, development and demonstration resources are needed in the next two decades to ensure EGS becomes commercially viable by 2030.

To achieve this deployment, policy frameworks are needed that address technical barriers related to resource assessment, accessing and engineering the resource, geothermal heat use and advanced geothermal technologies. Frameworks are also needed to deal with barriers related to economics, regulations, market facilitation and RD&D support. Policy makers, local authorities and utilities need to be more aware of the full range of geothermal resources available and of their possible applications. This is particularly true for geothermal heat, which can be used at a range of temperatures for a wide variety of tasks.

Important R&D priorities for geothermal energy include accelerating resource assessment, developing more competitive drilling technology and improving EGS technology, as well as managing environmental concerns.

Advanced technologies for offshore, geo-pressured and super-critical (including magma) resources could unlock a huge additional resource base. Co-produced hot water from oil and gas wells could also be utilised economically.

Key Short-Term Actions

Establish medium-term targets for mature and nearly-mature technologies, and long-term targets for advanced technologies; thereby increasing investor confidence and accelerating expansion of geothermal heat and power.

Introduce economic incentive schemes for both geothermal heat (which has received less attention to date) and geothermal power, with incentives phasing out as technologies reach full competitiveness.

Develop publicly available databases, protocols and tools for geothermal resource assessment and reservoir management to help spread expertise and accelerate development.

Introduce streamlined and efficient procedures for issuing permits for geothermal development.

Provide funds for sustained and substantially higher research, development and demonstration (RD&D) activities to plan and develop at least 50 more EGS pilot plants during the next 10 years.

Expand and disseminate information on EGS technology to enhance production, sustainable resource utilization, and management of environmental performance.

In developing countries, expand the efforts of multilateral and bilateral aid organisations to develop rapidly the most attractive available hydrothermal resources, by addressing economic and non-economic barriers.

Summary

Geothermal energy deployment is progressing rapidly in many countries and has significant potential for greater, widespread development. In order to assist future decision makers, a Technology Roadmap for Geothermal Heat and Power, with global deployment projections, has recently been published by the IEA, with the assistance of the IEA-GIA. The Roadmap envisages geothermal contributing about 3.4% of global electricity needs, and 3.9% of global heating demand, by 2050, displacing equivalent fossil-fuel CO_2 emissions. For more information on the document, contact Milou Beerepoot, Renewable Energy Division, IEA, Paris Headquarters, (Milou.Beerepoot@IEA.org).

References

IEA, 2011, Technology Roadmap, Geothermal Heat and Power. Publication of the International Energy Agency, 9 rue de la Federation, Paris, France (www.iea.org).

Goldstein, B., G. Hiriart, R. Bertani, C. Bromley, L. Gutiérrez‐Negrín, E. Huenges, H. Muraoka, A. Ragnarsson, J. Tester, V. Zui, 2011: Geothermal Energy. In IPCC Special Report on Renewable Energy Sources and Climate Change Mitigation [O. Edenhofer et al, (eds)], Cambridge University Press, Cambridge, United Kingdom and New York, NY, USA.

Geoscience Australia's Onshore Energy Security Program: Geothermal Energy

Budd, A.R.*, Gerner, E., Meixner, A.J., Kirkby, A.L., Weber, R. and Spring, J.
Anthony.Budd@ga.gov.au
Geoscience Australia
GPO Box 378, Canberra, ACT 2601.

Geoscience Australia's $58.9M 5-year Onshore Energy Security Program began in 2006 and included a new Geothermal Energy Project. The OESP concluded in June 2011 but the Geothermal Energy Section continues albeit with reduced funding.

The project aims to assist the development of a geothermal industry in Australia by: providing precompetitive geoscience information, including acquisition of new data; informing the public and government about Australia's geothermal potential; providing technical advice to government; and partnering with industry in international promotional events for the purpose of attracting investment.

This abstract gives a brief summation of activities undertaken by Geoscience Australia within the Onshore Energy Security Program potentially of interest to geothermal explorers.

Keywords: data acquisition, modelling, Geothermal Play Systems

Geothermal Energy Project

Following consultation with industry and State and Northern Territory geological surveys, a number of activities were identified where Geoscience Australia could either fill gaps where no other organisation was able to, or could complement activities by other partners.

Advice to government

Geoscience Australia (GA) is a prescribed agency within the Department of Resources, Energy and Tourism. GA provides advice to government on geoscience-related matters, including resources. GA participated in the development of the Geothermal Industry Development Framework and Geothermal Industry Technology Roadmap. GA was involved in the program design and subsequent technical assessment of the Geothermal Drilling Program. GA co-authored (with the Australian Bureau of Agriculture and Resource Economics) the Australian Energy Resource Assessment which included a chapter on geothermal energy. GA has been involved in the development of the Australian Code for Reporting of Exploration Results, Geothermal Resources and Geothermal Reserves, and sits on the Joint AGEA-AGEG Code Committee for the purpose of one day compiling and reporting geothermal resource and reserve estimates in the same way as is done for mineral and oil & gas commodities.

OzTemp

Geoscience Australia has released OzTemp, an updated dataset and map of predicted temperatures at 5 km depth, available from http://www.ga.gov.au/energy/geothermal-energy-resources.html. Extensive QA/QC was conducted on the dataset of bottom hole temperatures, and where available new data was included. For the map (Figure 1), the OZSeeBase dataset was used, and the Bureau of Metrology's Mean Annual Average Air Temperature was also used with a correction for surface temperature. For the first time, heat flow data was incorporated into the map.

Data acquisition

There is a paucity of temperature-specific data in Australia, and to address this Geoscience Australia has established a capability for measuring surface heat flow via thermal gradient logging and thermal conductivity measurement.

Thermal gradient logging

Without the possibility of drilling new holes, GA has worked with State geological surveys and minerals exploration companies to access exploration and water bores. Figure 2 shows the distribution of logged bores as of June 2011.

Thermal conductivity

Geoscience Australia operates an Anter 2022 Unitherm thermal conductivity meter and associated sample preparation equipment. Project staff have been involved in establishing operating procedures for the instrument, a process which has included inter-lab comparison testing with Torrens Energy, Hot Dry Rocks Pty Ltd, and Southern Methodist University. In addition, GA has engaged Hot Dry Rocks Pty Ltd to measure two batches of samples.

Samples have been taken from the majority of the bores measured for thermal gradient, as well as other bores for 'stratigraphic' conductivity values.

Heat Flow determinations

41 new heat flow determinations have been completed during the Program, providing a significant increase to the number of publicly

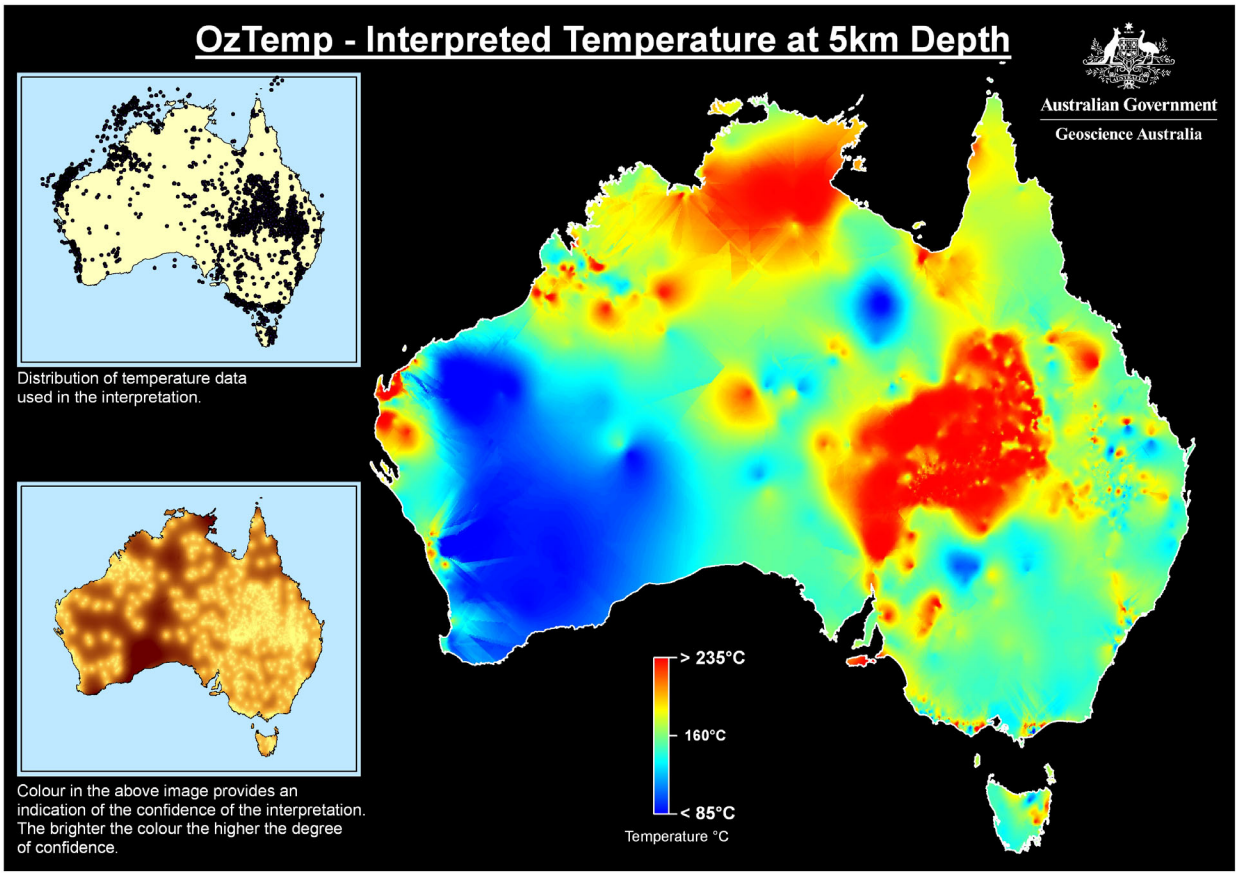

Figure 1: OzTemp map. An interpretation of the crustal temperature at 5km depth, based on the OzTemp bottom hole temperature database and additional confidential company data. A simple two layer model has been used for the extrapolation of the temperature to 5km depth; where the data quality and availability has allowed a slightly more complex three layer model using heatflow and thermal conductivity data was used for the extrapolation.

available heat flow data points. These determinations have been published in three Geoscience Australia records (Kirkby et al. 2010; Jones et al., 2011; Weber et al., 2011).

Promotion

Undoubtedly the greatest impediment to the development of the Australian industry since the Global Financial Crisis has been the lack of capital investment. Geoscience Australia has participated in "Team Australia Geothermal" events at the Geothermal Energy Expo (Reno 2009, Sacramento 2010 and San Diego 2011), and the World Geothermal Congress, Bali 2010. The collaboration of industry, government and associations has been aimed at portraying Australia as a favourable investment destination.

Resource assessments

In 2007 GA produced an estimate of the contained heat above 150°C in the top 5 km of the Australian crust. Understandably this produced a very large estimate of energy. To provide a degree of relevance and believability, an assumption was made that 1% of the resource would be accessible and convertible, and this therefore equates to ~26,000 years of energy consumption (Budd et al. 2008).

The production of the Australian Energy Resource Assessment (Geoscience Australia and ABARE, 2010) highlighted the need for a better understanding of Australia's geothermal resources potential. The knowledge of several other renewable energy resources is quite advanced, and there is a need for geothermal to be better understood so that it can be compared more directly to other energy sources. With a limitation on the availability of temperature data, other geoscience datasets must be used to inform or derive estimates of geothermal resource potential.

Geothermal Play Systems

It was mentioned above that there is a paucity of temperature-specific data publicly available in Australia. There is, however, a wealth of high-quality geoscientific data available throughout the country, much of which can be used to make assessments of geothermal potential from a conceptual view point. As have some companies and other organisations, GA has developed 2.5D and 3D methods for processing geological, geophysical and geochemical data to produce resource potential assessments and estimates. A 'systems' approach has been utilised to enable

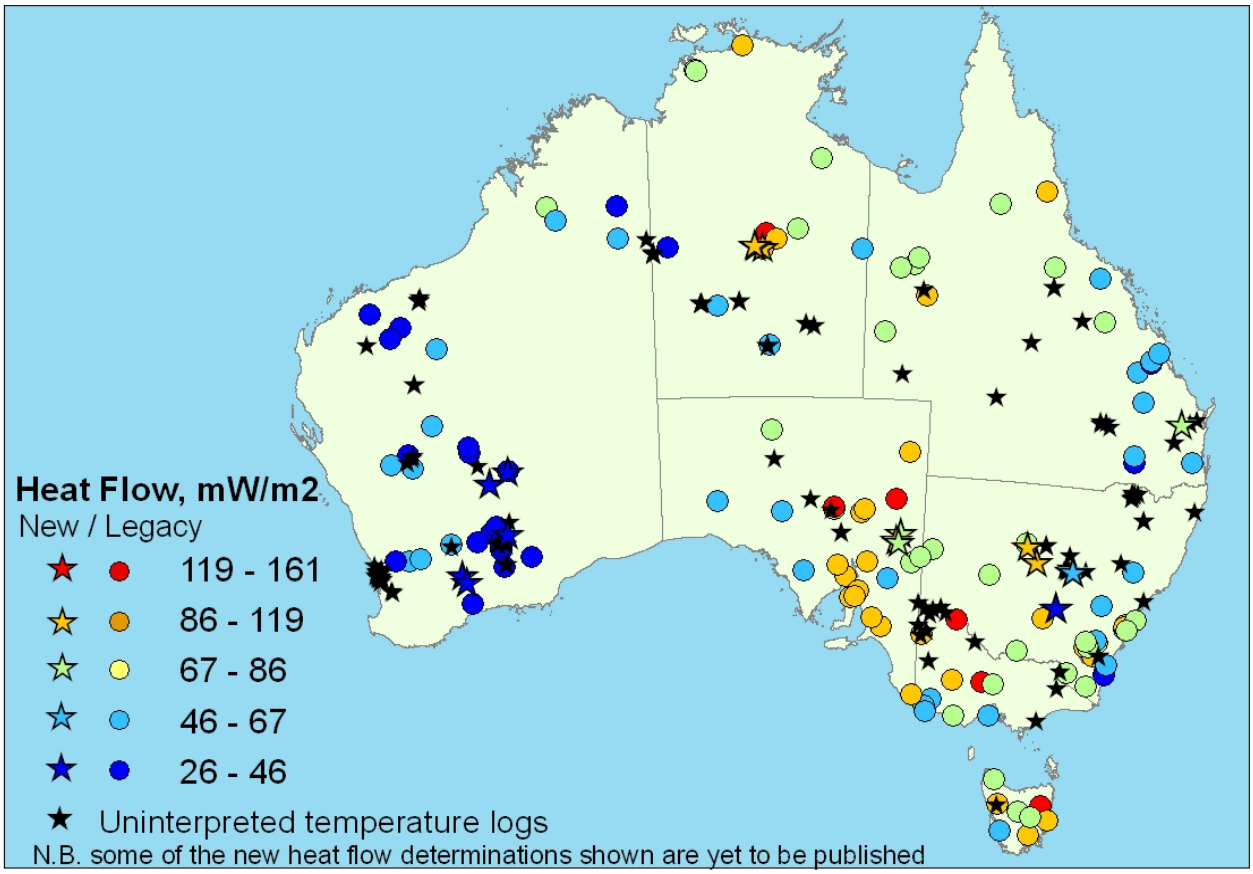

Figure 2: Heat flow data; published data in coloured circles; new data acquired by GA during OESP in stars.

these data sets to be used as 'mappable proxies' to estimate heat production and thermal insulation at regional scales (Budd et al. 2009). Conceptual and empirical methods of developing the Geothermal Play Systems approach have been pursued, and are still in further development.

3D thermal modelling

Through a Primary Industries and Resources South Australia (PIRSA) Australian Geothermal Energy Group (AGEG) Technical Interest Group 9 Tied Grant, a thermal calculation module for GeoModeller software was built by Intrepid Geophysics (e.g. Siekel et al. 2009). This has been used to develop thermal models of the Millungera Basin (Korsch et al., 2011), and the Cooper Basin (e.g. Gibson et al., 2010).

We have developed a synthetic grid of granites buried in flat-lying sediments that allows testing the effect of changing one variable at a time – the variables including thermal conductivity, density, heat production, and thickness of both granites and sediments, and additionally granite radius, granite thickness, and granite burial depth. This has resulted in 5,400 individual test models, and we are in the process of interpreting these results. These interpretations will then serve as a guide for a first-pass assessment of thermal potential of the whole content based on estimates of granite size and basin geometry and composition.

Energy Assessment

A GIS-based approach was used to qualify the Hot Rock and Hot Sedimentary Aquifer geothermal systems of northern Queensland (Huston, 2010).

A 3D thermal modelling approach was used to complete an assessment of geothermal potential in central-eastern South Australia (Huston and van der Wielen, 2011).

Seismic Acquisition and Processing

Geoscience Australia has more than 40 years experience in land seismic surveys and since 1980 has acquired in excess of 15 000 km of onshore deep crustal seismic reflection data and numerous 2D seismic refraction profiles. Since 2007, 13 seismic programs have been conducted through the OESP and ANSIR (see Figure 3) and the results of these surveys are being released progressively. Table 1 lists these surveys, their length, the data types acquired and the planned dates for release of the processed data.

Details of these surveys, and links to the results and interpretations can be found at http://www.ga.gov.au/minerals/projects/current-projects/seismic-acquisition-processing.html

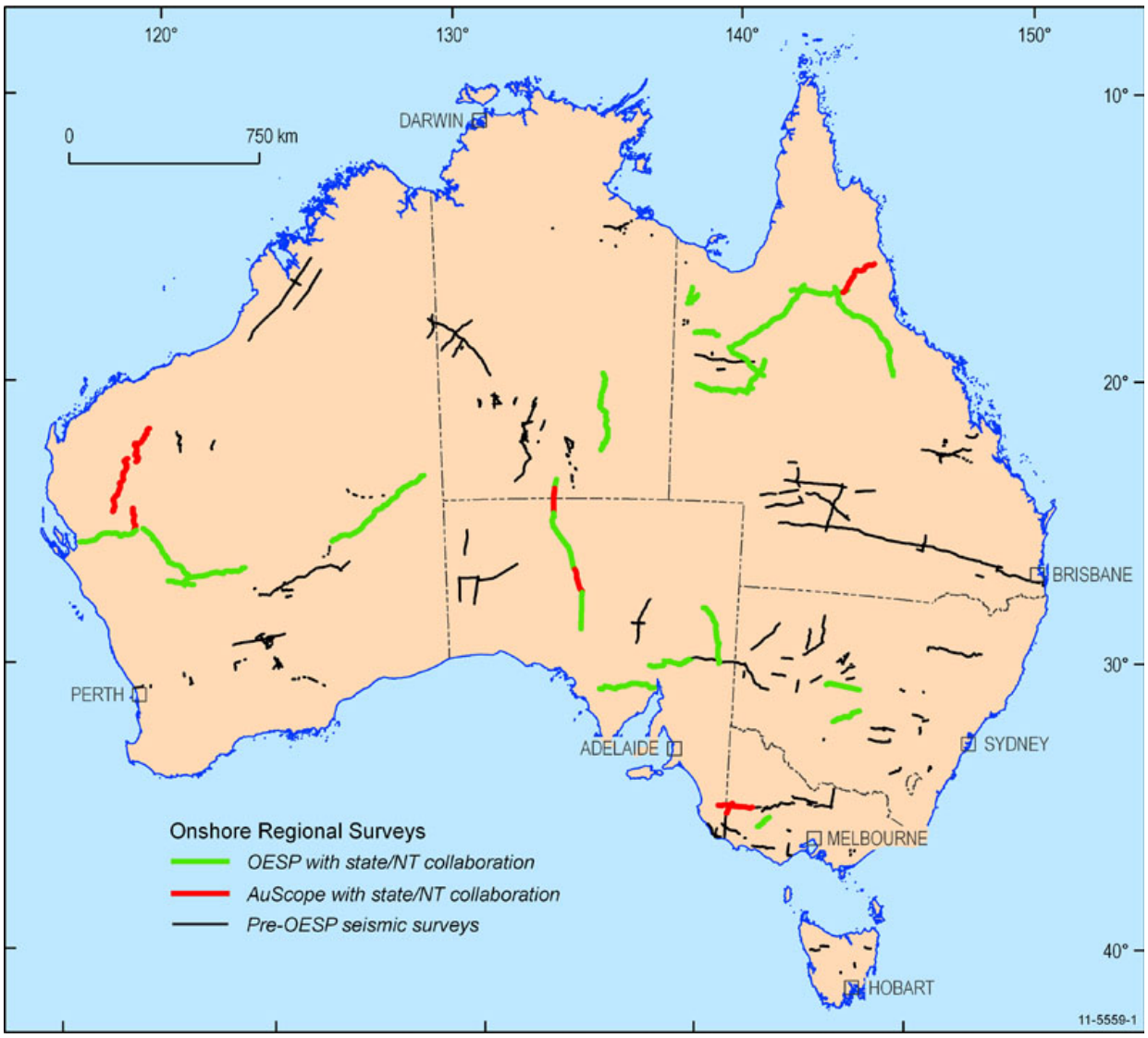

Figure 3. Map of Australia featuring seismic survey lines completed with OESP funding.

National Geochemical Survey of Australia

The primary aim of the NGSA is to provide pre-competitive data and knowledge to support exploration for energy resources in Australia. In particular, it will improve the existing knowledge of the concentrations and distributions of energy-related elements such as uranium (U) and thorium (Th) at the national scale.

The NGSA was initiated because of the realisation that there was no complete geochemical coverage available for Australia and because such a data layer is fundamental to successful exploration for energy-related and other commodities.

The objectives of the NGSA project are to:

- collect transported regolith samples at the outlet of large catchments covering more than 90 per cent of Australia using an ultra low sampling density approach;
- prepare and analyse the samples to extract the maximum amount of geochemical information (more than 60 elements) using internally consistent, state-of-the-art techniques;
- populate the national geochemical database with the resulting new data; and
- compile an atlas of geochemical maps for use by the exploration industry to identify areas of interest in terms of energy-related resources and other mineral commodities. These areas can then be the focus of targeted exploration efforts.

A sampling method has been adapted to Australian landscapes and climate conditions. It has been field-tested in the Riverina, Gawler and Thomson pilot projects. The cost of a national survey is kept reasonably low by applying an ultra low sampling density approach (1 site/1000 square kilometres to 1 site/10 000 square kilometres).

Details of these surveys, and links to the results and interpretations can be found at http://www.ga.gov.au/energy/projects/national-geochemical-survey.html.

Australia-Wide Airborne Geophysical Survey II

A common problem with past national airborne geophysical coverages is that the surveys were flown in patchwork fashion over many years and are not all registered to the same datum. In the case of airborne gamma-ray spectrometric data, acquisition equipment, system calibration and data processing procedures have changed significantly over time. Older surveys in Australia were reported in units of count per second, while modern surveys are reported in units of radioelement concentration. Also, environmental effects such as soil moisture and radon emanation can affect the base level of gamma-ray surveys. This means that gamma-ray spectrometric surveys seldom match exactly along their common borders, making it difficult to merge surveys into regional or continental-scale compilations. This limits the usefulness of these data because regional compilations facilitate the interpretation of large-scale features in the data and the comparison of features large distances apart.

A similar problem occurs with magnetic surveys, with inadequate reference field removal introducing base-level shifts. Also, the cross-over tie levelling procedure commonly applied to airborne magnetic data introduces a range of spurious wavelengths into the levelled data. Both gamma-ray spectrometric and magnetic surveys can be levelled and merged into continental-scale compilations by using the differences in areas where the surveys overlap to estimate correction factors. However, without independent control, this merging procedure can introduce long-wavelength errors into the merged data.

The Australian Government's solution to this problem was to acquire gamma-ray spectrometric and magnetic data over the entire Australian

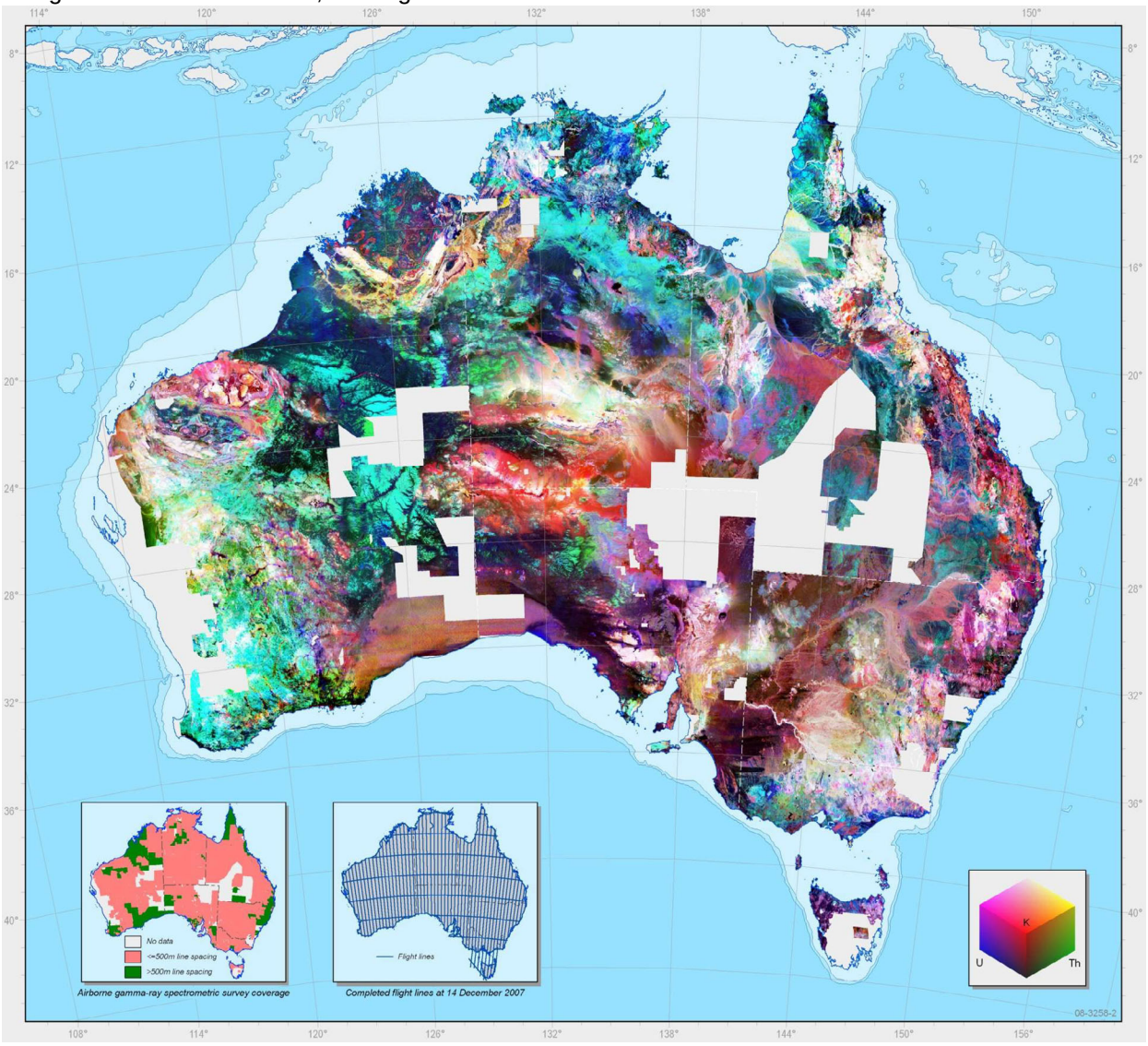

Figure 5: The new Radiometric Map of Australia (2010) has been compiled showing the distribution of airborne measured potassium (percent K), uranium (ppm equivalent U) and thorium (ppm equivalent Th) over 80 percent of the Australian continent at 100 metre resolution

continent at 75 km flight line spacing. These data (the Australia Wide Airborne Geophysical Survey - AWAGS) have been used to level and merge all public-domain gamma-ray spectrometric and magnetic data in Australia to common datums. The gridded merged data have been called the Radiometric and Magnetic Maps of Australia, respectively.

Project outputs

AWAGS survey

The AWAGS survey was completed in June 2008, and the project is continued as part of the Continental Geophysics Project. The data are available via the Australian Government's Geoscience Portal Geophysical Archive Data Delivery System (GADDS).

Radiometric Map of Australia

A new radioelement map of Australia, the Radiometric Map of Australia, has been compiled showing the distribution of airborne measured potassium (percent K), uranium (ppm equivalent U) and thorium (ppm equivalent Th) over 80 percent of the Australian continent at 100 metre resolution (Minty et. al., 2009). The map has been calibrated with the AWAGS to adjust all the public-domain radiometric surveys in Australia to the International Atomic Energy Agency's (IAEA) Global Radioelement Datum. The new datum provides a baseline for all current and future airborne gamma-ray spectrometric surveys in Australia.

Interpreters can use these grids of potassium, equivalent thorium and equivalent uranium to reliably compare the radiometric signatures observed over different parts of Australia. This enables the assessment of key mineralogical and geochemical properties of bedrock and regolith materials from different geological provinces and regions across the continent. These data support a range of different applications, including geological mapping, mineral and petroleum exploration, geomorphological studies and environmental mapping.

Magnetic Anomaly Map of Australia

A 5th edition full-colour Magnetic Anomaly Map of Australia at 1:5 million scale, and accompanying composite dataset with cell resolution of 3 seconds of arc, have been compiled. It is estimated that 27 million line-kilometres of survey data was acquired to produce this new edition, which is eight million line-kilometres more than for the previous edition released in 2004. New independent airborne total-field magnetic data acquired in 2007 during the AWAGS have been used to increase the accuracy of intermediate wavelengths of the continental-scale merge of the grids.

Information in the new magnetic anomaly map and associated grid database provides insights into the distribution of magnetically susceptible minerals within the Earth's crust. Such insights are of great value to energy and mineral exploration companies and for research into the solid Earth and the environment. Magnetic minerals in small amounts are widespread in the crust and become concentrated in zones which highlight the structure of the crust. This is particularly important for areas that have a significant thickness of surface cover (regolith and sedimentary basins) which can mask the underlying crystalline basement rocks. The magnetic signatures of the basement are measured through the cover and provide important information to help determine the nature and depth of the basement.

Details of these surveys, and links to the results and interpretations can be found at http://www.ga.gov.au/energy/projects/awags.html.

Conclusion

Precompetitive geoscience data can underpin investment decisions by both geothermal explorers and developers, and government.

References

Budd A.R., Holgate, F.L., Gerner, E.J., Ayling, B.F. and Barnicoat, A.C., 2008. Pre-competitive geoscience for geothermal exploration and development in Australia: Geoscience Australia's Onshore Energy Security Program and the Geothermal Energy Project, *in:* Gurgenci, H. and Budd, A.R. (*editors*), Proceeding of the Sir Mark Oliphant international Frontiers of Science and Technology Australia geothermal Energy Conference, Geoscience Australia, *Record 2008/18*, 1-8.

Budd, A.R., Barnicoat, A.C., Ayling, B.F., Gerner, E.J., Meixner, A.J., Kirkby, A.M., 2009, A Geothermal Play Systems approach for exploration, Australia, *in:* Budd, A.R. and Gurgenci, H. (*editors*), Proceedings of the 2009 Australian Geothermal Energy Conference, Geoscience Australia, **Record 2009/35**, 1-4.

Geoscience Australia and ABARE, 2010, Australian Energy Resources Assessment, Canberra.

Gibson, H., Seikel, R., and Meixner, T., 2010, Characterising uncertainty when solving for 3D temperature; new tools for the Australian geothermal energy exploration sector, 21st international geophysical conference and exhibition, ASEG-PESA 2010, Sydney, N.S.W., Australia, Aug. 22-26, **Australian Society of Exploration Geophysicists**.

Huston, D.L. (*editor*), 2010. An Assessment of the uranium and geothermal potential of north

Queensland. Geoscience Australia, **Record 2010/14**, 108pp.

Huston, D.L. and van der Wielen, S.E. (*editors*), 2011, An assessment of uranium and geothermal prospectiviety of east-central South Australia, Geoscience Australia, **Record 2011/34**, 229pp.

Jones, T., Gerner, E., Kirkby, A. and Weber, R., 2011. Heat flow determinations for the Australian continent: Release 2. Geoscience Australia, **Record 2011/28**.

Kirkby, A.L. and Gerner, E.J., 2010. Heat flow interpretations for the Australian continent: Release 1. Geoscience Australia, **Record 2010/41**, 28pp.

Korsch, R.J., Struckmeyer, H.I.M., Kirkby, A.L., Hutton, L.J., Carr, L.K., Hoffmann, K.L., Chopping, R., Roy, I.G., M. Fitzell, Totterdell, J.M., Nicoll, M.G., and Talebi, B., 2011. Energy potential of the Millungera Basin: A newly discovered basin in north Queensland. **APPEA Journal 51**, 37pp.

Minty, B., Franklin, R., Milligan, P., Richardson, L.M. and Wilford, J., 2009, The Radiometric Map of Australia, **Exploration Geophysics, 40/4**, pp. 325-333.

Seikel, R., Stüwe, K., Gibson, H., Bendall. B., McAllister, L., Reid, P., and Budd, A., 2009, Forward prediction of spatial temperature variation from 3D geology models: Adelaide: 20th **Australian Society of Exploration Geophysics Conference. Extended Abstracts**.

Weber, R., Kirkby, A.L. and Gerner, E., 2011. Heat flow determinations for the Australian continent: Release 3. Geoscience Australia, **Record 2011/30**.

Table 1. Sesimic reflection surveys acquired through the OESP.

Stakeholders	Survey Name	State	Traverse No	Length	Data Types	Survey Completed	Processed Data Release
OESP, GSQ Zinifex/pmd* CRC	L180 Mt Isa	Qld	06GA-M1	75km	Reflection, Gravity	Oct-07	Jun-08
		Qld	06GA-M2	62km	Reflection, Gravity	Oct-07	Jun-08
		Qld	06GA-M3	121km	Reflection, Gravity	Oct-07	Jun-08
		Qld	06GA-M4	200km	Reflection, Gravity	Dec-07	Jun-08
		Qld	06GA-M5	160km	Reflection, Gravity	Dec-07	Jun-08
		Qld	06GA-M6	283km	Reflection, Gravity	Nov-07	Jun-08
OESP/GSQ	L184 Isa-Georgetown	Qld	07GA-IG1	440km	Reflection, Gravity, MT	Aug-07	Dec-08
		Qld	07GA-IG2	243km	Reflection, Gravity, MT	Aug-07	Jun-09
OESP/GSQ	L185 Charters Towers	Qld	07GA-GC1	493km	Reflection, Gravity, MT	Sep-07	Jun-09
AuScope	L186 AuScope	Qld	07GA-A1	205km	Reflection, Gravity	Sep-07	Jun-09
OESP/NSW-DPI	L188 Rankins Springs	NSW	08GA-RS1	127km	Reflection, Gravity	Mar-08	Oct-08
		NSW	08GA-RS2	107km	Reflection, Gravity	Mar-08	Oct-08
	L188 Rankins Springs Extension (includes Line 08GA-RS2)	NSW	09GA-RS2	138km	Reflection, Gravity	Feb-09	Jun-09
OESP	L189 Gawler-Curnamona-Arrowie (Gawler province)	SA	08GA-G1	253km	Reflection, Gravity, MT	Jun-08	Dec-09
	L189 Gawler-Curnamona-Arrowie	SA	08GA-A1	60km	Reflection, Gravity	Jun-08	May-09

	(Arrowie Basin)						
	L189 Gawler-Curnamona-Arrowie (Curnamona province)	SA	08GA-C1	262km	Reflection, Gravity, MT	Jul-08	Sep-09
OESP/ AuScope/	L190 Gawler-Officer-Musgrave-Amadeus	SA/NT	08GA-OM1	634km	Reflection, Gravity, MT	Dec-08	Jul-10
PIRSA							
OESP/PIRSA	L191 Curnamona-Gawler Link	SA	09GA-CG1	144km	Reflection, Gravity	Jan-09	Jan-10
OESP/NTGS	L192 Georgina - Arunta	NT	09GA-GA1	373km	Reflection, Gravity, MT	Jul-09	Jan-11
AuScope/GSV/OESP	L193 Southern Delamerian	Vic/SA	09GA-SD1	146km	Reflection, Gravity	Nov-09	Jan-11
		Vic/SA	09GA-SD2	51km	Reflection, Gravity	Nov-09	Jan-11
GSV/OESP	L194 Ararat	Vic	09GA-AR1	69.6km	Reflection, Gravity	Nov-09	Jan-11
AuScope/GSWA/OESP	L195 Capricorn	WA	10GA-CP1	198km	Reflection, Gravity	May-10	Mid 2011
		WA	10GA-CP2	276.8km	Reflection, Gravity	May-10	Mid 2011
		WA	10GA-CP3	106.4km	Reflection, Gravity	May-10	Mid 2011
GSWA/OESP	L196 Youanmi	WA	10GA-YU1	302.2km	Reflection, Gravity, MT	Aug-10	Late 2011
		WA	10GA-YU2	282.8km	Reflection, Gravity, MT	Aug-10	Late 2011
		WA	10GA-YU3	109.8km	Reflection, Gravity, MT	Aug-10	Late 2011

The ARRC/Pawsey Geothermal Demonstration Project: An Example of How to Engage the Community

Simone Carr-Cornish*, Cameron Huddlestone-Holmes,
and Peta Ashworth
Simone.Carr-Cornish@csiro.au
Commonwealth Scientific Industrial Research Organisation (CSIRO)
CSIRO's Australian Rsource Research Centre (AARC) in Kensington, Perth.

The first deep well for CSIRO's ARRC/Pawsey Geothermal Demonstration Project is scheduled to be drilled in the second quarter of 2012. In Australia, this is the largest planned demonstration of direct use geothermal energy and one of the most suburban. It is likely there will be regulatory requirements to engage stakeholders, including the surrounding community. Outlined in this paper is how we will engage the community, through workshops with small groups of influential locals, a larger community workshop, a survey of local residents and a community meeting close to commencement of drilling. In addition to demonstrating how to engage the community, the project is an unprecedented opportunity to facilitate greater understanding of geothermal technology with the community, and the outcomes will help to inform future demonstrations.

Keywords: Community, engagement, stakeholders, Geothermal, perception,

What is the ARRC/Pawsey Geothermal Demonstration Project?

In June 2010, CSIRO was granted funding from the Australian Government's Education Investment Fund as part of the Sustainable Energy for the Square Kilometre Array to develop Australia's largest direct use geothermal demonstration site using geothermal energy from the deep underground aquifers. It is proposed that the project will provide heating and cooling for the ARRC facility and contribute towards the substantial cooling requirements of the Pawsey Centre supercomputer. This project, the largest direct use demonstration of geothermal energy sources in Australia, will essentially take place

Figure 1: Aerial view of ARRC/Pawsey Centre in Kensington Perth where drilling is taking place. Source: http://www.csiro.au/places/ARRC.html

under the backyards of Kensington, Perth residents and as such provides an unprecedented opportunity to raise awareness about geothermal energy with the Australian community.

Factors that will contribute to the success of this demonstration are the reservoir conditions as well as the community's response. Data from nearby deep petroleum wells indicate that the geological conditions have the potential to sustain a geothermal production system. If CSIRO proceeds with the full production system, it will involve an extraction and reinjection well. Extracted water is pumped through a heat exchanger where the required energy is removed and all the water is reinjected back into the aquifer. Drilling of the exploration well could take place as early as March 2012, depending on drill rig availability. In this paper we outline reasons for communicating directly with the community about the demonstration and how this engagement will take place.

Figure 1 is an aerial view of where the drilling will take place at the ARRC/Pawsey Centre in Kensington, Perth.

Current Legislation and Regulation Encourages Engagement

Both government and industry recognise the importance of effective engagement for minerals and energy projects to enable a social licence to operate (Ministerial Council on Mineral and Petroleum Resources, 2005). Openness and transparency are critical components of successful engagement and this is endorsed at the highest levels of government and by organisations such as the Organisation for Economic Cooperation and Development (1995). This recognition has been translated into various regulations such as the *South Australian Petroleum and Geothermal Energy Act* (State of South Australia, 2000) and the *Western Australian Petroleum and Geothermal Energy Resources Act* (PGERA; State of Western Australia, 1967). These Acts stipulate the minimum requirements for consulting with stakeholders and, as is the case for all energy projects, it is for the project proponents to decide whether they will go beyond compliance (Ashworth and Cormick, 2011).

In addition to the PGERA, the Western Australian Department of Mines and Petroleum have a Schedule of Geothermal Energy Exploration and Production Requirements (State of Western Australia, 2009). These outline that geothermal operations must be conducted in a consultative manner and comply with relevant Acts, rules, regulations, by-laws or directions applicable to host Shires and Districts.

Further to this, the Western Australian Department of Mines and Petroleum's, also through their *Guidelines for the Preparation and Submission of an Environmental Plan*, requires extensive documentation of community/ stakeholder interests including who should be consulted, the types of consultation, levels of information provided, issues and concerns raised, resolutions and what the process is for communicating throughout the ongoing operations (Department of Mines and Petroleum, 2005).

Consequently community engagement will be a key aspect of this demonstration, as this will comply with the Acts, the geothermal industry's own commitment to best practice (Primary Industries and Resources South Government of South Australia, 2011) and the values of CSIRO and their industry partner, GT Power Pty Ltd. Before outlining the community engagement activities that are planned for this demonstration, the next section describes existing research that documents current community sentiment towards geothermal energy.

Community Sentiment and Methods for Increasing Awareness

CSIRO aims to engage with the community that falls in the vicinity of the ARRC/Pawsey Geothermal Demonstration. The aim of the engagement process is twofold. First, to provide the local residents with information about the project, and second, to consult with them by accessing their opinions and identifying any potential concerns they may hold about the general technology or specific project. Previous research has demonstrated that early engagement helps to minimise the risk of opposition, while facilitating acceptance of the technology (Ashworth et al., 2011).

Furthermore, this engagement is of value because although geothermal technology has many promising benefits for society, one cannot assume automatic acceptance. There are numerous cases where community reactions have stalled or halted the implementation of low emission energy technologies. For example nuclear power projects have been hindered (Pickett, 2002), wind energy sites have been met with opposition (Devlin, 2005; Kaldellis, 2005), and concerns have also been raised about carbon capture and storage technology (Huijts et al., 2007; van Alphen et al., 2007). Geothermal has not been immune to incidents or negative reactions, as demonstrated in the media reporting of earthquakes from the hot fractured rock project in Basel, Switzerland (Swiss Info, 2007). Furthermore, it seems Australians are still making sense of the technology.

Australians are still making sense of geothermal energy

To date, there have been two small scale examples of geothermal technology in Australia. The town of Birdsville in Queensland uses

geothermal electricity sourced from hot water from the Great Artesian basin and the town of Portland in Victoria used geothermal district heating scheme for about twenty years, using hot water from the Otway Basin resource (Australian Geothermal Energy Association, 2010). There are also several exploration projects around Australia and in Western Australia geothermal energy is already being used to heat school and public swimming pools. However, on the whole Australian's have had little exposure to the technology.

To understand the public response to geothermal, along with other technologies and climate change, CSIRO's Science into Society Group (SISG) and Energy Transformed Flagship (ETF) have surveyed and conducted workshops with communities around Australia. The results of a survey conducted in June, 2011 of 2000 Australians showed that self-rated knowledge of geothermal energy (hot rocks) was lower than self-rated knowledge of most other energy sources/technologies (see Table 1; Hobman et al 2011:16).

Table 1. Self-rated knowledge of energy sources and related technologies

Knowledge* of:	Mean	Standard Deviation	Range
Wind	4.1	1.5	1-7
Solar (concentrating solar/solar-thermal)	3.8	1.6	1-7
Nuclear	3.7	1.6	1-7
Coal (without carbon capture and storage)	3.4	1.7	1-7
Geothermal (hot rocks)	3.0	1.7	1-7
Gas or coal (with carbon capture and storage)	2.9	1.5	1-7
Biomass	2.6	1.6	1-7

* Likert rating scale from 1(no knowledge) to 7(high knowledge), with midpoint 4(moderate knowledge).

Survey respondents were also asked to rate their support for technologies when presented with a brief definition of the energy source/technology. The definition for geothermal was:

> *"The energy available as heat extracted from within the earth's crust, usually in the form of hot water or steam. These resources are accessed by drilling wells into the earth and piping the steam or hot water to the surface, where the contained energy can be converted into electricity or used in processes that require heat"* (Hobman et al 2011:16).

Based on this description support for the use of geothermal was high but less than solar and wind (see Table 2; Hobman et al 2011:16).

Table 2. Support for energy sources and related technologies

Support* for the use of:	Mean	Standard Deviation	Range
Wind	5.7	1.4	1-7
Solar (concentrating solar/solar-thermal)	5.7	1.2	1-7
Geothermal (hot rocks)	4.9	1.5	1-7
Gas or coal (with carbon capture and storage)	4.2	1.4	1-7
Biomass	4.1	1.4	1-7
Coal (without carbon capture and storage)	3.6	1.5	1-7
Nuclear	3.6	2.0	1-7

* Likert rating scale from 1(strongly disagree) to 7(strongly agree), with midpoint 4(unsure).

Discussions in community workshops have highlighted that water usage and seismic activity are concerns the public genuinely hold (Dowd et al., 2011). Following are examples of comments made by participants.

Water usage:

> *"I am really concerned about the amount of water required for geothermal. If we already have a water problem aren't they just making things worse buy needing so much water for making the energy?"*

> *"Townships would need to be relocated for geothermal to ensure that there are plenty of hot rocks and water for operation and the effect it would have on industry, compared to clean coal"*

Seismic activity instigated by geothermal drilling:

> *"Geothermal is seen as better as it isn't treating a symptom by covering up a problem, it is actually a solution in that it produces little or no emissions but it is also a threat when looking at the possibility of seismic results due to drilling"*

> *"Wasn't there two large mistakes made overseas by geothermal drillers? Didn't they cause an earthquake? That really scares me to think that we are still creating destructive harm to the earth in search of energy"*

Additional information was also sought by participants:

> *"Not many people are aware of geothermal, unlike that of clean coal which has been discussed. I for one would really like more information and if possible to talk to someone from the industry itself"*

Communication and community-based workshops encourage understanding

The field of risk communication has been developed to explore ways to involve the public in decision-making. Risk communication is an interactive process of information and opinion exchange among individuals, groups and government institutions, involving multiple messages about the nature of risk (Committee on Risk Perception and Communication 1989). Dowd et al (2011) cautions that even sound scientific information is inclined to draw out challenging public discussion (Weber and Word 2001:448), often because how we perceive risk is actually very complex in that it is shaped by our attitudes, social values and cultural traditions (Renn et al 1996:178). The success of communication strategies are more likely if the factual and opinion based content can be differentiated; such strategies allow for dialogue, and build trust (Renn et al., 1996: 179).

The community workshops previously conducted by CSIRO follow the principles outlined by Renn et al (1996). Dowd et al. (2011) has reported on the efficacy of these workshops in not only identifying the community's understanding of geothermal energy technology but also increasing their knowledge of the technology. How supportive participants were initially at workshops (Dowd et al., 2011) was similar to that reported in the recent survey of the Australian public (Hobman et al., 2011); participants were mostly positive towards geothermal but did not rate the technology as highly as solar or wind. Although support was unlikely to shift significantly during the course of a day long workshop, changes in self-rated knowledge were immediate with the majority of participants shifting from low to moderate ratings.

Activities that will be used for Engaging Local Residents

Engagement is often described as being planned and deliberate, involving activities that promote public participation (Victorian Government Department of Sustainability and Environment, 2005). In order to engage with the residents living around the demonstration site we have planned: 1) workshops with small groups of influential locals; 2) a large community workshop; 3) a survey of local residents; and 4) a community meeting near the drilling site. Each activity, in varying ways, will serve to inform the local community about the project, consult with them to access their opinions and identify potential concerns. Public participation through informing and consulting are recognised forms of engagement by the International Association for Public Participation (IAP2, 2011). Informing involves providing the community with balanced and objective information to assist them in understanding the problems, alternative, opportunities and/or solutions. Consulting involves obtaining public feedback on analysis, alternatives and/or solutions.

Workshops with small groups of influential locals

Four workshops will be conducted prior to the large community workshop. These workshops will be conducted in the evening to make them more accessible for the majority of members of the community with each workshop involving 8-10 community members and take place over 2 hours. Influential locals will be invited including councillors, indigenous leaders, business leaders, teachers and nearby residents. Experts from the project will be present to describe the project and address questions that may arise.

Large community workshop

The community workshop, which could have as many as 100 attendees, will serve to significantly raise awareness of the demonstration project. The workshop will commence with expert presentations about climate change, low emission energy technologies and then present detailed information about the demonstration. Participants will have the opportunity to discuss the benefits and risks of the demonstration, and have their questions responded to by scientists and project experts. This opportunity for discussion with peers should contribute to greater awareness amongst the participants who are also likely to share their enhanced understanding with family and friends after the workshop.

Survey of local residents

Closely following the large community workshop surrounding, residents will be invited to participate in a survey. The survey will include details about the demonstration such as timing and benefits, along with information to address key concerns raised during other engagement activities. These details will contribute to increasing awareness, especially for residents who could not be involved in the earlier workshops. The survey will ask residents about whether they feel informed and are supportive of the project. The results will provide a representative indication of the local response to the demonstration.

Community meeting at the ARRC auditorium

To conclude the community engagement activities for this stage of the demonstration project, we will conduct a community meeting, close to the drilling site in the ARRC auditorium. This meeting will serve to validate the community's earlier input and concerns, while also adding to the transparency of the project. The engagement activities will complement the project's wider communication plan, which includes activities ahead of the test drilling such as consultation with the City of South

Perth Council and notices to the community through the local paper.

Conclusion

The ARRC/Pawsey Geothermal Project is an unparalleled opportunity to demonstrate the technology but also to build social momentum through direct engagement. In addition to increasing community understanding and meeting regulatory requirements, we aim to provide an example of how the community can be engaged about geothermal energy that will assist in preparing future demonstrations.

References

Australian Geothermal Energy Association (AGEA), 2011, Australian Projects Overview, visited September 6 2011, at http://www.agea.org.au/geothermal-energy/australian-projects-overview

Ashworth, P. and Cormick, C. 2011, Enabling the Social Shaping of CCS Technology in "Carbon Capture and Storage: Emerging Legal and Regulatory Issues", Eds I. Havercroft, R. Macrory, and R.B. Stewart. Hart Publishing: London.

Committee on Risk Perception and Communication National Research Council, 1989, Improving Risk Communication, National Academy Press: Washington DC.

Devlin, E., 2005, Factors Affecting Public Acceptance of Wind Turbines in Sweden. Wind Engineering, 29, 503-511.

Department of Mines and Petroleum (DMP), 2005, Guidelines for the Preparation and Submission of an Environment Plan, visited September 6 2011, at http://www.dmp.wa.gov.au/documents/081755_EP_Outlines.pdf

Dowd, A., Boughen, N., Carr-Cornish, S. and Ashworth, P., 2011, Geothermal Technology in Australia: Investigating Social Acceptance. Journal of Energy Policy, published online at http://dx.doi.org/10.1016/j.enpol.2011.07.029

Huijts, N.M.A., Midden, C.J.H. and Meijnders A.L.., 2007, Social Acceptance of Carbon Dioxide Storage, Energy Policy, 35, 2780–2789.

Hobman, V., Ashworth, P., Graham, P. and Hayward, J., 2011 Working Report, The Australian Public's Preference for Energy Sources and Related Technologies, CSIRO: Brisbane.

International Association for Public Participation (IAP2), 2011, IAP2 Spectrum of Public Participation, visited September 6 2011, at http://www.iap2.org.au/resources/spectrum.

Kaldellis, J.K., 2005, Social Attitudes Towards Wind Energy Applications in Greece, Energy Policy, 33, 595-602.

Ministerial Council on Mineral and Petroleum Resources (MCMPR), 2005, Principles for Engagement with Communities and Stakeholders, Union Offset Printers: Canberra.

Organisation for Economic Cooperation and Development (OECD), 2005, Guiding Principles for Regulatory Quality and Performance, visited September 6 2011, at http://www.oecd.org/dataoecd/19/51/37318586.pdf

Pickett, S.E., 2002, Japan's Nuclear Energy Policy: From Firm Commitment to Difficult Dilemma Addressing Growing Stocks of Plutonium, Program Delays, Domestic Opposition and International Pressure, Energy Policy, 30, 1337-1355.

Primary Industries and Resources South Government of South Australia (PIRSA), 2011, PIRSA Geothermal Energy, visited September 8 2011, at http://www.pir.sa.gov.au/geothermal/ageg/technical_interest_groups/group_1

Renn, O., Webler, Th. and Kastenholz, H., Perception of Uncertainty: Lessons for Risk Management and Communication, in V.H. Sublet, V.T. Covello and T.L. Tinker (eds.), Scientific Uncertainty and Its Influence on the Public Communication Process. Dordrecht (Kluwer 1996), pp. 163-182.

Swiss Info, 2007, Geothermal Project Shakes Basel Again, visited September 8 2011, at

http://www.swissinfo.ch/eng/Home/Archive/Geothermal_project_shakes_Basel_again.html?cid=46284

State of South Australia, 2000, Petroleum and Geothermal Energy Act, visited September 8 2011, at http://www.legislation.sa.gov.au/LZ/C/A/PETROLEUM%20AND%20GEOTHERMAL%20ENERGY%20ACT%202000.aspx

State of Western Australia, 1967, Petroleum and Geothermal Energy Resources Act (PEGRA), visited September 8, 2011, at http://www.austlii.edu.au/au/legis/wa/consol_act/pagera1967429

State of Western Australia, 2009, Schedule of Geothermal Energy Exploration and Production, visited September 8, 2011, at http://www.dmp.wa.gov.au/documents/PD-PTLA-TGR-142D.pdf

Van Alphen, K., van Voorst tot Voorst, Q., Hekkert, K.P., and Smits, R.E.H.M., 2007, Societal Acceptance of Carbon Capture and Storage Technologies, Energy Policy, 35, 4368–4380.

Victorian Government Department of Sustainability and Environment, 2005, Effective

Engagement: Building Relationships with Community and Other Stakeholders. The Community Engagement Network: Melbourne, Victoria.

Weber, J.R., Word, C.S., 2001, The Communication Process as Evaluative Context: What Do Nonscientists Hear When Scientists Speak? BioScience 51, 487–495.

Using stratigraphic forward modelling to characterise and identify geothermal reservoirs

Corbel, S.*[1,2], Griffiths, C.[2], Dyt, C.[2] and Ricard, L.P.[1,2]
soazig.corbel@csiro.au
[1] Western Australian Geothermal Centre of Excellence, Kensington WA 6151, Australia
[2] CSIRO Earth Sciences and Resource Engineering, PO Box 1130, Bentley WA 6102, Australia

The characterisation of geothermal reservoirs is a major issue for the geothermal industry, whether considering Hot Sedimentary Aquifers or Enhanced Geothermal Systems. Assessing the extractable heat from a reservoir requires knowing the extent and the rock properties of that reservoir. At the early stage of exploration, most geothermal companies cannot afford to acquire new data at and therefore rely on previously existing sparse well and seismic data. In those conditions, conventional characterisation techniques cannot be applied and new approaches are required.

In this study, we will explain the principles of stratigraphic forward modelling and how it helps characterise geothermal reservoirs. We will demonstrate the effectiveness of this technique on the Yarragadee Formation in the Perth Basin, and then go through the process of extracting the location and characteristics of potential geothermal reservoirs from the modelling results.

Keywords: geothermal exploration, Sedsim, stratigraphic forward modelling, Perth Basin

Sedsim stratigraphic forward modelling

Stratigraphic forward modelling is a process simulation approach that attempts to replay the way that sediments are deposited. It reproduces numerically the physical processes that eroded, transported, deposited and modified the sediments over varying time periods (Figure 1). Stratigraphic forward modelling has been used in the petroleum industry for more than a decade now (reference needed). It enables a better understanding of depositional mechanisms by testing different geological scenarios or conceptual models. It can predict facies and porosity distributions in areas where well data and seismic surveys are not available.

In this paper, we use the Sedsim three-dimensional stratigraphic forward modelling package that was developed originally at Stanford University by D. Tetzlaff and J. Wendebourg under the supervision of Prof. J. Harbaugh. It has since been modified and extended to the University of Adelaide and CSIRO by C. Dyt (Griffiths and Dyt, 2001). Sedsim enables the

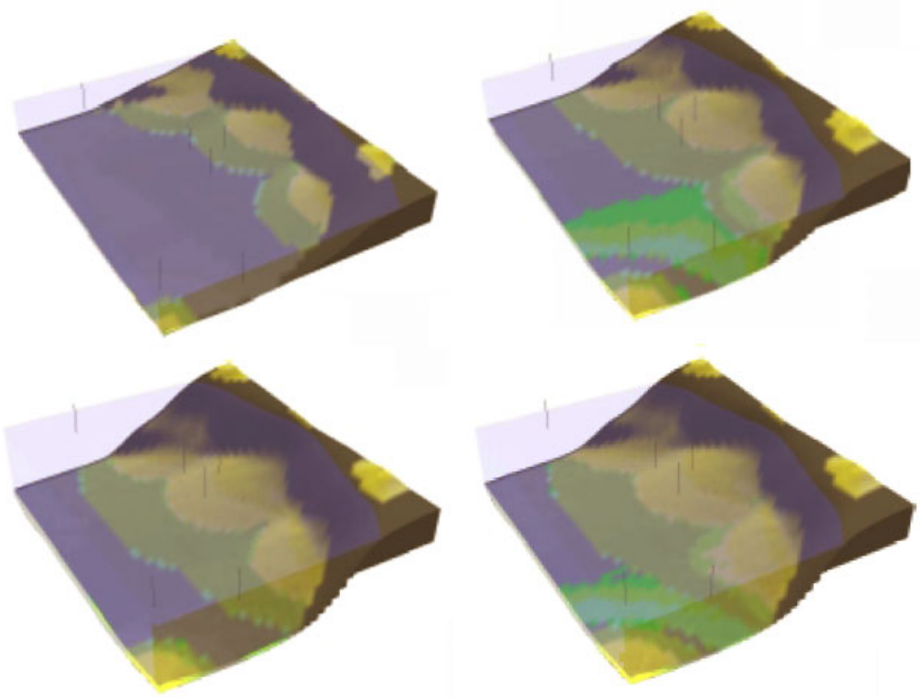

Figure 1: Example of stratigraphic forward modelling results at different time during the deposition (from Young and Griffiths, 2002).

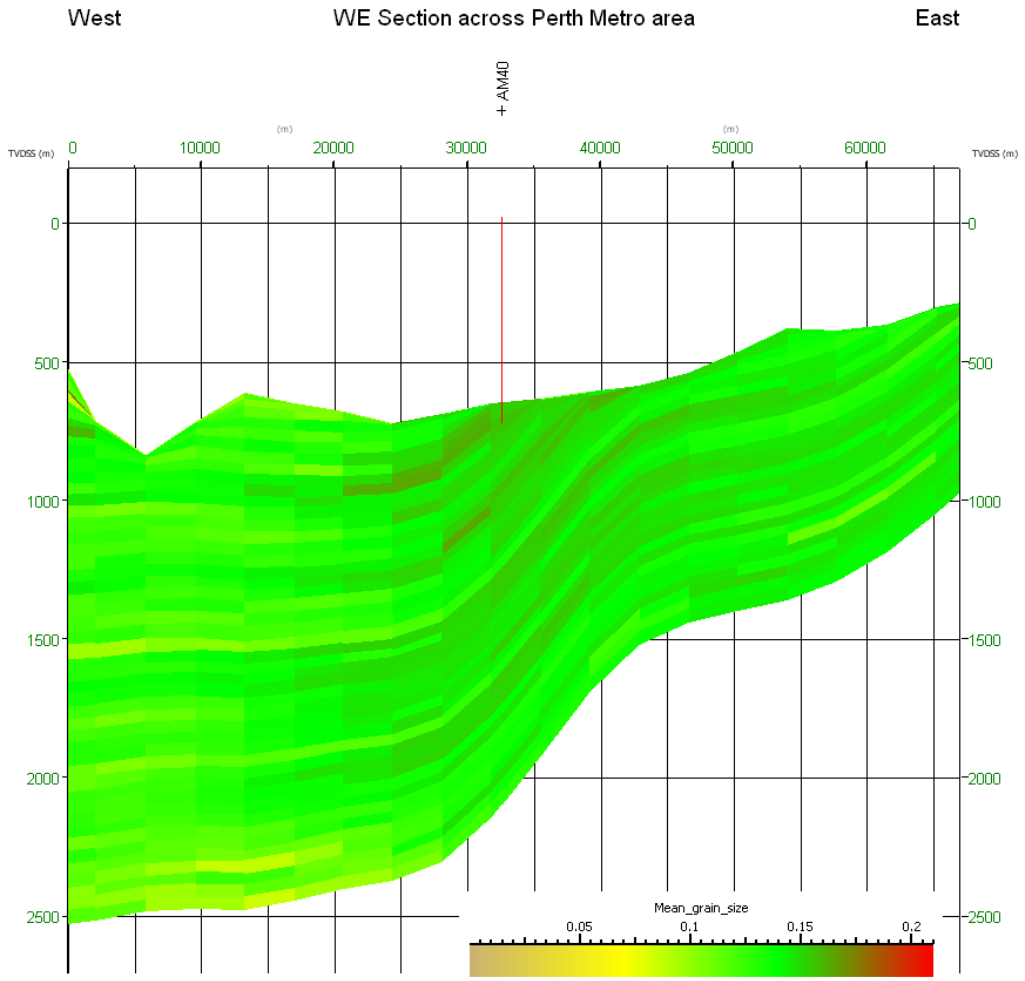

Figure 2: Section across Sedsim model showing mean grain size distribution. The only validation data available in this area was a water bore that only penetrated the first 40 meters of the Yarragadee Formation.

simulation of major depositional processes including marine, aeolian, fluvial, density flow, carbonate, vegetation and others.

Stratigraphic forward modelling of the Yarragadee Formation, Perth Basin

Sedsim stratigraphic forward modelling has been applied to the Perth Basin, in Western Australia, to characterise the Yarragadee Formation. The Yarragadee Formation contains most of the Yarragadee aquifer, which provides a major portion of Perth's drinking water and is currently involved in six direct use geothermal projects (Pujol 2011). Although those projects have demonstrated the geothermal potential of the Yarragadee aquifer, the deeper part of the aquifer is still poorly characterised. We used Sedsim to obtain a better reservoir characterisation without acquiring new data.

The Yarragadee Formation consists largely of sandstones fining up into claystones with coals. The sandstones range from fine to very coarse grains but are mostly medium to coarse with fine grained tops. The Perth Basin during Yarragadee deposition is believed to have been a vegetated floodplain traversed by meandering rivers transporting sediment from south to north, with local inputs of sediment along the sides of the rift forming small alluvial fans and tributary rivers (Tait 2007).

The Sedsim simulation was run over a period of 15.8 Ma, from Middle Jurassic to Late Jurassic. At that time Antarctica, Australia and Greater India still formed one continent. The major sediment source is a fluvial system originating from Antarctica, south of the current Perth Basin. Other minor sediment sources have been simulated originating in the Yilgarn Block, east of the basin and from Greater India, west of the basin. The simulations were run over a regular grid with a horizontal resolution of 3.71 km and a vertical resolution of 250,000 years. The final simulation was validated against well and seismic data where available.

The major outcomes of Sedsim simulations in term of reservoir characterisation are the grain size and porosity distributions. Even for cases where only a limited amount of direct measurements is available, porosity and grain size distributions can be predicted according to the geological history of the basin (see Figure 2).

Identifying geothermal reservoirs from stratigraphic forward modelling

A major question in the assessment of regional geothermal potential is the estimation of the quantity of the accessible resource base that can be extracted, and of the time during which such an extraction can be economically maintained (Gringarten 1978). In this paper, we therefore define a geothermal reservoir based on the amount of heat available in a reservoir and its extractability over a period of time.

To identify geothermal reservoirs, we will compute heat in place and sustainable pumping rates (Wellmann et al., 2011) from the Sedsim forward stratigraphic model results. Heat in place estimates will enable the definition of reservoir bodies. Once the different reservoir bodies are identified, we will compute for each of them sustainable pumping rate for a defined well spacing. We will then combine the sustainable pumping rates of each reservoir with the heat in place estimates to derive a potential recovery factor for the geothermal resource. The recovery factor will then enable the ranking the different reservoirs from an extractability point of view.

Discussion

We successfully applied stratigraphic forward modelling to characterise a poorly quantified sedimentary system in the Perth Basin. Starting from the geological history of the system, stratigraphic modelling simulates the sedimentation through geologic time. It therefore provides a way to estimate the grain size distribution, porosity and permeability based on geological reasoning rather than interpolation between sparse data. The simulated values have been validated against available data from well and seismic surveys. The stratigraphic forward modelling therefore provides insight into, and numerical predictions of, the distribution of sediments and their properties below ground, based on an understanding of the depositional processes involved. These properties can then be analysed to estimate geothermal reservoirs using heat in place and sustainable pumping rates estimates. We anticipate that stratigraphic forward modelling will therefore provide a valuable approach to understanding the subsurface distribution of properties, specifically in areas where data is sparse such as deep aquifers.

To date, stratigraphic forward modelling has already been successfully applied in the petroleum industry. We think that it could also be beneficial for geothermal applications. This will provide a novel way forward for a geologically controlled characterisation of geothermal reservoirs in poorly explored areas.

Acknowledgments

The Western Australian Geothermal Centre of Excellence (WAGCoE) is a collaboration between CSIRO, the University of Western Australia and Curtin University. WAGCoE is funded by the government of Western Australia, and also received additional support from industry partners Green Rock Energy and GT Power.

References

Griffiths, C., Dyt, C., Paraschivoiu, E. & Liu, K. 2001. Sedsim in hydrocarbon exploration. In: Merriam, D. & Davis, J. (Eds.), Geologic Modeling and Simulation. Kluwer Academic,New York, 71–97.

Gringarten, A.C., 1978, Reservoir lifetime and heat recovery factor in geothermal aquifers used for urban heating, Pure and Applied Geophysics, 117 (1) 297-308

Pujol, M., 2011, Examples of successful hot Sedimentary Aquifer direct-use projects in Perth, Western Australia, in Middleton, M and Gessner, K. (eds.) Western Australian Geothermal Energy Symposium Abstracts v. 1: p23.

Tait, A., 2007, A study of the Yarragadee Formation based on cores from Cockburn 1, Gage Roads 1, Gingin 1, Quinns Rock 1, Sugarloaf 1, Warnbro 1 and Whicher Range 1. Unpublished Report

Wellmann, J.F., Reid, L.B., Horowitz, F.G., Regenauer-Lieb, K., 2011, Geothermal Resource Assessment: Combining Uncertainty Evaluation and Geothermal Simulation, AAPG/SPE/SEG Conference

Young, H. and Griffiths, C., 2002, Sedsim Simulation of the Eastern Gregory Sub-basin, Canning Basin, WA.

Development of Geothermal Waters for Recreational Purposes – Mornington Peninsula Australia

Davidson. C.*, Peninsula Hot Springs, Anderson, T., GHD Pty Ltd, Stanley, D.R, GHD Pty Ltd.
charles@peninsulahotsprings.com
Peninsula Hot Springs
140 Springs Lane, FINGAL, VICTORIA 3939

Peninsula Hot Springs is Victoria's first hot spring and spa facility that uses naturally elevated temperature groundwater. This paper presents an overview of the spa development, from its original conception through to the technical summary of the facility's production bores.

Keywords: Groundwater, Recreational Waters, Victoria

Introduction

Peninsula Hot Springs is a relaxation and recreation facility with a source of 47ºC thermal water drawn from an aquifer located 600 metres below the surface. Purchased in 1997 the 42 acre (17 hectare) property is located in Fingal on the Mornington Peninsula, approximately one and a half hour's drive south from Melbourne.

After eight years of planning, drilling and raising finance, the first trial phase of the facility opened in June 2005. The initial stage provided facilities including public and private hot spring pools, a massage spa centre, relaxation rooms, a café and gift shop. A second phase of development commenced operation in December 2009 with the opening of a large Bath House bathing facility.

Future stages will see a further expansion in bathing, 126 rooms of accommodation, a Wellness centre and a planned geothermal demonstration of greenhouse and aquaculture operations.

Conception and Inspiration

The inspiration for Peninsula Hot Springs came from a 1992 bathing experience in the Japanese town of Kusatsu. Laying in the hot thermal waters, with snow all around, Peninsula Hot Spring founder Charles Davidson wondered why hot springs were not available in Australia and became inspired. A chance conversation with the head of the Victoria State office in Tokyo in 1997 revealed the existence of thermal waters deep underground on the Mornington Peninsula. By December that year, a 17 hectare site was purchased at the northern end of Davenport Drive, Rye, and the master planning was under way.

As there was no hot spring bathing culture in Australia at the time, and as Australia was home to people from all cultures of the world, the idea became to blend the best of world bathing cultures within the unique natural Australian environment. Travels to 18 countries to research the bathing and spa cultures lead to the development of a global hot springs spa.

Facility Development

Peninsula Hot Springs has two bores which are constructed into the Lower Tertiary age Werribee Formation, the basal unconsolidated sedimentary sequence of the Port Phillip Basin. The original steel cased production bore is used to supply geothermal waters of in excess of 47^{o}C to the recreational complex for bathing and hydronic heating.

To enable further increase in bathing offerings and to create a sustainable business, a re-injection bore began construction soon after the opening of the stage two facility. The bore was completed in October 2010 and the re-injection system was commissioned in May 2011. The system installed is designed to provide sufficient capacity for the projected geothermal requirements for the completion of the facility.

Community Impact and Investment

Peninsula Hot Springs employs 143 staff and is attracting over 250,000 visitors annually. The on-going development of the site has been driven by the huge demand for bathing in thermal waters and the significant growth in the spa and well being industry over the past 10 years.

Annual turnover was $11.5 million in 2010/11 and will be more than $14 million in 2011/12. Many of the visitors to Peninsula Hot Springs stay in the region, dine at restaurants and cafes and visit wineries, golf courses and other tourism attractions during their stay. This provides flow on economic benefit to the local economy. In its six years of operation Peninsula Hot Springs has grown to be the most visited tourism attraction in the region.

Geothermal Resort Potential in Victoria

Victoria's Spa and Wellness Tourism Action Plan (2005 – 2010), a first for Australia, emphasised the under development of spa and recreational facilities in the Victoria. With over 100 recognised mineral springs, Victoria has by far the highest number of natural springs in the country. An update of this plan for the years 2011-2015 was

released in September, 2011 emphasizing the ongoing commitment of the Victorian Government to the growth of the spa and wellbeing market. Together with the launch of the spa and wellness action plan (Tourism Victoria 2011), a business case for geothermal spa development in coastal Victoria aiming to attract new investment in the industry.

The development of the geothermal resource and the spa facility has been a massive undertaking by Peninsula Hot Springs. Eight years in the start up phase and the subsequent 6 years of operation and ongoing development have seen over $14 million invested in the facility. Peninsula Hot Springs pioneered geothermal development in the Mornington Peninsula and established a premier Victorian tourist attraction.

Development of Peninsula Hot Springs predates the proclamation of the *Geothermal Energy Resources Act* (2005), a framework that provides resource security, allocation and environmental planning. Projects that involve bores at temperatures less than 70°C or where the heat source is less than 1 km below the earth's surface, will not require an exploration permit. This Act greatly encourages investment.

Other developments have subsequently occurred in Warrnambool in the States southwest, relying on similar age (Tertiary - Eocene) geological formations (Dilwyn, Pebble Point Formations) within the Otway Basin. Potential also exists elsewhere in the Port Phillip and Gippsland Basins, and to a lessor extent in the Murray Basin owing to its distance from major tourism centres.

Geological Targets

Stratigraphy

Peninsula Hot Springs is located at the southern end of the Mornington Peninsula, and lies within the geological structure referred to as the Port Phillip Basin. The basin has been infilled with several phases of volcanics and sediments during the Tertiary and Quaternary periods.

The general stratigraphic sequence for the Port Phillip Basin has been described by many (e.g. Birch, 2003) and a summary has been provided in Table 1.

Previous Drilling

The characteristics of the basin on the eastern side of Port Phillip Basin was determined through the drilling of two deep investigation (Nepean 37 and Nepean 38) drilled by the former Mines Department of Victoria. These bores, drilled at Sorrento and Rye respectively, extended to depths of 1,273 metres and 942 metres respectively. Nepean 38 was constructed for groundwater observation purposes and remains an integral bore in the State observation network. Nepean 37 was not constructed and was plugged and abandoned following the completion of drilling.

Period	Formation	Lithology
Quaternary (Pleistocene)	Bridgewater Fm	Variable mixtures or sands, clays, calcareous aeolinites
Tertiary (Pliocene)	Wannaeue Fm.	Shelly sandstones and calc-arenites
Tertiary (Miocene – Pliocene)	Brighton Group	Sands, clays
Tertiary (Miocene)	Fyansford Fm / Demons Bluff	Marls (marine deposition)
Tertiary (Eocene)	Werribee Fm	Sands, silts, clays and coals (fluviatile origin)
	Older Volcanics	Basalt
Palaeozoic	Basement	

Table 1 Port Phillip Basin Stratigraphy

Information gathered during the drilling and monitoring of these bores provided valuable information as to the potential for low grade geothermal development in this region. This information was listed in King *et al,* 1987 who noted that elevated groundwater temperatures and geothermal gradients were present along the Mornington Peninsula.

Geothermal Gradients

King *et al* (1987) reported a geothermal gradient of 5 ^{o}C/100 m depth. The source of the elevated geothermal gradient is believed to be the Selwyn Fault.

The Lower Tertiary age sedimentary sequence therefore presented itself, based on the historical drilling information, as being a potential low grade geothermal prospect for development for recreational purposes. In addition, being within the Mornington Peninsula tourism region, and the proximity to Melbourne provided added marketing opportunities for a spa development.

Licensing and Approvals

Victoria Groundwater Licensing Overview

The Victorian Department of Sustainability and Environment (DSE) have recognised areas of intensive groundwater use throughout Victoria. The principle management unit for groundwater resources in Victoria is the Groundwater Management Unit or GMU. A GMU may be a Groundwater Management Area (GMA), a Water Supply Protection Area (WSPA) or an Unincorporated Area. These are declared under the *Water Act* (1989) to ultimately provide sustained management of the groundwater resources.

The Peninsula Hot Springs facility is located within the Nepean GMA. The GMA was initially

defined to manage the surficial aquifers e.g. Bridgewater and Wannaeue Formation. No depth limit has been applied to the formation, and therefore management controls also apply to all aquifers in the vertical profile including the target aquifer for this project the deeper Werribee Formation.

Licensing

A groundwater extraction licence was issued by Southern Rural Water to 'take and use' groundwater under the *Water Act* (1989).

The groundwater licensing process involved referrals to South East Water and the Victorian Environment Protection Authority (EPA), and therefore a condition of the extraction licensing was the subsurface disposal of waste water.

Peninsula has installed a second production (injection) bore with the ultimate objective of returning their waste stream to the source aquifer.

Production Bores

Bore Design

The original bore installed on the property (bore 144197) was constructed with mild steel casing. The objective of this bore was to prove up the geothermal resource. It was completed in early 2002. The second production (injection) bore installed at the site (WRK056027) has been constructed with Fibre Reinforced Plastic (FRP) casing and stainless steel. It was completed in mid 2010.

The shallow groundwater resources within the Bridgewater and Wannaeue Formations are widely developed for irrigation use, hence the declaration of the Nepean GMA. Groundwater quality in the shallow aquifers is often less than 300 mg/L TDS (Birch ed, 2003). The groundwater in the deeper Werribee Formation is of poorer quality, approximately 3,000 mg/L TDS (Laing, 1980).

Casing Annular Seals

Owing to the differing water qualities, casing in both bores (144197 and WRK056027) was pressure cemented to provide a seal to hydraulically isolate the shallow and deeper aquifer system. Whilst this was a mandatory of the bore construction license issued by Southern Rural Water, it also provided confidence to local irrigators that their shallow resource would not be adversely impacted by the development.

Development Zones

Wireline geophysical logging (e.g. natural gamma, neutron, density and temperature) was used during the pilot hole drilling to identify permeable, coarse grained lenses within the Werribee Formation for development. The basal lenses within the Werribee Formation were selected to maximise the temperature of the production water.

Bore 144197 is screened over two intervals between whereas the second bore WRK056027 has a single 20 m screen (refer Table 2).

Screen Designs

Lithological samples collected during the drilling program underwent particle size distribution testing to determine appropriate sizes for screen apertures. Stainless steel screens were specifically designed to maximise production. The screen intervals are summarised in Table 2.

Bore	Screen From - To	Aperture
144197	533 m to 540 m (7 m)	0.635 mm
	612 m to 622 m (8 m)	0.76 mm
WRK056027	521 m to 541 m (20 m)	0.3 mm

Table 2 Bore screen intervals

Production Bore Testing

Performance (pumping) tests have been conducted on both bores. Bore WRK056027 was capable of flow rates in excess of 30 L/s and sustained flow rates rate over 1 ML/day over a 24 hour period.

Conclusions / Learnings

Peninsula Hot Springs has successfully developed the low grade geothermal groundwater resources of the Werribee Formation on the Mornington Peninsula.

Peninsula Hot Springs are the first to develop the deep geothermal groundwater resources in this region which came at some risk due to the paucity of deep drilling information in the region.

There were difficulties in securing competent drilling contractors during the period owing to prevailing drought conditions throughout Victoria. The timing of the second borehole was delayed by drilling contractor unavailability, and drilling difficulties were experienced during its drilling.

Geochemical modelling was undertaken to assess the compatibility of re-injection waters. Numerical groundwater modelling was also undertaken to determine the potential for recycling of waters and long term impacts on the heat resource. Peninsula Hot Springs are undertaking a comprehensive monitoring program for their re-injection bore to assess and monitor its performance.

References

Birch, W. D.,(Editor), 2003, Geology of Victoria. Geological Society of Australia Special Publication 23. Geological Society of Australia (Victoria Division).

King, R. L., Ford., A. J., Stanley, D. R., Kenley, P. R., and Cecil, M. K., 1987, Geothermal Resources of Victoria, Department of Industry, Technology and Resources, Victorian Solar Energy Council.

Laing, A. C. M., 1980, Groundwater in Nepean 37 (Sorrento). Victorian Geological Survey Unpublished Report 1980/38.

Tourism Victoria, 2011, Victoria's Geothermal & Natural Mineral Water Tourism Investment Opportunities

Latrobe Valley Shallow Geothermal Project

Driscoll, J.P.* & Beardsmore, G.R.
jim.driscoll@hotdryrocks.com
Hot Dry Rocks Pty Ltd
36 Garden Street, South Yarra, VIC 3141

The Latrobe Valley Shallow Geothermal Project (LVSGP) aims to demonstrate fluid circulation and heat extraction from moderate temperature groundwater resources at less than 1,000 m depth in the Latrobe Valley and establish the technical and commercial viability of this renewable resource for small-scale electricity production.

Hot Dry Rocks Pty Ltd (HDR) undertook a Geothermal Systems Assessment (GSA) to assess the potential for moderate temperature geothermal energy targets within the Morwell–Traralgon area of the Latrobe Valley, onshore Gippsland Basin, Victoria. The principal risk areas addressed in the GSA include the presence of an adequate thermal insulating cover sequence (hence adequate temperatures for geothermal prospectivity), the presence of a suitable reservoir unit (a sedimentary aquifer), and the availability of water.

Successful demonstration of the LVSGP will translate to similar geological settings in Australia and overseas.

Keywords: Latrobe Valley, Geothermal Systems Assessment, Hot Sedimentary Aquifer

Introduction

Geothermal exploration aims to identify areas where the main components of a geothermal system are present or can be engineered. Namely: the availability of water, in situ permeable aquifers or rock units and elevated temperatures at drillable depth.

Hot Dry Rocks Pty Ltd (HDR) is the operator of the Latrobe Valley Shallow Geothermal Project (LVSGP). The aim of the LVSGP is to install a 500 kW (gross; 350 kW net) pilot electrical power generator to demonstrate the potential of using moderate temperature groundwater to generate baseload electricity. The generator is being developed and constructed by HDR's partner in the LVSGP, Green Thermal Energy Technologies (gTET).

In November 2010 the Victorian Government's Department of Primary Industries (DPI) awarded HDR a $217,500 grant under the Energy Technology Innovation Strategy (ETIS) Sustainable Energy Research & Development (SERD 2) program to progress the LVSGP.

A key element of this grant was a Geothermal Systems Assessment (GSA) of the coal-bearing

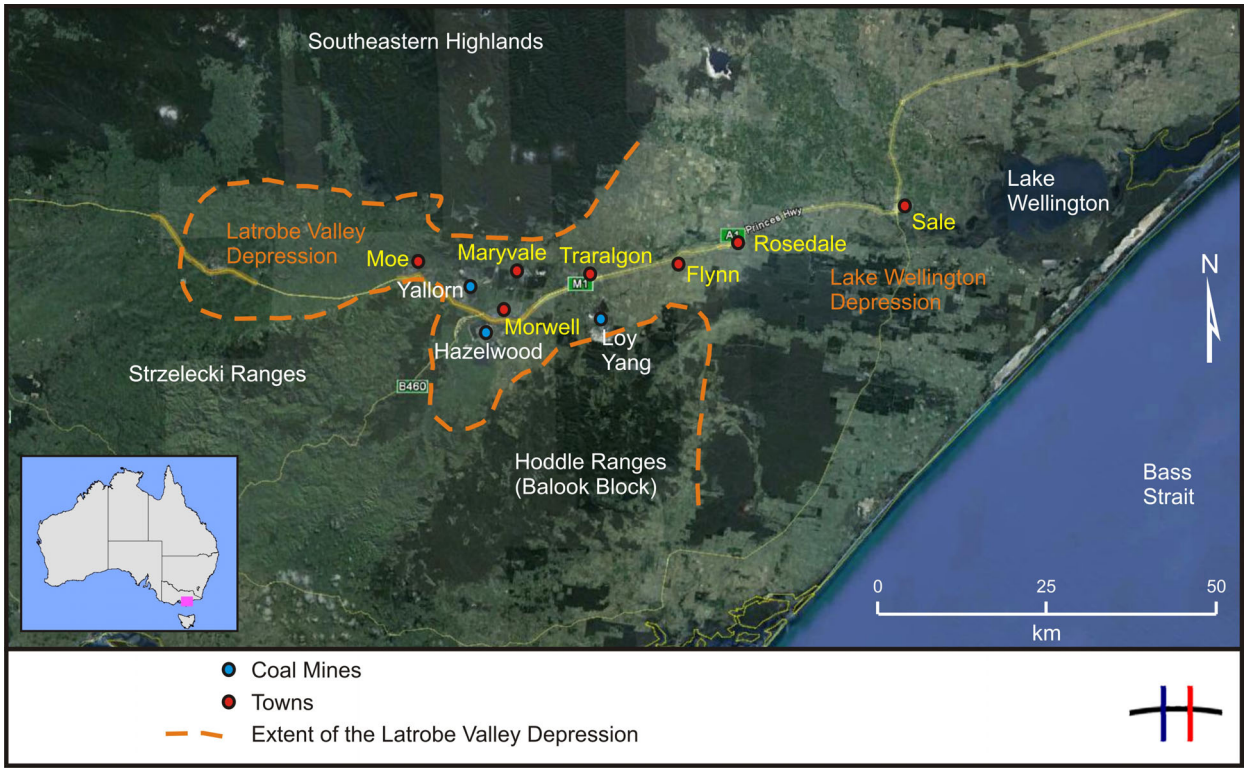

Figure 1: Location of the Latrobe Valley (background image courtesy of Google Earth).

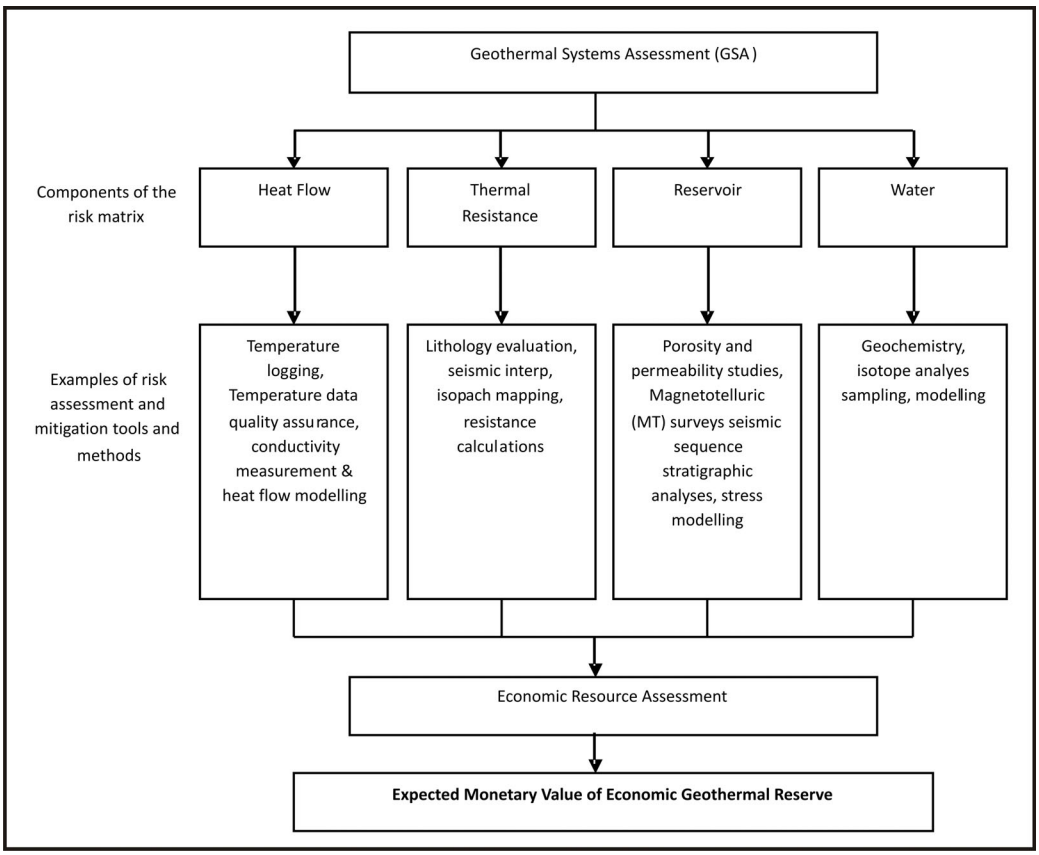

Figure 2: The GSA Framework as described by Cooper and Beardsmore (2008).

region of the Morwell–Traralgon area of the Latrobe Valley. This assessment was primarily based on existing geotechnical datasets. However, HDR undertook a Precision Temperature Logging (PTL) work program to provide further data on the sub-surface temperature profile of key areas. A key deliverable of the GSA was to identify a preferred site for the initial LVSGP exploration bore.

Since the LVSGP is targeting hot water shallower than 1,000 m, the project falls outside the regulations of the Victorian Government's Geothermal Energy Resources Act (2005). However, the project is still subject to the usual planning and environmental legislation and regulation.

Location

The study area of the GSA broadly covered the coal-bearing sequences of the onshore Gippsland Basin, Victoria—specifically the Morwell–Traralgon area of the Latrobe Valley (Figure 1), located approximately 140 km ESE of Melbourne.

Brown coal resources are prevalent throughout the Latrobe Valley, extending from Moe to Rosedale, and include open-cut coal mines at Loy Yang, Hazelwood and Yallourn. These include large coal resource areas yet to be allocated for development. The coal mining industry dominates the Latrobe Valley landscape, both geographically and politically, being a major employer in the region. Strategically, the Latrobe Valley is the centre of Victoria's electricity generating industry, supplying approximately 85% of Victoria's electricity needs.

The geothermal potential of coal-bearing basins

The most prospective regions for high geothermal temperatures are those that have geological units of sufficiently low conductivity (high thermal resistance) in the cover sequence combined with high heat flow. Thick intervals of coal- and clay-rich sequences provide excellent thermal insulation properties; thus heat is trapped below the sequences. Coal-rich sequences are also commonly interbedded with sandstone horizons that often have excellent reservoir characteristics, such as high porosity and permeability. The coincidence of elevated temperature and shallow reservoirs makes an ideal geothermal energy target.

Occurrences of relatively high temperature groundwater flowing at high yields from shallow depths in the Latrobe Valley are well known. Jenkin (1962) noted two bores with elevated temperatures in the Maryvale area, one of which recorded a well yield of 69.5 L/s at 70 °C from a depth of 524.5 m.

Geothermal Systems Assessment

The Geothermal Systems Assessment (GSA) offers a holistic approach to delineating geothermal resources with a methodology synonymous to that proposed by Magoon and Dow (1994) in their Petroleum Systems Analysis volume. The GSA framework (Figure 2), first described by Cooper and Beardsmore (2008), addresses principle geological risks at basin or tenement scale. Further detailed work at a play scale is recommended to progress exploration in areas that a GSA might highlight.

Four critical geothermal risk areas relate to four geological factors. These are summarised below:

1. Heat flow: Probability that heat flow measurements or assumptions reliably characterise the play under investigation. Estimated from geographic coverage and 'uncertainty' of heat flow estimates.
2. Thermal resistance: Probability that thermal resistance and heat transfer mechanism beneath the level of well intersects are as assumed (purely conductive, convective component, advective component).
3. Reservoir: Probability that reservoir properties and volumetric extent are as assumed. Estimated from geographic coverage, data type and reservoir type. Includes void connectivity and prevailing stress regime.
4. Water: Probability that water supply or chemistry will not adversely impact on the project.

The GSA methodology assesses each component of the risk matrix, and places a confidence rating on the data used based on experience and current understanding of the area of interest. Some aspects of risk in the geothermal system share varying degrees of co-dependence. For example, heat flow and thermal resistance risk share a common link via rock thermal conductivity measurements.

By understanding and quantifying the risk elements of each critical technical area, steps can be taken to mitigate the risk prior to significant expenditure (being proactive rather than reactive). For example, if heat flow is uncertain, it can be measured prior to significant expenditure.

Available data sets

Well data

Many petroleum wells, coal bores and water bores have previously been drilled within the Latrobe Valley (Figure 3).

Hydrogeological data were sourced from several publications and included information such as groundwater models, well pump tests, and core porosity and permeability estimates. However, the vast majority of hydrogeological data known to exist for the region are non-published, proprietary information not available for this study.

Seismic data

Seismic data in the Latrobe Valley are relatively

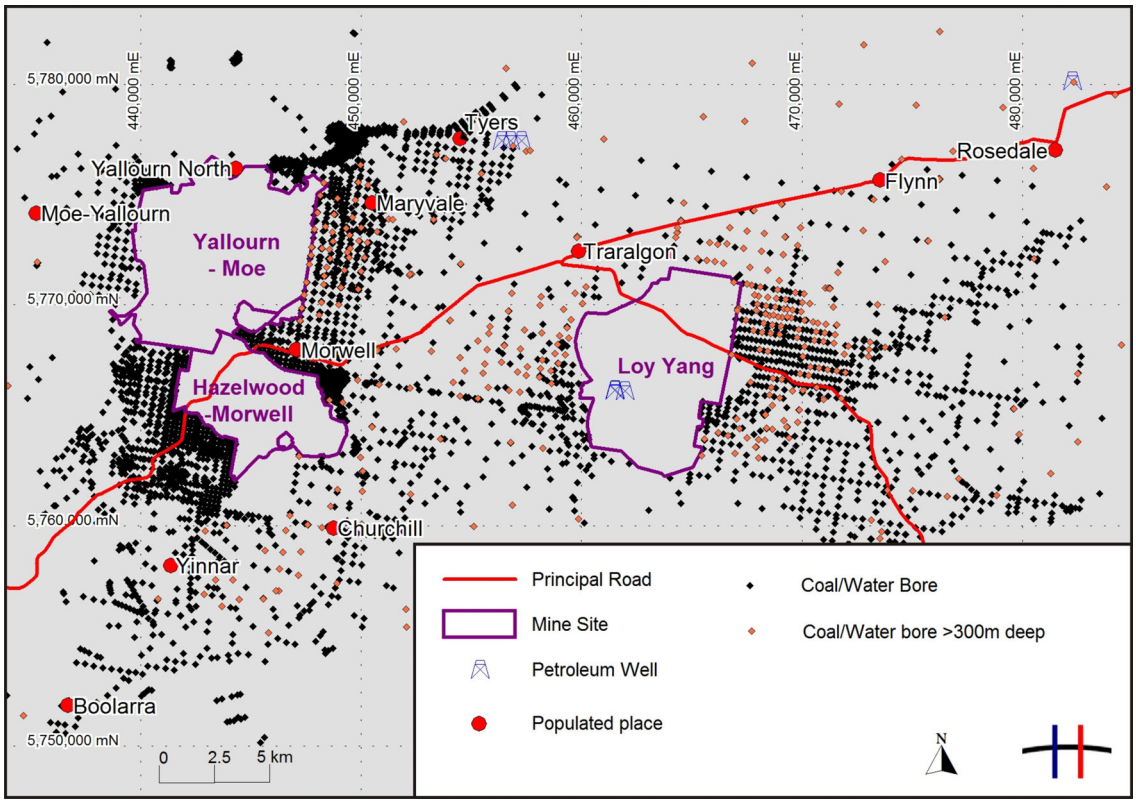

Figure 3: The geographical distribution of all petroleum wells and coal/water bores in the Latrobe Valley.

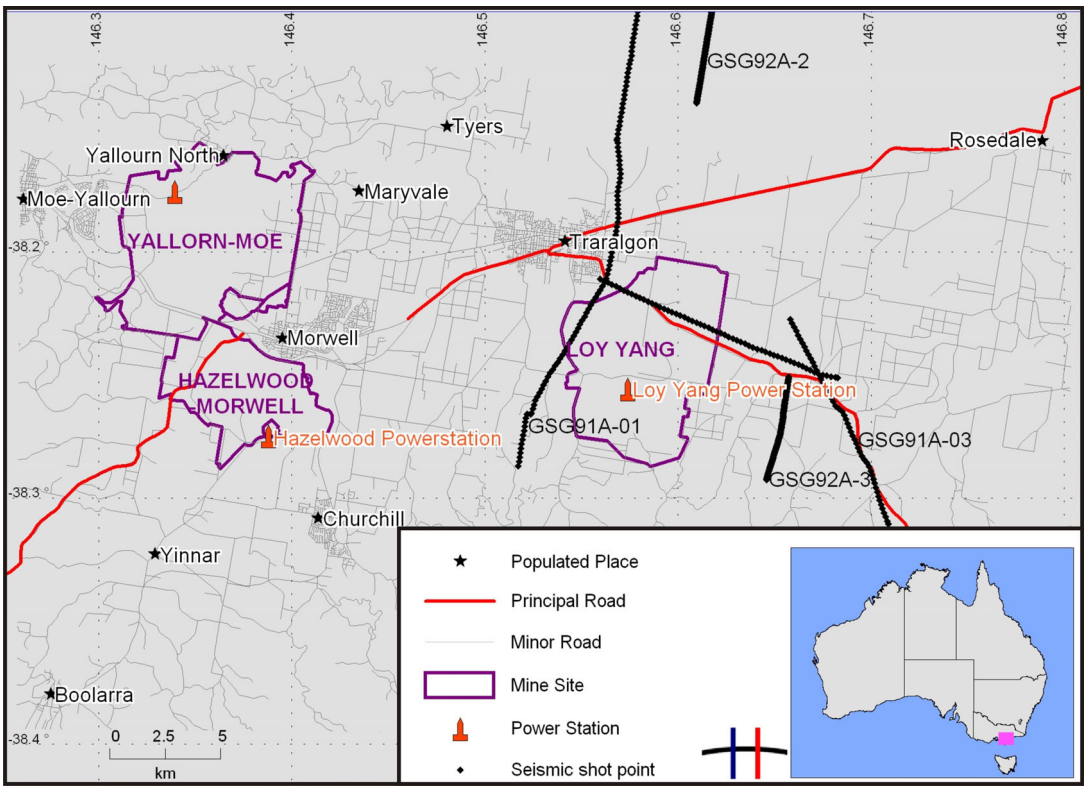

Figure 4: Location of seismic lines in the Latrobe Valley.

sparse with just four regional reflection seismic lines acquired in 1991 (Figure 4). The lines (GSG91A-01, GSG91A-03, GSG92A-2, GSG92A-3) have data to a depth of 3.8 seconds TWT and are of reasonable quality, although quality deteriorates at depths greater than 1 second TWT, probably due to signal attenuation through the Cainozoic coal succession. However, a number of key reflections and faults beneath this depth remain interpretable.

Latrobe Valley Coal Measures 3D Model data

HDR was able to interrogate DPI's 2003 Latrobe Valley Coal Measures 3D Model to quantify the depth to base Cainozoic and estimate the cumulative thickness of coal sequences in the area. DPI released a revised Latrobe Valley Coal Measures 3D Model in May 2011. The new model covered an expanded geographical area, included previously confidential datasets, and incorporated geotechnical data collected between 2003 and 2011.

Geology of the Latrobe Valley

The Gippsland Basin was formed during the Jurassic–Early Cretaceous continental breakup of Gondwanaland in the initial phase of the rifting of Australia from Antarctica (Duddy, 2003). During this rifting E–W orientated en echelon grabens formed along southern Australia and rapidly filled with sediments. The Gippsland Basin began to rapidly subside as a result of crustal extension and fluvial non-marine sediment loading. The separation of Antarctica from Australia along western Tasmania in the mid-Cretaceous (~95 Ma) resulted in the Gippsland Basin becoming a failed rift (Duddy, 2003; Webb et al., 2011).

In the Late Neogene (~10 Ma) the Gippsland Basin was subjected to tectonism and deformation associated with the Kosciuszko Uplift (Webb et al., 2011). This period of tectonism reactivated early rift features converting them to features of compression. Throughout the Cainozoic post-rift failure, the Gippsland Basin became a rapidly subsiding sag basin (Holdgate, 2005; Webb et al., 2011).

The Gippsland Basin covers 56,000 km², of which approximately 16,000 km² is situated onshore, and contains a succession of non-marine Cretaceous to early Cainozoic sediments (Holdgate et al., 2000). A generalised cross section of the onshore Gippsland Basin is presented in Figure 5.

Temperature Data

One of the primary aims of a GSA is to quantify the value and uncertainty of the temperature of key reservoir targets. Direct measurements of temperature at the target depth are rarely available for geothermal energy projects targeting resources down to 5,000 m depth. However, the LVSGP is targeting shallow reservoirs previously drilled at depths <1,000 m and thus directly measured datasets are available.

Temperature data are important pieces of information for assessing the commercialisation of any geothermal resource. However, caution should be maintained with respect to the validity

of pre-existing temperature datasets as they are usually collated for other purposes—most notably petroleum exploration—and collected as ancillary data.

Temperature data reported in petroleum and coal/water bore reports are often of unknown quality. Petroleum 'bottom hole temperature' (BHT) are usually recorded a short time after the circulation of drilling fluid in a hole, and therefore represent disturbed thermal conditions. Likewise, temperature logs collected immediately after drilling has ceased in other types of bores are prone to similar errors.

Historical data from a number of boreholes in the Latrobe Valley suggest that elevated temperatures at shallow depths are a common occurrence. Driscoll (2006) conducted a geothermal assessment of Victoria and collated all published temperature data from boreholes drilled in Victoria. A core component of that particular study was establishing the source of temperature data reported in earlier reports and borehole completion reports. However, in many instances, the process of how and when data were collected could not be verified. Much of the temperature data collected from coal and petroleum reports are thus of unknown quality. This information is critical since well temperatures measured during the drilling process can underestimate the virgin rock temperature of the formations at depth.

Discussions between HDR and a number of engineering and coal companies yielded further temperature data that were only recently made available. However, once again, the details of how the data were recorded were not provided.

Thermal resistance

Thermal resistance is the 'blanket' that traps heat underground. It is synonymous with the 'trap' and 'seal' concepts of petroleum systems analysis. Thermal resistance (m^2K/W) is the cumulative sum of overburden thickness (m) divided by thermal conductivity (W/mK). A geothermal prospect must have an adequate 'thermal blanket' to retain heat at depth. This is best provided by a thick sequence of low conductivity lithologies such as coals, carbonaceous shales or fine-grained siltstones.

The Latrobe Valley hosts a world-class brown coal deposit comprising up to five individual seams, each in excess of 100 m. These thick multi-stacked coal units—the Hazelwood Formation, Yallourn Formation, Morwell Formation and upper portions of the Traralgon Formation—are widely distributed throughout the Latrobe Valley. HDR's thermal conductivity analysis in DPI's Geothermal Atlas of Victoria (2010) confirmed the brown coal sequences exhibit low conductivity and thus provide excellent insulatory cover.

HDR calculated that approximately 350 m cumulative thickness of coal would provide insulation properties to achieve a 90 °C temperature.

Given the plethora of geotechnical data confirming the thickness and lateral extent of thick coal measures in the Latrobe Valley, the known presence of elevated temperature in the Latrobe Valley, and the directly measured thermal conductivity results from the coal measures, HDR is confident that thermal resistance poses a low risk.

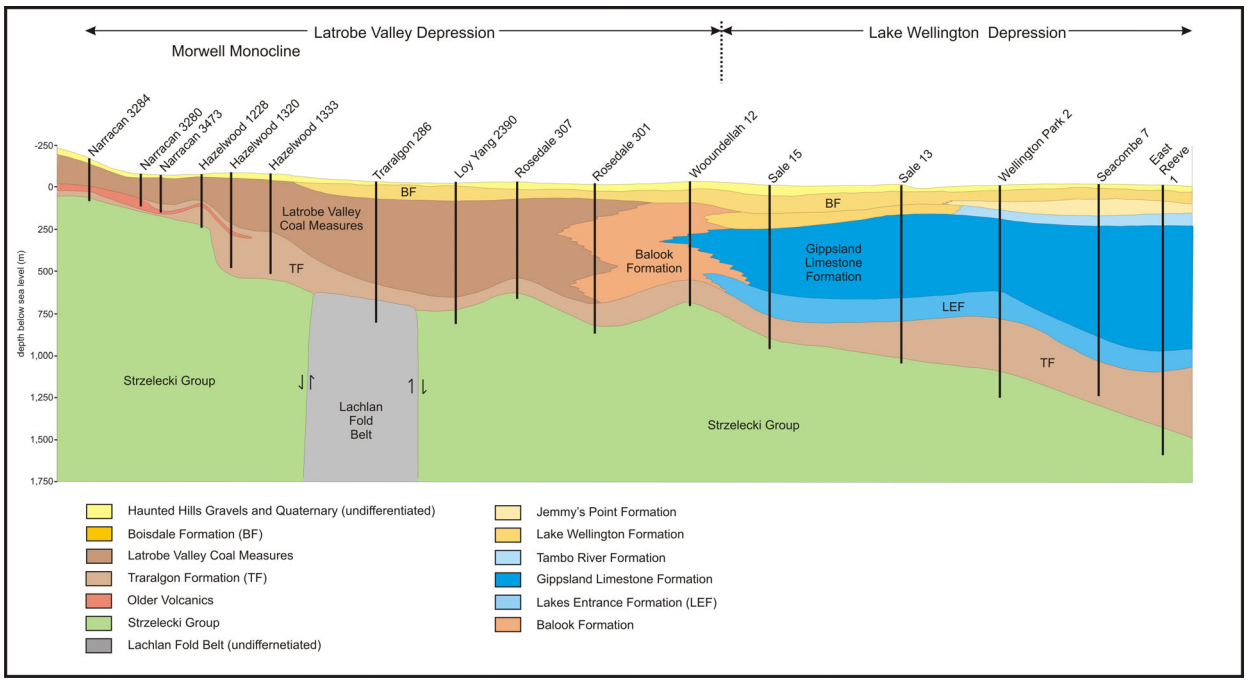

Figure 5: Generalised cross section across the Latrobe Valley (modified from King et al. 1987).

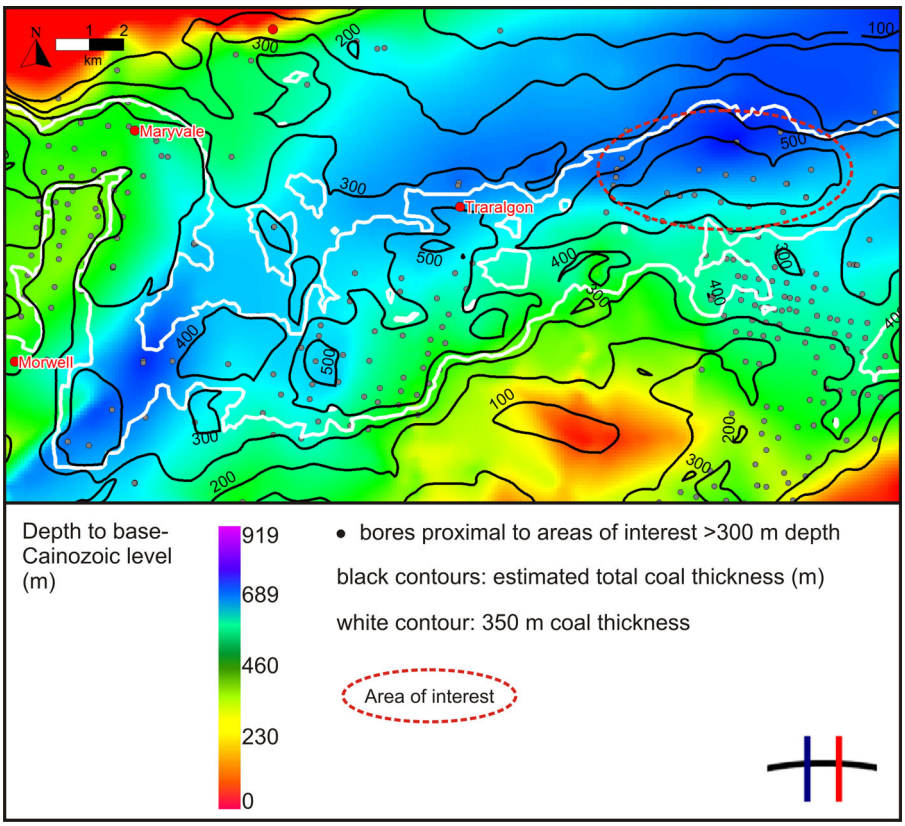

Figure 6: Contour of the 350 m cumulative coal isopach (white line) based on DPI's 2011 Latrobe Valley Coal Measures 3D Model, superimposed on an estimated depth to base-Cainozoic level (basement) colour grid in the Latrobe Valley (values indicate metres below ground level). The areas with a purple hue indicate the thickest Cainozoic sequences. The main area of interest delineated, based on the sedimentary succession thickness and cumulative coal thickness, is east of Traralgon.

Precision Temperature Logging

In light of the temperature data issues, HDR undertook Precision Temperature Logging (PTL) in late May 2011 to confirm prior reports of the subsurface temperature regime.

HDR interrogated DPI's 2011 Latrobe Valley Coal Measures 3D Model to identify the most geologically favourable area for exploratory drilling, namely where the Cainozoic sedimentary fill is thickest and where the cumulative coal measure thickness is greatest (Figure 6). The most prospective area based on the geological constraints was immediately east of Traralgon where the cumulative coal thickness was predicted to exceed 350 m and the sedimentary fill equates to approximately 800 m.

Boreholes in excess of 300 m depth were selected since shallower wells might be affected by both diurnal and seasonal effects and by abnormal climatic trends. Details of the selected bores are included in Table 1 and Figure 7.

Bore Number	Logged Depth (m)	Maximum Temperature (°C)
Loy Yang 1675	628.0	63.2
Loy Yang 2268	439.9	52.2
Loy Yang 2269	244.9	35.0
Loy Yang 2390	683.0	62.6

Table 1: Temperature data collected from the Precision Temperature Logging work program.

Results

The temperature profile from the Traralgon–Flynn area (Figure 8) were encouraging and showed a steep and steady increase with depth through the coal-rich sequence.

Loy Yang 1675 is shown in detail below as an example of further analysis of the PTL data.

Loy Yang 1675

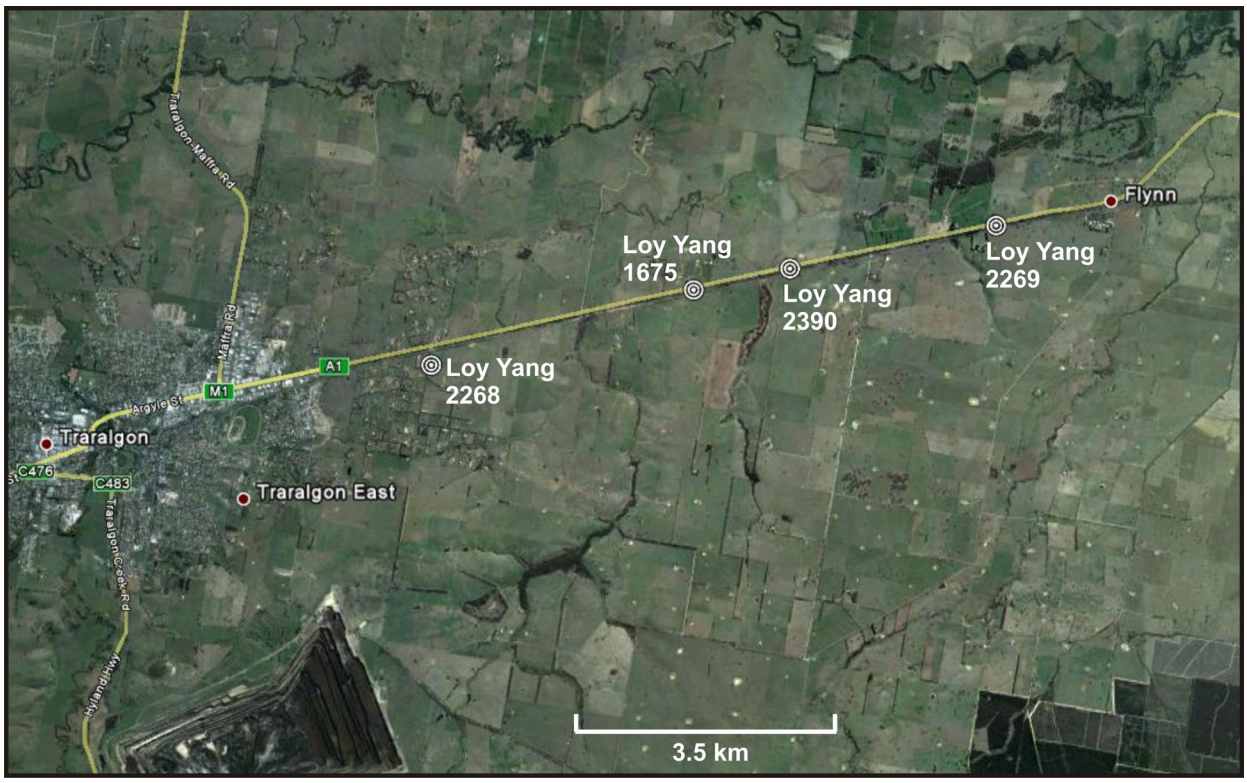

Figure 7: Precision Temperature Logging was performed on four bores in the Traralgon–Flynn area (background image courtesy of Google Earth).

The precision temperature log and derived thermal gradient log for Loy Yang 1675 are shown in Figures 9 and 10. Whilst the bore is 825 m deep, our temperature probe met an obstruction at 628 m, where a temperature of 63.2 °C was recorded, and was unable to descend any further.

The temperature gradient log (Figure 10) indicates approximately 250 m of coal-rich sediment had been penetrated down to 628 m. DPI's 2003 Latrobe Valley Coal Measures 3D Model (Figure 6) had suggested over 350 m of coal-rich sediment would be penetrated at the bore site, and HDR thus initially anticipated that a further ~100 m of coal might lie between 628 m and 825 m. DPI subsequently supplied wireline logs for the Loy Yang 1675 bore down to a total depth of 825 m. These logs include the Gamma

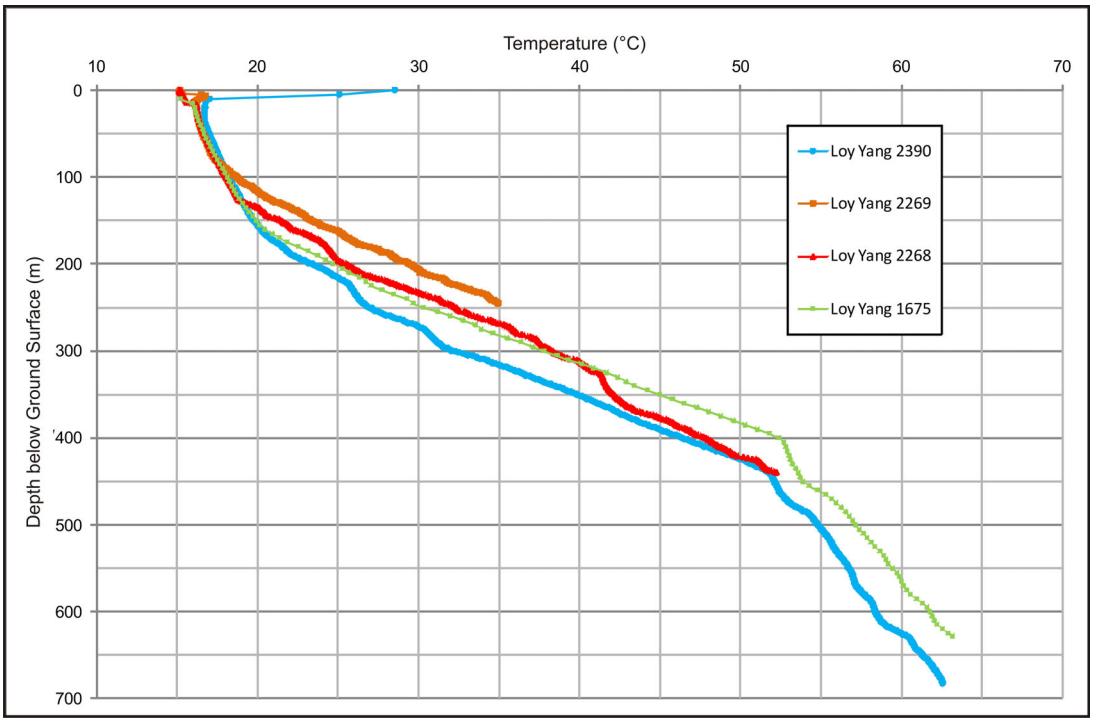

Figure 8: Precision Temperature Logs for the four Loy Yang bores.

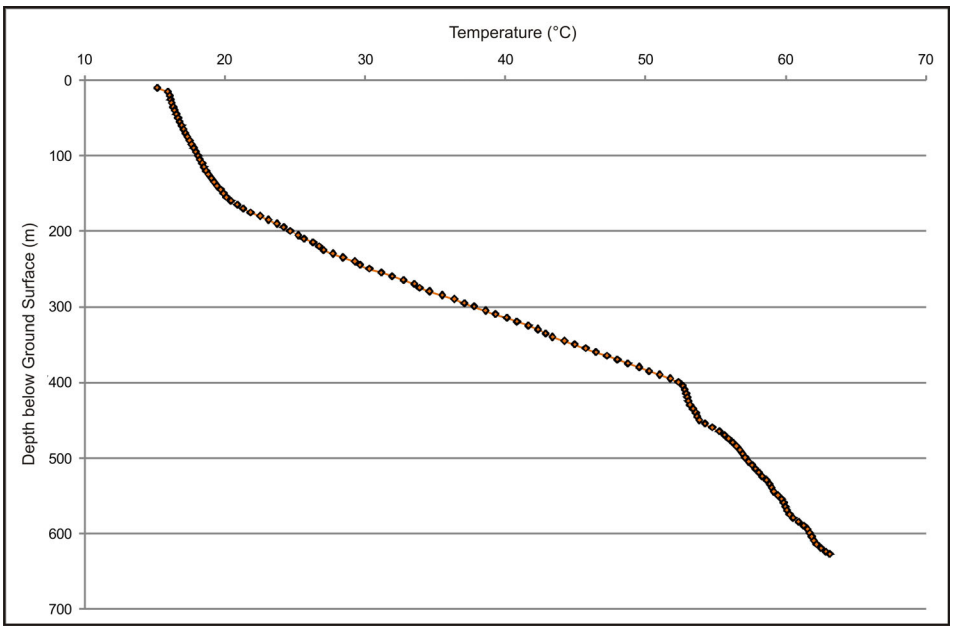

Figure 9: Precision Temperature Log for the Loy Yang 1675 bore. The maximum temperature of 63.2°C was recorded at 628 m.

Ray (GR) which can be used as a proxy for delineating lithologies in a bore. The GR log strongly suggested that the deeper stratigraphic section comprises sandstone, siltstone and carbonaceous mudstone rather than coal-rich lithologies. HDR therefore considered 350 m cumulative coal thickness unlikely. It is likely the temperature at the base of the Cainozoic will be ~75 °C at that location.

Evidence from the other three Traralgon–Flynn bores suggested a similar geological scenario, where the cumulative coal thickness interpreted from wireline logs is substantially less than the 2003 Latrobe Valley Coal Measures 3D Model suggests.

Reservoir

Reservoir risk has many guises, and is dependent on the type of geothermal resource being targeted. In the case of the LVSGP, the target is a hot sedimentary aquifer (HSA). The key criteria for an HSA are porosity, permeability, transmissivity (i.e. permeability x aquifer thickness), storage and yield. These criteria determine reservoir 'deliverability' and whether sustainably high groundwater production and injection flow rates can be achieved for an economically viable geothermal power plant. HDR estimates that a flow rate of approximately 100 L/s will be required for target production levels for the LVSGP.

Within the study area the lowest technical reservoir risk lies with HSA targets of the Traralgon Formation. Favourable properties include its likely existence below the minimal target isotherm and its indicative primary porosities and permeabilities. The greatest uncertainty lies with its actual thickness, which can strongly impact reservoir transmissivity. Ideally, a reservoir thickness in the order of 100 m is required.

Working fluid

For the proposed geothermal plant, if the target of 100 L/s is sustained then the amount of fluid cycled though the aquifer would be in the region of 3.2 GL/year. Existing hydrogeological evidence (e.g. porosity, permeability) indicates that units of the Traralgon Formation Aquifer System can act as high-yielding aquifers.

Across the entire onshore Gippsland Basin a significant long-term trend of declining water table levels has been recorded (GHD, 2010). However, the proposed geothermal electricity generation operation will involve reinjection of the water in a 'closed loop' circuit and its potential impact in terms of pressure effects are expected to be contained to the local site (on the order of 100s of metres radius). To properly evaluate potential production/injection effects HDR intends to complete numerical aquifer modelling to simulate the response of the aquifer to the proposed production-injection scenarios over a 20-30 year operation life span.

The Stratford Groundwater Management Unit (GMU) covers the LVSGP groundwater resources. The Stratford GMU has been fully allocated, thus HDR will be required to trade water entitlements if consumption of groundwater is necessary.

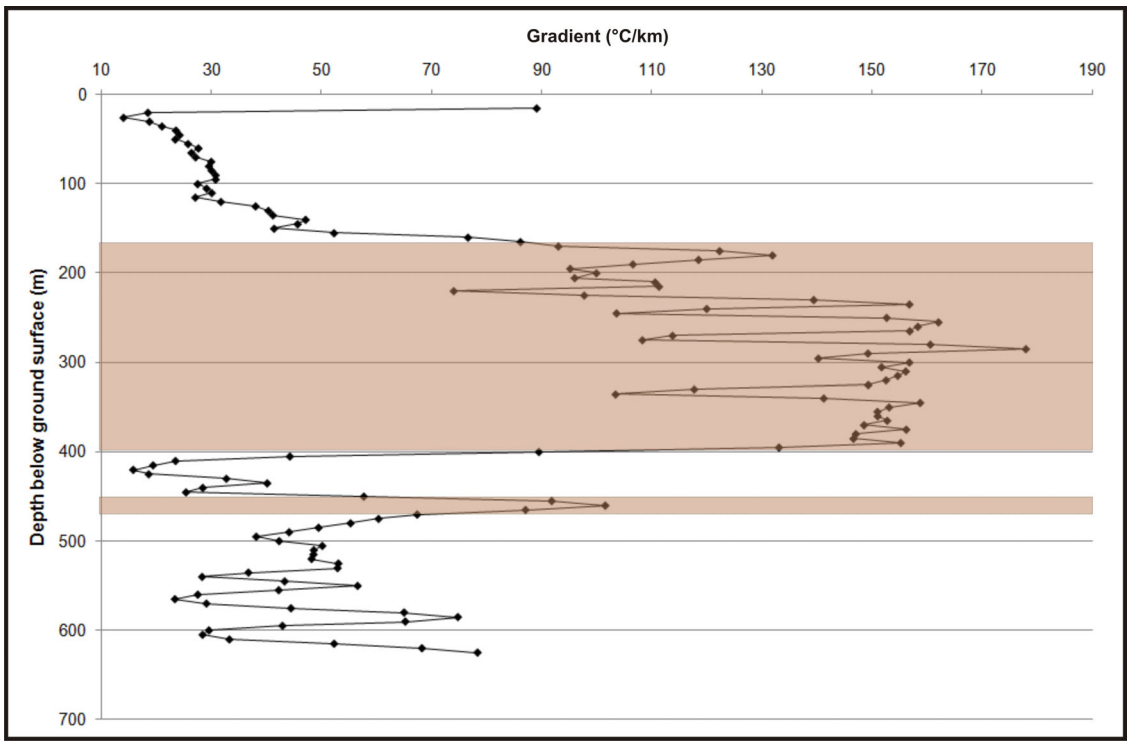

Figure 10: Temperature gradient profile of Loy Yang 1675. Brown shaded areas indicative of coal-rich sequences, at total thickness of ~250 m.

Results

The GSA identified thermal resistance as the greatest risk in that the total coal thickness is uncertain down to the base Cainozoic. To mitigate this risk HDR chose to target an area with existing boreholes into the Traralgon Formation. A productive HSA reservoir at a temperature of 70–75 °C is the lowest risk geothermal target within the Cainozoic section of the Latrobe Valley. Existing borehole data suggest that such reservoir conditions occur in the vicinity of Maryvale.

gTET is designing an optimal power generation system for the LVSGP.

Conclusions

The principle findings of the LVSGP GSA are:

1. A lack of quality, reliable temperature data from deep wells in the Latrobe Valley required that HDR undertake precision temperature logging (PTL).
2. The target geothermal resource for the LVSGP is groundwater at 70–75°C from 600–700 m.
3. HDR considers the risk of insufficient reservoir temperature as low for the LVSGP since the target temperature has previously been intersected in a bore within the target depth interval and location.
4. HDR considers the lowest technical reservoir risk for the LVSGP to be the lower Traralgon Formation. Favourable porosity and permeability attributes are likely to exist within the 600–700 m target depth. The greatest uncertainty lies with its actual thickness which can strongly impact reservoir transmissivity. A reservoir thickness on the order of 100 m is targeted.

References

Cooper, G.T. and Beardsmore, G.R., 2008. Geothermal systems assessment: understanding risks in geothermal exploration in Australia. Proceedings of PESA Eastern Australasian Basins Symposium III, Sydney 14–17 September, (2008), 411–420.

Department of Primary Industries (DPI)., 2003. Digital Geological Model of the Latrobe Valley Coal Resource. Geological Survey of Victoria Unpublished Report 2003/2 – Basic CD Package.

Department of Primary Industries (DPI)., Geothermal Atlas of Victoria.

Department of Primary Industries (DPI)., 2011. Digital Geological Model of the Latrobe Valley Coal Resource. Geological Survey of Victoria.

Driscoll, J., 2006. Geothermal Prospectivity of Onshore Victoria, Australia. Victorian Initiative for Minerals and Petroleum Report 85, Department of Primary Industries. 88pp.

Duddy, I.R., 2003. Mesozoic. In: Birch W.D. ed. Geology of Victoria, pp. 239-288. Geological Society of Australia Special Publications 23. Geological Society of Australia (Victoria Division).

GHD., 2010. Latrobe Valley regional groundwater and land level annual monitoring report, July 2008

to June 2009. Sourced January 2011: http://groundwater.geomatic.com.au/Main.aspx.

Holdgate, G.R., 2005. Geological processes that control lateral and vertical variability in coal seam moisture contents-Latrobe Valley (Gippsland Basin) Australia. International Journal of Coal Geology 63, 130–155.

Holdgate, G.R., Wallace, M.W., Gallagher, S.J. and Taylor, D., 2000. A review of the Traralgon Formation in the Gippsland Basin – a world class brown coal resource. International Journal of Coal Geology 45, 55–84.

Jenkin, J.J., 1962. Underground water in east Gippsland. Victorian Department of Mines Underground Water Investigation, Report 6.

King, R.L., Ford, A.J., Stanley, D.R., Kenley, P.R. and Cecil, M.K., 1987. Geothermal Resources of Victoria. Department of Industry Technology and Resources and Victorian Solar Energy Council. 134pp.

Magoon, L.B. and Dow, W.G., 1994. The Petroleum System. In: Magoon, L.B. and Dow, W.G. (Eds), The Petroleum System–from source to trap, American Association of Petroleum Geologists, Memoir 60, 3–24.

Webb, J.A., Gardner, T.W., Kapostasy, D., Bremar, K.A. and Fabel, D., 2011. Mountain building along a passive margin: Late Neogene tectonism in southeastern Victoria, Australia. Geomorphology 125, 253–262.

Geothermal Water Use: Requirements and Potential Effects

[1]Driscoll, J.P.*& [2]Middlemis, H.
jim.driscoll@hotdryrocks.com
[1]Hot Dry Rocks Pty Ltd, 36 Garden Street, South Yarra, VIC 3141
[2]RPS Aquaterra, Level 6, 33 Franklin Street, Adelaide, SA 5000

Geothermal projects require access to water during development and operation. Some current geothermal exploration and development activity is in areas of low water supply potential and/or high water demand.

The National Water Commission contracted Hot Dry Rocks and RPS Aquaterra to consider water use implications relating specifically to the geothermal industry. This extended abstract provides a summary of water requirements by various geothermal operations, and potential effects on water resources.

Keywords: Water Use, Engineered Geothermal Systems, Hot Sedimentary Aquifers, Low Enthalpy Systems, Ground Source Heat Pumps

Introduction

The Intergovernmental Agreement on a National Water Initiative (NWI) was signed at the 25 June 2004 Council of Australian Governments meeting. Through the NWI, the Commonwealth and State governments have agreed on actions to achieve a more cohesive national approach to the way Australia manages, measures, plans for, prices, and trades water. The National Water Commission (NWC) commissioned Hot Dry Rocks (HDR) and RPS Aquaterra (RPS) to provide some insight into how to address the water planning, management and use implications relating to the geothermal industry (RPS Aquaterra & Hot Dry Rocks, 2011).

Geothermal Energy Potential

In essence, the geothermal energy potential in Australia can be best viewed as a continuum between high enthalpy, deeply buried resources (3,000–5,000 m) suitable for large-scale commercial electricity generation (Engineered Geothermal Systems, EGS, and Hot Sedimentary Aquifers, HSA), through to low enthalpy, shallow resources, suitable for small-scale Low Enthalpy Aquifer (LEA) (direct use heating and industrial processes), Ground Source Heat Pumps (GSHP) and Aquifer Thermal Energy Storage (ATES) applications (Figure 1).

EGS and HSA: Water planning issues

Pressure management of the subsurface reservoir is of critical importance to EGS and HSA projects. EGS projects will always require circulation of an introduced working fluid through the engineered reservoir to convey heat energy to the surface as well as to maintain reservoir pressure and inhibit

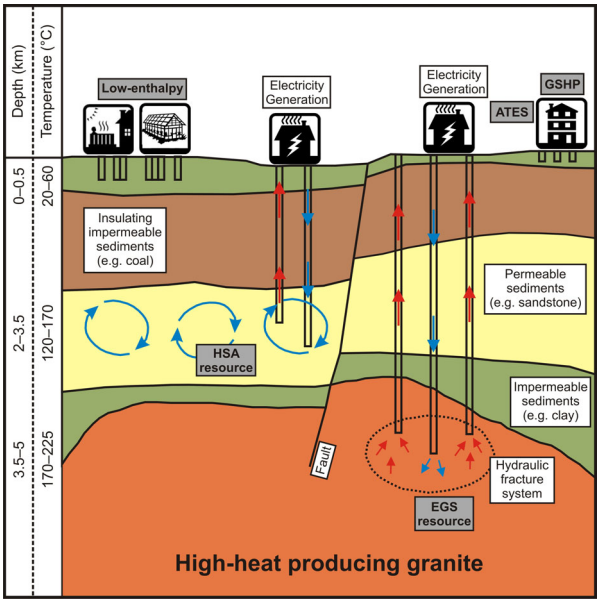

Figure 1: Geothermal energy applications in Australia (modified after Ayling, 2007).

fracture closure. HSA developments use in situ working fluids to maintain reservoir pressures and permeability. In both instances, an inability to maintain and manage reservoir pressures and the efficient circulation of the working fluid will ultimately lead to a decreased operational lifespan of the project. From the geothermal operator's viewpoint, it would be ill-advised to introduce fluids with varying hydrogeochemical properties into the reservoir system as this may well lead to complications with precipitation and scaling of the reservoir and/or bore network. Regulators would also have similar concerns and would be unlikely to allow re-injection that may substantially affect the pressure characteristics and/or the water quality of a valued resource.

It is for these reasons that most, if not all, EGS and HSA projects in the planning and development stages within Australia are designed to be closed-loop systems, with very low consumptive use during scheme operation. Any fluid produced from the production well is reinjected to the same subsurface aquifer (or engineered reservoir in the case of EGS projects).

Water demand is highest in geothermal projects where the volumes of in situ fluids contained within the formations are inadequate to stimulate and operate an engineered underground reservoir. Water consumption for EGS should be controlled by using closed-loop systems (i.e. re-injecting to the same hydrogeological unit), non-

evaporative cooling (for electrical power generation plants) and general aquifer pressure management.

EGS and HSA: Exploration stage

The general progression of an exploration program in Australia includes the following steps:

1. Desktop geothermal systems assessment (GSA) (Cooper & Beardsmore, 2008).
2. Shallow 'heat flow' drilling.
3. Deep 'appraisal' drilling.

Once a GSA of an area has been completed, several areas of interest are typically identified. A drilling program is designed for a series of shallow 'heat flow' bores to obtain objective data on local heat flow and other geological information of the area.

Cordon & Driscoll (2008) cite two exploration companies that provided details of water usage from their respective shallow 'heat flow' drilling programs in South Australia, estimating 50–85 kL for a single shallow bore. Whilst these companies were exploring in sparsely populated parts of South Australia, they both faced logistical and environmental issues with sourcing the water. By working with the local community and government, the companies were able to minimise real and perceived environmental impacts of the drilling program.

Once a company has achieved a level of confidence in defining its geothermal resource, deep drilling is planned to appraise the reservoir characteristics—typically to a depth of 3,000–5,000 m. This marks the beginning of the development stage. Drilling costs dictate that the first deep exploration well is converted into either an injection well or production well (drilling one well to 3,000–5,000 m is widely anticipated to cost A$12m–A$15m).

Cordon & Driscoll (2008) cite Petratherm's plan to drill two wells at its Paralana project to a depth of approximately 4,000 m. Four local water bores were being drilled at the project site to meet drilling requirements. Whilst the water bores were targeting shallow, non-prescribed aquifers rather than the deeper prescribed artesian water, Petratherm still required a permit for the construction of a bore.

EGS and HSA: Development stage

Water use in the development stage of an EGS project includes such activities as sumps for drilling fluids, hydraulic permeability tests, fracture stimulation of the reservoir section to develop the underground heat exchanger, tracer tests and circulation tests, and reservoir charging with working fluid. Cordon & Driscoll (2008) comprehensively reviewed water requirements and volumes utilising technical data from Mil-Tech UK Ltd (2006) to predict the development stage as requiring a total of about 280,000 m^3 (280 ML) of water per EGS 'module'. This is based on the assumption that an EGS module consists of one injector (1st well) and two producers (2nd and 3rd well) of 8.5" open-hole diameter. EGS bores are typically drilled to a depth of 3,000–5,000 m with an assumed separation between bores of about 600 m.

HSA projects require substantially less water since they do not require fracture stimulation or reservoir charging. Cordon & Driscoll (2008) estimated approximately 2,000 m^3 (2 ML) of water for each of the HSA deep bores to be drilled.

EGS and HSA: Operational stage

As there are only a handful of operational EGS plants in the world, and none yet in Australia, conventional geothermal projects are generally used in comparison to provide an estimate of water usage for the production phase of EGS and HSA energy projects. In a typical, successful conventional geothermal reservoir, individual production wells can produce 5 MW or more of net electric power through a combination of high temperatures and high flow. Minor volumes of water are required for periodic maintenance activities during operation of a conventional geothermal system.

The production and/or reinjection capacity from an individual well tends to decrease with time, depending on a number of variables including changes within the reservoir, rates of chemical deposition and mechanical conditions of the well. To restore or regain some of the capacity, well maintenance/rehabilitation is undertaken with a work-over drilling rig, as this is much cheaper and shorter (typically one week) than drilling a new well. Acid cleaning is another rehabilitation method that involves injecting an acid solution into the production or reinjection zone for a short period of time (hours) to dissolve any build-up of scaling products within the formation around the well.

The primary use of water in power plants is cooling, although there are other ancillary uses related to power generation. There are a number of different types of cooling systems and the selection of these is based on the type of power plant, geothermal resource chemistry, site meteorological conditions and access to a cooling source such as a river or aquifer.

Controlling EGS water losses

Controlling water losses is an important aspect of developing a geothermal energy project particularly in areas of restricted water availability. Such losses can have significantly negative economic and environmental impacts if not managed. Australian EGS projects are likely to encounter risks associated with water supply in terms of access to water (licences, allocations,

etc) and related management of impacts due to pumping. Consider, for example, a hypothetical EGS project consisting of six wells each producing hot water at 100 L/s. If all the water is reinjected with 1% loss per cycle (estimate based on international experience), the project has to make up 6 L/s, or 0.5 ML per day (182 ML/annum), throughout its entire life. While that may not necessarily be a problem, it does imply that a permanent supply of water might be required for many EGS projects.

Water loss mitigation strategies can be employed. In the case of shallow 'heat flow' bores, the main water losses can be attributed to evaporation on the surface of the sumps or water filtrating out of the sumps as very little water is lost down hole. In one drilling project, sumps were resealed which resulted in significant decreases in water loss from 8–16 kL to 2–8 kL in a 24 hour period during drilling (Cordon & Driscoll, 2008).

EGS field projects carried out throughout the world have experienced the impact of water losses through trial production testing. Tester et al. (2006) reports anecdotal details from several R&D projects, summarised below.

Fenton Hill, USA

The reservoir could be circulated in such a manner that the fractured volume did not continue to grow and, thus, water losses were minimised. If water was injected at high enough pressures to maintain high flow rates, the reservoir continued to grow and water losses were high. The fractures were being jacked open under high-injection pressures, causing extension of the fractures and increased permeability. At lower pressures, this did not happen, so the permeability was lower and flow rates much lower.

Rosemanowes, UK

An experimental proppant (sand) was carried into the joints as part of a secondary stimulation using high viscosity gel. Proppants are small-sized particles that are mixed with hydrofracturing fluids to hold fractures open after a hydraulic fracturing treatment (proppant materials are carefully sorted for size and shape, hardness, and chemical resistance to provide an efficient conduit for production of fluid from the reservoir to the wellbore). This stimulation significantly reduced the water losses and impedance, but encouraged short circuiting and lowered the flow temperature in the production borehole.

Ogachi, Japan

Fluid losses within the reservoir were high during injection testing, because the wells were not properly connected. Once connection between wells was improved, fluid loss was reduced.

Low enthalpy geothermal systems: Water planning issues

Direct heat use from low enthalpy aquifers by ground source heat pumps (GSHP) and aquifer thermal energy stabilisation (ATES) schemes have similar water requirements and effects.

The potential impacts on groundwater via utilisation of low enthalpy geothermal systems can be classed as either hydrogeological or thermogeological events. The lack of information from an Australian context of low enthalpy geothermal systems necessitates the use of international examples.

For the current and envisaged scale of development (limited/isolated), the issues discussed below should be manageable within existing arrangements for bore licensing and water allocation planning, provided they are implemented carefully. Should there be an intense concentration of development, then specific water management arrangements may need to be developed (eg. considering the thermal energy balance of an urban aquifer, as well as its water and salt balance).

Hydrogeological impacts

Potential hydrogeological impacts relating to low enthalpy systems can be grouped into drilling-related issues, and water balance and aquifer hydraulic issues. There are three main drilling-related hydrogeological scenarios that may result in adverse impacts from the drilling of low enthalpy geothermal systems (Banks, 2008):

1. Inadvertent penetration of artesian conditions.
2. Drilling through two aquifers, inducing leakage from one to another.
3. Drilling on contaminated land sites, thus resulting in conduits for contaminants to the aquifer.

In regard to aquifer and hydraulic issues, if the scheme is a single bore or open-loop scheme, then there will be discharge to a receiving water body that is either different to the extraction water body, or the extraction/discharge water body itself may be an open-ended system. This can lead to potential impacts on the water body that might be due to temperature or water chemistry.

In a dual/multi-bore or closed-loop scheme (essentially non-consumptive), where water is being re-injected to the aquifer or circulated through closed pipe networks, there will be localised drawdown or mounding of water levels/pressures around wells, which could affect existing users (Banks, 2008).

The re-injection of water can cause increased rates of dissolution where the formation is susceptible (notably carbonate-type formations). For example, Younger (2006) investigated the

potential for limestone dissolution as a result of cooling by low enthalpy geothermal schemes. Injection of warm water could also result in the clogging of pore space (Banks, 2008) through dissolution and redeposition. It should be noted that much of this is speculative at this stage, as the research is yet to be undertaken.

Thermogeological impacts

Thermogeologically, the primary constraint on the capacity of an area or location to support low enthalpy geothermal systems is the number of schemes that can be installed without thermal interference between the schemes.

The lack of information from an Australian context of low enthalpy aquifer geothermal systems necessitates the use of international examples. Since 2003, the Spatial Strategy for London requires onsite generation of renewable energy, with GSHPs recognised as such a technology. This has resulted in a major uptake in London of open-loop systems. To begin with these were consumptive (single bore or open-loop), but the majority are now non consumptive (multi-bore or closed-loop).

Though closed-loop, it is recognised that there is now a developing density of schemes that may be affecting the overall temperature of the main chalk aquifer from which the groundwater is being sourced. A study on the regional distribution of ground temperature in the chalk aquifer of London (Headon et al, 2009), indicated that there is potential modification of the subsurface thermal regime as a result of re-injection. Elsewhere, such as in Winnipeg (Canada), research has also been undertaken to try to determine the extent of the merging of thermal plumes in the carbonate aquifer beneath the city (Ferguson & Woodbury, 2005).

This is not to suggest that all centres of growth are now having adverse impacts on the aquifers from which they are sourced. However, Australia has the opportunity to learn from the experiences of those places that have already undergone growth.

Consents to investigate and discharge to the aquifer are the main requirement in the UK for potential installers. As the applications become more complex, it is expected that the granting of future licences will depend on the quality and thoroughness of the supporting assessments (Fry, 2009).

Geothermal power plants and cooling systems

Binary cycle systems are expected to be used to generate electricity for Australian conditions (somewhat lower enthalpy than other international projects).

A binary cycle unit uses a working fluid with a low boiling point and high vapour pressure, heated in the heat exchanger by the geothermal fluid until it boils and changes state to a gas. The binary working fluid is then expanded through a turbine generator where power is generated. The binary working fluid is then condensed back to a liquid in a cooler before being pressurised back to working pressure by a pump.

Many of the power plants in Australia are likely to be located in remote areas away from water sources and in hot climates. A hot climate and a lower enthalpy resource is likely to restrict the use of air-coolers and a lack of water for cooling would result in hybrid cooling systems being the most probable application for binary power plants in Australia.

The amount of cooling water required will vary substantially between plants, being a function of the technologies selected, resource chemistry and local meteorological conditions.

Conclusions

Projections of water requirements in an expanding geothermal sector are primarily restricted to electricity generating developments associated with EGS and HSA, since low enthalpy geothermal systems are generally multi-bore or closed-loop systems that require negligible water for well development or for operations.

The water requirements for EGS and HSA developments are substantially different since HSA operations do not usually require fracture stimulation nor initial fluid charging of the reservoir (i.e. HSA systems make use of the in situ aquifer properties) where EGS uses water for engineering effective circulation of the working fluid.

For an EGS development, the reported average water requirement for drilling and construction of 280,000 m^3 (280 ML) (Cordon & Driscoll, 2008) is based on a three bore configuration (a ‘triplet’) comprising two production bores and one injection bore. Such a triplet would normally be expected to supply approximately 10 MWe of power—dependent on resource flow rate and temperature characteristics. Thus, an average of 280,000 m^3 (280 ML) of water might be consumed for each 10 MWe EGS development.

For an HSA triplet construction, Cordon & Driscoll (2008) estimated approximately 2,000 m^3 (2 ML) of water for each of the bores to be drilled; thus 6,000 m^3 (6 ML) might be consumed for each 10 MWe HSA development.

The Waterlines report to the National Water Commission by RPS Aquaterra and Hot Dry Rocks (2011) considered a likely range of EGS and HSA systems that may be developed in Australia, and related growth projections. A broad index of water use was devised that could be

applied to water planning studies, accounting the development and operational water needs of EGS/HSA, but not for the cooling needs for electrical power plants. It is estimated that 1 GL per annum is required to sustain 40 MW installed capacity (assuming HSA amounts to 25% to 50% of the combined EGS/HSA mix). With allowance for low to high growth into the 2020s, this indicates that water consumption in the order of 30–60 GL per annum may support 1,200–2,400 MW of generating capacity (plus water for cooling the power plants).

References

Ayling, B.F., 2007. Electricity Generation from Geothermal Energy in Australia. Geoscience Australia, Educational Factsheet GA10662, 2pp.

Banks, D., 2008. An Introduction to Thermogeology: Ground Source Heating. Blackwell Publishing. 339pp.

Cooper, G.T. and Beardsmore, G.R., 2008. Geothermal systems assessment: understanding risks in geothermal exploration in Australia. Proceedings of PESA Eastern Australasian Basins Symposium III, Sydney 14–17 September, (2008), 411–420.

Cordon, E. and Driscoll, J.P., 2008. Full Life-Cycle Water Requirements for Deep Geothermal Energy Developments in South Australia. Department of Primary Industries and Resources (South Australia) and the Australian School of Petroleum, 50pp.

Ferguson, G. and Woodbury, A.D., 2005. Thermal sustainability of groundwater-source cooling in Winnipeg, Manitoba. Canadian Geotechnical Journal, 42(5), 1290–1301.

Fry, V., 2009. Lessons from London: Regulation of open loop ground source heat pumps in Central London. Quarterly Journal of Engineering Geology and Hydrogeology, 42, 325–334.

Headon, J., Banks, D., Waters, A.J. and Robinson, V.K. 2009. Regional distribution of ground temperature in the Chalk aquifer of London, UK. Quarterly Journal of Engineering Geology and Hydrogeology, 42, 313–323.

MIL-TECH UK Ltd., 2006. Assessment of water requirement and storage aspects for a development of a deep Hot Dry Rock (HDR) system Olympic Dam, South Australia. Report prepared for Green Rock Energy Ltd., 17pp.

RPS Aquaterra and Hot Dry Rocks, 2011, Geothermal Energy and Water Use, Waterlines report, National Water Commission, Canberra (in press).

Tester et al., 2006. The Future of Geothermal Energy – Impact of Enhanced Geothermal Systems (EGS) on the United States in the 21st Century, MIT Press, pp. 1-9; 2-29; 4-1–4-52.

Younger, P.L., 2006. Potential pitfalls for water resources of unregulated development of ground source heating resources. Proceedings of the Annual Conference of the Chartered Institute of Water & Environmental Management.

Large scale integration of geothermal energy into the Australian transmission network

Mehdi Eghbal*[1] and Tapan Kumar Saha[1,2]
m.eghbal@uq.edu.au saha@itee.uq.edu.au
[1] Queensland Geothermal Energy Centre of Excellence (QGECE)
[2] School of Information Technology and Electrical Engineering
The University of Queensland, St Lucia, 4072, Queensland, Australia

Enhanced geothermal systems are expected to have significant potential for generating electricity in Australia, however two types of challenges need to be addressed. One is technological developments in converting the heat from hot granites 4-5 km below the earth's surface to electricity. The other is efficiently delivering the generated electricity to end users located far away from the generation zone. The aim of the transmission research program of the Queensland Geothermal Energy Centre of Excellence (QGECE) is to investigate the technical aspects of connecting remote geothermal power plants to the existing high voltage transmission network. This paper presents an overview of the transmission program by briefly explaining the challenging issues of large scale integration of geothermal energy into the Australian network and introducing the research projects of the transmission program. Details of each study can be found in the cited published papers.

Keywords: Large scale geothermal energy, reliability analysis, transmission expansion planning, voltage stability

1. Challenges

The following subsections briefly discuss the challenges of large scale integration of geothermal energy into the Australian electricity network.

1.1 Remote location

Major geothermal energy sources in Australia are located in remote areas far away from the high voltage transmission network. Hence, long transmission lines are required to deliver the power to major load centres. Apart from huge investment in building new lines, the operation of long transmission lines carrying bulk amount of power has technical issues such as voltage and small signal stability.

One of the challenges of transmitting power through long HVAC transmission lines is power losses. Ohmic power losses increase significantly when length of the line increases. This means the generation of geothermal power located in remote areas should be large enough to overcome the significant power loss problem.

1.2 Uncertainties

This section explains major uncertainties involved in the future planning for transmitting large scale geothermal power to the national grid.

Generation technology

Extracting heat from hot granites located 4-5km below the earth's surface to generate electricity is the main concept behind enhanced geothermal systems. Small scale power generation based on this concept has been successfully proved in 2009 (Geodynamics 2009). It is estimated that the Cooper and Eromanga Basins could generate 4000 MW power to supply base-load by 2030. There are uncertainties in the technology required to realise this potential and also make it competitive against electricity from other sources.

Emission trading scheme

Currently in Australia, similar to other electricity markets, the generation cost of electricity from renewable sources is comparatively higher than that from fossil fuels. Emerging carbon pricing and/or emission trading schemes are expected to change this trend and makes the cost of electricity from renewable sources of energy competitive against that from other sources such as conventional coal power plants.

Transmission regulatory frameworks

Major renewable sources of energies such as geothermal are located in remote areas from the existing transmission infrastructure. The huge investment cost of building long transmission lines is a hurdle for large scale integration of geothermal energy (and other renewable energies) into the national grid. Policy changes in current connection arrangements for remote renewable generators are required to facilitate large scale penetration of renewable energies and meet the renewable energy target by 2020. Approval of proposals such as *scale efficient network extensions* can be beneficial to the geothermal industry as well as other renewable generators.

2. Industry engagement

Planning experts from Powerlink Queensland and the Australian Energy Market Operator (AEMO)

are members of an industry advisory committee of the transmission research program. The role of this committee is to provide technical advice and feedback for the research projects (QGECE 2010).

To determine the most efficient connection options for connecting large scale geothermal energy into Queensland network, Powerlink Queensland in 2010 provided the QGECE with the Queensland transmission network power flow data based on a confidentially agreement. As part of the current transmission research program, possible scenarios of connecting prospective geothermal power plants to the Queensland electricity grid are being investigated. In this study the most efficient transmission option for each scenario is determined by taking into account the optimum voltage level, transmission line configuration and transmission technologies (HVAC versus HVDC).

Also, in order to be able to explore the connection options to South Australia, QGECE is in contact with ElectraNet to access the South Australia's network data.

Small scale geothermal energy is one of the renewable sources of energy that can be used to supply remote area off-grid electricity networks. To overcome the capacity limit of the geothermal reservoir to supply the peak demand, other renewable sources of energy such as solar together with diesel and energy storage can be used. In addition, demand response programs can also be utilised to maintain the balance between demand and supply. Currently authors are conducting a research project for TransGrid, the transmission service provider in New South Wales, to investigate the impact of demand response programs on transmission network planning.

3. Transmission research program

The aim of the transmission research program is to analyse large scale integration of geothermal power scenarios into the Australian electricity network with acceptable reliability and economical way considering foreseeable carbon pricing schemes.

The following sub-sections briefly introduce the main focuses of the transmission program. Details of each project can be found in (Bui et al., 2011; Eghbal et al., 2011; Eghbal et al., 2010; Hasan et al., 2011a,b; Nguyen et al., 2010a, b; Nguyen et al., 2011). It should be mentioned that the feasibility of the developed methodologies are first validated by implementation on simplified test power systems. The ultimate aim of the transmission project is to apply the developed methodologies to the Australian electricity network.

3.1 Voltage stability

One of the challenging issues of operating a long transmission line is voltage stability. When the line is transferring bulk amount of power, any voltage instability problem could jeopardise the security of the network. The stability project of the transmission program addresses steady state voltage stability, small signal stability and transient stability issues.

Voltage stability studies on Australian South East (SE) 14 generators test system show that bipolar HVDC transmission lines are more stable compare to HVAC (Nguyen et al., 2010a). Also it has been demonstrated that stability of the HVDC interconnection is not deteriorated when the length of the line increases. On the other hand, the stability margin of HVAC interconnection decreases proportionally when the length of the interconnection increases.

Inter-area oscillations are caused by interactions among large groups of generators at two ends of an interconnection. Small signal stability analysis on HVAC interconnections shows that the inter-area mode becomes less stable when the length of the interconnection increases (Nguyen et al., 2010b). Simulation results of connecting a remote generator to the simplified South East Australian power system (Gibbard, 2010) have shown that power system stabiliser and power oscillation damping controller can effectively damp the oscillations (Nguyen et al., 2011).

To improve the transient stability of the simplified South East Australian power system (Gibbard 2010), a new supplementary control for current source converter HVDC has been developed (Bui et al., 2011). Three phase balanced fault analysis has shown that the proposed rectifier controller model improves the transient stability of the system. Also, it has been observed that the connection point of the HVDC interconnection has a significant impact on the power loss.

3.2 Reliability analysis

Geothermal energy is a base-load renewable source of electricity. Large scale integration of geothermal energy can affect the reliability of the network. Basically, connecting a large base-load power plant improves the generation adequacy. Distance between the generation zone and the load centres, transmission configuration and technology (HVAC/HVDC) are factors that affect the reliability. There are few candidate connection points in each state for connecting the prospective geothermal generation zone in Innamincka to the national transmission network. Random outages in the long distance lines carrying bulk amount of power can seriously deteriorate network reliability and result in power flow congestion in other parts of the network. Price spikes in the electricity market are also one of the consequences of transmission congestion.

The aim of the QGECE's reliability analysis project is to develop a probabilistic reliability analysis tool for studying the impacts of future large scale geothermal generation capacity on the Australian electricity market. Simulation results on IEEE 24 bus reliability test system confirm that the following issues have an impact on the locational marginal price of the electricity in the electricity market (Hasan et al., 2011a):

- connection point of new renewable generators
- configuration of future network expansion
- generation technology
- future load growth

Further analysis on possible transmission configurations has proved that proper selection of the hub location (in case of connecting remote generators to a network) could be useful to justify the investment cost. Moreover, considering emission cost in the market benefit analysis also makes remote renewable generation options more competitive against traditional sources of generation (Hasan et al., 2011b).

3.3 Transmission expansion planning

Two types of transmission projects are required to transfer base load power from prospective geothermal power plants to major load centres. One is extending the existing transmission network to reach the geothermal generation zone (in Cooper Basin) and the other is increasing the power transfer capability of the existing interconnections. The Australian Energy Market Operator (AEMO) has identified a few connection points in South Australia, Victoria, New South Wales as well as Queensland (Silva and Robbie, 2009). The proposed transmission line between Innamincka and South Australia has the shortest distance (about 450 km). However, the current capacity of the interconnections between states and future wind generation expansion plans in South Australia make it impossible to deliver bulk amount of geothermal power from this state to major load centres in Victoria and New South Wales without major transmission augmentations.

Each transmission project requires an enormous investment cost and takes a considerable amount of time. Therefore, determining the most efficient transmission expansion scenario is very important to AEMO, transmission service providers as well as renewable energy generators including the geothermal industry.

The transmission expansion planning project aims to determine the optimal location and size of the new transmission lines considering possible generation expansion scenarios and forecasted demand. The objective is to economically upgrade the network in order to supply future demand in the most reliable way. In this project, the problem is formulated as a mixed integer nonlinear programming problem and solved by using meta-heuristic optimisation techniques such as genetic algorithm (GA), particle swarm optimisation (PSO) and shuffled frog leaping algorithm (SFLA) (Eghbal et al., 2011). Simulation results show that not only optimal location and number of new transmission lines are important but also increasing the voltage level of new lines can reduce the total cost by reducing the power losses and enhancing available transfer capability. In systems with an uneven distribution of generation and load centres, the impact is more significant.

Implementing some form of carbon pricing is expected to make the generation cost of electricity from renewable sources more competitive to that from fossil fuels and consequently facilitates the penetration of renewable generators into the current power system. As such a change in the future generation portfolio will affect transmission planning, it is important to consider the uncertainties associated with the carbon price and emission trading schemes. Currently, authors are developing a multi-objective planning framework to address the impact of CO_2 price on transmission expansion planning.

3.4 Connection to Queensland

The transmission network in Queensland is a HVAC network with 330 kV, 275 kV and 132 kV lines. Powerlink recommended constructing a new Halys to Blackwall 500 kV transmission line in order to address the forecasted thermal and voltage stability limitations in south east and west Queensland (Powerlink 2009).

To investigate the feasibility of connecting large scale geothermal power plants in Innamincka to the Queensland network, the current 275 kV substation in Western Down is considered as the connection point. It is also assumed that the 500 kV network in Queensland is in place. Different scenarios for connecting 1000 MW and 600 MW geothermal power are chosen and then analysed. Simulation results show that 500 kV double circuit line and 275 kV double circuit line are the most likely HVAC options for connecting 1000 MW and 600 MW geothermal power to the Queensland network, respectively. Since geothermal power plants are base load generators, active power loss and reactive power compensations are important issues. Preliminary results show that it is economical to increase the voltage level of the new interconnection up to 500 kV and consequently increase the investment cost in order to reduce the operating cost over the life time of transmission lines.

The feasibility of using recent HVDC transmission technologies will also be studied. Recent technological developments as well as lower power loss make HVDC a competent option to

HVAC for transmitting bulk amount of power over long distances.

4. Conclusions

Connecting remote geothermal generation power to the national grid is a challenging issue. Large investments are required and different uncertainties are involved in the transmission planning problem.

Thertansmission research program at the Queensland Geothermal Energy Centre of Excellence focuses on addressing the stability and reliability issues of connecting remote large scale geothermal power plants to the national grid. Feasibility of HVAC and HVDC transmission technologies are being investigated.

Uncertainties affecting the transmission project are identified and being considered in developing a new transmission planning framework.

References

Bui, M. X., Nguyen M. H., and Saha,T. K., 2011, Dynamic simulation of HVDC interconnection in large power system, IEEE Power and Energy Society General Meeting, Detroit, MI, USA, p. 1-6.

Eghbal, M., Saha, T. K. and Hasan, K. N. 2011, Transmission Expansion Planning by Meta-heuristic Techniques: A comparison of Shuffled Frog Leaping Algorithm, PSO and GA, IEEE Power and Energy Society General Meeting, Detroit,Michigan, USA, p. 1-6.

Eghbal, M., Saha, T. K. and Nguyen, M. H., 2010, Optimal voltage level and line bundling for transmission lines: 20th Australasian Universities Power Engineering Conference (AUPEC), p. 1-6.

Geodynamics 2009, ASX Announcement 31 March 2009 Stage 1- Proof of Concept Complete. Available at http://www.geodynamics.com.au/IRM/Company/ShowPage.aspx?CPID=1947&EID=33944995&PageName=Proof+of+Concept+Complete (accessed on 27/06/2011).

Gibbard, M. and Vowels, D., 2010, Simplified 14-generator model of the SE Australian power system, The University of Adelaide, South Australia, pp.1-45

Hasan, K. N., Saha, T. K. and Eghbal, M., 2011a, Renewable Power Penetration to Remote Grid-Transmission Configuration, Investment Allocation and Net Benefit Analyses: IEEE Power and Energy Society Innovative Smart Grid Technologies (ISGT) Conference, Perth, Australia, p. 1-8.

Hasan, K. N., Saha, T. K. and Eghbal, M., 2011b, Tradeoffs in Planning Renewable Power Generation Entry to the Electricity Market: IEEE Power and Energy Society General Meeting, Detroit, MI, USA, p. 1-6.

Nguyen, M. H., Eghbal M., Saha T. K. and Modi N., 2011, Investigation of Oscillation Damping for Connecting Remote Generators into an Existing Power System: IEEE Power and Energy Society Innovative Smart Grid Technologies (ISGT) Conference, Perth, Australia, p. 1-8.

Nguyen, M. H., Saha, T.K. and Eghbal, M., 2010a, A comparative study of voltage stability for long distance HVAC and HVDC interconnections: IEEE Power and Energy Society General Meeting, p. 1-8.

Nguyen, M. H., Saha, T. K. and Eghbal, M., 2010b, Impacts of HVAC interconnection parameters on inter-area oscillation: 20th Australasian Universities Power Engineering Conference (AUPEC), p. 1-6.

Powerlink 2009, Powerlink Annual Planning Report 2009. Available at http://www.powerlink.com.au/asp/index.asp?sid=5056&page=Corporate/Documents&cid=5250&gid=597(accessed on 27/06/2011).

QGECE 2010, Queensland Geothermal Energy Centre of Excellence Annual Planning Report 2009-2010. Available at http://www.uq.edu.au/geothermal/docs/QGECE-ANNUAL-REPORT-2009-2010-TP.pdf (accessed on 27/06/2011).

Silva., R. d., and Robbie A. , 2009, Network extensions to remote areas Part 2 - Innamincka case study. Available at http://www.aemo.com.au/ (accessed on 27/06/2011).

A Mathematically Perceptive Approach for the Classification, Coordination, Prioritisation and Selection of Drillhole Targets

Farrar, L.J.D and Holland, M.A.

farrar3@hotmail.com

PO Box 194, Roseville, NSW 2069.

The opportunity to consider the potential of geothermal energy was presented to us in 2010. We have chosen to take the view that exploration and exploitation of this resource will evolve rapidly and that a sturdy knowledge of the nature of granite emplacement will play a central role.

A mathematically perceptive approach that coordinates the granite theme at several relevant scales can count and mark opportunities and their status with a view to developing a complementary mathematical modelling strategy.

The geothermal energy potential of a radiogenic granite body and its disposition as a conduit to deeper opportunity has been engaged with regard to both empirical and theoretical considerations.

Empirically, the application of geophysics to mineral prospecting has revealed geological insights that demand theoretical attention.

Theoretically, mathematical insight has been underutilised as a means to address both intrinsic and extrinsic qualities that are apparent in survey data.

Technologically, the acquisition, compilation, transformation and presentation of geophysical data has been impressive.

Commercially, the technological momentum has managed to overshadow analytic potential.

We wish to introduce and illustrate some aspects that have emerged as a consequence of our outlook and experience.

Keywords: granite emplacement, modelling, icosahedral division, continental facets, regional pic-cells, gravity anomaly, heat, confocal, PDE.

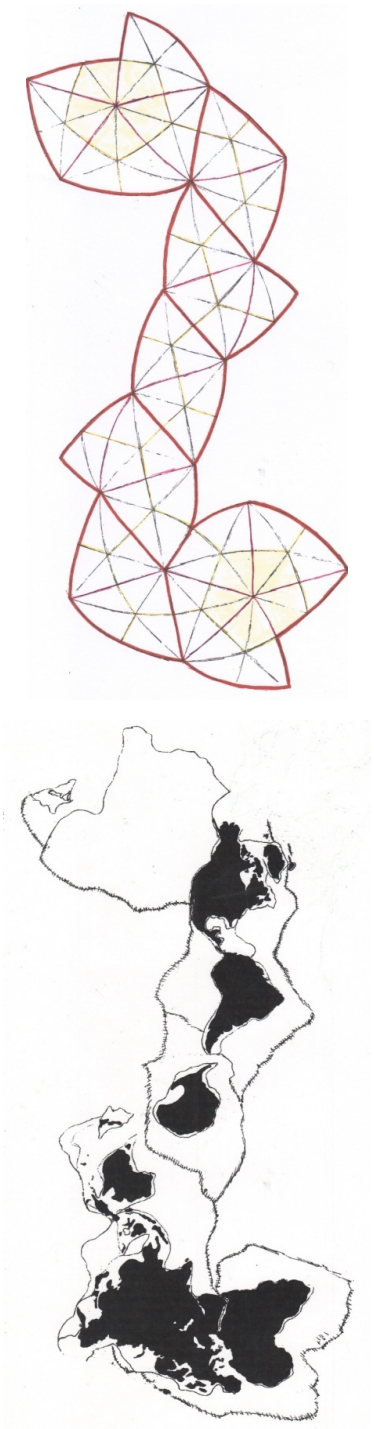

Figure 1 Map showing icosahedrally geometric basis for a plate tectonic projection of the Earth's surface

Coordination

Any process, involving combinations of models, tends to identify common attributes from which a recomposite form of the modelling strategy may emerge.

Mathematical analysis of geophysical information has emphasised the merits of geometric organisation in nature, and the value in taking advantage of it.

Empirical and theoretical examination of data may be coordinated by utilising a well-conceived frame of reference. Figure 1 illustrates icosahedral division of the lithosphere as a basis for modelling plate tectonics. Figure 2 illustrates subdivision as continental facets, based on the location and distribution of geological provinces that are classified as shield, platform, orogen and basin.

Further subdivision identifies a model based on 60750 regional pic-cells of the order of 50 kilometre extent.

Individual regional models may be constructed in this way, retaining lithospheric, atmospheric, near-neighbour and planetary reference.

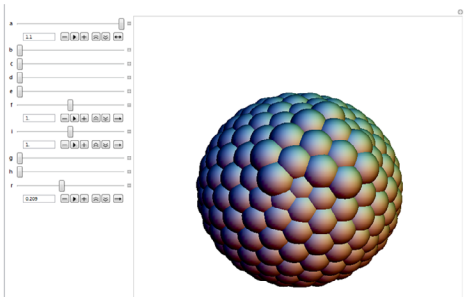

Figure 2 Continental Facets – developed using “Mathematica”. The Australian facets are highlighted. ‘Yilgarn’ and ‘Pilbara’ can be identified on the western side. ‘Eromanga’, “Murray’ and ‘Gawler’ form a triangular group to the South. The ‘Gondwana’ group is manipulated by controls on the left.

Granite Emplacement

The relationship between stratigraphic deformation and granite emplacement was given attention as a basis for the analysis of a seismic survey that was conducted at the Woodcutters Mine [8]. The magnetic and radiometric character of the stratigraphic column, in conjunction with the prominent gravity anomaly of the Rum Jungle granite complex was utilised for the purpose of quantifying the setting to some degree.

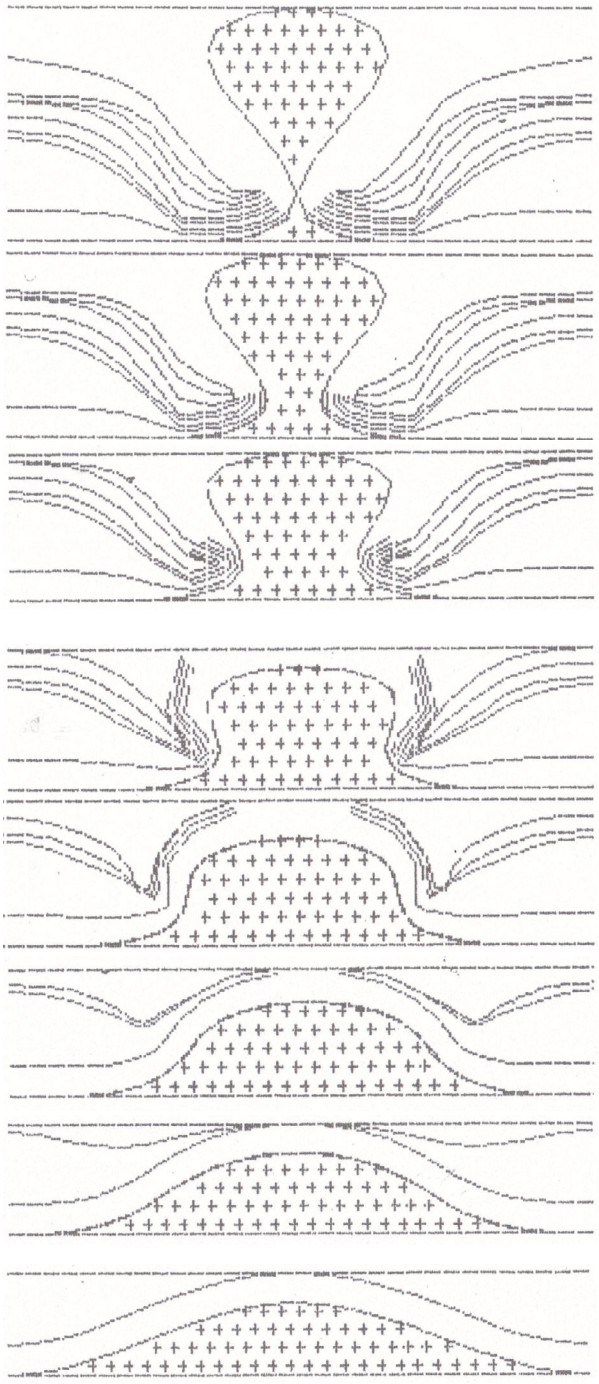

Figure 3 Diagram that depicts granite emplacement

Based on work presented by Ramberg [1], Stephansson [1,10], Fletcher [6], Berner, Ramberg and Stephansson [1] and Park [9], the simple geometric model, Figure 3 was developed in order to appreciate spatial considerations.

Deformed magnetite bearing stratigraphic units and the density contrast of granitic bodies create a very useful combination when applied to the interpretation of concealed or subsurface geology. Regional interpretation of the Pine Creek Geosyncline [8], the Tennant Creek Inlier [3] and many other examples are suggestive of a method that involves “regional pic-cells”.

Figure 4 Theoretical gravity expression for an elliptical cylinder of infinite extent.

Gravity Expression

An expression for the gravity due to the variations on an elliptical theme (Fig. 5) using the convention in Figure 4 is:

$$g = GM_l \frac{r}{nf^2}\left((r^2/(r^2 - f^2))^n - 1\right) \qquad (1)$$

n	cross section
1	doublet
-1/2	elliptic
-1	circular

The magnetic equivalent of this expression was conceived by identifying the common attributes of different magnetic models [5] and was utilised repetitively in the analysis of drillhole surveys for the investigation of the extensive population of gold-bearing magnetite bodies at Tennant Creek [4].

An empirically derived basis for appreciating variation emerged from the repetitive application of this mathematical expression. In conjunction with the confocal property, the intrinsic form of an enclosure can be perceived as a function of its remote appearance.

The intrinsic form of an enclosure can establish requisite constraint when dealing with its internal character.

$$g = 2GM_l\left(\frac{r-\sqrt{r^2-f^2}}{f^2}\right) \qquad (2)$$

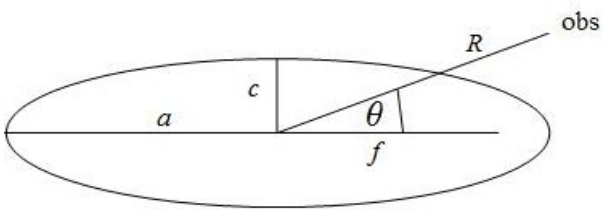

$r = Re^{-i\theta}$

$f = \sqrt{a^2 - c^2}$

G- Gravitational Constant

M_l- Mass per unit length

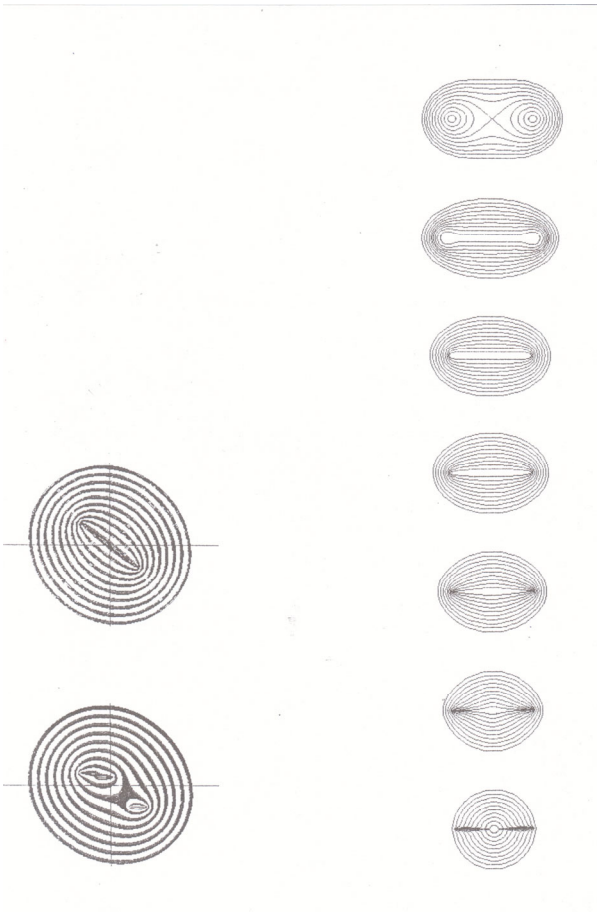

Figure 5 Confocal variation on an elliptical theme. The series on the right are derived from a common mathematical identity. A realistic confocal form is compared with that of the ellipse, on the left.

Form and the Confocal Property

Gravity and magnetic field character produced by an elliptic source with uniform internal density or magnetisation is a function of focal dimension. (See Fig. 4). This provides a particular analytic advantage when drill testing a concealed body of undetermined properties and volume.

The value of *n* in equation (1) is valid for (n=-1,-½,+1) and can be utilised with caution for the range (-1<n<1). Repetitive application to the analysis of drillhole magnetic surveys facilitated a strong empirical basis, worthy of further theoretical investigation.

Currently, the mathematical nature of heat and gravity are being examined in this way. Divergence from the ellipsoidal uniformity is taken toward ovoid and doublet, and to lenticular and spherical forms (Fig. 5).

It is anticipated that two diverse heat distribution themes will emerge, and this will reinforce the manner by which the vast population of granite bodies are explored and exploited.

Heat

Appreciation of geographic division and subdivision, granite emplacement, recomposite modelling, and their influence on strategic drillhole location and trajectory creates the basis for an analysis of the intrinsic properties of the potential resource.

Beyond this a perceptive knowledge of thermodynamic principles can benefit from recent developments in the exact solutions of a class of nonlinear heat equations.

$$u_t = u_{xx} + f(u)$$

The method of differential Gröbner bases is used both to find the conditions on *f(u)* under which classical and non-classical symmetries other than the trivial spatial and temporal exist, and to solve the determining equations for the infinitesimals [2,7].

The classical method for finding symmetry reductions of PDEs is the Lie group method of infinitesimal transformations. These must all have the Painlevé property for the PDE to be completely integrable – i.e. they must pass the Painlevé ODE test.

The non-classical method involves an assumption about the form of an unknown function, made to facilitate solutions of an equation. Recent developments in a particular class offer novel approaches to overcome major scalability and tractability problems through mathematical insight. This can be extended to 3 dimensions and developed as efficient algorithms. The formulation is sufficiently general to model a wide variety of physical characteristics such as temperature and space dependent heat reaction.

Concluding Remarks

Simultaneously objective and subjective, the modelling and analysis of remote and drillhole-derived information can induce a need for frequent adaptation of its theoretical base. In this presentation, we have attempted to honour the qualitative theoretical features, as assumptions are subjectively adjusted.

[1] Berner, H., Ramberg, H. and Stephansson, O., 1972, Diapirism in Theory and Experiment. Tectonophysics, v.15: p. 197-218

[2] Clarkson, P.A., and Mansfield, E.L., 2008, Symmetry Reductions and Exact Solutions of a class of Nonlinear Heat Equations.

[3] Donnellan, N., Hussey, K. J. and R. S. Morrison, 1995, Flynn 5759, Tennant Creek 5758, 1:100000, Geological Map Series, Department of Mines and Energy, Northern Territory Geological Survey. (Geophysics by L. J. D. Farrar), and Tennant Creek SE S3-14, 1:250000 geological series.

[4] Farrar, L. J. D., 1979, Some Comments on Detailed Magnetic Investigations of Ellipsoidal Bodies at Tennant Creek: Exploration Geophysics,v.10,p. 26-33.

[5] Farrar, L. J. D., 1985 Model Shape, Dipole Moment and the Analysis of Geophysical Anomalies. Australian Society of Exploration Geophysicists. 4th Geophysical Conference and Exhibition, Sydney Australia.

[6] Fletcher, R.C., 1972, Application of a Mathematical Model to the Emplacement of Mantled Gneiss Domes. American Journal of Science, v.272, p. 197-216.

[7] Harris, S.E., and Clarkson, P.A., 2008, Painlevé analysis and similarity reductions for the magma equation. Symmetry, Integrability and Geometry Methods and Application, v.2

[8] Nicholson, P.M., Ormsby, W.R. and Farrar, L. 1994, A Review of the Structure and Stratigraphy of the Central Pine Creek Geosyncline. AusIMM Annual Conference, Darwin.

[9] Park, R.G., 1980, Origin of Horizontal Structure in High-Grade Achaean Terrains, Geological Society of Australia. Second International Symposium, Perth Australia.

[10] Stephansson, O., and Johnson, K., 1976, Granite Diapirism in the Rum Jungle Area, Northern Territory Australia. Precambrian Research, v.3, p.159-185.

Geothermal Simulation, Perth Basin, Western Australia

[1]Ghori, K.A.R. and [2]Gibson, H*.
Ameed.Ghori@dmp.wa.gov.au and helen@intrepid-geophysics.com
[1]Geological Survey of Western Australia, Department of Mines and Petroleum, East Perth, Western Australia.
[2]GeoIntrepid, 2/1 Male Street, Brighton, Victoria, 3186, Australia.

One-dimensional (1D) and three-dimensional (3D) thermal modelling indicates that the highest geothermal anomalies in the Perth Basin occur in the Coomallo and Beermullah Troughs, Bookara Shelf, and north of Moora township. The modelled temperatures and recorded temperatures are up to 154 and 150°C at 4 km, respectively. These are based on temperatures in 253 petroleum wells, 1D modelling of 162 wells, and temperature simulation directly from a 3D geology model centred on the Dongara to Eneabba region (which the earlier 1D modelling indicated as having the highest simulated and recorded temperatures within the Perth Basin).

Introduction

Petroleum wells and water bores drilled in the search for petroleum and groundwater resources provide first-hand information on subsurface temperatures and geology, which aids evaluation of geofluid systems of the Perth Basin's petroleum, groundwater and geothermal systems.

Exploration for geothermal energy in Western Australia was formalized in January 2008, with the first geothermal acreage released in the Perth Basin. Presently, the Perth Basin is the state's most attractive target for geothermal energy research, exploration, development and utilization. Six companies and two research institutions hold 31 Geothermal Exploration Permits (GEPs). The Perth Basin has favourable geology, well-developed infrastructure and proximity to commercial markets (Fig. 1).

Previous multi-disciplined published work includes that of: Crostella (1995), Mory and Iasky (1996), Crostella and Backhouse (2000), Owad-Jones and Ellis (2000) addressing petroleum geology; and work by Thorpe and Davidson (1991), and Davidson (1995) investigating groundwater resources. Studies addressing geothermal energy potential in the Perth Basin include those by: Bestow (1982), Chopra and Holgate (2007), Ghori (2007, 2008a, 2008b, 2009), Hot Dry Rocks Pty Ltd (2008), and Gibson et. al. (2010).

Geology

The Perth Basin is a northerly elongated rift-trough extending along the west coast of Australia (Fig. 1); the major tectonic units include the Darling Fault and Dandaragan Trough in the east and the offshore Abrolhos and Vlaming sub-basins in the west. The Dandaragan Trough is the major depocentre containing up to 12 km of sedimentary succession, predominantly Permian to Cretaceous in age, with only a veneer of younger rocks (Fig. 2).

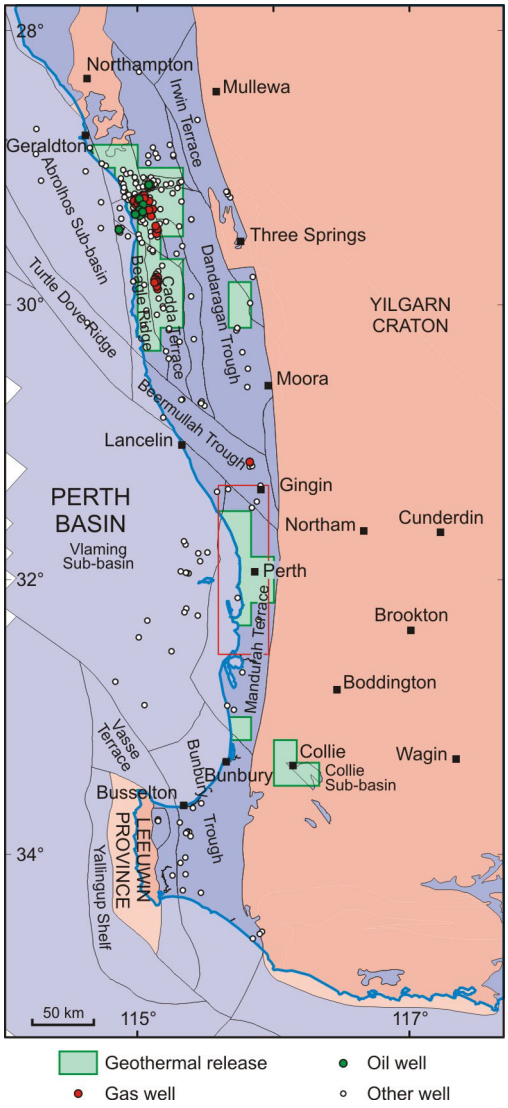

Figure 1. Perth Basin Map showing petroleum wells and Geothermal Exploration Permits.

Approach

GSWA aims to develop a reliable subsurface dataset of temperatures, basement depths, rock types and in-situ stress conditions to analyse geothermal and petroleum systems of the Perth Basin. First, raw temperature data was compiled from 253 petroleum wells and 47 artesian monitoring water-bores. Temperature gradients were then calculated and mapped, including an evaluation of data quantity and quality, ready for follow-up interpretation studies. Next, 253 wells were further assessed for data quality, and

equilibrium temperatures were calculated for the purpose of 1D heat-flow modelling of 162 selected wells (Chopra and Holgate, 2007; Hot Dry Rocks Pty Ltd, 2008). Finally, 3D geological, temperature and heat-flow modelling were undertaken by Gibson et. al. (2010) for the northern Perth Basin were the highest predicted temperatures of the basin occur.

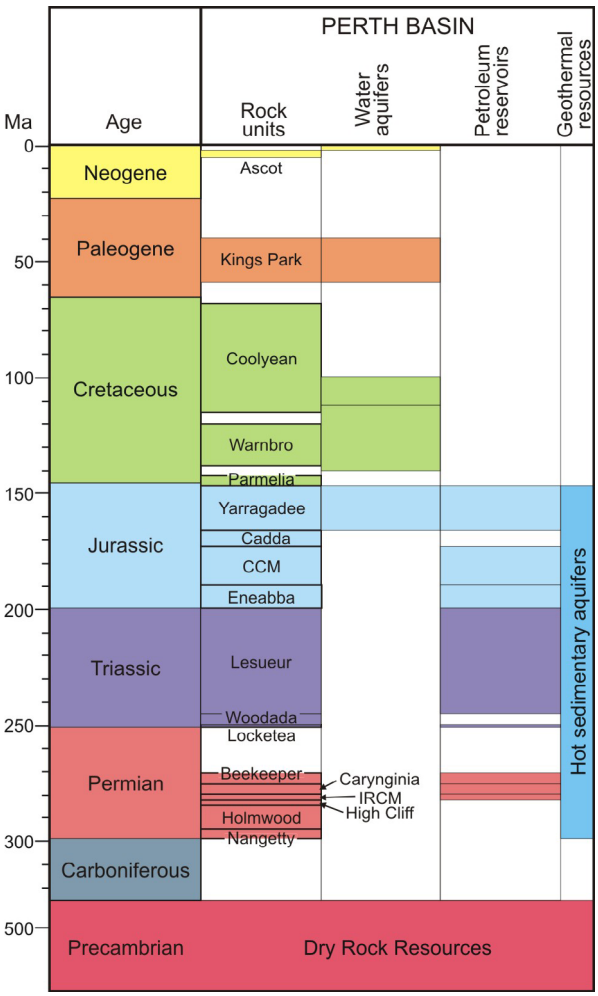

Figure 2. Generalised time-stratigraphy showing ground water and petroleum reservoirs, and potential geothermal resources.

Temperatures

Temperatures from the 253 petroleum wells are mostly from maximum bottom hole temperatures (BHTs) recorded during logging, with limited temperatures from drill stem tests (DSTs), and production tests (PTs). BHTs are lower than equilibrium temperatures and require more positive corrections compared to temperatures from DSTs and PTs. Horner and semi-log plots were used to estimate equilibrium temperatures for wells where sufficient data were available to apply these corrections. Ground surface temperatures are from the Australian Bureau of Meteorology (Chopra and Holgate, 2007; Hot Dry Rocks, 2008). The estimated equilibrium temperatures are up to 160ºC between 3.5 and 4.5 km (Fig. 3a). Normal and higher geothermal gradients are found at depths <2.8 km, due to thick sedimentary cover of low thermal conductivity rocks. Normal and lower gradients occur in deeper wells, down to 4.8 km (Fig. 3b).

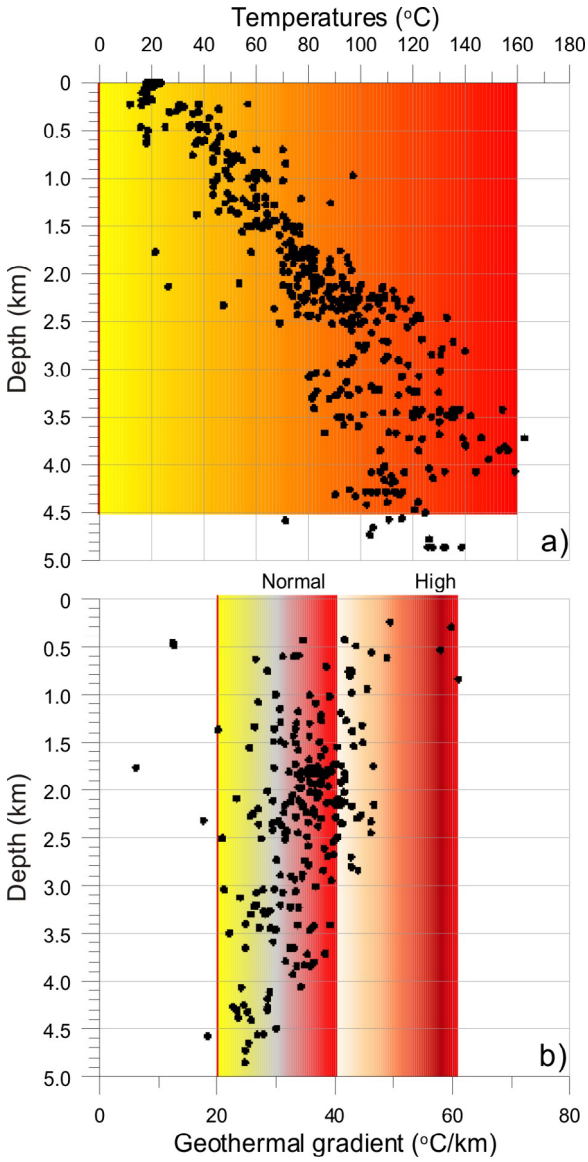

Figure 3. Recorded: a) temperatures, b) geothermal gradients versus depth.

Heat-flow modelling

1D conductive heat flow modelling was performed for 162 wells for the purpose of estimating temperatures at depth. Heat flow outcomes ranged from 30 to 140 mW/m², with values <65 mW/m² estimated in the Bunbury Trough, and values >90 mW/m² estimated towards the Eneabba and Dongara region (Hot Dry Rocks Pty Ltd, 2008). Estimated temperatures at 5 km are up to 250 ºC in the north, and as low as 110 ºC in the south (Fig. 4). This confirms the north Perth Basin, where basement is at comparatively shallow depths, has the highest heat flows and temperatures. The north Perth Basin also hosts the oil and gas fields discovered within the basin.

3D conductive heat flow modelling (Gibson el al, 2010) was performed to characterize the

geothermal anomaly in the Dongara to Eneabba region, where high temperatures occur at comparatively shallow depths.

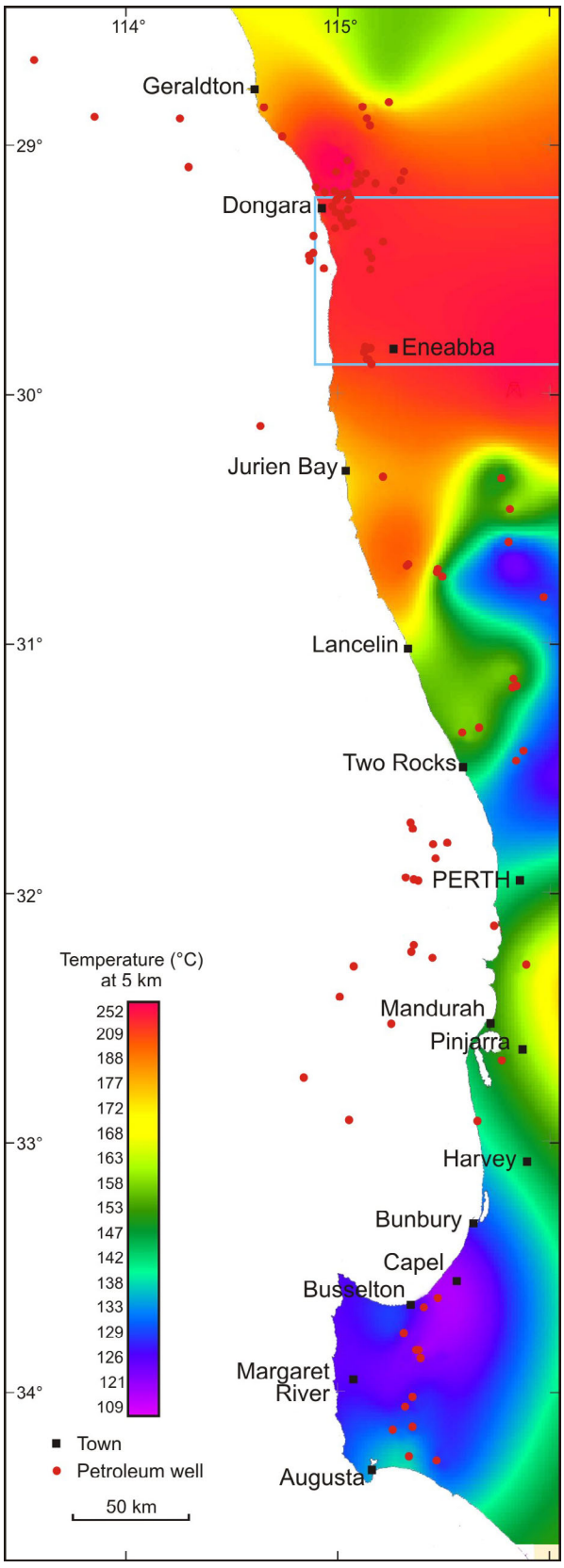

Figure 4. Shows the distribution of subsurface temperatures at 5 km, estimated from 1D heat-flow modelling (Hot Dry Rocks Pty Ltd, 2008).

3D geological, temperature and heat-flow modelling utilised constraints from previous GSWA studies by Mory and Iasky (1996), Chopra and Holgate (2007), and Hot Dry Rocks Pty Ltd (2008), including adopting formation tops and temperature data from 96 wells in the region.

First, a geological model for a 3D area about 140 km wide, 280 km long and 16 km deep was built, and later gridded to a low resolution constant cell size (X 1000; Y 1000; Z 100 m), and a high resolution cell size (X 500; Y 500; Z 50 m). These voxel models were basis on which 3D simulation of temperatures could be performed throughout a 3D grid, directly from the geology model. Following calibration in which measured BHT temperatures where validated, temperature outcomes ranged from 22 to 380 ºC, throughout the model including depths up to 15 km below SL.

3D modelling identified high-temperature anomalies on the Bookara Shelf in the north, the Coomallo Trough (central), and the Beermullah Trough in the south (Fig. 5). Across the Coomallo Trough temperatures range from ~100 to 154 ºC at 4 km (Fig. 5). Within the model depth-limits, estimated vertical heat flows range from 50 to 102 mW/m² (Fig. 6) and vertical temperature gradients range from 15 to 40 ºC/km (Fig. 7).

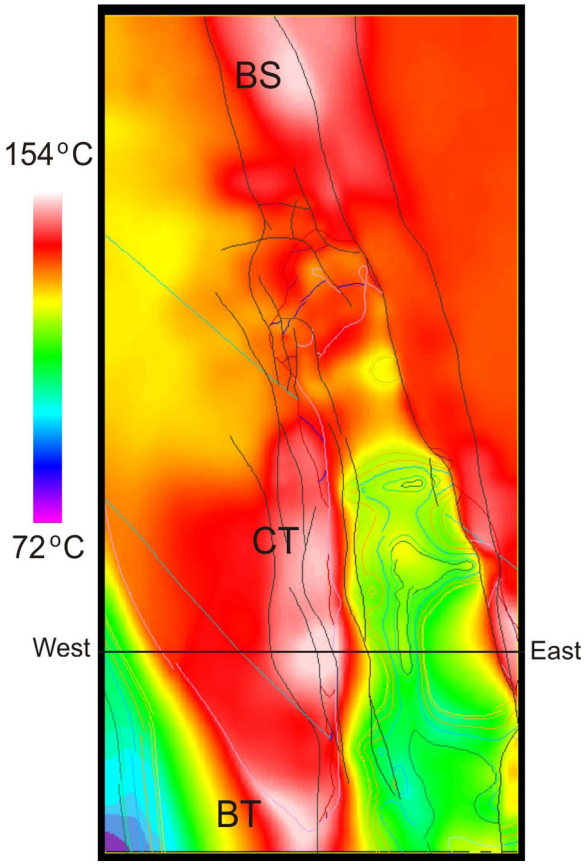

Figure 5. Estimated temperatures at 4 km below sea level derived from 3D modelling (BS = Bookara Shelf; CT = Coomallo Trough and BT = Beermullah Trough), from Gibson et. al. (2010).

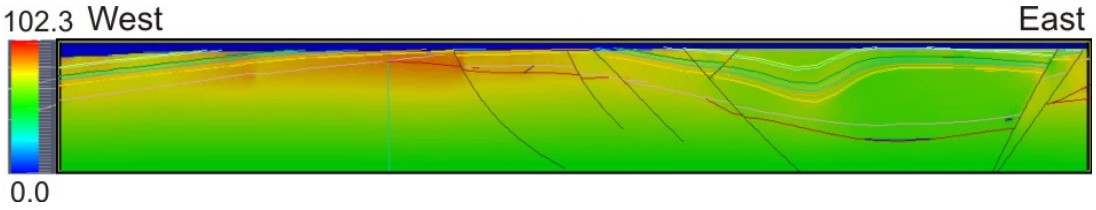

Figure 6. Modelled vertical heat flows across the Coomallo Trough range from 50 to 102 mW/m² (see fig. 5 for section location), from Gibson et al (2010).

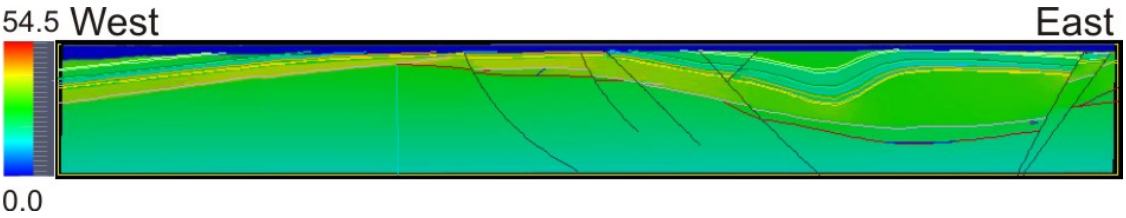

Figure 7. Modelled vertical temperature gradients across the Coomallo Trough range from 15 to 40ºC/km (see fig. 5 for section location), from Gibson et al (2010).

Conclusions

The Coomallo Trough, Beermullah Trough, Bookara Shelf, and north of Moora areas have the highest estimated temperatures within shallow locations, in the Perth Basin. The modelled 3D temperatures and the measured temperatures are up to 154 ºC and up to 150 ºC at 4 km, respectively. In conclusion, the northern Perth Basin has the best temperatures for direct and electric generation applications from its geothermal systems. It also has favourable geology, and well-developed infrastructure and commercial markets within reach.

Acknowledgments

This paper is published with the permission of the Director, Geological Survey of Western Australia

References

Chopra, P.N. and Holgate, F., 2007, Geothermal energy potential in selected areas of Western Australia, a consultancy report by Earthinsite.com Pty Ltd for Geological Survey of WA, Geological Survey of WA, Statutory petroleum exploration report G31888 A1, unpublished.

Crostella, A., 1995, An evaluation of the hydrocarbon potential of the onshore Perth Basin, WA Geological Survey, Report 43, 67pp.

Crostella, A. and Backhouse, J., 2000, Geology and petroleum exploration of the central and southern Perth Basin, Western Australia, Western Australian Geological Survey, Report 57, 85pp.

Davidson, W.A., 1995, Hydrogeology and groundwater resources of the Perth Region, Western Australia, Western Australia Geological Survey, Bulletin 142, 257pp.

Ghori, K.A.R., 2007, Search for energy from geothermal resources in Western Australia, Sept. 2007 Petroleum in WA, WA's Digest of Petroleum Exploration, Development and Production, Depart. of Industry and Resources, Perth, 36–39.

Ghori, K.A.R, 2008a, The search for Western Australia's geothermal resources, Geological Survey of Western Australia, Annual Review 2006–07, 25–31.

Ghori, K.A. R, 2008b, Extended abstract, Western Australia's geothermal resources, 2008 American Association of Petroleum Geologists Conference and Exhibition, San Antonio, April 20–23, 2008, http://www.searchanddiscovery.net/documents/2008/08032ghori/index.htm.

Ghori, K.A.R, 2009, Petroleum data: leading the search for geothermal resources in Western Australia, Australian Petroleum Production and Exploration Association, Journal 49, 359–379.

Gibson, H., Bonet, C., Seikel, R. and Hore, S., 2010, 3D geological model building, and 3D temperature and heat flow calculation of the northern Perth Basin, Geological Survey of Western Australia, Record 2011/16, 76pp.

Mory, A.J. and Iasky, R.P., 1996, Stratigraphy and structure of the onshore northern Perth Basin, WA Geological Survey, Report 46, 102pp.

Hot Dry Rocks Pty Ltd, 2008, Geothermal energy potential in selected areas of WA (Perth Basin), a report prepared for the Department of Industry and Resources, Western Australia, Geological Survey of Western Australia, Statutory petroleum exploration report G31888 A2, unpublished.

Owad-Jones, D. and Ellis, G., 2000, Western Australia atlas of petroleum fields, Onshore Perth Basin, Petroleum Division, Department of Mineral and Energy Western Australia, volume 1, 114pp.

Thorpe, P.M. and Davidson, W.A., 1991, Groundwater age and hydrodynamics of the confined aquifers, Perth, Western Australia. Proceedings, International Conference on Groundwater in Large Sedimentary Basins, Perth, WA, 1990. Australian Water Resources Council Series 20, 420–436.

What will make EGS geothermal energy a viable Australian renewable energy option?

Hal Gurgenci
h.gurgenci@uq.edu.au
Queensland Geothermal Energy Centre of Excellence, The University of Queensland, St Lucia, QLD 4072

There are good reasons to expect the Australian geothermal sector to be able to provide zero-emission electricity for the country at an affordable cost, once certain technical challenges are overcome. This paper presents cost estimates for geothermal electricity using the present technology and identifies the areas where technical improvements are anticipated in the next couple of years and how they should influence that cost.

The present proven cost of EGS geothermal electricity is too high to be commercially feasible but is expected to come down to parity with gas-fired electricity provided successful outcomes are achieved in some of the current research programs in Australia and elsewhere.

Challenges for the Australian geothermal energy sector

While Australia is not known as a traditional geothermal energy country, high radiogenic heat production within large sections of the Australian continental crust offers a significant geothermal power potential (McLaren et al., 2003). There has been considerable interest in recent years toward realising at least part of this potential. In fact, according to the Australian Geothermal Implementing Agreement Annual Report, more than AU$450 million have been spent on studies, geophysical surveys, drilling, reservoir stimulation and flow tests in the geothermal energy area in 2002 to 2009 (Goldstein 2009).

In spite of this effort, the only geothermal power plant in the country is still the Birdsville geothermal power station, which owes its existence to a combination of local factors which may be difficult to be repeated elsewhere.

After Birdsville, the early commercial geothermal projects in Australia targeted Engineered Geothermal Systems (EGS) also known as Hot Dry Rock (HDR) resources (Chopra, 2005). Currently, two companies have such projects at advanced levels of development: Geodynamics Cooper Basin and Petratherm Paralana projects.

In recent years, a new form of geothermal play has attracted commercial attention in Australia. The term Hot Sedimentary Aquifers (HSA) is used to refer to those resources located in sedimentary basins insulated by an impermeable layer at the top and heated by the basement rock underneath. The underlying heat source for Australian HSA is radiogenic rather than magmatic, although there may be exceptions (see, for example Uysal et al, 2011).

In both HSA and EGS, the two essentials for a commercially viable operation are the flow rate and the temperature. The latter is relatively easier to achieve. There are good scientific tools to predict the temperature and to target the location of the high temperature resource. Consequently, there have not been many recent failures to find these temperatures after drilling to the target locations. A flow rate high enough to enable viable power generation however has been more elusive to achieve.

In a recent workshop in the United States (Renner 2011), the following areas were identified for improvement before EGS becomes commercially viable in USA:

- 20% reduction in drilling costs;
- Increasing the production flow rate to 80 kg/s; and
- 20% improvement in conversion efficiency.

In this paper, an estimate is presented for what the cost of geothermal electricity could be in Australia for a high-temperature EGS resource using the state-of-the-art EGS technology and what improvements are required to make it commercially viable.

To represent the state-of-the-art, the Geothermal Electricity Technology Evaluation Model (GETEM) will be used. This is an economics/performance spreadsheet model developed by the US Department of Energy Geothermal Technologies Program to assess power generation costs and the potential for technology improvements to impact those generation costs. The GETEM Version 2009-A15 was used. This was the most recent GETEM model before the beta version of a new version was released at the GTP Review in Maryland in June 2011.

At what price is the geothermal electricity commercially viable? The answer of course depends on a number of variables including future incentives for renewable electricity and a possible carbon tax regime. A rigorous analysis of these factors is beyond the scope of this paper. Therefore, quite arbitrarily, the cost of electricity from a Combined Cycle Gas Plant (CCGT) including a carbon tax of $30/tonne of CO_2 was set as a commercially viable aspirational cost

target for the geothermal electricity. A past study by Energy Supply Association of Australia (ESAA) provides this cost as 8.5 ¢/kWh, based on a discount rate of 10% (IEA 2010).

The Case Study

The present cost of geothermal electricity is calculated for a hypothetical geothermal resource as defined in Table 1.

Table 1. Case Study Definition

Brine temperature	250 °C
Well depth	4500 m
Reservoir type	EGS
Power plant	State-of-the-art binary plant with air-cooled condensers

The State of the Art

Drilling Costs

GETEM has three cost curves for drilling geothermal wells. These high, medium, and low cost curves were worked out by Sandia. The lower cost wells are more likely to have been drilled in "softer" formations, and experienced few troubles. The high cost wells are more likely to have been drilled in harder formations, or had more troubles, or both.

For the state-of-the-art cost calculations, it is assumed that the geothermal well costs will follow the high cost curve option. For a 4500-m deep EGS well, the cost calculated using the high-cost curve is US$22.3m in 2008 US dollars.

Production Flow Rates

The limited experience with EGS makes it difficult to select a production flow rate as the state of the art. In the only Australian EGS project that produced brine flow at the surface, Geodynamics reported the flow rate from Habanero #2 to be in excess of 25 kg/s, with lower flow rates achieved in 2009 during the closed-loop circulation tests. In this paper, I will assume 30 kg/s as the present achievable production flow rate. This is higher than what has actually been experienced but is justifiable as the state-of-the-art production flow rate for the purpose of the present analysis (this agrees with Petty 2010).

Binary Plant

The power conversion efficiency in GETEM is represented by specifying the net kilowatts produced per unit brine flow rate. The power generation efficiency in GETEM is represented by a parameter called brine effectiveness with the units of kW per kg/s (or kJ/kg) of the geothermal fluid. I used a brine effectiveness of 90 kJ/kg and 10% for parasitic losses. The cycle efficiency is based on the steam cycle shown in Figure 1. The upper figure shows the block diagram of a binary plant with preheater (PRE), evaporator(EVA), and superheater(SUP) for steam, which is expanded through a turbine (TUR) and condensed in a condenser(CON) and pumped back to the turbine inlet pressure in a pump (PUM). The lower figure is the cycle plotted on a temperature-entropy (T-s) diagram. The numbers on the T-s diagram correspond to the positions in the upper figure, e.g. 1 and 2 are before and after the pump. The calculations are based upon steam properties from the NIST property database REFPROP (NIST, 2011).

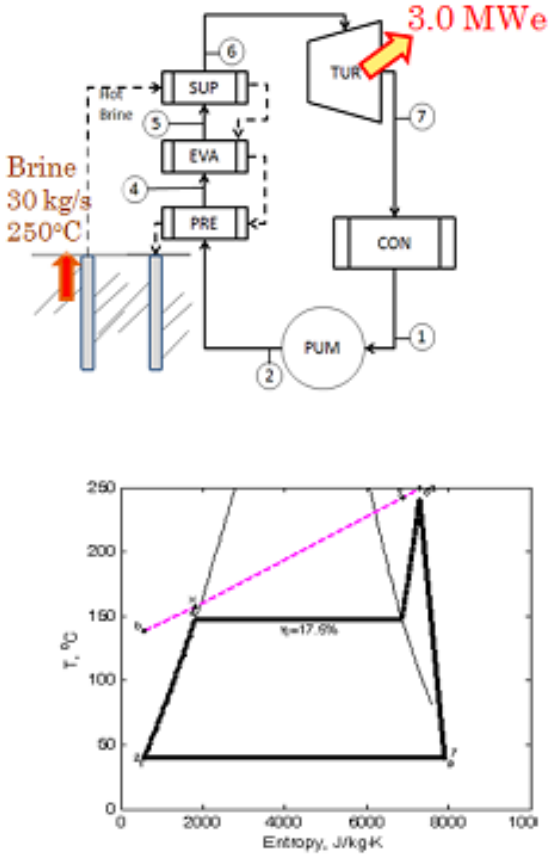

Figure 1. Steam cycle representative of state-of-the-art for geothermal brine at 250°C.

I assumed a heat exchanger pinch point difference of 10 °C (which is a heat exchanger design constraint and refers to the minimum temperature difference between the brine and the cycle fluid). The net power generation (not including the brine circulation pumping) is 3000 kWe for a brine flow rate of 30 kg/s, corresponding to a brine effectiveness of 100 kW/(kg-s). Assuming air-cooled condensers and about 10% for the fan parasitic losses, the net brine effectiveness is 90 kW/(kg-s), which is the number I used in GETEM to represent the state of the art EGS power generation. The plant costs are calculated as $2488/kWe using the default curves embedded in GETEM.

Other Costs

Other cost entries used to calculated the levelised cost of electricity (LCoE) were assumed to be 10% for the cost of the capital and 3 ¢/kWh for annual operations and maintenance. This is

composed of 2 ¢/kWh for the power plant and 1 ¢/kWh for the field (including the production pumps). These are the suggested default values by GETEM adapted from hydrothermal data, which I adopted in this analysis. There is not enough EGS experience to suggest different values.

The LCoE

The levelised cost of electricity using the above assumptions were calculated by GETEM as 26.9 ¢/kWh. The breakdown of this cost is given in Figure 2.

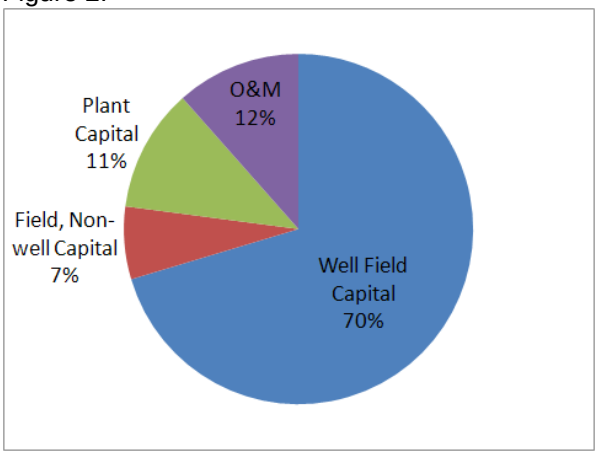

Figure 2. State-of-the-art LCOE components

I created this pie chart by using the results from GETEM. The O&M share has already been explained. The other components in Figure 2 correspond to the cost of the capital for the well field, other field investment and the power plant.

Future Improvements

The effect of the following technology improvements on the LCoE has been calculated using GETEM:

- Drilling Cost
  - Cheaper wells (Medium-Cost curve)
- Power Conversion
  - Supercritical cycles
  - Natural Draft Dry Cooling Towers
- Production flow rate
  - Double the flow
  - Triple the flow

The results are summarised in Figure 3.

All of the above technology improvements are targets of ongoing research projects. it can be expected to see significant progress towards these aims in the next two years and achieve the targets in less than five years. The power plant projects are well-advanced in QGECE and other places in the world. We expect to have supercritical power cycles available for commercial use in the next few years. Similar expectations apply to natural draft dry cooling towers. The aim of cheaper wells is a common subject for several DOE-funded projects in United States. Progress is expected but it is difficult to see how quickly this would occur and at what scale. The flow rate issue is probably the most critical aim. Based on the author's own observations, the issue is similar to what faced the coal seam gas industry 15 years ago in terms of low permeability of the seam and low gas flow rates and it took about 8-10 years for that industry to develop commercial tools to increase flow rates to acceptable levels. A similar time scale may apply here.

Conclusions

The present proven cost of EGS geothermal electricity is 26.9 ¢/kWh but this is expected to come down to as low as 8.5 ¢/kWh provided successful outcomes are achieved in some of the current research programs in Australia and elsewhere, which are targeting the technology improvements considered in Figure 3.

Finally, the focus in this paper has been on EGS. More experience with HSA is needed to carry out similar calculations.

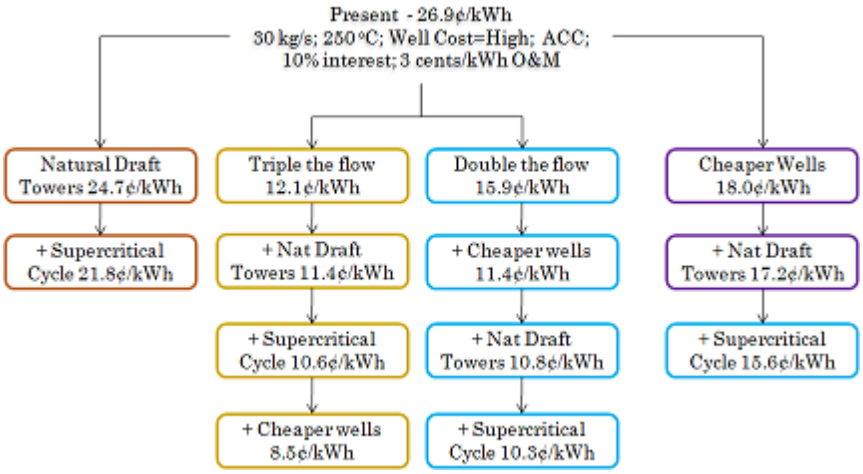

Figure 3. Expected cost reductions by future technology improvements

References

Goldstein, B. Australian Geothermal Implementing Agreement Annual Report – 2009 http://www.agea.org.au/news/2011/australian-geothermal-implementing-agreement-annual-report-2009/ .

IEA/NEA/OECD Publication. Projected Costs of Generating Electricity, 2010.

McLaren, S, Sandiford, M et al. 2003. In: R.R. Hillis and R.D. Müller (Eds.), Geol. Soc. of Aust. Spec. Pub. 22 and Geol. Soc. Am. Spec. Pap. 372

NIST Standard Reference Database REFPROP – Reference Fluid Thermodynamic and Transport Properties (2007).

Petty, S., Bour, D., Nordin, Y., Nofziger, L. Multiple Zone Stimulation of EGS Wells – Key to reservoir Optimisation, SMU Workshop, 13-15 June 2011

Renner,J.L. EGS – Status and Technology needs, AAPG/SPE/SEG Hedberg Research Conference on Enhanced Geothermal Systems, March 2011, Napa, California (quoting Susan Petty, GRC Webinar/Workshop Series, July 2009. http://www1.eere.energy.gov/geothermal/egs_webinar.html)

Uysal, I.T., Yuce, G., Italiano, F., and Gasparon, M. (2011). Noble gas isotopic studies of CO_2 –rich waters in Australian sedimentary basins with a geothermal energy potential. *International Conference on Gas Geochemistry 2011*, San Diego, California, USA, 28 Nov-2 Dec 2011.

Real-Time Induced Seismicity Monitoring During Wellbore Stimulation at Paralana-2 South Australia

Michael Hasting[1&4], Julie Albaric[2], Volker Oye[2], Peter Reid[3], Mathieu Messeiller[3], Ella Llanos[3], Peter Malin[4], Eylon Shalev[4], Mathew Hogg[4], Mark Alvarez[4], Alex Miller[4], Christina Walter[4], Carolin Boese[5], Nora Voss[6]

m.hasting@auckland.ac.nz or hasting.michael@gmail.com

[1]Hasting Micro-Seismic Consulting, 1233 Quail Way, Ridgecrest CA 93555 USA +1-760-608-7542

[2]NORSAR, Gunnar Randers vei 15, 2007 Kjeller, Norway

[3]Petratherm Ltd, Australia, Level 1, 129 Greenhill Road Unley SA 5061, Australia

[4]IESE and the University of Auckland, 58 Symonds Street, CBD Auckland, 1142, New Zealand

[5]Victoria University, School of Geography, Environment and Earth Sciences, Kellburn Parade, Victoria University of Wellington, Wellington 6012, New Zealand

[6]GZB, International Geothermal Center, Hochschule Bochum, Lennershofstraße 140, 44801 Bochum, Germany

In 2009 the Paralana JV, drilled the Paralana-2 (P2) Enhanced Geothermal System (EGS) borehole east of the Flinders Range in South Australia. Drilling started on June 30th and reached a total depth of 4,003m (G.L AHD) on Nov 9th. A 7- inch casing was set and cemented to a depth of 3,725m and P2 was officially completed on the 9th Dec 2009. On Jan 2nd 2011 a six meter zone was perforated between 3,679 and 3,685 mRT. A stimulation of P2 was carried out on Jan 3rd by injecting approximately 14,668 litres of fluid at pressure of up to 8.7 kpsi and various rates up to 2 bpm. During the stimulation ~125 micro-earthquakes (MEQ) were triggered in the formation. Most of the MEQ events occurred in an area about 100 m wide and 220 m deep at an average depth of 3,850 m. The largest event, a M_W 1.4, occurred after the shut-in.

Between 11th and 15th of July 2011, the main fracture stimulation was carried out with ~3 M litres injected at pressures up to 9 kpsi and rates up to 10 bpm. Over 11,000 MEQ were detected by the seismic monitoring network. This network consisted of 12 surface and 8 borehole stations with sensor depths of 40 m, 200 m and 1,800 m. Four accelerometers were also installed to record ground motions near key facilities in the case of a larger seismic event. MEQ were automatically triggered and located in near-real-time with the software MIMO provided by NORSAR. A traffic light system was in operation and none of the detected events came close to the threshold value. More than ½ of the detected events could be processed and located reliably in the full automatic mode.

Selected MEQ events were also manually picked on site in order to improve the location accuracy. A total of 875 MEQ events were picked, located and plotted on site to give the operator, Petratherm, a sense of the fracture created while post processing yielded another 1,025 events. After a data download in mid August an additional 750 events were located from this data set. As such over 2,600 events were hand-picked and located to form the final picture of the stimulation fracture. Results show that fracturing occurred in three swarms. The 1st swarm occurs near the well and deepened with time from 3.7 km to over 4.1 km. The 2nd swarm occurred a few days in and shows as a circular patch extending a few hundred meters east of the 1st one. The 3rd swarm occurred after shut-in and extends downwards to the NNW and reaches 4.4 km depth. Petratherm believes that there is a primary NE/SW structure that takes most of the fluid. Then, two NNE/SSW structures are highlighted after day 5 to 6 and continue growing after shut-in. The first fracture appears to have a sygmoidal pattern. The two later structures appear to act as boundaries to the East and West and are subparallel to the major faults that define the graben in which P2 was drilled. They appear to deepen towards the north. A later shallower structure is highlighted to the SE of the well. Overall, it appears that at least 4 structures have been enhanced and stimulated. The well head pressure after the minifrac and after the main frac shows a value of about 3940 psi. This shows that the injection of fluids in P2 has connected into a naturally fractured network, with *in situ* fluid. While drilling P2, overpressured brines were intersected at depths between 3680 and 3860m. We believe that this zone of fracture permeability has been connected to and enhanced. The MEQ cloud shows a complex fracture network of at least 4 structures that can be interpreted as conjugated faults/fractures. Refer Figure 1a and 1b below:

The “Post” injection seismicity also shows that events occurred on the outer edges of the main injection swarm and that there are four distinct areas of continued seismicity. All events form primarily along a northeast trending structure that is steeply dipping to the northwest with a total length of over 1,350 m and depth of between 3,200 m and 4,200 m.

Assuming that injected fluids went into opening of new fractures a volume change must occur. Using a variation of the Brune formula (JGR, VOL. 73,

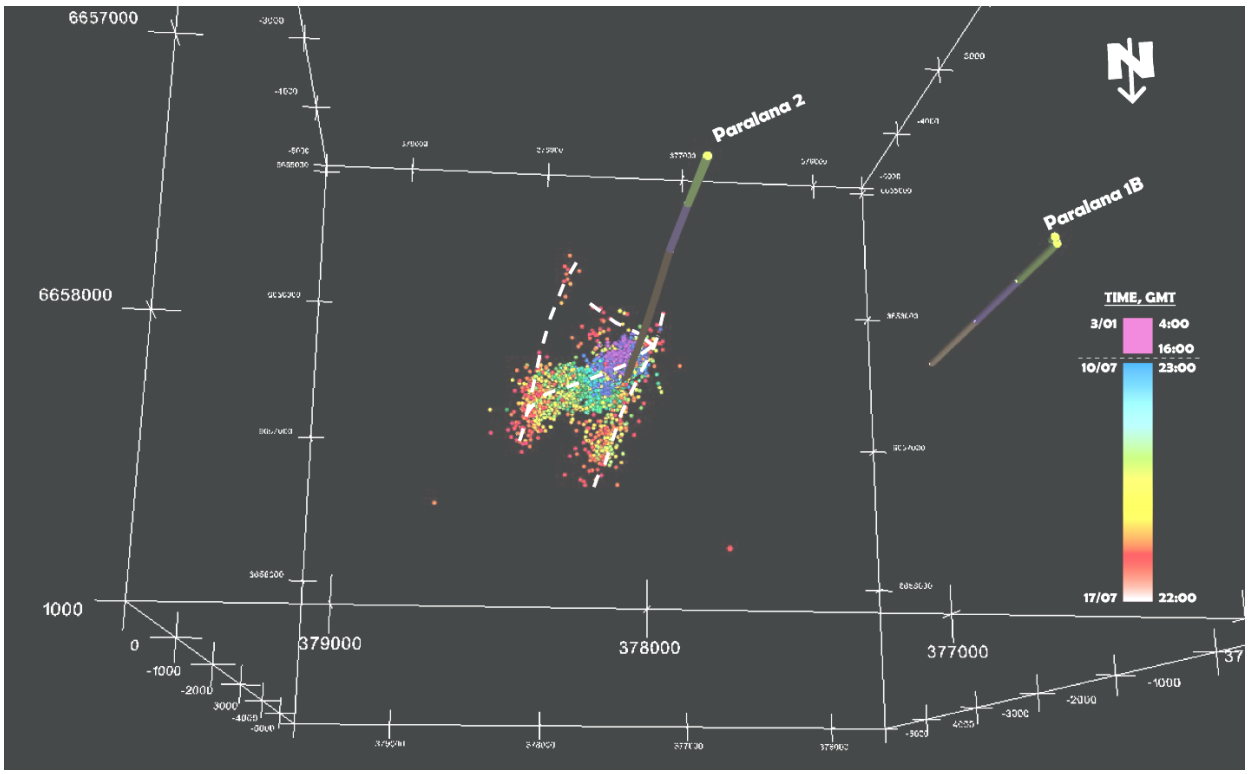

Figures 1a: 3D Plots Showing Induced Seismic Events

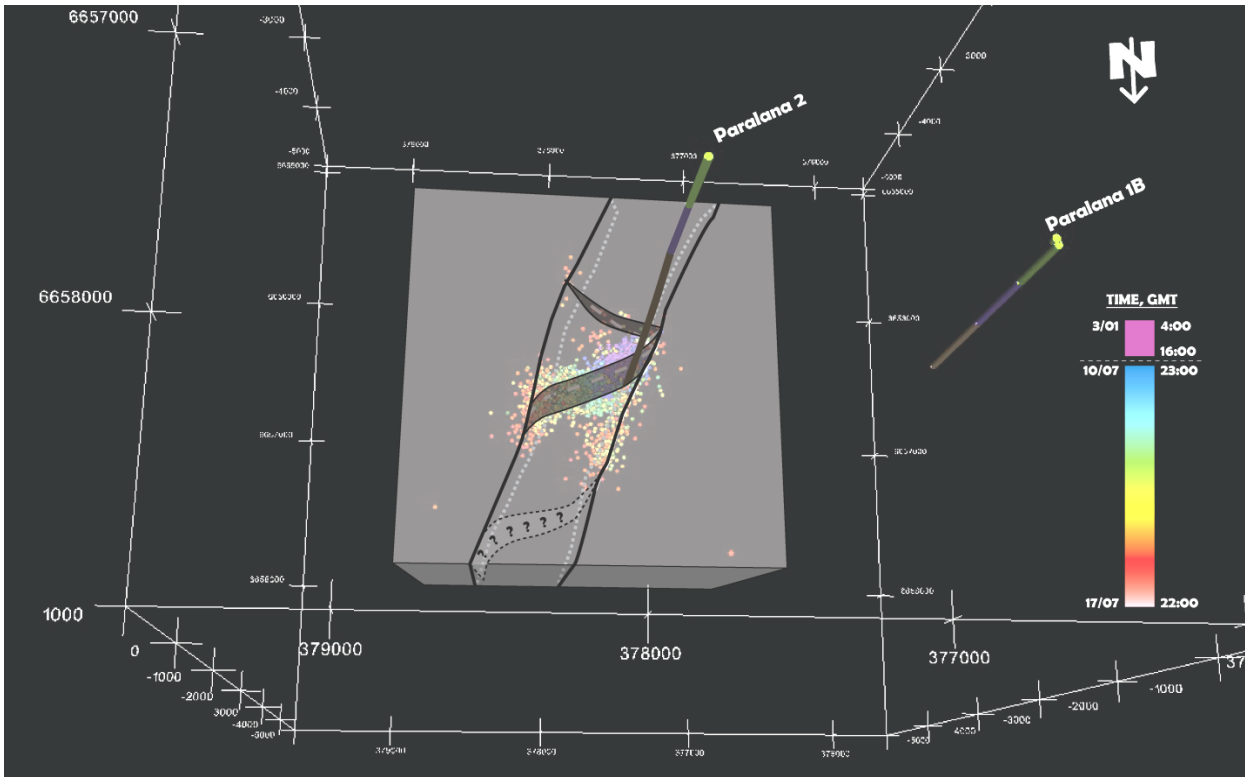

Figures 1b: Geological interpretation of main fractures based on the seismicity and a 2D seismic survey of the area

NO. 2, PP. 777-784, 1968) for estimating seismic moment and converting to a “Moment Magnitude”, M_W, we estimated that a total M_W=3.12 is needed to accommodate the fluids. Summing the M_W of the 2,600 hand-picked events yields a total measured M_W=3.05. As such most of the fluids must have gone into the opening of fractures and have created a new geothermal reservoir.

Keywords: Induced Micro Earthquakes, MEQ, EGS, Stimulation, Injection, Paralana, Petratherm, IESE, MIMO, NORSAR, Reftek

Introduction

Between April 2008 and January 2011 the Institute of Earth Science and Engineering (IESE) conducted a background micro-seismic study of the area around the Paralana geothermal project area. Results of this study showed very little seismic activity within the footprint of the seismic array. However during the drilling of the Paralana-2 (P2) borehole we did see several micro-seismic events associated with the cementing of the casing. On 3 January 2011 a stimulation experiment of P2 was carried out. During this experiment, a mini-frac, the Paralana MEQ network detected over 300 seismic events in a four hour timeframe around the stimulation. Of the 300 seismic events approximately 125 were large enough to be located. During this phase of operations the network consisted of twelve stations, four at the surface and eight in boreholes (Figure 2). It should be noted that six of the borehole stations were installed at a depth of 200 m below surface, one at a depth of 40 m and one at a depth of 1,797 m.

All sensors measured three components and were configured in a traditional X, Y, and Z configuration. The surface station used 2Hz sensors while most of the borehole station used a 4.5Hz borehole SONDE. For station B05, deployed into the bottom of the Paralana-1B borehole, due to the size of the casing a custom built 15Hz sensor was deployed measuring 1.75 in (44.45 mm) OD and including the coupling weights over 9 ft (2.75 m) long. Figure 3 shows this sensor being deployed. Sampling rate on the data loggers were set to 1000 Hz to record the maximum frequency content of the earthquake during the fracture. Post processing of the data showed that for most all stations a sampling rate of 250 Hz would have been acceptable due to the strong attenuation of the signals in the softer sediments in the area.

During the July 2011 main stimulation, the MEQ network was upgraded using 900 MHz spread-spectrum radios to a real-time network and nine more stations were added to the array. Of the nine new stations, four of these were strong motion accelerometers while the rest were standard 2 Hz velocity sensors. Figure 4 shows the configuration of the Paralana MEQ network during the main stimulation. Due to the limitation on the real-time communications, and the results of the mini-frac, a sampling rate of 250 Hz was used on all station in the network. During the main stimulation of P2 over 11,000 events were detected by the MEQ network with over 6,000 events being automatically located by the MIMO software. Approximately 875 events were also manually phase picked and located by IESE staff while on site and an additional 1,725 events were hand-picked during post processing. Figure 5 shows a plot of all events manually picked and located by IESE.

Results of the main stimulation event locations show that primary fracturing occurred along a generally northeast to southwest structure steeply dipping to the northwest. Later development of the fracture network involves two NNE/SSW

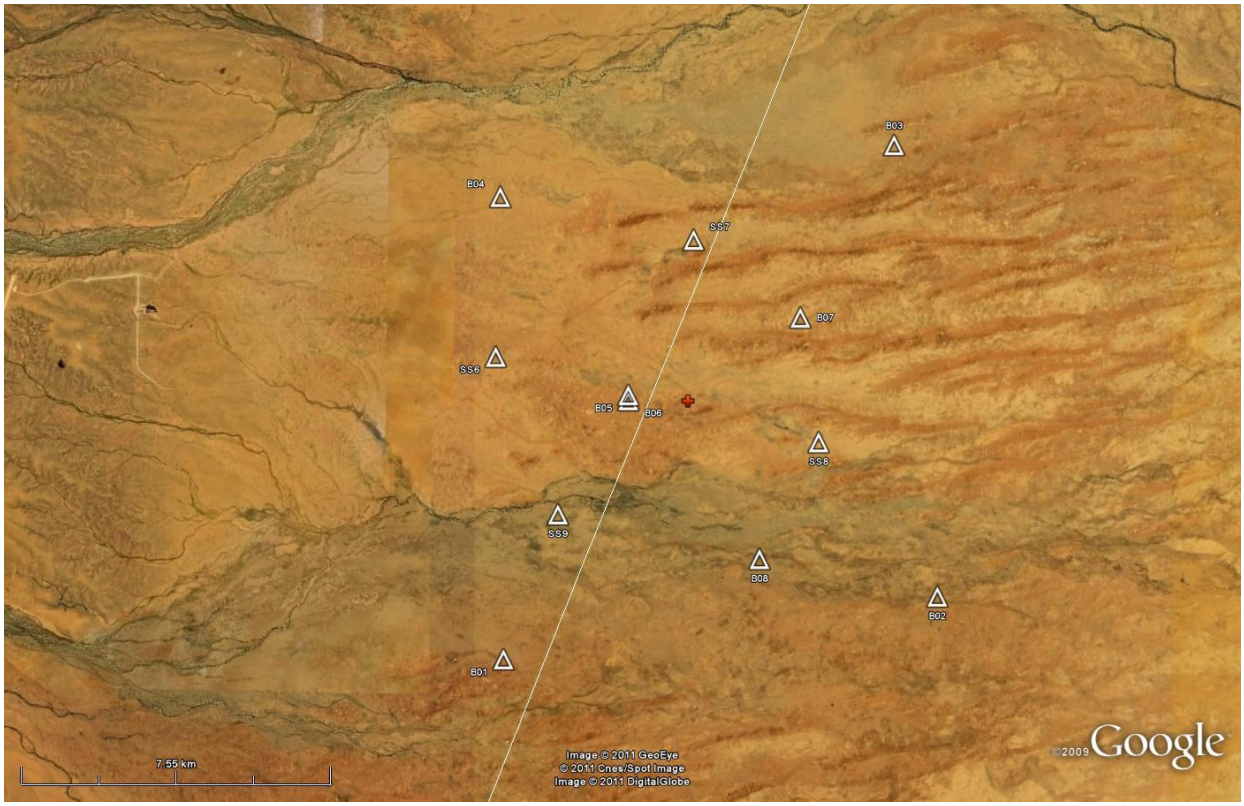

Figure 2: Paralana MEQ network station layout for mini frac. Top of Paralana-2 borehole is represented by a red cross.

Figure 3: 15Hz Sensor being deployed into the Paralana-1b borehole. Station name = B05

structures. In figure 5 the events plotting north of the main injection event swarm are deeper events along the main fracture and will be shown in cross-sections in later plots. Additionally the fracturing during pumping operations was significantly different than fracturing while the wellhead was shut-in under pressure. Most of the events occurring after the shut-in of the wellhead occurred on the outer edges of the main swarm. This will be shown in later figures. It should be noted that fracturing of the rock was still occurring more than 30 days after P2 was shut-in and as such the figures in this paper will be updated as data is downloaded and events are located.

Mini Stimulation

The primary purpose of the mini-frac experiment was to determine the pressures and flow rates needed for achieve the main stimulation. It gave IESE the ability to evaluate the network performance and determine the recording parameters needed for the main-frac monitoring program. From the results of the mini-frac monitoring we were able to determine the best location for new stations and the level of effort it would take to provide Petratherm with the necessary onsite support for recording and locating events in near-real-time.

As noted above, during the mini-frac of the P2 borehole ~125 seismic events were located (Figure 6). As shown in the figure, the events occurred vertically over a range of about 300m and align roughly along the path of the borehole. The largest event, a M_W1.45, occurred in the middle of the swarm. From figure 7 it can be seen that the main event occurred at, or just after, the time of shut-in and just as the pressure started to decrease. It should be pointed out that while

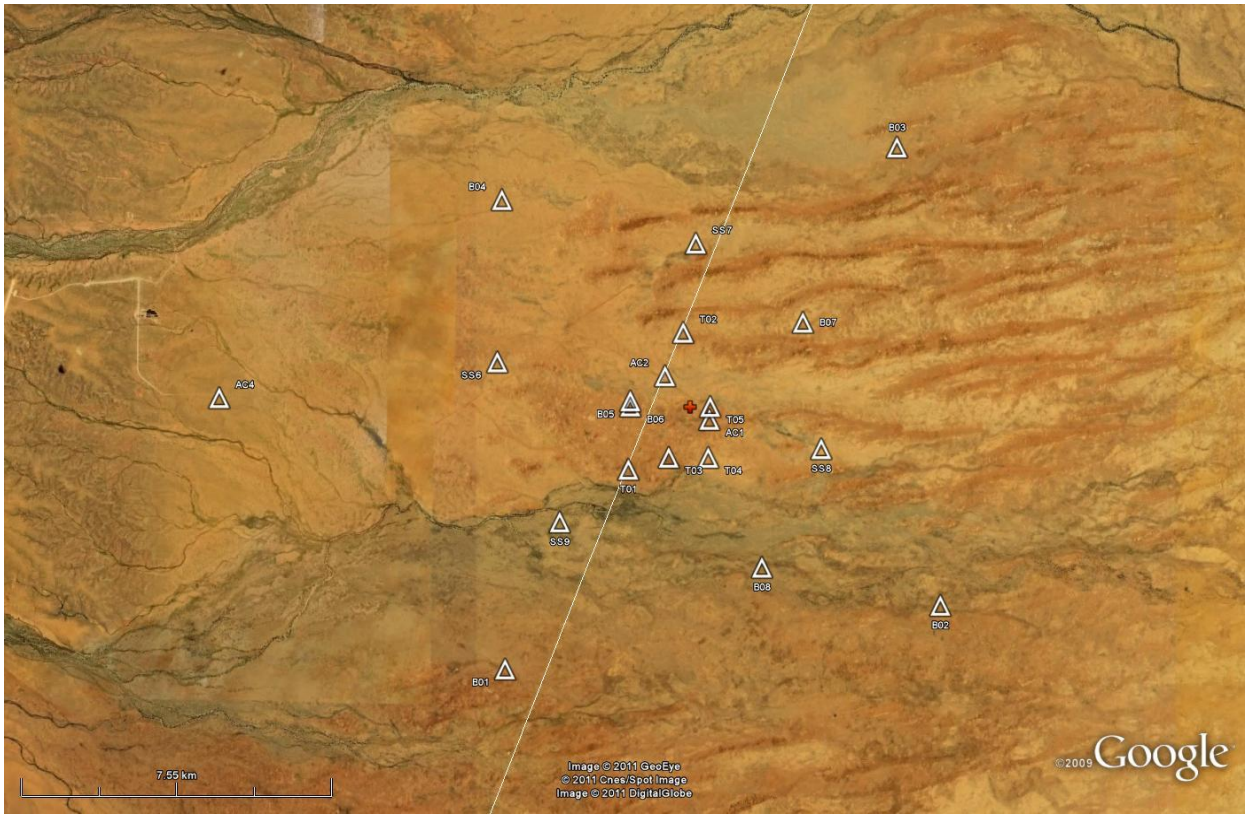

Figure 4: Paralana MEQ network station layout for main frac. Top of Paralana-2 borehole is represented by a red cross.

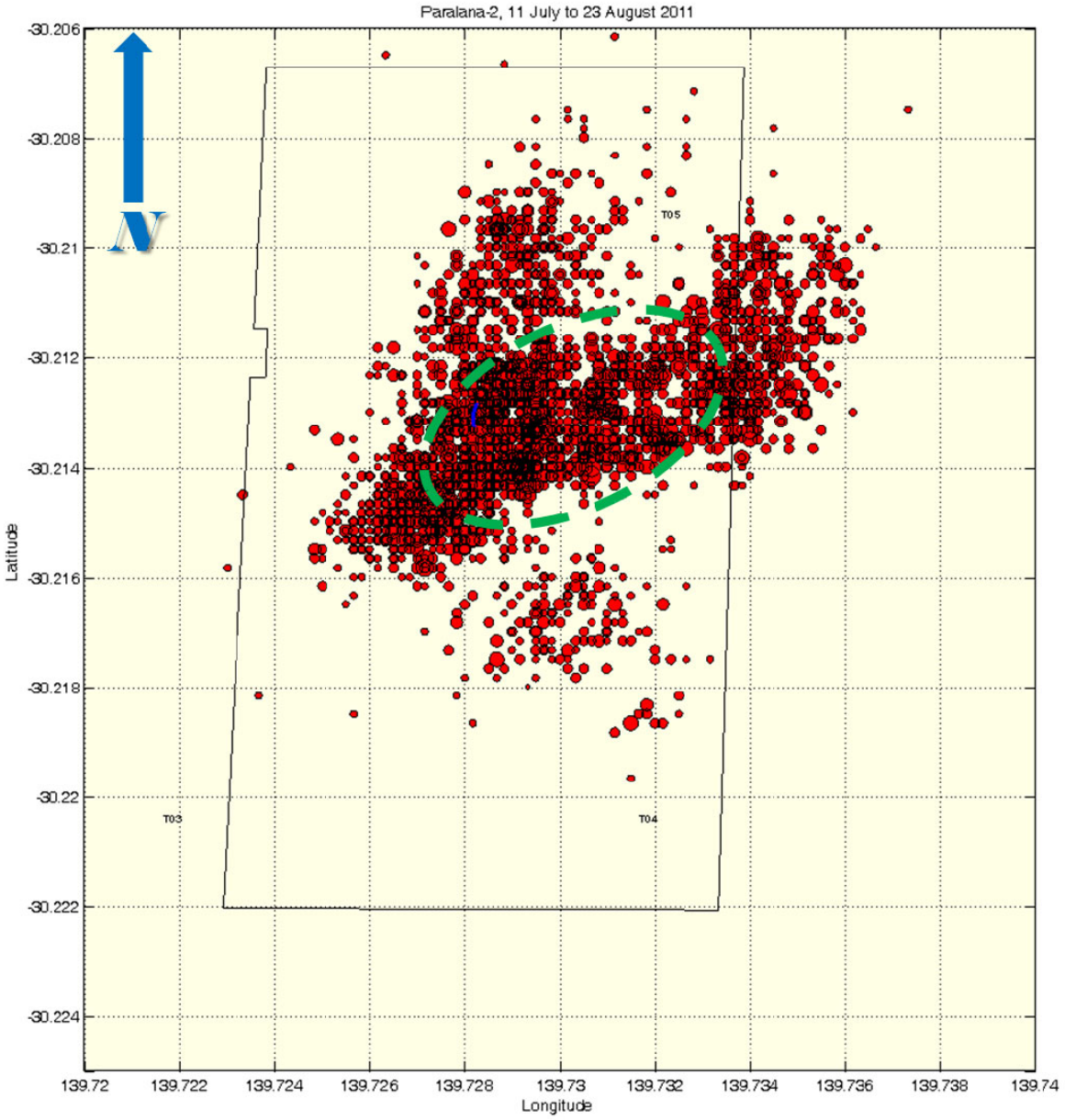

Figure 5: Plot showing map view of all +2,600 seismic events recorded during and after the main stimulation/injection of the Paralana-2 borehole. Black line is the Paralana-2 fence boundary. Events to the north are deeper than the main northeast-southwest trend. Green dashed line = main injection swarm area

seismic recordings were timed by GPS, it is not known if there was a timing offset on the computer used to record the pressure data. This may indicate the collapse of a larger section of fracture rock that was being held open by the increased pressure and when the pressure decreased it could no longer support the opening of the fracture. Note that the equilibrated wellhead pressure after the minifrac was 3940 psi, suggesting that P2 was connected to a natural fracture with overpressured brine.

Main Stimulation

The primary objective of the main stimulation was to generate a fracture with a minimum length of about 500 meters and width/depth of between 200 to 300 meters in size. This would provide a minimum surface area of 100,000 to 150,000 sq-meters. This objective was exceeded and an area of approximately 850,000 sq-meters was generated.

Event Locations

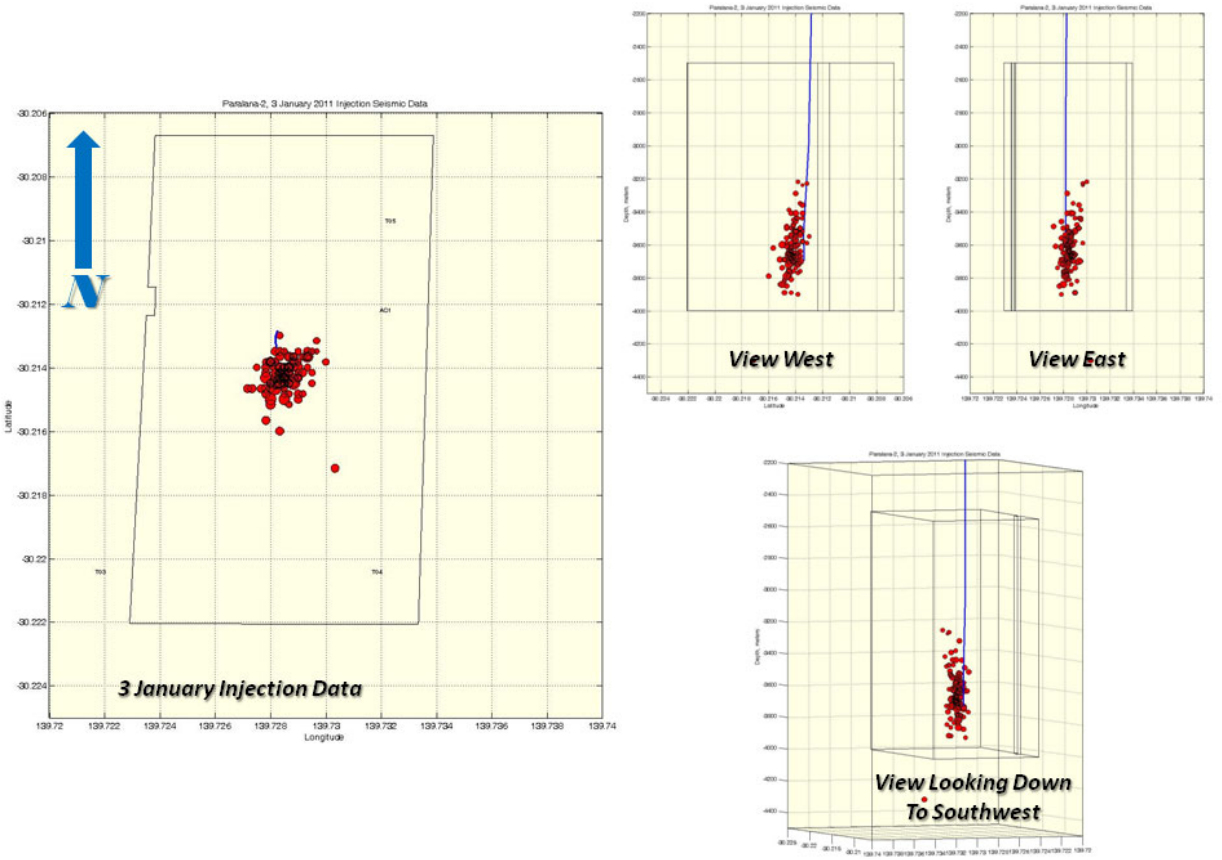

Figure 6: Mini-frac seismic events; blue trace on cross section plots is the Paralana-2 wellbore location. Inner box is for reference only and is a subsurface projection of the Paralana-2 fenced boundary.

During the main stimulation of the P2 borehole, the Paralana MEQ network was run in a continuous recording mode with all data from each station being sent to the central site for real-time processing. For the real-time data processing we used both the Refraction Technologies (RefTek) software RTPD for recording the data, RTCC for controlling the station, and RTMonitor for viewing the data in real-time. IESE staff also provided the fracing operators with a real-time feed of the seismic waveforms so that they could view the events as they happened. As such they were able to follow the seismicity and make adjustments as

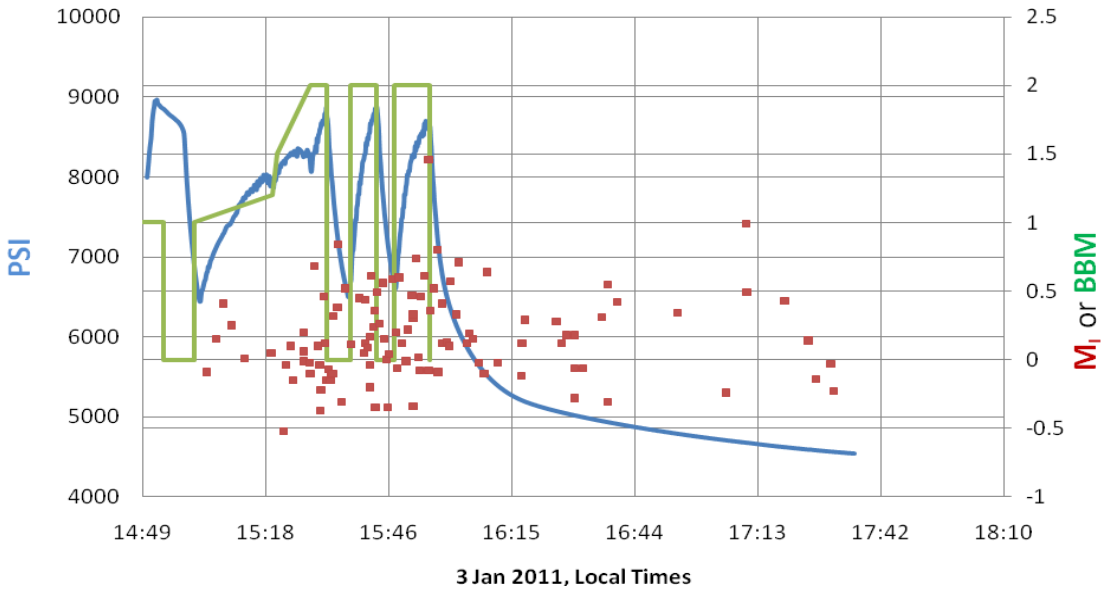

Figure 7: Plot of injection pressure (blue line) vs. seismic data (red dots) and pumping rates (green line)

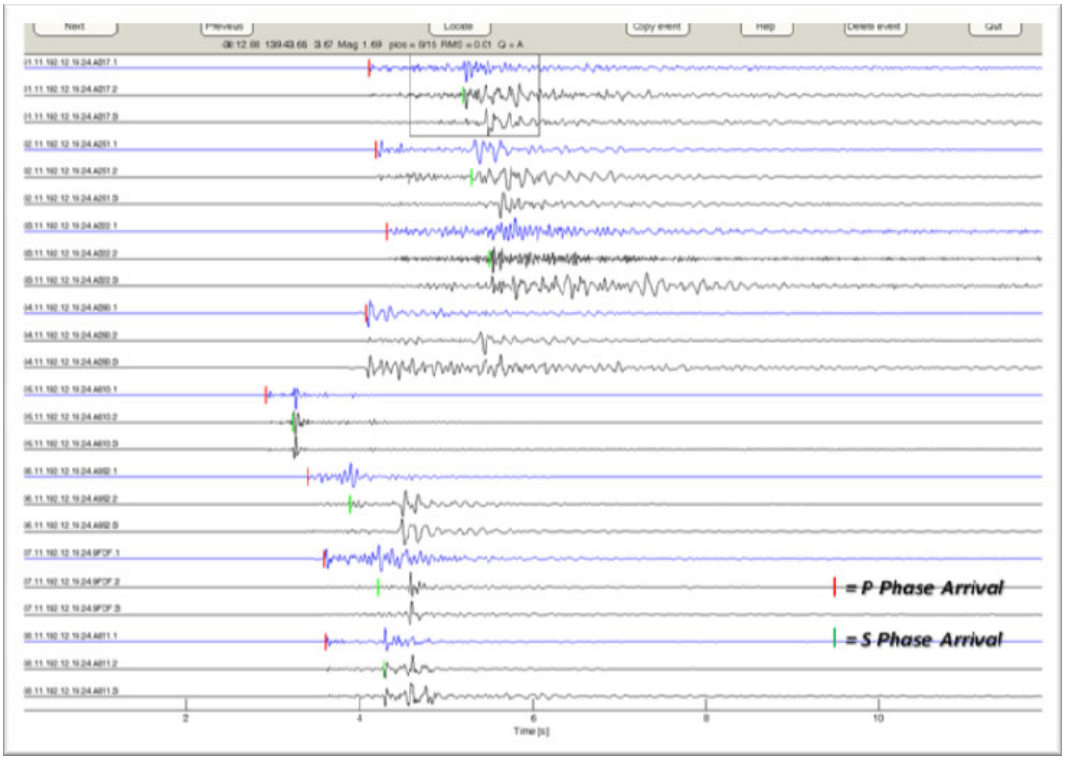

Figure 8: M_W 1.69 event located near the beginning of the main stimulation.

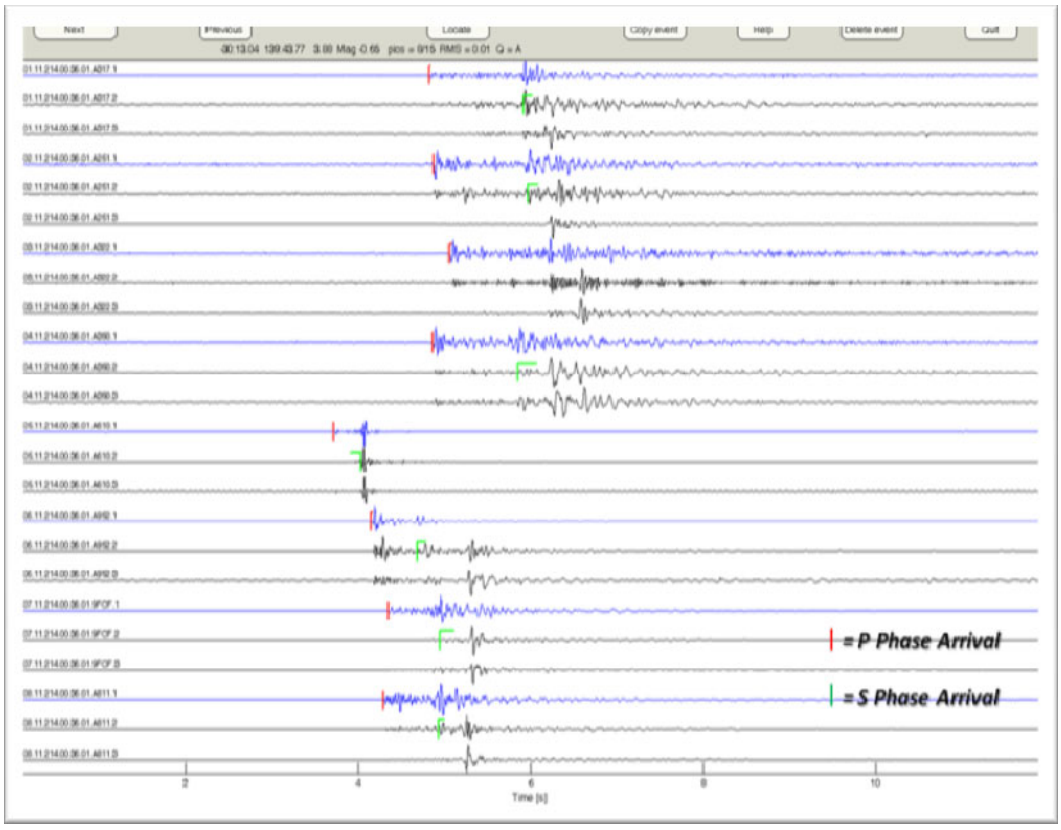

Figure 9: M_W -0.65 event that occurred several days after the stimulation had been completed.

necessary during the fracing operations.

During the real-time monitoring efforts onsite we ran a program (RTP2SEGY) which converted the raw RefTek data packages and converted them to a SEGY data stream and segmented them into 2 min data files. These SEGY files were then processed by MIMO to provide near-real-time event triggering, detection and preliminary locations and magnitudes. Since we had to wait for each 2 min file to be completed, there was a small delay in the event processing. MIMO was

provided by NORSAR and helped give the operators a feel as to the size of the fracture being created in near-real-time. However, because it was set to trigger on very small events and tried to locate them, over 11,000 events were triggered on and located. Of these automatically triggered events, about 5,000 were so small that they were hard to locate and as such made the image harder to read. Post processing of the automated data locations helped to clear up the image of the fracture.

While MIMO was processing data in near-real-time every few hours, IESE onsite staff would download the raw RefTek data and run the raw data through a set of triggering MATLAB algorithms developed by IESE staff. Since we were dealing with a large number of events, the triggering ratios were set to detect the larger events (M_W > -0.5). Triggers were associated into events and then "event files" were generated. These event files were typically only 12 second in length. Figures 8 and 9 show examples of some of the event file waveforms for a M_W 1.67 and M_W -0.65 events respectively. As you can see, even the smallest events recorded by the Paralana MEQ network show a good signal to noise ratio, making it easy to pick the phase arrivals. While on site over 875 events were hand-picked using the IESE software and an additional 1,725 events were hand-picked in post processing.

While on site the Paralana Picking Crew (Figure 10) hand-picked over 875 of the larger events using the IESE software, along with help from the onsite Petratherm staff (Figure 11). An additional 1,725 events were hand-picked in post processing by Michael Hasting to help form the final picture of the fracture pattern generated by the main stimulation.

Figure 12 shows the final event locations after post processing for all hand-picked events. The events in Red are seismic events recorded and located during the actual injection of fluid into the P2 borehole at pressures up to 9,000 psi. The Stimulation, or Injection, of fluids started at about 23:00GMT on the 10th of July and ended at about 09:00GMT on the 15th. The events in Green are seismic events recorded and located after the shut-in of the injection stimulation of P2 with pressures ranging from 9,000 psi to just over 4,000 psi. As shown in Figure 12, many of the events during injection occurred in the center of the seismic swarm, while events after shut-in occurred on the outer edges of this central swarm. The extent of the seismic swarm is approximately 1,350 m in the northeast to southwest and has a vertical extent ranging in depth from 3,400 m to over 4,200 m.

We compared the events from the mini-frac experiment to the start of the main stimulation. Figure 13 shows the locations of the mini-frac events (Red) and events from the first few hours

Figure 10: Paralana picking crew, from left to right, Dr Julie Albaric NORSAR, Alex Miller, Christina Walter, Michael Hasting IESE, Carolin Boese VUC and Nora Voss Hochschule Bochum.

Figure 11: Petratherm onsite crew, from left to right, Peter Reid, Ella Llanos, Mathieu Messeiller

during the main stimulation (Green). As you can see in Figure 13, during the main stimulation seismicity first occurred in the same area as the mini-frac experiment. After a few hours of pumping during the main stimulation, the fracture pattern started extending to the northeast and downward, forming an ellipsoid. Over time, this ellipsoid had a breakout on the fourth day of pumping shooting outwards further to the northeast by about 300-400 m and downward to the northwest by about 250 m. This can be seen clearer in later figures.

Event Locations over Time

As noted above, over 2,600 seismic events were hand-picked and located during and after the main stimulation of P2. Figure 14 shows map view plots by day of these event locations. The events start near the wellbore of P2 and work out in a general northeast trend. On 14 July we start to see the development of events north of the main swarm of events. These events are located deeper and are still basically on strike with the main swarm. There was also a breakout of events to the northeast during a standby where pumping was not taking place but pressure was held on the wellhead. This northeast breakout occurred over a six to eight hour period and almost doubled the fracture area and extending it out by about 300 to 400 meters during that period. Both these breakout are circled on the 14 July figure below. On 16 July, after shut-in, we start to see the development of a small cluster southeast of the main swarm. This cluster becomes more

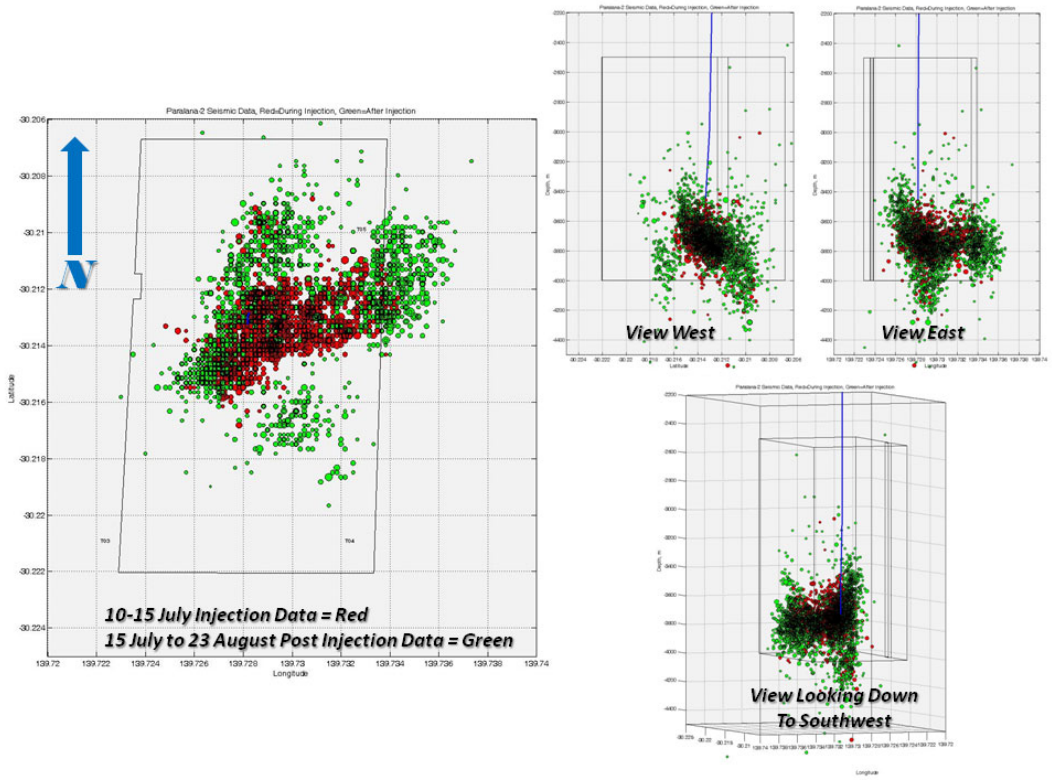

Figure 12: Paralan-2 micro-seismic events during and after stimulation, red = during stimulation, green = post stimulation

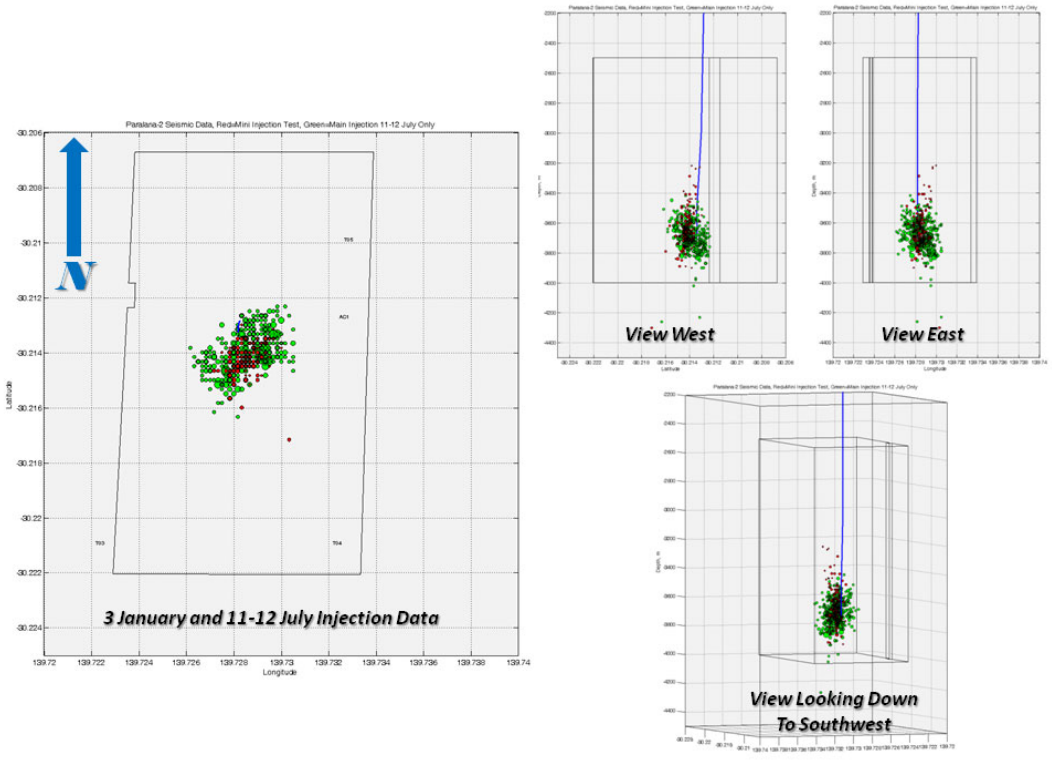

Figure 13: Mini-frac event in red and first few hours of the main-frac in green

pronounced over time and is off the main fracture swarm.

Over time, we see the continued growth of the main swarm to the northeast and southwest, as well as the deeper events located north of the main swarm. We believe the events to the west and east from the 14th of July are part of a second set of fractures. The preliminary frac is orientated on a NE/SW trend. Later events follow a different set of fractures, orientated NNE/SSW. There is a later frac to the SE. This growth, as well as the smaller cluster to the southeast, shows up as four cluster areas in the last plot of Figure 14. From figure 14 you can see that the lateral extent of the

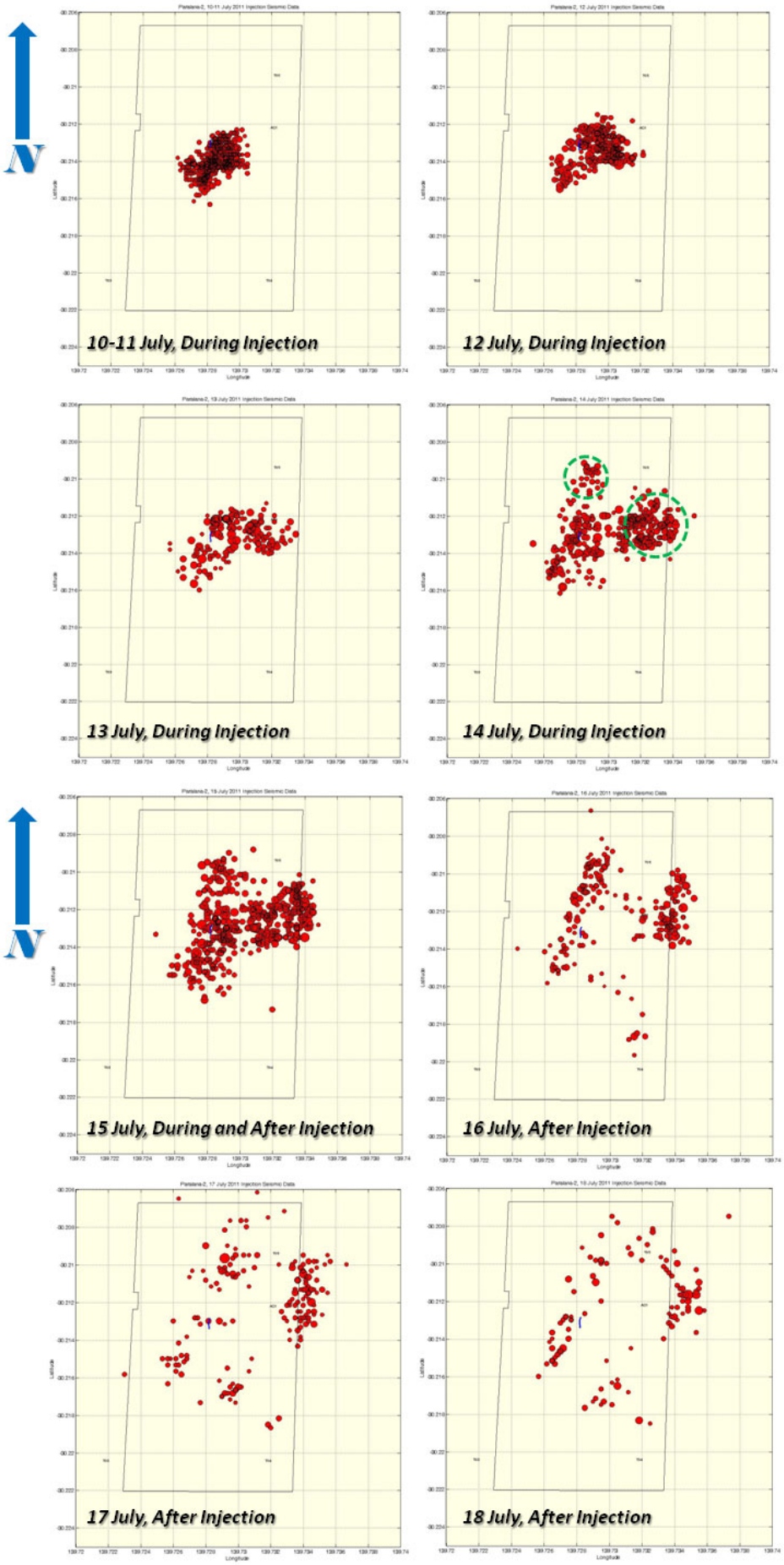

Figure 14: Map plot of hand-picked event location recorded by the Paralana MEQ network during and after stimulation. Note breakout on the 14th, green circles

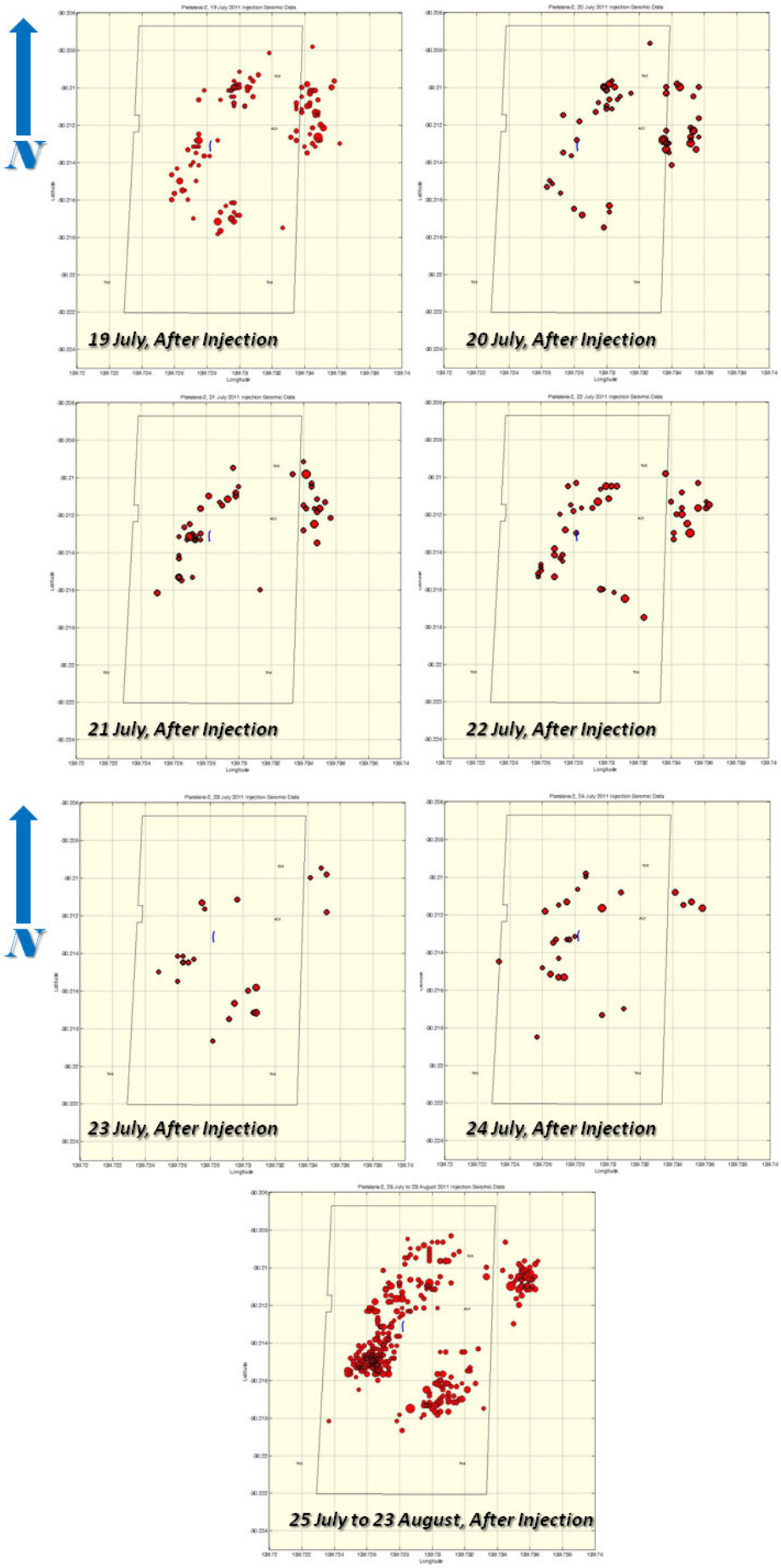

Figure 14 *(continued)*: Map plot of hand-picked event location recorded by the Paralana MEQ network during and after stimulation. Note breakout on the 14th, green circles

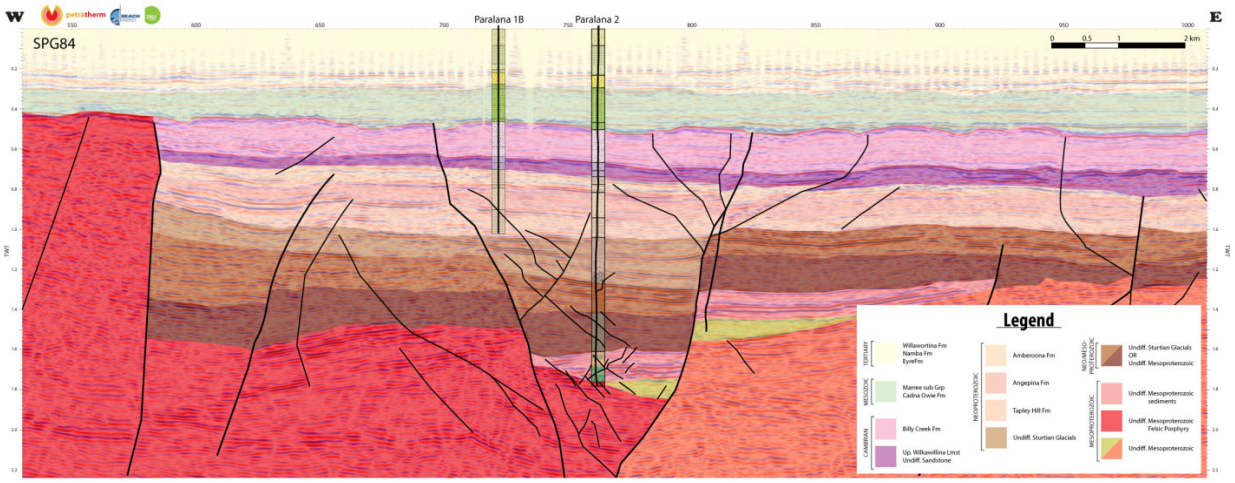

Figure 15: 2D seismic cross section showing mapped faults. Stimulation may have intercepted the main fault to the east of Paralana-2, as well as to the west.

faulting is about 1,350 m long and from figure 12 above you can see that the depth range of fracturing is between 3,400 m and 4,200 m in depth. Based on the SPG84 2D seismic crosssection (Figure 15) it appears that the fracturing to the northeast may have stopped near the mapped fault located about 1km to the east of the P2 trace outlined in the figure. On the 3D model, Figure 16, the frac stops before the main faults mapped on the seismic cross section. The structure acting as a boundary to the East is not the main fault, but is sub parallel to it. As you can see from the figures below, it seems there is still a few hundred meters before hitting the fault.

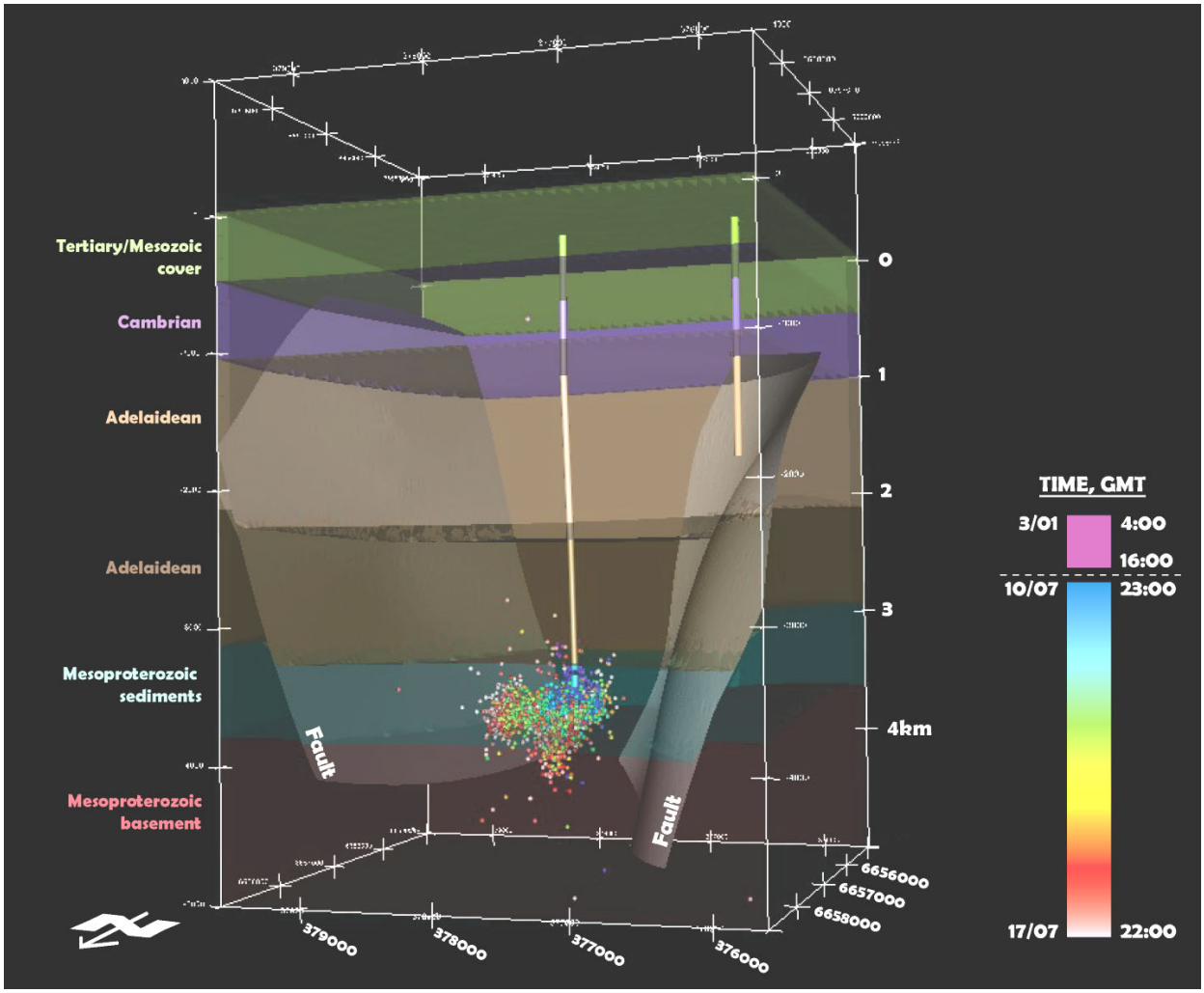

Figure 16: 3D model of the Paralana site

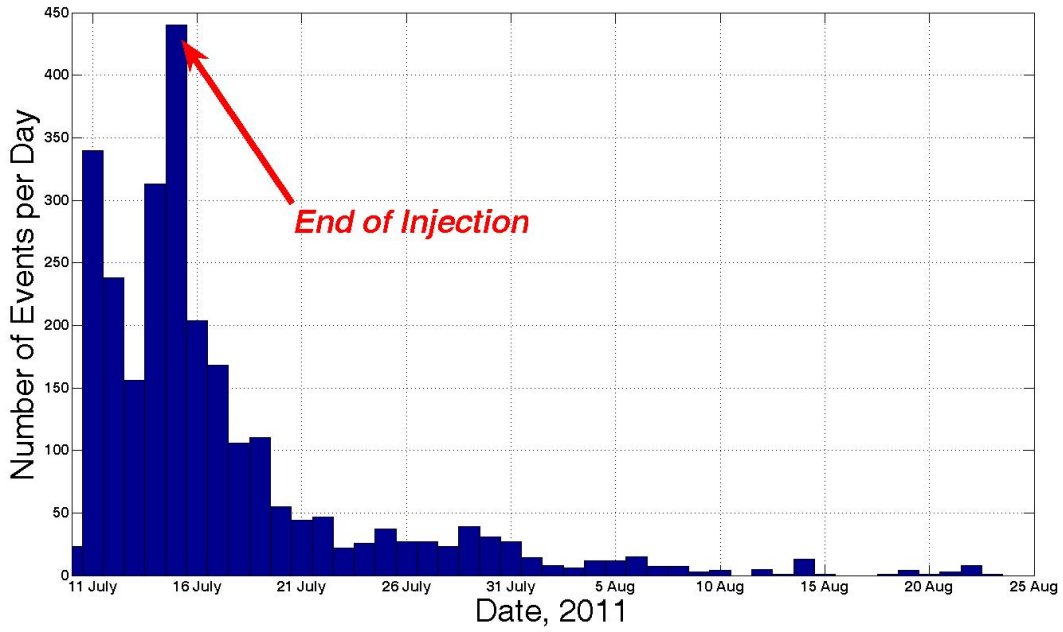

Figure 17: Decay plot of Paralana-2 seismic events over time between 10 July and 23 August

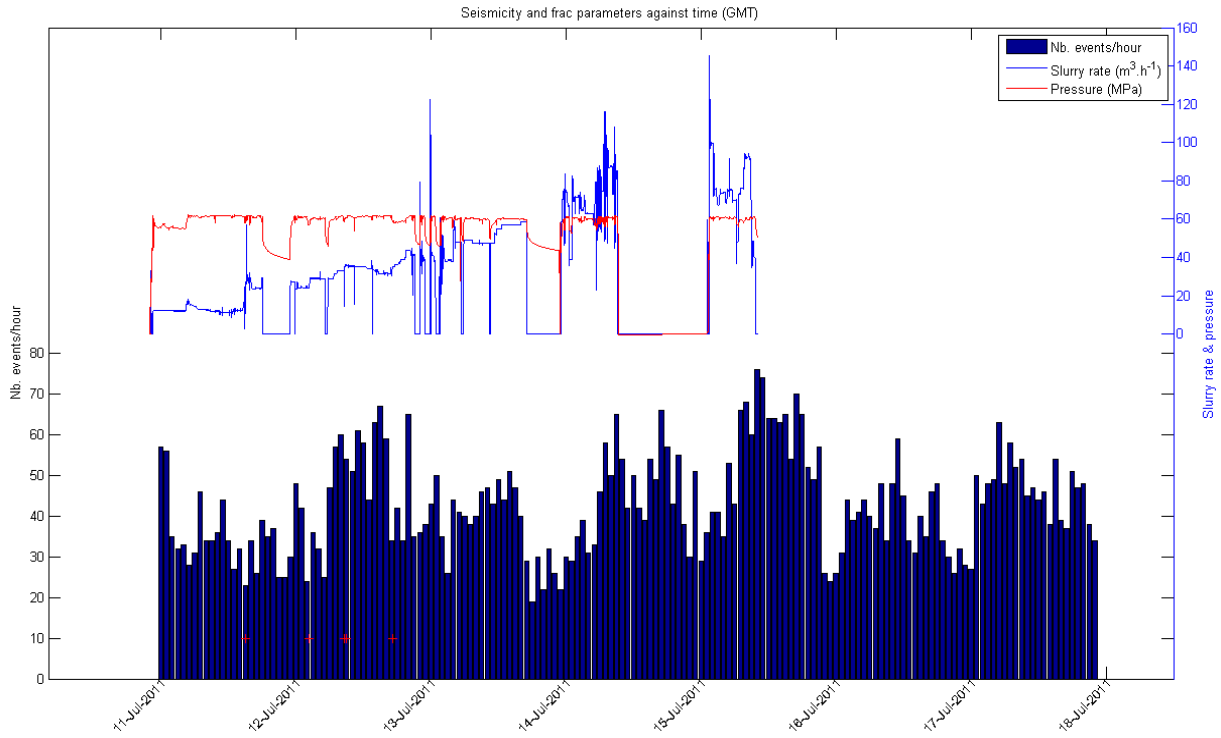

Figure 18: events per hour during and just after the main stimulation as recorded by MIMO

Additionally, the smaller fault to the west of P2 may have stopped the progression of fracturing to the southwest. Additional work is being on the integration of this 2D seismic cross section and the event locations.

In Figure 17 we show the rate of the seismicity during the main stimulation and the decay rate after injection was stopped. As you can see, as of the last data download on 23 August 2011 there were still small events occurring at an average rate of one to two per day. It should be pointed out that figure 17 shows only the events that we were able to locate and that there were about five times as many events that we were not able to locate due to their small size. Figure 18 shows a plot during and just after the main stimulation by hour as recorded by MIMO, along with the pumping pressures and rates provided by Halliburton.

Form the maximum length and depths measured for the fracturing, we get a minimum fracture area of around 875,000 m^2 generated during the main

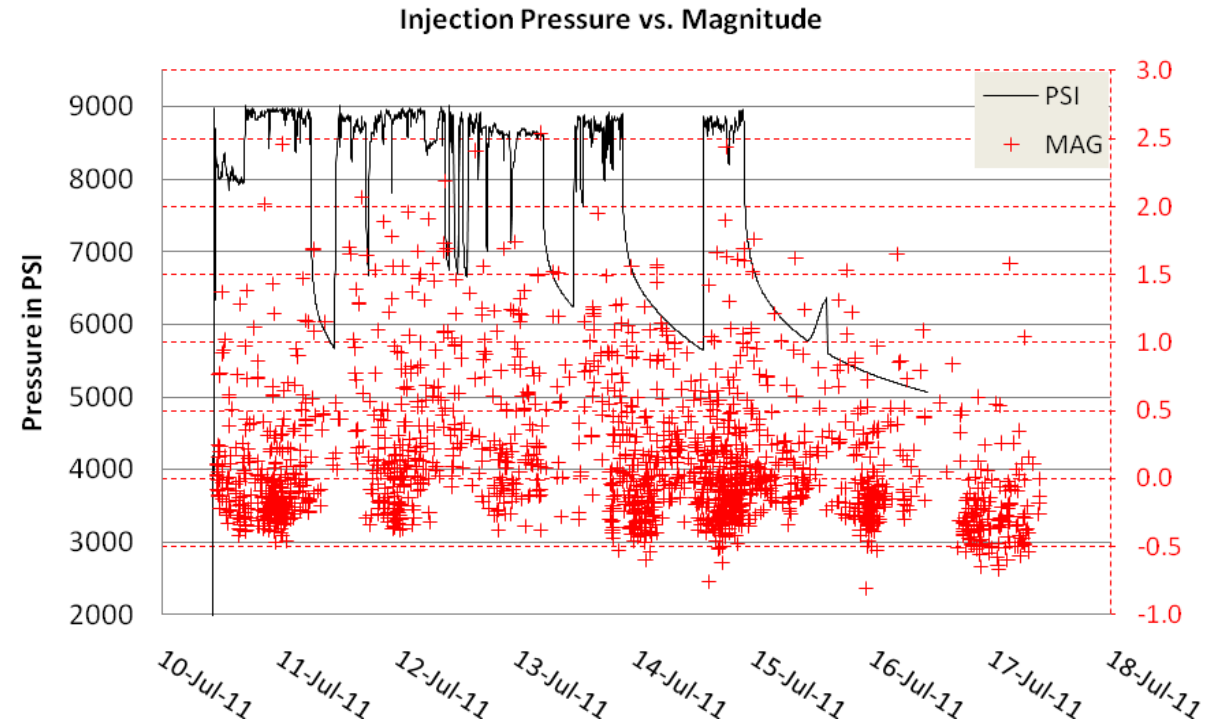

Figure 19: Injection pressure vs. magnitude during and just after pumping. Note lower limit due to triggering threshold used at the time the plot was made; smaller events were still occurring and located in post processing. Actual minimum limit of located events in post processing were ~M_l-1.4.

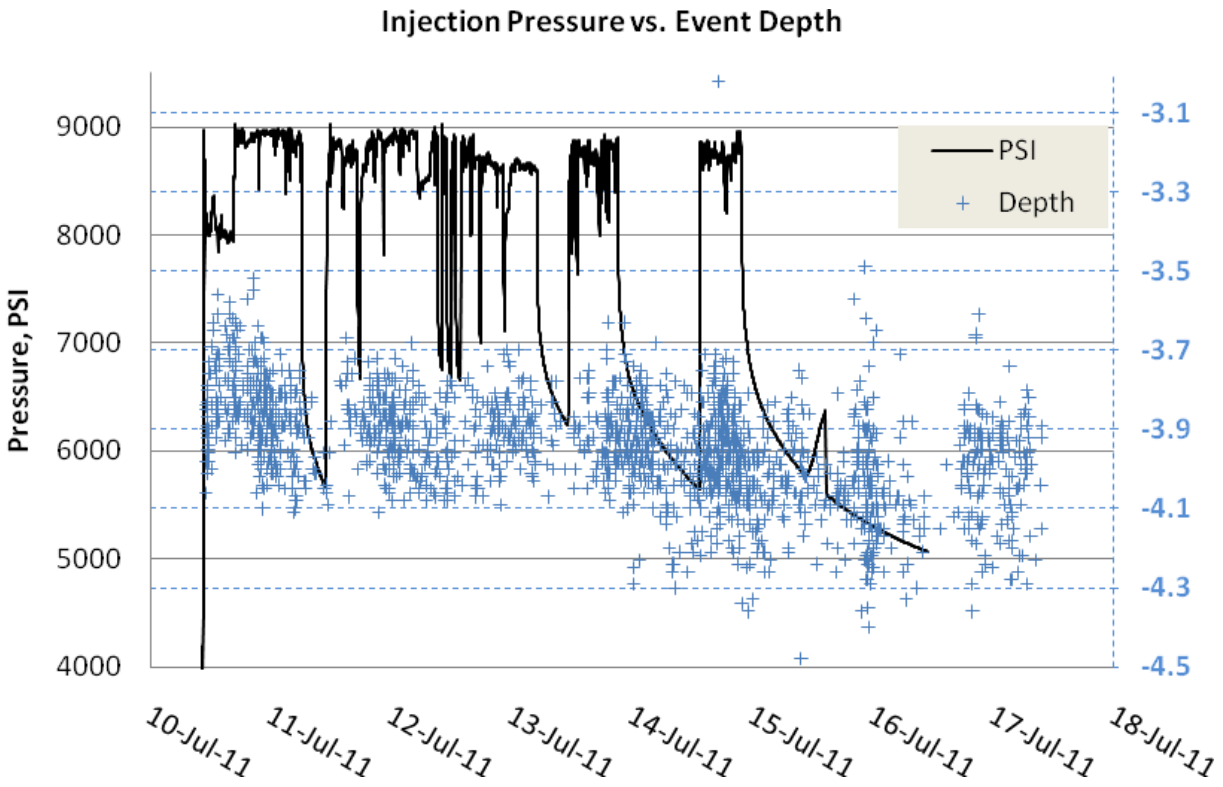

Figure 20: Injection pressure vs. depth during and just after pumping. Same dataset used in Figure 19.

stimulation. Dividing this into the total volume of injection (~3 M litres) we estimated that an average fracture displacement of between 3.5 and 4.5 millimeters would be required to accommodate the entire volume of injection over this area. While fractures may be larger or smaller throughout the volume, this gives us a good first approximation of the fracture density needed to accommodate the fluids. However it should be pointed out that due to the uncertainty

of the event locations we cannot at this point tell if there were multiple parallel fractures occurring during the stimulation. As such, the estimation of 3.5 to 4.5 millimeters should be considered a maximum displacement value and the actual may be, and most likely is, less than this.

Injection Pressure vs. Magnitude and Depth

During the main injection test, of the hand-picked events, only seven events had a magnitude greater than M_W = 2.0, with the largest being a M_W 2.6 which occurred near the end of pumping, on the 13th of July (figure 19). Over 95% of the hand-picked events which occurring during the injection test were smaller than M_W 1.5 and over 50% were smaller than M_W = 0.0. However, if we take into account the results from MIMO, over 90% of the "total" seismic events detected were smaller than M_W 0.0. As can be seen in figure 19, most all seismicity occurred during injection of fluids. It should be pointed out that figure 19 only shows the larger events that IESE triggered on, so the detection threshold limit was set to about M_W = -0.5 in size. Figure 20 shows injection pressure vs. event depth during and just after injection for the same events in figure 19. As can be seen in figure 18, events deepened over time by 250 to 350 meters, with the mean depth of events occurring at about 3.95 km depth.

Seismic Moment vs. Injection Volume

During the main stimulation injection over 19,000 barrels, or just over 3 M litres, of fluid were injected during the five day period between the 11th and 15th of July 2011. Assuming that all the fluids must be accommodated in the opening of fractures, a net volume change must occur. As such, we feel that the only way to accommodate this volume change is through the "opening" of fractures and not through slip along a fault. Using Brune's (1968) formula we can estimate the total seismic moment needed for the opening of the fractures:

$$M_O = \mu * L * W * D$$

Where M_O = the seismic moment, μ = the rigidity of the rock, and L, W and D are the length width and displacement respectively along the fault. If we assume L*W*D = the Volume of Injection then we can rewrite this as:

$$M_O = \mu * \text{Volume of Injection}$$

Using an average value of $\mu = 2.0 \times 10^{11}$ dyne-cm^2 (typical for a depth of 4 to 5 kilometers below surface but can vary from 1.0 to 3.0 x 10^{11} dyne-cm^2) we get a total seismic moment for the opening of the fractures during the injection of ~6.08 x 10^{20} dyne-cm. We can further convert this seismic moment estimation to a moment magnitude, M_W, using the Kanamori's (1983) formula where:

$$M_W = (\log(M_O) - 16.1)/1.5$$

Kanamori formula shows that a M_W = 3.12 is required to accommodate the total volume injected based on the assumed rigidity of 2 x 10^{11} dyne-cm^2. Summing up the total seismic moment from each event in the seismic catalogue of hand-picked events, we get a total seismic moment of M_O = 4.23 x 10^{20} dyne-cm released during the injection, 10 July to 09:00 on the 15th of July. We get a further seismic moment release of M_O = 5.24 x 10 ^{19} dyne-cm after the injection stopped, 09:00 on the 15th of July to 23 August, for a total seismic moment released between 10 July and 23 August of M_O = 4.76 x 10^{20} dyne-cm. Using the Kanamori equations yields a total magnitude of M_W 3.02 for the injection, M_W 2.41 for post injection and M_W 3.05 from 10 July to 23 August 2011. These magnitudes match nicely with the estimation of M_W = 3.12 for the total seismic moment needed to accommodate the injected volume of fluid as we have not included all the smaller events, which will make up much of the difference of M_W = 0.07 difference.

Future Work

Future work on the Paralana-2 seismic data will involve calculation on the first motion for the larger events where we have good phase arrivals. Fault plane solution will be generated and plotted to see how, or if, there are any changes in polarity between injection events, post injection events and for events occurring outside the main fracture area (i.e. cluster to the southeast of the main swarm). We will additionally undertake a study of stress drop for events occurring during and after the injection to see if there are any differences, and if we can connect these differences to different zones, as well as a tomographic inversion of the data to generate a better 3D velocity model around the wellbore.

We will also be looking at any event associated with the first flow testing of the Paralana-2 borehole, which has yet to be completed as of the writing of this paper. Additionally, while not reported in this paper, we will be investigating various late phase arrivals seen in the waveform data. These late phase arrivals most likely have to do with reflections in the subsurface structures and could be used to help map the area around the Paralana-2 borehole. Additionally during the main stimulation a 4D Magnetotelluric (MT) study was being carried out by the University of Adelaide. We plan to integrate our finds with the results of the 4D MT survey.

Conclusions

Based on the seismicity recorded during and after the main injection testing at the Paralana-2 borehole, we can conclude that most of the fluids injected opened fractures. While at this point in time we cannot say if these are new fractures, or

older fractures that have been reopened, the well head pressure post stimulation suggests that there is a connection to a natural fracture network. But at this time we cannot quantify the volume of new fracture vs volume of enhanced existing fractures. However we can conclude that most all the injected fluids did produce a net volume change and went into the opening of fractures. As of this writing, we have yet to find any correlation between pumping rates, pressures and the size of the seismic events, except to say that the largest events occurred during or just after pumping and at pressures near 9,000PSI. However, we can conclude that in the Paralana region it is highly unlikely that a larger seismic event can be generated.

From the seismicity plots, we can see that a fracture system was created that is approximately 1.35km long and ruptured predominantly to the northeast of the borehole, with some extension to the southwest after pumping ceased. We can also see that at least 4 structures have been enhanced by the fracture stimulation. The fracture network extended mostly downward and to the northwest along a steeply dipping plane with a vertical extent of approximately from a depth of 3,400 m to over 4,200 m. Additionally, we estimated that a maximum fracturing displacement of 3.5 to 4.5 millimeters is required to accommodate the injected volume of fluid.

Based on 2D seismic cross section, we think that the northeastern extent of the fracturing stopped at a structure subparallel to the mapped fault defining the eastern boundary of the graben. This structure appears to have acted as a hydrological barrier. Why the events went deeper over time and did not extend to the southwest is still not clear and may have been constrained by another barrier to the southwest of P2 (i.e. the smaller faults mapped in the 2D seismic cross section).

Overall, the authors feel that the injection of +3M litres of fluid into the Paralana-2 borehole was a success as the fracture volume generated was greater than planned by almost 800 %. Additionally, the Paralana-2 borehole took all the fluids injected. Therefore a new geothermal reservoir has been created and/or existing fractured permeability has been enhanced at the Paralana site. Future testing will show whether a true EGS system can be maintained. Testing of the injected fluids through a flow tests will help planning the next steps of the Paralana Geothermal Project by collecting data on pressure, flow rates, temperature and fluid chemistry.

Additionally the Paralana-2 stimulation showed the necessity for having a suitable micro-seismic monitoring network in place before, during and after any wellbore stimulation. Additionally having a real-time network running during the main stimulation should be required for any stimulation project carried out whether for EGS applications or other such operations, i.e. carbon sequestration, coal seam gasification and even oil/gas well fracing. The application of a real-time network during stimulation projects provides the operator, as well as the state/government, real-time feedback on what is happening several kilometers below them.

References

Brune, J., 1968, Seismic Moment, Seismicity, and Rate of Slip along Major Fault Zones, Journal of Geophysical Research, VOL. 73, NO. 2, 777-784pp

Kanamori, H., 1983, Magnitude Scale and Quantification of Earthquakes, Tectonophysics, 93, 185-199pp

Acknowledgements

On behalf of all the authors on this paper I, Michael Hasting, would like thank Petratherm LTD, Beach Energy Limited and TRUEnergy (the JV Partners) for selecting IESE to be part of the Paralana project and the monitoring of the induced seismicity. In particular, I would like to single out Terry Kallis, Managing Director of Petratherm, and Derek Carter, Chairman of Petratherm, as well as the other board members (Simon O'Loughlin, Richard Hillis, Lewis Owens and Richard Bonython) for all their support over the years. I would like to give a special thank you to Louise McAllister, Betina Bendall, and Brett Meredith, former staff members of Petraherm, who were instrumental in the development and deployment of the MEQ array. Additionally, I would like to single out the efforts of Trevor Wadham, Alex Silz and Mark Pitkin of Beach Energy for arranging the actual onsite support for the fracing program at the Paralana-2 site. This was a hard job well done.

I want to thank the entire IESE staff back in Auckland, as well as the staff of Auckland UniServices and the University of Auckland, for all their support in getting this project completed. I would like to acknowledge the efforts of Lianne Skinner for getting all the people where they needed to be and when they needed to be there; this was not an easy job and I thank you for doing it. Additionally, I would like to thank Drs. Peter Malin and Eylon Shalev for their continued support; I/we could not have done it without your input and insight. To Matt, Zhan, Annie, Alex, Christina, Reid, Marcos, Lake, Liam: Alan and others, thanks for getting me the equipment and helping with the deployments when I needed it the most. To Gary Putt, Analeise Murahindy and Kelvin Keh of UniServices: thanks for the contract support and making sure the bills were paid.

I would also like to take the opportunity to personally thank Craig Bartels, President of Heathgate Resources PTY LTD, for letting us stay

at the Beverly Mining camp during the perforation and main fracing operations, as well as the Wooltana and Wertaloona stations, and for supporting the Paralana Geothermal Project. I would also like to thank his staff at Beverly for the great meals, accommodations and conversations. And to Peter and Debbie Moroney, station managers for Wertaloona and Wooltana, and Lindsay and Sian Mengerson of Wooltana; a special thanks for all the, support, chin wags and X^4, may we have many for in the future, next one is on me.

I would like to give a big thank you to the Doug and Marg Spriggs and the entire staff at the Arkaroola Wilderness Sanctuary. Doug and Marg have been a big supporter of the Paralana project over the years and provided sanctuary when Matt Hogg and I were stranded by a flashflood…..many thanks for helping us out, for the loan of the truck and for the great meals. Doug, you still owe me a flight over the Flinders….or maybe it is I who owes you.

I want to thank all the authors on this paper. This was a large and important project and I could not have done any of it without your support. This was truly a global effort with help from Norway, Germany, France, USA, New Zealand, Kenya and Australia. And finally, to my wife, Judith, thanks for putting up with all my long absence while working in the outback of OZ and your support at home. Again thank you to all and to those that I have not mentioned.

QGECE Research on Heat Exchangers

K. Hooman* and Z. Guan

Queensland Geothermal Energy Centre of Excellence, The University of Queensland, Brisbane, Australia

The aim of this paper is to give an overview of the research conducted at QGECE on air-cooled heat exchangers, in general and condensers in particular, for their application in geothermal power plants. The application of metal foam heat exchangers in natural draft dry cooling towers has been studied in detail. Furthermore, the design of a steel cooling tower is proposed and analysed. Solar-enhanced dry cooling tower, a concept put forward by QGECE, is examined here. This paper also provides an update on our research on the issue of fouling and dust deposition on air-cooled heat exchangers.

Keywords: Air-cooled condensers, cooling towers, heat exchangers

Introduction

Air-cooled heat exchangers are the main focus of our research at QGECE mainly because of the scarcity of water or high humidity in locations where the geothermal power plant is built [1, 2]. Air can be either forced through the heat exchanger or driven by buoyancy. Fan-cooled systems can lead to high parasitic losses especially on hot days. This makes Natural Draft Dry Cooling Towers (NDDCT) an ideal option for such cases. The reason for QGECE's interest in NDDCT is obvious. Most of our geothermal resources are located where there is no water. Besides, the thermal efficiency of our binary power plants is so low that we cannot afford fan parasitic losses.

Research activities

This paper offers a brief overview of different research activities conducted at QGECE as follows.

Dust monitoring in Innamincka

One way to increase the air-side heat transfer coefficient is to maximise the surface area density by applying fins with pin pitch of around 2mm. One of the main problems with enhanced surface heat exchanger is the tendency of airborne foreign material to foul its external surface. It is well known that the fouling on heat exchanger surface have a deleterious effect on the performance of enhanced surface heat exchangers. Fouling affects the heat transfer coefficient, reduces air flow rate, and increases energy consumption and the cost of maintenance services.

For instance, Bell and Groll [3] found that the air-side pressure drop could increase up to 200% and heat transfer rate could decrease by more than 10% on the microchannel heat exchangers they tested due to the fouling caused by ASHRAE dust buildup on heat exchanger surfaces. Therefore, a deep understanding of the effects of airborne dust on air-cooled heat exchangers is essential for the future application of such systems in geothermal power plants.

Air-side fouling on heat exchanger surface can be classified into air dust deposition fouling, and the microorganism growth fouling (biofouling). The purpose of this study is focus on the air dust deposition fouling only by monitoring the dust concentration and its particle distribution in Innamincka, one of the Australian geothermal power plant sites. The particle size study will also distinguish the particles which rise from soil dust from those which rise from plant pollen.

The first stage of the study is to install a dust monitoring device in Innamincka to collect real time data of dust concentration, dust sample (for size analysis), wind speed, wind direction and ambient temperature. The monitoring device used in this study is E-Sampler which is a product of Met One Instruments, Inc. sold in Australia by Ecotech. The whole system includes E-Sampler, Solar power panel, wind speed and direction sensor, and mounting frame. The monitoring device has been installed in Innamincka in May as shown in Figure 1.

Figure 2 shows dust concentration, temperature, wind speed and wind direction collected on 22nd May 2011 from about 11:30 am to 14:30 pm. It should be noted that the Innamincka was still in a clear season and the spike shown in the figure were caused by the road dust when trucks drive cross. The north-west wind (300 deg) was blowing with speed of about 6 m/s.

After the real time dust data have been collected on site, concentration, particulate size and chemical composition of the dust will be analysed. Tests on heat exchangers in laboratory will be carried out with the similar dust conditions obtained in site (concentration, size distribution and wind speed). The dust deposition and its effect on the heat exchangers (finned-tune and metal foam) will be identified by measuring the heat transfer rate as well as the external and internal pressure losses of the heat exchanger.

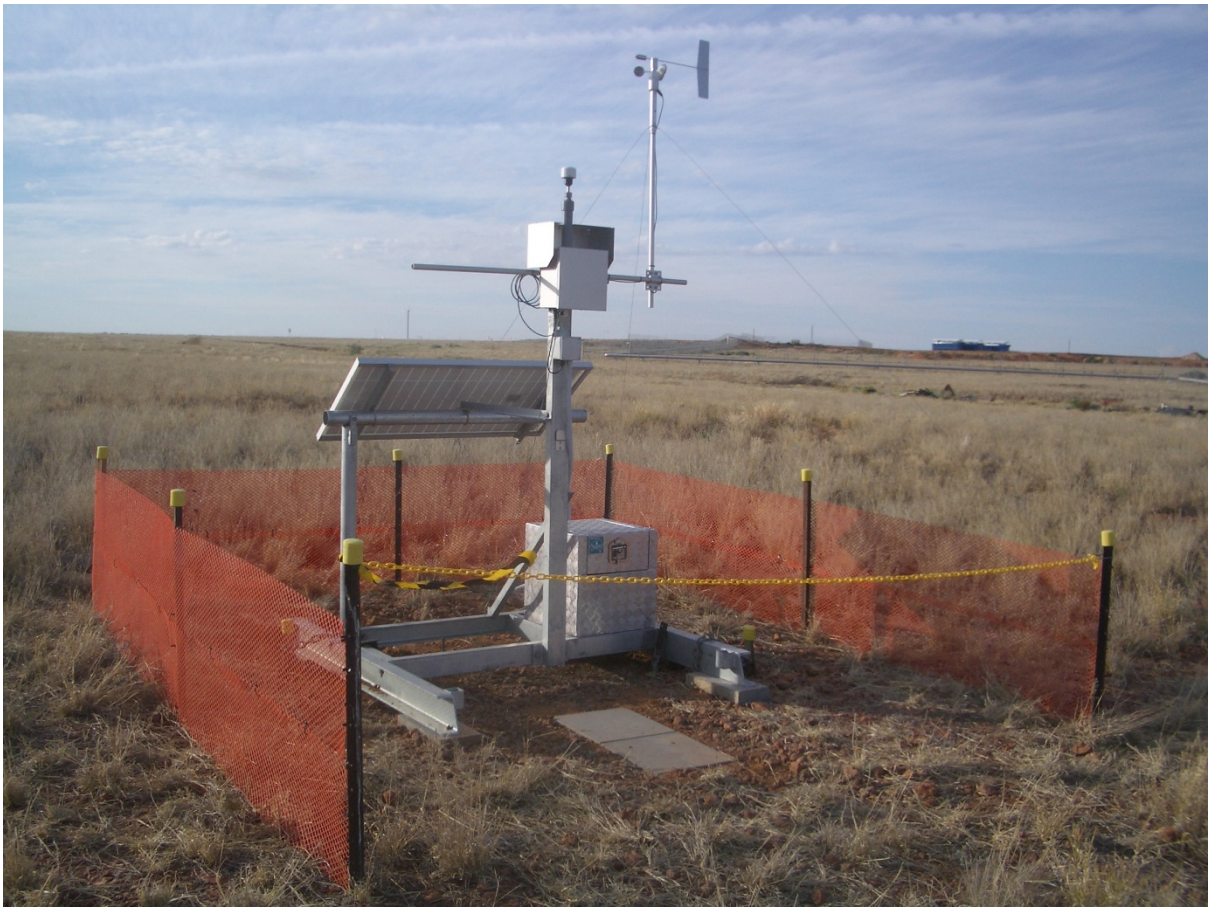

Figure 1: Dust monitoring system installed in Innamincka (Photo provided by Geodynamics Ltd)

Model prediction of the fouling by dust deposition can then be established and verified.

Once the effect of dust on the performance of metal foam heat exchanger has been identified, the final goal of the project is to find methods of mitigation of the dust on the heat exchanger.

Steel tower design

It is either water or air which is mostly used in power plant condensers. From water consumption standpoint, the major categories of cooling systems can be characterised as recirculating wet cooling and dry cooling. The choice among the cooling systems involves a number of tradeoffs. The primary tradeoffs are among water use, environmental effect and the cost of electric power. Since a geothermal power plant has much lower efficiency than its coal-fired counterpart, it would require larger cooling system if the same power is to be generated. For example, a typical geothermal power plant needs to have a heat sink more than five times its generating capacity. If wet cooling system is used, it would consume a larger quantity of water. Gurgenci [4] argues that water consumption was about 0.4kg/s per MW of heat dumped. A 25-MW geothermal power plant running at 15% efficiency will need to dispose of 142 MW of heat. The wet cooling tower water consumption for this plant would be 56.8 kg/s or 1.8 million tonnes per year. It will be either difficult or expensive to get such amount of water for geothermal power plants normally located in arid areas. Therefore, dry cooling seems to be the only option for condensers.

With mechanical draft systems a large portion of power consumption will be required by the fans (about 5-8% of net output). This leaves NDDCTs as cost-saving solutions for the geothermal power plants.

The material of natural cooling tower is mostly made of reinforced concrete (RC) except for a few other options (such as rope and steel cooling towers have been built for seismic active areas). The erection of reinforced concrete tower shell must be with high accuracy in the shape and wall thickness needs to be designed for bending and buckling strength. This requires advanced construction methods and skilled work force. The RC towers are heavy (usually 15 times heaver than steel cooling towers) which increases the costs of material transportation to the remote sites. One of the reasons behind the use of reinforced concrete construction as a method of building natural draft dry cooling towers in coal-fired power plants is the concern about corrosion caused by exposure to some of the elements in the flue gases in combination with the ambient effects. These concerns do not apply to a binary

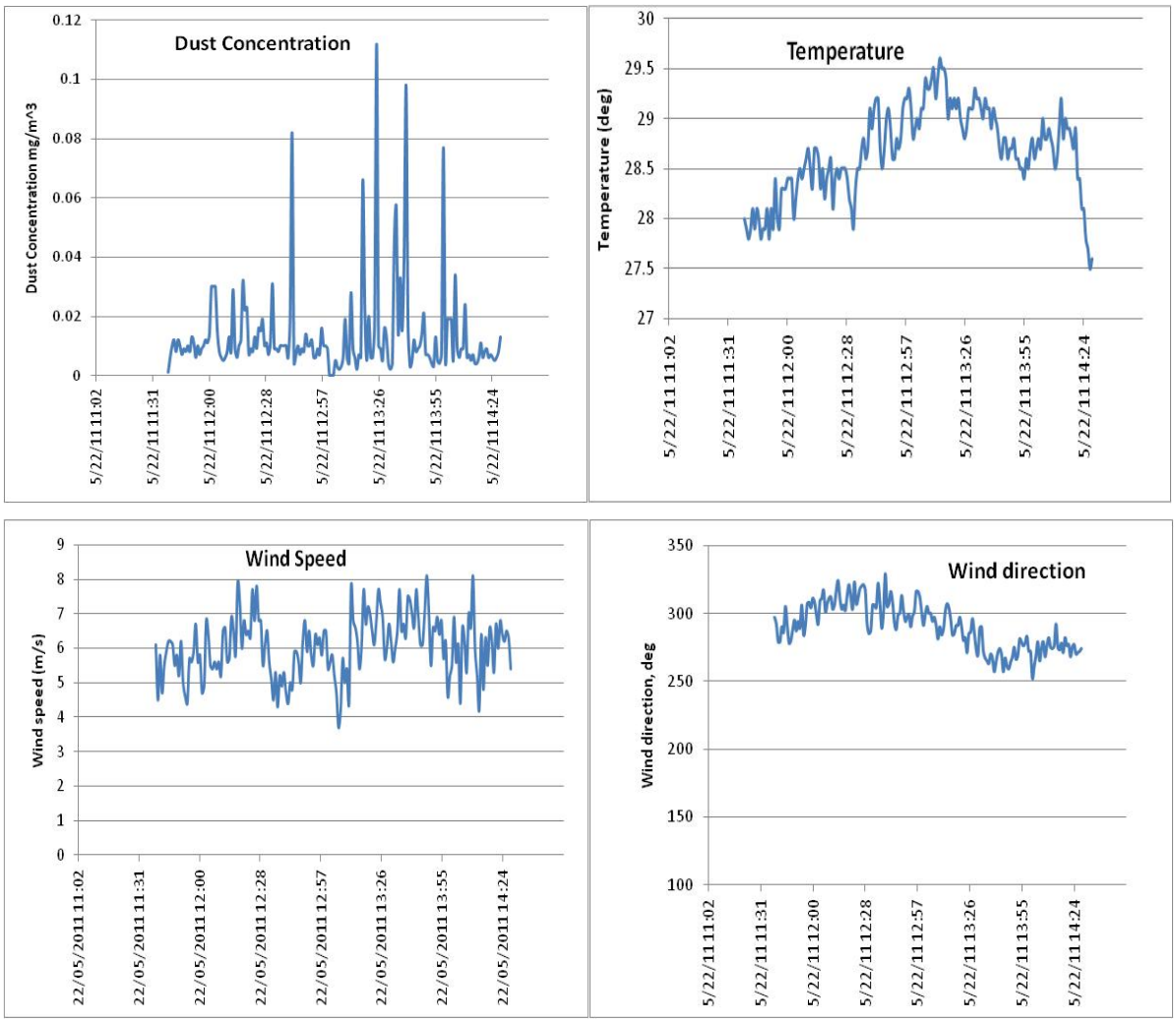

Figure 2 Data collected on 22nd May

geothermal plant. Therefore, the use of steel towers in geothermal plants may offer new options that are not available to fossil fuel power plant designers.

The benefits of using steel cooling tower are the short construction time and less skilled workers requirement. The individual member of the steel cooling tower can be factory made and installed in site quickly. Construction of steel cooling tower does not need highly skilled working force specialised in the same field as the reinforced concrete cooling tower. The erection methods of steel tower are simple and quick which are attractive for the remote areas such as geothermal power plant sites.

QGECE is developing steel cooling tower for geothermal power industries in Australia. One of the footprint designs of this steel cooling tower is based on the 25MW geothermal power plant. Thermal analysis results are shown in Table 1 for the required heat exchangers area and tower dimension.

Based on the tower dimension shown in Table 1, the design and analysis of the steel tower are shown in figures 3-5. The stress and buckling analysis results are based on the maximum pressure caused by wind speed of 162 km/h. The total weight of the steel tower is about 950 t.

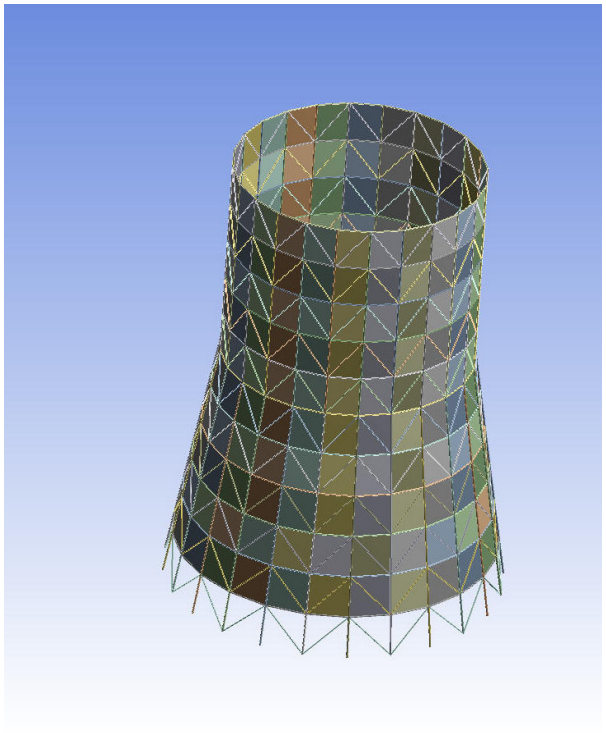

Fig. 3 Geometrical of steel cooling tower for 25MW geothermal power plant

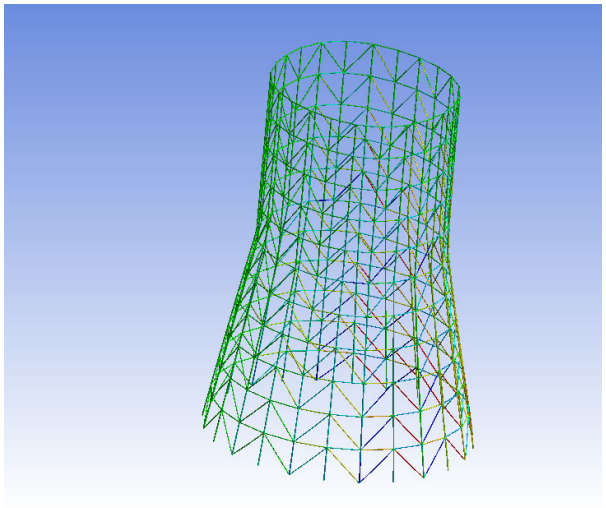

Fig. 4 Stress analysis results

The natural draft dry cooling tower project received a major boost by the QGECE participation in the University of Queensland collaboration with the Solar Dawn consortium in the successful Solar Flagship project to build a 250 MWe solar thermal plant in Chincilla. Initially the Solar Dawn Power Station will incorporate wet cooling (using treated water from coal seam methane) but will need to consider a requirement for transition to air or hybrid cooling in future years. To develop and test options for the consortium towards this end, QGECE will design and build a natural draft dry cooling tower test station on site that will be fed by part of the solar collector array. The objective will be to optimise air and hybrid cooling concepts (including natural draft cooling) for the main Solar Dawn Plant.

Finally, a current QGECE project is considering the use of shallow aquifers as buffer for dumping waste heat. Research this year has been limited to investigation of potential size of such aquifers in areas where hot rock resources are located. The preliminary results suggest significant potential in the use of this concept as a supplement to the above air cooling options.

Solar-enhanced cooling towers

A solar enhanced natural draft dry cooling tower (SENDDCT) would enhance the performance of a normal natural draft dry cooling tower (NDDCT) by adding solar heat after the heat exchangers and thus increases the buoyancy of the air inside

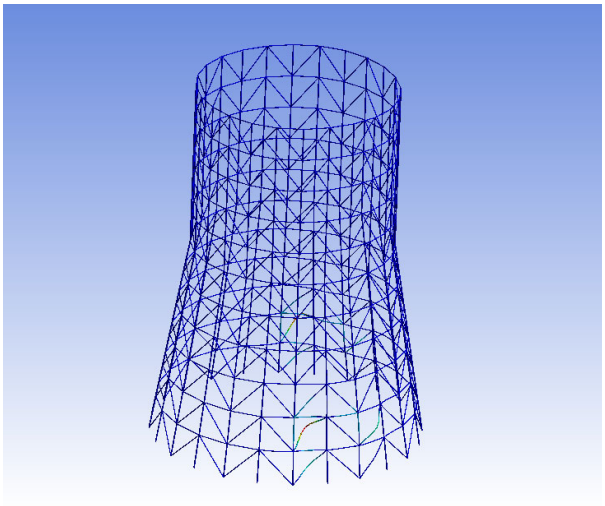

Fig. 5 Buckling analysis results (first mode)

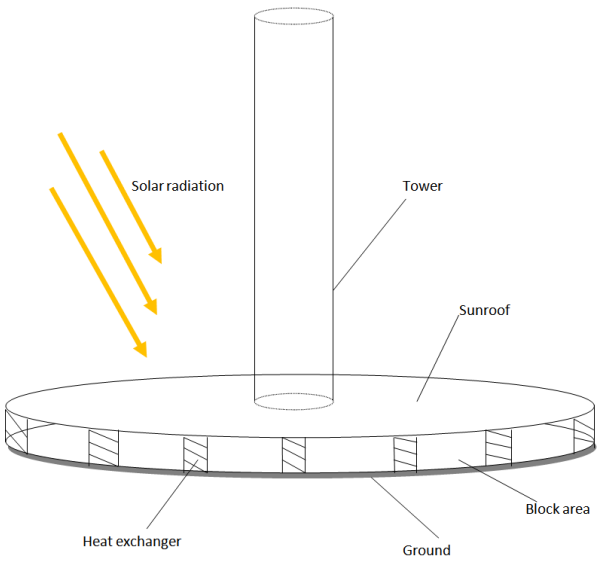

Fig.6 Configuration of solar enhanced natural draft dry cooling tower

Table 1. Thermal analysis results for the design point of 25MW geothermal power plant

	Case I ITD = 30	Case II ITD = 25	Case III ITD = 20
Tai	20	20	20
Twi	50	45	40
Q (MW)	142	142	142
P (MW)	25	25	25
Mw (kg/s) Water	4380	4700	5600
Ma (kg/s) Air	6540	8050	10000
No. of tubes (15m)	12680	16100	21750
Tube bundles 2.52x15m 4 rows	76	96	130
Total fin tube area (m^2)	2868	3638	4915
Tower height (m)	100	110	120
Tower inlet diameter (m)	60	70	80
Tower outlet diameter (m)	60	60	65

the tower and helps to drive more air through the heat exchangers. The improved heat transfer rates caused by the higher air flow rates can be exploited to build a cooling system with either less heat exchanger areas or smaller tower sizes resulting in a reduced capital cost.

Three major components for a solar enhanced natural draft dry cooling tower are the heat exchangers, the solar collector (sunroof and ground), and the tower as shown in figure 6. The sunroof is a transparent circular roof which is placed around the foot of the tower at the tower inlet height. Heat exchangers are placed vertically along the outer edge of the solar collector. As sun heats the sun roof, the air under the roof is heated. Warm air naturally rises through the tower and fresh air is sucked in thus providing a cooling air flow through the heat exchanger bundles. The total heat exchange area may be less than the area offered at the perimeter of the solar collector. If this is the case, the rest of the perimeter of the solar collector needs to be blocked.

The performance of this new design concept has been compared with the one of conventional natural draft cooling tower through the tower height needed for certain heat dumped as shown

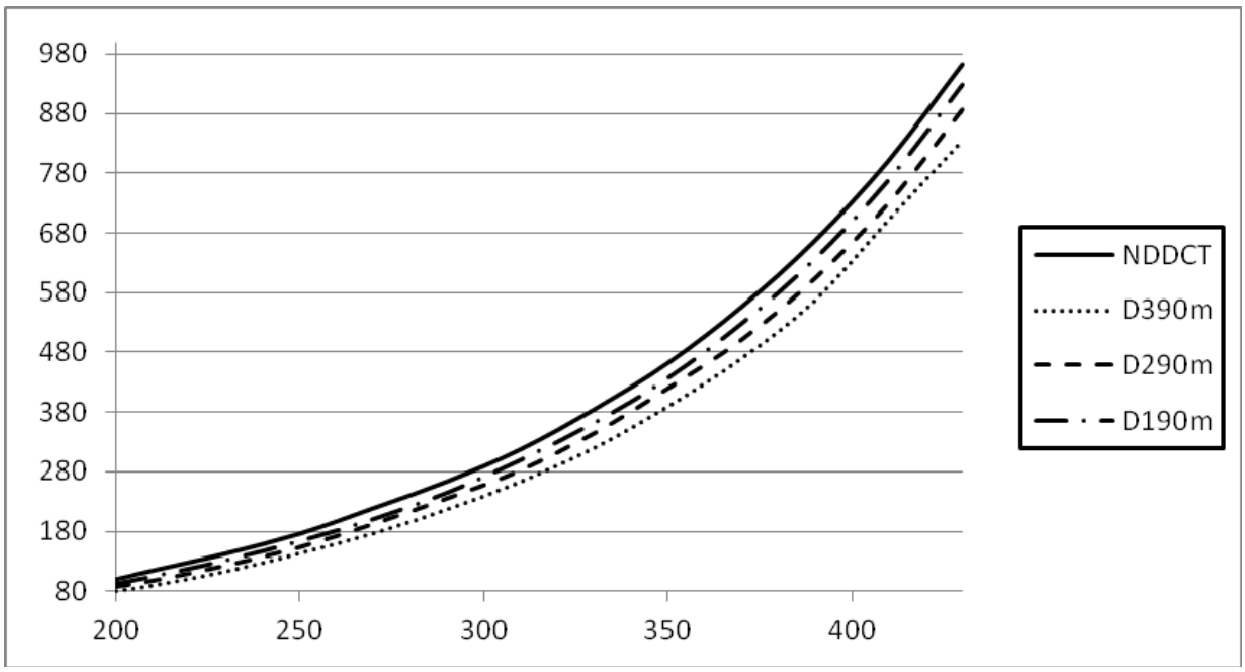

Fig.7 Tower height comparison required for both towers

Figure 8 The lab scale model for a NDDCT

in figure 7. It clearly shows that the tower height for solar enhanced cooling tower is smaller than the height required for the conventional natural draft cooling tower.

Scaling of cooling towers

QGECE is investigating efficient heat exchangers to reduce the cost of towers. This would have been impossible unless a proper test bed is provided. In doing so, a 2 m height cooling tower is built and is operational at our QGECE lab, see Fig. 8. The tower has a square cross-section with a base-throat area ratio of 2. Initial experiments are conducted to evaluate the tower frictional (shape) resistance, i.e. by excluding the heat exchanger resistances. At the same time, a 3D numerical model is built so that parametric study of the problem is possible [5]. Parallel to these tests and simulations a theoretical model is developed to shed some light on the scaling of such NDDCTs [6].

Metal foam heat exchangers

A new design for tubes in air-cooled condensers is currently being examined at QGECE. The idea is to replace the fins by a layer of metal foams, see figure 9, to increase the heat transfer area and, hence, reduce the total tube numbers and heat exchanger size/cost [2]. This can significantly reduce the cost as an efficient heat exchanger will lead to a less expensive (and shorter) cooling tower. A photo of our test section is presented in figure 9.

Conclusion

A summary of our current research activities on air-cooled heat exchangers at QGECE is presented. Numerical, theoretical, and experimental approaches have been undertaken to tackle the problems addressed here. Some new concepts proposed by QGECE are examined and analysed. Quantitative results will be presented in detail during the oral presentation.

References

[1] Kroger DG. Air-cooled heat exchangers and cooling towers Tulsa, Okl.: Pennwell Corp., 2004.

[2] Hooman K, Gurgenci H. Different heat exchanger options for natural draft cooling towers. World Geothermal Congress Nusa Dua, Bali, Indonesia 2010: Paper # 2633.

[3] Ian H. Bell and Eckhard A. Groll, 2011, Experimental comparison of the impact of air-side particulate fouling on the thermo-hydraulic performance of microchannel and plate-fin heat exchangers, Purdue e-Pubs.

[4] Gurgenci, H. 2010. www.uq.edu.au/geothermal/latest-news-and-highlights/Hal Gurgenci's geothermal blog.

[5] Hooman K, Gurgenci H. Porous Medium Modeling of Air-Cooled Condensers. Transport in Porous Media; 84 (2010) 257-273.

[6] Hooman K. Dry cooling towers as condensers for geothermal power plants. International Communications in Heat and Mass Transfer; 37 (2010) 1215-1220

What Does the Future Hold for Geothermal Energy?

Roland N. Horne

horne@stanford.edu

Stanford Geothermal Program

Energy Resources Engineering Department, Stanford University, CA 94305-2220, USA

The past five years have brought considerable changes to geothermal development. Historically high oil prices since 2005 have focused attention on renewable energy, supported by a global ambition to address greenhouse gas reduction. Geothermal developments have accelerated in many parts of the world, both in countries (such as New Zealand, Indonesia and the US) that have a traditional interest in "conventional" geothermal resources, as well as countries without a historical interest in geothermal energy (such as Australia and Germany). Some new developments have followed well-worn paths using conventional hydrothermal resources in volcanic regions, while others have struck out in new directions in Enhanced Geothermal System (EGS) projects in nonvolcanic regions. Technology has allowed for developments of conventional resources with lower temperature, restricted water access, and constrained surface utilisation. EGS projects have launched in a variety of different directions and places (the US currently has six active EGS developments).

In this context, the future expansion of geothermal developments depends on exploring for new fields and overcoming technical challenges in known but not-yet-exploited fields. Two issues that are currently being addressed by the world geothermal community are: (1) the "productivity gap" in the exploitation of fields that are too hot for downhole pumps, but too cool for flash production, (2) the development of reliable EGS development procedures that can ensure sustainable flow rates and assure the public that induced seismicity will not be a problem.

Keywords: future, well productivity, EGS.

1. Introduction

The past five years have represented a boom time for geothermal energy development in the world, with substantial interest and activity in many countries. As an example, the resurgence of interest in geothermal energy is evident in Figure 1, from the Geothermal Energy Association (GEA) April 2011 Annual U.S. Geothermal Power Production and Development Report. Although slowed somewhat by the financial crisis of 2008-2009, installed capacity in the USA rose steadily during this period.

Furthermore, it is clear that this new development was not merely “sweeping up the crumbs” – projects that had been set aside for later years before – as Figure 2 shows, there is a large number of projects under development in areas that are classified as “unproduced”. These are defined by GEA (2011) as:

> *“Conventional Hydrothermal (Un-produced Resource): the development of a geothermal resource where levels of geothermal reservoir temperature and reservoir flow capacity are naturally sufficient to produce electricity and where development of the geothermal reservoir has not previously occurred to the extent that it supported the operation of geothermal power plant(s).”*

So the 111 projects in conventional/unproduced resources represent exploration and development in new areas not currently under production.

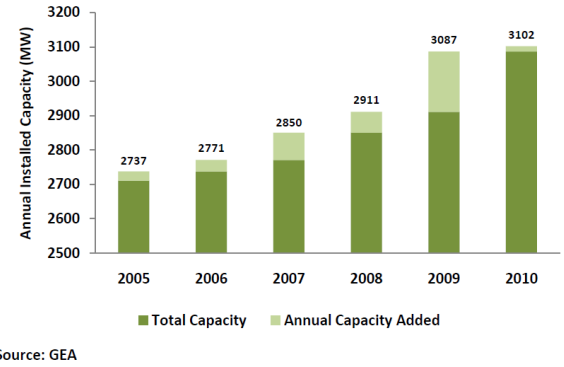

Figure 1: Installed capacity in the USA, 2005-2010, from GEA, April 2011.

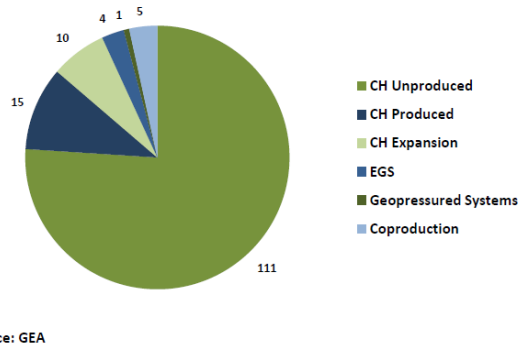

Figure 2: A total of 146 projects under development in the USA, and their category (CH = conventional hydrothermal), from GEA, April 2011.

Similar expansions have been seen in many other countries, with a total increase of installed capacity worldwide of 1782 MWe (from 8933 to 10,715 MWe) between 2005 and 2010 (Bertani, 2010). Figure 3, from Bertani (2010), shows the increase in installed capacity and produced

electricity from 1950 to 2010, with a projection to 2015. Although the 2015 figure of 18,500 MWe is a projection only, the number of projects under development (as shown for example in Figure 2) leads credence to the number. It should also be noted that historically high oil prices in the early 1980s also stimulated a substantial expansion of geothermal capacity.

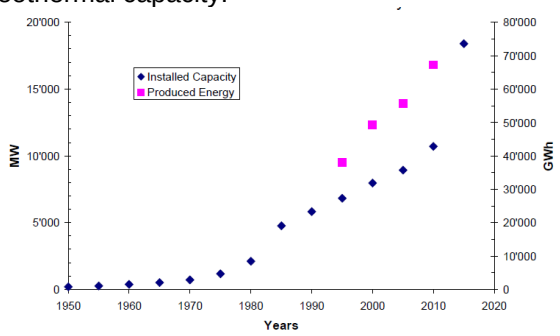

Figure 3: World geothermal electricity, installed capacity (MW) and produced electricity (GWh), 2005-2010, from Bertani (2010).

This renewed interest is the result world economic and political forces (mainly increased oil price and moral preference for renewable energy) combined with advances in technology that make geothermal energy more accessible (for example, power plant efficiency increases and utilisation of lower temperature fluids).
Innovations in utilisation technologies have included:

- Increasing use of innovative power plants, often by marrying flash plants with binary bottoming cycles. The result is an increased recovery of the thermal energy in the resource.

- Use of fluids of lower temperature, with refined binary cycle power plants. The result is a wider availability of producible resources. A noteworthy example is the 250 kW organic Rankine cycle plant in Chena Hot Springs, Alaska, which produces electricity from a very low temperature (74°C) geothermal resource (Lund et al., 2010).

- Reservoir enhancement techniques. The world has seen the first commercial Enhanced Geothermal System (EGS) plant at Landau, Germany, started in 2008 (Schellschmidt et al., 2010). Multiple EGS projects are now under development in the world, including six in the US alone.

This paper will discuss these three issues, as a path to understanding where they may take the geothermal energy industry in the future.

2. Innovative Plants

For many years, geothermal power plants had a degree of uniformity based on the adoption of strategies that had worked in the small number of flash plants in early developments. Based on experience at The Geysers, in the US the 55 MW plant came to be accepted as “normal” in size. Apparently this was often found to be a comfortably sized unit in many other parts of the world too. Based on reservoir temperatures common at the time, turbine inlet pressures tended to be in the vicinity of 600 kPa.

However in the more recent past, considerably wider variation in the design strategy of the plant has been seen. A good example is the combined cycle plant at Rotokawa in New Zealand (Figure 4), which was one of the first developments built with a binary bottoming cycles supplied from the exhaust of a steam flash plant. This plant combines a back pressure steam turbine with a very high inlet pressure (2550 kPa) with three binary plants into which the exit steam is sent (Legmann and Sullivan, 2003). This combined cycle unit has a steam consumption of around 5 kg/kWhr, which is very favourable compared to steam consumption at The Geysers of about 8 kg/kWhr (computed from data shown in Sanyal and Enedy, 2011) or around 9 kg/kWhr at Ahuachapán, El Salvador (Handal et al., 2007).

Combinations of binary and flash plants are now found in several other projects too.

Figure 4: Rotokawa geothermal plant, a combined cycle flash-steam/binary station (photo: Mighty River Power).

The innovation already extends beyond the combination of different geothermal generation technologies. The past few years has seen an interest in the combination of geothermal generation with other sources, for example the combined geothermal-solar operation at Ahuachapán, El Salvador (Handal et al., 2007, and Alvarenga et al., 2008), and one announced in August 2011 by ENEL Green Power for the Stillwater project in Nevada (see also Greenhut et al., 2010). The combination of geothermal with solar thermal energy provides an opportunity to raise source fluid temperatures and even out the intermittency in insolation.

In the future, energy combinations, such as the electricity and hot water supply projects common in Iceland, will certainly continue the innovation.

3. Lower Resource Temperatures

The increasingly common use of binary power plants has expanded the range of geothermal resource temperatures from which electricity can be generated usefully. Although not yet common, there are specific examples of isolated electrical loads such as at Chena Hot Springs, Alaska, shown in Figure 5, which produces electricity from a very low temperature (74°C) geothermal resource (Lund et al., 2010). Chena Hot Springs is more than 100 km from the closest electrical transmission line, so would otherwise be dependent on diesel-fuelled generation. In fact, there are many off-grid communities in the state of Alaska that could benefit from geothermal electricity generation in place of diesel fuel that is supplied at extremely high cost due to their remoteness. Similar advantages are to be gained in island communities such as in the Caribbean (Huttrer, 2010). Figure 6 shows an active drilling program at Akutan Island in the Aleutian chain of Alaska (Kolker and Mann, 2011).

Figure 5: Binary power plant at Chena Hot Springs, Alaska. Photo: Roland Horne, 2007.

Figure 6: Drilling at Akutan, Alaska, from Kolker and Mann (2011). Photo: Amanda Kolker, 2010.

As electricity production from lower temperatures becomes more feasible, another intriguing possibility is the recovery of geothermal energy from coproduced fluids, for example those brought to the surface with oilfield water. Pilot projects are already in operation in Wyoming (Johnson and Walker, 2010) and Huabei, China (Gong et al., 2011). Figure 7, from Johnson and Walker (2010) shows the organic Rankine cycle plant in Wyoming, which has been in operation since September 2008. The worldwide oil industry produces as much as 300 million barrels of water per day (540,000 kg/sec) and in many places the temperatures are within the range of operational geothermal power plants. Oil field operations are often also substantial consumers of electrical power, so the generation of electricity local to the operation is of particular benefit.

Figure 7: Binary plant recovering heat from coproduced oilfield water at Rocky Mountain Oilfield Testing Center RMOTC in Wyoming, Johnson and Walker (2010).

The importance of resource temperature is somewhat more complex than appears at first glance. Although in simple terms it is true that hotter is better, there remains a “hole” in resource accessibility, due to the fact that self-flowing wells drop substantially in productivity at temperatures below a certain range, while downhole pumps are only effective up to a specific temperature range. This was described very succinctly by Sanyal et al., (2007), who illustrate the “hole” in a figure repeated here as Figure 8. As shown in the figure, there is a gap that lies roughly between 190 and 220°C, within which neither pumped nor self-flowing wells are completely effective.

This resource temperature gap represents a technological challenge that is in the process of being addressed by the geothermal industry.

4. Enhanced Geothermal Systems

Although new conventional geothermal reservoirs are being both discovered and exploited, the fact remains that the likelihood of major conventional resource discoveries is diminished. The world is not likely to find another resource like The Geysers. So the prospect for major expansion of geothermal development lies in Enhanced Geothermal Systems (EGS).

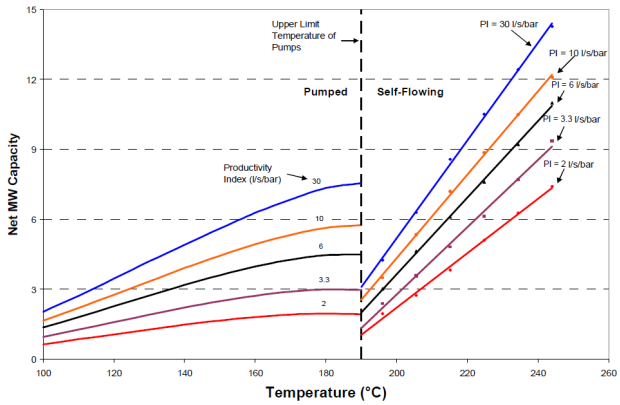

Figure 8: Net MW capacity of a geothermal well as a function of temperature, from Sanyal et al. (2007).

The "MIT Report" of Tester et al. (2007) undertook an extensive study of the promise of EGS for the USA, and this document proved very influential in swaying political and investment favor towards EGS. In the four years that have followed, at least six EGS projects have been initiated in the US, as well as several in other countries. Although some may choose to argue about the definition of EGS, by the definition of many the first commercial EGS development has been in operation at Landau in Germany since 2008 (Schellschmidt et al., 2010).

The successful stimulation of hot rock has been achieved in many "research" EGS projects dating back to the Fenton Hill, New Mexico, project in the 1970s. However it is only as the number of projects has grown that a more routine understanding of their creation and management has expanded.

In August 2011, Doone Wyborn presented a summary of experiences in EGS stimulations, providing a very useful side-by-side comparison of EGS projects in different environments. Some of Wyborn's tables are reproduced here, with permission. It is important to note that success can be claimed if considerable seismic activity was achieved with water injection at pressures below the minimum principal stress at the particular site. This process has been well known for some time (Pine and Batchelor, 1984).

Table 1 reproduces Wyborn's summary of projects that reported both successful stimulation and production. Table 2 reproduces his summary of stimulation projects that did not have production or had minimal production.

It is also instructive to compare projects in granite to projects in other kinds of rocks (generally either sandstone or volcanics). In general the experiences of granite EGS stimulations (which have been the most common) differ from fracture stimulation in sandstones and volcanic tuffs.

The stimulation at Groß Schönebeck in Germany, reported by Zimmermann et al. (2008) was an especially interesting one in that the fracturing involved distinct and independent injections into one formation that was sandstone and another that was volcanic. In this case the stimulation treatment was a propped fracture, presumably tensile, unlike the unpropped, slip fractures generally created in granite. Zimmermann et al. (2010) summarised the results, including that of a

Project	Years	Rock type	Depth (m)	Production Temperature (°C)	Production (l/s)
Fenton Hill, New Mexico	72-96	granodiorite	3,600	191	13
Rosemanowes UK	78-91	granite	2,200	70	16
Le Mayet, France	84-94	granite	800	22	5.2
Hijiori, Japan	85-02	tonalite	2,200	180	12.8
Soultz, France	87-95	granite	3,800	135	21
Soultz	96-present	granite	5,000	155	25
Landau, Germany	05 - present	granite/faults	2,600	160	76
Habanero, South Aust	03-present	granite	4,250	212	30

Table 1: EGS projects with successful stimulation and production, from Doone Wyborn (August 2011).

Project	Years	Rock type	Depth	Temperature of reservoir
Falkenberg Germany	78-85	granite	250	13
Hachimantai, Japan	83-88	granodiorite	400	60
Fjalbacka, Sweden	84-89	granite	500	15
Ogachi, Japan	89-01	tonalite	1000	250
Basel, Switzerland		Granite	4500	180
Bad Urach, Germany	06-08	Granite gneiss	4500	180
Jolokia 1	09-10	granite	4500	265

Table 2: EGS projects with successful stimulation (no production reported), from Doone Wyborn (August 2011).

subsequent acidisation treatment. Well productivity index was increased from 2.4 m^3/(hr.MPa) before stimulation to 10.1 m^3/(hr.MPa) by hydraulic fracturing, and to around 15 m^3/(hr.MPa) by acidisation (Zimmermann et al., 2010, quote this later number as tentative). Following the stimulation, the flow rate was around 16 kg/sec.

A hydraulic stimulation at Berlin, El Salvador, was into volcanic rocks (not granite) and has been described by Rivas and Torres (2003). Injectivity was improved only modestly, from 0.67 to 0.84 kg/(sec.bar) (0.24 to 0.30 m^3/(hr.MPa)). Microseismicity was observed, but was not major.

Although EGS developments continue to show promise, there remain several technological advances to be made. The MIT Report (Tester et al., 2007) made projections of EGS penetration into the US energy mix, based among other things on a flow rate per well of around 80 kg/sec (l/s). An examination of Table 1 shows that only one EGS project (Landau) has achieved such a flow rate. Improvement of well production rates will be dependent of making more connections in the reservoir, by better control of the fracturing process, for example by use of diverting agents to produce multiple fractures (Petty et al., 2011). Such efforts are ongoing.

Conclusion

Geothermal energy has undergone a renaissance over the past ten years, as many new technologies and new countries have joined the industry. The use of innovative hybrid plants, lower resource temperatures and enhanced reservoir stimulation has made geothermal energy accessible in a much wider variety of places.

Acknowledgements

The author would like to thank those who granted permission for the inclusion of their results, diagrams and photographs in this paper.

References

Y. Alvarenga, S. Handal, and M. Recinos, “Solar Steam Booster in the Ahuachapán Geothermal Field,” Geothermal Resources Council Transactions, Vol. 32, 2008, 395-399.

Ruggero Bertani, “Geothermal Power Generation in the World, 2005–2010 Update Report,” Proceedings World Geothermal Congress 2010, Bali, Indonesia, 25-29 April 2010.

Geothermal Energy Association (GEA), Annual U.S. Geothermal Power Production and Development Report, April 2011. http://www.geo-energy.org

Bin Gong, Hongbin Liang, Shouliang Xin, and Kewen Li, “Effect of Water Injection on Reservoir Temperature during Power Generation in Oil Fields,” Thirty-Sixth Workshop on Geothermal Reservoir Engineering, Stanford University, Stanford, California, January 31 - February 2, 2011.

Andrew D. Greenhut, Jefferson W. Tester, Ronald DiPippo, Randall Field, Christopher Love, Kenneth Nichols, Chad Augustine, Fausto Batini, Bill Price, Gianluca Gigliucci, Irene Fastelli, “Solar-Geothermal Hybrid Cycle Analysis for Low Enthalpy Solar and Geothermal Resources,” Proceedings World Geothermal Congress 2010, Bali, Indonesia, 25-29 April 2010.

S. Handal, Y. Alvarenga, and M. Recinos, “Geothermal Steam Production by Solar Energy,” Geothermal Resources Council Transactions, Vol. 31, 2007, 503-510.

Gerald W. Huttrer, “2010 Country Update for Eastern Caribbean Island Nations,” Proceedings World Geothermal Congress 2010, Bali, Indonesia, 25-29 April 2010.

Lyle A. Johnson and Everett Walker, “Oil Production Waste Stream, a Source of Electrical Power,” Thirty-Fifth Workshop on Geothermal Reservoir Engineering, Stanford University, Stanford, California, February 1-3, 2010.

Amanda Kolker and Ray Mann, “Akutan Geothermal Project,” Renewable Energy Alaska Project (REAP) Forum, March 2011. http://alaskarenewableenergy.org

John W. Lund, Karl Gawell, Tonya L. Boyd, Dan Jennejohn, “The United States of America Country Update 2010,” Proceedings World Geothermal Congress 2010, Bali, Indonesia, 25-29 April 2010.

Hilel Legmann, Phillip Sullivan, “The 30 Mw Rotokawa I Geothermal Project Five Years of Operation,” International Geothermal Conference, Reykjavík, Sept. 2003.

Susan Petty, Laura Nofziger, Daniel Bour, Yini Nordin, “Fluid Diversion in an Open-Hole Slotted Liner,” Thirty-Sixth Workshop on Geothermal Reservoir Engineering, Stanford University, Stanford, California, January 31 - February 2, 2011.

R.J. Pine and A.S. Batchelor, “Downward Migration of Shearing in Jointed Rock During Hydraulic Injections,” Int. J. Rock Mech. Min. Sci. & Geomech. Abstr. (1984) Vol. 21, No. 5, pp. 249-263.

Jose Rivas and Rodolfo Torres, “Seismic Monitoring of a Well Stimulation Operation at the Berlin Geothermal Field, El Salvador,” Geothermal Resources Council Transactions, Vol. 27, October 12-1 5, 2003, p. 365-368.

Subir K. Sanyal, James W. Morrow, and Steven J. Butler, “Net Power Capacity of Geothermal Wells Versus Reservoir Temperature – a Practical Perspective,” Thirty-Second Workshop on Geothermal Reservoir Engineering, Stanford University, Stanford, California, January 22-24, 2007.

Subir K. Sanyal and Steven L. Enedy, “Fifty Years of Power Generation at the Geysers Geothermal Field, California – the Lessons Learned,” Proceedings, Thirty-Sixth Workshop on Geothermal Reservoir Engineering Stanford University, Stanford, California, January 31 - February 2, 2011.

Rüdiger Schellschmidt, Burkhard Sanner, Sandra Pester, Rüdiger Schulz, “Geothermal Energy Use in Germany,” Proceedings World Geothermal Congress 2010, Bali, Indonesia, 25-29 April 2010.

Jefferson Tester, David Blackwell, Susan Petty, Maria Richards, Michal Moore, Brian Anderson, Bill Livesay, Chad Augustine, Ron DiPippo, Ken Nichols, Ralph Veatch, Elisabeth Drake, Nafi Toksoz, Roy Baria, A.S. Batchelor, John Garnish, “The Future of Geothermal Energy: an Assessment of the Energy Supply Potential of Engineered Geothermal Systems (EGS) for the United States,” Thirty-Second Workshop on Geothermal Reservoir Engineering, Stanford University, Stanford, California, January 22-24, 2007, http://geothermal.inel.gov/publications/future_of_geothermal_energy.pdf

Doone Wyborn, “EGS Concept,” a presentation to the US Department of Energy EGS Road-Mapping Workshop, San Francisco, August 3-4, 2011.

Zimmermann, G., Reinicke, A., Brandt, W., Blöcher, G., Milsch, H., Holl, H.-G., Moeck, I., Schulte, T., Saadat, A., Huenges, E, “.Results of Stimulation Treatments at the Geothermal Research Wells in Groß Schönebeck/Germany,” Thirty-Third Workshop on Geothermal Reservoir Engineering, Stanford University, Stanford, California, January 28-30, 2008.

Zimmermann, G., Reinicke, A., Blöcher, G., Moeck, I., Kwiatek, G., Brandt, W., Regenspurg, S., Schulte, T., Saadat, A., Huenges, E., “Multiple Fracture Stimulation Treatments to Develop an Enhanced Geothermal System (EGS) - Conceptual Design and Experimental Results,” Proceedings World Geothermal Congress 2010 Bali, Indonesia, 25-29 April 2010.

Experiences, Learnings and Developments of Surface Operations in a High Pressure Enhanced Geothermal System (EGS)

Humphreys, B.*, Roe, A., Gray, T., Hirsinger, L., Fischmann, I., Schmidt, P.
ben.humphreys@geodynamics.com.au
Geodynamics Limited.
19 Lang Parade, PO Box 2046, Milton, QLD 4064.

Geodynamics has obtained significant experience and learnings in the design and operations of surface equipment in a high pressure Enhanced Geothermal System (EGS) in three key areas. These are:

- Pumping and sealing
- Closed loop pressure behaviour
- Mineral deposition

The aim of this paper is to share Geodynamics' experiences, learnings and developments in the design and operations of surface equipment for EGS applications. It is intended that the industry as a whole will benefit from the knowledge sharing and that it will assist the industry towards demonstrating the viability of EGS technology in Australia.

Keywords: Geothermal, EGS, Power Plant, Reinjection, Stibnite, Explosive Decompression

Closed Loop Circulation

Geodynamics has obtained significant experience in the design and operations of surface equipment from an EGS closed loop circulation test and subsequent studies into issues identified. The closed loop circulation test was carried out in a hot granite rock reservoir at the Habanero EGS field near Innamincka, South Australia. The test was carried out between December 2008 and February 2009 and was the first of its kind in Australia and one of the few in the world.

The EGS field at Habanero is considered unique due to the extremely high reservoir pressure, circa 730 Bar at 4,200 m (measured depth), which is about 340 Bar at the shut in production wellhead.

During the test, hot geothermal brine was produced from one well, Habanero 3, and reinjected into another well, Habanero 1. The wells were connected underground via the hot rock reservoir creating a closed loop. This was proved by pressure relationships and a tracer test. A large majority (75%) of the tracer was recovered during the 6-week circulation test.

During the circulation test a maximum flow of 15.2 kg/s at temperatures up to 216°C were achieved for a thermal output of about 14 MW_{th}. The test circulated an accumulated quantity of about 50,000 tonnes which is equivalent to 926 operational hours at 15 kg/s (Chen, 2010). Open flows of up to 30 kg/s, 219°C were also achieved with a thermal output of about 28 MW_{th} (Chen, 2010). The closed loop flow was restricted by high injection pressures at Habanero 1. The restriction is believed to have been caused by the presence of a mud ring resulting from drilling mud lost into the fracture system.

Surface Equipment

The high pressure does not favour traditional direct flash steam plant due to the requirement to subsequently pump the flashed brine back up to 450 Bar for reinjection. The consequence is that piping, heat exchangers and pumps must be designed and operate reliably at very high pressures. The reservoir operating philosophy is to reinject all the production fluid, this combined with the remote, arid location means that there is little fluid available for evaporative cooling. This means that air cooled condensers are used with a separate, closed circuit power cycle, i.e. a binary cycle (See Figure 1).

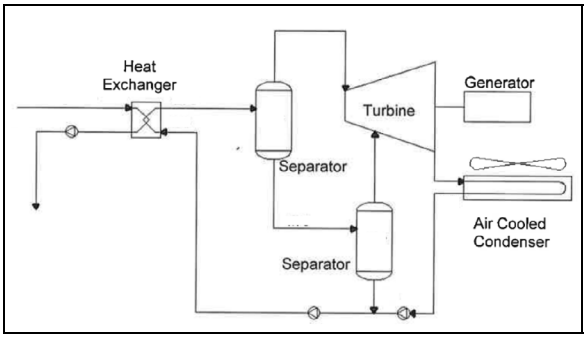

Figure 1: Schematic of power plant arrangement

There are several advantages of this arrangement over a direct flash plant; one is that issues of chemical scaling such as silica and calcite can be avoided. Another feature of the closed brine system is that the circulation is assisted by the difference in density of the water columns in the production and reinjection wells (natural circulation or buoyancy drive). The disadvantages are the high capital cost of equipment, dissolved gases at high partial pressures, and other minerals such as antimony which can deposit on heat exchanger tubes as stibnite.

In order to conduct the closed loop test the production well was connected to the reinjection well via; a high pressure pipeline (about 600m), an air-cooled heat exchanger that cooled the brine, and a reinjection pump. This arrangement

of the surface equipment was selected to replicate the type of closed system intended for future commercial plants. The high pressures involved, 340 Bar inlet and 450 Bar outlet, and the brine constituents including minerals and dissolved gases provided some challenges for the design and operation of the plant.

In order to solve the reliability issues as well as take steps to develop the technology required for commercial sized EGS plants Geodynamics' has carried out extensive investigations of the issues observed.

Pumping and Sealing

A 41 stage centrifugal mixed flow pumping system with a dual mechanical seal was used to reinject the brine into the reservoir (See Figure 2). The pump suffered one major failure during a rapid shutdown caused by an elastomer failure. The post mortem revealed; (i) extensively damaged elastomers (See Figure 3), (ii) the diffusers had imploded (See Figure 4), and (iii) the bearings (or sleeves) were cracked along the keyway.

The pump also suffered ongoing reliability issues due to elastomer failures through extrusion and explosive decompression because of the high pressures and dissolved gases.

The mechanical seal suffered a series of failures due to operator error, elastomer issues and what is thought to be movement of the seals sleeve relative to the main body.

Elastomer issues

In an attempt to resolve the elastomer issues, the original ones were upgraded to ones of higher shore hardness and with greater resistance to explosive decompression and extrusion. This was done in a staged approach, increasing the quality and cost of elastomers. This was done to identify the most cost effective solution and prevent delays to the circulation test as some elastomers had significant lead times. This approach increased the life of the elastomers to about 6 weeks and appeared to resolve the extrusion issues. However, even with the highest grade of elastomers available explosive decompression issues continued.

Geodynamics engaged BHR Group in the UK to carry out a review of the suitability of elastomers at the process conditions and the issue of explosive decompression.

Explosive decompression in this context (or rapid gas decompression) is defined by Monaghan (2009) as: *"…..an operational condition during which the applied system pressure is quickly released, resulting in the expansion of absorbed gas which can lead to damage of elastomeric seals."* However, as stated by Monaghan (2009), "*the prefix "explosive" can be misleading, since decompression damage can occur even when pressure is bled down over many hours or even days."*

Elastomers are especially susceptible to explosive decompression in high pressure gas and supercritical fluid environments (Eldevik, 2008). The precise details of the interaction between the elastomers and fluid at Habanero are under further investigation as the gases at Habanero are considered dissolved, at normal operating conditions, and not present as free gases.

For the purpose of this paper it is sufficient to say that the high pressures and presence of dissolved CO_2 (and other gases) at Habanero are such that explosive decompression tends to occur. On one occasion, gases could be clearly observed diffusing out of an elastomer causing explosive decompression damage. This was observed after the pump was disassembled and probably an hour or more after complete depressurisation of the system.

Generally, the extent of damage due to explosive decompression is related to the gas composition and conditions, exposure time, properties of the elastomer, and the duration of pressure release. Monaghan (2009) explains further: *"Damage normally occurs internally due to the presence of voids from the curing process. These voids act as stress concentrations when the operational pressure is released and the resultant strain at the void wall increases during gas expansion. Degassing is a slow process and is governed by the diffusion coefficient for the given material and absorbed gas composition".*

The findings of the review basically concluded that no commercially available elastomers are likely to be able to provide reliable service in the Habanero process conditions.

To prevent future elastomer issues spring energised PTFE seals will be used in a new mechanical seal and the existing pump. This technology has been proven in high pressure gas compressor applications.

Pump issues

The analysis of the major pump failure showed that the diffusers failed due to an inability to equalize pressures quickly enough on a rapid loss of suction pressure. The pump supplier was able to solve this problem by incorporating balancing holes in each stage. The holes had negligible impact on pump performance.

The sleeves of the pump were found to be commonly cracked along the keyway. This was believed to be caused by inadequate lubrication. This issue was resolved by modifying the design to a keyless type of sleeve and changing the sleeve material.

The pump performed well after the modifications however a full internal inspection is yet to be done

to confirm that the modifications have completely resolved the issues. This is planned to be done prior to recommissioning of the 1MW Plant.

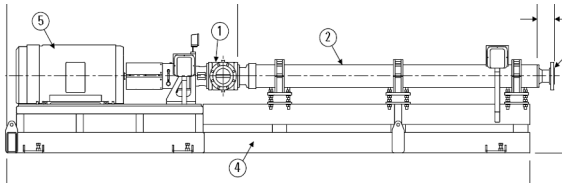

Figure 2: Schematic of Reinjection Pump

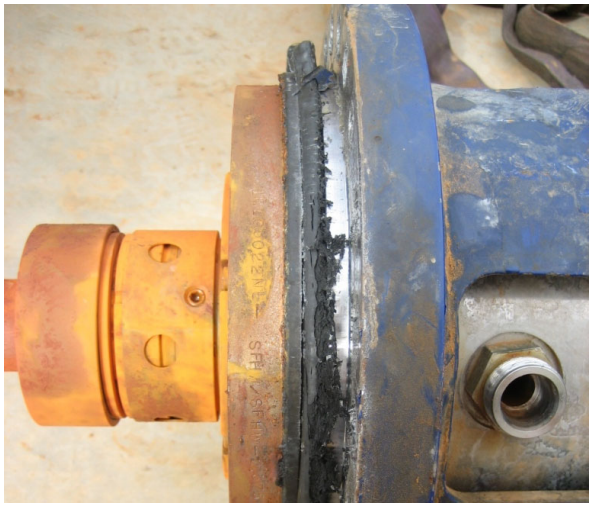

Figure 3: Elastomer showing explosive decompression and extrusion damage

Figure 4: Imploded diffusers

Seal issues

The existing seal has two sealing faces with the brine used as a barrier fluid. The high pressure drop is distributed across the two seal faces using a pressure reducing valve. Although the barrier system was cost effective it proved troublesome in operation and precipitated minerals could be found in the seal during overhauls.

The initial seal failures were caused by operator error, whereby full system pressure was applied to the barrier system, and a reverse pressure situation caused by a rapid loss of pump inlet pressure. These issues were easily resolved but they highlighted the operational complexity of having the barrier system directly connected to the process fluid.

Later seal failures were much more complex and are still not fully understood. There is strong evidence to suggest that the sleeve of the seal is moving axially relative to the body of the seal. This is thought to have separated the sealing faces and moved elastomers out of position causing damage. A common observation has been that the seal setting plate which holds the sleeve in position prior to installation has not been able to be reinstalled after a failure.

Due to the troublesome barrier system and the inability to eliminate elastomers from the existing seal it was decided to purchase a new seal to increase reliability and prove technology for future plants.

A new mechanical seal that uses existing gas compressor and CO_2 reinjection technology is in the design phase and will replace the existing seal. This dual seal will use an over pressurised barrier system to eliminate the issues with using the brine, utilise spring energised PTFE seals, and extra focus is being applied to the design of the seal sleeve and shaft joining method.

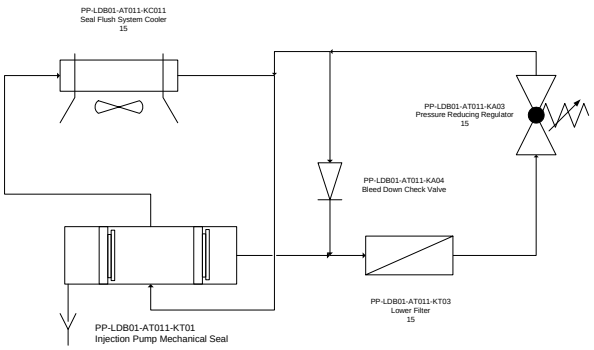

Figure 5: Schematic of existing seal barrier system

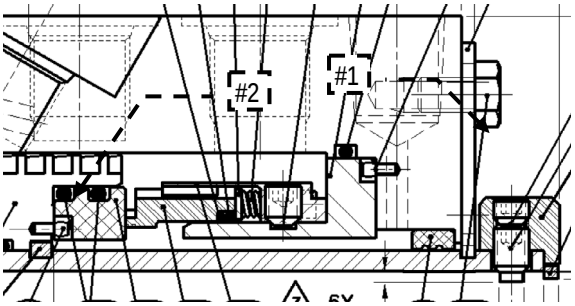

Figure 6: Schematic of secondary sealing face showing the setting plate that was unable to be reinserted upon failure (#1) and the elastomer observed to be pushed out of position (#2)

Figure 7: Photo of secondary sealing face showing elastomer pushed out of position and squashed

Closed loop pressure behaviour

A complex phenomenon was observed during the closed loop test in which high pressure events occurred upstream of the pump during shut downs. These events exceeded the normal operating pressure and lifted the pressure relief valve. Two distinct types of shut down, a manual stop and a trip, could be observed in the pressure data and the behaviour showed good repetition in each case.

Analysis of the pressure data versus operational events showed that the manual shut down caused the high pressure events. The pump trip case showed some interesting behaviour but did not seem to cause high pressure events.

SVT Consultants were engaged to develop hydraulic models and attempt to replicate the actual closed loop behaviour. The model was then used to run scenarios to attempt to identify the cause/s of the behaviour and identify solutions. SVT used a one dimensional surge analysis model to simulate the system.

It was found that the actual behaviour could not be replicated with the wells as fixed boundary conditions, validating further the closed loop theory. The magnitude of the high pressure events also could not be replicated without the inclusion of a large volume of fluid at the bottom of the injection well and large restriction between this volume and the reservoir, and restricting the pressure relief valve (PRV) flow. This provided evidence to support the theory of the presence of a mud ring in Habanero 1 restricting closed loop circulation. Operational issues were experienced with the PRV and upon overhaul significant corrosion was observed so it is plausible that the PRV was sticking or jamming. The final model replicated the actual behaviour quite well in both a manual shut down and trip event.

Figure 8 shows recorded operational data during a manual shutdown where the suction pressure exceeds the design pressure after about 15s. Figure 9 shows the model output for the same scenario with good similarity and a peak after about 19 – 20s.

The model could also estimate the effect of the natural circulation drive due to the different fluid densities in the production and injection well. With the mud ring restriction included, the brine system started natural circulation about 3 mins after a pump trip. Without the mud ring restriction the model showed natural circulation should start after only 30s. 100% natural circulation flow was about 13 kg/s without the mud ring and only 5 kg/s with it. The model also showed closed loop flow rates of 25 kg/s with the mud ring removed compared to the 15 kg/s actually achieved (Lawrenz, 2011).

The models were able to reasonably accurately match the actual closed loop behaviour and have identified potential cost effective and simple solutions. They showed that the root cause of the pressure surges was when the system was manually shut down and the production well emergency shut down valve was closed first. The combination of this and the restriction in the injection well caused reverse flow and significant overpressure (Lawrenz, 2011).

It is confidently believed that the issues will be resolved with the addition of a non-return valve and a change to operating procedures.

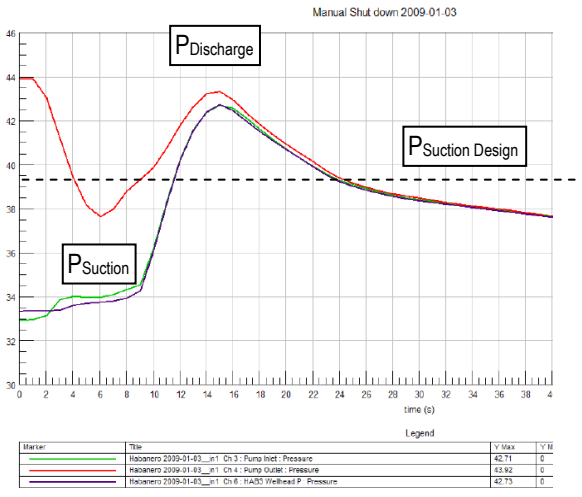

Figure 8: Recorded operational data for manual shutdown (Lawrenz, 2011)

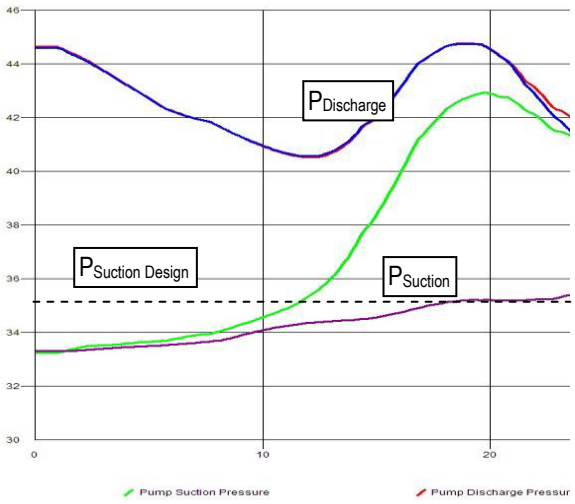

Figure 9: Data from hydraulic model showing similar behaviour (Lawrenz, 2011)

Mineral deposition

During closed loop circulation the deposition of stibnite (antimony sulphide) on the inner surface of the brine cooler tubes caused rapid and significant reduction in heat transfer (See Figure 10). This is of concern for future power plant operations due to the associated reduced performance.

Stibnite deposition is not a well-known issue in geothermal plants and of the literature reviewed only three operational references could be identified. Two of the identified geothermal plants are in New Zealand, Ngawha and Rotokawa (Brown, 2007). The other reference identified was an exploratory well in the Mt.Amiata area in Italy. The stibnite fouling here occurred mainly in the pressure separator and started in the production well (Capetti et al, 1995).

Geodynamics engaged an acknowledged expert on the topic to help evaluate the problem and identify solutions.

Antimony is a naturally occurring mineral and can be found as several different compounds, such as stibnite, or can exist in its elemental state. At Habanero 3, the antimony is believed to precipitate as stibnite due to the presence of H_2S. Metallic antimony was identified during earlier tests at Habanero 2, this is believed to be due to a lower concentration of H_2S.

Stibnite as defined by Brown (2011): "*Stibnite is antimony(III) sulphide Sb_2S_3. It occurs naturally as a mineral that normally forms acicular (long, needle-like) black crystals. Like arsenic, antimony has two oxidation states Sb^{3+} and Sb^{5+}. Thus stibnite has antimony in the reduced oxidation state of +3. Crystalline stibnite is soft (mohs hardness = 2), and has a density of 4.63 g/ml. The melting point is 550 ºC.*"

The precipitation of stibnite is directly related to pH and temperature (See Figure 11 and Figure 12). The higher the temperature and higher the pH the less likely stibnite is to precipitate (Brown, 2009). While raising the pH to prevent precipitation seems attractive this would be very costly at Habanero due to the presence of dissolved CO_2 and would most likely cause problems with calcite and in particular silica precipitation after the heat exchangers.

The New Zealand plants typically use hot caustic solutions to dissolve the stibnite and clean the heat exchangers. This method has been trialled at Habanero once and a caustic cleaning system is intended to be used for the 1MW plant.

Figure 10: Brine cooler tube showing stibnite deposition

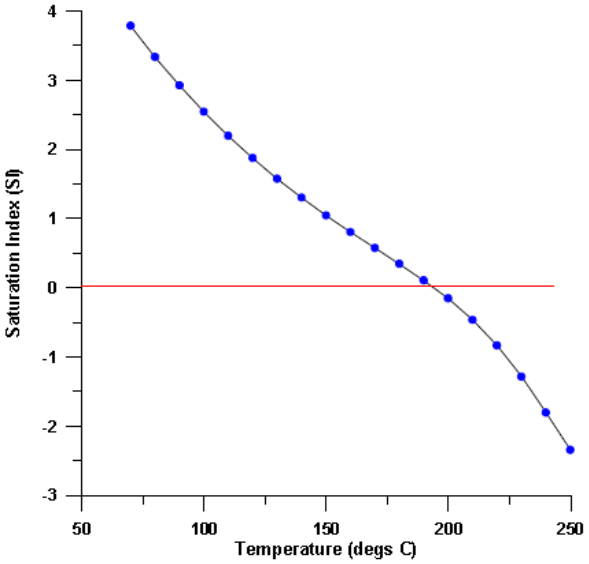

Figure 11: Effect of Brine Temperature on theSolubility of Stibnite in Habanero 3 Brine (pH ≈ 6) (Brown 2009)

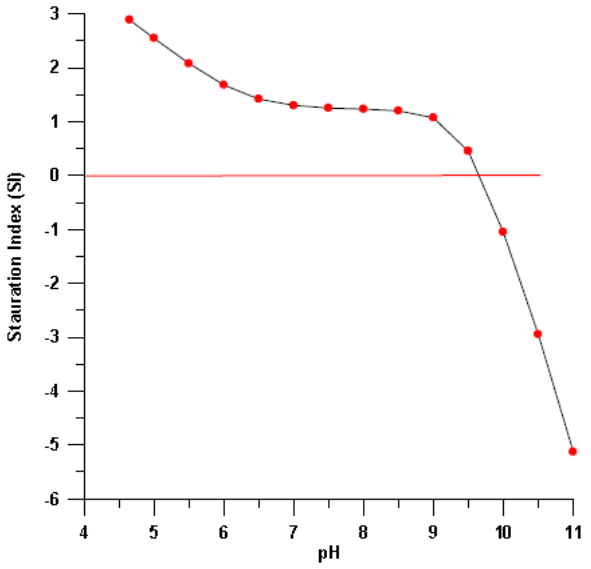

Figure 12: Effect of pH on the Solubility of Stibnite in Habanero 3 Brine (Brown 2009)

Conclusions

The unique high pressure conditions at the Habanero EGS field create a challenging environment for the reliable operation of surface equipment in the brine system.

This paper has outlined several key issues identified during circulation testing of an EGS system and stated the proposed solutions for these issues.

When designing surface equipment for high pressure EGS systems particular attention should be applied to; pump and seal selection, material selection, the use of elastomers, potential pressure transients, fluid chemistry and potential precipitants.

GDY has progressed significantly on the path of developing reliable and cost effective solutions for surface equipment in EGS applications.

References

Brown, K., 2009. Stibnite Fouling and Mitigation. Report prepared for Geodynamics Limited by GEOKEM.

Brown, K., 2011. Antimony and Arsenic Sulfide Scaling. In: Proceedings International Workshop on Mineral Scaling 2011 Manila, Philippines, 25-27 May 2011.

Cappetti, G., D'Olimpio, P., Sabatelli, F., Tarquini, B., 1995. Inhibition of antimony sulphide scale by chemical additives: laboratory and field test results. In: Proceedings of the 1995 World Geothermal Congress, Florence, Italy, May 18–31,1995, pp. 2503–2507.Ca

Chen, D. B., 2010. Habanero Closed-Loop Circulation Test Interpretations. Version 1.0, 25 August 2010, Geodynamics Ltd.

Dorrington, P., Brown, K.L., 2000, Management of stibnite deposition at Ngawha. In: Proceedings of the 22nd New Zealand Geothermal Workshop, Auckland, New Zealand, November 8–10, 2000, pp. 163–167.

Eldevik, F. 2008, Safe Pipeline Transmission of CO2. In: Pipeline & Gas Journal, Vol. 235, No. 11, November 2008.

Firth, D.,Lichti, K., Ko, M., Julian, R., 2010, Risk Assessment 1MW Plant Above Ground Components in the Brine System at Habanero. Report for Geodynamics Limited by Quest Reliability.

Lawrenz, H., 2011, Habanero Brine System Surge Analysis. Report for Geodynamics Limited by SVT Engineering Consultants.

Monaghan, K., 2009, Reinjection Pump Sealing Assessment in Geothermal Hot Fractured Rock (HFR) Facility. Report CR8189 for Geodynamics Limited by BHR Group.

Rushton, H., Scrase, G., Lichti, K., Ko, M., Julian, R., 2010, Phase 3 Review of Corrosion Rates and Damage Mechanisms 1 MW Plant – Final Predictions. Report for Geodynamics Limited by Quest Integrity Group.

Wilson, N., Webster-Brown, J., Brown, K., 2007, Controls on stibnite Precipitation at two New Zealand geothermal power stations. School of Geography, Geology and Environmental Science, University of Auckland, Auckland, New Zealand, GEOKEM, Swanson, Auckland, New Zealand.

Tracer testing at the Los Humeros, Mexico, high-enthalpy geothermal field

Iglesias, E.R.* [1] , Ramírez-Montes, M. [2], Torres, R.J. [1], Cruz-Grajales, I. [2], Reyes-Picasso, N. [1]
iglesias @iie.org.mx
[1] Instituto de Investigaciones Eléctricas; [2] Comisión Federal de Electricidad

We conducted a tracer study in the high-enthalpy Los Humeros, Mexico, geothermal reservoir to assess the effects of produced-brine injection in a major part of the field. A liquid-phase tracer, 2,6 naphthalene disulfonate, was used. Our results revealed that injection in well H-13 recharges the feeding zones of the nine monitored producing wells. Our results also indicate there is negligible risk of thermal interference in the observed wells at the injection rates of this study. The observed small aggregated tracer recovery suggests that most of the injected fluid, perhaps up to about 99%, flows to the deep reservoir, recharging it and enhancing its economic life.

Keywords: tracer testing, fractured reservoir, high-enthalpy field

Background

Los Humeros geothermal field sits atop of a volcanic caldera. It is a high-enthalpy geothermal resource emplaced in fractured volcanic formations. The current installed capacity is 40 MWe which will increase to 75 MWe by 2012.

The Mexican Comisión Federal de Electricidad (CFE), owner and operator of the field, currently injects about 4.2 kg/s of separated brine, produced in different parts of the field, in well H-13. The destination of the injected fluids as well as their likely capacity to produce unwanted thermal interference with producing wells is of considerable economic interest for CFE.
To investigate these questions teams of the

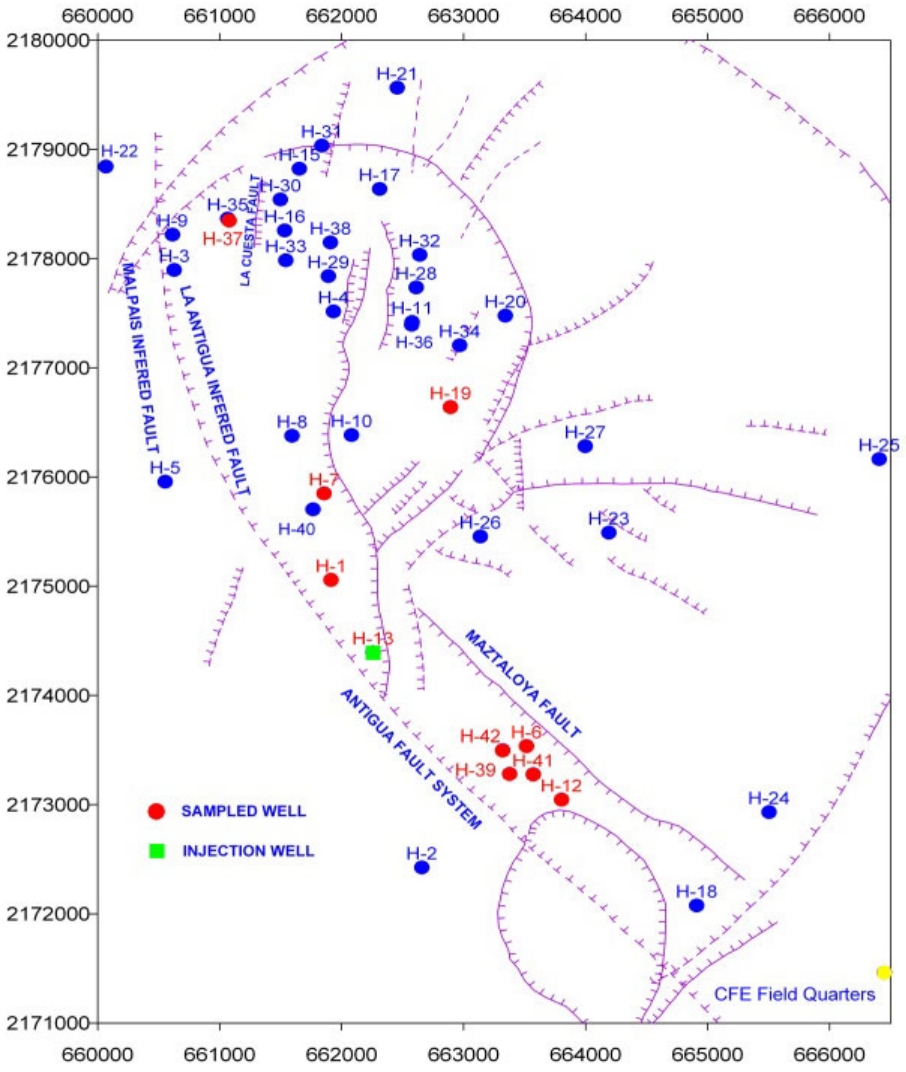

Figure 1.Los Humeros geothermal field well locations.

Instituto de Investigaciones Eléctricas (IIE) and CFE jointly designed, implemented and analysed the results of the study described in this paper.

Materials and method

Nine production wells in the ample area of interest (Fig. 1) were selected for this study. Their names, distances to the injector H-13 and respective discharge quality are shown in Table 1.

Well	Distance to H-13 (m)	Mean discharge quality
H-01	748	0.55
H-06	1,523	0.91
H-07	1,509	0.92
H-12	2,050	0.94
H-19	2,334	0.94
H-39	1,579	0.85
H-41	1,724	0.95
H-42	1,391	0.88
H-37	4,125	0.62

Table 1. Well information

We chose 2,6 naphthalene disulfonate (2,6 nds) as our liquid-phase tracer considering its high-temperature thermal stability, low detection limit, negligible risk to the environment, simple logistics, commercial availability and affordable price. Naphthalene sulfonates were studied by Rose et. al (2001; 2002) who demonstrated their usefulness as high-temperature geothermal tracers.

On July 30, 2010 we injected 300 kg of 2,6 nds dissolved in 1,500 l of injection brine, in well H-13. The injection operation lasted 18 minutes. Sampling of the participating wells, including H-13 started 4 hours later. For convenience the wells were sampled with diminishing frequency, a standard procedure for this kind of tracer test.

Recovery curves were computed numerically integrating the product of the liquid flow rate times the concentration of the residence curves over the observation period.

Results and discussion

Figures 2-4 present the tracer residence curves and the corresponding recovery curves for each monitored production well. As shown in these figures, the sampling period covered 272 days. Eighty samples were taken in each well.

The tracer was detected in all nine monitored wells, as depicted in Figs. 2-4. This demonstrated that injection in well H-13 recharges the feeding zones of the nine wells monitored in this study.

Note that, with the exception of well H-01D, the recovery curves in Figs, 2-4 were monotonously

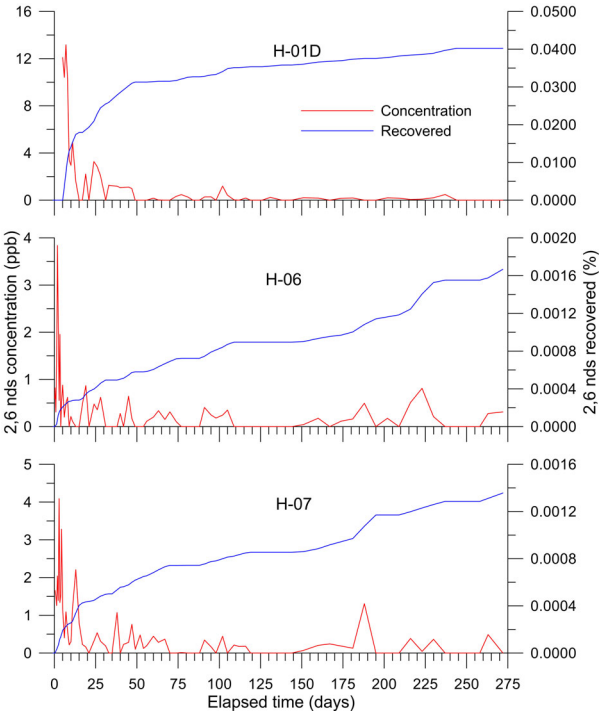

Figure 2. Residence and recovery curves of wells H-01, H-06 and H-07

increasing during the sampling period, indicating that the tracer was still arriving to the wells when sampling concluded. In well H-01D, the closest to the injector, the recovery curve reached a final plateau and tracer arrival seems to be essentially completed.

Table 2 presents the percentage of tracer recovery for all wells during the sampling period.

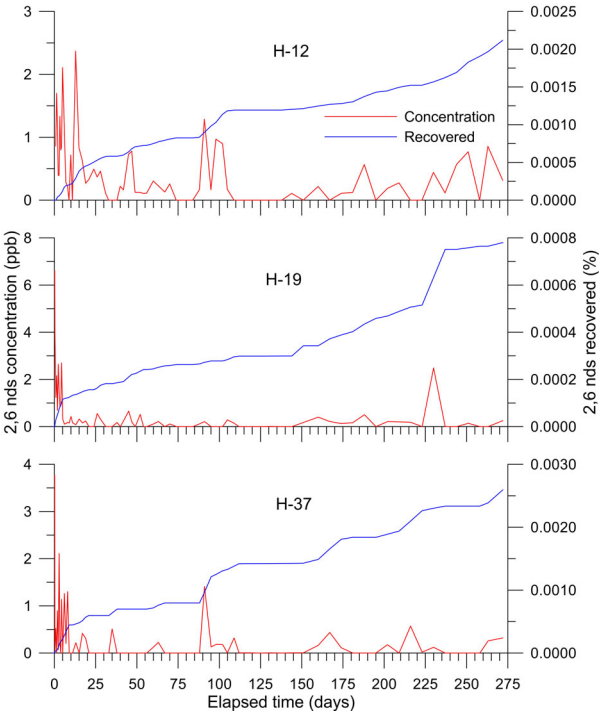

Figure 3. Residence and recovery curves of wells H-12, H-19 and H-37

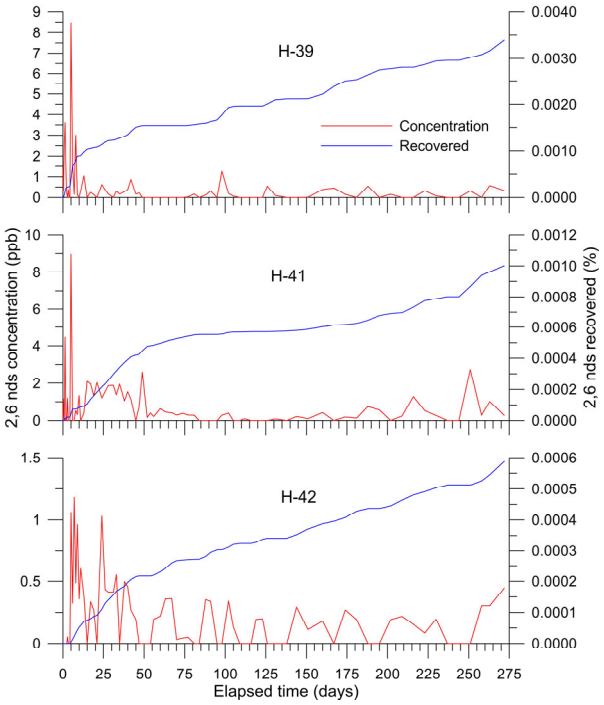

Figure 4. Residence and recovery curves of wells H-12, H-19 and H-37

Well	Distance to H-13 (m)	Tracer recovery (%)
H-01	748	0.0402
H-06	1,523	0.0017
H-07	1,509	0.0014
H-12	2,050	0.0021
H-19	2,334	0.0008
H-39	1,579	0.0026
H-41	1,724	0.0034
H-42	1,391	0.0010
H-37	4,125	0.0006
Aggregated recovery		0.0537

Table 2. Tracer recovery

In order to check for tracer recirculation we sampled the injection well simultaneously with the other wells. The corresponding results are presented in Fig.5. The total recirculated tracer amounted to 0.0076 % of the injected tracer, which represents 14.15% of the total recovered tracer in the production wells. Therefore significant tracer recycling occurred during the sampling period.

The figures in Table 2 and in Figs. 2-5 are not corrected for recirculation of the tracer. However, for the discussion following this paragraph the lack of correction does not preclude reaching reasonable conclusions, because corrected recoveries would be smaller than the observed ones.

The observed aggregated tracer recovery from the producing wells is small and comparable to a

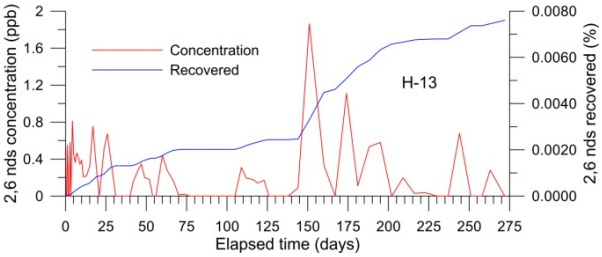

Figure 5. Results for the injection well.

previous result (0.131%) obtained in the Northern part of this field (Iglesias et. al., 2008b) over a smaller area and a shorter period (205 days); in that case tracer recovery reached completion in all but two wells. In the current study most wells did not reach recovery completion; only H-01D did. Thus, in principle one can hardly conclude anything about what would have been the total recovery if sampling had continued until all wells reached recovery completion. However, in previous tracer studies on fractured geothermal fields, including this one (Iglesias et al, 2007; 2008a; 2008b; 2010; 2011), we found that, generally, tracer recovery diminishes rapidly with distance to the injector well. In this case H-01, the closest well to the injector, recovered about 75% of the recorded total. This and Fig. 6 suggests a similar pattern to that found in previous studies prevails in this one.

Assuming that to be the case, it is reasonable to expect that, once completed in all the wells, total tracer recovery would be of the same or similar order of magnitude as the recovery found for well H-01. Furthermore, it seems very likely that part of the injected tracer would be produced by wells not monitored in this study, as suggested by the detection of the tracer in wells H-19 and H-37 located far from the injection well, at 2,334 and 4,125 m from it respectively. Even so, the small magnitude of the aggregated recovery indicates that most of the injected fluid is dispersed in the reservoir. A reasonable scenario for this to happen is that most of the injected brine, being colder and denser than the reservoir fluid, flows downwards to depths greater than those corresponding to the feeding zones of the wells, recharging the deep reservoir and enhancing its economic life.

The small recovery percentages found in this study also suggest that thermal interference due to injection in well H-08 is unlikely for the monitored wells, at the injection rates of this study.

Our results reveal the existence of horizontal permeability over a wide area of the field (e.g., wells H-12 and H-37 are 6 km apart). There is no perceptible correlation between this permeability distribution and the known distribution of faults in Los Humeros (Fig. 2). We suggest this permeability distribution may be associated with

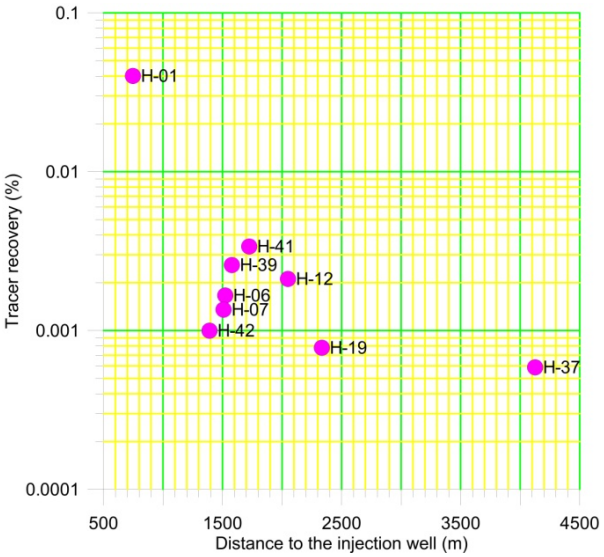

Figure 6. Tracer recovery vs. distance to the injection well.

contacts between different geologic formations in the caldera.

Summary and conclusions

We performed a tracer study in the high-enthalpy Los Humeros geothermal field, which sits atop a volcanic caldera. The reservoir is emplaced in fractured volcanic formations. A high-temperature, liquid-phase tracer was injected in well H-08. Liquid samples were obtained from nine producing wells and from the injection well, for a period of 272 days. These wells cover a significant fraction of the current field area.

The tracer was detected in all the monitored producing wells, proving that injection in well H-08 recharges their feeding zones.

The aggregated tracer recovery was small, comparable with previous results obtained in a smaller area in the Northern part of the field. This result suggests that most of the injected fluid, perhaps up to about 99%, flows to the deep reservoir, recharging it and enhancing its economic life.

The small recovery percentages found in this study also suggest that thermal interference due to injection in well H-08 is unlikely for the monitored wells, at the injection rates of this study.

Our results revealed the existence of horizontal permeability over a wide area of the field, with no perceptible correlation between it and the known distribution of faults in Los Humeros. We suggest this permeability distribution may be associated with contacts between different geologic formations in the caldera.

References

Iglesias, E.R., Flores-Armenta, M., Torres, R.J., Ramírez-Montes, M., Reyes-Picasso, N., Reyes-Delgado, L., 2011, Estudio con trazadores de líquido y vapor en el área Tejamaniles del campo geotérmico de Los Azufres, Mich.: Geotermia vol. 24, No. 1, 38-49.

Iglesias, E.R., Flores-Armenta, M., Torres, R.J., Ramírez-Montes, M., Reyes-Picasso, N., Reyes-Delgado, L., 2010, Simultaneous liquid- and vapor-phase tracer study in the Tejamaniles area of the Los Azufres, Mexico, geothermal field,: Proceedings of the World Geothermal Congress 2010, Bali, Indonesia, 25-29 April 2010.

Iglesias, E.R., Flores-Armenta, M., Quijano-Leon, J.L., Torres-Rodriguez, M.A., Torres, R.J. and Reyes-Picasso, N., 2008b, Estudio con trazadores de líquido y vapor en la zona Marítaro – La Cumbre del campo geotérmico de Los Azufres, Mich.: Geotermia vol. 21, No. 1, 12-24.

Iglesias, E.R., Torres, R.J. and Reyes-Picasso, N., 2008a, Estudio con inyección de trazadores en la zona Sur del campo geotérmico de Los Azufres: Instituto de Investigaciones Eléctricas, Report IIE/11/13360/I-02/F, 56 pp.

Iglesias, E.R., Torres, R.J. and Reyes-Picasso, N., 2007, Estudio con trazadores en la zona Norte del campo geotérmico de Los Humeros, Puebla – Primera etapa: Instituto de Investigaciones Eléctricas, Report IIE/11/13360/I-02/F, 105 pp.

Rose, P.E., Capuno, V., Peh, A., Kilbourne, P.M., Kasteler, C., 2002, The use of naphthalene sulfonates as tracers in high temperature geothermal systems: Proceedings of the 23rd Annual PNOC-EDC Geothermal Conference, 53-58.

Rose, P.E., Benoit, W.R., Kilbourne, P.M., 2001, The application of polyaromatic sulfonates as tracers in geotermal reservoirs: Geothermics vol. 30, 617-640.

The QGECE Power Conversion Group

P.A. Jacobs*, A. Rowlands, H. Gurgenci, E. Sauret, P. Petrie-Repar,
A. Atrens, C. Ventura, R. Singh, J. Czapla, H. Russell, B. Twomey, J. Zhang
peterj@mech.uq.edu.au
Queensland Geothermal Energy Centre of Excellence.
The University of Queensland, Brisbane, 4072.

The Power Conversion Group within the Queensland Geothermal Energy Centre of Excellence (QGECE) has the task of developing analysis and design capability for elements of the surface plant associated with exploitation of geothermal energy resources. Since there is a separate heat exchangers group, our focus is on the turbomachinery components of the power plant. Our activities fall into two broad categories: (1) analytical and computational modelling, and (2) experimental studies. The analytic and computational modelling enables the design and evaluation of concept machines while the experimental studies anchor the modelling tools in reality.

Keywords: power conversion, turbine, modelling, experimental demonstration.

Analytical Studies

A study of available fluids has been undertaken for potential power cycles. This study considered a range of temperatures for the various geothermal resources and a selection of subcritical and transcritical cycle options. For temperatures up to 150 °C cycles based on a range of hydrofluorocarbons look promising. At higher temperatures, on the order of 250 °C, a transcritical CO^2 cycle is being considered as a solution, provided there is access to a cooling medium to condense the carbon dioxide. Alternatively, a fully supercritical Brayton cycle could be used when condensing is not an option.

As well as steady state cycle analysis, we have been building dynamic simulation capability for both supercritical CO_2 and lower temperature refrigerant-based cycles. We have made a significant investment in the Dymola simulation software which is based on the Modelica programming language. Figure 1 shows the flow sheet for the supercritical CO_2 (Brayton) cycle that is the focus of our control studies. One of our interests is in the system response to sudden

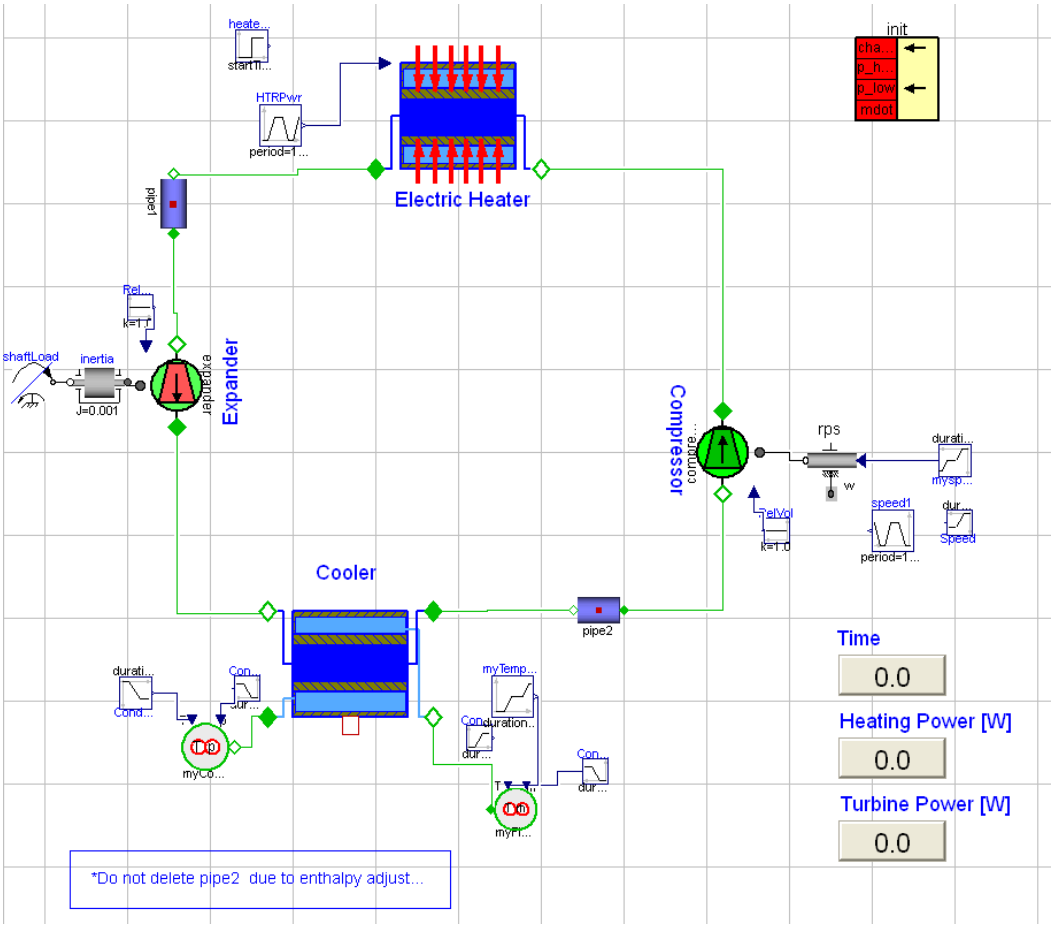

Figure 1: Dymola-based simulation of the CO_2 Brayton cycle.

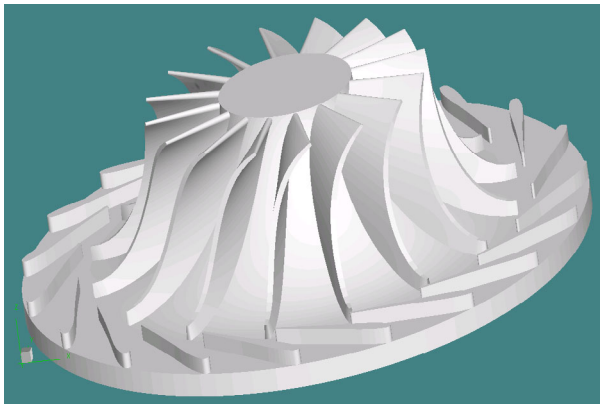

Figure 2: Model of stator and rotor for a candidate radial-inflow turbine.

change in load, and might be experienced by small off-grid power generators but also the more general study of control strategies for Brayton cycles. Strategies include the addition and removal of mass of cycle fluid to facilitate optimum operation of the cycle in the presence of part-load conditions.

Turbine Analysis and Design

Radial-inflow turbines have been our initial focus for expanders because they are expected to have good performance for output powers up to a few hundred kilowatts. They are also simpler to design and manufacture on a small scale than axial-flow machines.

For turbine design and analysis, we have been using the RITAL and AXCENT programs from Concepts NREC. We are now able to carry out preliminary design and CFD analysis of proposed radial-inflow turbines and have been investigating the export of parameters defining the geometry of the turbine for use with the in-house analysis software as well as for manufacture. Figure 2 shows one of the geometries for both inlet guide vanes and rotor for a characteristic machine.

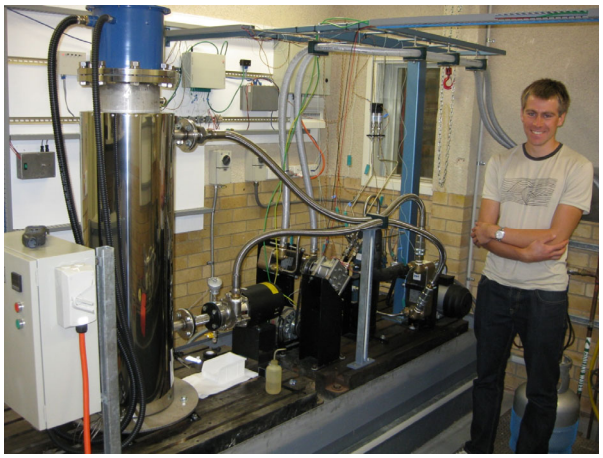

Figure 3: Small-scale power loop in UQ laboratory (and group member Hugh Russell).

To complement the use of commercial analysis and design codes, we are developing an in-house turbine-performance code and a more detailed flow simulation code. The turbine-performance code is able to be extended to dense-gas behaviour and will eventually be integrated into the cycle analysis programs. The Eilmer3 flow solver is capable of handling fully three-dimensional geometries and dense-gas equations of state, as required for the detailed flow analysis within a fixed or rotating frame of reference. It is intended for the flow path optimisation within a particular candidate turbine.

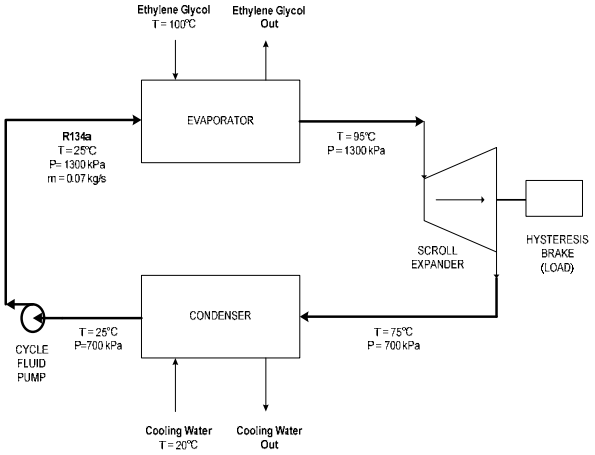

Figure 4: Small-scale power loop with R134a working fluid.

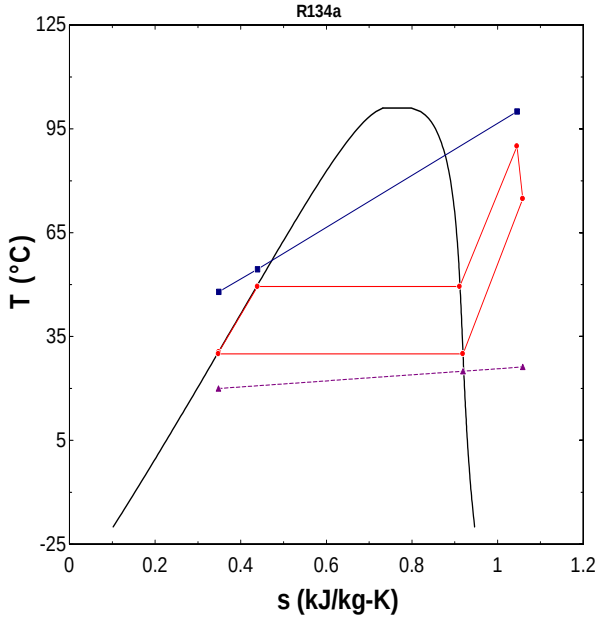

Figure 5: Thermodynamic cycle for the small-scale power loop.

Experimental Verification

In the QGECE laboratory on the University of Queensland campus, we have been building some small-scale hardware demonstration rigs.

As one of our first experimental activities, we have constructed a small-scale power loop with R134a as the working fluid and a typical mass flow of 0.07 kg/s (Figure 3). This is our practice test-bed for dense-gas expanders and has initially been

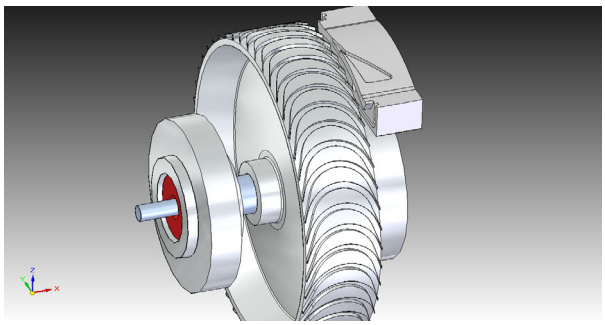

Figure 6: Internal view of the initial impulse turbine to be manufactured for the dense-gas power loop.

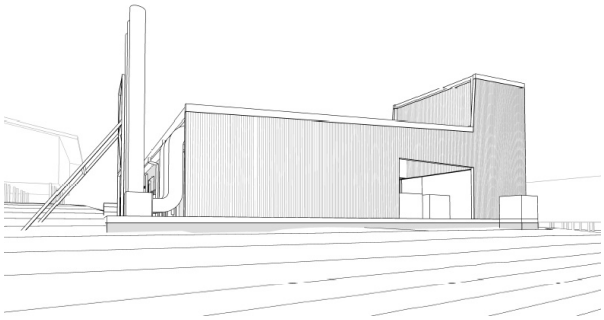

Figure 7: Sketch of the proposed QGECE test laboratory at Pinjarra Hills campus of UQ.

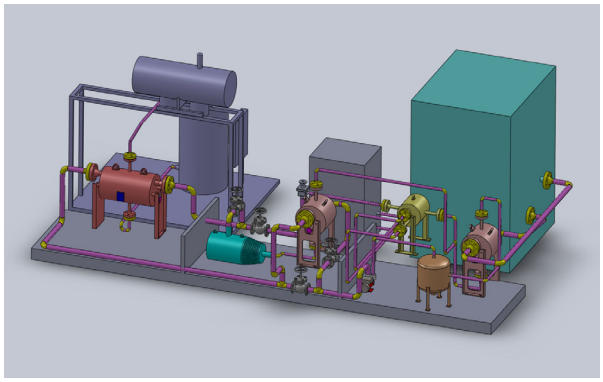

Figure 8: High-pressure loop.

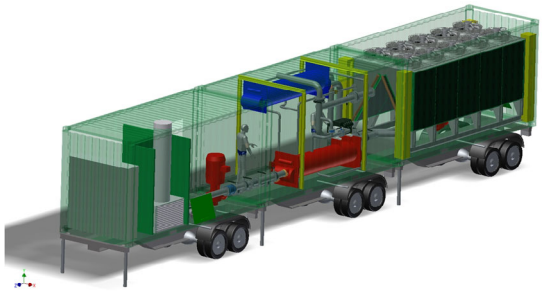

Figure 9: View of the components comprising the Terragen power-loop.

run with a Rankine cycle as shown in Figures 4 and 5.

The principal components are a reciprocating pump, plate heat exchangers, for the evaporator and condenser, and a scroll expander that is coupled to a load through a torque meter. Not shown in Figure 4 is the collection to temperature, pressure and mass-flow and speed sensors. These are monitored via a serial network and the data are displayed in real time and recorded for later analysis.

The scroll-expander is soon to be replaced by our first, in-house designed turbine. Although much of our turbine analysis and design efforts are focused on radial-inflow machines, this first expander will be a small impulse turbine as shown in Figure 6. Choice of an impulse turbine allowed the construction of a reasonable-sized machine for the very small mass flow in the loop. The machine been designed with the aid of the CFD codes to specify the shape of the supersonic nozzle expansion and the inter-blade passages. It is to be manufactured in the next few weeks so we should be able to report on its performance at the conference in November.

The selection of working fluid, operating temperatures and pressures are quite limited for QGECE lab located on the UQ campus so we are shifting our efforts to establishing a larger and more versatile test facility at the UQ Pinjarra Hills site, a few kilometers west of the main UQ campus. See Figure 7.

Work has recently started on the design and construction of a high-pressure loop (Figure 8) that will eventually (January 2011) be housed at the Pinjarra Hills site. This test loop will allow the use of a range of working fluids at supercritical pressures and temperatures, although power output will still be a few kilowatts.

A much larger test loop, with an output power on the order of 100 kW is presently being developed by Verdicorp, Florida, USA. It is based on R245fa as the cycle fluid and uses a radial-inflow turbine with a high-speed alternator and magnetic bearings. See Figure 9.

This facility will be the focus of on-going collaboration with our turbine-design activities leading to the design of new turbines for this machine. Initially the rig will operate with a moderate-pressure Rankine cycle but the components of the rig have been designed to operate at supercritical conditions for a range of interesting working fluids and at an output power of interest to geothermal applications.

Integration of In-Situ Stress Analysis and Three-Dimensional Seismic Mapping to Understand Fracture Networks in Australian Basins

*King, R., Abul Khair, H., Bailey, A., Backé, G., Holford, S. and Hand, M.
rosalind.king@adelaide.edu.au
South Australian Centre for Geothermal Exploration and Research
and Centre for Tectonics, Resources and Exploration
University of Adelaide, SA 5005

Understanding natural fracture networks is becoming increasing important to the geothermal industry due to their control on subsurface porosity and permeability. To understand fluid flow in a natural fracture network in a basin at present day, it is vital to determine the in-situ stress regime. Previous studies have shown that fluid flows in the direction of the maximum horizontal stress (σ_H; Heffer & Lean, 1993). However, natural fracture networks can be more complex than this. Therefore, it is vital to map them at all scales to understand their connectivity and potential fluid flow pathways.

Faults and fractures trending approximately NW-SE and NE-SW in the Cooper Basin and N-S and NW-SE in Northern Perth Basin have been identified using image logs. In-situ stress analysis demonstrates that these faults and fractures are optimally oriented for reactivation and are thus, open to fluid flow. However, the fault and fracture networks are not visible on the amplitude seismic data, making fracture connectivity and potential fluid flow pathways difficult to map and model. Here, we use analysis of the seismic attributes from three-dimensional seismic cubes in the Cooper and Northern Perth basins to identify and map these fault and fracture networks. In both the Cooper and Northern Perth basins, seismic attribute mapping has demonstrated good connectivity between the optimally oriented faults and fractures, and thus, providing excellent fluid flow pathways within the basins.

Keywords: In-Situ Stress, Seismic Attributes, Fractures, 3D Mapping, Cooper Basin, Northern Perth Basin, Fluid flow

Geological setting of the Cooper and Northern Perth Basin

The Warburton, Cooper, Eromanga and Eyre basins are successive stacked basins located in central-eastern Australia separated by two major unconformities (Figure 1). The Late-Carboniferous to Middle-Triassic Cooper Basin is composed of non-marine, characterized by fluvial, lacustrine and swamp deposits with coal measures (Hill and Gravestock, 1995; Alexander, 1998; Van Ruth et al., 2003).

The Perth Basin is located in southern Western Australia. It is a N-S trending rift basin, extending approximately 1000 km from north to south and is both onshore and offshore (Figure 1). The basin displays two major phases of rifting and subsequent infill from the Late Carboniferous to Early Permian, in both onshore and offshore parts of the Northern Perth Basin (Mory & Iasky, 1994; Quaife et al., 1994; Song & Cawood, 2000; Hodge, 2005).

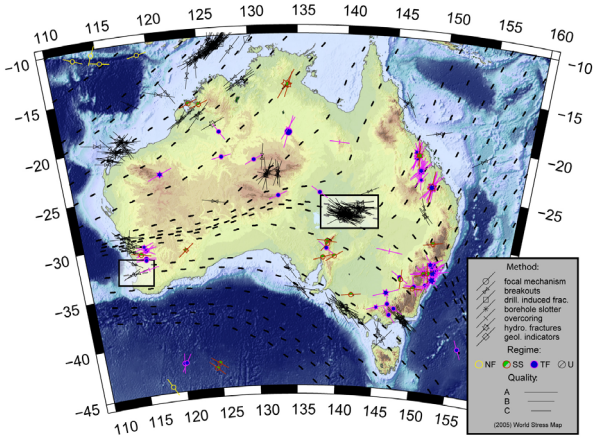

Figure 1: Australian Stress Map (Hillis & Reynolds, 2000) and location of the Cooper Basin and Northern Perth Basin

Elevated heatflows are observed in both basins. In the Cooper Basin these heat flows are associated with basement granites, possible from the Mount Painter Suite. Combined with the presence of natural fracture networks and extensive petroleum exploration data, these factors make the Cooper and Northern Perth basins significant geothermal prospects.

In-Situ Stress Analysis

The three principal stresses ($\sigma_1 > \sigma_2 > \sigma_3$) can be resolved into a vertical stress (σ_v) and two horizontal stresses (a maximum, σ_H, and a minimum, σ_h) within the Earth's crust (Anderson, 1951). The orientations and magnitudes of these three stresses control the orientation of newly forming fractures and the reactivation of pre-existing fractures. The in-situ stress tensor for a given region can be defined using borehole failure observed on image logs, as well as density logs and leak-off tests (LOTs).

Borehole breakouts are stress-induced elongations of a borehole cross-section (Figure 2b), which occur when the maximum circumferential stress exceeds the compressive rock strength; resulting in spalling of the borehole

wall (Bell, 1996a; Bell, 1996b). Borehole breakouts occur perpendicular to the present-day σ_H orientation (Kirsch, 1898; Bell & Gough, 1979; Figure 2b). On electrical resistivity images produced from FMI logs borehole breakouts appear as dark, electrically conductive areas separated by 180° (Figure 2c).

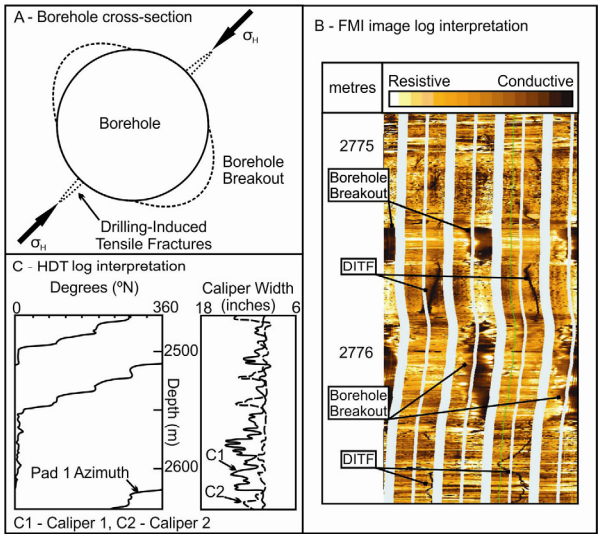

Figure 2: Northern Perth Basin: a) HDT logs exhibiting borehole breakouts (Reynolds & Hillis, 2000). b) A cross-section of a borehole illustrating the position of borehole breakout and DITFs relative to present-day σ_{Hmax} in a vertical wellbore. c) FMI image from Kingia-1 showing borehole breakout and DITFs separated by 90° around the borehole wall. Note the gamma ray corresponds to the position of borehole breakouts and DITFs; borehole breakouts are confined to low gamma ray (<100 gpi) horizons and DITFs to high gamma ray (>100 gpi) horizons. From King et al., 2008.

Drilling-induced tensile fractures form when the minimum circumferential stress becomes tensile (i.e. negative) and exceeds the tensile strength of the borehole wall (Peška & Zoback, 1995; Brudy & Zoback, 1999; Figure 2b). Such DITFs are parallel to the present-day σ_H orientation in vertical wells. On image logs DITFs appear as dark electrically conductive fractures, usually not longer than 2.0 m, often with small jogs or kinks and separated by 180° (Brudy & Zoback, 1999).

Maximum horizontal stress orientations in the Cooper and Northern Perth basins

Previous studies of the present-day stresses in the Cooper Basin and Northern Perth Basin used high resolution dipmeter logs and image logs (Reynolds & Hillis, 2000; Reynolds et al., 2004; King et al., 2008). In this study, image logs from a further 5 petroleum wells in the Cooper Basin have been analysed demonstrating a mean regional σ_H orientation in the Cooper Basin is approximately E-W at ~100. In the Northern Perth Basin, a further 8 petroleum wells have been analysed; demonstrating 302 BOs and 75 DITFs, giving an E-W σ_H orientation, at ~080.

In-situ stress magnitudes in the Cooper and Northern Perth basins

The magnitude of σ_v was calculated by integration of density logs from petroleum wells. The vertical stress magnitude at a specific depth is equivalent to the pressure exerted by the weight of the sediment overburden; and water column for offshore wells (Engelder, 1993).

The magnitude of σ_h was calculated using leak-off tests (LOTs) and formation integrity tests (FITs). The tests involve increasing the pressure of the borehole fluid in a small section (<10 ft) of newly drilled well, immediately after the casing has been set (Dickey, 1986). During the test, the pressure is increased until a fracture has formed at the borehole wall (Dickey, 1986). Fracture formation is marked by a change in slope on a pressure versus time plot. In most cases the fracture forms in the direction of σ_H and opens against (orthogonal to) σ_h. Leak-off test pressures provide the best estimate of σ_h (Bell, 1996b).

Table 1: In-situ stress magnitudes in the Cooper and Northern Perth basins

Vertical Stress	Maximum Horizontal Stress	Minimum Horizontal Stress
Cooper Basin at 1 km depth		
17.0-20.4	26.9	14.8
Cooper Basin at 3 km depth		
54.1-65.1	79.2	60.0
Northern Perth Basin at 1 km depth		
21.1-22.8	22.5	21.0
Northern Perth Basin at 3 km depth		
69.1-69.6	71.0	65.0

In the Cooper Basin, the magnitude of σ_H was constrained by 'Frictional Limits', which gives an upper limit to possible values of σ_H (Jaeger & Cook, 1979). The magnitude of σ_H was calculated in the Northern Perth Basin using the relationship between σ_h and σ_H in the presence of DITFs, including the pore pressure (Pp) and mud weight (Pw; after Brudy & Zoback, 1999).

The stress magnitudes in the Cooper Basin and Northern Perth Basin broadly define strike-slip fault stress regimes ($\sigma_H > \sigma_v > \sigma_h$), consistent with previous studies. However, the magnitude of σ_h, approaches σ_v inferring that the stress regimes are transitional between strike-slip fault and reverse fault ($\sigma_H > \sigma_v \approx \sigma_h$) in both of the basins; consistent with previous studies (King et al., 2008; Reynolds et al., 2004; Reynolds et al., 2006).

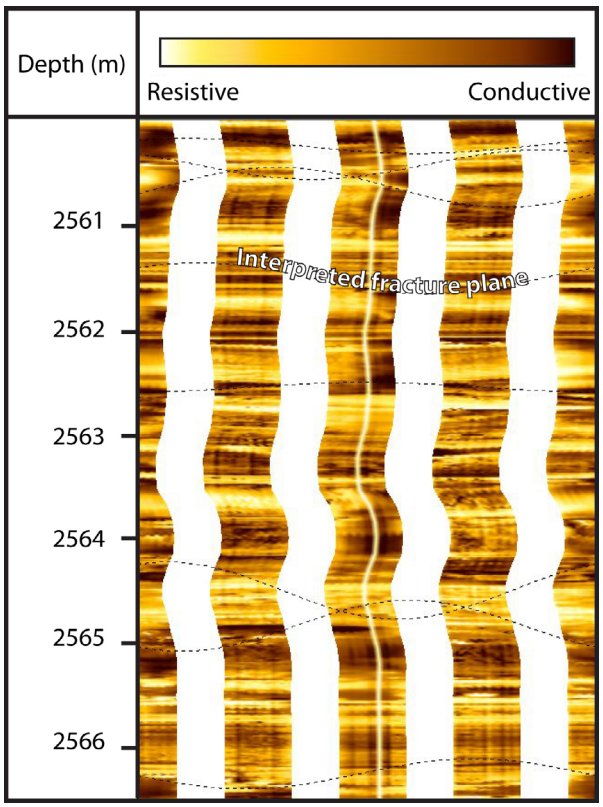

Figure 3: Electrically resistive fractures (closed to fluid flow) in the Cooper Basin (Backé et al., 2010).

Natural Fractures

Observed natural fractures in the Cooper and Northern Perth basins

Natural fractures were interpreted on the image logs in the Northern Perth Basin and Cooper Basin. Natural fractures are distinguished from DITFs on image logs by their continuous nature; natural fractures are often seen as continuous sinusoids whereas DITFs are discontinuous because they only propagate in the tensile region of the borehole wall (hence separated by 180°; Barton, 2000). Where DITFs are always electrically conductive, natural fractures can be both electrically conductive and resistive (Barton, 2000).

In this study both electrically conductive fractures and electrically resistive fractures were observed on FMI and FMS logs from the Northern Perth Basin and Cooper Basin (Figures 3 and 4). Conductive fractures are considered to be open and filled with drilling mud, giving them a dark, electrically conductive appearance on FMI images. Resistive fractures are thought to be closed and/or cemented producing the light, electrically resistive appearance on FMI images.

Wells analysed for natural fractures in the Cooper Basin demonstrate conductive fractures striking NE-SW and NW-SE, forming a conjugate set (Figure 3; Backe et al., 2010). A second smaller E-W striking set is also observed in the Cooper Basin (Back et al., 2010).

In the Perth Basin electrically resistive and conductive fractures closely parallel observed N-S to NW-SE striking fault sets and E-W striking faults (King et al., 2008). Resistive fractures are observed in all three orientations. Conductive fractures are only observed to strike N-S and NW-SE (Figure 4).

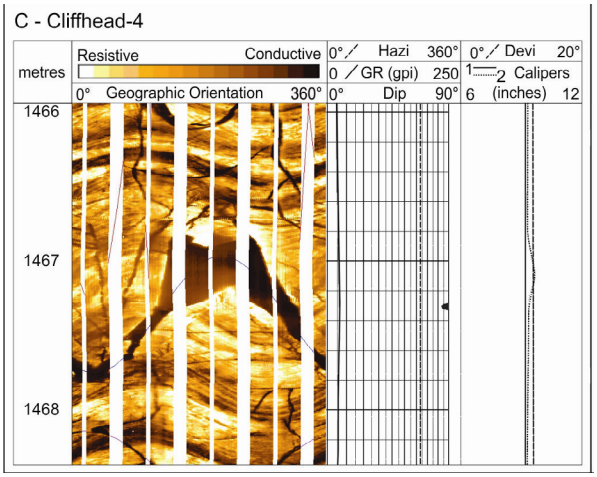

Figure 4: Electrically conductive fracture (open to fluid flow) in the Northern Perth Basin (King et al., 2008).

Prediction of fluid flow through natural fractures

The formation of new faults and fractures and reactivation of pre-existing faults and fractures is controlled by the in-situ stress regime. In a strike-slip fault stress regime new faults and fractures form approximately 26-30° to σ_H (Anderson, 1951; Healy et al., 2006).

A transitional reverse fault to strike-slip fault stress regime is inferred in both the Cooper and Northern Perth basins. Figure 5 is a fracture susceptibility plot demonstrating a transitional reverse fault to strike-slip fault stress regime (σH > σv ≈ σh) at 1 km depth and an E-W σH azimuth, consistent with the two basins. Reactivation potential plots use the same principals as Mohr Circles (e.g. Means, 1976) to assess which orientations of pre-existing faults and fractures are most likely to be critically stressed, and therefore, most likely to be active and open to fluid flow. Red areas on the diagram illustrate the orientations of faults and fractures (poles to planes) most susceptible to reactivation and blue areas exhibit fault and fracture orientations least likely to reactivate (closed to fluid flow). Pre-existing faults and fractures that strike N-S and have horizontal or vertical to steep dips are the least likely to reactivate in the two basins (Figure 5). However, fractures striking N-S, NW-SE and NE-SW with moderate dips are the most prone to reactivation in the two basins. Therefore, the N-S, NE-SW and

NW-SE fractures are thus, most likely to be open to fluid flow (Figure 5).

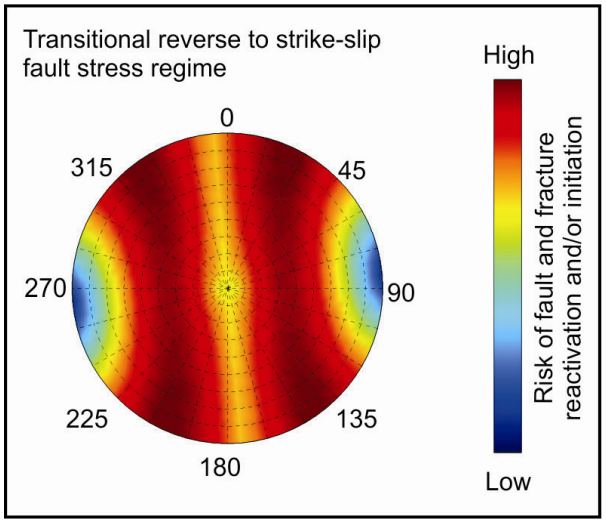

Figure 5: Fracture susceptibility plot for a transitional reverse fault to strike-slip fault stress regime, with an E-W maximum horizontal stress orientation. This represents the orientations of fractures and faults (as poles to bedding) most likely to be active (red) and least likely to be active (blue) for the Cooper and Northern Perth Basins.

Here we have demonstrated the use of the in-situ stress regime to understand the potential for fluid flow through pre-existing fractures observed on image logs in the Cooper and Northern Perth Basins. However, natural fracture networks are often more complex. The limitations associated with interpreting natural fractures on image logs are: 1) coverage controlled by well location; 2) all observations are at a metre-scale, and; 3) wells only provide two-dimensional visualisation of the fracture network. In this study we use seismic attribute mapping to develop our models of the natural fracture networks in the Cooper and Northern Perth basins.

Three-Dimensional Seismic Mapping

Different techniques based on either structural or on geophysical methods can be used to improve the interpretation of seismic data, whether 2D or 3D. Calculating, displaying and interpreting seismic attributes have been a large component for any geophysicist toolbox for the past couple of decades. For detecting potential fractures at depth in both the Cooper and North Perth Basins, we followed a three-step methodology, using the OpenDetect™ software. First, a steering cube of the dip of the seismic events in inline and crossline direction at every sample point was created from the amplitude cube using the Fast Steering algorithm, later filtered by a median filter (Fig. 6). This steering cube is the base for the structural oriented filtering of seismic volumes, enhancing multitrace attributes and eventually curvature attribute generation. The attributes calculated from the dip-steering cube are guided along a three dimensional surface on which the seismic phase is approximately the same. The dip/azimuth information stored in the steering cube is used to create a virtual horizon at each position, thus effectively filtering the data from noise when used in conjunction with a median filter. This allows the removal of random noise in the dip steering cube, and enhances laterally continuous seismic events by filtering noise along the structural dip. In median filtering, the centre amplitude in a dip-steered circle is replaced by the median amplitude within the extraction volume; the effect is an edge-preserving smoothing of the seismic data.

Finally, several volumetric dip-steered-curvature attributes were computed from the seismic volume and the dip-steering volume, following the method of Al-Dossary and Marfurt (2006). This method uses a sub-volume of data to compute the curvature at every point in the 3D seismic cube, in multiple wavelengths. Shorter wavelengths denote intense and highly localized fracture patterns and longer wavelengths correspond to broader fractures.

Natural fracture networks in the Cooper Basin

This study, using both seismic amplitude and attributes mapping, allowed us to map and to better constrain the structure and the natural fracture network in the region covered by the 3D seismic cubes in the Cooper and Northern Perth basins.

The Cooper Basin is affected by numerous structures of various scales. At the levels of the Roseneath and Murteree Shale Formations, to the southeast of the study area is the regional-scale Moomba-Big Lake fault, trending SW-NE. This high-angle fault is dipping to the southeast, with the folded hanging-wall being uplifted by roughly 0.1s to 0.2s. A series of more spatially limited folds also appear in the footwall of the Moomba-Big Lake fault, away from the fault itself. These folds appear to be symmetrical in section-view, and present generally four-way closure geometries in map view. The top of the Cooper Basin sediments is a regional unconformity, which also marks a boundary in the deformation style. Above at this level, the beds appear less deformed, with some very subtle low amplitude folds of kilometric-scale.

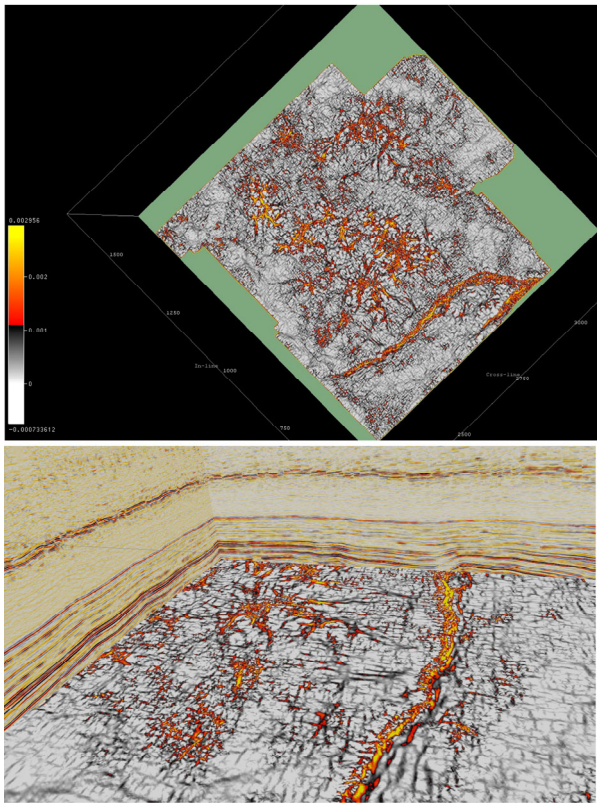

Figure 6: Top: Attributes maps at 2000ms across the Moomba Big Lake 3D seismic cube; Bottom: 3D view of the 2s time-slice with the amplitude inline and crossline for visual comparison.

A clear pervasive fabric is evidenced by the most positive curvature attribute (Fig 6), but remains invisible on the amplitude time slices or extraction along the horizons. This fabric consists of linear features with various lengths, mainly orientated along two directions, NW-SE and SW-NE. These fabrics are visible on time slices between the 1.7s and 2.2s, as well as along the horizon extraction maps. The density of this fabric is variable on both the Roseneath and the Murteree Shales. It appears that this fabric is generally denser close to the faults and at the apex of the mapped folds. However, other areas characterized by a low intensity of deformation also display a strong fabric as well. A drawback of this analysis is the potential limited detection of the acquisition footprint, reducing the resolution and scale of the fracture analysis.

This pervasive fabric displayed using the seismic processing and imaging techniques is parallel to the fractures observed on image logs in the Cooper Basin. It is therefore possible that the seismic attributes display actual fractures. This approach is currently being applied in the Northern Perth Basin, which we suggest will display a similar correlation with fractures mapped using image logs.

Summary

Different methods, valid for different observation scales, can be used to characterise in-situ stress and natural fracture networks. In this work, we have focussed on well-derived data, such as geophysical logs, and three-dimensional seismic data.

The Cooper Basin is a Late-Carboniferous to Middle-Triassic intraplate sag basin. The maximum horizontal stress orientation has been determined using image logs at ~100. Stress magnitudes in the Cooper Basin demonstrate a transitional strike-slip fault to reverse fault stress regime. Conjugate natural fractures striking NW-SE and NE-SW are considered to be active and open to fluid flow in this present-day stress regime. Seismic attribute mapping has identified a structural fabric in the same orientation as these fractures. Thus, implying good connectivity between these open fractures and numerous potential fluid pathways.

The Northern Perth Basin is part of the larger Late-Carboniferous to Early-Permian rift basin. The maximum horizontal stress orientation has been determined using image logs at ~084. Stress magnitudes in the Northern Perth Basin demonstrate a transitional strike-slip fault to reverse fault stress regime. Natural fractures striking N-S and NW-SE are considered to active and open to fluid flow in this present-day stress regime.

For completeness, the description of the fracture network should be combined with direct observation along oriented core and field work. However, this study demonstrates the importance evaluating both seismic data and well log data to understand in-situ stresses and the associated fracture networks where these direct data are not available.

References

Al-Dossary, S., and K. J. Marfurt, 2006, Multispectral estimates of reflector curvature and rotation: Geophysics, v. 71, p. 41-P51.

Alexander, E.M., 1998, Lithostratigraphy and Environments of Deposition, in Gravestock, D.I., Hibburt, J.E., and Drexel, J.F., eds., The Petroleum Geology of South Australia, Cooper Basin, Volume 4: South Australian Department of Primary Industries and Resources, Report Book, 98/9 PIRSA Adelaide, Australia, p. 69–115.

Anderson, E.M., 1951, The dynamics of faulting and dyke formation with applications to Britain: Oliver Boyd, Edinburgh.

Backé, G., Abul Khair, H., King, R., and Holford, S., 2010, Fracture mapping and modelling in shale-gas target in the Cooper Basin, South Australia: Australian Petroleum Production and Exploration Association Journal, v. 51.

Barton, C.A., 2000, Discrimination of natural fractures from drilling-induced wellbore failures in wellbore image data – implications for reservoir permeability: Society of Petroleum Engineers International Petroleum Conference and Exhibition, Mexico.

Bell, J.S., 1996a, In situ stresses in sedimentary rocks (part 2): applications of stress measurements: Geoscience Canada, v. 23, p. 135-153.

Bell, J.S., 1996b, In situ stresses in sedimentary rocks (part 1): measurement techniques: Geoscience Canada, v. 23, p. 85-100.

Bell, J.S., and Gough, D.I., 1979, Northeast-southwest compressive stress in Alberta: Evidence from oil wells: Earth and Planetary Science Letters, v. 45, p. 475-482.

Brudy, M., and Zoback, M.D., 1999, Drilling-induced tensile wall-fractures: implications for determination of in-situ stress orientation and magnitude: International Journal of Rock Mechanics and Mining Sciences, v. 36, p. 191-215.

Dickey, P.A., 1986, Petroleum development geology: 3rd edn. Pennwell Books, Tulsa.

Engelder, T., 1993, Stress Regimes in the Lithosphere: Princeton University Press.

Healy, D., Jones, R.R., and Holdsworth, R.E., 2006, Three-dimensional brittle shear fracturing by tensile crack interaction: Nature, v. 439, p. 64-67.

Heffer, K.J., and Lean, J.C., 1993. Earth Stress Orientation – A control on, and guide to, flooding directionality in a majority of reservoirs, in, W. Linville, ed., Reservoir Characterisation III: Pennwell Becks, Tulsa, p. 799-822.

Hill, A.J. and Gravestock, D.I., 1995, Cooper Basin, in, Drexel, J.F., and Preiss, W.V., eds., The Geology of South Australia, Volume 2: The Phanerozoic. South Australian Geological Survey Bulletin, pp. 78–87.

Hillis, R.R., and Reynolds, S.D., 2000,The Australian Stress Map: Journal of the Geological Society, London, v. 157, p. 915-921.

Hodge, C. C., 2005, Seismic evidence for reverse and wrench fault tectonics - Cliff Head Oil Field, Perth Basin. Australian Petroleum Production and Exploration Association *Journal*, 381-398.

Jaeger & Cook, 1979

King, R.C., Hillis, R.R. & Reynolds, S.D. (2008) In situ stresses and natural fractures in the Northern Perth Basin, Australia: Australian Journal of Earth Sciences, v. 55, p. 685-701.

Kirsch, V., 1898, Die Theorie der Elastizität und die Beddürfnisse der Festigkeitslehre: Zeitschrift des Vereines Deutscher Ingenieure, v. 29, p. 797-807.

Means, W.D., 1976, Stress and Strain: Springer-Verlag, Berlin.

Mory, A.J., and Iasky, R.P., 1994, Structural evolution of the onshore Northern Perth Basin, Western Australia, in, Purcell, P.G. and Purcell, R.R., eds., The Sedimentary Basins of Western Australia: Perth, Western Australia, Proceedings of the West Australia Basins Symposium, p. 781-789.

Peška, P., and Zoback, M.D., 1995. Compressive and tensile failure of inclined well bores and determination of in situ stress and rock strength: Journal of Geophysical Research, v. 100, p. 12791-12811.

Quaife, P., Rosser, J., and Pagnozzi, S., 1994, The structural architecture and stratigraphy of the offshore Northern Perth Basin, Western Australia, in, Purcell, P.G. and Purcell, R.R., eds., The Sedimentary Basins of Western Australia: Perth, Western Australia, Proceedings of the West Australia Basins Symposium, p. 811-822.

Reynolds, S.D., and Hillis, R.R., 2000. The in situ stress field of the Perth Basin, Australia: Geophysical Research Letters, v. 27, p. 3421-3424.

Reynolds, S.D., Mildren, S.D., Hillis, R.R., and Meyer, J.J., 2004, The in situ stress field of the Cooper Basin and its implications for hot dry rock geothermal energy development: PESA Eastern Australian Basins Symposium II, p. 431-440.

Reynolds, S.D., Mildren, S.D., Hillis, R.R. and Meyer, J.J., 2006, Constraining stress magnitudes using petroleum exploration data in the Cooper-Eromanga Basins, Australia: Tectonophysics, v. 415, p. 123-140.

Song, T., and Cawood, P. A., 2000, Structural styles in the Perth Basin associated with the Mesozoic break-up of Greater India and Australia: Tectonophysics, v. 217, p. 55-72.

Van Ruth, P., Hillis, R., Tingate, P., and Swarbrick, R., 2003. The origin of overpressure in 'old' sedimentary basins: an example from the Cooper Basin, Australia: Geofluids, v. 32, p. 125-131. DOI:10.1046/j.1468-8123.2003.00055.x.

A Comprehensive 3D Thermo-poroelastic Numerical Model for Evaluation of Heat Recovery Potential from Enhanced Geothermal Systems

Joshua Koh, Abdul Ravoof Shaik and Sheik S Rahman*
sheik.rahman@unsw.edu.au
School of petroleum Engineering, University of New South Wales, Sydney, Australia

A 3D numerical geothermal reservoir model has been developed for the purpose of studying coupled changes in reservoir permeability, heat transfer and fluid flow due to long term production and thermal drawdown (Koh et al., 2011). This study integrates four key elements: a natural fracture characterization model, a fluid flow simulation model, a heat transfer model and a geomechanical stimulation model. Fluid flow is simulated by fully coupling stresses and temperature to the flow equations. The heat transfer model is based on conductive heat transfer within the reservoir rock, convective heat transfer through the reservoir fluid and time dependent thermal equilibrium between the rock and fluid. The stimulation model simulates the shearing of fractures and the stress dependent permeability changes in a dynamic process by coupling the thermo-poroelastic fluid flow and the shear dilation analysis.

Patchwarra geothermal reservoir was used as a field case to study the degree of stimulation that can be achieved and subsequent thermal drawdown over a productive life. A stochastic fracture network (Tran and Chen, 2007) of the Patchwarra field was generated based on the data available in the open literature (Mildren et al. 2007). The reservoir was subjected to different pressure cycles to determine the degree of permeability enhancement that could be achieved. Stress changes due to thermal drawdown and consequent change in permeability over the reservoir's productive life was monitored. Flow rates and corresponding pressure losses between the injector and producers as well as heat recovery of the produced water were calculated to assess the geothermal potential of the reservoir. Different well placement scenarios were examined to assess the impact of directional fracture interconnectivity on production rates. The results of this study has shown that directional fracture interconnectivity and injection schedule has a profound effect on heat recovery from enhanced geothermal systems. This has allowed us to select an optimum well placement scenario which maximises the production rate with minimum pressure loss.

We have also observed that effective tensile normal stresses induced by the injected cold fluid tends to increase fracture apertures, and hence, increase fracture permeability within the zone of cooling (Ghassemi and Kumar, 2007).

Keywords: Geothermal, EGS, stimulation, thermal drawdown

Results and Discussion

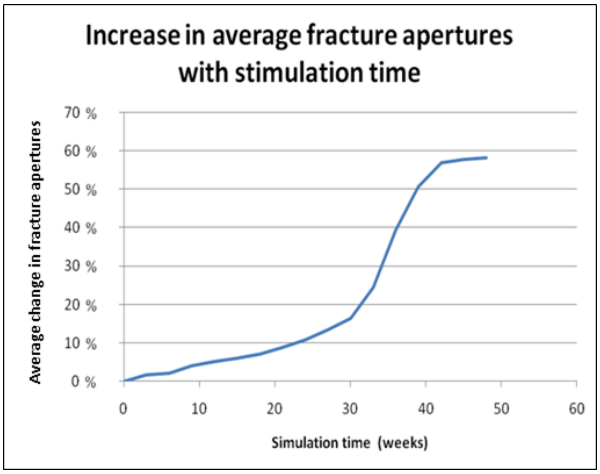

Figure 1: Average increase in fracture apertures due to stimulation

Results of shear dilation are presented as average percentage increase in fracture aperture and dilation events with time. From **Fig. 1**, it can be seen that there exists three distinct periods: 0-28 weeks, 28-42 weeks and greater than 42 weeks. Until about 28 weeks, the rate of occurrence of dilation events due to induced fluid pressure remains fairly constant. Following this time, the rate of occurrence of shear dilation increases sharply until about 42 weeks. This phenomenon can be explained as follows. Due to the anisotropic stress state of the reservoir rock, there exists resultant shear and normal traction components along variably oriented fracture planes. When the reservoir pressure increases (due to stimulation pressure), the normal traction components (compressive initially) on the fracture planes diminish, however, the shear components prevail. Eventually, the fracture shear dilation pressure is reached, whereby the normal (compressive) traction on the fracture plane is insufficient in preventing shear failure and the fracture undergoes slip in shear and dilates. This results in a large fold increase in permeability and allows rapid propagation of fluid pressure through the fracture network. Eventually, reservoir permeability increases significantly, both due to

pressure induced inflation (temporary) and shear dilation (retainable) of the fracture network. At this time, as seen through the 2nd inflexion point in Fig. 1, most fractures have been jacked open and all the shear tractions on the fracture planes have been mobilized for shear dilation. Thereafter, no significant dilation events can be observed (a plateau of events is reached).

Pore Pressure and Fluid Velocity Distribution

The fluid pore pressure distribution and the RMS fluid velocity profile in the reservoir after 5 years are presented in **Figs. 2** and **3** respectively. In Fig. 2, the pressure profile between injector and producer is reasonably smooth as the pore pressure has had time to establish a quasi-steady state. The velocity profile shown in Fig. 3 illustrates the ability of the model to retain a high level of heterogeneity and regions of high and low velocities are clearly seen distributed throughout the flow domain. The fluid velocities distributed through the fracture network become concentrated close to the injection and production wells.

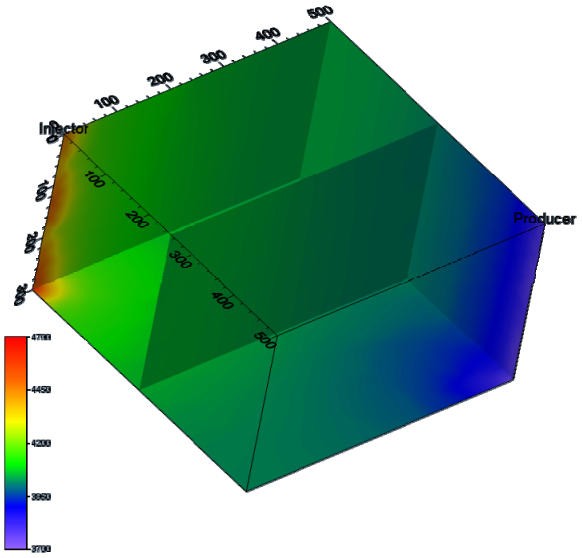

Figure 2: Reservoir pore pressure profile after 5 years of production with 1000 psi pressure loss between injector and producer.

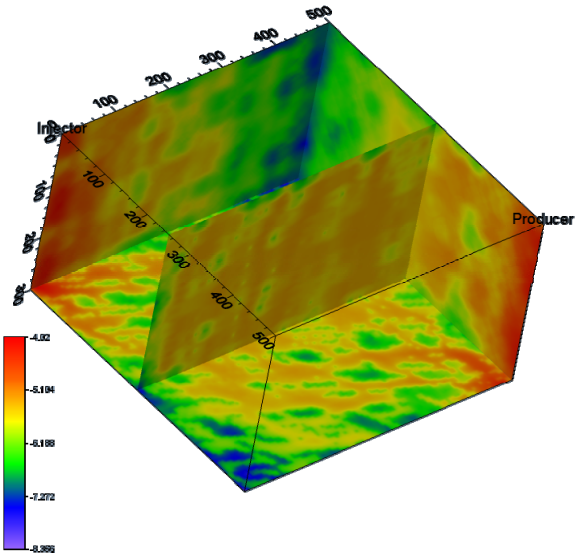

Figure 3: Rms fluid velocity profile after 5 years of production with 1000 psi pressure loss between injector and producer.

Rock and Fluid Temperature Distribution

In **Figs. 4** and **5**, the changes in rock temperature over a period of 5 and 20 years respectively are presented. It can be seen from these figures that at early time, the temperature of the rock body remains quite high. During late time (20 years), the rock body cools down and the direction of cooling is influenced by the fracture orientations.

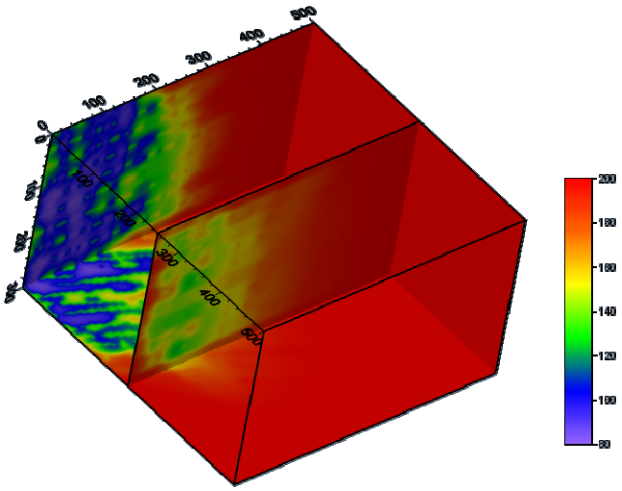

Figure 4: Reservoir temperature profile after 5 years of production with 1000 psi pressure loss between injector and producer.

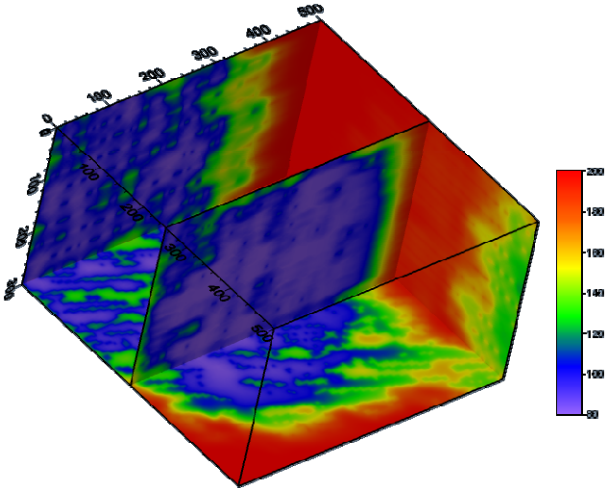

Figure 5: Reservoir temperature profile after 20 years of production with 1000 psi pressure loss between injector and producer.

Effect of Increased Production Rate

It is observed that with increase in production rate, the rock body cools at an increasing rate, which in turn results in faster thermal breakthrough of the production fluid (see **Fig. 6**). Net effect of rapid thermal breakthrough as such is derived from the fact that the residence time of fluid within the fracture network is insufficient to capture sufficient heat from the hot rock matrix.

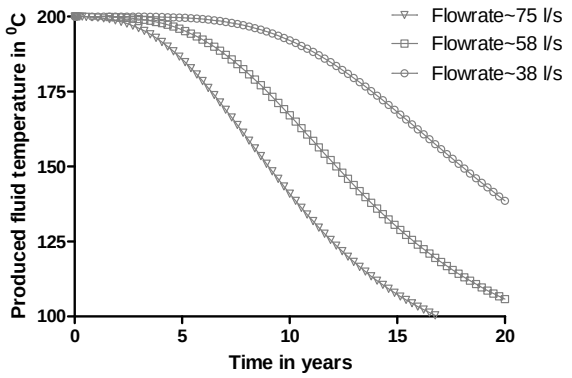

Figure 6: Dynamic produced fluid temperature for different flow rates

Effect of Thermal Stresses

The effective stresses in the reservoir rock at early production time (3 years) and late production time (10 years) are presented in **Fig. 7** (x direction). It should be noted that a geomechanics sign convention is adopted for stresses (positive for compression). From both plots, it is apparent that the effective stresses in reservoir at late time (10 years) are significantly less compressive than those at early time. The decreases in effective stresses causes fracture dilation and therefore permeability enhancement.

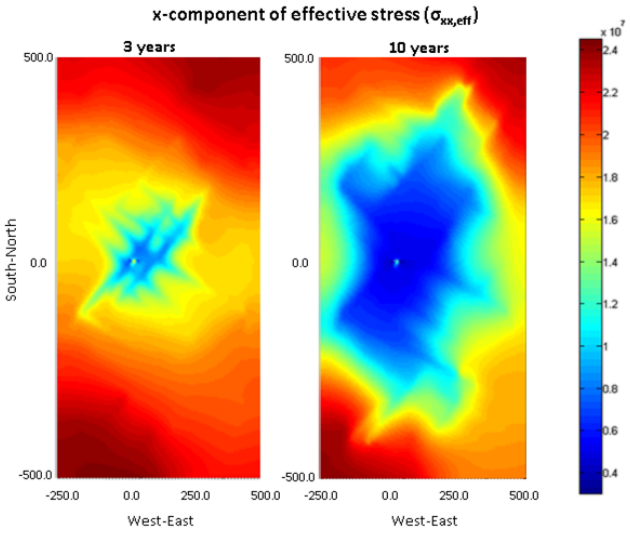

Figure 7: Effective stresses in the x direction at 3 years (left) and 10 years (right) injection time at mid reservoir plane showing decrease in effective stress due to matrix cooling.

Conclusions

In this paper, a thermo-poroelastic reservoir model is developed and used to study the effect fluid induced pressure on the stimulation of naturally fractured geothermal reservoirs.
The Patchwarra Formation in the Cooper Basin, Central Australia was used in the numerical study.

The effect of varying the production rate for a given pressure drop between the injector and producer was assessed. The net effect of increased flow rate is correlated with a more rapid thermal breakthrough and production fluid cooling. This can be attributed to the thermo-hydro-mechanical coupling in the simulation model.
The circulation of cold water induces tensile thermal stresses which allow residing fractures to dilate and enhance permeability.

References

Ghassemi, A. and G. Suresh Kumar (2007). “Changes in fracture aperture and fluid pressure due to thermal stress and silica dissolution/precipitation induced by heat extraction from subsurface rocks.” Geothermics **36**(2): 115-140.

S. Mildren, J. Burgess and J. Meyer, (2005). “Multiple Application of Image Log Data to EOR Operation in the Cooper Basin Australia.” SPE 97792.

Tran, N., Z. Chen, et al. (2007). "Characterizing and modelling of fractured reservoirs with object-oriented global optimization." Journal of Canadian Petroleum Technology **46**(3): 39-45.

Koh, Joshua, Roshan, Hamid, Rahman, Sheik S. (2011) ”A numerical study on the long term thermo-poroelastic effects of cold water injection into naturally fractured geothermal reservoirs.” Computers and geotechnics, **38**(5): 669-682

Mid West Geothermal Project, North Perth Basin, Australia

Adrian Larking*, Gary Meyer, Mark Ballesteros
alarking@greenrock.com.au
Green Rock Energy Limited, 6/38 Colin Street, West Perth, Western Australia 6005, Australia

Green Rock Energy Limited (Green Rock) recently shifted its focus from direct heat projects in the central Perth Basin to concentrate on more commercially attractive electricity production opportunities in the northern Perth Basin, Western Australia. This area has the highest heat flows in the Basin, and the natural geothermal waters contained in hot sedimentary aquifers provide a significant potential resource.

Green Rock holds seven Permits (the Mid-West Geothermal Project) occupying 2,094 km^2 in the north Perth Basin which the Company considers contain good geological resource potential for power generation (Figure 1). These Permits are located near oil and gas fields, close to power infrastructure in a region with rapid growth of power demand where there is an extensive power distribution network. The Mid West region has the fastest growing power demand in the State. Development of magnetite iron ore mining and processing will require several hundreds of MWe and potentially over 1GW of baseload electricity supply in the next 5-10 years.

The Company's near term aim is to find the optimum location to drill the first two wells to recover geothermal energy for commercial generation of electricity to supply this burgeoning growth from major mining developments planned in the MidWest region.

Keywords: Perth Basin, Mid West WA geothermal system, permeability.

Regional Setting

The Perth Basin is a 1,000 km long N-S trending extensional rift containing a thick sequence of sediments in places up to 15 kilometres deep (Figure 2). The structure of the Perth Basin is the product of multiple rifting events during the Permian, Late Triassic to Early Jurassic and Middle Jurassic to Early Cretaceous. Rifting produced the series of deep, north-south trending basins along the western margin of the Yilgarn Craton. The Basin is an intensely faulted half-graben comprised of a series of sub-basins, troughs, shelves and ridges containing predominantly Early Permian to Late Cretaceous sedimentary sequences. Sediment deposition in the Basin commenced with extension during the Permian (~290 Ma) and continued to the Early Cretaceous (~138 Ma) (Figure 3). The Basin was uplifted during the final separation of Western Australia and greater India during the breakup of Gondwana. To the west the rift sediments extend offshore beneath the Indian Ocean to the continental–oceanic boundary.

The structural setting of the Perth Basin is characterised by its extensional tectonic origins, thick sedimentary successions which overlie apparently hot crystalline basements, high heat flows and evidence of the existence of substantial geothermal energy resource potential. The Perth Basin has a vertical structural asymmetry with the sedimentary fill being thicker towards the east of the half graben. The hills marking the eroded NS trending Darling Fault form the eastern boundary of the Perth Basin. This asymmetry may influence the ground water flow which in places is known to flow westwards into the sea from the land.

The early extensional tectonic regime of the Perth Basin is now overprinted by an essentially compressional setting. Stress field data for the Perth Basin are derived mainly from petroleum well borehole breakouts and drilling-induced tensile fractures from 34 measurements as illustrated in the World Stress Map. These data suggest the contemporary stress regime for the Perth Basin is transitional reverse to strike-slip with an approximate east-west maximum horizontal compression direction.

Three major fault trends have been observed across the Northern Perth Basin:

- E-W (275°) striking listric normal faults were associated with the first phase of rifting during north-south extension initiated in the Early Permian;
- The 2nd phase of rifting during the break-up of Gondwana in the Jurassic produced the most dominant structural trends in the Perth Basin, with major N-NNW (~360°-345°) striking listric normal faults and several large N-S striking anticlines.
- NW (~310°) trending strike-slip transfer faults were the latest stage of basin evolution and were caused by major basin inversion and seafloor spreading in the Indian Ocean during the Early Cretaceous.

East and N-NW striking faults are currently critically stressed and have been re-activated. Open fractures were observed in several wells and are commonly orientated in directions NNE and NNW as well as near E-W.

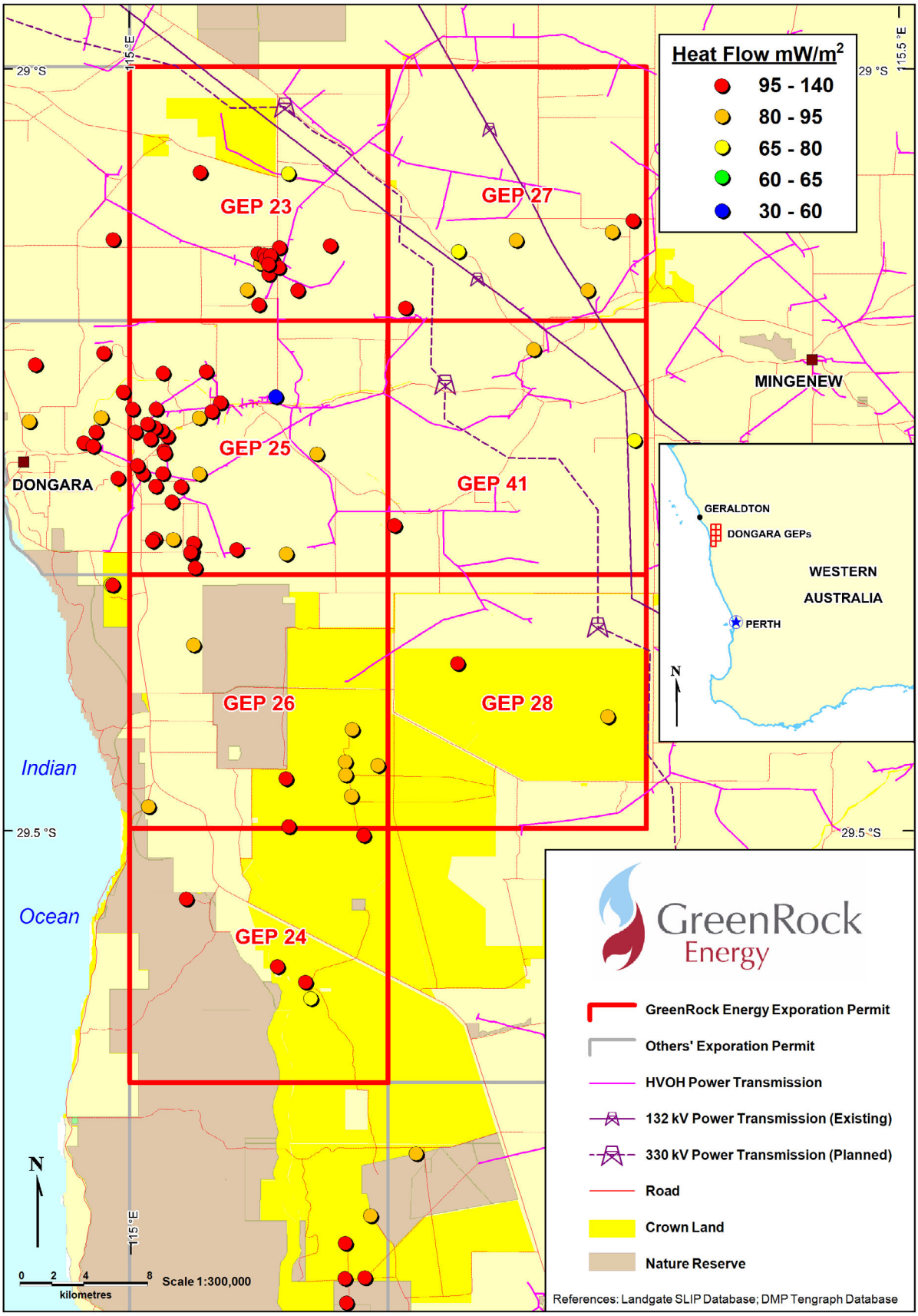

Figure 1. Heat Flow in Green Rock Permits (after unpublished report by Hot Dry Rocks Pty Ltd).

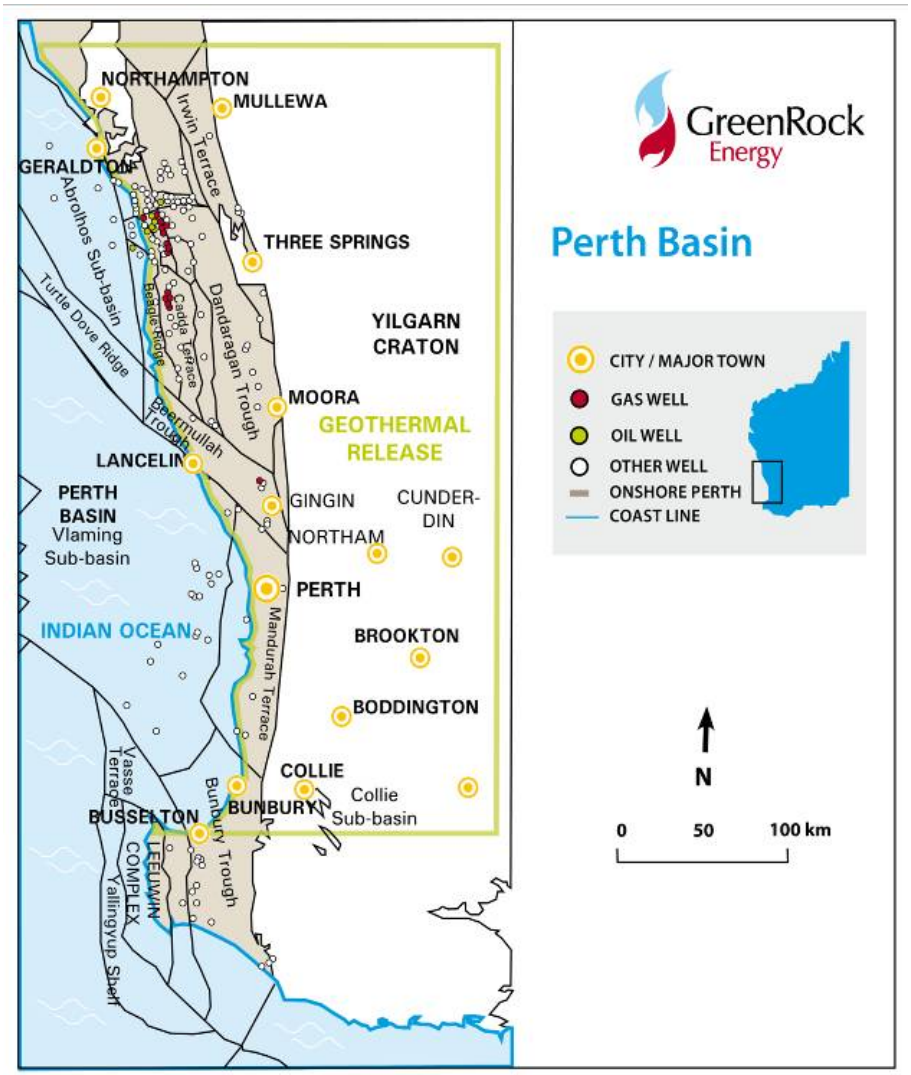

Figure 2. Perth Basin Structural Elements

Geothermal System

Data derived mainly from petroleum wells indicate there is an active *geothermal system* in the northern Perth Basin. There are a number of key elements required for a viable geothermal system in hot sedimentary aquifers. There must be a supply of natural water in sufficient volume, trapped in an extensive permeable reservoir which has been heated sufficiently by a sub-surface heat source so the heat is retained beneath thermally insulating impermeable sealing sediments. A viable reservoir requires an extensive interconnected network of matrix, intergranular, vuggy or fracture porosity with capacity to hold large volumes of geothermal water with permeability to facilitate flow of the water at commercial rates to the well bore.

With its thick sequences of sandstones, impervious and thermally insulating shales and coals, the Perth Basin has potential to house hot sedimentary aquifer (HSA) geothermal energy resources. This is borne out by high geothermal gradients and heat flows determined by independent observers (Chopra and Holgate, 2005 and HDRPL, 2008). There is considerable evidence from drilling of hot geothermal water trapped in sediments in the northern Perth Basin but the origin of its heat content has not been resolved. The source of the high heat flows in the Perth Basin may be radioactive crystalline rocks and radiogenic sedimentary horizons however any direct evidence is lacking. Granites in the Archean Craton bordering the Perth Basin contain abundant radiogenic minerals and sources (Middleton, 2010) and at shallow depths the Basin contains some of the world's largest mineral sands deposits many of which are rich in radiogenic minerals.

The geothermal systems in the north Perth Basin have little surface expression hence deep drilling is required to map the distribution of sub-surface heat resources. Most geological knowledge of the north Perth Basin was derived from the petroleum industry where there is a history of petroleum exploration and drilling starting in the 1950s. Around 250 petroleum wells have been drilled and 23,985 km of 2D seismic and 2,838 km^2 of 3D seismic acquired in all of the Perth Basin. Although data derived from petroleum wells are

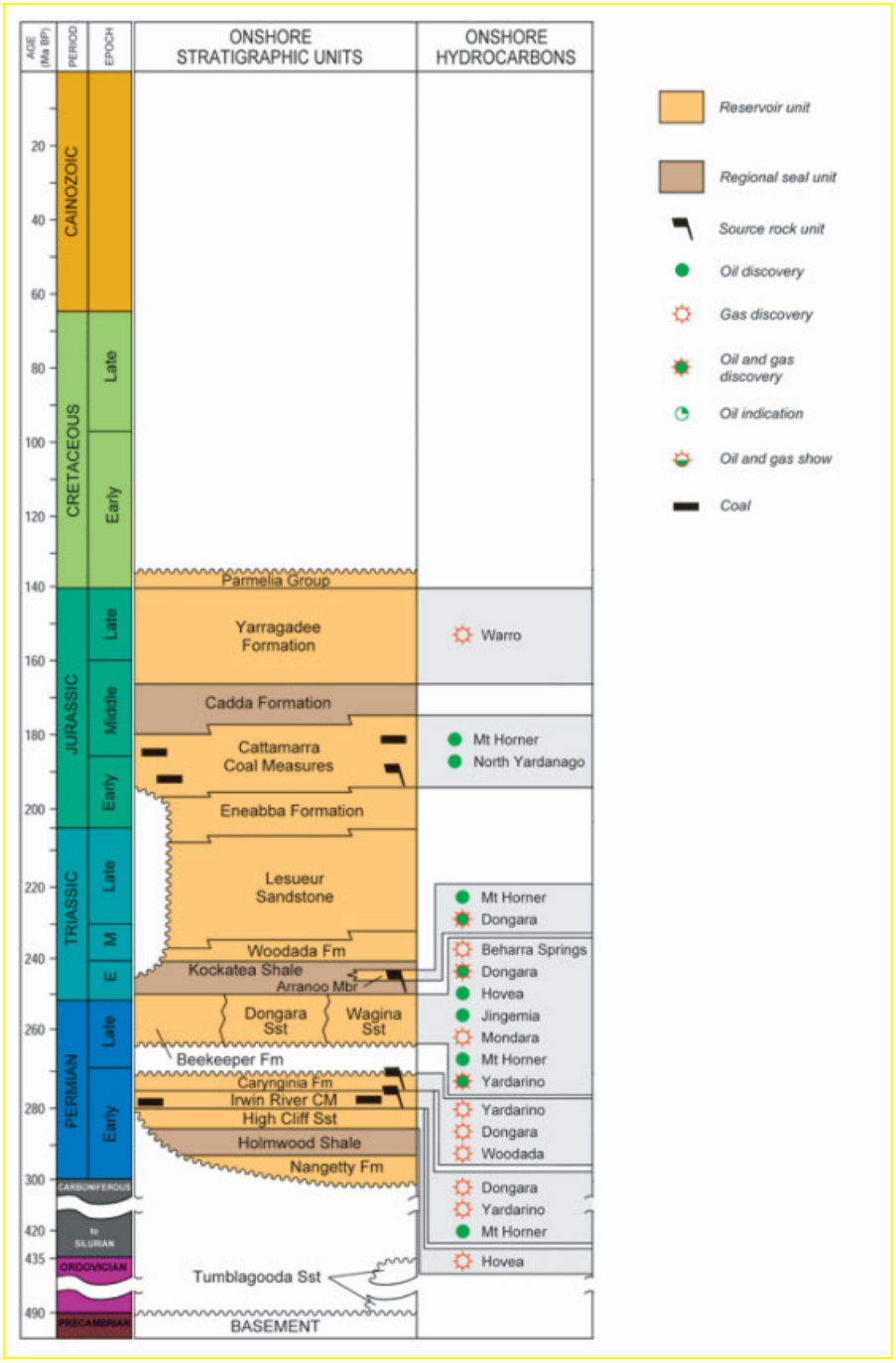

Figure 3. Perth Basin Generalised Stratigraphy of North Perth Basin (Ghori, Khwaja, 2008 Geological Survey of Western Australia).

rather sparsely distributed, a substantial portion is concentrated in and around Green Rock's exploration permits in the northern Perth Basin, where 13 oil and gas fields have been discovered to date. New activity exploring for tight gas and shale gas in the north Perth Basin is set to add substantially to the amount of 3D seismic acquired and petroleum wells drilled in the region.

To maximise flow rates from these anomalously hot sedimentary reservoirs Green Rock is targeting the combination of natural matrix and fracture permeability in favourably oriented structural corridors where the fractures are most likely to remain open at depth in the Permits. To achieve this, the Company is focussing on the hottest locations in sediments shallower than 4,000 metres with good 3D seismic coverage and access to high voltage power lines. Based on past experience in the area, drilling to these depths is should be relatively fast and should not present any particular technical difficulty.

Until this year Green Rock has concentrated on using existing petroleum wells and water bores to define the temperature and heat flow distribution over the Permits and identify areas where potentially permeable sediments occur within the areas of highest heat flow. Heat flows in Green Rock's Permits are amongst the highest determined in the Basin averaging above 90 mW/m^2 and in places substantially exceeding 100

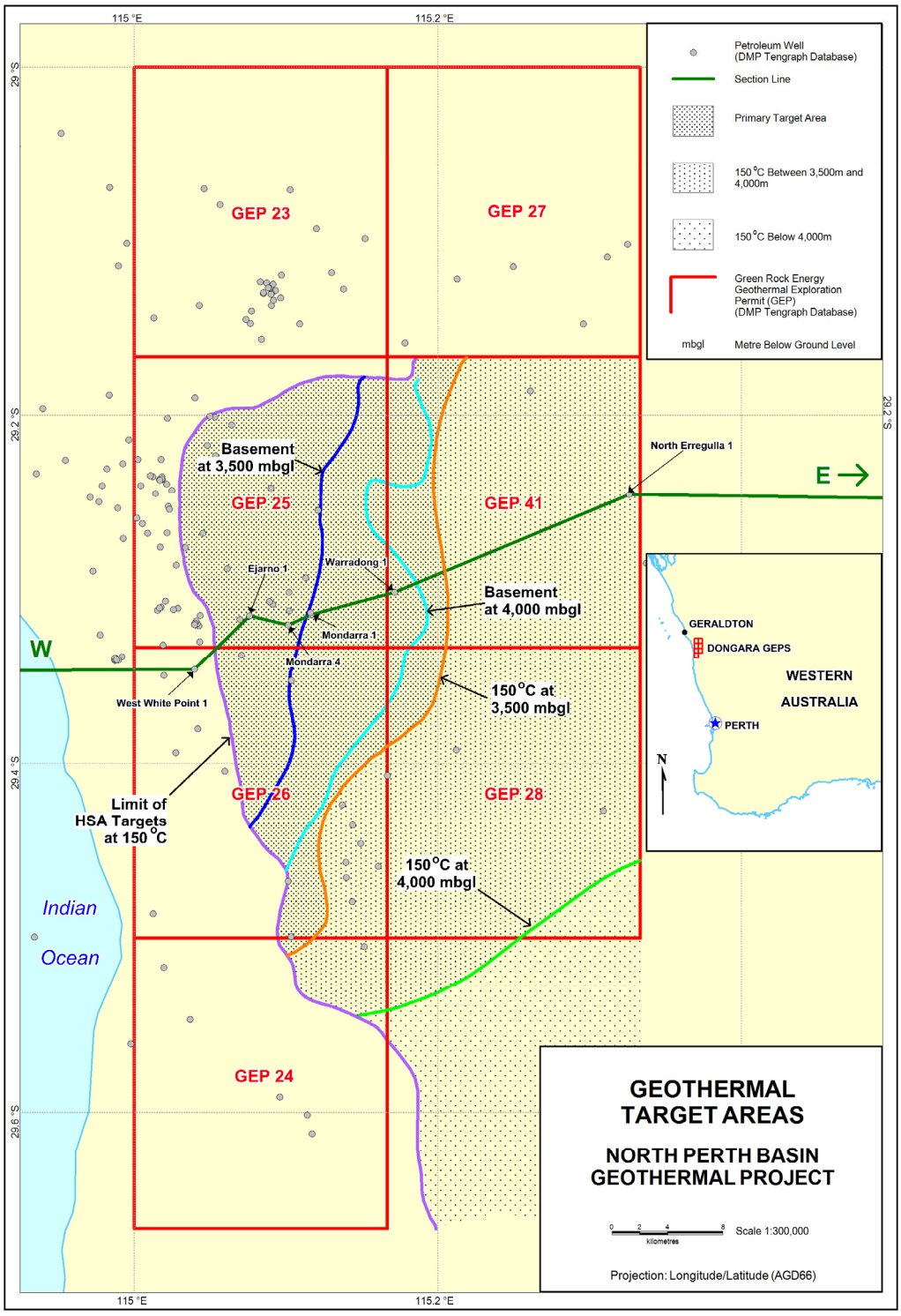

Figure 4: Green Rock Geothermal Target Areas

mW/m^2. This is anomalously high compared to Australian average surface heat flows. The highest heat flows may be due to the contribution of some convective heat flow but to date there is no definitive evidence for this. There are 132 petroleum wells in the Permit areas including 39 where the temperature in sediments has been estimated to be over 150 °C at depths less than 3,500 metres. This temperature is sufficient to generate electricity commercially provided that sufficient geothermal water recovery flow rates can be achieved.

This year the Company concentrated on mapping the distribution of natural matrix and fracture permeability within these regions of highest heat flows with a view to selecting suitable drilling locations near existing power transmission lines for easy access to market. To identify where natural permeability is likely to be highest, reinterpretation of 3D seismic survey data collected within the Permits is underway. A number of potentially permeable intervals has been identified, primarily in the Triassic and

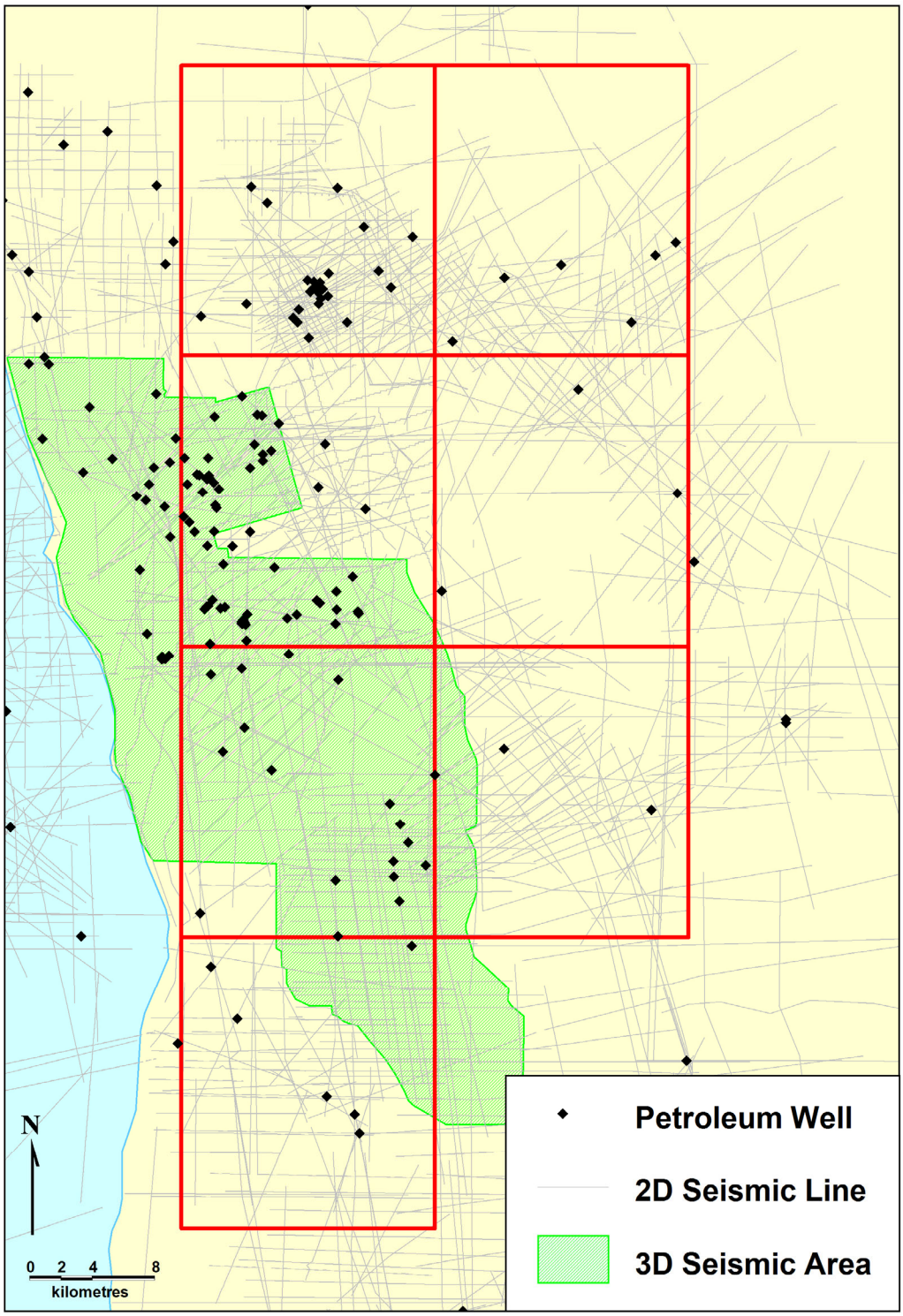

Figure 5: Seismic surveys & wells in Permits

Permian formations. Mapping efforts will focus on defining the depth and temperature associated with these formations over the Permit areas, the structural fabric of the Basin and the distribution of potential flow paths within the sediments. This work has involved mapping geological stratigraphy, structure and natural fault and fracture patterns together with analysis of data derived from petroleum wells to detect and distinguish natural open fractures and barriers to fluid flow in relation to the existing structures and stratigraphy and the sub-surface stress field.

Fortunately, the Department of Mines and Petroleum (DMP) in Western Australia supplied the Company with around 780 km^2 of 3D seismic data acquired by the petroleum industry within the regions in the Permits with the highest heat flows.

Seismic data can be used to map the location of sediments formed in a depositional environment with the best potential to have high porosity and matrix permeability. Some seismic sequence stratigraphic studies have been undertaken for this purpose by the petroleum industry to

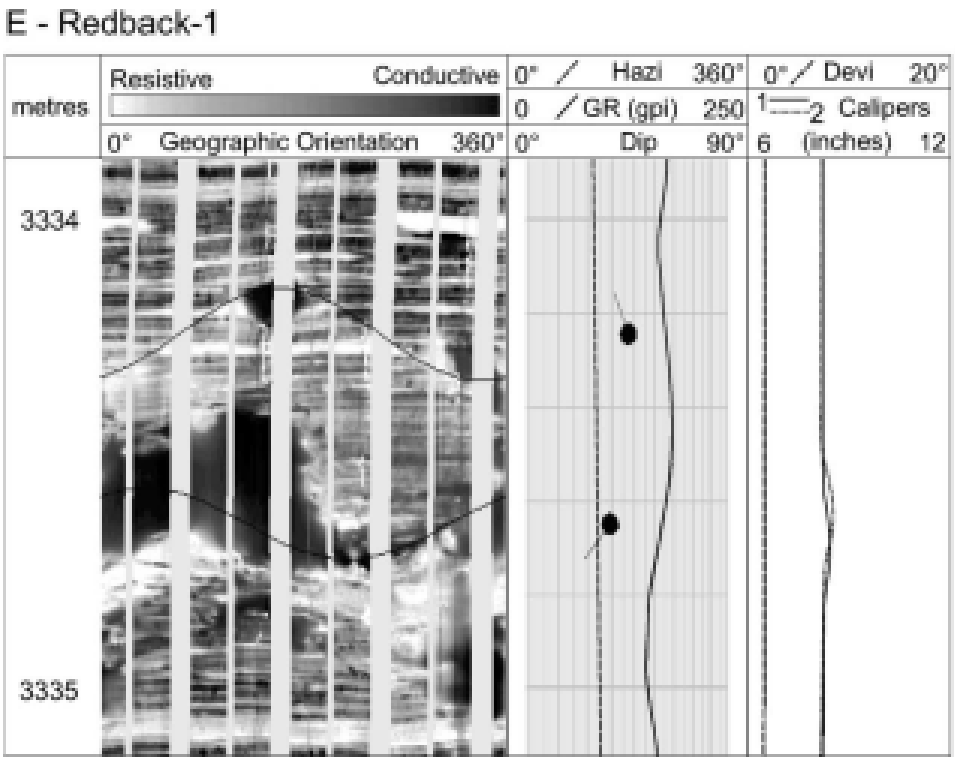

Figure 6: FMI Image from Redback 1 (King et al 2008)

reconstruct the depositional environment of the sedimentary sequences. One limitation is that most of these studies concentrated on the existing productive petroleum reservoirs such as the Permian Wagina Sandstone to the exclusion of other potential HSA reservoirs in the same areas.

Porosity and permeability commonly deteriorate with increasing depth in sedimentary basins due to compaction and diagentic cementation. Within Green Rock's permits in the North Perth Basin, petroleum wells have demonstrated good matrix permeabilities in Permo-Triassic sandstone reservoirs down to depths of around 2,700 metres but persist to significantly greater depths in some areas where conditions are favourable (Laker, 2000). There is some limited evidence of substantially lower permeabilities at greater depths where temperatures above 150ºC would be expected and chemical reactions may be more active. Much less is known about the potential for high water flows from natural fault or fracture permeability as this has not been targeted by the petroleum industry in this area.

This is not the full picture, as the amount of post-depositional uplift varies widely across the Permit areas; some parts of the Basin are currently at maximum depth of burial while other areas have experienced over 2000 metres of uplift (Laker, 2000). This has resulted in a complex relationship between porosity and permeability versus current subsurface depth. Consequently, the Company believes it is important to reconstruct the structural history of the Basin to properly map and understand reservoir compartmentalisation by faulting and variations of porosity and permeability with depth. In limited places there is evidence from well cores in the north Perth Basin of preservation of matrix porosity at depth by the presence of hydrocarbons or chlorite coatings in saline formation waters near petroleum fields. Protection against the effects of permeability destruction by silica cementation would require the hydrocarbons or chlorite grain coatings to have been in place before the onset of silica diagensis. So an understanding of the Basin history is important for mapping of porosity and permeability with depth (Laker, 2000).

At Landau in the Rhine Graben in Germany substantial volumes of geothermal water are produced via fracture permeability in sediments having very low matrix permeability (Schindler, et. al., 2010). Likewise in the northern Perth Basin it may be necessary to target fracture permeability at the depths required to obtain temperatures above 150 °C where matrix permeability alone may be insufficient for commercial geothermal fluid flow rates.

Reinterpretation of the 3D seismic to date has resulted in significant revisions by the Company to published information about locations and orientations of major faults. In addition, fault imaging and fracture analysis techniques are being utilised to provide finer resolution of faults and fracture networks from 3D seismic data. Although many natural fractures may be below the apparent size for resolution by seismic techniques they may still be detectable and

Figure 7: MT research survey in Dongara area, North Perth Basin.

recognisable by modern seismic imaging techniques. Also various seismic attribute analytical techniques can be used with 3D seismic to map fracture permeability by measuring different properties or attributes in different directions. This means it may be possible to map small fracture networks which may be important to understanding fluid flow in the sediments and to design wells to intersect the fracture networks in the optimum orientation. Green Rock is utilising these approaches in the north Perth Basin (eg. Opperman, 2011).

Knowledge of the location of natural fracture networks in the sub-surface is not sufficient for siting of wells to optimise geothermal fluid recovery. The geothermal productivity in natural fractures is dependent on whether the fractures remain open or are tight and sealed to flow. This depends on their orientation with respect to the structural fabric and orientation and magnitude of the current stress field in the sub-surface. To assist with resolving this, a geo-mechanical model of the current tectonic stress fields from various depths can be constructed. This can assist with orienting wells to tap critically stressed faults and fractures which are most likely to be reactivated and open and to avoid faults which may act as barriers to fluid flow. The model is also useful to ensure production and injection wells are aligned optimally in the sub-surface with respect to the direction of fluid flow. In this respect the Permits contain a major fault zone known as the Abrolhos Transfer Zone where the favourable alignment of this structural corridor relative to the current stress field should favour the formation and retention of open permeable faults.

There is evidence of conductive open fractures at depth in Green Rock's Permits. For example an image from a FMI log from the Redback #1 petroleum well shows an electrically conductive fracture about 25 cm wide at a depth of 3,334 metres. In view of this, an evaluation of logs and drilling data from existing petroleum wells is being carried out by the Company in association with the University of Adelaide in an attempt to detect open conductive fractures intersected in the wells and relate them to the mapped faults/fracture sets and the stress field. Fourteen wells have been evaluated to date for this purpose.

Magneto-tellurics (MT) is another technique being trialled by the Company to determine if it can assist to detect water saturated zones and fracture networks at depth. As at October 2011 the results of a MT research survey carried out by Institute of Earth Science & Engineering (IESE) at the University of Auckland (Figure 7) are being analysed and evaluated to identify broad zones at depth which are water saturated. MT has proven to be very effective elsewhere and is commonly used to locate water saturation in fractured hydrothermal reservoirs.

References

Chopra P.N. and Holgate, F. (Earthinsite Pty Ltd) (2005): Geothermal Energy Potential in Selected areas of Western Australia, a Report commissioned by Western Australian Department of Industry and Resources 2007; and also – A GIS Analysis of Temperature in the Australian Crust; Proceedings of World Geothermal Congress, Antalya, Turkey 2005, pp 7.

Davidson, W.A.(1995) Hydrogeology and groundwater resources of the Perth Region, Western Australia: Western Australia Geological Survey, Bulletin 142, 257 pp

Freeman, M.J., and Donaldson, M.J (2006): Geology of the southern Perth Basin and Margaret River wine district, southwestern Western Australia – a field guide: Western Australia Geological Survey, Record 2006/20

Gori, K.A.R. (2008): Perth Basin's Geothermal Resources, Australian Geothermal Energy Conference 2008, Extended Abstract. Geological Survey, Department of Industry and Resources

Hot Dry Rocks Pty Ltd (2008): Geothermal Energy Potential in Selected Areas of Western Australia, Perth Basin, pp 270.

Hot Dry Rocks Pty Ltd (2009): Western Perth Geothermal project, Geothermal Exploration Stage 2, unpublished report for Green Rock Energy Limited, pp28.

King, R. C., Hillis, R. R. and Reynolds, S. D.(2008) 'In situ stresses and natural fractures in the Northern Perth Basin, Australia, Australian Journal of Earth Sciences,55:5,685 — 701

Laker, Neil (2000): Sedimentological and Petrographic Review of the Permo-Triassic Sandstones of the Northern Perth Basin, Oolithica Geoscience Ltd report for AWE Ltd. 39pp.

Middleton, Mike F, (2010) Temperatures within Outcropping Radiogenic Granites, Implications for geothermal energy in Western Australia. Unpublished presentation at Geothermal Open Day, Department of Mines & Petroleum, Western Australia.

Mory, A.J., Haig, D.W., Mcloughlin, S., and Hocking, R.M (2005): Geology of the northern Perth Basin, Western Australia – a field guide: Western Australia Geological Survey, Record 2005/9

Mory, R.J, and Iasky, R.P.(1996): Stratigraphy and Structure of the Onshore Northern Perth Basin, Report 46, Geological Survey of Western Australia pp 126

Opperman, Ralf, (2011): A revolution in seismic visualisation of fault networks – implications for the drilling and production of resources, Gas & Oil Expo & Conference, North America 2011.

Origin Energy (2011): poster at APPEA Conference Perth, Australia

Regenauer-Lieb, Prof. K, Horowitz Dr F (2007), The Perth Basin Geothermal Opportunity, The University of Western Australia & CSIRO, p42-44, April 2007

Schindler, M., Baumgartner, J., Gandy, T., Hauffe, P., Hettkamp, T., Menzel, H., Penzkofer,P., Teza, D. Tischner, T. and Wahl, G, (2010): Successful Hydraulic Stimulation Techniques for Electric Power Production in the Upper Rhine Graben, Central Europe, Proc. World Geothermal Congress 2010, Bali, Indonesia.

Well Log and Core Based 3D EGS Flow Simulation – Application to the Raton Basin Thermal Anomaly, CO, USA

Leary PC*[1], Malin PE[1], Pogacnik J[1] & Macartney H[2]
p.leary@auckland.ac.nz
[1] Institute of Earth Science and Engineering, University of Auckland, New Zealand
[2] Pioneer Natural Resources USA, Inc, Denver CO, USA

Enhanced/Engineered Geothermal Systems (EGS) are conceptually simple but have long defied cost-effective field realization. The chief difficulties appear to be

- The high cost of drilling
- Difficulties in predicting flow.

While drilling costs continue to resist significant reduction, we believe important progress is at hand for addressing flow uncertainty *in situ* – the latter meaning at the drilling target itself. Accurate handling of *in situ* flow uncertainty can thus in principle reduce risks to EGS drilling.
Key to EGS progress is recognizing:

- the specific physical origin of *in situ* flow uncertainty on all scale lengths;
- the fact that *in situ* flow uncertainty admits no statistical/sampling/averaging solution;
- *in situ* flow uncertainty is amenable to numerical modeling;
- modeling *in situ* flow uncertainty can be integrated into well-log analysis;
- increased applications of horizontal drilling to hydrocarbon recovery provide a technology base relevant to EGS.

We discuss this sequence of points in the context of an EGS project centered on a pair of parallel horizontal wells. The wells are modeled as located in a rock volume with well log and core determined flow uncertainty. Focusing on *in situ* flow heterogeneity between the EGS well pair, we find an approximate scale-relation,

$$a^2\ell \sim Qr_0 / 2\pi\varphi v \sim O(10^6 m^3)$$

between a wellbore length ℓ and separation 2a and two EGS flow factors. These factors are: wellbore flow Q ~ 25L/s and mean *in situ* flow velocity v ~ 10-8m/s. The latter velocity allows sustained conductive heat recharge of the EGS volume. The other terms in this relation are wellbore radius r0 ~ 0.1m and mean porosity φ ~ 0.06. With these factors, sustained heat exchange can be realized, for example, for ℓ ~ 400m and 2a ~ 75m.

In this presentation we use well log-determined flow-uncertainty models to design wells for the Raton Basin that satisfies the scaling relation.

Key words: EGS, *in situ* permeability, fluid flow modeling, heat transport modeling

Introduction

Previous approaches to *in situ* flow modeling have assumed that spatial variation in porosity φ and permeability κ can be ignored in favor of using the mean values of φ and κ ($\underline{\varphi}$ and $\underline{\kappa}$). Corollary to this assumption is that a handful of small scale well-log and/or well-core samples adequately fix the *in situ* flow properties.

This mean-value approach to *in situ* flow is widely applied, for example, to time-dependent wellbore pressure data in hydrology (Theis 1935; Heath 1989; Ingebritsen, Sanford & Neuzil 2006), the oil and gas industry (Earlougher 1977), and geothermal fields (Grant et al. 1982; Edwards et al. 1982; Sanyal & Butler 2010). In particular, wellbore pressure histories are typically interpreted in terms of mean formation 'storage capacity' $\underline{\varphi}ch$' and 'flow capacity' $\underline{\kappa}h$, h = mean formation thickness and c = formation compressibility.

In the '$\underline{\kappa}h$' picture, fractures are typically inserted as large-scale, quasi-planar breaks in an otherwise quasi-uniform poroelastic 'matrix'. Fluid flow in such fractures is parameterised as laminar in a complex of intersecting fracture planes (e.g., Gringarten & Witherspoon 1973; Sayers & Schutjens 2007; Sayers 2007).

As obvious as such a picture appears, it has proved difficult to establish a coherent, systematic, quantitative measure of *in situ* fractures. This includes not only their distribution, but also their connectivity and transport of heat or solutes. Symptomatic of this difficulty is that wellbore pressure history data yield little insight into fracture-controlled heterogeneity. This is because a wide range of *in situ* fracture heterogeneity models return essentially the same time-pressure histories as a uniform '$\underline{\kappa}h$' medium (Leary and Malin 2011). The confusion wrought by such models has not helped make the case for investment in EGS projects.

We present here instead a 3D fracture-flow model based on well log and core data. The resulting time-pressure histories match data without any assumptions about storage or flow capacity uniformity. This well-data-driven approach produces flows that match the actual natural variability of the EGS site. As a result, both the expected flow of a given well design and its response to EGS enhancements can be 'honestly'

estimated. We illustrate this approach by applying it to the Raton Basin in Colorado.

The physical nature of *in situ* fluid flow based on well-logs and cores

Setting formation characteristics aside, the manner in which rock properties change as seen in well-logs and cores show that fluids percolate through spatially-correlated networks of grain-scale fractures. Such networks erratically link up in unpredictable fluid pathways at all scale lengths - from mm (grains) to km (reservoirs and above). The larger the spatial scale on which these fluid flow pathways function, the larger the volume of flow the pathways carry. However, at no point in such networks is it 'predicatable' how the flow connects further along. In contradiction to the 'uniform κh' picture of fluid flow, well-log and well-core data indicate that this spatial uncertainty is the primary feature of *in situ* flow.

The problem with the 'uniform κh' picture arises from the view of Biot (1962) and subsequent authors that *in situ* variations in fluid flow paths are uncorrelated. (See for example Thomsen (1985), Berryman and Wang (1995), Sayers (2007), Sayers and Schutjens (2007)) The assumption of uncorrelated variation of rock properties places a testable condition on the Fourier spectra of well-logs, namely

$$S(k) \sim \text{const}, \qquad (1)$$

Where S(k) = well-log fluctuation power at spatial frequency k. Despite its logical force and clarity, however, spectral condition (1) is rarely if ever encountered in well-log data. Instead, Fourier power spectra for well logs recorded in a range of physical properties, rock types, tectonic settings, and well trajectories consistently vary inversely with spatial frequency,

$$S(k) \sim 1/k. \qquad (2)$$

This relation holds over as many as ~ five decades of scale length, from ~1 cycle/km to ~1 cycle/cm (Leary, 2002). Fig 1 illustrates (2) for a suite of well logs from a reservoir outcrop.

The well-log "power-law" systematics in (2) (and the related well-core evidence discussed below) indicate that the grain-scale microphysics centers on a "critical-state" grain-scale fracture density n_{crit} (Leary 2002). As most crustal rocks are made of tough grains bonded by weak cements that fracture easily at small strains, grain-scale fractures are fundamental to crustal properties. Well-log power-law spectral like (2) show that grain-scale fractures build long-range correlation networks of fractures at all scale lengths. In particular, above critical density n_{crit}, through-going fracture pathways become highly probable at all scales within a crustal volume.

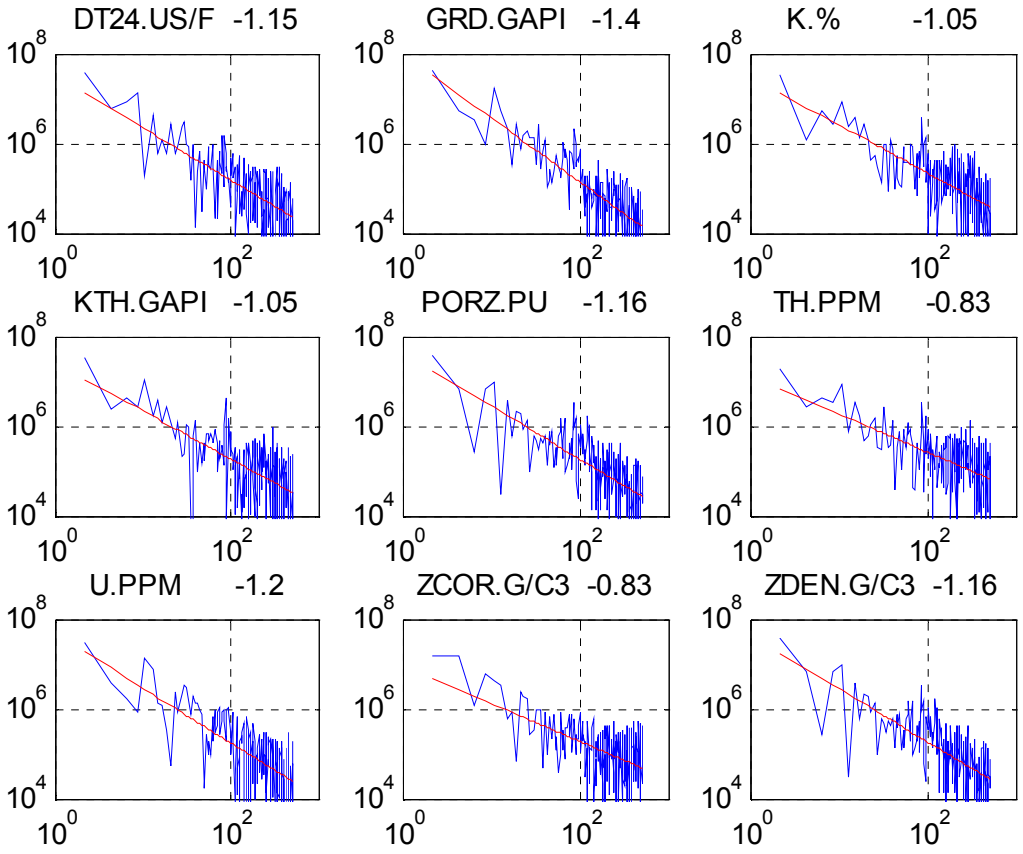

Fig 1 – Fourier power spectra for suite of well logs recorded at a Wyoming sand/shale formation. Red lines fit spectra to form $S(k) \sim k^{\beta}$, with fit exponent $\beta \sim -1$ given above each plot. Well-log data courtesy of R Slatt; cf.Leary (2002).

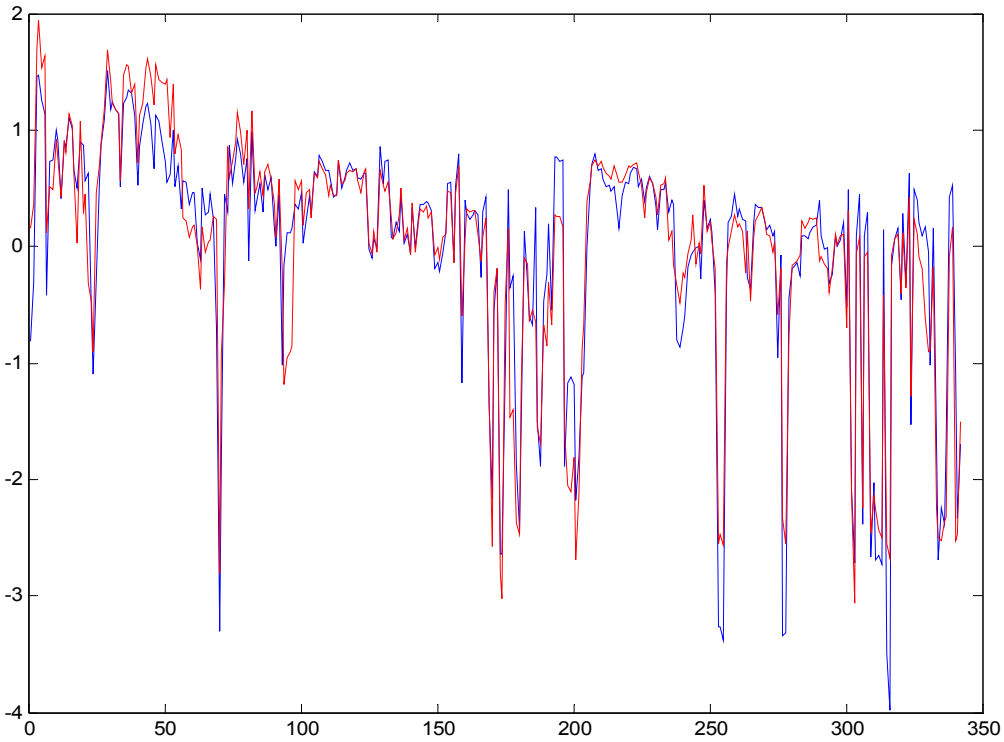

Fig 2 – As the fracture porosity changes, so does the fracture permeability. Show here is the superposition of zero-mean/unit-variance well-core porosity (blue) and log (permeability) (red) sequence of 350 well-core samples from a South Australia tight gas province. The zero-lag cross-correlation for these sequences is ~ 87%.

A number of well known features of crustal rock are linked to fracture density distributions like (2): (i) microearthquake activity in the crust; (ii) dam impoundment-induced microearthquakes from ~ 1-3 bar increases in crustal loading; (iii) scale independence of earthquake processes.

Well-core data from clastic reservoirs support the grain-scale fracture-density picture of crustal rock. This derives from an empirical relation between changes in porosity and changes in permeability found both in data and in fracture connectivity models:

$$\delta\varphi(i) \sim \delta\log(\kappa(i)). \qquad (3)$$

In (3) porosity and log(permeability) changes between samples i = 1…n are reduced to zero-mean unit-variance form (Leary and Walter, 2008). Fig 2 illustrates relation (3) for a suite of 350 well-core samples from South Australia.

This observed relation can be deduced from the density of fracture-porosity. If the porosity of two samples are associated with n and n+δn grain-scale fractures, and if the number of pathways within the two samples is proportional to n! and (n+δn)!, then the empirical relation (3) is equivalent to the identity (Leary & Walter 2008),

$$\delta n \sim \delta\log(n!). \qquad (4)$$

Identity (4) 'explains' the empirical "poroperm" relation (3) in terms of grain-scale flow as percolation between grain-scale fracture sites. As such it provides a well-log- and core-validated means to compute *in situ* flow. In this model fluid percolates along long-range spatially-correlated fracture networks governed by relations (2) and (4).

Applying poroperm relations to EGS flow

It is straightforward to numerically simulate what well-logs and core data tell us happens in clastic rock at all scale lengths *in situ*. Using relations (2) and (3), we can simulate flow as it applies, for instance, to the EGS heat transport arrangement illustrated in Fig 3.

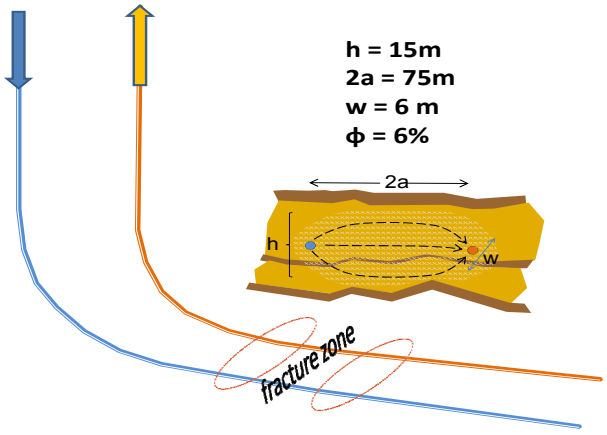

Fig 3 – Generic EGS horizontal wellbore pair intersecting zones of spatially correlated fracture density; the given wellbore pair dimensions are characteristic of tight-gas extraction in the Raton Basin, Colorado, USA.

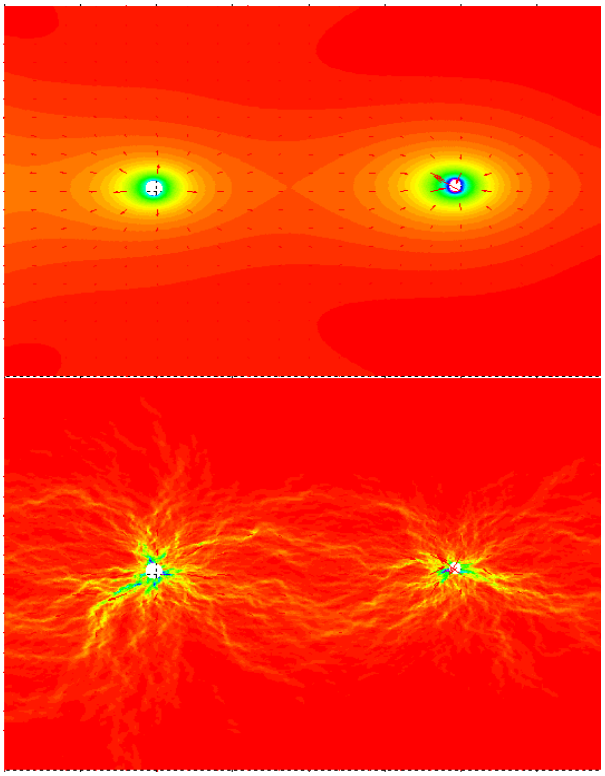

Fig 4 – 2D well-to-well flow velocity section for quasi-uniform 'κh' poroperm distribution (above) and poroperm distribution obeying empirical spatial fluctuation empirics (2)-(3) (below).

EGS flow geometry is a 'closed' system between a pair or more of wellbores. An injection bore feeds heat-depleted water from the surface into a heat exchanger crustal volume and the other bores return heat-replenished water to the surface. Horizontal drilling and logging are currently standard wellbore operations. Thus a simple geometry to analyze is a pair of parallel horizontal wellbores of length ℓ and separation 2a, $\ell >> a$.

Horizontal wellbores simplify models by remaining in a given aquifer/formation and/or at relatively steady pressure-temperature conditions. At many EGS sites, fractures are likely to be sub-vertical to vertical, and aligned to open against the least principal horizontal stress. As pictured in Fig 3, the wellbore azimuth can be assumed to be normal to the fracture faces so that the fractures transect the wellbore and promote wellbore fluid transfer into/out of the formation.

Fig 4 shows 2D-section fluid velocity fields for interwell flow across the Fig 3 well geometry. Flow in a standard 'κh' poroperm distribution (the top plot) is contrasted with flow a poroperm distribution obeying *in situ* relations (2)-(3) (the lower plot). The later velocity field illustrates the spatial erratic nature of fracture-borne flow. Where the 'κh' poroperm distribution velocity field is conveniently uniform, the flow velocity field governed by (2)-(3) varies unpredictably along the length of wellbores as well as between the wellbores.

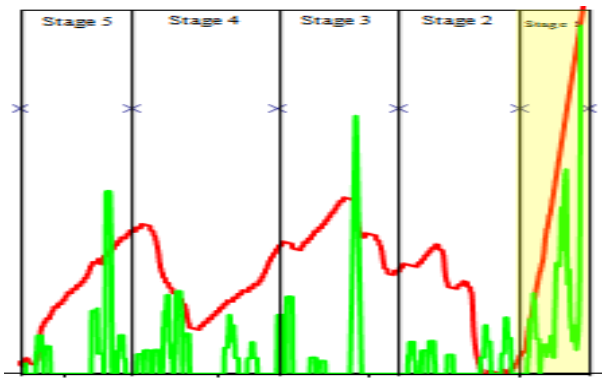

Fig 5 – Horizontal wellbore fracture density (green) and gas production (red) spatial fluctuations recorded along a 650m wellbore interval. These data do not fit a uniform kh picture of flow, but more like shown in Fig. 4.

The erratic flow paths of Fig 4 illustrate in 2D the degree to which EGS heat transport by interwell fluid flow is likely to vary in space. Such spatial variation in flow is documented in the well data shown in Fig 5. This Fig. shows how gas flow into a producer well varies along the length of the wellbore.

In both the model in Fig. 4 and data in Fig. 5, it can be seen how *in situ* spatial fluctuations in poroperm properties render EGS wellbores into discrete source/sink volumes of variable strength rather than smooth source/sink volumes of uniform strength.

The spatial variability of *in situ* poroperm distributions illustrated Figs 4-5 means that EGS sites are likely to have a 3D pressure $P(r) \sim P_0 r_0/r$ dependence on radial offset. This is in contrast to a logarithm dependence $P(r) \sim P_0 \log(r_0/r)$ characteristic of a 2D cylindrically-symmetric source/sink distribution.

We propose that this inherently 3D nature of *in situ* flow establishes a revised picture of *in situ* EGS flow fundamentally different from the 'κh' matrix plus discrete fracture approach. In the new picture, each EGS wellbore must flow at a volumetric rate Q consistent with power generation. Thus Q needs to be more than ~ 25L/s ~ $0.025 m^3/s$. At the same time, heat extraction must be sustained over the project lifetime. Hence interwell fluid mean flow rate cannot exceed a design limit. A safe estimate of design-limit interwell fluid flow rate is $v \sim 10^{-8} m/s$ ~ 0.3m/yr. At this heat-extraction flow rate, heat is reliably restored to the EGS volume by thermal conduction (Ingebritsen et al. 2006).

Consider a 3D source/sink radial pressure dependence of $P(r) \sim P_0 r_0/r$ normalised to r_0 = wellbore radius and P_0 = wellbore pressure. In this case the associated fluid flow velocity field is

$$v \sim \kappa/\mu \, \partial_r P \sim \kappa/\mu \, P_0 r_0/r^2$$

where $\kappa(x,y,z)$ = formation permeability distribution and μ = dynamic viscosity of water at the reservoir temperature. First we equate wellbore flow Q to change in external water content of the rock adjacent to the wellbore. Assuming a well length ℓ and radius r_0, wellbore flow rate equals the *in situ* flow rate

$$Q = \varphi dV/dt = 2\pi\varphi\ell r\, dr/dt = 2\pi\varphi\ell r v$$

$$v(r_0) = \kappa/\mu\, P_0/r_0 = Q/2\pi\varphi\ell r_0,$$

from which we find $\kappa/\mu\, P_0 = Q/2\pi\varphi\ell$. The *in situ* 3D radial pressure dependence gives a median far-field flow velocity as $v \sim v(a) = \kappa/\mu P_0 r_0/a^2 = Q/2\pi\varphi\ell\, r_0/a2 = Qr0/2\pi\varphi/\ell a^2$, whence

$$\ell a^2 \sim Q r_0/2\pi\varphi v. \qquad (5)$$

Assume Q ~ 25L/s = 0.025 m^3/s, r_0 ~ 0.1m, φ ~ 0.06, v ~ 10^{-8}m/s, ℓa^2 ~ 6.7 $10^5 m^3$. Then this relation balances for ℓ ~ 400m and 2a ~ 75m. The resulting sustainable *in situ* heat-exchange flow rate is v ~ 10^{-8}m/s. This wellbore geometry is the one illustrated in Fig 3.

Application to the Raton Basin

The Raton Basin of southern Colorado and northeastern New Mexico is a geothermal anomaly with temperature gradients ~ 55°C/km evident from bottom hole temperatures (Macartney & Morgan 2011). The anomaly spans much of the basin, with projected temperatures of 150°C at 2.5km depth over more than 350 square miles (Figure 6).

Extensive Raton Basin horizontal wellbores have been logged for fracture content and associated gas production, e.g., Fig 5. Such *in situ* horizontal well flow data exist in profusion. Finite-element 3D flow/transport simulation code such as *Sutra* (Voss and Prevost 2008; Leary & Malin 2010) allow realistic flow and heat transport modeling of poroperm spatial fluctuations within potential EGS crustal volumes on spatial scales consistent with current drilling and fracture stimulation practice.

Conclusion

We conclude by stating that the business case for the economic extraction of 150°C water at 2.5km in the Raton Basin with horizontal well drilling and fracture stimulation can be supported through well log- and core-based modelling.The inherent spatial uncertainty associated with *in situ* flow can be understood in terms of the variability of grain scale and larger fractures. The evidence for this is documented *in situ* in Fig 5, and numerically modeled in 2D in Fig 4. Eq. (5) can be deduced from these results as the basis for sustainable 3D heat transport in a generic Raton EGS well pair (Fig 3).

References

Berryman, J. G., and H. F. Wang, 1995, The elastic coefficients of double porosity models for fluid transport in jointed rock, *Journal of Geophysical Research*, **100**, 24611-24627.

Biot, M. A., 1962, Mechanics of deformation and acoustic propagation in porous media, *Journal of Applied Physics*, **33**, 1482-1498.

Edwards L.M., G.V. Chilingar, H.H . Rieke III & W.H. Fertl, 1982, *Handbook of Geothermal Energy*, Gulf Publishing Company, Houston, pp613.

Earlougher R.C., 1977, *Advances in Well Test Analysis*, Society of Petroleum Engineers, Dallas, pp264.

Grant M.A., I.G. Donaldson & P.F. Bixley, 1982, *Geothermal Reservoir Engineering*, Academic Press, New York, pp369.

Gringarten A.C. & P.A. Witherspoon ,1973, Extraction of Heat from Multiple-Fractured Dry Hot Rock, *Geothermics*, v.2 No. 3-4, 119-122.

Heath R.C., 1989, *Basic Ground-Water Hydrology*, USGS Water-Supply Paper 2220, pp84.

Ingebritsen S, W. Sanford & C. Neuzil, 2006,

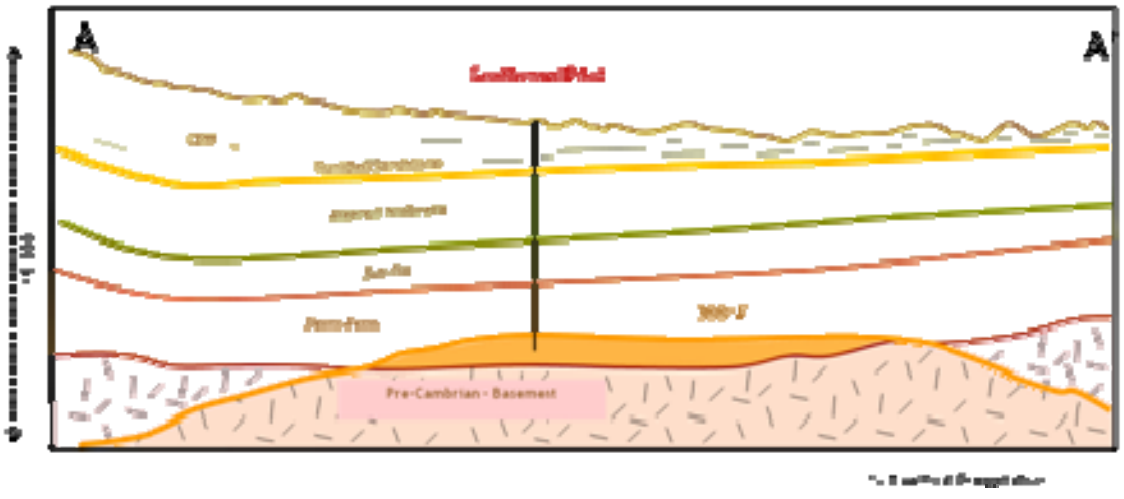

Fig 6 – Projected 150°C thermal anomaly at 2.5km depth in the Raton Basin, Colorado, USA.

Groundwater in Geological Processes, Cambridge University Press, pp536.

Leary P. & P. Malin, 2011, Is Theis flow modelling sufficient for EGS/HSA geothermal, *Proceedings Geothermal Resources Council*, San Diego, 23-26 October.

Leary P. & P. Malin, 2010, The Nature of Reservoir Fracture Heterogeneity: II -- Rapid Interwell Connectivity Simulation for Reservoir-scale Structure Modelling, *Proceedings World Geothermal Congress*, Bali, Indonesia, 25-30Apr.

Leary, P. C., and L. A. Walter, 2008, Crosswell seismic applications to highly heterogeneous tight gas reservoirs, *First Break*, **26**, 33-39.

Leary, P.C., 2002, Fractures and physical heterogeneity in crustal rock, in Goff J.A. and Holliger K, (Eds.) *Heterogeneity of the Crust and Upper Mantle - Nature, Scaling and Seismic Properties*, Kluwer/Academic/Plenum Publishers, New York, 155-186.

Macartney H. and P. Morgan, 2011, The Potential for Geothermal Energy Recovery from Enhanced Geothermal Systems in the Raton Basin of Southern Colorado, USA, *AAPG Hedberg Research Conference, Enhanced Geothermal Systems, Napa CA,* 14-18 March.

Sanyal S. & S.J. Butler, 2010, Geothermal power capacity of wells in non-convective sedimentary formations, *Proceedings World Geothermal Congress*, Bali, Indonesia, 25- 30 April.

Sayers, C. M., and P. M. T. M. Schutjens, 2007, Special Section: Geomechanics, The Leading Edge, **26**, 582-662.

Sayers, C. M., 2007, Special Section: Fractures, The Leading Edge, **26**, 1102-1202.

Theis C.V. (1935) *Transactions American Geophysical Union* **16**, 519-524.

Thomsen, L., 1985, Biot-consistent elastic moduli, *Geophysics*, **50**, 2797-2807.

Voss, C. I., and A. M. Provost, 2008, *Water Resources Investigations Report 02-4231*, United States Geological Survey, Reston VA; http://water.usgs.gov/nrp/gwsoftware

Induced Seismicity: Issues and the Path Forward

E.L. Majer
elmajer@lbl.gov (510) 486-6709
Earth Sciences Division
Lawrence Berkeley National Laboratory

Microearthquake monitoring for fracture enhancement and imaging of fracture systems will play a crucial role in the success of EGS, both from a reservoir management and public acceptance point of view. As with the development of any new technology, however, some aspects are accepted, and others need clarification and study. Although induced seismicity has occurred in many different energy and industrial applications (reservoir impoundment, mining, construction, waste disposal, conventional geothermal), it is important to point out that in all cases, with proper study and engineering controls, induced seismicity issues have never stopped the eventual implementation of any of these technologies. In addition, microseismicity is now being used as a tool for understanding and measuring the success of injecting fluid into the subsurface in a variety of applications. However, recent publicity surrounding induced seismicity at several geothermal sites points out the need to develop more rigorous standards and practices to avoid any potential problems with induced seismicity. It is critical that the policy makers and the general community be assured that EGS, CO_2 sequestration, and other technologies relying on fluid injections will be engineered to avoid any unacceptable seismicity and be developed as a safe and cost effective technology. In a broad sense there are two different needs that must be met to make fluid injection technology a safe and cost effective practice: technical and general policy. Both are equally important and are tightly linked together. Over the past several years the U.S. Department of Energy (USDOE) has been developing two companion documents to address both of these issues. The first is the EGS induced Seismicity Protocol and the second is the EGS Induced Seismicity Best Practices. The protocol was developed for all stakeholders involved with EGS, recommending seven critical steps to be considered before during and after EGS activities. It was written as a guideline, versus a requirement, that would be useful for the public, regulators, policy makers, the public and the operators. The purpose being to gain public acceptance as well outline procedures for dealing with technical issues associated with induced seismicity. The best practices was written mainly for the operators to provide a more detailed description and guidelines with specific recommendations on how to implement such activities as monitoring , risk analysis, and public interaction. Presented will be an over view of both the protocol and best practices, as well current gaps and needs in advancing the knowledge and practices associated with making induced seismicity a useful tool instead of a roadblock.

Zircon chronochemistry of high heat-producing granites in Queensland and Europe

V. Marshall*[1,2], K. Knesel [2] and S.E. Bryan[1, 3]
v.marshall@uq.edu.au
1. Queensland Geothermal Energy Centre of Excellence, The University of Queensland, St Lucia, QLD 4072
2. School of Earth Sciences, The University of Queensland, St Lucia, QLD 4072
3. Biogeoscience, Queensland University of Technology, GPO Box 2434, Brisbane, QLD 4001

High heat-producing granites (HHPGs) are reservoir rocks for enhanced geothermal systems (EGS), yet the origins of their anomalous chemistry remain poorly understood.

To gain a better understanding of the characteristic distribution of elemental depletions and enrichments (focussing on U, Th & K) within granite suites of different heritage and tectonic setting, and the processes that lead to these enrichments, we are undertaking a systematic accessory-mineral chronochemical study of two suites of S- and I-type granites in northern Queensland, as well as two archetypal HHPGs in Cornwall, England (S-type) and Soultz-sous-Forêts, France (I-type).

Novel zircon LA-ICP-MS chronochemical methods will later be underpinned by a systematic petrographic, scanning electron microscope (SEM), and electron microprobe (EPMA) study of all the REE-Y-Th-U-rich accessory minerals to fully characterise how the composition, textural distributions and associations change with rock chemistry between and among the suites.

Preliminary results indicate that zircons with inherited ages do not have anomalously high U (>1000 ppm) & Th (>400 ppm) values (Ahrens, 1965). Instead, enrichment in these HPE is seen in zircons dated to around the time of magmatic emplacement. These results indicate that enrichment arose primarily through fractional crystallisation of the granitic magmas.

Our results support the suggestion that a source pre-enriched in the HPEs does not appear to be fundamental for the formation of all HHPGs. Instead fractional crystallisation processes, and the accessory minerals formed in magmas of differing initial compositions, are the key controls on the levels of enrichment observed (e.g. Champion & Chappell, 1992; Chappell & Hine, 2006). One implication is that the most fractionated granites may not be the most enriched in the HPEs and therefore prospective to future EGS development.

Keywords: High heat-producing granites (HHPGs); heat-producing elements (HPEs); source composition; fractional crystallisation; zircon

Introduction

The generation and emplacement of granitic magma as plutonic and volcanic rocks is fundamental to the evolution of the continental crust (Coleman et al., 2004; Glazner et al., 2004; Annen, 2011). The formation of granitic magma through partial melting of crustal material and subsequent cooling and fractional crystallisation of this magma, which may or may not include a component of mantle-derived melt, results in chemical differentiation of the continents (Petford et al., 2000).

In some cases this magmatic differentiation results in the production of granites with extreme enrichment in the HPEs U, Th and K well above the upper continental crustal average of 2.7 ppm U, 10.7 ppm Th and 3.4 wt% K_2O (Taylor and McLennan, 1985; Champion, 1991; Chappell and Hine, 2006).

Despite their distinctive chemistry (Willis-Richards and Jackson, 1989; Champion, 1991; Förster et al., 1999b), the origin of HHPGs remains enigmatic. The geochemical characteristics of granitic magmas are generally accepted to reflect the composition of the source rocks and petrogenetic processes involved in the formation, differentiation and emplacement of granitic melt (Ishihara, 1977; Hyndman, 1981; Chappell, 2010), although the relative importance of these factors in the compositional diversity of granites is unclear.

The fundamental aim for this work is to address this uncertainty and, in doing so, to unravel the factors governing the relative material vs. process contributions to the distinctive geochemical characteristics of HHPG.

Background

The influence of source (material) vs. differentiation (process) on HPE enrichments in granites

Lithological and chemical composition of the source

The idea that granites 'image' their source (Chappell, 1979) was first proposed in 1974 when Chappell & White stated that S- (supracrustal) and I- (infracrustal) type granites must be generated from rocks of differing compositions. S-type magmas are peraluminous

[Al_2O_3/(Na_2O+K_2O+CaO), ASI >1], and originate from a supracrustal source that has experienced weathering of feldspars to clay minerals, with a consequent loss of sodium (NaO) and calcium (CaO) (Chappell and White, 1974; Chappell, 1999). I-type magmas generally contain less Al [Al_2O_3/(Na_2O+K_2O+CaO), ASI <1] and are generally weakly peraluminous to metaluminous (an ASI of <1 is metaluminous) as the source has not experienced significant weathering (Chappell and White, 1974).

It is therefore natural to question whether the lithological characteristics of the crustal source play a role in the enrichments of U, Th & K characteristic of HHPGs. A survey of the literature reveals, however, that HHPG have a variety of compositional affinities and thus appear to be derived from a variety of possible sources (Chappell and Hine, 2006). This observation is compatible with the suggestions that many 'S-' and 'I- type' granitoids may simply reflect mixtures of igneous and sedimentary source types, such that compositional differences are representative of a sliding scale rather than having a definitive chemical and mineralogical difference based on their source (Collins, 1998; Kemp et al., 2007). Perhaps more importantly, it also implies that, at least with respect to bulk lithological characteristics, there is no "special" source rock required for the generation of HHPG (e.g. Chappell and White, 2001).

However, many Paleozoic examples of HHPGs in Queensland appear to be spatially associated with Proterozoic basement (Champion, 1991; Bryan et al., 2002), which itself is enriched in U, Th & K (McLaren et al., 2003). In the Proterozoic terranes within the Mount Painter Region, South Australia, present day heat production is measured to be ~16 μWm^3 (McLaren et al., 2002), 6.4 times that of the 'average' granite (2.5 μWm^3, Haenel et al. 1988), with U, Th & K contributing two to three times as much to heat production in the crust during the Proterozoic (McLaren et al., 2003). This association begs the question as to whether derivation from an enriched source is a general geochemical prerequisite for generation of HHPG. In other words, does melting of a source enriched in U, Th & K produce granitic melt enriched in these heat-producing elements?

Magmatic differentiation during ascent and emplacement

Crystal fractionation undoubtedly plays an important role in the compositional spectrum of granitic rocks, and this includes the HPE elements U, Th, & K (Bea et al., 1994a; Chappell and Hine, 2006). However, the critical question that remains is which factors lead to (i.e., govern) this enrichment through fractional crystallisation.

In this context, it is useful to propose two end-member scenarios, though it is acknowledged that no single model will likely explain all cases. At one end of the spectrum, the enrichment may be governed by some overriding external factor, such as magma ascent pathway, and emplacement environment and history. In this case, strong enrichments may simply reflect extreme crystal fractionation (e.g., Halliday et al., 1991), which could in theory occur in any granitic magma regardless of its source. If so, we might expect that strongly enriched granites (both S- and I-type) follow some broadly similar fractionation paths. At the other end of the spectrum, the differentiation history and resulting elemental enrichments (and depletions) might be governed by the initial composition of granitic melts as inherited from their source (e.g., Chappell, 1999). In this scenario, we should expect that each granite type follows a characteristic (distinctive) chemical evolutionary path as shown in Figure 1.

Hydrothermal alteration

An additional process which can overprint the original chemical composition of granite is post-magmatic alteration by hydrothermal fluid flow. Low-temperature hydrothermal events are capable of introducing and/or redistributing elements (such as K^+ & U^{6+}) within a granitic system (Förster et al., 1999b; Chappell and Hine, 2006). However, strong evidence exists that to a first order the extreme enrichments in many archetypal HHPGs primarily reflects a magmatic origin (Förster et al., 1999b; Chappell and Hine, 2006)

Methodology

To investigate the importance of the source controls - both in terms of the HPE budget inherited during melt production and its indirect control on subsequent differentiation pathways leading to HPE enrichments - a systematic accessory-mineral chronochemical study of two suites of S- and I-type granites in northern Queensland (N QLD), as well as two archetypal HHPGs in Cornwall, England (S-type) and Soultz-sous-Forêts (Soultz), France (I-type) is underway. All of the granites are generally geochemically well-characterised; this affords the opportunity to focus on a detailed study of the residence history of phosphate and silicate accessory minerals, which govern the behaviour of U, Th, Y and REE in granites. The main focus will be application of novel zircon LA-ICP-MS chronochemical methods (following the methods outlined in Harris et al. 2004 and Bryan et al., 2004). Although uncertainties exist with regards to the relationship between zircon and magma chemistry (Hoskin et al., 2000), this will be tested as part of this study. These results will be underpinned by a systematic petrographic, scanning electron microscope (SEM), and electron microprobe (EPMA) study of all the REE-Y-Th-U-rich accessory minerals to fully characterise how the composition, textural

distribution and associations change with whole-rock chemistry and texture between and among the suites.

The bulk of the mineralogical work will concentrate on the Queensland granites, but the two European granites (one S- and one I-type) will provide a critical point for comparison with sites of past and ongoing feasibility studies of hot dry-rock, enhanced geothermal systems. The N QLD S- and I-type suites were chosen to provide a range of relatively unenriched to extremely enriched compositions (Fig 1), as well as excellent vertical and lateral sample coverage across the targeted bodies. These characteristics are critical to examine: (1) how, when and why elemental enrichments develop during differentiation, and (2) the distinct spatial distribution of HPE enrichment that arises in each granite type.

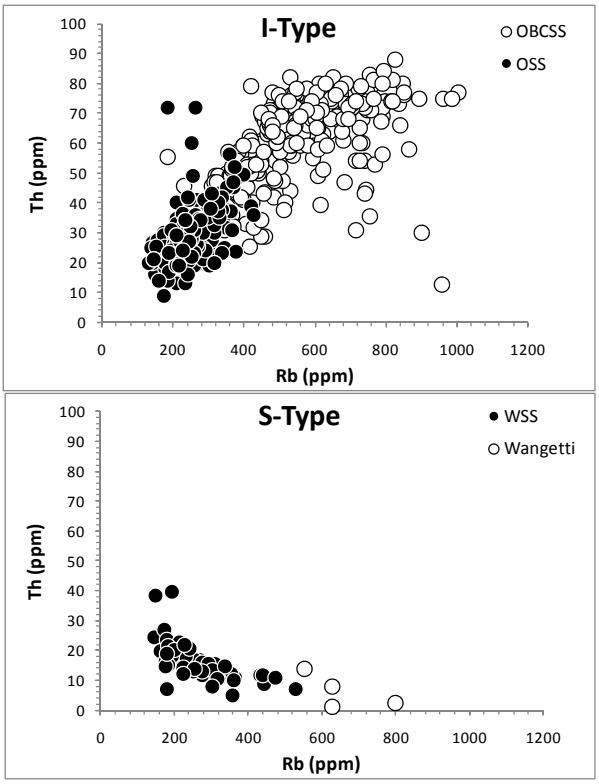

Figure 1: Variation diagrams for the I- (O'Briens Creek and Ootann Supersuites) and S-type granites (Whypalla and Wangetti Supersuites) of the Hodgkinson Province, N QLD. Variations between the granite types are seen when using Rb as an index of differentiation, suggesting there was no accessory phase present in the I-types to remove Th from the magma, whereas in the S-types Th was removed with increasing differentiation.
Data compiled from Champion (1991).

Preliminary results

Approximately 60 laser ablation "spot" analyses of zircons were conducted per whole-rock sample, with nine rock samples so far examined (one from Soultz, three from Cornwall, and five from N QLD). Utilising zonation patterns as revealed through cathodoluminescence (CL) imaging, distinct domains within zircon crystals were identified and dated; where possible both cores and rims were targeted. Obvious inherited cores (e.g., Fig 2) have been found in eight of the nine samples. The 208-based common Pb correction was applied to all age calculations; the $^{238}U/^{206}Pb$ age is used where grains are <1000 Ma, whereas the $^{207}Pb/^{206}Pb$ age is used for older grains.

Figure 3 illustrates the general range of age populations revealed by the zircon U/Pb LA-ICP-MS analysis of three examples for the previously dated S-type Carnmenellis and Land's End plutons, Cornwall, UK, and I-type granite from Soultz, France. Our concordant $^{238}U/^{206}Pb$ emplacement ages for the Cornubian granites (298 ± 3 Ma and 276 ± 4.4 Ma) are similar to those obtained through previous thermal ion mass spectrometry (TIMS) U/Pb dating of monazites which produced ages of 293.7 ± 0.6 Ma and 277-274.5 ± 1.4 Ma for the Carnmenellis and Land's End plutons, respectively (Chen et al., 1993). However, in contrast to the TIMS analyses of bulk mineral separates, our in-situ results also allow us to identify and characterise inherited zircon cores in these samples.

In the Carnmenellis pluton at Carnsew, 22 inherited zircons were dated ranging from 1593 ± 40 Ma to 441 ± 8 Ma (Fig 3). In contrast, fewer inherited zircons were found in the younger Land's End pluton, but inherited ages do extend back to 918 ± 13 Ma. At face value, the presence of clearly identifiable inheritance is consistent with the lower temperature, S-type character of these granites (Miller et al., 2003). The survival of inherited zircons in these highly fractionated magmas (Chappell and Hine, 2006) likely reflect the Zr saturated characteristics of these magmas (Watson and Harrison, 1983) as well as derivation from a "water-rich" metasedimentary source rock (i.e., rich in muscovite and biotite), which likely melted at relatively low temperature.

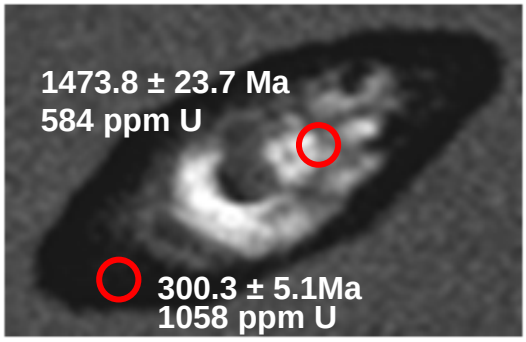

Figure 2: CL image of a 235µm zircon with a U-poor inherited core and U-rich magmatic rim, as determined through LA-ICP-MS analyses (circles mark the laser ablation site). Carnmenellis, Cornwall, UK.

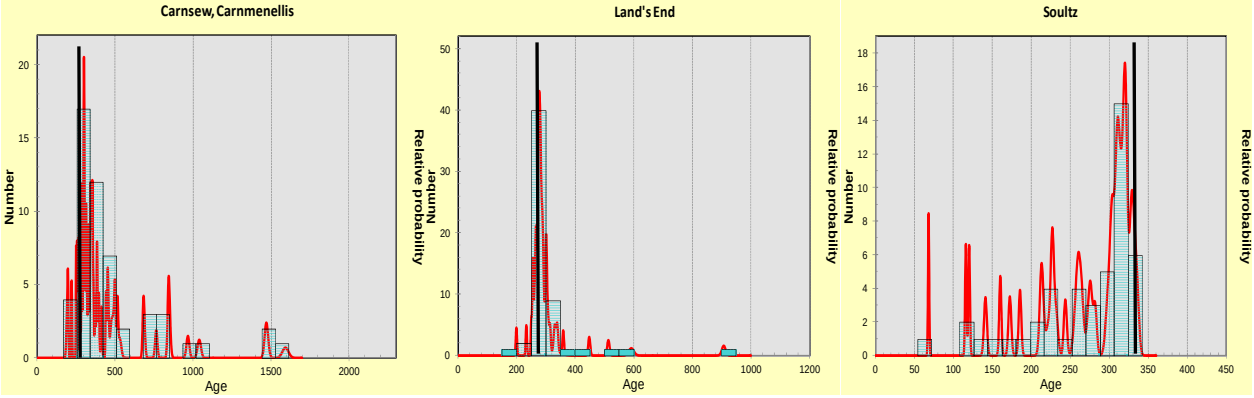

Figure 3: Probability density plots of ^{208}Pb corrected U/Pb zircon ages, illustrating significant levels of inheritance (Carnmenellis, Cornwall, UK), minimal inheritance (Land's End, Cornwall, UK), and no inheritance but alteration to the elemental abundances, as evidenced by ages younger than that of magmatic emplacement (Soultz, France). Solid black lines indicate dates obtained by previous studies (Chen et al., 1993; Alexandrov et al., 2001).

Our ^{238}U/^{206}Pb emplacement age for the Soultz intrusion (320 ± 4 Ma) also agrees, within error, with the published ion probe U/Pb zircon age of 331 ± 9 Ma (Alexandrov et al., 2001). However, the LA-ICP-MS results highlight two interesting features in the Soultz zircons.

Firstly, they do not show any evidence of obvious inheritance (agreeing with previous zircon investigations by Cocherie et al. 2004). This could imply a contribution from a mantle-derived melt undersaturated in Zr resulting in dissolution of existing zircon grains and no new zircon crystallisation (Robinson and Miller, 1999). A mantle-derived chemical signature could also be explained by the melt having a meta-igneous source (as proposed for Soultz, Stussi et al., 2002 and references therein), as the resultant melt would be less saturated in Zr and melt at a higher temperature (Miller et al., 2003). This is supported by experimental zircon studies which have found mafic melts can dissolve greater amounts of zircon at a given temperature than silicic melts (Watson, 1979; Watson and Harrison, 1983). A mantle-derived melt contribution has been proposed for the Soultz monzogranite on the basis of the presence of enclaves (Stussi et al., 2002) and relatively low ^{87}Sr/^{86}Sr (Rummel, 1991). Hf-isotopic analysis of the zircons should help resolve the possibility of a mantle signature to the granitic magmas and is work planned for 2012.

The second important feature of the Soultz zircon ages is the strong age disturbance (Fig 3), despite residing at a depth of 1608.1 m at ~30°C (Hooijkaas et al., 2006). The significant population of 'young' ages indicate that Pb loss has likely occurred within some of the higher U grains; sixteen of the twenty 'young' ages are analyses from zircon cores, thus scenarios such as later U enrichment through hydrothermal fluid flow are unlikely. High U contents can promote radiation damage and metamictisation of the grains, resulting in the destruction of the zircon crystal structure and leaving it open to modification of initial element abundances (Chakoumakos et al., 1987). The U content of the Soultz zircons increases systematically with decreasing U-Pb age in the younger, discordant analyses (Fig 4). In contrast to the European samples, inherited grains of Proterozoic age are seen in I- as well as the S-type granites of N QLD. This may signify a lack of a mantle input in the N QLD granites and/or variable contributions from biotite and amphibole between the Soultz and N QLD I-type granites. All of the granites show a large range of chemical compositions. However, the inherited populations have relatively low U (<1000 ppm) and Lu (<200 ppm) concentrations, with a few exceptions of moderately elevated U in the S-type Carnmenellis (UK) and Mount Carbine (N QLD, Whypalla Supersuite) granites. Importantly, the very high U and Lu zircons (> 8000 ppm and > 400pm, respectively) in the Nettle Granite (N QLD, O'Briens Creek Supersuite, Fig 5) comprise analyses from the concordant age population, indicating that the extreme enrichment in the zircon from this granite is a result of magmatic crystallisation (as suggested by Pollard, 1988).

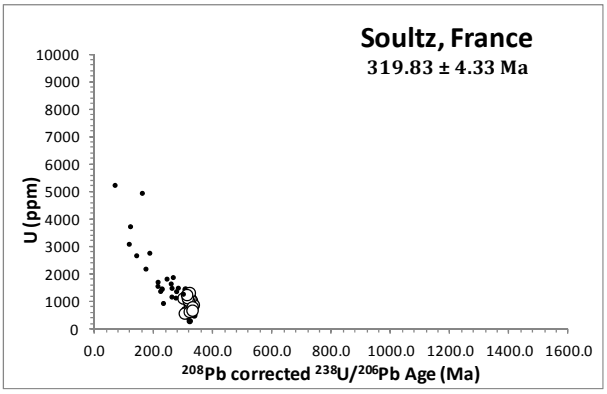

Figure 4: Zircon U/Pb ages vs. U concentration for the Soultz-sous-Forêts granite, France. The analyses with high U concentrations and apparently younger ages are likely representative of Pb-loss from the grain. Data used in age calculations are shown in large unfilled circles; analyses excluded from age calculation are shown as smaller filled circles (based on sample related or statistical criteria). Age errors are smaller than the symbol size.

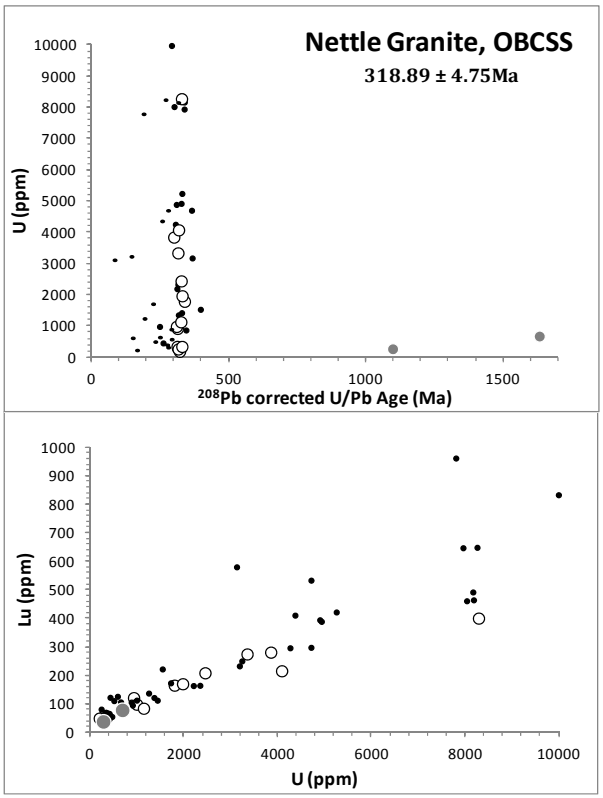

Figure 5: Zircon U/Pb Age vs. U and U vs. Lu concentration for Nettle Granite, N QLD. $^{238}U/^{206}Pb$ age used for grains<1000 Ma, $^{207}Pb/^{206}Pb$ age for older grains. Data symbols same as in Figure 4. Analyses excluded from age calculations are shown as grey circles if they reflect significant inheritance.

Elevated U contents (> 2000 ppm) are also present in concordant data in the Land's End.

Implications

The preliminary zircon chronochemical results show that a source component substantially enriched in U & Th is not readily identifiable in any of the S- or I-type granites examined thus far. This observation certainly requires additional testing for the suites targeted here, as well as for other HHPGs in additional settings where there is an unequivocal spatial association between high heat-producing Proterozoic granitic basement and younger HHPG (e.g., South Australia). Nevertheless, our preliminary results confirm the suggestion that most of the U & Th enrichments in the I-type granites examined here (thus far) are derived through strong fractional crystallisation (e.g. Champion, 1991; Chappell and Hine, 2006). While the post-magmatic alteration may locally and variably redistribute U in some of the granites (e.g., Cornwall, Chappell & Hine, 2006), it is not responsible for the underlying enrichment in heat-producing elements in the majority. The question that then arises again is what factors lead to (and govern) this enrichment through fractional crystallisation.

One possibility is that the distinctive initial melt (bulk) compositions, which arise from different source rocks, may impart a type of "genetic" code that governs later differentiation. For instance, the degree of aluminium saturation of the original (unfractionated) S- and I-type granitic melts depends in large part on the nature of the source (e.g., Bea, 1996). S-type granites are always oversaturated in Al and thus peraluminous. In contrast, I-types are metaluminous to weakly peraluminous.

Experimental studies show that the solubility of the most important phosphate mineral, apatite $[Ca(PO_4)_3(OH,F,Cl)]$, is low in metaluminous granites and increases with increasing aluminosity (Harrison and Watson, 1984; Pichavant et al., 1992; Wolf and London, 1995). As a result, peraluminous magmas have higher phosphorous contents than metaluminous granites with the same silica content (e.g., Bea *et al.* 1992; Chappell 1996).

Experimental studies also suggest that, unlike apatite, the solubilities of other phosphate accessory minerals, such as monazite ($LREEPO_4$) and xenotime ($Y\text{-}HREEPO_4$), remain low regardless of the degree of Al saturation (Rapp and Watson, 1986). Therefore, P-rich peraluminous granitic magmas may become saturated in monazite and xenotime at low REE concentrations. If so, fractionation of even minute quantities of these accessory minerals, which are typically included along with zircon $[ZrSiO_4]$ in co-precipitating biotite grains, should result in significant removal of REE and U & Th from the residual melt. This suggestion is supported by suppression of enrichment or even decreases of U, Th and the REE with increasing Rb (a sensitive measure of the extent of fractional crystallisation) displayed by the S-type granites of N QLD (Fig 1).

In contrast, because of the scarcity of phosphate anions in metaluminous melts, precipitation of REE phosphates requires higher REE concentrations than in peraluminous melts. As a result, allanite $[Ca, LREE)_2(Fe^{2+}, Fe^{3+})Al_2O(Si_2O_7)OH]$ and titanite $[CaTiSiO_4(O, OH, F)]$ become the main carriers of REE, U, & Th (again along with zircon), and they do so at a more advanced stage of fractionation. These silicate minerals are less effective than the phosphates (monazite and xenotime) at removing these elements from the melt (Bea, 1996). This may then allow U, Th and the REE to remain "incompatible" and to become strongly enriched in highly fractionated metaluminous to weakly peraluminous granites, as seen in the N QLD examples (Fig 1).

A key factor in understanding the origin of HPE enrichments may therefore be the control of initial melt composition, particularly the degree of Al saturation (or "aluminosity") on the relative stability and composition of phosphate vs. silicate REE-Y-Th-U accessory mineral phases in S- and I-type granites (e.g., Chappell, 1999). Although these minerals occur in trace amounts, they

largely govern the behaviour of U & Th during critical stages of differentiation simply because they contain most of these elements (Bea, 1996).

One important implication that emerges from this discussion is that the most fractionated (e.g., Rb-rich) granites do not necessarily represent those that are the most enriched in U & Th. For instance, when using Rb as an index of differentiation (Fig 1), we see a 10 fold increase in Th with increasing differentiation in metaluminous melts, yet over the same amount of differentiation we see an 18 fold decrease in Th content in peraluminous melts. This contrasting behaviour may have important consequences for the heat production through contrasting vertical and lateral distributions of HPE in zoned and composite plutons.

References

Ahrens, L.H., 1965, Some observations on the uranium and thorium distributions in accessory zircon from granitic rocks: Geochimica et Cosmochimica Acta, v. 29, p. 711-716.

Alexandrov, P., Royer, J.-J., and Deloule, E., 2001, 331 +/- 9 Ma emplacement age of the Soultz monzogranite (Rhine Graben basement) by U/Pb ion-probe zircon dating of samples from 5 km depth: Earth and Planetary Sciences, p. 747-754.

Annen, C., 2011, Implications of incremental emplacement of magma bodies for magma differentiation, thermal aureole dimensions and plutonism-volcanism relationships: Tectonophysics, v. 500, p. 3-10.

Bea, F., 1996, Residence of REE, Y, Th and U in granites and crustal protoliths; Implications for the chemistry of crustal melts: Journal of Petrology, v. 37, p. 521-552.

Bea, F., Fershtater, G., and Corretgé, L.G., 1992, The geochemistry of phosphorous in granite rocks and the effect of aluminium: Lithos, v. 29, p. 43-56.

Bea, F., Pereira, M.D., Corretgé, L.G., and Fershtater, G., 1994a, Differentiation of strongly peraluminous, perphosphorous granites. the Pedrobernardo pluton, central Spain: Geochimica et Cosmochimica Acta, v. 58, p. 2609-2628.

Bryan, S.E., Allen, C.M., Holcombe, R.J., and Fielding, C.R., 2004, U-Pb zircon geochronology of Late Devonian to Early Carboniferous extension-related silicic volcanism in the northern New England Fold Belt: Australian Journal of Earth Sciences, v. 51, p. 645-664.

Bryan, S.E., Holcombe, R.J., and Fielding, C.R., 2002, Revised Middle to Late Palaeozoic tectonic evolution of the northern New England Fold Belt, Queensland, Abstracts & Programme, GSNZ Annual Conference 'Northland 2002', Geological Society of NZ Miscellaneous Publication, p. 9.

Chakoumakos, B.C., Murakami, T., Lumpkin, G.R., and Ewing, R.C., 1987, Alpha-decay-induced fracturing in zircon: The transition from the crystalline to the metamict state: Science, v. 236, p. 1556-1559.

Champion, D.C., 1991, The felsic granites of far north Queensland, The Australian National University.

Champion, D.C., and Chappell, B.W., 1992, Petrogenesis of felsic I-type granites: an example from northern Queensland: Transactions of the Royal Society fo Edinburgh: Earth Sciences, v. 83, p. 115-126.

Chappell, B., 2010, High- and low- temperature granites: The Ishihara Symposium: Granites and associated metallogenesis, p. 35-36.

Chappell, B.W., 1979, Granites as images of their source rocks: Geological Society of America Abstracts with Programs, v. 11, p. 400.

Chappell, B.W., 1996a, Compositional variation within granite suites of the Lachlan Fold Belt: its causes and implications for the physical state of the granite magma: Transactions of the Royal Society fo Edinburgh: Earth Sciences, v. 87, p. 159-170.

Chappell, B.W., 1999, Aluminium saturation in I- and S-type granites and the characterization of fractionated haplogranites: Lithos, v. 46, p. 535-551.

Chappell, B.W., and Hine, R., 2006, The Cornubian Batholith: an example of magmatic fractionation on a crustal scale: Resource Geology, v. 56, p. 203-244.

Chappell, B.W., and White, J.R., 1974, Two contrasting granite types: Pacific Geology, v. 8, p. 173-174.

Chappell, B.W., and White, J.R., 2001, Two contrasting granite types: 25 years later: Australian Journal of Earth Sciences, v. 48, p. 489-499.

Chen, Y., Clark, A.H., Farrar, E., Wasteneys, H.A.H.P., Hodgson, M.J., and Bromley, A.V., 1993, Diachronous and independent histories of plutonism and mineralisation in the Cornubian Batholith, southwest England: Journal of the Geological Society, v. 150, p. 1183-1191.

Cocherie, A., Guerrot, C., Fanning, C.M., and Genter, A., 2004, Datation U-Pb des deux faciès du granite de Soultz (Fossé rhénan, France): C.R.Geoscience, p. 775-787.

Coleman, D.S., Gray, W., and Glazner, A.F., 2004, Rethinking the emplacement and evolution of zoned plutons: Geochronologic evidence for incremental assembly of the Tuolumne Intrusive Suite, California: Geology, v. 35, p. 433-436.

Collins, W.J., 1998, Evaluation of petrogenetic models for Lachlan Fold Belt granitoids: Implications for crustal architecture and tectonic models: Australian Journal of Earth Sciences, v. 45, p. 483-500.

Förster, H.-J., Tischendorf, G., Trumbull, R.B., and Gottesmann, B., 1999b, Late-collisional granites in the Variscan Erzgebirge, Germany: Journal of Petrology, v. 40, p. 1613-1645.

Glazner, A.F., Bartley, J.M., Coleman, D.S., Gray, W., and Taylor, R.Z., 2004, Are plutons assembled over millions of years by amalgamation from small magma chambers?: GSA Today, v. 14, p. 4-11.

Haenel, R., Rybach, L., and Stegena, L., 1988, Handbook of terrestrial heat-flow density determination: with guidelines and recommendations of the International Heat Flow Commission: Dordrecht, Kluwer Academic Publishers.

Halliday, A.N., Davidson, J.P., Hildreth, W., and Holden, P., 1991, Modelling the petrogenesis of high Rb/Sr silicic magmas: Chemical Geology, v. 92, p. 107-114.

Harris, A.C., Allen, C.M., Bryan, S.E., Campbell, I.A., Holcombe, R.J., and Palin, J.M., 2004, ELA-ICP-MS U–Pb zircon geochronology of regional volcanism hosting the Bajo de la Alumbrera Cu–Au deposit: implications for porphyry-related mineralization: Mineralium Deposita, v. 39, p. 46-67.

Harrison, T.M., and Watson, E.B., 1984, The behaviour of apatite during crustal anatexis: Equilibrium and kinetic considerations: Geochimica et Cosmochimica Acta, v. 48, p. 1467-1477.

Hooijkaas, G.R., Genter, A., and Dezayes, C., 2006, Deep-seated geology of the granite intrusions at the Soultz EGS site based on data from 5 km-deep boreholes: Geothermics, p. 484-506.

Hoskin, P.W.O., Kinny, P.D., Wyborn, D., and Chappell, B.W., 2000, Identifying accessory mineral saturation during differentiation in granitoid magmas: an integrated approach: Journal of Petrology, v. 41, p. 1365-1396.

Hyndman, D.W., 1981, Controls on source and depth of emplacement of granitic magma: Geology, v. 9, p. 244-249.

Ishihara, S., 1977, The magnetite-series and ilmenite-series granitic rocks: Mining Geology, v. 27, p. 293-305.

Kemp, A.I.S., Hawkesworth, C.J., Forster, G.L., Paterson, B.A., Woodhead, J.D., Hergt, J.M., Gray, C.M., and Whitehouse, M.J., 2007, Magmatic and crustal differentiation history of granitic rocks from Hf-O isotopes in zircon: Science, v. 315, p. 980-983.

McLaren, S., Dunlap, W.J., Sandiford, M., and McDougall, I., 2002, Thermochronology of high heat-producing crust at Mount Painter, South Australia: Implications for tectonic reactivation of continental interiors: Tectonics, v. 21, p. 1-17.

McLaren, S., Sandiford, M., Hand, M., Neumann, N., Wyborn, L., and Bastrakova, I., 2003, The hot southern continent: heat flow and heat production in Australian Proterozoic terranes, *in* Hillis, R., and Muller, D., eds., The Evolution and Dynamics of the Australian Plate, Geological Society of Australia, p. 151-161.

Miller, C.F., Meschter McDowell, S., and Mapes, R.W., 2003, Hot and cold granites? Implications of zircon saturation temperatures and preservation of inheritance: Geology, v. 31, p. 529-532.

Petford, N., Cruden, A.R., McCaffrey, K.J.W., and Vigneresse, J.-L., 2000, Granite magma formation, transport and emplacment in the Earth's crust: Nature, v. 408, p. 669-673.

Pichavant, M., Montel, J.M., and Richards, L.R., 1992, Apatite solubility in peraluminous liquids:experimental data and an extension of the Harrison-Watson model Geochimica et Cosmochimica Acta, v. 56, p. 3855-3861.

Pollard, P.J., 1988, Petrogenesis of tin-bearing granites of the Emuford district, Herberton tinfield, Australia: Australian Journal of Earth Sciences, v. 35, p. 39-57.

Rapp, R.P., and Watson, E.B., 1986, Monazite solubility and dissolution kinetics: Implications for the thorium and light rare earth chemistry of felsic magmas: Contributions to Mineralogy and Petrology, v. 94, p. 304-316.

Robinson, D.M., and Miller, C.F., 1999, Record of magma chamber processes preserved in accessory mineral assemblages, Aztec Wash pluton, Nevada: American Mineralogist, v. 84, p. 1346-1353.

Rummel, F., 1991, Physical properties of the rock in the granitic section of borehole GPK1, Soultz-sous-Forêts: Geothermal Science and Technology, v. 3, p. 199-216.

Stussi, J.-M., Cheilletz, A., Royer, J.-J., Chèvremont, P., and Féraud, G., 2002, The hidden monzogranite of Soultz-sous-Forêts (Rhine Graben, France). Mineralogy, petrology and genesis: Géologie de la France, v. 1, p. 45-63.

Taylor, S.R., and McLennan, S.M., 1985, The Continental Crust: its Composition and Evolution, Blackwell Scientific Publications.

Watson, E.B., 1979, Zircon saturation in felsic liquids: Experimental results and applications to

trace element geochemistry: Contributions to Mineralogy and Petrology, v. 70, p. 407-419.

Watson, E.B., and Harrison, T.M., 1983, Zircon saturation revisited: temperature and composition effects in a variety of crustal magma types: Earth and Planetary Science Letters, v. 64, p. 295-304.

Willis-Richards, J., and Jackson, N.J., 1989, Evolution of the Cornubian ore field, southwest England: Part I. Batholith modelling and ore distribution: Economic Geology, v. 84, p. 1078-1100.

Wolf, M.B., and London, D., 1995, Apatite dissolution into peraluminous haplogranitic melts: an experimental study of solubilities and mechanisms: Geochimica et Cosmochimica Acta, v. 58, p. 4127-4146.

Legal Issues

McKenzie, G. C., Schultz, JG and Reznikov, KN.
george.mckenzie@finlaysons.com.au
Finlaysons
GPO Box 1244, Adelaide, SA 5000

The Australian geothermal sector currently faces significant challenges relating to available sources of private sector and government funding and capital as the Australian economy and the sector emerge from the GFC.

The sector is epitomised by ASX listed entities in the small to medium cap range. The challenges faced by the sector are particularly acute for these companies.

However, these challenges also provide opportunities to companies operating in the sector who are proactive in meeting the challenges.

The paper will examine in a practical and informative way the legal avenues open to companies to maximise opportunities arising out of the current economic climate affecting the country and the sector. These will include:

- Mergers and takeovers – tips for bidders and targets;
- Asset acquisitions/disposals -
- Foreign investment – what are the hurdles for incoming and outgoing investment and how to overcome them
- Dealing with large utilities – protecting your company in joint venture arrangements

Keywords: legal, mergers, takeovers, asset acquisition and disposal, foreign investment and joint ventures

Synchysite from the Soultz high-heat producing monzogranite, Soultz-sous-Forêts, France: Implications for titanite destabilisation and differential REE and Th mobility in hydrothermal systems

Alexander W. Middleton*[1,3], I. Tonguc Uysal[1], H.-J. Förster[2] and Suzanne D. Golding[3]

[1] Queensland Geothermal Energy Centre of Excellence, The University of Queensland, Brisbane, QLD. 4072

[2] GeoForschungsZentrum Potsdam, Telegrafenberg, 14473 Potsdam, Germany

[3] School of Earth Sciences, The University of Queensland, Brisbane, QLD. 4072

In order to better understand the relatively unstudied high heat producing granites (HHPG) of the Australian continent, this project has focused on the European analogue: Soultz-sous-Forêts (France). HHPGs are characterised by their radiogenic element (U, Th and K) content, which is higher than average continental crust values.

In a similar manner to ore deposit exploration where intrusive bodies are partially characterised by their alteration assemblages, this hot-dry rock geothermal research will also attempt to characterise the alteration of HHP felsic igneous rocks. Hydrothermal alteration (metasomatism) is classed as the chemical, textural and mineralogical changes ensuing from mineral-fluid interaction in a hydrothermal system. As the pervasiveness of metasomatism can be dependent on the degree of natural fracturing within the granitic body, the understanding of alteration mineralogy and its position within the granitic body could prove integral when locating sites for ensured forced circulation during geothermal energy exploitation. Moreover, as metasomatic phases indicate palaeo-hydrothermal temperature and chemistry it may thus illuminate potential impacts arising from injecting saline solutions whilst utilising the EGS. This paper may therefore illuminate such impacts, including mobilisation of rare earth elements and thorium entrained within conduits of high fluid-flow as well as has implications to the greater understanding of Th mobility in hydrothermal solutions, a conventionally considered “immobile” element. This will be done by analysing the various heat-producing metasomatic accessory phases, with focus on synchysite, found in the Soultz-sous-Forêts monzogranite, a subject which has received no previous attention.

Keywords: Rare earth elements, Soultz-sous-Forêts, titanite

Introduction

Geological Setting

The Soultz monzogranite (Stussi et al., 2002) is situated in the western district of the Rhine Graben (40km NW of Strasbourg), proximal to the Vosges fault and is overlain by Mesozoic to Cenozoic sedimentary cover. The monzogranite was drilled with borehole EPS1 as part of European investigations into enhanced geothermal systems (EGS) and was found to have highly fertile values of radiogenic elements, K (~4%), Th (24-35ppm) and U (6-13ppm (Hooijkaas et al., 2006). The enrichment in radiogenic as well as REE (rare earth elements) may be related to assimilation-fractional crystallisation as postulated by Stussi et al. (2002). Zircon U/Pb work by Alexandrov et al. (2001) dates the monzogranite at 331 ± 9 Ma indicating a possible early Namurian emplacement (Gradstein and Ogg, 1997). The monzogranite is porphyritic, consisting of 1-8cm K-feldspar megacrysts within a phaneritic matrix of quartz, plagioclase, biotite, hornblende with accessory apatite, allanite, titanite, zircon and magnetite (Genter and Traineau, 1991). Further whole-rock geochemistry by Stussi et al. (2002) showed that distinctive geochemical enclaves existed within the monzogranite. These ranged from monzogabbrodiorite- quartz-monzodiorite-quartz-monzonite and quartz syenite and are believed to be mantle-derived.

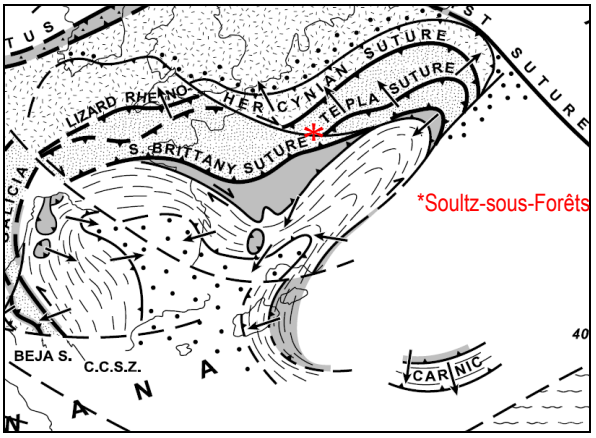

Fig 1: Possible tectonic suture configuration of Hercynian orogeny from Matte (2001).

Titanite

As one of the Soultz monzogranite principle REE (and Y) and Th-bearing phases in the Soultz monzogranite, titanite is known to have a highly variable composition which can depend on the composition of the host rock. Where basic rocks show a classic $CaTi[SiO_4]$ (O,OH,F) composition, highly evolved (Pollard et al., 1987) granitic rocks

are likely to bear titanite with a more chemically exotic composition. For example, the Skye Granite contain titanites with REE_2O_3 (rare earth element) values of up to 46.1 per cent (Exley, 1980). This may result from a $Ca^{2+} + Ti^{4+} = REE^{3+} + (Al, Fe)^{3+}$ (Exley, 1980; Vuorinen and Hålenius, 2005) substitution allowing for a balance in valency. This lithological dictation on composition is due to the relative enrichment in incompatible elements available in the late stages of melt evolution. In hydrothermal environments titanite may destabilise in the presence of Ca-poor, moderate pCO_2 fluids forming: calcite + quartz + rutile ± REY-bearing phases including allanite, bastnaesite, monazite and xenotime (Hunt and Kerrick, 1977; Bancroft et al., 1987; Pan et al., 1993). The assemblage was also postulated to contain fine grains of synchysite ($Ca(REE)(CO_3)_2F$) however this was never confirmed (Pan et al., 1993). This paper therefore not only holds implications to lower temperature destabilised titanite assemblages but also records the first, to date, analysable example of synchysite from titanite destabilisation in the literature.

Hydrothermal Alteration

Three predominant alteration styles have been identified in the Soultz pluton: minor “pervasive” propylitic, vein-related and weathering-related argillisation to haematisation (Genter, 1991). Although the primary K-feldpsar and quartz appear unaltered, the primary ferromagnesian minerals (biotite and hornblende) have undergone almost complete chloritisation forming assemblages of: chlorite + siderite + opaque (haematite-magnetite) and chlorite + epidote (Genter and Traineau, 1991). Plagioclases show a similar extent of selective alteration, forming needles of illite. Zones proximal to fracture networks appear pervasively altered with varying degrees illitisation and carbonatisation. For this study we will focus on this varying pervasive alteration and its chemical influence on the monzogranite.

Analytical Work

Samples K102, K108, K177 and K206 were provided by the Soultz-sous-Forêts Hot-Dry Rock project and represent granite of increasing depth and varying alteration intensity. Samples were cut and made into polished thin-sections.

EDS (enhanced dispersive spectroscopy) and BSE (back scattered electron) images were acquired using the JEOL XL30 SEM at the CMM, Hawken Lab, University of Queensland, Brisbane. Operating parameters were kept at 20kV and spot size 5. Low vacuum analysis was performed on JEOL 6460 SEM in the same facility.

Electron-microprobe analyses of samples were performed in the wave-dispersive mode of the JEOL JX-8500F at the GeoForschungsZentrum, Potsdam, Germany. ZAF oxide corrections were employed with specific operating conditions to minimise degradation of the sample. Operating conditions were: acc. Volatage 15kV, beam diameter 10µm and beam current 5 nA.

Results

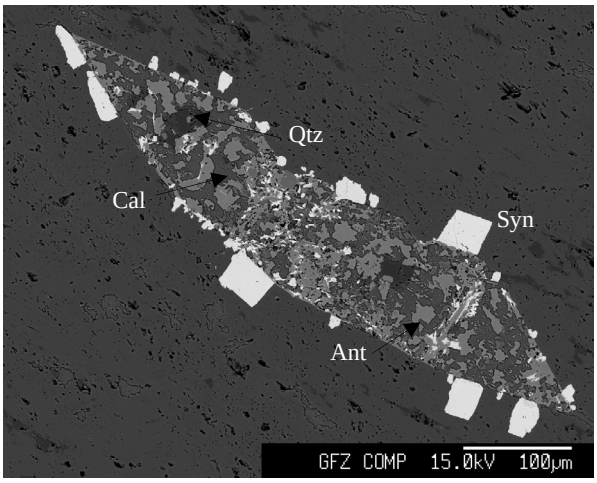

Fig 2: PPA replacing titanite. Cal = calcite, Qtz = quartz, Ant = anatase, and Syn = synchysite.

Titanite is readily identifiable in the Soultz pluton and whether or not it appears as unaltered, highly birefringent rhombic crystals or as polyminerallic, pseudomorph assemblages (PPA) is dependent on the proximity to fracturing. With increasing fracturing and hence fluid/rock ratio samples show an increasing degree of alteration. Under transmitted-light microscopy altered titanites are present as either “dusted-opaque” rhombs or as euhedral-subhedral alteration pseudomorphs. The mineralogy of the “dusted” grains are difficult to identify under transmitted or reflected light due to the nature of formation. The subhedral pseudomorphs, on the other hand, were less difficult allowing accurate identification of the subhedral anatase with supporting quartz-carbonate matrix. EDS and microRAMAN analysis identified the assemblage: anatase + calcite +quartz + synchysite ± bastnaesite.

Synchysite either formed highly birefringent, tabular sub- to euhedral crystals or anhedral-subhedral acicular laths with nano-scale intergrowths of anatase. The acicular laths appear to concentrate within the titanite void, whereas the tabular phases either rim or are proximal to the mineral void. The formation of euhedral laths can be traced to the pooling of hydrothermal fluids following vein-directed fluid movement. Analysing synchysite grains proved difficult as samples were either too small or were decomposed under the electron beam too readily. Those most appropriate for analysis occurred as sub- to euhedral tabular 15-50 by 30-40 micron grains. Although commonly present in PPA from K177, it is rare and almost exclusive to one PPA from K108, where monazite is the predominant REE-

bearing phase. Monazite, xenotime and thorite are the principle REE and Th-bearing phases found in samples K108 and K206 representing a different fluid chemistry. Although not analysable, due to its grain size, synchysite was also identified as a common phase in Mn-rich zones of carbonate veinlets of K108.

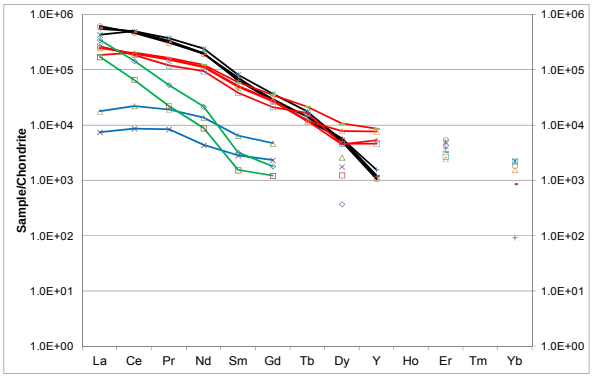

Fig 3 showing REE and Y plot for monazite (black), synchysite (red), allanite (green) and titanite (blue).

Synchysite was confirmed as a REE fluorocarbonate by identifying C, O and F peaks in low vacuum SEM EDS. Trace element concentrations of synchysite were determined using EPMA as seen in Table 1 and Figure 3.

Table 1. Trace element concentration (wt%) of synchysite in sample K177

Sample	K177G	K177G	K177G	K177G
P_2O_5	0.02	0.02	0.00	0.02
SiO_2	0.82	0.40	0.34	0.34
TiO_2	0.45	0.39	0.81	0.51
ZrO_2	0.00	0.00	0.00	0.00
ThO_2	0.69	1.18	0.81	1.23
UO_2	0.08	0.00	0.04	0.00
Al_2O_3	0.27	0.59	0.23	0.25
Y_2O_3	2.42	3.02	0.94	1.73
La_2O_3	9.70	7.19	8.46	8.00
Ce_2O_3	21.56	21.09	22.26	22.88
Pr_2O_3	2.33	2.86	3.00	2.62
Nd_2O_3	8.79	10.30	10.59	10.21
Sm_2O_3	1.29	1.44	1.58	1.57
Gd_2O_3	1.08	1.39	0.89	1.24
Tb_2O_3	0.11	0.15	0.06	0.14
Dy_2O_3	0.44	0.60	0.23	0.46
Ho_2O_3	-	-	-	-
$Er2O_3$	0.19	0.33	0.00	0.09
Tm_2O_3	-	-	-	-
Yb_2O_3	0.06	0.07	0.00	0.00
Lu_2O_3	-	-	-	-
CaO	17.08	16.66	16.67	16.68
FeO	0.00	0.35	0.08	0.23
F	5.44	5.70	5.77	5.86
$F=O_2$	2.29	2.40	2.43	2.47
Sum	70.53	71.34	70.33	71.62

After chondrite normalisation REE and Y patterns indicate a relative enrichment of LREE to HREE in titanite, allanite, synchysite and monazite. For La-Sm titanite, synchysite and monazite share similar patterns, whereas allanite patterns are steeper. Patterns of synchysite and monazite appear to diverge at Sm with significant divergence at Y. Similarly, synchysite shows relatively lower La/Dy of 38.5 to monazite, 77.4, as well as higher average Y_2O_3 values of 1.2 wt% and 0.24 wt%, respectively. As predominant REE in synchysite, La_2O_3 and Ce_2O_3 are on av. 10.9 wt% and 22.3 wt% respectively. The remaining REE_2O_3 wt% is on av. 14.9 wt%.

Analysed grains had CaO values of 16-17 wt% and average F values of 5.4 wt%. The average 0.4 wt% TiO_2, has been attributed to nano-scale inclusions of anatase inclusions.

Discussion

Titanite Destabilisation from CO_2-F-rich fluid

REE and Th Source

The peraluminosity, as defined by its aluminium saturation index (Zen, 1986), and hence the CaO content (Cuney and Friedrich, 1987) of granite can dictate the primary accessory phases to uptake incompatible elements such as REEs and HFSE (Watt and Harley, 1993; Wolf and London, 1994). As shown by Wolf and London (1994) whilst the peraluminosity tends towards an ASI index of >1, the solubility of apatite will increase therefore promoting both P_2O_5 in the melt and the likelihood of phosphates being the primary carrier of REE and HFSE. However, the Soultz ASI indicates a metaluminous (<1) and CaO-rich melt (~2%) (Stussi et al., 2002) within the stability field of Ca-bearing silicates (Cuney and Friedrich, 1987) such as titanite and allanite. As these phases require a stability limit of 1.5% CaO, they, along with thorite (Bea, 1996) and minimally apatite ,will act as the predominant incompatible element-bearing minerals. With the above in mind, the most likely parent-source of REE for the pseudomorph assemblages will be titanite as shown from the synchysite and bastnaesite grains within or rimming the parent-mineral void. This is further substantiated by EPMA mapping in the present study indicating the presence of REE within the crystal structure as well as an almost identical REE pattern between titanite and synchysite. Discrepancies of REE pattern symmetry do however; lie in the La and to a lesser extent Ce contents with % values of synchysite being enriched with respect titanite, relative to ΣREE (Fig 4). Elevated values of lanthanum and cerium are due to sourcing from a relatively enriched source of LREE with respect to titanite, such as allanite or LREE-rich uranopolycrase. Enrichment of LREE in allanite (Fig 3) can be traced to the timing of crystallisation within the chamber (Gromet and

Silver, 1983). As titanite crystallised first, it produced relative depletion in HREE and allowed a now LREE-enriched melt to crystallise allanite. The topic of primary magmatic enrichment is however beyond the scope of this project and will not be discussed further. Apatite may take up REE and HFSE in metaluminous granites (Watt and Harley, 1993); petrographic analyses of K177 in the current study found shielded quartz-bound euhedral apatite with no to minimal evidence of dissolution. Those apatite grains with minor dissolution-reprecipitation structures generally contain monazite or synchysite within voids indicating minimal if any release of REE into the surrounding rock (cf. Harlov et al, 2005). Those released into solution are unlikely to have been mobilised significant distances due to the presence of Ca^{2+} (Salvi and William-Jones, 1996), a common cationic ligand destabiliser of REE and HFSE that have complexed with bi-ligands such as $F^{-}HCO^{3-}$(Wood, 1990b). The only other potential source of REE and Th is thorite; this is however, rather unlikely as thorite grains appear minimally, if at all, affected by the degree of alteration found in the CO^{2-}F-dominated K177.

The origin and role of volatiles

With the appearance of contemporaneous synchysite and ankerite, one must assume the availability of CO_2 in the metasomatic system (Förster, 2001). Moreover, fluid inclusion (FI) studies by (Dubois et al., 1996)on carbonate-quartz veins from EPS1-2052.1 m (10m above this study's sample site) found CO_2-rich solutions within isolated and euhedral quartz FI clusters, with homogenisation temperature-pressure pairs of ~350°C -~2.2kbar and 295°C -0.6kbar (± 0.06kbar) respectively. This may be sourced from either pressure and crystallisation related-degassing from deeper mafic enclaves (Lowenstern, 2001; Stussi et al., 2002) or from the influx of meteoric water that has interacted with carbonate/organic-rich sedimentary units (Fouillac and Genter, 1992).

Upon ingress of a CO_2-rich solution, chloritisation of biotite would have liberated portions of Fe and Mg cations, now available for ankerite formation. Similarly, CO_2 is integral to the formation of this assemblage as it may not only account for the destabilisation of the primary parent phase, titanite (Corlett and McIlreath, 1974; Hunt and Kerrick, 1977; William-Jones, 1981) after chloritisation, but also the transport of REE in aqueous phase (Wood, 1990b).

Works by Hunt and Kerrick (1977) found that at 0.5 XCO_2, <500 °C and 2 kbar, titanite will destabilise by the following equation:

$$\text{Titanite} + CO_2 \longrightarrow \text{Rutile} + \text{Calcite} + \text{Quartz}$$

$$CaTiSiO_5 \longrightarrow TiO_2 + CaCO_3 + SiO_2 \quad (1)$$

This formula however uses an idealised composition for titanite which is uncommon in most igneous bodies especially those of evolved felsic granites such as the Soultz monzogranite (Stussi et al., 2002; Xie et al., 2010) where titanites contain recognisable concentrations of incompatible elements. Taking into account the mineralogy seen at Soultz as well as notably similar geochemical occurrences found by Pan et al. (1993), a more likely equation will result:

$$\text{Titanite} + CO_2 + F \longrightarrow \text{Anatase} + \text{Calcite} + \text{Quartz} + \text{Synchysite} \pm \text{Bastnaesite}$$

$$(Ca, REE, Ti, Th)SiO_5 \longrightarrow TiO_2 + CaCO_3 + SiO_2 + CaCe(CO_3)_2F \pm REE(CO_3)F \quad (2)$$

REY and Th mobility

REE and Y (hereafter REY) are variably mobilised by hydrothermal fluids depending on a number geochemical parameters such as pH, composition and Redox conditions (Wood, 1990b, a; Bau, 1991; Uysal et al., 2011). The composition of the hydrothermal fluid, for example, will preferentially mobilise HREE and Y over LREE when dominated by hard ligands like F^{-}, but will mobilise HREE in solutions dominated by soft, bicarbonate ligands (Bau and Dulski, 1995). Conversely, Wood (1990b) found in fluids rich in chlorine above "geologically unimportant" temperatures (25 °C), LREE will have higher Cl-ligand stability constants. The LREE will therefore be entrained in solution as $REECl^{2+}$ or $REECl_30$ with the latter being prevalent at temperatures above 300 °C. This theory could also be invoked for the introduction of La and Ce into synchysite contemporaneously with titanite destabilisation. As seen from Fig. 4a, there is a substantial increase in the percentage of La in the REE from "parental" titanite to synchysite or monazite, indicating the destabilising fluid was enriched in the very LREE. This enrichment may originate from high concentrations of Cl^{-} in solution during allanite destabilisation. Upon precipitation of resultant metasomatic phases, residual La and Ce in solution may have complexed with available Cl^{-} as $REECl^{2+}$ or $REECl_30$ (Wood, 1990b) and been transported to the site of titanite dissolution. Consequent breakdown of chloride complexes would then have freed-up La and Ce to be incorporated in synchysite permitting free Cl^{-} to remain in the fluid phase (Förster, 2001). An alternative theory of enrichment arises from REE transport by sorption over complexation. Assuming a mildly acidic pH (Bau and Möller, 1991; Sanematsu et al., 2011), hydrothermal fluids may be depleted in HREE as their sorption strength is higher than that of their lighter counterparts in the presence of certain sheet

silicates allowing preferential mobilisation (Coppin et al., 2002) in aqueous phase. Since CO_2 is present in the system, the acidity can be inferred from the formation of carbonic acid (Barclay and Worden, 2000) and may therefore allow sorption to dominate as the REY transportation mechanism, hence enriching the newly forming synchysite in La and Ce.

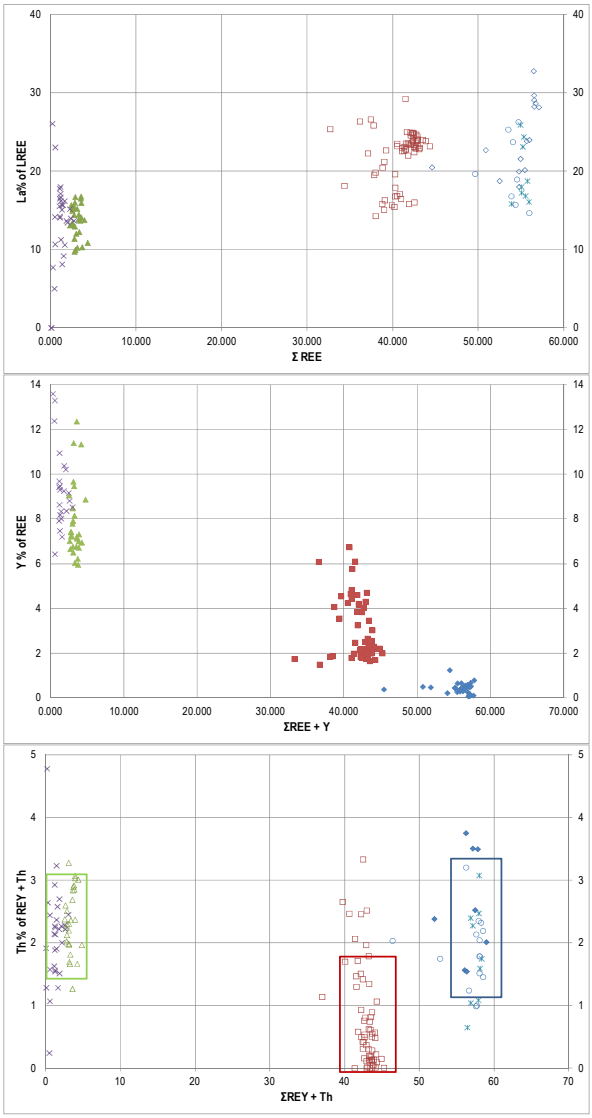

Fig. 4 (a) La % of REE against ΣREE, (b) % of REE + Y against Σ REE + Y and (c) Th % of REY + Th against ΣREY + Th. Green and Purple = titanite, synchysite = red and blue = monazite.

Following destabilisation of titanite, REY and Th may have been held in aqueous phase via speciation with soft ligands (Bau, 1991; Bau and Möller, 1991) such as (bi)carbonate or fluorocarbonate complexes (Wood, 1990b, a; Förster, 2000) as insinuated by the presence of synchysite and bastnaesite. These species are likely to prevail over the more stable single ligand F^- complex (Wood, 1990b) as the abundance of free fluorine would trigger the precipitation of fluorine-bearing phases such as fluorite (Förster, 2001). As most synchysite grains form part of the pseudomorph or are either proximal to the attributing PPA the distance of transport of REY and Th via ligand complex was, on the most part, minimal. The apparent immobility is however expected as calcium's strong affinity for CO32- and F- will buffer the concentration of ligands available for complexation causing mineral precipitation (Salvi and William-Jones, 1990, 1996). HREE (including Y; HREY) and Th on the other hand, show an increased mobility as seen by the relative depletion of Y and Th in synchysite (Fig 4b and c). The loss of HREY and Th may be attributed to not only the preferential incorporation of LREE (Wang et al., 1994; Förster, 2000, 2001) into its crystal structure but also the comparatively higher stability constants for HREY (Wood, 1990b). Furthermore, the particularly large depletion in yttrium may indicate that in the presence of bi-ligand complexes such as fluorocarbonates, it will act as a "heavy pseudolanthanide" (Bau and Dulski, 1995) and hence be highly mobile. The unusual depletion of Th in synchysite and therefore increased mobility of Th is potentially due to the lack of accommodation space in synchysite resulting from La and Ce abundance but also the availability of residual $F\text{-}CO_2^{3-}$ to mobilise the Th from the site of precipitation. This finding is of great importance, as it not only implies the mobility of Th in fluorocarbonate ligand-rich solutions but also, if fluorocarbonate phases are destabilised during forced circulation-based fluid-rock interaction, there may be regional mobilisation of Th within the system.

Implications and Conclusions

Following emplacement at approx. 331 ± 9 Ma (Alexandrov et al., 2001) the Soultz monzogranite (Stussi et al., 2002) underwent a succession of hydrothermal alterations. Ignoring the preceding ubiquitous propylitic alteration (Ledésert et al., 2010), vein-fracture-related alteration significantly modified the original mineralogy with varying degrees of intensity. Co-genetically with carbonate and illite precipitation, multiple accessory phases have undergone destabilisation. Titanite, allanite and previously unfound uranopolycrase have been altered to, among other minerals various incompatible element-bearing phases. This may therefore provide initial insight into potential metasomatic phases by which characterise HHPGs. These products are not only dependent on the fluid/rock ratio and the availability of fixing anions, in this instant CO_2-F and PO_4^{3-}, but also the degree of REY, Th and U enrichment. In K177 where alteration was limited as low to moderate degrees of selective alteration, CO_2-F prevailed due to the metastability of apatite.

Reactant	Product
Titanite	Synchysite ± Bastnaesite
Allanite	Synchysite + Bastnaesite +Thorite
Uranopolycrase	Rutherfordine

Due to its lower degree of LREE enrichment, titanite showed a smaller diversity in the destabilisation products. The conclusive identification of synchysite however, represents its first documented citing from titanite destabilisation in the literature. Moreover, as anatase acted as the principle TiO_2, our results expand on previous works (Hunt and Kerrick, 1977; William-Jones, 1981; Pan et al., 1993; Troitzsch and Ellis, 2002) and, in a qualitative manner, expand on the stability field in which titanite may destabilise under moderate pCO2.

Where alteration was pervasive and texturally destructive from high f/r (K_20_6), we assume a low pH, from abundant CO_2, led to the increased solubility of apatite. This would have allowed HPO_4^{2-} (Harouiya et al., 2007) in solution therefore contributing to the prevalent phosphate-silicate over fluorocarbonate metasomatic phases. K108 represents a mixture of end-member products as seen by the presence of REY and Th-bearing fluorocarbonates and phosphates. With the exception of one quartz-shielded titanite grain, all synchysite grains are found in Mn-rich zones of complex ankerite-illite veinlets. This coupled with semi-quantitative mass balance studies (Fig 4b), and the known presence of Th in synchysite can infer the mobility of Th in solution where $F\text{-}CO_2^{3-}$ acts as the principle ligand complex. We stipulate that, based on the enhanced mobility of HREE and Y in F-bearing solutions (Bau and Dulski, 1995) as seen in Fig 4b, thorium may also be mobilised in solutions where F acts a significant component, such as in low pH hydrothermal solutions rich in fluorocarbonate or bicarbonate ligands. This, in combination with previous works indicating fluorine and CO_2 loss during forced re-injection (Pauwels, 1997), may therefore indicate potential thorium mobilisation during exploitation of geothermal energy. This is under the premise that forced re-injection occurs through fracture networks accommodating carbonates ± synchysite.

Moreover, as EPMA results prove titanite to be a substantial sink of Ca (20 wt%), this work illuminates an alternative source for numerous permeability-reducing (self-sealing) calcite veins (Pauwels, 1997; Ledésert et al., 1999). As such, understanding the degree of titanite and whole rock alteration is of great importance as it may not only influence permeability but also the chemical stimulation required for efficient hydraulic connection (Ledésert et al., 2009).

References

Alexandrov, P., Royer, J.-J., and Deloule, E., 2001, 331 ± 9 Ma emplacement age of the Soultz monzogranite (Rhine Graben basement) by U/Pb ion-probe zircon dating of samples from 5km depth: Comptes Rendus de l'Acedémie des Sciences, v. 332, p. 747-754.

Bancroft, G.M., Metson, J.B., Kresovic, R.A., and Nesbitt, H.W., 1987, Leaching studies of natural and synthetic titanties using secondary ion mass spectrometry: Geochimica and Cosmochimica Acta, v. 51, p. 911-918.

Barclay, S.A., and Worden, R.H., 2000, Geochemical modelling of diagenetic reactions in a sub-arkosic sandstone: Clay Minerals, v. 35, p. 57-67.

Bau, M., 1991, Rare-earth element mobility during hydrothermal and metamorphic fluid-rock interaction and the significance of the oxidation state of europium: Chemical Geology, v. 93, p. 219-230.

Bau, M., and Dulski, P., 1995, Comparative study of yttrium and rare-earth element behaviours in fluorine-rich hydrothermal fluids: Contributions to Mineralogy and Petrology, v. 119, p. 213-223.

Bau, M., and Möller, P., 1991, REE systematics as source of information on minerogenesis, *in* Pagel, M., and Leroy, J.L., eds., Source, Transport and Deposition of Metals: Rotterdam, A. A. Balkema.

Bea, F., 1996, Residence of REE, Y, Th and U in Granites and Crustal Protoliths; Implications for the Chemistry of Crustal Melts: Journal of Petrology, v. 37, p. 521-552.

Coppin, F., Berger, G., Bauer, A., Castet, S., and Loubet, M., 2002, Sorption of lanthanides on smectite and kaolinite: Chemical Geology, v. 182, p. 57-68.

Corlett, M.I., and McIlreath, I.A., 1974, An authigenic Quartz-Calcite-Rutile Assemblage in Ordovician Limestones: Canadian Mineralogist, v. 12, p. 411-416.

Cuney, M., and Friedrich, M., 1987, Physicochemical and crystal-chemical controls on accessory mienral paragenesis in granitoids: implications for uranium metallogenesis: Bulletin de Minéralogie, v. 110, p. 235-247.

Dubois, M., Ayt Ougougdal, M., Meere, P., Royer, J.-J., Boiron, M.-C., and Cathelineau, M., 1996, Temperature of palaeo- to modern self-sealing within a continental rift basin: The fluid inclusion data (Soultz-sous-Forêts, Rhine graben, France): European Journal of Mineralogy, v. 8, p. 1065-1080.

Exley, R.A., 1980, Microprobe studies of REE-rich accessory minerals: implications for Skye granite

petrogenesis and REE mobility in hydrothermal systems: Earth and Planetary Science Letters, v. 48, p. 97-110.

Förster, H.-J., 2000, Cerite-(Ce) and Thorian Synchysite-(Ce) from the Niederbobritzsch Granite, Erzegebirge, Germany: Implications for the Differential Mobility of the LREE and Th during Alteration: Canadian Mineralogist, v. 38, p. 67-79.

Förster, H.-J., 2001, Synchysite-(Y)-synchysite-(Ce) solid solutions from Markersbach, Erzgebirge, Germnay: REE and Th mobility during high-T alteratio of highly fractionated aluminous A-type granites: Mineralogy and Petrology, v. 72, p. 259-280.

Fouillac, A.M., and Genter, A., 1992, An O, D, C isotopic study of water/rock interactions in the Soultz-sous-Forêts granite, *in* Bresee, J.C., ed., Geothermal Energy in Europe: The Soultz hot dry rock project, Volume 2: Montreux, Gordon and Breach Science Publishers, p. 105-118.

Gradstein, F.M., and Ogg, J., 1997, A Phanerozoic timescale: Episodes, v. 19, p. 3-5.

Gromet, L.P., and Silver, L.T., 1983, Rare earth element distributions amoung minerals in a granidiorite and their petrogenetic implications: Geochimica and Cosmochimica Acta, v. 47, p. 925-939.

Harouiya, N., Chaïrat, C., Köhler, S.J., Gout, R., and Oelkers, E.H., 2007, The dissolution kinetics and apparent solubility of natural apatite in closed reactors ar temperatures from 5 to 50°C and pH from 1 to 6: Chemical Geology, v. 244, p. 554-568.

Hooijkaas, G.R., Genter, A., and Dezayes, C., 2006, Deep-seated geology of the granite intrusion at the Soutlz EGS site based ondata from 5km-deep boreholes: Geothermics, v. 35, p. 484-506.

Hunt, J.A., and Kerrick, D.M., 1977, The stability of sphene: experimental redetermination and geologic implications: Geochimica and Cosmochimica Acta, v. 41, p. 279-288.

Ledésert, B., Berger, G., Meunier, A., Genter, A., and Bouchet, A., 1999, Diagenetic-type reactions related to hydrothermal alteration in the Soultz-sous-Forêts Granite, France: European Journal of Mineralogy, v. 11, p. 731-741.

Ledésert, B., Hebert, R., Genter, A., Bartier, D., Clauer, N., and Grall, C., 2010, Fractures, hydrothermal alterations and permeability in the Soultz Enhanced Geothermal System: Comptes Rendus Geoscience, v. 342, p. 607-615.

Ledésert, B., Hébert, R., Grall, C., Genter, A., Dezayes, C., Bartier, D., and Gérard, A., 2009, Calcimetry as a useful tool for a better knowledge of flow pathways in the Soultz-sous-Forêts Enhance Geothermal System: Journal of Volcanology and Geothermal Research, v. 181.

Lowenstern, J.B., 2001, Carbon dioxide in magmas and implications for hydorthermal systems: Mineralium Deposita, v. 36, p. 490-502.

Pan, Y., Fleet, M., and MacRae, N., 1993, Late alteration in titanite ($CaTiSiO_5$): Redistribution and remobilisation of rare earth elements and implications for U/Pb and Th/Pb geochronology and nuclear waste disposal: Geochimica and Cosmochimica Acta, v. 57, p. 355-367.

Pauwels, H., 1997, Geochemical results of a single-well hydraulic injection test in an experimental hot dry rock geothermal reservoir, Soultz-sous-Forêts, Alsace, France: Applied Geochemistry, v. 12, p. 661-673.

Pollard, P.J., Pichavant, M., and Charoy, B., 1987, Contrasting evolution of fluorine- and boron-rich tin systems: Mineralium Deposita, v. 22, p. 315-321.

Salvi, S., and William-Jones, A.E., 1990, The role of hydrothermal processes in the granite-hosted Zr, Y, REE deposit at Strange Lake, Quebec / Labrador: Evidence from fluid inclusions: Geochimica and Cosmochimica Acta, v. 54.

Salvi, S., and William-Jones, A.E., 1996, The role of hydrothermal processes in concentrating high-field strength elements in the Strange Lake peralkaline complex, northeastern Canada: Geochimica and Cosmochimica Acta, v. 11, p. 1917-1932.

Sanematsu, K., Kon, Y., Imai, A., Watanabe, K., and Watanabe, Y., 2011, Geochemical and mineralogical characteristics of ion-adsorption type REE mineralization in Phuket, Thailand: Mineralium Deposita, p. 1-15.

Stussi, J.-M., Cheilletz, A., Royer, J.-J., Chèvremont, P., and Féraud, G., 2002, The hidden monzogranite of Soultz-sous-Forêts (Rhine Graben, France). Mineralogy, petrology and genesis: Géologie de la France, p. 45-64.

Troitzsch, U., and Ellis, D.J., 2002, Thermodynamic properties and stability of AlF-bearing titanite $CaTiOSiO_4$-Ca-$AlFSiO_4$: Contributions to Mineralogy and Petrology, v. 142, p. 543-563.

Uysal, I.T., Gasparon, M., Bolhar, R., Zhao, J.-X., Feng, Y.-X., and Jones, G., 2011, Trace element composition of near-surface silica deposits - A powerful tool for detecting hydrothermal mineral and energy resources: Chemical Geology, v. 280, p. 154-169.

Vuorinen, J.H., and Hålenius, U., 2005, Nb-, Zr- and LREE-rich titanite from the Alnö alkaline complex: Crystal chemistry and its importance as a petrogenetic indicator: Lithos, v. 83, p. 128-142.

Wang, L., Ni, Y., Hughes, J.M., Bayliss, P., and Drexler, J.W., 1994, The atomic arrangement of synchysite-(Ce), $CeCaF(CO_3)_2$ The Canadian Mineralogist, v. 32.

Watt, G., and Harley, S., 1993, Accessory phase controls on the geochemistry of crustal melts and restites produced during water-undersaturated partial melting: Contributions to Mineralogy and Petrology, v. 114, p. 550-566.

William-Jones, A.E., 1981, Thermal Metamorphism of Siliceous Limestone in the Aureole of Mount Royal, Quebec: American Journal if Science, v. 281, p. 673-696.

Wolf, M., and London, D., 1994, Apatite dissolution into peraluminous haplogranitic melts: An experimental study of solubilities and mechanisms: Geochimica and Cosmochimica Acta, v. 58, p. 4127-4145.

Wood, S.A., 1990a, The aqueous geochemistry of the rare-earth elements and yttrium, 1. Review of available low-temperature data for inorganic REE speciation of natural waters: Chemical Geology, v. 82, p. 159-186.

Wood, S.A., 1990b, The aqueous geochemistry of the rare-earth elements and yttrium: 2. Theoretical predictions of speciation in hydrothermal solutions to 350°C at saturation water vapour pressure: Chemical Geology, v. 88, p. 99-125.

Xie, L., Wang, R.-C., Chen, J., and Zhu, J.-C., 2010, Mineralogical evidence for magmatic and hydrothermal process in the Qitianling oxidised tin-bearing granite (Hunan, south China): EMP and (MC)-LA-ICPMS investigations of three types of titanite: Chemical Geology, v. 276, p. 53-68.

Zen, E.-A., 1986, Aluminium Enrichment in Silicate Melts by Fractional Crystallisation: Some Mineralogic and Petrogrpahic Constraints: Journal of Petrology, v. 27, p. 1095-1117.

An analytical model of coupled fluid flow and heat transfer through a fracture with permeable walls in an EGS

Mohais, R.[1], Xu, C.[1]* and Dowd, P.A.[2]
cxu@civeng.adelaide.edu.au
[1] School of Civil, Environmental and Mining Engineering,
[2] Faculty of Engineering, Computer and Mathematical Sciences
and
South Australian Centre for Geothermal Energy Research
University of Adelaide, SA 5005

The cubic law is commonly used to describe flow within fractures with walls that are impermeable (Witherspoon and Long, 1987). However existing experimental evidence conducted on natural fractures in granite cores shows significant deviations from the cubic law (Abelin et al. (1985), Raven and Gale (1985)). Published research reveals that when granite is heated to high temperatures, pores may develop along the fracture walls (Vaughn et al. (1986)) and there may be a large increase in inter-crystalline crack density at temperatures between 200°C and 300°C (Atkinson et al. (1984), Fredrich et al. (1986)). In light of this, we modelled fractures as channels with parallel permeable walls to take into account existing microcracks, fissures and pores in the granular material that comprise the walls.

We formulated a 2-d model of coupled flow and heat transfer by means of a system of four equations including the Navier-Stokes equations, the continuity equation and the energy equation. Our technique included the use of similarity parameters and perturbation analysis, followed by the application of slip boundary conditions at the interface of the free fluid and fracture walls. The results obtained showed that wall permeability affects the flow and heat transfer for small wall Reynolds numbers. In this paper, we will present axial velocity and temperature profiles for fractures with apertures ranging from 0.01 to 0.001 m and permeability in the range from 10^{-6} to 10^{-12} m^2.

Keywords: fracture, similarity solution, wall permeability

Mathematical Interpretation of a fracture

Beavers and Joseph hypothesized that when a viscous fluid in a channel flows parallel to the permeable medium, the effects of viscous shear propagate across the interface and results in thin layer of streamwise moving fluid lying just below the permeable layer (Beavers and Joseph, 1967; Beavers et al., 1970). This fluid layer is pulled along by the free fluid external to the permeable layer. The tangential component of the velocity of the free fluid, u_f at the boundary of the permeable material is considerably higher than the mean filter velocity (seepage velocity), u_m, within the permeable body. This is the Beavers-Joseph slip flow hypothesis which is valid for common viscous liquids at low Reynolds number (Neale and Nadar, 1974). Slip generally results from fluid properties, interactions between the fluid and the wall, the shear rate at the wall and surface roughness (in the case of liquid flows) (Ligrani et al., 2010).

The slip boundary condition can be defined as

$$\frac{\partial u_f}{\partial y} = \frac{\alpha}{\sqrt{k}}(u_f - u_m) \quad (1)$$

Experiments have shown conclusively that once the walls of a channel are comprised of permeable material of permeability, k, then slip boundary conditions should be incorporated in the flow model (Beavers and Joseph, 1967; Beavers et al., 1970). This condition is evaluated at a boundary limit point from the exterior of the fluid. The parameter, α, is a dimensionless quantity that characterizes the material properties of the permeable medium. It can be determined through flow simulations and measurements. It can be determined through flow simulations and measurements.

Crandall et al., (2010) performed numerical computations of flow within open fractures and confined fractures surrounded by permeable medium using an interface condition and found an increase in flow volume of about 10%. Berkowitz (1989) incorporated Brinkman's slip boundary conditions in 1-d modeling of fractures with permeable walls. He showed that the omission of slip leads to underestimation of volumetric flow as high as 19%.

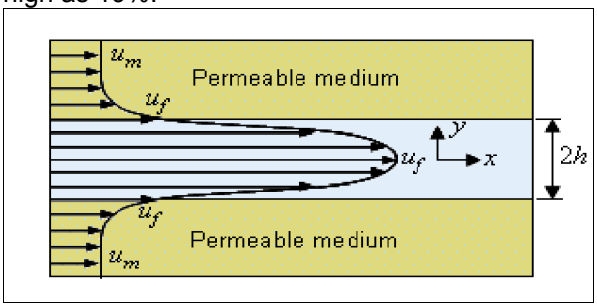

Figure 1. Velocity profile for coupled parallel flows within a channel and bounding porous medium according to the slip

flow hypothesis of Beavers and Joseph (after Beavers and Joseph (1967) and Neale and Nadar (1974)

Analysis of flow

We consider a single horizontal fracture that connects the injection and production wells in an EGS. We neglect end effects at the entry and exit points and model the fracture as a channel with horizontal parallel walls. We define the distance between the channel walls to be *2h*. Assume that both walls have a permeability, *k*. The effects of permeability enter through the slip boundary conditions at *y*=±*h*. We define the non-dimensional distance *y**=*y*/*h*.

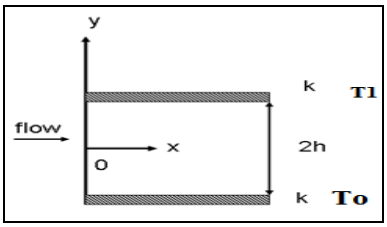

Figure 2. Interpretation of a fracture with plane parallel, permeable walls. The lower wall is at temperature To and the upper wall at temperature T1

We can write the stream function in terms of the entrance velocity, u_o,, a constant wall velocity, v_w, and a similarity function *f* according to Terrill and Shrestha, (1965).

$$\psi(x,y^*) = (hu_0 - v_w x) f(y^*) \quad (2)$$

The velocity components become

$$u(x,y*) = \left(u_0 - \frac{v_w}{h}x\right) f'(y^*) \quad (3)$$

$$v(y*) = v_w f(y^*) \quad (4)$$

We define a wall Reynolds number by

$$Re_w = \frac{v_w h}{\nu} \quad (5)$$

Where $\nu = \frac{\eta}{\rho}$.

The Navier-Stokes equations reduce to:

$$\left(u_0 - \frac{v_w x}{h}\right)\left(\frac{-v_w}{h}((f')^2 - ff'')\right) - \frac{\nu}{h^2} f''' = -\frac{1}{\rho}\frac{\partial P}{\partial x} \quad (6)$$

$$\frac{v_w}{h} ff' - \frac{\nu v_w}{h^2} f''' = -\frac{1}{\rho h}\frac{\partial p}{\partial y*} \quad (7)$$

Eqn. (7) is a function of y* only and so we have

$$\frac{\partial^2 p}{\partial y* \partial x} = 0 \quad (8)$$

This is a useful result which can be used in Eqn. (6) to give after integration

$$f'''+Re_w(-ff''+(f')^2)=C \quad (9)$$

Here *C* is a constant of integration. This third order non-linear ordinary differential equation together with the boundary conditions will yield an exact solution for the equations of motion and the continuity equation. We have expanded the function *f(y*)* and the constant of integration using the wall Reynolds number as follows:

$$f(y^*)=f_0(y^*)+f_1(y^*)Re_w+f_2(y^*)Re_w^2+ \ \dots \ +f_n(y^*)Re_w^n+\dots \quad (10)$$

$$C=c_0+c_1Re_w+c_2Re_w^2+ \dots +c_nRe_w^n+\dots \quad (11)$$

The symmetric properties of the upper and lower walls of the channel were used in determining the boundary conditions:

$$u(x,1) = -\frac{\sqrt{k}}{\alpha h}\frac{\partial u}{\partial y*} = -\phi\frac{\partial u}{\partial y*} \quad (12)$$

$$\left.\frac{\partial u}{\partial y*}\right|_{y*=0} = 0 \quad (13)$$

$$v(x,0)=0 \quad (14)$$

$$v(x,1)=v_w \quad (15)$$

The slip coefficient is defined as:

$$\phi = \frac{\sqrt{k}}{\alpha h} \quad (16)$$

Further details of similarity solution are given in Mohais et al. (2011). We obtained after solving up to first order solution:

$$f_0 = y^{*3}\left(\frac{-1}{2(1+3\phi)}\right) + y^*\left(\frac{3+6\phi}{2+6\phi}\right) \quad (17)$$

$$f_1 = \frac{-y^{*7}}{840}\left(\frac{3}{2(1+3\phi)^2}\right) + y^{*6}\frac{3(7\phi+1)}{280(3\phi+1)^3} + y^*\left(\frac{1}{280(1+3\phi)^2} - \frac{3(7\phi+1)}{280(1+3\phi)^3}\right) \quad (18)$$

$$c_0 = \frac{-3}{1+3\phi} \quad (19)$$

$$c_1 = \frac{9(7\phi+1)}{140(1+3\phi)^3} + \left(\frac{3+6\phi}{2+6\phi}\right)^2 \quad (20)$$

Analysis of heat transfer

The energy equation can be coupled to the momentum equations through the velocity variations with wall permeability.

$$\rho c_p \left(u\frac{\partial T}{\partial x} + v\frac{\partial T}{\partial y}\right) = K_t\left(\frac{\partial^2 T}{\partial x^2} + \frac{\partial^2 T}{\partial y^2}\right) \quad (21)$$

We use the non-dimensional parameter, θ, and write

$$\theta' = \frac{T - T_0}{T_0 - T_1} \quad (22)$$

We substitute the θ parameter into the energy equation and after some re-arrangement, arrive at,

$$\rho c\left(v_w f\theta'\right) = \frac{K_t}{k}\theta'' \quad (23)$$

Using the Prandtl number, Pr, we can then write,

$$Re_w Pr f\theta' = \theta'' \quad (24)$$

In a similar manner to the flow analysis, we presented a similarity solution of the form

$$\theta(y^*)=\theta_0(y^*)+\theta_1(y^*)Re_w+\theta_2(y^*)Re_w^2+ \ \dots \ +\theta_n(y^*)Re_w^n+\dots \quad (25)$$

We conducted analysis up to the first order term. The results and similarity solution are presented in Mohais et al. (2011).

$$\theta = -\frac{y^*}{2} - \frac{1}{2} + Re_w Pr\left(\frac{y^{*5}}{80+240\phi} - \frac{y^{*3}(1+2\phi)}{8+240\phi} + y^*\left(\frac{-1}{80(3\phi+1)} + \frac{1+2\phi}{8+24\phi}\right)\right) \quad (26)$$

Results and Discussion

Based on the above framework, we proceed to examine the effect of changing fracture aperture on the axial flow profiles. In the first instance, we use a relatively large wall permeability of k=10^{-8} m^2, Re_w= 0.5, and α=1.

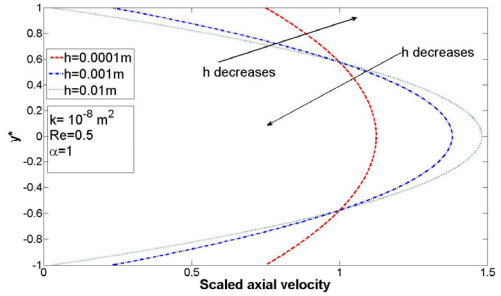

Figure 3: Axial flow profiles of flow in a channel with permeable walls: Effects of channel aperture with α value of 1

We propose that in the hydro-fracturing process, flow channels are created with walls that are not smooth. Cracks and fissures created in the walls during hydro-fracturing can be thought of as thin permeable layers that line the channel wall. Fluid is able to seep into these layers.

Fig. 3 shows three different axial flow profiles, each for a different half-width, within channels with permeable parallel walls. At each wall, there is a slip velocity. The slip velocity at the walls is larger for narrow channels. There is also a lower minimum velocity at the mid-point of the channel for smaller half-widths.

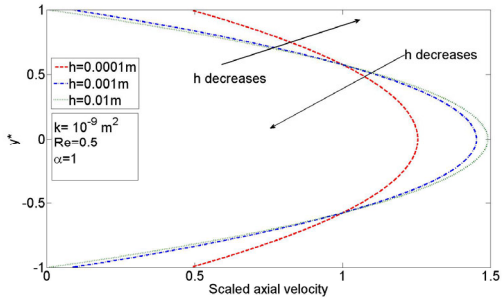

Figure 4: Axial flow profiles of flow in a channel with permeable walls of k=$10^{-9}$$m^2$

Fig. 4 shows the axial flow profiles within a channel with permeable walls one order of magnitude less than those shown in Fig. 3. The scaled axial velocity at the walls in channels of the same half-width, decreases with decreasing permeability. This is particularly pronounced in the channel of half-width 0.0001m.

As the permeability decreases further, the axial velocity profiles for the various apertures are coincident. This is shown in Fig. 5. For a permeability of k=$10^{-12}$$m^2$, the channel behaves as though the walls are essentially impermeable and a parabolic flow profiles emerge. In Fig. 5, the effect of the slip velocity at the walls has essentially been negated.

We next consider the effect of α on the flow profiles. The parameter α is unique to different materials. In their experiments on slip boundary conditions, Beavers and Joseph used two materials, foametal and aloxite (Beavers and Joseph, 1967; Beavers et al., 1970). Foametal

has a cellular structure with irregular pores with an α value that ranges from 0.78 to 4.0. Aloxite is made from fused crystalline aluminium oxide grains held together with a ceramic bond. The experimental value may be as low as 0.1.

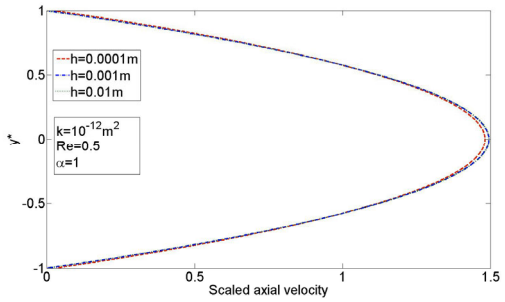

Figure 5: Axial flow profiles of flow in a channel with permeable walls of $k=10^{-12}$m^2

We investigated the effect of changing α on the flow profiles within a channel of varying half-widths. Since no experimental work has yet been conducted to determine the effect of permeable walls on fluid flow within parallel walled channels, we considered the two extreme values of 0.1 and 4.0, until such time that an appropriate α value be determined for fractures in granite.

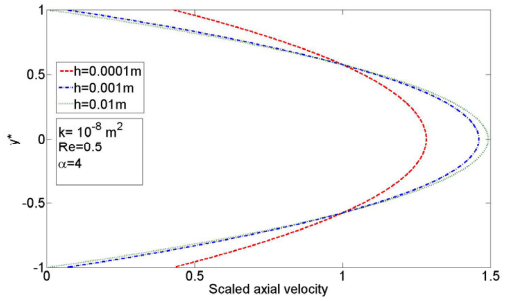

Figure 6: Axial flow profiles of flow in a channel with permeable walls: Effects of channel aperture with wall α value of 4

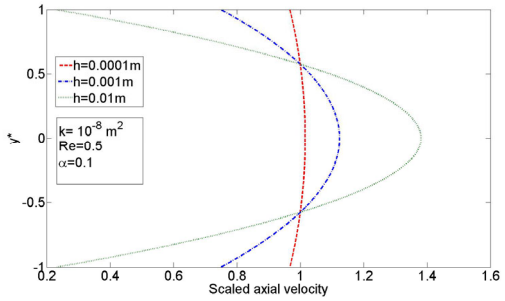

Figure 7: Axial flow profiles of flow in a channel with permeable walls: Effects of channel aperture with wall α value of 0.1

Figs. 6 and 7 show the effect of changing the parameter α on the flow profiles within channels of varying half-width.

Let us first consider the (wide) channel of half-width 0.01 m. In Figs. 3, 6 and 7, the flow profile within this wide channel is represented in green. There is no significant slip velocity at the channel walls regardless of the α value. The large width of this channel affords easy flow-through without significant loss of fluid to the permeable layers at the walls. A smooth parabolic profile of axial flow velocity arises.

In the case of a channel of half-width 0.001 m, there is slip velocity at the channel walls. A smaller value of α gives rise to a larger slip velocity, a smaller mid-line velocity and a flatter flow profile (Fig. 7). For a large value of α, the axial flow profile is almost identical to that of the wider channel (Fig. 6).

For narrow channels, when α is small, plug flow occurs where the maximum velocity at the channel mid-line is practically equal to the slip velocity within the channel walls (Fig. 7). As α increases, the slip velocity decreases (Fig. 3) and when α=4, then the velocity profile assumes a definite parabolic shape (Fig. 6), however there is still slip velocity at the walls and the profile is not identical to that of wider channels.

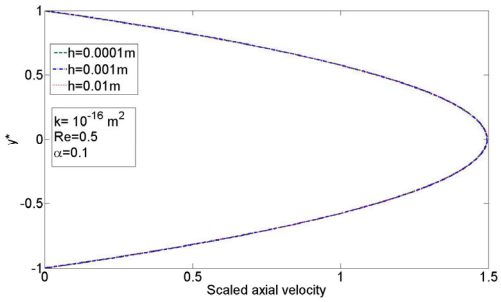

Figure 8: Axial flow profiles of flow in a channel with permeable walls: Effects of channel aperture with wall α value of 0.1 and permeability of 10^{-16} m^2

For small α values and extremely small permeability, parabolic profiles with no slip velocity at the walls arise. The profiles obey the cubic law for these conditions (Fig.8).

The variation of temperature profile from the mid-line of the channel to the lower wall is presented in Fig. 9. θ is relatively insensitive to wall permeability, even as high as 10^{-6}m^2. Perhaps this warrants further investigation through a new similarity parameter for temperature. Further analysis into the temperature profile and heat transfer profiles is presented in Mohais et. al (2011).

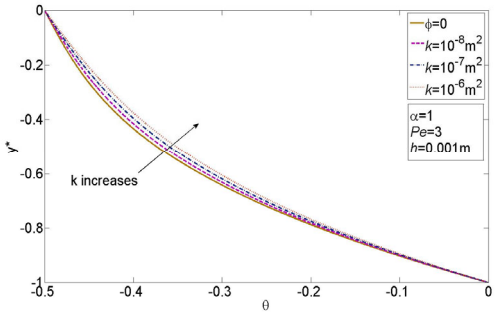

Figure 9: Variation of temperature profile (θ) of fluid for the lower half of a channel of varying permeability Pe=1.25

Conclusions

We hypothesise that flow channels created during the hydro-fracturing process in an EGS possess walls which are permeable in nature. The existing cubic law that is commonly used to describe flow within fractures does not apply to channels like these. We have presented an analytical solution to accommodate wall permeability. We have coupled the Navier-Stokes and energy equations in 2-d and developed a similarity solution with boundary conditions followed from the work of Beavers and Joseph (1967, 1970).

In this paper, we present the flow profiles for walls of varying permeability. We showed that two main parameters that should be investigated are α and h. The next phase of this work involves supporting the current analytical solution with experimental results.

References

Abelin, H., I. Neretnieks, S. Tunbrant, L. Moreno. Final report on the migration in a single fracture; Experimental results and Evaluations. Svensk, Kärnbränsleförsorjning Tech. Rep. 85-03. Nucl. Fuel Safety Proj. Stockholm, Sweden 1985.

Atkinson, B.K., D. MacDonald, P.G. Meredith. Acoustic response and fracture mechanics of granite subjected to thermal and stress cycling experiments. In Proc. 3rd Int. Conf. on Acoustic Emission and Microseismic activity in geological structures and materials. Eds. H.R. Hardy and F.W. Leighton. Trans. Tech. Pubs., Clausthal, N. Germany, 5-18, 1994.

Berkowitz, B. (1989), Boundary conditions along permeable fracture walls: Influence on flow and conductivity, Water, Resour. Res., 25(8), 1919-1922.

Beavers, G.S and D.D. Joseph (1967), Boundary conditions at a naturally permeable wall, J. Fluid Mech., 30, 197-207.

Beavers, G.S. and Sparrow, E.M. and Magnuson, R.A. (1970), Experiments on coupled parallel flows in a channel and a bounding porous medium, ASME J. Basic Eng., 92, 843-848.

Crandall, D. and G. Ahmadi and D.H. Smith (2010), Computational modelling of fluid flow through a fracture in permeable rock, Transp. Porous Media, 84, 493-510.

Fredrich, J.T., T-F Wong. Micromechanics of thermally induced cracking in three crustal rocks. J. Geophys. Res. 91, 12764, 1986.

Ligrani, P., Blanchard, D. and B. Gale (2010), Slip due to surface roughness for a Newtonian liquid in a viscous microscale pump, Phys. Fluids, 22, 0520021-15.

Mohais, R., Xu, C. and P.A. Dowd (2011), Fluid flow and heat transfer within a single horizontal channel in an Enhanced Geothermal System, ASME J. Heat Transf., 133(11), 112603 (8 pages)

Neale, G. and Nader, W., Practical Significance of Brinkman's extension of Darcy's Law: Coupled parallel flows within a channel and a bounding porous medium (1974), Can. J. Chem. Eng., 52, 475-478.

Raven, K.G. and J.E. Gale. Water flow in a natural rock fracture as a function of stress and sample size. Int. J. Rock Mech. Min. Sci. and Geomech. Abstr. Vol. 22, No. 4, 251-261, 1985.

Terrill, R.M., Shrestha, G.M. (1965), Laminar flow through parallel and uniformly porous walls of different permeability, ZAMP, 16, 470-482.

Vaughn, P.J., D.E. Moore, C.A. Morrow, J.D. Byerlee. Roles of cracks in progressive permeability reduction during flow of heated aqueous fluid through granite. J. Geophys. Res. Vol. 91, No. B7, 7517-7530, 1986.

Witherspoon, P.A. and Long, J.C.S. (1987) Some recent developments in understanding the hydrology of fractured rocks, 28thUS Symposium on Rock Mechanics

Hydrothermal fluid flow during mineral alteration reactions in geothermal and other systems: An overview

Allan Pring[1,2]*, Barbara Etschmann[1,2,3,] Joel Brugger[1,2] and Yung Nogthai[3]
Allan.Pring@samuseum.sa.gov.au
[1]Department of Mineralogy, South Australian Museum, North Terrace, Adelaide, SA 5000, Australia
[2]School of Earth and Environmental Sciences, University of Adelaide, Adelaide, SA 5005, Australia
[3]School of Chemical Engineering, University of Adelaide, Adelaide, SA 5005, Australia

It is well established that mechanical fracture systems play an important part in controlling the flow of hydrothermal fluids in geothermal systems and more generally in the mid- to upper crust. However, fracture systems are not the only factor controlling fluid transport in pervasive fluid flow systems. When a hydrothermal fluid travels through the crust, unless it is in chemical equilibrium with the minerals in the surrounding rocks, a chemical reaction will occur between the fluid and the minerals. This process is known in the hydrological literature as "reactive fluid flow" and these fluid-rock interactions have been studied principally using numerical modelling methods, as it has been widely thought that the time scales of reactive fluid-rock interactions in nature are incompatible with laboratory-scale experiments (Berkowitz 2002). At a fundamental level, these fluid-rock interactions are mineral replacement reactions and the kinetics and properties of the processes of mineral dissolution and precipitation are key to their understanding **(**Putnis 2009, Brugger et al. 2010a**)**. We have been studying the physics and chemistry of mineral replacement reactions, principally in relation to ore formation processes and geothermal energy systems. We have found that the product minerals are always initially porous and remain porous while the reaction proceeds (be it alteration, ore deposition, or recrystallisation) (Xia et al. 2009, 2010, Qian et al. 2010). Changes in volume associated with replacement reactions, either positive or negative, introduce stress into the system leading to microfracture and the micro-cracks and porosity that increase the permeability of the system **(**Xia et al. 2009). At some time after the reaction has finished the porosity ripens (or anneals out). This is a general process caused by the fact that as the new mineral assemblage equilibrates with the fluid, the driving force for textural equilibration becomes the reduction of interfacial surface area (Putnis 2009). Thus the porosity and micro-cracking disappear, and reaction-driven porosity is transient in nature on a geological time scale.

This transient porosity should have significant effects on rock permeability and hence on fluid flow and mass transport in hydrothermal systems, including geothermal systems. Few studies on the effects of reaction-generated permeability on fluid flow have been reported (Zhang et al 2000, Tenthorey and Cox 2003). The reason given for this lack of data in recent reviews is that these reactions occur on a geological rather than laboratory time scale (Berkowitz 2002). However, our recent research has proven that such replacement reactions can be studied on a laboratory time scale at least for model geological systems; they are much more rapid than previously thought (Xia et al. 2009, 2010, Qian et al. 2010).

We have recently designed and constructed a flow-through cell to measure the change in permeability during and after a mineral replacement reaction under hydrothermal conditions. With this apparatus we can measure and determine the properties and processes responsible for changes in permeability during mineral replacement/alteration over a wide range of solution conditions up to 350 ˚C and 0.7 kbar. While our focus is on processes on a fundamental level, there are obvious applications to geothermal energy and ore formation systems.

In the geothermal systems the flow of hydrothermal fluids is commonly localized along faults and fractures both natural and generated by stimulation. These fracture systems carry the high fluid fluxes and are the primary fluid circulation mechanism in geothermal systems. Cox (2010) noted that permeability enhancement in fault zones is associated with the formation of porous and permeable wear products along fault slip surfaces. There is also substantial permeability enhancement associated with grain-scale micro-crack networks (Zhang et al. 1995). The opening of fractures, be they large-scale faults or micro-cracks, brings hydrothermal fluids into contact with rocks that might otherwise be dry. In such cases the rock and the fluid will not be in equilibrium, prompting mineral replacement, alteration, or recrystallisation as the fluids interact and equilibrate with the rocks. The precipitation of minerals can be triggered by changes in volume and pressure, as the nucleation of minerals from hydrothermal fluids is volume- and pressure-dependent. Such nucleation and mineral growth leads to the sealing, or closure, of fractures, cracks and even pipes. Mineral replacement reactions are coupled: the dissolution of one group of minerals effectively changes the local solution composition and at the same time creates space, promoting the precipitation of another

mineral or assemblage (a coupled dissolution-reprecipitation (CDR) reaction; Xia et al. 2009). The distance, or length scale, between the dissolution front and the point of precipitation can vary from metres to nanometres. The former describes the process of scaling in pipes and the latter case leads to interface-coupled dissolution-reprecipitation reactions (ICDR). ICDR often results in pseudomorphic replacement, a common phenomenon in mineralogy. In addition, processes such as fossilisation and metal corrosion can be considered as ICDR reactions (Fig. 1) The coupling of the replacement is controlled by the relative solubilities of the parent and product minerals, which depends not only on P, T, but also on solution composition (e.g., pH, redox, ligand concentrations) and the path to nucleation of the product mineral. In all cases, the product mineral when formed is porous and it is this porosity that enables fluid transport to and from the reaction front (Putnis, 2009; Xia et al. 2009).

Micro-cracks and grain boundaries also play an important role in these reactions on the microscale. As noted above, the change in volume associated with mineral replacement can introduce stress into the system and can cause micro-fracturing. The relative contributions to fluid flow or permeability of micro-cracks and reaction-generated porosity are unknown. Because it is transient by nature, their relative contributions to fluid flow in hydrothermal systems change over time, and their contribution may be heavily underestimated when modelling is based on 'fossil' systems. We are conducting experiments which aim to address these questions in a quantitative manner using several mineralogical transformations as model systems for laboratory studies.

In-situ flow-through reactors.

We have developed the simple flow through cells, to probe mineral formation under low to moderate hydrothermal conditions (up to 350 °C, 700 bar) by *in-situ* experiments (Fig. 2). The cells use a HPLC pump and a back pressure regulator to generate fluid flow at pressures up to 700 bars and we have a small heating element on the sample cell which provides local temperature control. By measuring the pressure changes

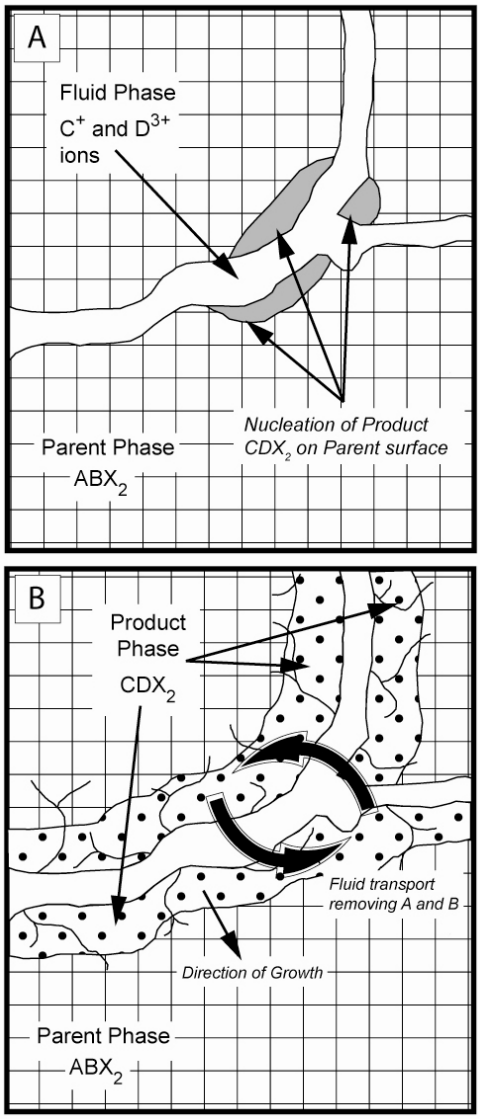

Fluid transports through pores and cracks to reaction interface - adding C^+ and D^{3+}

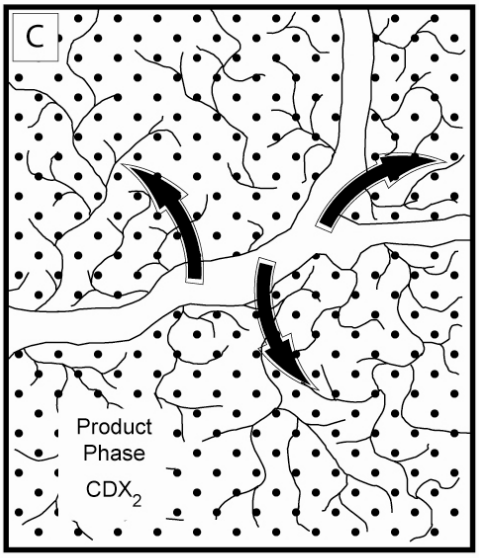

Curved arrows show direction of fluid flow

Figure 1 Schematic diagram showing the essential features of reactive fluid-flow. A) A mineral replacement reaction initiates at a number of sites along a microfracture, because the fluid is not in equilibrium with the mineral. (B) The replacement reaction proceeds at the reaction front between phase ABX_2 and CDX_2. CDX_2 is porous and contains micro-cracks that facilitate mass transport to and from the reaction front. C) The replacement reaction is complete, phase CDX_2 is in equilibrium with the fluid, and the porosity starts to ripen due to reduction of interfacia surface area during textural equilibration. While the mineral remains porous enhanced fluid transport continues through the grains.

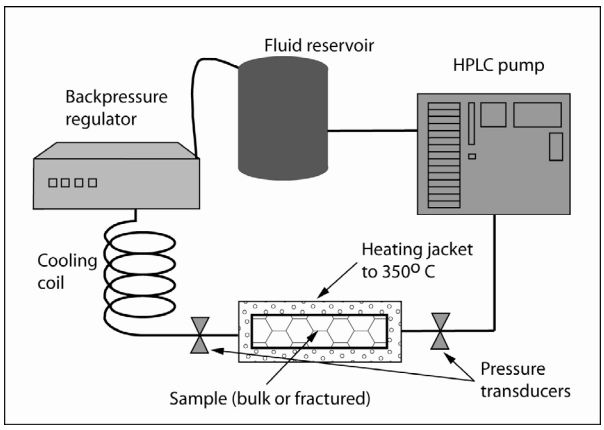

Figure 2 Schematic diagram of flow-through hydrothermal cell for in-situ measurement of changes in permeability.

across a sample during a mineral replacement reaction, we can determine the permeability from Darcy's law. Similar techniques, known as "core flooding" are commonly used in the petroleum industry to study the permeability of reservoir sediments, albeit generally at room temperature and in the absence of significant fluid-rock interactions. Darcy's law is a simple proportional relationship between the instantaneous discharge rate through a porous medium, the viscosity of the fluid and the pressure drop over a given distance.

$$Q = \frac{-kA}{\mu} \frac{(P_b - P_a}{L}$$

Darcy's Law

The total discharge, *Q* (units of volume per time, e.g., cm^3/s) is equal to the product of the permeability of the medium, *k*, the cross-sectional area to flow, *A*, and the pressure drop, all divided by the viscosity, μ and by the length over which the pressure drop is taking place, *L*. The negative sign is needed because fluids flow from high pressure to low pressure. So if the change in pressure is negative, the flow will be positive (in the *x* direction).

With a modified *in-situ* hydrothermal flow reactor (Fig. 2), we can measure the pressure drop (ΔP) across a sample continuously during a mineral replacement reaction at elevated PT and thus establish the permeability *k*. We can do this with bulk samples and pre-fractured samples and we can also allow samples to anneal in the reaction solution, under the appropriated solution and PT conditions, for periods of up to several months.

The choice of model systems for investigation is driven by the necessity of working at time-scales and PT conditions practicable for laboratory study. While ideally we would have liked to study processes such as albitization and sericitization (sodic and potassic alteration), the PT ranges for rapid reaction in these systems (>500 °C and >1 kbar) are not readily amenable to laboratory-scale *in-situ* fluid flow experiments. In addition to the appropriateness of the kinetics of the reactions under accessible PT conditions, the selected primary minerals need to be readily available in suitably sized samples, i.e. as pieces (both single crystal and monolithic polycrystalline form) that can be cut into self-supported discs ~10 to 20 mm in diameter and 2 to 5 mm in thickness. With these constraints in mind, we selected three mineralogical systems:

1) The KBr-KCl system. The replacement of KBr by KCl is an ideal model system to establish general experimental methods and refine equipment design. The reaction takes place a room temperature and a 10 mm thick disc of KBr will be transformed to K(Cl,Br) by immersion in a saturated solution of KCl in less than 10 h. The rate of the reaction can be increased or decreased by manipulating temperature and the Cl/Br ratio of the solution. Large transparent KBr crystals are readily available, as they are widely used in infrared spectroscopy. It is possible to observe the progress of the transformation optically: the KBr crystals are colorless and transparent, but freshly formed K(Cl,Br) is highly porous and white in color. The porosity starts to ripen after 24 hours if these milky K(Cl,Br) crystals are left in solution: the edges of the crystals become transparent after a few days and the crystals become completely clear, with large fluid inclusions after 3 months (Fig. 4). (Putnis et al. 2005).

2) The calcite ($CaCO_3$)–dolomite ($CaMg(CO_3)_2$) system. Dolomitisation is an important alteration reaction in many diagenetic and hydrothermal systems; it is closely associated with ore formation in Mississippi Valley-type Pb-Zn systems (MVT). Carbonate scaling also is a significant problem in geothermal production wells. Calcite (and aragonite) can be transformed to magnesium calcite and ultimately to dolomite at relatively low PT conditions (<0.5 kb and <200 °C) through the action of a $MgCl_2$–rich brine. Large transparent calcite and aragonite crystals and cleavage fragments are readily available on the commercial mineral market (natural calcite is still used in various optical devices). The transformation reaction is relatively rapid, taking place over a 7-day period (at 180 °C and 30 bars); the reaction is considerably faster under the same conditions for aragonite (Brady et al. 1996).

3) The celestite ($SrSO_4$) – strontianite ($SrCO_3$) system. Celestite is the commonest Sr mineral and a common scaling and fouling mineral in the petroleum and geothermal industries. Strontium carbonate is an important reagent in the production of colour TV screens and ferrite magnets, and is produced on a commercial scale by conversion from celestite (Suarez-Orduna et al. 2007). Celestite can be converted to strontianite by reaction with a hydrothermal fluid

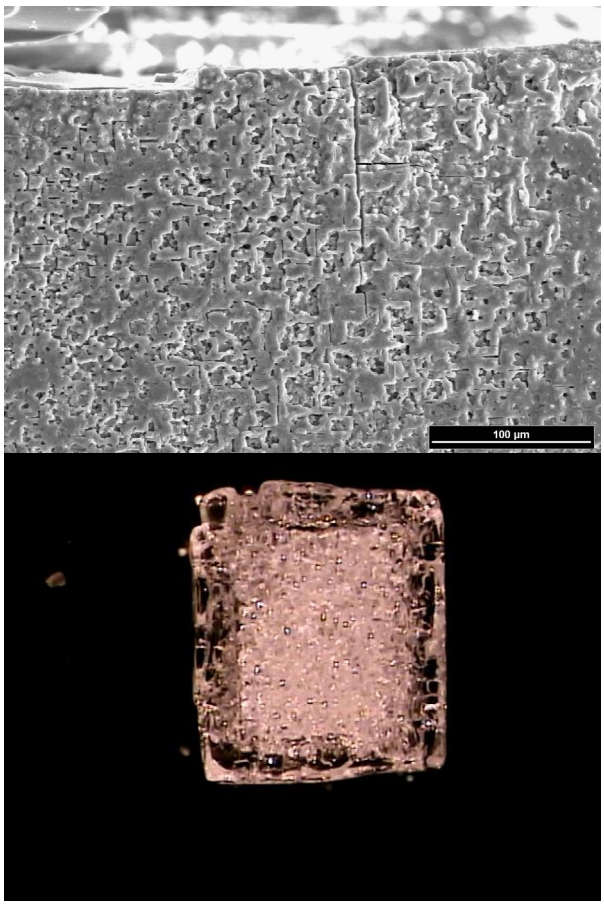

Figure 3. Images of KBr replacement by KCl SEM images showing porosity in a freshly made KCl (top). Optical micrograph of a transformed crystal after 12 days in solution showing ripening of porosity at the crystal edges (bottom)

rich in Na_2CO_3 or K_2CO_3 at 150-250 °C at autogenous pressures. Suarez-Orduna et al. (2004) showed that a 10 mm single crystal of celestite can be transformed to strontianite in 4 days, yielding a pure porous product.

Minerals formed in nature by replacement reactions such as dolomite and strontianite are generally not porous when mined; this suggests that the porosity of the mineral has ripened with time. In the simple KBr-KCl system, porosity ripening is observed after 24 h when the product mineral is left in contact with the equilibrated fluid, and the porosity completely disappears after 3 months (Fig. 4). The mechanism of porosity ripening is not fully understood, but it would appear that the connectivity of the porosity breaks down due to the sealing or blocking of some pores, due to crystal growth within the pore channels. This process seals off some of the pores, trapping fluid within the crystal. The rate of ripening is driven by minimizing the free energy of the system by reduction of interfacial surface area in textural equilibration. (Putnis 2009). In the KBr-KCl system this is about two orders of magnitude slower than the mineral replacement. The kinetics of coarsening in other systems is unknown and is likely to depend on the free energy associated with the reduction of the interfacial surface area. The replacement reaction and the subsequent ripening of the porosity and the micro-cracking may be critical in controlling fluid flow during mineral alteration. If we can elevate the relationship between the rate of transformation and the rate of porosity ripening in the 3 systems to be studied in this project them we should be able to establish a general relationship that can be used in reactive flow modelling.

Acknowldegements.

Thanks are due to Dr Christine Putnis of the University of Münster for the images in Figure 3

References

Barnhoon, A., Cox S.F., Robinson, D.J and Senden, T. (2010) *Geology* 38, 779-782.

Brady, P.V., Krumhansi, J.L. and Paenguth, H.W. (1996) *Geochimica et Cosmochimica Acta* 60, 727-731.

Berkowitz, B., (2002) *Advances in Water Resources* 25, 861-848.

Brugger, J., Pring, A., Ryan, C., Reith, F, Etschmann, B., Lui, W., ONeill, B., and Ngothai, Y..(2010) *Journal of Radiation Physics and Chemistry*, 79, 151-161, 2010.

Cox, S.F., (2010) *Geolfluids* 10, 217-233.

Putnis A., (2009) *Reviews in Mineralogy and Geochemistry* 70, 87-124.

Putnis, C. V., Tsukamoto, K., and Nishimura, Y.,(2005). *American Mineralogist,* 90, 1909-1912.

Qian, G, Brugger, J., Skinner, W.M., Chen, G., and Pring, A.(2010) *Geochimica et Cosmochimica Acta* 74, 5610-5630.

Suarez-Orduna, R., Rendon-Angeles, J.C, Lopez-Cuevas, J. and Yanagisawa, K (2004) *Journal of Physics: Condensed Matter* 16, S1331-1344.

Suarez-Orduna, R., Rendon-Angeles, J.C and Yanagisawa, K (2007) *International journal of Mineral Processing*, 83, 12-18.

Tenthorey,E, and Cox S.F. (2003) *Geology* 31, 921-924.

Xia F., Brugger, J., Ngothai, Y., O'Neill, B, Chen, G., Putnis, A., and Pring, A., (2009) *Geochim. Cosmochim. Acta*, 73, 1945-1969.

Xia, F. O'Neill, B, Ngothai, Y., Peak, J., Tenailleau, C.,Etschmann, B, Qian, G., Brugger, J., Struder, A., Olsen, S., and Pring, A. (2010) *Journal of Applied Crystallography*, 43,

Zhang, S., Cox, S.F., Paterson, M.S., (1995) *Journal of Geophysical Research*, 99, 15761-15775.

Zhang, S., Fitz Gerald, J.D., and Cox, S.F (2000) *Geology*, 28, 911-914.

Geothermal Cities

Klaus Regenauer-Lieb* and the Team of the Western Australian Geothermal Centre of Excellence:
CSIRO, The University of Western Australia and Curtin University
Klaus.Regenauer-Lieb@csiro.au
The University of Western Australia.
35, Stirling Avenue, 6009 Crawley

The US Geothermal Energy Association has identified Perth as one of the top ten "Geothermal Cities" on the grounds of "entering the geothermal community with a new twist – as the first geothermally cooled city with commercially powered heating and air-conditioning units." This announcement reports on the proposal of the WA Geothermal Centre of Excellence (WAGCoE) for CSIRO to cool and heat the Australian Resources Research Centre (ARRC) and the adjacent Pawsey Centre with heat from a deep aquifer below the building. This Education Investment Fund supported project is the first demonstration of a novel WAGCoE developed, patented geothermal cooling technology that has the potential to displace 60 per cent of the electricity needed for conventional heating, ventilation and air conditioning for modern cities by a clean geothermal solution.

By working with CSIRO on this project, WAGCoE aims to take the first step towards providing geothermal desalinated water, air conditioning and power to our cities with zero emissions. The Centre will achieve this by supporting a series of geothermal demonstration projects demonstrating exploitation of convective geothermal fields in sedimentary aquifers.

Successful completion of the ARRC/Pawsey Centre Geothermal Project is expected to lead to adoption of this technology by the wider community, notably in industrial and commercial buildings, schools, shopping centres and government buildings with cooling capacities ranging from 300 kW to several MW. The proposed technology does not occupy a substantial aboveground footprint, thereby making it amenable to existing building retrofit. The standard and existing chillers in buildings simply need to be replaced by adsorption chillers.

Installing or retrofitting this technology on to only 300 buildings in the Perth metropolitan area with a required cooling capacity of 1 MW each would lead to 724,000 tonnes of CO_{2e} abatement per annum. The same technology can also be applied in new townships, such as Alkimos with 20,000 dwellings and the township in Pilbara, with 50,000 dwellings being planned. The adoption of the first demonstrator (Fig. 1) alone, can in both the Perth metropolitan area and in new Western Australian townships, abate 82 million tonnes of CO_{2e} over 20 years.

Keywords: Geothermal Cities, direct heat, power generation, zero emission

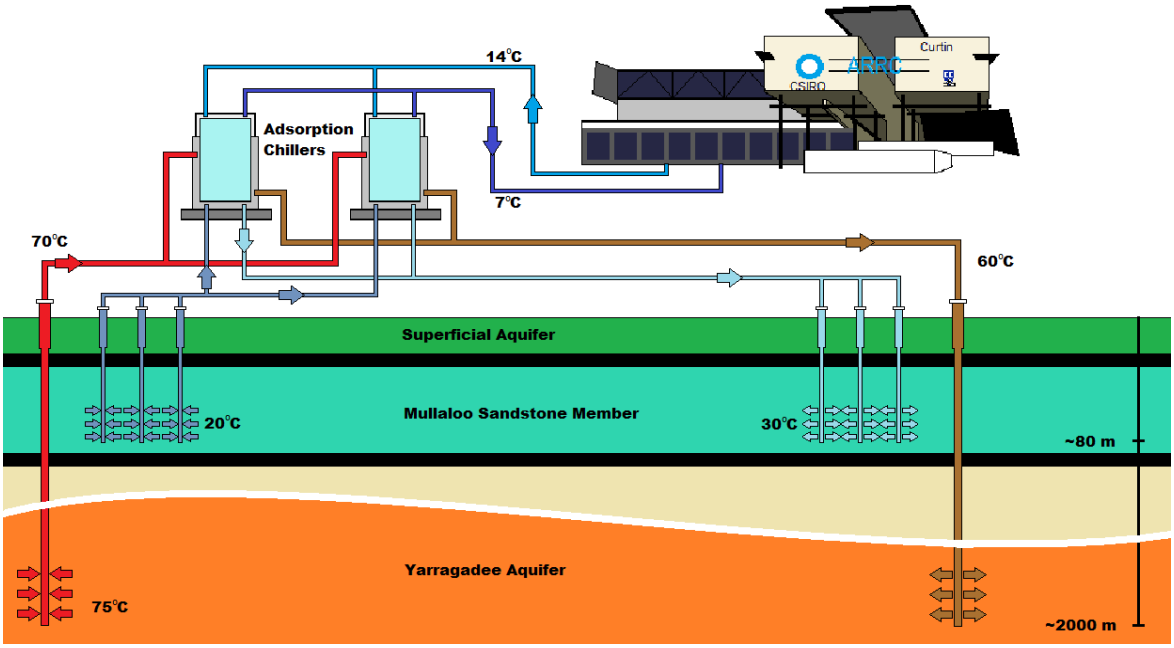

Figure 1. Proposed geothermal heating and cooling solution for the Australian Resource Research Centre. Geothermal heat is being harvested from the deeper Yarragadee aquifer to power the adsorption chiller, which provides cooling to the ARRC building, and all the heat is then rejected into the shallower Mullaloo aquifer.

Dual Heat Abstraction-Heat Rejection Solution

The first innovative component of the ARRC/Pawsey Centre geothermal demonstration project is the novel coupling of adsorption chiller technology to a geothermal heat source. This part of the demonstration hinges on the abstraction of heat from a deep aquifer. Wherever water in excess of 60 degrees Celsius is available (not only from a geothermal but also from another waste heat source), its widespread use in this way can displace significant amount of electricity use in modern cities.

The second innovation is the new concept of a coupled heat rejection into the shallow aquifer using the method of chaotic mixing. This component is often overlooked but probably the most relevant for broadening the footprint of geothermal worldwide and not only for direct heat use. All geothermal implementations, including so-called high temperature resources, have to tackle the problem that they provide temperatures that are still lower than those obtained from burning fossil fuels. Therefore, the lack of efficiency of geothermal energy is always compounded by the need to reject large amounts of energy as heat. Since most geothermal applications are water-cooled it implies in practical terms that the cooling towers have to often waste twice the amount of water produced by the geothermal system or more. Our below ground heat rejection solution solves this problem.

The proposed ARRC/Pawsey Centre geothermal demonstration project shown in Fig. 1 will introduce a tight-knit combination of three components (i) deep geothermal abstraction (ii) shallow geothermal heat rejection and (iii) adsorption chiller as an end-user of this novel concept. For the geothermal city concept we see the adsorption chiller as interchangeable with any of the cascaded heat solutions from electric power production, to HVAC, to desalination and city farming.

Heat Abstraction

The activities of the WAGCoE in this field have been reported on in previous conferences e.g. [Regenauer-Lieb et al., 2008] and are summarized here in brief. We are focussing particularly on the overlooked potential of hot sedimentary basins, which provide typically lower temperature than the hot rock or volcanic plays. The two key challenges involve geological targeting of the heat sources; and combating the engineering challenges of using the low-grade heat directly. This has been accomplished by:

- assessing the geological and geophysical data from the Perth Basin to identify geothermal targets and thereby construct digital geological models of the basin
- Delivering two patents for utilising heat directly from low temperature geothermal sources and establishing a geothermal desalination facility and a geothermally powered adsorption cooling device (described in more detail later)
- Developing a complex system design that combines surface engineering and the underground heat exchanger for optimal tradeoffs and for infrastructure sustainability

WAGCoE also has a fundamental research program that pushes for hotter and deeper resources. We investigate deeper below the sedimentary cover and address the challenges of extracting heat from the granitic basement. Novel multiscale methods for data assimilation in geosciences have been developed from 4D-synchrotron tomography to large-scale geophysical, geological and geochemical data sets which are reported in one of the premier science journals *Nature* [Fusseis et al., 2009; Regenauer-Lieb et al., 2006; Schrank et al., 2011].

Heat Rejection

Recently, a patented technology for efficient heat rejection has been developed based on a controlled laboratory experiment performed in CSIRO's Division of Material and Engineering Science in the Highett labs, Melbourne [Metcalfe et al., 2010; Metcalfe et al., 2010]. A numerical approach has been developed that allows optimisation of subsurface chaotic mixing which has many potential applications, e.g. for treating contaminant sites, for in-situ leaching, in the petroleum industry, CO_2 sequestration, nuclear waste disposal and geothermal energy extraction and heat rejection.

Heat rejection installations into shallow aquifers are also sometimes known as "aquifer thermal storage" or "open loop groundwater systems". They classically consist of a pair or several pairs of extraction/injection well dipoles. These are often designed and operated in a loop, where the extraction well and the injection well are considered to be fixed for the lifetime of the operation. Thermal breakthrough, where disposed hot water from the injector reaches the extraction well, poses a serious risk for these operations. This risk limits the optimal design life of the pair. The design life and the maximum amount of heat that can be rejected can be increased significantly through a simple switching protocol that efficiently mixes the water between the dipoles. An example is shown in Figure 2 [Trefry et al., 2011] for an arrangement of injection-extraction pairs verified in laboratory and numerical experiments Figure 3 [Lester et al., 2010]; see also Trefry et al. this vol.)

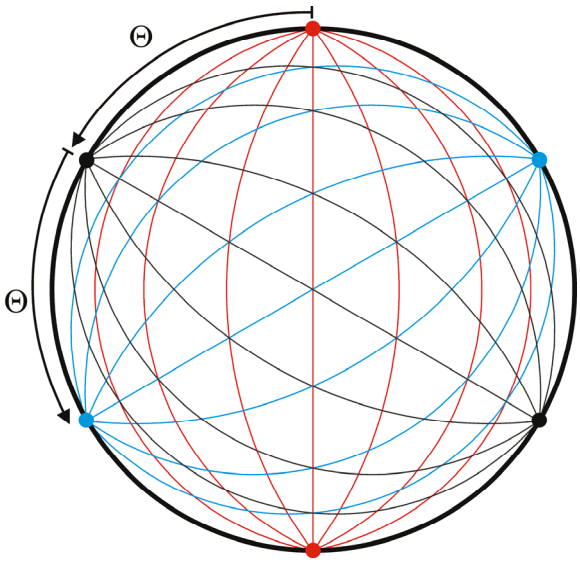

Figure 2. Example programmed dipole sequence for a chaotic switching protocol (rotated potential mixing). The red streamlines show the flow regime induced by one well dipole, then, after some programmed duration t, this dipole is deactivated and another dipole at jump angle Θ is activated (black streamlines), then deactivated at time $2t$ and a third dipole is immediately activated (blue streamlines), and so on.

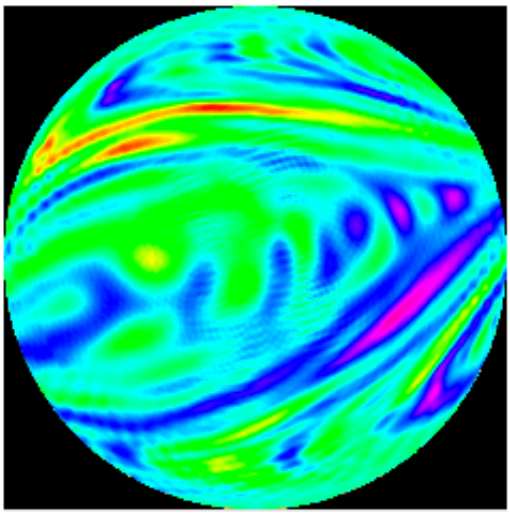

Figure 3. Example of optimal mixing eigenmode (Lester et al. 2010.)

This technology is particularly useful for the heat rejection side since, owing to thermodynamic efficiencies, more heat must be rejected than is extracted. The desire would be to operate such a geothermal well field beyond the classical engineering lifetime of 20 years. The lifetime requirement arises because of the substantial capital investment for drilling the wells and the above ground infrastructure. A significant problem on this time scale is the problem of chemical precipitation around the injection boreholes. This is because the deep aqueous chemistry often can be saline/acidic with dissolved gases. The mixing protocol also has the potential to address this problem since the chemical potentials are switched.

Adsorption Chillers

Adsorption chillers form a relatively new class of heat driven chillers first patented in the 1980's. Compared with absorption chillers, which are the conventional alternative, adsorption chillers rely on a solid rather than a liquid phase to drive the heat exchange. The solid adsorbent can be either silica gel or zeolite. The key virtues of adsorption chillers are that they can be powered by heat sources with temperatures as low as 65 °C and there is no risk of solution crystallization. Compared with absorption chillers, which typically require a heat source temperature of 90 °C, adsorption chillers are viable with geothermal resources at shallower depths. This drastically reduces the risk and cost of drilling and improves reservoir performance, which translates to a lower ongoing pumping cost for extraction of the groundwater. There is a trade-off between reservoir accessibility and required flow rate. Being a relatively new technology with a smaller consequent market penetration, the unit cost of an adsorption chiller (currently twice that of an absorption chiller) are expected to reduce significantly over time. However, in terms of net project capital costs they are already competitive because of the below ground advantages.

For installations where space is an issue the adoption of zeolite-water as the working pair provides a far more compact option than the standard silica gel-water technology, which therefore requires a smaller aboveground footprint. To the best of our knowledge this technology has not been deployed in Australia, but has been tried and tested commercially chiefly in Japan and Europe since late 1980's in the paint industry, iron refineries and process industry where low grade heat is abundant. WAGCoE's manager of the above ground engineering program Prof. Hui Tong Chua is international leader in this technology, and holds an adsorption chiller patent granted in Singapore, US and Europe which has been successfully licensed to the industry since 2003. His adsorption chiller design model is used by Mayekawa, the world-leading manufacturer for adsorption chillers, in its in-house product prototyping. He is currently developing a new generation of compact adsorption chiller which can operate at temperatures as low as 55 °C. This will conceivably boost the viability and uptake of geothermal adsorption chiller technology.

Heat driven chillers, absorption and adsorption regardless, reject significantly more heat to the environment than standard electricity driven chillers. In standard engineering design, cooling towers are used for heat rejection to the atmosphere. They consume a significant amount of fresh water, discharge a considerable amount of spent water to the sewerage which produce significant emissions and require ongoing

chemical treatment. A key innovation of our proposed ARRC/Pawsey Centre geothermal demonstration project is that we replace this standard design protocol with the novel ground-source heat rejection design described above. So instead of rejecting heat to the atmosphere, the same amount of heat is rejected to a shallow aquifer at a depth of about 80 m. This innovative scenario consumes essentially the same amount of electricity as the standard cooling tower design, but it does not consume any fresh water, nor does it require any ongoing chemical treatment. In addition, the perennially cool groundwater offers 2 °C and 6 °C temperature drop on top of what cooling towers can offer, in winter and summer, respectively, thereby further improving chiller efficiency.

Research Partners

CSIRO, Curtin University, The University of Western Australia

Industry Collaborators: GTPower, Green Rock Energy Ltd, New World Energy, Geodynamics, BHP, Newcrest, Geowatt (Switzerland)

The Geothermal Research Initiative (GRI): A collaborative network of the Australian geothermal energy research community involving CSIRO, Western Australian Geothermal Centre of Excellence, Queensland Geothermal Energy Centre of Excellence, South Australian Centre for Geothermal Energy Research, Melbourne Energy Institute, Priority Research Centre for Energy at University of Newcastle, Geoscience Australia, The Institute of Earth Science Engineering at the University of Auckland (NZ)

Institutional Collaborators: Geological Survey of WA, WA Department of Water, Institute for Geothermal Resource Management (Germany), Sustainable Energy Association Australia (SEA), Australia-US-Switzerland-Iceland International Partnership for Geothermal Technology (IPGT)

References

Fusseis, F., Regenauer-Lieb, K., Liu, J., Hough, R. and deCarlo, F., 2009. Creep Cavitation can establish a granular fluid pump through the middle crust Nature, 459: 974-977.

Lester, D., M. Rudman, G. Metcalfe, M.G. Trefry, A. Ord, and B. Hobbs, 2010. Scalar dispersion in a periodically reoriented potential flow: Acceleration via Lagrangian chaos. Physical Reviews E, 81(4): 046319.

Metcalfe, G., D. Lester, A. Ord , P. Kulkarni, M. Rudman, M. Trefry, B. Hobbs, K. Regenauer-Lieb, and J. Morris, 2010. An experimental and theoretical study of the mixing characteristics of a periodically reoriented irrotational flow. Philosophical Transactions of the Royal Society A, 368: 2147–2162

Metcalfe, G., Lester,D, Ord,A , Kulkarni,P, Trefry, M , Hobbs, B, and Regenauer-Lieb, K., Morris, J, 2010. A Partially Open Porous Media Flow Towards Visualization of Coupled Velocity, Concentration, and Deformation Fields. Philosophical Transactions of the Royal Society London, A, 368: 217-230.

Regenauer-Lieb, K., Chua, H., Wang, X., Horowitz, F. and Wellmann, F., 2008. Direct-Heat Use for Australia, Australian Geothermal Energy Conference. AGEC.

Regenauer-Lieb, K., Weinberg, R. and Rosenbaum, G., 2006. The effect of energy feedbacks on continental strength. Nature, 442: 67-70.

Schrank, C., Fusseis, F., Karrech, A. and Regenauer-Lieb, K., 2011. Thermal elasticity is a booster for failure in the brittle-ductile crust Nature, in review.

Trefry, M.G., Lester, D.R., Metcalfe, G., Ord, A. and Regenauer-Lieb, K., 2011. Toward enhanced subsurface intervention methods using chaotic advection. Journal of Contaminant Hydrology, - In Press,

Geothermal Logging in Perth, Western Australia

Reid, L.B.[*1,2], Bloomfield, G.[2], Ricard, L.P.[1], Wilkes, P.[1,3] and Botman, C.[3]
Lynn.Reid@csiro.au
[1] Western Australian Geothermal Centre of Excellence, CSIRO, Bentley WA 6102, Australia
[2] University of Western Australia, Crawley WA 6009, Australia
[3] Curtin University, Bentley WA 6102, Australia

The principle aim of geothermal exploration is to discover high subsurface temperatures in a location both economically and technically viable for drilling and usage. In the Perth Metropolitan Area (PMA), temperatures suitable for low-grade direct-heat use operations are provided by hot groundwater in sedimentary aquifers. Although several commercial projects utilise hot water from the Yarragadee Aquifer [Pujol, 2011], there has been no systematic study of subsurface geothermal conditions in the PMA to support future schemes.

Exploration of Perth's geothermal potential has been performed by the Western Australian Geothermal Centre of Excellence (WAGCOE) and students from the University of Western Australia and Curtin University [Reid et al., 2011]. The study aimed to gain true formation temperatures from shallow sediments by detailed temperature and gamma ray logging within water bores up to 800 metres deep. The project was part of a broader initiative within WAGCOE to characterise the geothermal resource in the Perth Basin.

Keywords: Temperature logging, geothermal gradients, radiogenic heat production

Geologic Background

The city of Perth sits atop the Perth Basin, a sedimentary rift basin approximately 1000 km long extending in a north-northwesterly orientation between latitudes 27°00'S and 34°00'S. The Perth Basin is bounded by the Darling Fault to the east and the continental slope to the west. Basement lithology consists of Precambrian rocks of the Pinjarra Orogen [Mory et al., 2005]. Early Permian to Late Cretaceous sedimentary sequences up to 15 km thick occupy the series of sub-basins, troughs, shelves and ridges comprising the basin. Native permeabilities of the aquifer sediments throughout the Perth Basin are high [Davidson & Yu, 2006], thus facilitating groundwater circulation through these aquifers at relatively shallow depths. The attainable pumped flow rate of the Perth Basin's heated water resources may therefore be practical for hot sedimentary aquifer (HSA) geothermal use.

Descriptions of the shallow (<1 km) stratigraphic units of the Perth Region are found in Davidson [1995]. The shallow portion of the Perth Basin comprises three major aquifers: the Superficial, Leederville and Yarragadee aquifers; as well as several minor aquifers: the Rockingham, Kings Park, and Mirrabooka aquifers.

Logging Campaign

Detailed vertical temperature and gamma ray logging of seventeen WA Department of Water (DoW) Artesian Monitoring (AM) wells was performed throughout the PMA. The probe was an A626-4 Conductor Gamma/Temperature Sonde, with a temperature range of 0-70 °C, and a precision of approximately 0.007 °C. Equipment was provided by Geoscience Australia.

Sampling was conducted at 5 cm intervals with a 5 m min^{-1} descent. The data were recorded as digital LAS files and are stored in the WAGCOE Data Catalogue [Corbel & Poulet, 2010] at http://geothermal.org.au/Catalogue.htm. The temperature probe was calibrated before and after logging. Data was quality controlled by correcting for effects of basal silting, water table elevations, and seasonable ground surface temperature fluctuations [Reid et al., 2011].

In addition to the direct measurements, temperature logs from fifty-three DoW AM wells measured in the 1980s were digitised into LAS format [Reid et al., 2011]. The digitised data were calibrated to temperature point values recorded at the time. These wells greatly extend the spatial scope of quality data available in the PMA.

Temperatures at Depth

The temperature logs provide a picture of true formation temperatures within shallow sediments in the Perth Basin. A three-dimensional model of the temperature distribution was created and used to produce maps of temperature at depth and within the major aquifers. Figure 1 shows the temperature distribution at 250 metres below the ground surface. Figure 2 shows temperatures at the top of the Neocomian Unconformity, an erosional surface roughly representing the top of the Yarragadee Formation, the top of the major water-bearing permeable Yarragadee Aquifer. Three dimensional models in PDF format of the subsurface temperatures are available online at http://www.geothermal.org.au/Catalogue.htm.

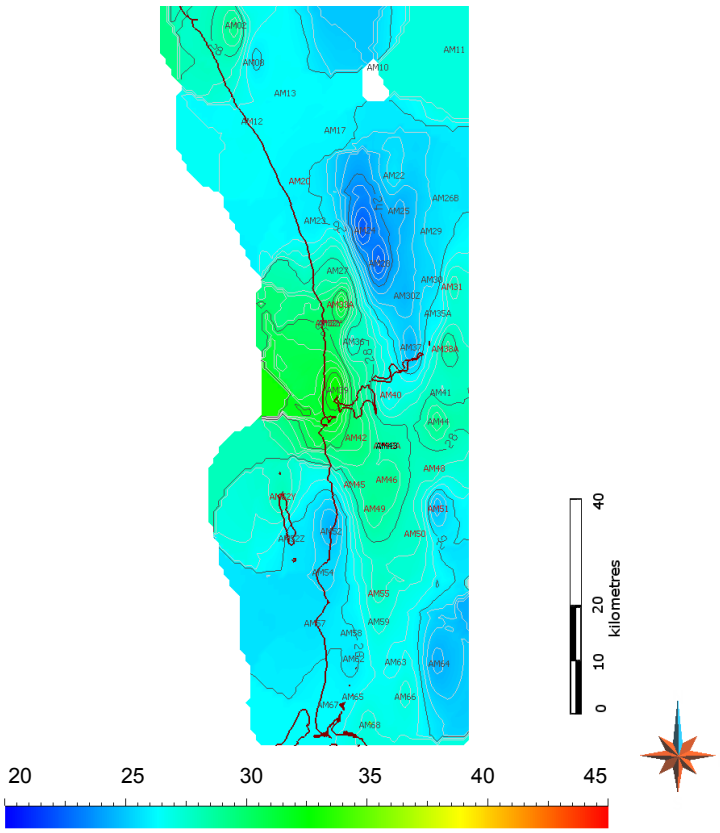

Figure 1: Temperature (°C) at 250 metres below AHD. Wells used in the analysis are shown.

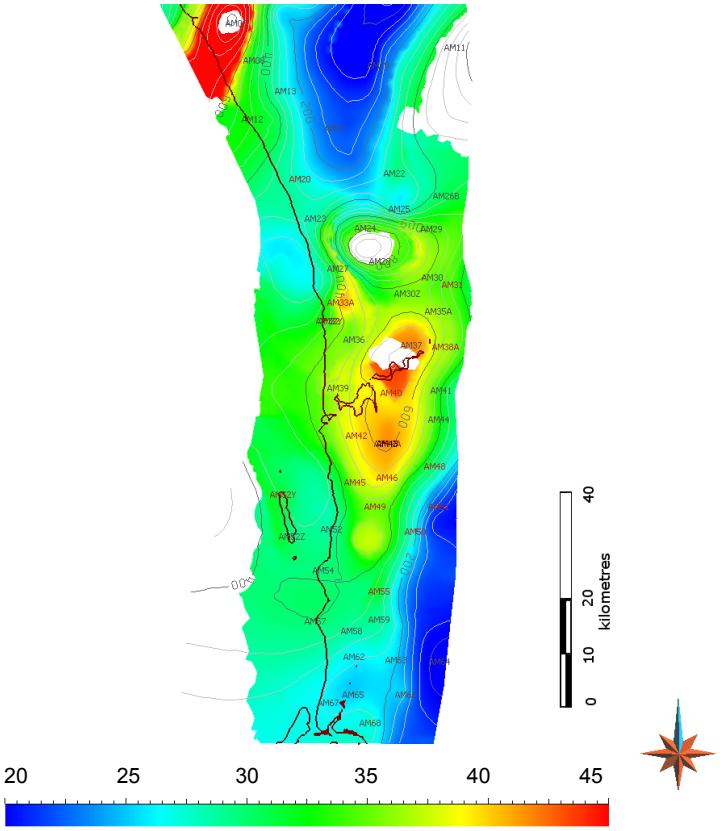

Figure 2: Temperature (C) at the top of the Neocomian Unconformity. Contours indicate depths (m) of unconformity below AHD.

Non-conductive heat flow

The temperature data were interpreted with a one-dimensional conductive heat model using the GeoTemp package [Ricard et al., 2011]. Significant difference (> 5%) between the model and the observations was deemed indicative of heat moving via non-conductive mechanisms, such as advection or convection. Evidence of non-conductive or advective heat flow is demonstrated in most formations in the PMA, with significant effects in the aquifers.

Geothermal Gradients and Heat Flow

Average geothermal gradients were calculated for each formation from the logged and digitised data and are shown in Table 1. In general, the gradients vary with lithology, with sandstone formations exhibiting average gradients of approximately 25 °C km^{-1}, while insulating silt/shale formations show higher average gradients of over 30 °C km^{-1}. For this gradient analysis, vertical conductive heat flow was assumed and wells exhibiting advective flow in that formation were excluded from the calculation. The last column of Table 1 indicates the fraction of wells crossing each formation included in the average conductive geothermal gradient estimates.

Table 1: Average geothermal gradient by formation

Formation	Geometric Mean (°C km^{-1})	Std. Deviation (°C km^{-1})	Fraction of wells used
Superficial	11.4	6.9	19/40
Rockingham	15.5	5.6	7/8
Kings Park	27.4	13.2	10/10
Mullaloo	23.3	16.8	4/6
Como	28.4	3.7	3/4
Lancelin	24.7	6.0	3/4
Poison Hill	16.0	2.6	6/6
Gingin	16.8	12.1	7/10
Molecap	20.8	7.0	8/11
Mirrabooka	24.5	13.1	5/6
Kardinya	29.8	9.7	22/36
Henley	22.7	7.7	18/29
Pinjar	25.2	8.9	32/47
Wanneroo	25.1	6.9	55/62
Mariginiup	30.8	7.9	51/53
South Perth	38.3	8.4	42/46
Gage	25.0	5.7	34/37
Parmelia	36.1	13.6	2/3
Yarragadee	25.1	4.7	26/31
Cattamarra	23.8	3.2	6/9

Preliminary heat flow estimates were calculated from these average conductive gradients and thermal conductivities measured by HDRPL [2008] for formations considered applicable to the PMA. The geometric mean heat flow estimates range between 64 mW m^{-2} to 91 mW m^{-2}, with the standard deviation of the arithmetic mean heat flow ranging between 15 and 23 mW m^{-2}.

Radiogenic Heat Production

Analysis of the gamma ray logs yielded the first estimates of radiogenic heat production in Perth Basin formations. Using an empirical correlation [Bücker & Rybach, 1996], bulk values by formation ranged between 0.19 and 0.85 μW m^{-3} and are shown below in Table 2. Matrix values are obtained by correcting with porosity. Here, porosity is assumed to be 0.20 in sandstone formations and 0.05 in shaly formations; sources of more precise porosity estimates are noted in the table. Matrix radiogenic heat production values range from 0.23 to 1.06 μW m^{-3}, similar to other values reported in the worldwide literature.

Table 2: Radiogenic Heat Production by formation. Porosity estimates obtained from α:Davidson [1995]; β: Leyland [2011]; χ: Israni & Delle Piane [2011].

Formation [Member]	Bulk Radiogenic Heat Production (μW m^{-3})		Matrix Radiogenic Heat Production (μW m^{-3})
	Mean	Std. Deviation	
Superficial	0.19	0.07	0.24$^{\alpha}$
Kings Park [Mullaloo Sandstone]	0.19	0.05	0.23
Kings Park	0.32	0.02	0.34
Kings Park [Como Sandstone]	0.19	0.02	0.23
Osborne [Mirrabooka]	0.19	N/A	0.23$^{\alpha}$
Osborne [Kardinya Shale]	0.57	0.14	0.60
Osborne [Henley Sandstone]	0.35	0.07	0.44
Leederville [Pinjar]	0.85	0.15	1.06$^{\beta}$
Leederville [Wanneroo]	0.58	0.09	0.73$^{\beta}$
Leederville [Mariginiup]	0.78	0.11	0.98$^{\beta}$
South Perth Shale	0.82	0.08	0.87
Gage	0.54	0.17	0.68
Yarragadee	0.45	0.08	0.57$^{\alpha}$
Cattamarra Coal Measures	0.45	N/A	0.47$^{\chi}$

Radiogenic heat production is not a significant source of heat within shallow Perth Metropolitan area sediments, producing less than 1% of total estimated heat flow. Analysis of the gamma ray logs also helped produce a consistent set of

stratigraphic formation elevations in the PMA [Reid et al., 2011].

Discussion

For the first time, an extensive database of temperature measurements and maps of the temperature distribution in three dimensions in the Perth Metropolitan Area are available. Average geothermal gradients of 25 °C km^{-1} , to 30 °C km^{-1} indicate that subsurface temperatures can be reasonably well predicted for direct use applications. However, non-conductive heat flow is widespread across the area and these effects should be considered in any permeable setting. Geothermal gradients and estimates of conductive vertical heat flow exhibit considerable variability within formations, which points out the need for mapping of thermal rock properties. Radiogenic heat production rates for Perth Basin sediments are shown to be an insignificant part of this variability.

Additional work led by WAGCOE and CSIRO is currently underway to further characterise the thermal regime in the area. Temperature and three-component gamma ray logging is focusing on areas of significant anomalies indicated in this analysis. Older datasets are being digitised to provide inexpensive, albeit less accurate, spatial coverage. The movement of heat by advective groundwater flow is being quantified to determine the significance of this mode of heat transport. Thermal properties such as thermal conductivity, and specific heat are being measured through laboratory studies and numerical model calibration. This coordinated effort is leading to a good understanding of geothermal prospects in the Perth area.

Acknowledgements

The Western Australian Geothermal Centre of Excellence is funded by the Western Australian government, CSIRO, the University of Western Australia, and Curtin University. This work was supported by Green Rock Energy Ltd. and GT Power, Ltd. Geoscience Australia graciously provided the logging equipment.

References

Bücker C. and Rybach, L., 1996. A simple method to determine heat production from gamma ray logs, *Marine and Petroleum Geology*, 13(4) 373-375.

Corbel, S. and Poulet T., 2010, WAGCoE data catalogue for geothermal exploration, *2010 IEEE Sixth International Conference on eScience*, pp 89—94.

Davidson W. A., 1995. Hydrogeology and groundwater resources of the Perth Region, Western Australia: Western Australia. Western Australia Geological Survey Bulletin 142.

Davidson W. A. & Yu X., 2006. Perth regional aquifer modelling system (PRAMS) model development: Hydrogeology and groundwater modelling. Western Australia Department of Water Hydrogeological Record Series HG 20.

HDRPL [Hot Dry Rocks Pty. Ltd.], 2008. Geothermal energy potential in selected areas of Western Australia (Perth Basin): A report prepared for the Department of Industry and Resources, Western Australia. Hot Dry Rocks Pty Ltd.

Israni, S.R. and Delle Piane, C., 2011, Rock Physics and Petrophysical characterization of units from the Perth Basin, CSIRO Confidential Report Number EP113342, 42 pp.

Leyland, L., 2011, Hydrogeology of the Leederville Aquifer, central Perth Basin, Western Australia, Ph.D. Thesis, School of Earth and Environment, University of Western Australia.

Mory A. J., Haig D. W., Mcloughlin S. & Hocking R. M., 2005. Geology of the northern Perth Basin, Western Australia – a field guide. Western Australia Geological Survey 2005/9.

Pujol, M., 2011, Examples of successful hot Sedimentary Aquifer direct-use projects in Perth, Western Australia, in Middleton, M and Gessner, K. (eds.) *Western Australian Geothermal Energy Symposium Abstracts v. 1*: p23.

Reid, L.B., Bloomfield, G., Botman, C., Ricard, L.P., and Wilkes, P. Temperature Regime in the Perth Metropolitan Area. Results of temperature and gamma logging and analysis, June/July 2010. 2011. CSIRO Report EP111422, 197 pp.

Ricard L.P., Chanu J-B and Pons G., 2011, Temperature interpretation and modelling for geothermal applications: GeoTemp, in: Middleton, M. and Gessner, K. (eds.) *Western Australian Geothermal Energy Symposium Abstracts, v.1*: p 26.

Paralana 2 – Well Testing and Stimulation

Reid P. W.[1], Messeiller M.[1], Llanos E. M.[1] and Hasting, M.[2]

[1] Petratherm Limited, 129 Greenhill Rd, Unley 5061, South Australia,

[2] Hasting Micro-Seismic Consulting, 1233 Quail Way, Ridgecrest CA 93555 USA

Corresponding Author: preid@petratherm.com.au

The Paralana Engineered Geothermal Project is located 600 km north of the city of Adelaide in South Australia (Figure 1). The project is testing for viable geothermal sources generated by the radiogenic decay of high heat producing Mesoproterozoic basement rocks of the Mt Painter Complex (Figure 2). Petratherm Limited in joint venture with a major oil and gas (Beach Energy) and power industry energy utilities (TRUenergy) are initially seeking to build a 7.5 MWe commercial power development to supply a local off-grid mine, with the long term objective of providing large scale (260 MWe)power through the national grid.

In the second half of 2009 a deep geothermal well, Paralana 2, primarily designed to be an injector well, was drilled to 4003 metres (G.L) AHD (Figure 2). During drilling of the well, several zones of over-pressured fluid between 3670 - 3864 metres were encountered. The well was originally designed to be steel cased but due to well breakout issues in the lower portion of the well, a result of the abovementioned over-pressured brines, the final casing string was set at 3725 metres. The strategy is to perforate the casing at selected target intervals and perform hydraulic stimulations to increase the chance of achieving a commercial flow rate, a key commercial barrier for EGS developments around the world.

Keywords: Paralana, Hydraulic Fracture Stimulation, Micro-seismic array

Micro-Seismic Array

The Paralana micro-earthquake (MEQ) monitoring array has been operational since April 2008, initially recording the background seismicity in the region, prior to ground operations. The array was established and is monitored by seismologists from the Institute of Earth Science and Engineering, Auckland, New Zealand. The array combines sensitive downhole sondes with surface seismometers to enable the interpretation of a wide spectrum of seismic events (Figure 3). For the recent hydraulic stimulation In July 2011 the array was upgraded to a real-time monitoring network to enable analysis of micro-seismic events and to manage induced seismic risk.

Four ground accelerometers were also added to the array and were located to measure peak ground velocity with respect to local surface infrastructure. The ground accelerometer data was used in real time to manage the injection operating process and induced seismic risk (Figure 3). In addition to hand picking of seismic events during the stimulation, events were analysed with auto-picking software, MIMO, developed by the Norwegian Seismic Array (NORSAR).

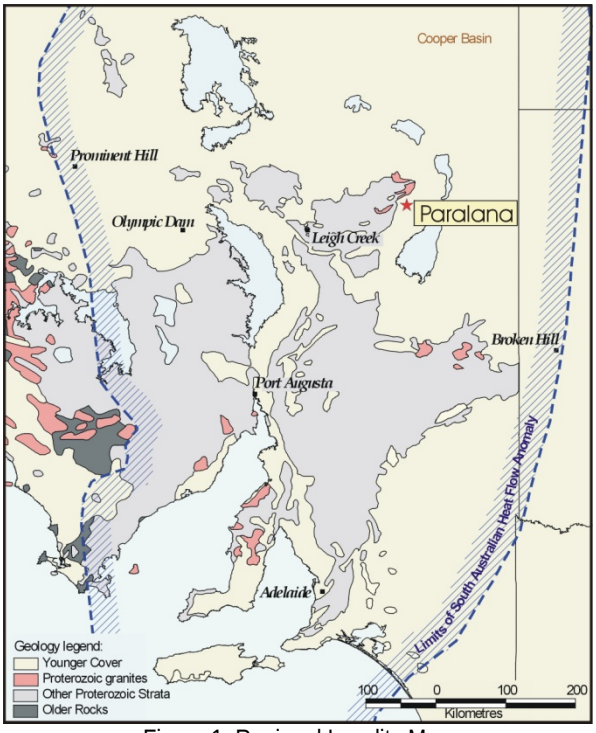

Figure 1. Regional Locality Map.

Diagnostic Fracture Injection Test (DFIT) – January 2011

In January 2011, the Paralana 2 deep well's casing was perforated over the 3679 - 3685 metres interval, corresponding to the zone where the wireline logging did not indicate the presence of a permeable structure. This was trialled to initiate a complex frac in competent formations around the well bore. The perforation was followed by a small volume stepped injection test that successfully broke down the formation. Injection rates ranged between 1.3 and 5.3 l/sec providing base information to plan the main fracture stimulation works. On completion of the injectivity test, the measured stable well head pressure was 3,940 psi. The high pressure suggests connection to a pre-existing over-pressured zone contained in the reservoir rock.

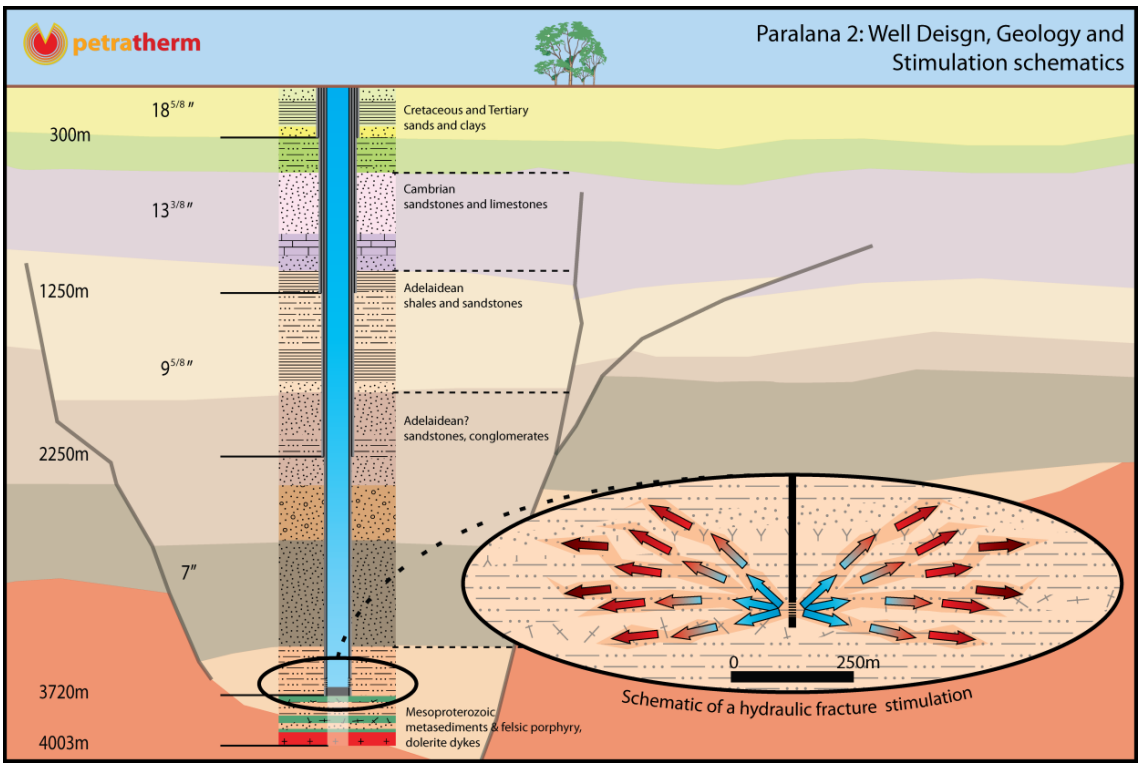

Figure 2. Paralana Well Completion and Geological log.

During the 2 hour DFIT injection period, approximately 300 seismic events, with about 125 large enough to be located were recorded. The event magnitudes were small ranging between -1 to 1 on the Richter magnitude scale. The fracture cloud extended approximately 300 metres to the North East, and is 200 metres wide and is approximately 130 metres thick. The injection survey was used in part to calibrate the micro-seismic array.

Fracture Stimulation – July 2011

In July 2011 fracture stimulation works were successfully completed. Over a five day period, 3.1 million litres of fracturing fluid were pumped into the Paralana 2 well at pressures up to 9,000 psi. Initial injection rates were low (3 l/sec), but steady improvement occurred over the period principally through the injection of several acid treatments. The reservoir rock sequence contains only trace carbonate so it thought the increased injection rates are principally due to the breakdown of casing cement in and around the injection zone. Near the end of the injection period a maximum sustained pump rate of 27 litres per second was achieved.

The stimulation produced over 11,000 micro-earthquakes detected by the micro seismic network (Figure 4). The primary aim of the fracture stimulation, which was to create fractures in the subsurface at least 500 metres from the Paralana 2 well, was achieved with stimulated zone extending approximately 900 metres to the northeast and east of the Paralana 2 well and at a depths ranging between 3,500 to 4,100 metres.

The fracture network comprises at least 4 main structures, with the principal area of growth, a northeast trending en-echelon style tensile opening fracture which dips steeply to the northwest. This feature seems to be bounded either side by steep north-northeast trending structures.

On completion of the stimulation, the calculated stable wellhead pressure remained at approximately 4000 psi. Hence it appears that the stimulated volume is over-pressured and connected into a naturally over-pressured zone. This may assist in the recovery of hot fluids from the reservoir.

The largest seismic event detected during the stimulation was magnitude 2.6 on the Richter scale with 98% of the micro-seismic events detected being below 1.0. The magnitude 2.6 was felt as a short and slight vibration by some staff members near the well bore. Companies and people in the surrounding area did not feel the event.

The Richter Magnitude 2.6 event corresponded with a peak particle velocity of 2.36 mm per second, which falls within the green operating zone of the induced seismicity risk management plan.

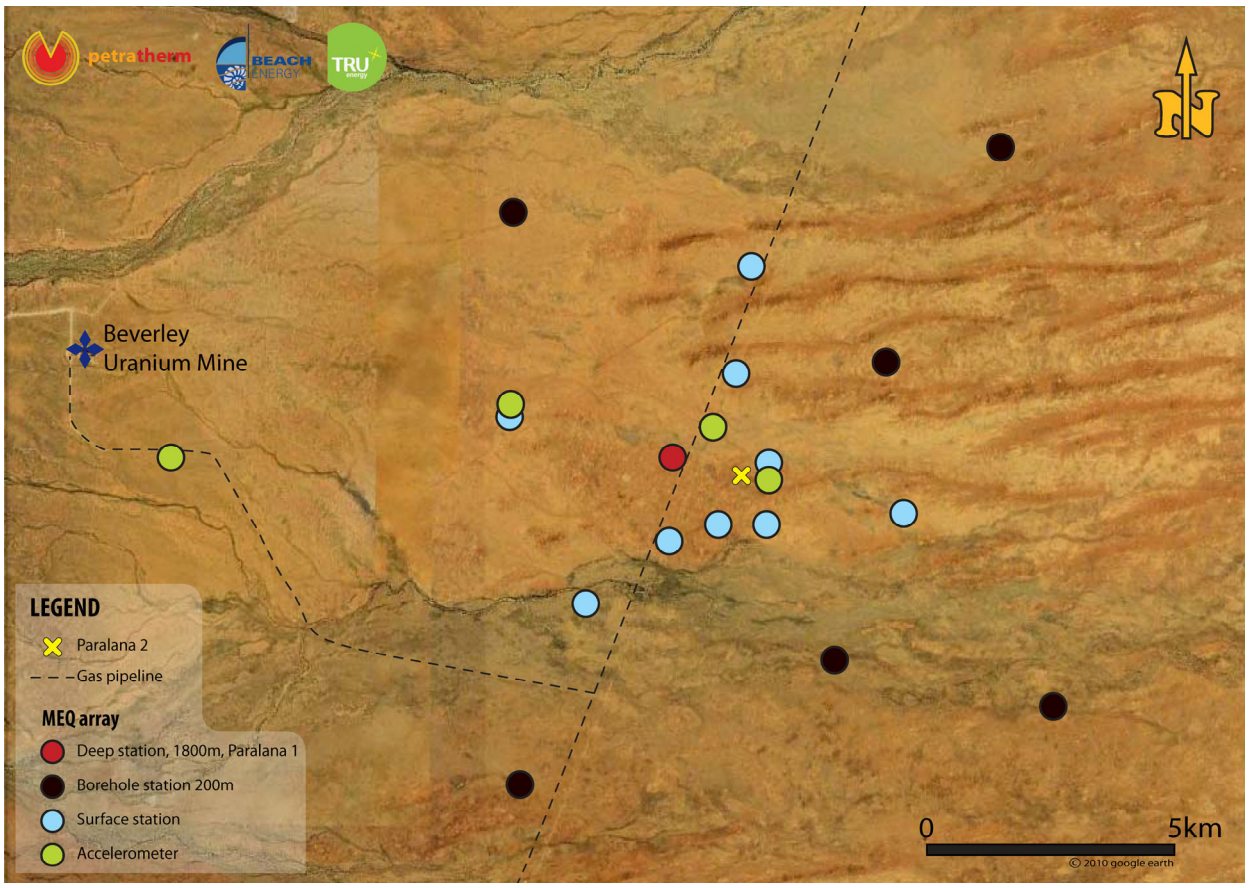

Figure 3. Google Earth Image of Paralana area, showing distribution of the Micro Seismic Array

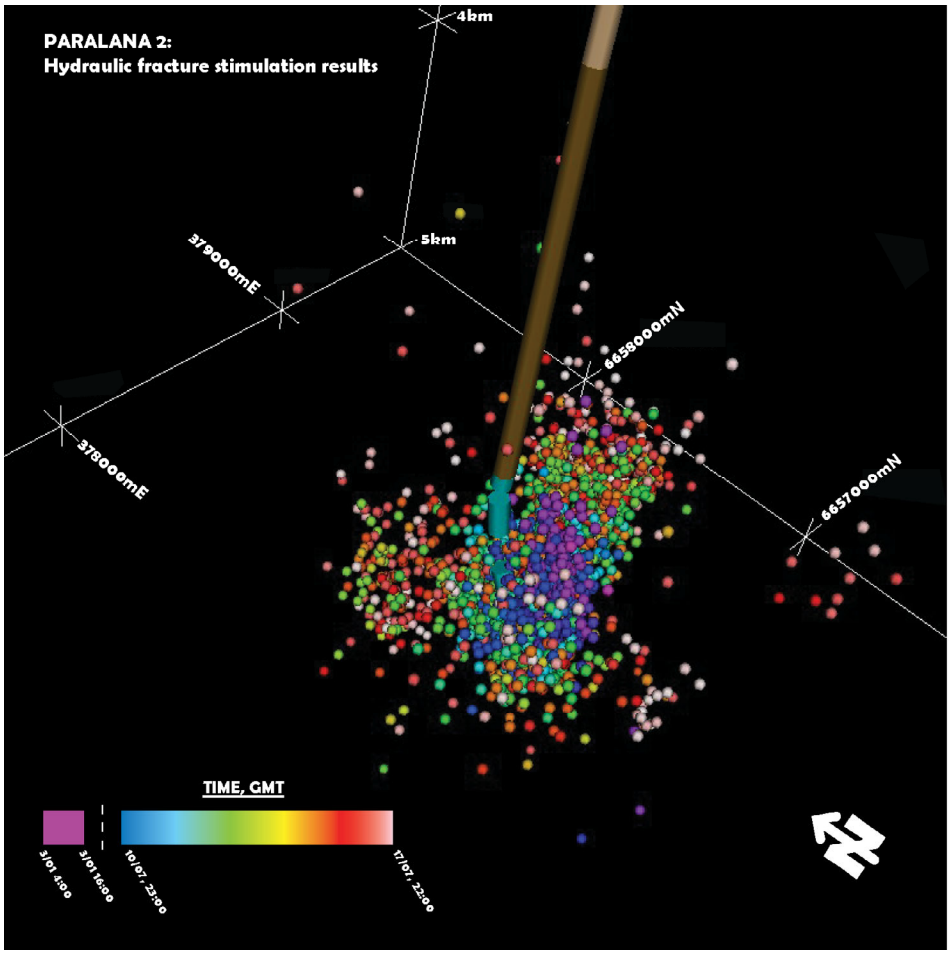

Figure 4. Oblique view of the fracture cloud looking down and towards the northeast.

Huge untapped geothermal reserves in New Zealand

A. G. Reyes
a.reyes@gns.cri.nz
GNS-Science
1 Fairway Drive, Avalon, Lower Hutt, New Zealand

New Zealand is one big geothermal system with pockets of subsurface high temperatures where heat can be mined economically from fluids and/or rock. However, there is difficulty in truly estimating the overall geothermal potential of a region especially where most of the heat reserves are "locked" in deep low-permeability rock formations that only nascent or yet-to-be developed technology can harness for economic use, e.g., as in Enhanced Geothermal Systems (EGS). The main objectives of this study are to propose a grading system for heat reserves for geothermal purposes, document the conventional and unconventional sources of geothermal energy in New Zealand, and roughly estimate the potential heat reserves in both conventional and unconventional sources.

At present, New Zealand has 600 MWe capacity of geothermal power installed in Ngawha and five geothermal systems in the Taupo Volcanic Zone, with a further 1000 MWe within the Taupo Volcanic Zone, alone, that remain untapped (http://www.eeca.govt.nz, 2011).

Keywords: conventional, unconventional, New Zealand, heat grade

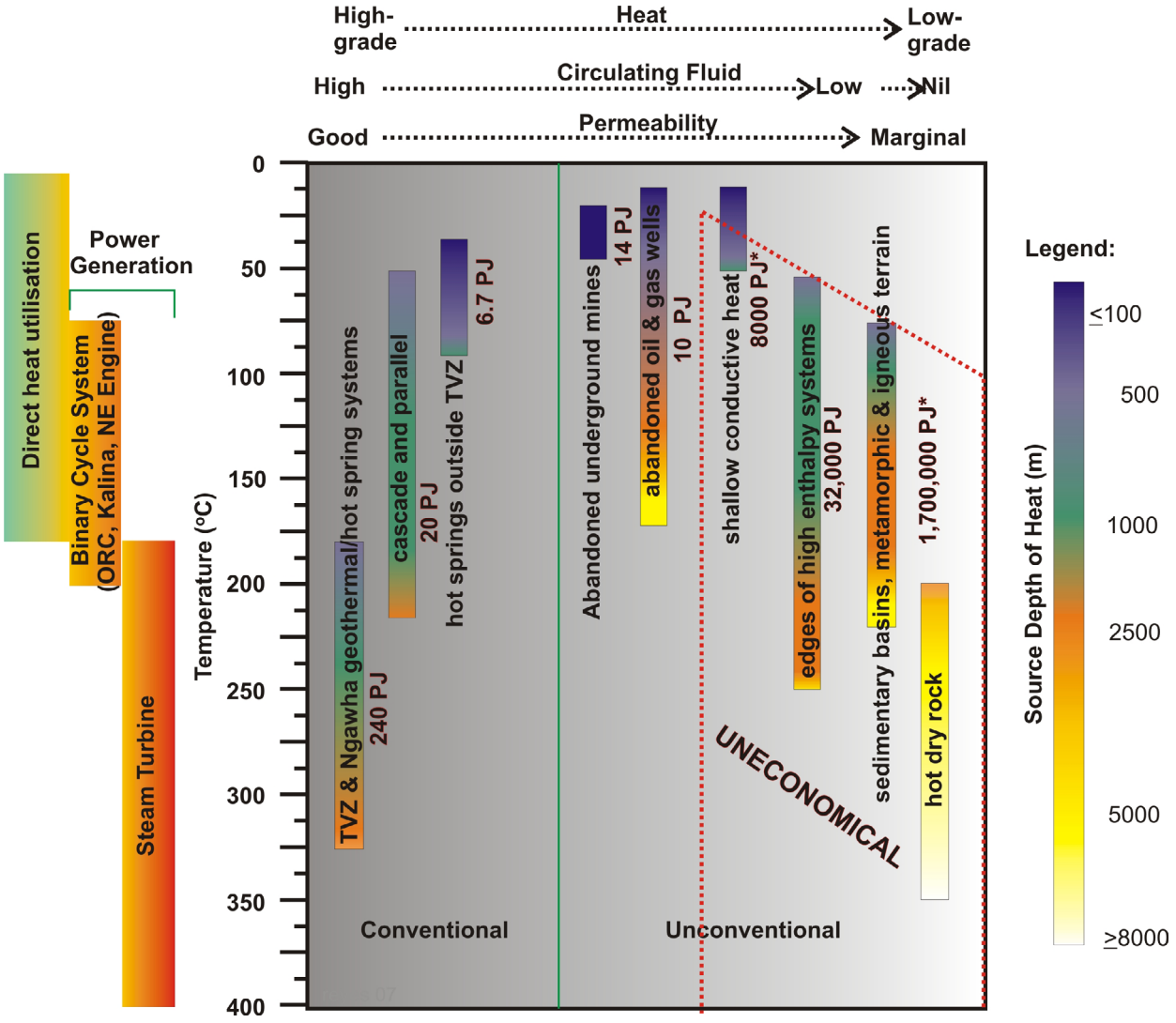

Figure 1: A geothermal grading system for conventional and unconventional sources of geothermal energy in New Zealand for direct use and power generation and their general temperatures, source depths, permeability, heat grade and volume of circulating fluids. Also shown is the estimated potential energy from each source. Technological difficulties render some sources uneconomical at present. ORC= Organic Rankine Cycle; NE= Natural Energy engine (from Reyes, 2007a,b).

Heat grading system

A geothermal resource is a volume of rock where heat can be economically harnessed for conversion to power or for direct utilization. Heat is mined from fluids circulating in the rock, or in the case of geothermal ground source heat pumps, directly from the ground or circulating groundwater. Because of technological advances in harnessing heat, e.g., heat pumps (Lund and Freeston, 2001, Yasukawa and Takasugi, 2003) and even improvements in drilling and well maintenance techniques (e.g., Lund, 2007) in the last 20 years, exploitable geothermal temperatures have been extended to as low as <10 ^{o}C to as high as about 350 ^{o}C. In these systems, natural permeability and the presence of circulating fluids can range from high to nearly nil (Figure 1). Conventional geothermal systems contain large quantities of hot water or steam that can be tapped economically from permeable zones at <3500 m for direct use of power generation. These systems usually discharge from hot springs and fumaroles on the surface. Conventional sources of geothermal energy for power generation and direct heat utilisation in New Zealand occur in (1) high-temperature geothermal systems of the Taupo Volcanic Zone and in Ngawha, Northland (including waste water from power generation) and (2) about 140 low-temperature thermal spring systems (with one or more springs) outside these two regions. In conventional geothermal systems, heat resources are high grade because heat is effectively transferred to exploitable depths by large volumes of fluids circulating in permeable zones. High-grade heat can be harnessed economically from circulating fluids using conventional extraction and energy conversion techniques as shown in Figure 1.

Unconventional geothermal sources include any source of heat outside hot spring systems where permeability and fluid flow may be marginal and heat low-grade. These resources include conductive systems at the edges of high temperature geothermal systems (e.g., Taupo Volcanic Zone and Ngawha) or within sedimentary basins, metamorphic and igneous terranes including hot rock at >3500 m. In some of these geological settings, heat may be more readily available because of conductively-heated waters circulating in abandoned oil and gas wells or accumulating in abandoned underground mineral and coal mines.

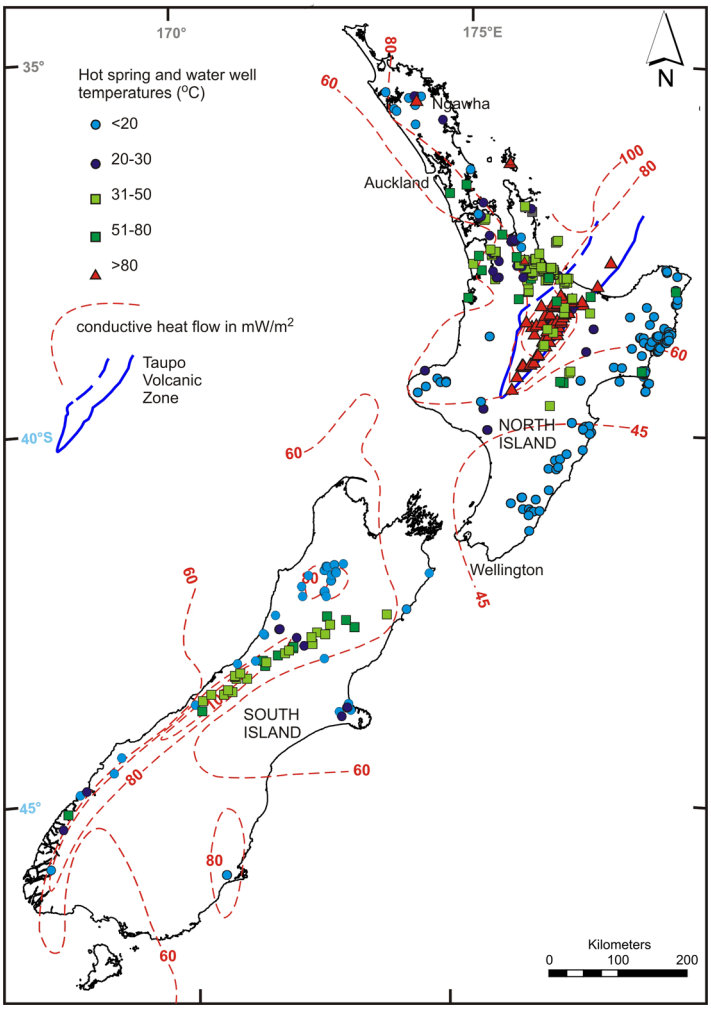

Figure 2: Discharge temperatures of mineral springs in New Zealand. Heat flow contours are from Allis et al, 1998. Because of the low annual ambient air temperature in some South Island sites, springs with discharge temperatures <20 ^{o}C are sometimes considered thermal; but not in the North island where ambient temperatures are higher (adapted from Reyes, 2007a.).

The term “low-grade heat” in unconventional geothermal systems refers to the economic extractability of heat and not to temperature. As shown in Figure 1, unconventional sources of geothermal energy can have temperatures up to >350 ^{o}C. The low-grade heat of some unconventional geothermal systems stems from insufficient permeability to induce flow, low fluid volume circulating in the rock formation and/or location at depths >3500 m, requiring unconventional or experimental techniques such as EGS (Engineered or Enhanced Geothermal Systems (Lund, 2007) to harness. Thus, in most cases, unconventional geothermal sources are not economically viable at present, except probably for cases where heat can be extracted by heat pumps at relatively shallow depths; or made more accessible for extraction by pre-existing structures, for example, such as abandoned oil and gas wells and underground mineral and coal mines.

Hot spring systems- a conventional source of geothermal energy

To evaluate the potential for low-temperature geothermal utilization in New Zealand, a survey of low-temperature thermal spring systems outside the high-temperature Taupo Volcanic Zone and Ngawha was carried out by GNS-Science (Reyes, 2007a, Reyes et al, 2010).

In this paper a mineral spring is considered thermal when its discharge temperature is 4 ^{o}C above the annual ambient air temperature (Reyes

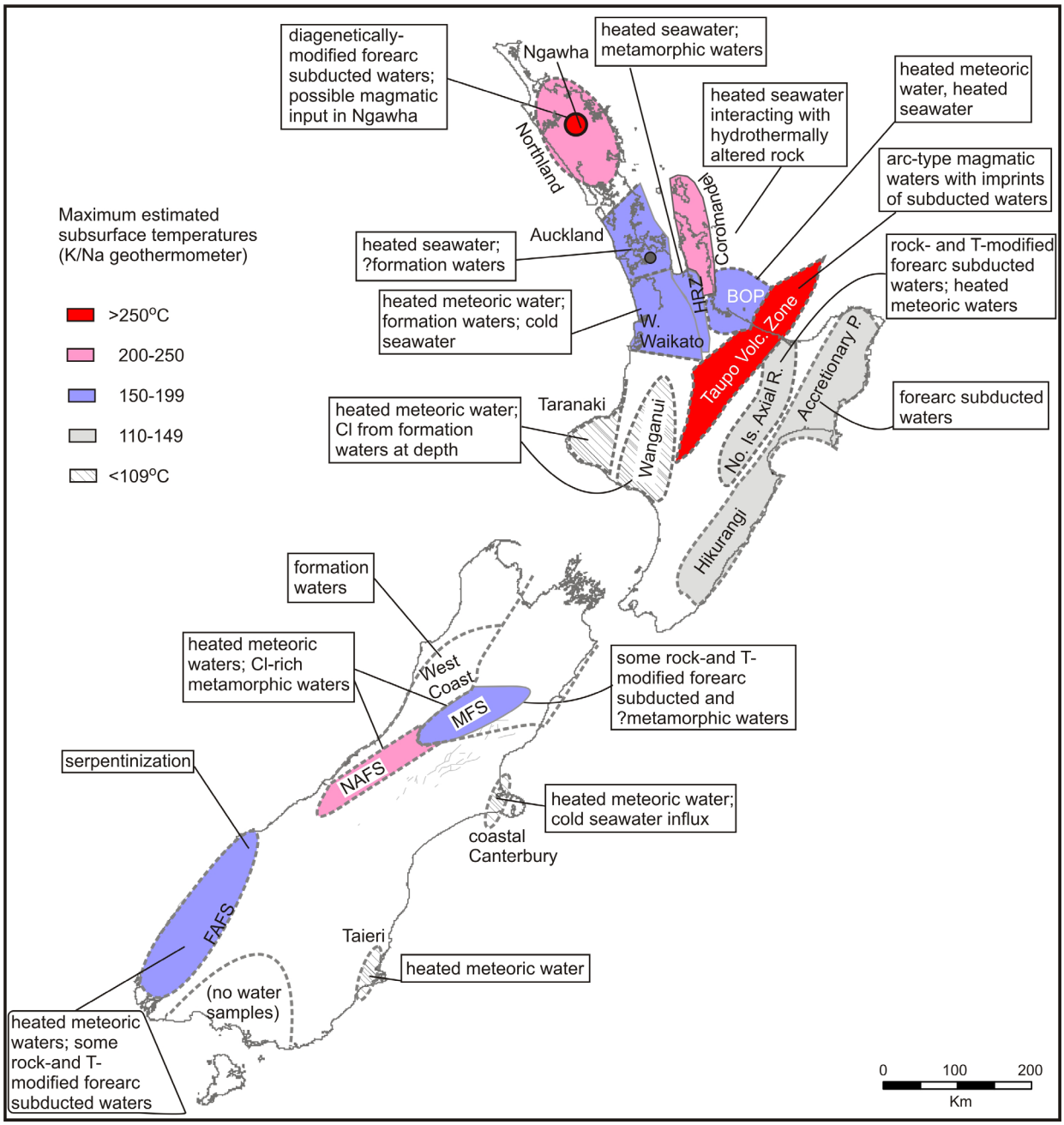

Figure 3: Variations in fluid compositions of discharge waters from mineral springs located in 18 tectono-geographic regions in New Zealand and estimated subsurface temperatures based on the K/Na geothermometer. NAFS- North Alpine Fault System, MFS= Marlborough Fault System, FAFS = Fiordland Alpine Fault System, P.= Prism (adapted from Reyes et al, 2010).

et al, 2011). Discharge temperatures from thermal springs range from 17 ^{o}C in the Cascade Terraces in Fiordland in South Island, where annual ambient air temperature is about 12 ^{o}C, to local boiling (98 ^{o}C to 100 ^{o}C) in the Taupo Volcanic Zone. The highest spring discharge temperature in low-temperature geothermal systems, outside the Taupo Volcanic Zone and Ngawha, is 87 ^{o}C with a median value of 50 ^{o}C (Figure 2). Apart from hot springs, another 12 major areas of warm water upflow were discovered during drilling of wells for domestic or industrial use and during exploration for coal, oil and gas (in blind thermal regions).

Thermal mineral spring occurrences in New Zealand are clustered in 18 different tectono-geographic regions characterised by specific fluid chemical and isotopic compositions attendant to the different tectonic settings as summarised in Figure 3.

Subsurface temperatures estimated from the K/Na ratio of spring waters range from <109 ^{o}C inTaranaki, Wanganui, Taieri and coastal Canterbury to >250 ^{o}C in the Taupo Volcanic Zone and Ngawha. Measured well temperatures are as high as >320 ^{o}C in the Taupo Volcanic Zone and Ngawha (Thain et al, 2006).

In the low-temperature thermal spring systems, outside the Taupo Volcanic Zone and Ngawha, the highest subsurface temperatures occur in Northland and the Coromandel Peninsula in the North Island; and in the Northern Alpine Fault System (NAFS) in the South Island where K/Na ratios indicate 200–250 ^{o}C at depth (Figure 3).

Because of differences in heat sources (ranging from magmatic to conductive heating of deeply circulating waters) and variations in the permeability of tectonic structures, the estimated annual flow of thermal waters and subsurface temperatures vary widely in the low-temperature hot spring systems.

The available energy from the TVZ surface springs is at least 7500 MWt (Bibby et al, 1995) or about 237,000 TJ, more than 200 x the energy from low-temperature hot spring systems in the North and South Islands where the minimum estimated energy is only about 33 MWt (1042 TJ) in the North Island and 1.5 MWt (47 TJ) in the South Island.

Unconventional sources of geothermal energy

In estimating the heat in place for unconventional sources of geothermal energy, a porosity of 0.01 is used for hot rock and 1.0 for flooded underground mines where heated flood waters fill mine caverns.

Hot rock

Apparently, estimates of the geothermal potential of hot rock of a region are fraught with assumptions, and in the end, could merely be a futile unrealistic academic exercise. In attempts to estimate the geothermal potential of hot rock from near surface to about 4000 m several assumptions were made: (1) recovery is 1%, (2) 70 % of the country is available for heat extraction (about 185,000 km^2) at shallow depths (<250 m) and at deep levels (3) the composition of the rock remains the same from surface to about 4000 m and thus the heat capacity and density of the rock are constant, (4) the country is divided into two major regions: low heat flow (<70 mW/m^2; thermal gradient is <33 ^{o}C/km; Figure 2) and high heat flow (>70 mW/m^2; thermal gradient is >33 ^{o}C/km), and (5) the base temperature all over the area of interest is 15 ^{o}C. Thus, at shallow depths (<250 m), the estimated heat energy is about 8,000 PJ and at deep levels, >1,000 EJ (Figure 1). Thus, the heat calculations merely prove the enormous geothermal potential of the ground beneath our feet.

Heated water in abandoned hydrocarbon wells

Abandoned hydrocarbon wells and underground mineral and coal mines provide access to conductively heated waters at depth.

There are 349 onshore abandoned hydrocarbon wells in New Zealand that might potentially be harnessed for geothermal energy for direct use of heat, power production and development as pseudo hot springs for tourism (Reyes 2007b). Well depths range from 17 m to 5065 m vertical. Estimated bottom hole temperatures range from ambient (12 ^{o}C to 18 ^{o}C) to 172 ^{o}C. The K/Na ratios of waters in some oil and gas wells indicate subsurface temperatures of 180 $\pm$ 20 ^{o}C.

Of these wells 40% are located in Taranaki (Figure 3), the only producer of oil, gas and condensate in New Zealand at present. The rest of the wells are distributed in the North and South Island sedimentary basins. Although the requisite temperature may be present in abandoned hydrocarbon wells for a wide range of geothermal energy uses, there are many geoscientific, technical and non-technical problems to be considered before these wells could be used for geothermal power generation or cogeneration (Reyes, 2007b). Waters from an abandoned hydrocarbon well in Taranaki are presently being used for a bathing complex and to produce mineral waters.

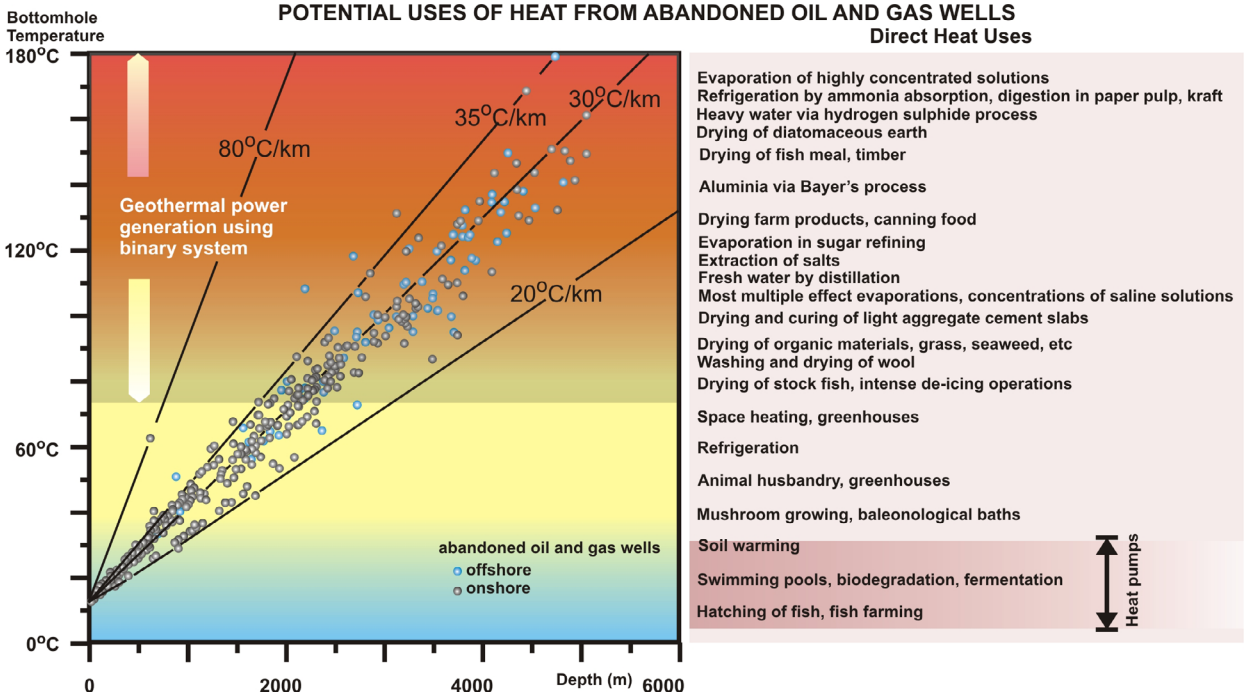

Figure 4: Cross plot of depth (m) and estimated bottom hole temperatures (°C) of abandoned offshore and onshore hydrocarbon wells in New Zealand and possible uses of thermal fluids (adapted from Lindal, 1973; Reyes, 2007b).

The use of abandoned hydrocarbon wells, with bottom hole temperatures ranging from about 30°C to 170°C, for direct heat utilisation and power generation could add, at least, another 6,000 TJ to the geothermal energy potential of New Zealand. The energy would be harnessed from shallow depths using ground source heat pumps for space heating and heating of domestic water (Figure 4). Twenty wells have been identified in Taranaki and the Hikurangi Accretionary Prism (Figure 3) which, if converted, could potentially be used for geothermal power generation using a binary system.

Heated water in abandoned underground mines

There are about 20 abandoned underground coal mines and at least 10 underground mineral (gold and/or base metals) mines that have been evaluated (Reyes, 2007a).

Estimated and measured temperatures of waters accumulated in sealed parts of coal mines range from 18°C to 26°C at depths of 80m to 300m. Projected temperatures are higher in mineral mines at 19°C to 35°C because of deeper levels (as deep as 700 to 850m) and also because some are located in high heat flow areas in the Coromandel Peninsula and the South Island (Figure 2) where the thermal gradient is 35 to 40°C/km. Very rough estimates of the volume of heated water in the abandoned mines yield an estimate of about 4000 TJ of potential geothermal energy from old abandoned underground mines. Again, like geothermal production from abandoned hydrocarbon wells, there are technical and non-technical factors to be considered in using mines as sources of geothermal energy, including safety, distance from populated areas environmental considerations, long-term sustainability and economic viability. However one coal company in the Waikato region of the North Island has shown interest in using heated waters (as high as 26°C) discharging from orifices from abandoned sealed mines as a source of alternative energy.

Summary and conclusions

Conventional sources of geothermal energy with high grade heat reserves have an energy potential of at least 265 PJ, mostly occurring in the Taupo Volcanic Zone. However, only about 5-10% of this energy is being used at present. There is also a wide range of unconventional sources of geothermal energy with enormous heat potential (Figure 1) but <0.1 PJ of these are being harnessed at present. Thus, more than 90% of New Zealand's geothermal reserves remain unexploited at present.

References

Allis, R.G., Funnell, R.H., and Zhan, X., 1998, From basins to mountains and back again, NZ basin evolution since 10 Ma: Proceedings 9th International Symposium on Water–Rock Interaction, A.A. Balkema, Rotterdam, New Zealand, pp. 3–9.

Bibby, H.M., Caldwell, T.G., Davey, F.J., and Webb, T.H., 1995, Geophysical evidence on the structure of the Taupo Volcanic Zone and its hydrothermal circulation: Journal of Volcanology and Geothermal Research, v. 68, p. 29–58.

Lindal, B., 1973, Industrial and other applications of geothermal energy. In: Geothermal Energy: Review of Research and Development, Paris, UNESCO, LC No. 72-97138, pp.135-148.

Lund, J.W., 2007, Characteristics, development and utilization of geothermal resources: Geo-Heat Centre Quarterly Bulletin, Oregon Institute of Technology, v. 28(2), pp. 1–9.

Lund, J.W. and Freeston, D., 2001, World-wide direct uses of geothermal energy 2000, Geothermics, v. 30, pp. 29-68.

Reyes, A.G., 2007a, A preliminary evaluation of sources of geothermal energy for direct use: GNS-Science Report 2007/16, 42 p.

Reyes, A.G., 2007b, Abandoned oil and gas wells- a reconnaissance study of an unconventional geothermal resource: GNS-Science report 2007/23, 41 p.

Reyes, A.G., Christenson, B.W. and Faure, K., 2010, Sources of solutes and heat in low-enthalpy mineral waters and their relation to tectonic setting, New Zealand: Journal of Volcanology and Geothermal Research, v. 192, p. 117-141.

Thain, I., Reyes, A.G. and Hunt, T., 2006, A practical guide to exploiting low temperature geothermal resources: GNS-Science Report 2006/09.

Yasukawa, K. and Takasugi, S., 2003, Present status of underground thermal utilization in Japan: Geothermics, v. 2, pp. 609-618.

GeoTemp: A framework for temperature interpretation and modelling

L.P. Ricard*[1,2], J-B. Chanu[2], L. Esteban[2]
Ludovic.Ricard@csiro.au
[1] Western Australian Geothermal Centre of Excellence, CSIRO, Kensington, WA 6151
[2] CSIRO Earth Science and Resources Engineering, Kensington WA 6151

One of the fundamental parameters controlling the viability of any geothermal project is the temperature of the reservoir. At the early exploration stage, it is unlikely to have access to accurate temperature data. To estimate it, engineers rely mainly on temperature data such as wireline temperature logs, Drill Stem Tests, Repeated Formation Tests and Bottom Hole Temperatures which usually arise from geographically sparse measurements, often from shallow depths or have low reliability. The reservoir temperature distribution is intrinsically related to the thermal properties of the rock and formation chemistry and dynamics. Different thermal regimes such as conduction, advection and conduction with heat production could take place, depending on the local geology, structures and hydrogeology.

This work defines an integrated data analysis workflow for temperature interpretation, modelling and estimation based on the interpretation of geophysical wireline logs, sparse temperature data, core sample measurements, geology and hydrogeology. This workflow is packaged into the software GeoTemp.

Keywords: Temperature, thermal regime, logging, modelling, predictions, thermal conductivity, heat flow

1 Introduction

Exploration for geothermal energy resource aims to locate and evaluate potential geothermal reservoirs in economically viable locations. To proceed to a thermal characterization for temperature prediction at depth, we rely on existing thermal related data. The existing temperature data sources include Bottom Hole Temperature, Drill Stem Test and Repeated Formation Test temperature and wireline temperature logs. The first sources are generally geographically and vertically sparse (often only a few data points for the whole depth of a well) and of low reliability (usually gather through petroleum exploration rather than geothermal characterization). Wireline temperature logs are extremely rare for deep wells (e.g. petroleum wells) but fortunately are more common for shallow wells (water monitoring and mining bores). An extensive temperature logging campaign is currently being undertaken in Australia by Geoscience Australia (Kirkby *et al.*, 2011) and state agencies such as the Victorian Department of Primary Industry, the Queensland and the Western Austrlian Geothermal Centre of Excellence (Reid et al., 2011). PressureDB/ PressurePlot (PressurePlot, 2007) and OzTemp (Holgate and Gerner, 2010) provide database of temperature data from petroleum wells. By early March 2011, for Western Australia, only 36 sample measurements of thermal conductivity were publicly available for the Perth Basin (HDRPL 2008) and 50 measurements for the Canning Basin (HDRPL 2009). These measurements were done on cores in laboratory without in-situ conditions from petroleum wells spread all over the basins.

Heat is transported inside rocks by a combination of processes such as conduction, advection and radiation, defining the thermal regime. At a first approximation, for mildly heterogeneous formations, the thermal regime can be assumed to be constant. Therefore thermal characterization of a stratigraphic sequence could be achieved by assessing thermal regimes for each formation (Fig. 1).

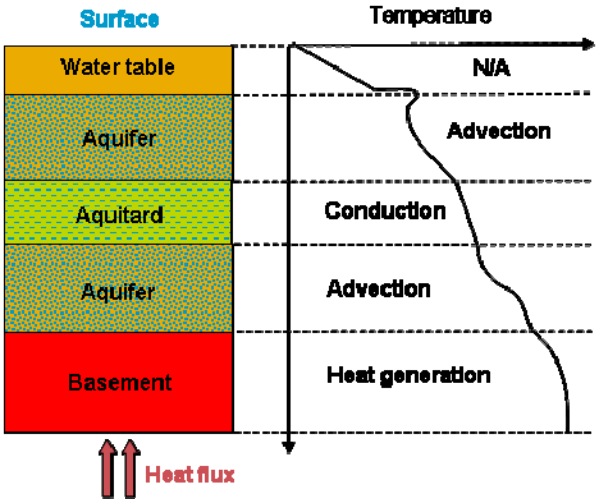

Figure 1: Schematic of hydrogeological stratigraphy with thermal regime and temperature by formation

To proceed towards temperature prediction at depth, quality control of the available data is required prior to any interpretation or modelling.

To help to reach temperature prediction with associated uncertainties, we present a workflow from the processing towards quality control, interpretation, modelling and quantitative extrapolation and finally spatially interpolations of wireline temperature logging measurement for geothermal reservoir engineering purposes. This software, GeoTemp, proposes several independent tools to manipulate the data and

proceed to some simple geographical understanding. GeoTemp accepts standard input files and exports pictures in common formats for visualization and reporting.

2 General framework

GeoTemp aims to set a protocol for inferring underground temperature and estimating rock thermal parameters based on the analysis, interpretation and modelling of wireline temperature logs and core sample data.

The GeoTemp was built with three distinct components: (i) Wireline workflow, (ii) Wireline workflow support and (iii) PressurePlot analysis.

Wireline workflow is formed of 6 modules corresponding to the different steps of the process: Processing, Data evaluation, Heat Production, Conduction, Conduction Modelling and Risk.

Each module is independent from the others, however, they are linked in an integrated framework that facilitates the workflow from processing to interpretation and then to modelling with prediction (Fig. 2).

Wireline workflow support proposes four modules for data handling: Viewer, Formation Management, Guided Analysis and Regional Assessment.

PressurePlot analysis represents its own module for simple petroleum data analysis.

All the components accept widely used file formats and well defined input/output files (Ricard and Chanu, 2011). Each module incorporates automatic procedures for loading and interpreting the data with visualization of intermediate and final results which may be exported for reporting purposes.

3 GeoTemp Wireline Workflow

3.1 Processing

GeoTemp Processing handles three functionalities: calibration of the temperature data, depth conversion from Measured Depth (MD) to True Vertical Depth (TVD) and quality control of the Gamma-ray and local temperature gradient.

Every temperature probe has a natural drift over time, so regular temperature calibrations need to be performed and temperature data must be corrected. The GeoTemp Processing module gives the user the ability to calibrate the temperature data using a set of calibration data.

The non-perfect verticality of wells imposes to correct the depth from Measured Depth (MD) to True Vertical Depth (TVD) by loading temperature log (.LAS file) and survey data (.XLS file) in the TVD Calculations frame (Fig. 3). Using survey data, GeoTemp Processing allows the user to

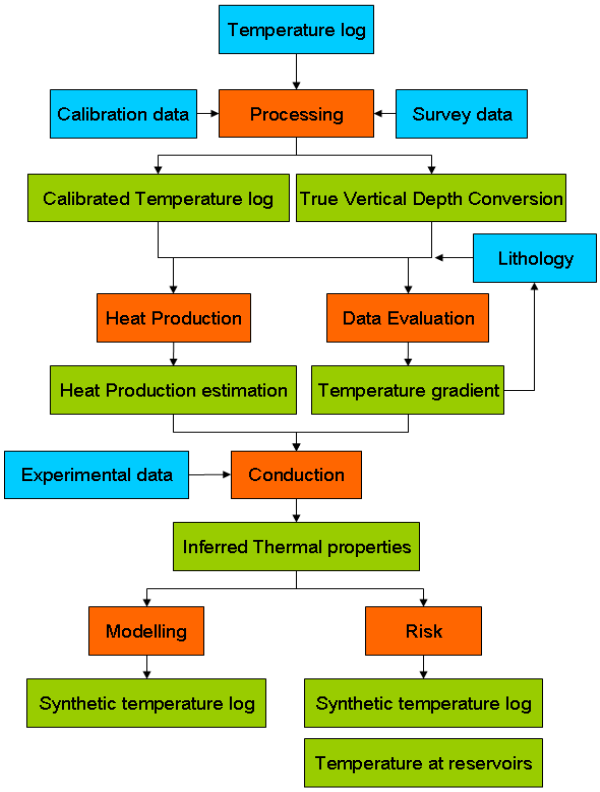

Figure 2: GeoTemp wireline workflow for thermal reservoir characterisation. Blue boxes represent input data, orange boxes represents the modules, green boxes represents output data.

convert the depth from MD to TVD by simple orthogonal projections.

The link between Measured Depth and True Vertical Depth is expressed as follow (equation 1):

$$TVD = \sum_{i=1}^{N} MD_i \sin\left(\theta_i\right) \qquad (1)$$

where *TVD* is the True Vertical Depth in meters, and for each deviated segment *i*, MD_i is the Measured Depth in meters and θ_i is the angle in degrees.

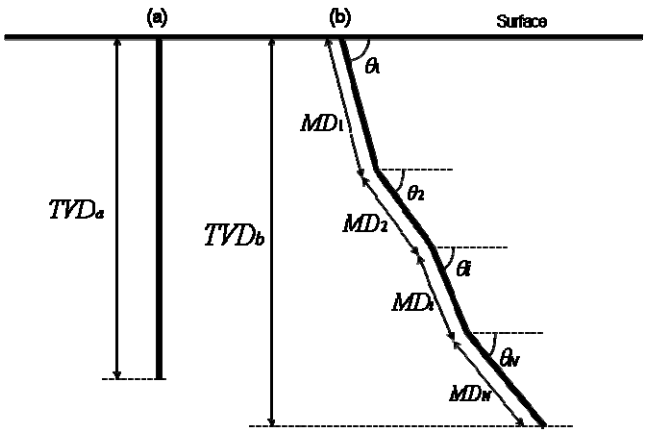

Figure 3. MD/ TVD correction: (a) vertical well MD = TVDa and (b) deviated well, MDi corrected to TVDb.

A third functionality of GeoTemp Processing is the quality control of gamma ray and local temperature gradient data (Fig. 4) and the ability to graphically display. It also provides real and filtered temperature gradient values as geometric, arithmetic and harmonic means, median, standard deviation, minimum, maximum and number of values in two separate frames. These features allow the user to inspect the temperature and gamma-ray data in detail.

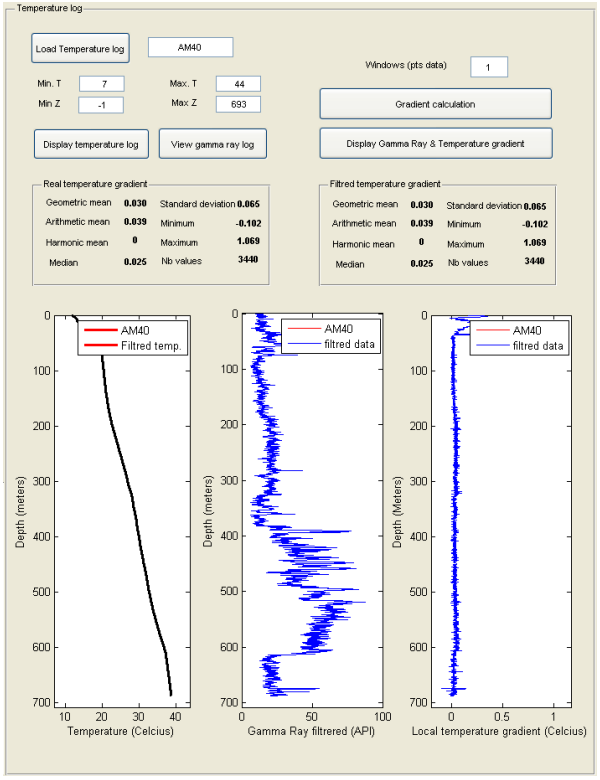

Figure 4: Temperature log frame screenshot

3.2 Evaluation

The second module of the workflow provides the tools to perform quality control of thermal profiles with respect to a vertical conduction model, check the consistency of the temperature, lithology and gamma ray data. It also evaluates thermal regimes by formation units and finally calculates their corresponding temperature gradients (Fig. 6).

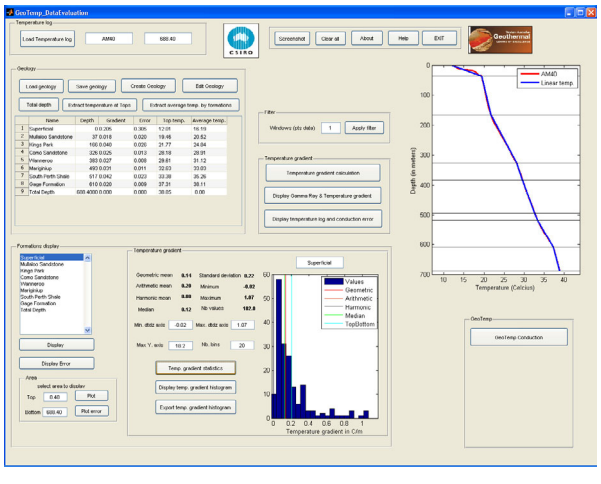

Figure 5: Data evaluation module screenshot

Gamma Ray (GR) can be analysed and displayed within each formation units to link the unit limits with GR markers.

If inconsistency is detected, unit limit can be adjusted. Linear temperature gradients can then be calculated by formation. In the case of vertical heat conduction with no heat production, the temperature profile obeys to (equation 2):

$$T(z) = T_0 + q_0 \sum_{i=1}^{N} \left(\Delta z_i / \lambda_i \right) \qquad (2)$$

where T is temperature (Celsius degree), T_0 is surface temperature or another reference temperature, q_0 is the constant heat flow density, z is depth below ground level (metres) and λ_i is thermal conductivity (W/m/K) in the depth interval Δz_i (Kutasov, 1999).

For each formation, a normalized quadratic error between the linear temperature gradient and the real temperature data is calculated to quantify the suitability of the conductive thermal regime assumption. If the quadratic error is satisfactory by the user, the vertical conduction assumption is accepted and used for the further modules.

3.3 Heat Production

The rate of radiogenic heat generation within rocks is related to the quantity of radioactive material present, the rate of decay and the energy of the emitted particles. Gamma-ray spectrometers provide the most direct method for measuring the abundance of uranium, potassium and thorium in rock (Beardsmore and Cull, 2001) The estimation of heat production rate by formations is done from the Gamma-ray wireline log using the empirical equation (equation 3):

$$A = 0.0158(GR - 0.8) \qquad (3)$$

where *A* is the heat generation count in μW m^{-3} and *GR* is the gamma ray count in API units.

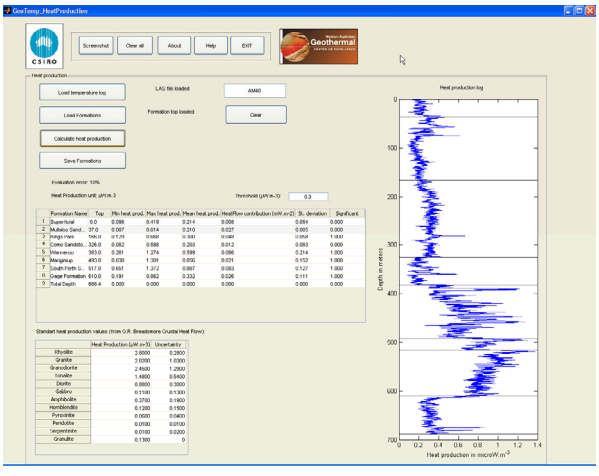

Figure 6: Heat production module screenshot

3.4 Conduction

Assuming a vertical conduction regime, a conductive interpretation of temperature logs can be performed using GeoTemp Conduction. In this module, the temperature gradient combined with experimental thermal conductivity measurements can be used to calculate the vertical heat flow and double-check the consistency of thermal conductivity, vertical heat flow and temperature gradient.

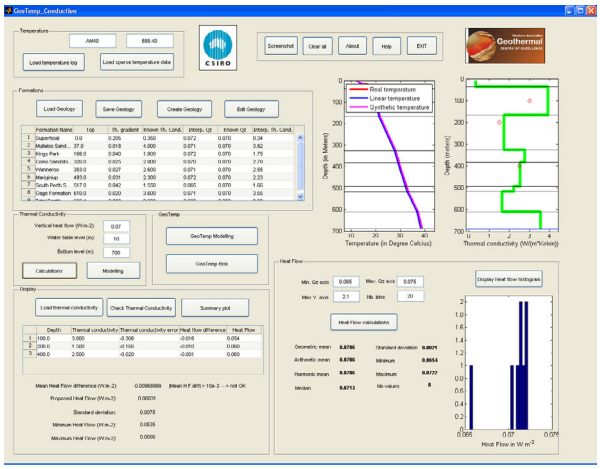

Figure 7: Conduction module screenshot

3.5 Conduction Modelling

The fifth component focuses on conductive modelling and temperature prediction at target reservoir depth.

Interpreted parameters such as thermal conductivities by formation, vertical heat flow and temperature at a given depth are used to calculate a synthetic temperature log. Normalized quadratic error between the real and the synthetic temperature logs is calculated for quality evaluation of the interpretation/ modelling process. Temperature predictions can be made for depths below the supporting measurement data if vertical heat conduction is assumed.

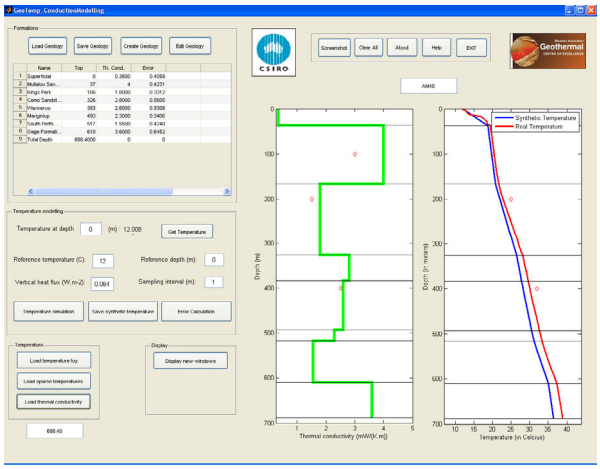

Figure 8: Conduction Modelling module screenshot

3.6 Risk

Uncertainties linked to the measurements, to the interpretation and to the modelling have to be taken into account in the prediction process. GeoTemp Risk allows the user to specify for a conductive system along with uncertainties on the heat flow and the thermal conductivities. Given those uncertainties, an envelope temperature log could be defined as uncertainty range on the temperature prediction. By specifying reservoir depth interval, average temperatures could be calculated.

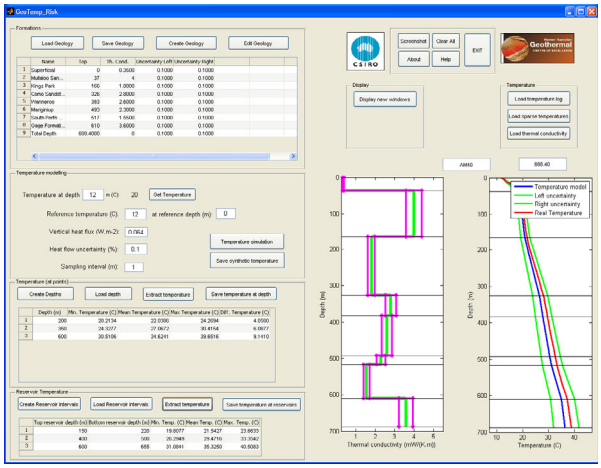

Figure 9: Risk module screenshot

4 GeoTemp Wireline Workflow Support

4.1 Formation Management

Geology management module enables the user to create or edit a lithology. Accesses to this module are from GeoTemp Framework but also from Geotemp Data Evaluation, Geotemp Conduction, Geotemp Modelling and Geotemp Risk. These modules are significantly different and the associated geology data inputs of these modules are varying. For each module, different parameters are needed if the user wants to create a new formation.

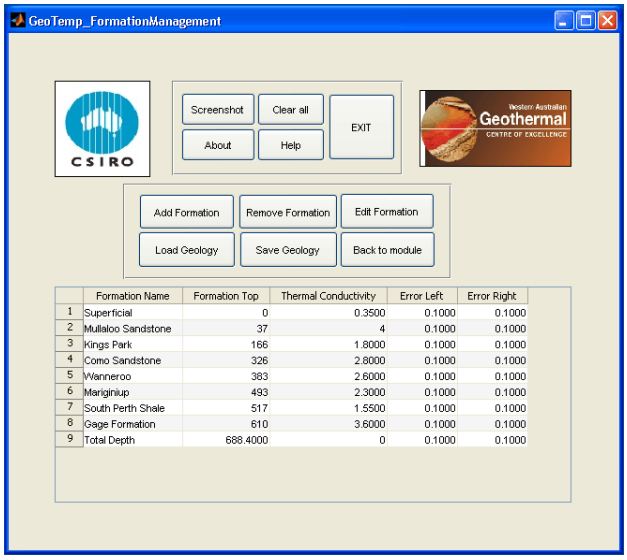

	Formation Name	Formation Top	Thermal Conductivity	Error Left	Error Right
1	Superficial	0	0.3500	0.1000	0.1000
2	Mullaloo Sandstone	37	4	0.1000	0.1000
3	Kings Park	166	1.8000	0.1000	0.1000
4	Como Sandstone	326	2.8000	0.1000	0.1000
5	Wanneroo	383	2.6000	0.1000	0.1000
6	Mariginiup	493	2.3000	0.1000	0.1000
7	South Perth Shale	517	1.5500	0.1000	0.1000
8	Gage Formation	610	3.6000	0.1000	0.1000
9	Total Depth	688.4000	0	0.1000	0.1000

Figure 10: Formation Management module screenshot

4.2 Viewer

GeoTemp Viewer allows the user to load and display several temperature logs at once (Figure 5). By plotting several temperature logs at once, the user can easily compare the temperature logs.

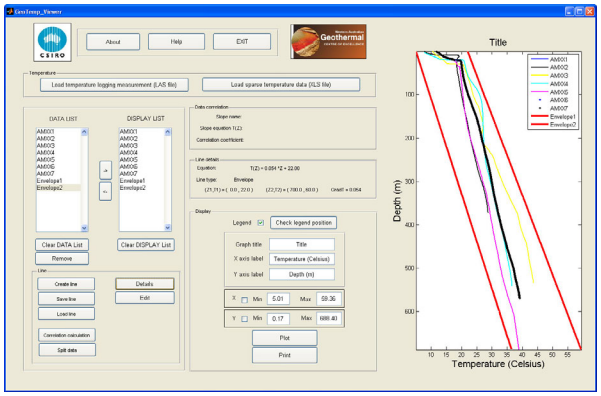

Figure 11: Viewer module screenshot

4.3 Regional assessment

In this module, a 2D spatial distribution analysis of the temperature field is calculated using the 1D temperature logs. Extraction of temperature at depths is also possible and exportable to Microsoft Excel spreadsheet.

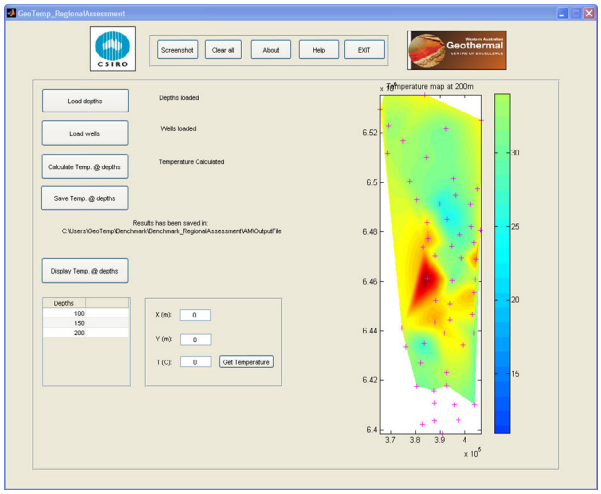

Figure 12: Regional Assessment module screenshot

4.4 Guided Analysis

Guided analysis makes calculation of conductivity, heat flow, heat production, temperature calibration, temperature gradient and true vertical depth for several wells in a same time. It need a list of file names as an input and then do calculations and may display results on graphs and table.

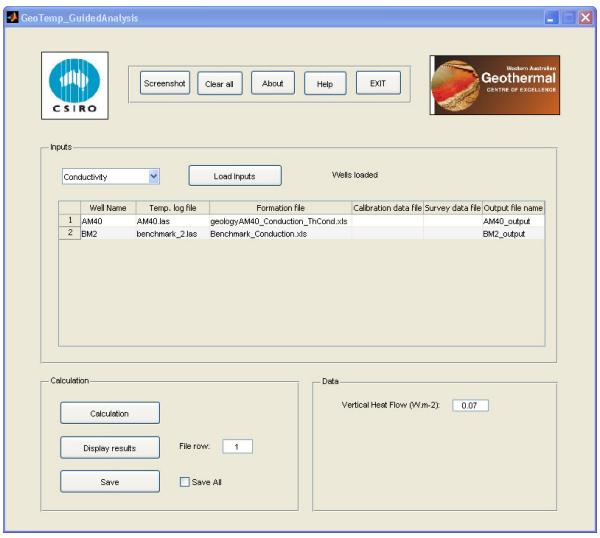

Figure 13: Guided Analysis module screenshot

5 GeoTemp PressurePlot

GeoTemp Pressure Plot allows the user to load and display temperature data and gives information about the data type and data reliability. This module, as the GeoTemp Viewer module, enables the user to create lines, especially envelope lines and linear regression lines of sparse temperature data.

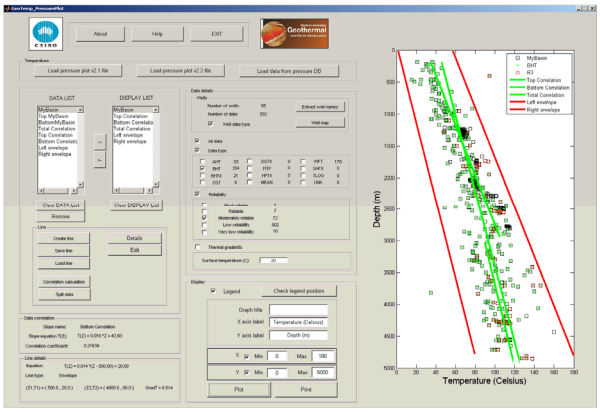

Figure 14: PressurePlot module screenshot

Acknowledgments

The Western Australian Geothermal Centre of Excellence (WAGCOE) is funded by the Western Australian government. This work has benefited from the CSIRO ESRE Petroleum Geoscience program Capability Development Fund.

The authors are grateful to Gemma Bloomfield, Guillaume Pons, Sebastian Gutbrodt, Lynn Reid and Mike Trefry for their inputs, tests or suggestions.

The authors also express their gratitude to Alison Kirky, Rikki Weber and Tim Jones from Geoscience Australia for the evaluation of the software at early stage of development.

References

Beardsmore, G.R., and Cull J.P., 2001, *Crustal heat flow a guide to measurement and modelling*. Cambridge University Press. ISBN: 0 52179289 4 hardback.

HDRPL, 2008, Geothermal energy potential in selected areas of Western Australia (Perth Basin): A report prepared for the Department of Industry and Resources, Western Australia. Hot Dry Rocks Pty Ltd, Report DOIR0060108.

HDRPL, 2009, Geothermal energy potential in selected areas of Western Australia (Canning Basin): A report prepared for the Department of Mines and Petroleum, Western Australia. Hot Dry Rocks Pty Ltd, Report DOIR0681008.

Holgate, F.L., and Gerner, E.J., 2010, OzTemp Well Temperature Data. Geoscience Australia, available from: https://www.ga.gov.au/products/servlet/controller?event=GEOCAT_DETAILS&catno=70604.

Kirkby, A.L., Gerner, E.J., Budd, A.R., Weber, R.D., Meixner, A.J., and Champion, D.C., 2011, *Heat flow data collection for the Australian continent: Support for an emerging geothermal industry*, in: Middleton, M. and Gessner, K. (eds.) West Australian Geothermal Energy Symposium Abstracts v. 1: p. 13.

Kutasov, I. M., 1999, *Applied geothermics for petroleum engineers*, Elsevier Science. ISBN: 0 444 82887 7.

PressurePlot, 2007. http://www.pressureplot.com/

Reid, L. B., Bloomfield, G., Botman, C., Ricard, L., and Wilkes, P., 2011, Temperature regime in the Perth metropolitan area. Results of temperature and gamma logging and analysis, June/July 2010. Report No: EP111422.

Ricard L. P. and Chanu J-B., 2011. *GeoTemp 1.0: User Manual*, WAGCOE/ CESRE report in preparation.

Temperature estimates for geothermal application: Cockburn 1, Perth Basin, Australia

Ludovic P. Ricard*[1,2], Lionel Esteban[2], Lucas Pimienta[2], Claudio Delle Piane[2], Cody Evans[2], Jean-Baptiste Chanu[2] and Joel Sarout[2]
Ludovic.Ricard@csiro.au
[1] Western Australian Geothermal Centre of Excellence (WAGCoE), CSIRO, Kensington, WA 6151
[2] CSIRO Earth Science and Resources Engineering, Kensington WA 6151

Core analyses, wireline temperature logging and lithology data provide information on the rock thermal properties at different scale, different level of accuracy and on the effects of potential heterogeneities. Estimations of temperature of deep geothermal reservoir remain a challenge. Recently temperature predictions techniques were developed and applied to the Jurassic sandstones of the Perth basin; these involved direct measurements of rocks' thermal properties and the joint-interpretation of geophysics-petrophysics-rock physics data. Special care was dedicated to the evaluation of consistency between different measurements and predictions and their interpretations. The present study focuses on an exhaustive interpretation of core measurements with new modelling approaches, local geology and wireline temperature logs applied to the evaluation of the geothermal potential of the Cockburn-1-well site in the Perth Metropolitan Area, Western Australia.

Keywords: Temperature, thermal characterisation, interpretation, modelling, predictions, thermal conductivity, heat flow

1 Introduction

Heat transport properties of geological formations are fundamental parameters in the assessment and successful planning of geothermal energy exploration. The inherent complexity of natural rocks brings drastic difficulty to the interpretation of data from direct measurements. To overcome these limitations several tools can be deployed in ground field, wells and laboratory experiments to constrain the range of rocks' thermal properties variability and understand their mechanisms. Despite the difficulty to measure in-situ thermal conductivity and diffusivity; the lack of down hole temperature probing beyond 700 m of depth; rare/sparse drilling data and other thermal-dynamic information, a new data set was collected and a new modelling approach developed to provide answers to some geothermal exploration issues.

Parallel tools such as thermal and basic petroleum logging tools, laboratory thermal conductivity and diffusivity measurements are investigated; and used to characterise the vertical Cockburn-1-well site in the South-West part of the Perth basin from the surface to 3.5 km depth; in addition we combine the rare data available at this site with information from surficial sub-wells in order to characterise the thermal behaviour and potential for geothermal viability in the Jurassic sandstone aquifer of the Perth basin.

It is also shown through a joint modelling approach that Thermal Conductivity (TC) may be directly predicted from the easily acquired Elastic Waves Velocities (EWV). Thus allowing to further refine our predictions.

2 Local settings

The Perth basin (West coast of Perth city) is isolated by the Darling fault to the East and composed of Precambrian basement crystalline rocks overlyed by Permian to Holocene sediments, mainly composed of sandstone-shale succession. The targeted geothermal aquifer in the Perth Basin is known for the presence of hot water in permeable clean sandstone of fluvial-marine origin with permeability > 1 Darcy (Regenauer-Lieb et al., 2009; Israni and Delle Piane, 2011). The local thermal gradient is estimated to be of 25 to 30 °C/km (Reid et al., 2011). The targeted geothermal reservoir is composed of clean Jurassic sandstones and spans across 3 formation units among the 5 crossed by Cockburn-1-well: Cattamarra Coal Measures [1914 to 3054.4 m], Cadda [1725 to 1914 m] and Yarragadee [313.3 to 1725 m] and sometimes affected by levels of shaly-coal rich layers acting as thermal and hydraulic barriers (Song and Cawood, 2000).

Temperature data on site consist of a Bottom Hole Temperature (BHT) value of 81.1ºC at 3048 m at the Cockburn 1 well and wireline temperature logging measurements available at the Artesian Monitoring wells AM42, AM45A, AM52, AM52Y and AM52Z located close to the Cockburn 1 well from temperature logging campaigns done in 1980 and in 2011 (Table 1 and Reid et al., 2011 for further details).

Thermal Conductivities were measured on core samples from the Perth Basin under room conditions in the laboratory (HDRPL, 2008) and more recently the measurement pool was extended to a wider collection (Delle Piane et al., 2011).

Local hydrogeology consists of three main aquifers (Davidson, 1995): the unconfined Rockingham superficial aquifer, the confined Leederville aquifer and the confined Yarragadee aquifer (Table 2). Both confined aquifers are widely produced for domestic use.

Table 1: Wireline temperature logging measurements *(AHD: Australian Height Datum)*

Well name	Property DoW – digitised WAGCOE - logged	Total Depth (mAHD)	Approximate distance (km) to Cockburn 1
AM42	DoW	562.5	11 NE
AM45A	WAGCOE	180.2	7 E
AM52	DoW	444	9.4 SE
AM52Y	DoW/ WAGCOE	381/ 376	11.5 SW
AM52Z	DoW	359.4	7 W

Table 2: Stratigraphic sequence

Aquifer	Formation
Superficial aquifer	Rockingham
Confining bed	Kings Park
Confining bed	Kardinya
Leederville aquifer	Henley
Leederville aquifer	Pinjar
Leederville aquifer	Wanneroo
Leederville aquifer	Mariginiup
Confining bed	South Perth
Yarragadee aquifer	Gage
Confining bed	Cattamarra Coal Measures

3 Wireline temperature analysis

In this section, we first assess the local thermal regime and then, evaluate thermal conductivities measurements, interpretation and modelling before proposing a temperature prediction at depth.

3-1- Local thermal regime

According to Reid et al., 2011, radiogenic heat production is not a significant source of heat within the shallow Perth Metropolitan Area sediments, producing less than 1% of total estimated vertical heat flow. Wireline temperature logging measurements are available in five Artesian Monitoring wells close to Cockburn 1 well (Fig. 1 and Table 1). While the geothermal gradient analysis (Table 3) shows that the thermal regime is apparently vertically conductive, the variability of the temperature at a given depth is already significant from 30m depth (Table 4).

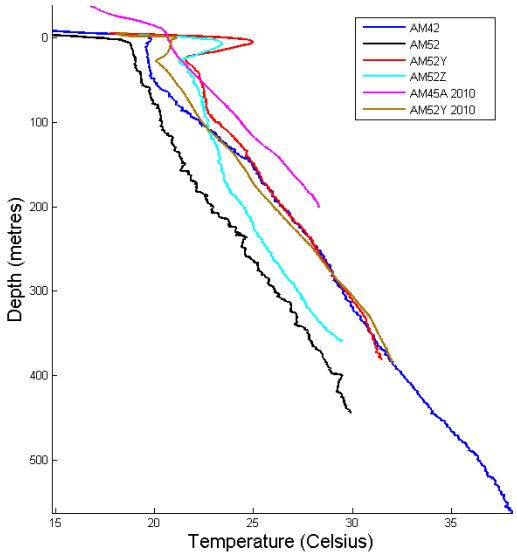

Figure 1: Wireline temperature log measurements for AM42, AM45A, AM52, AM52Y, AM52Y 2010 and AM52Z from AHD.

Table 3: Average geothermal gradient by formation for wells AM42, AM45A, AM52, AM52Y, AM52Y 2010 and AM52Z with relative error between linear gradient and real data (from Reid et al., 2011)

Formations	Thermal gradient average	Thermal gradient std	Cond. error average	Cond. error std
Superficial	N/A	N/A	N/A	N/A
Rockingham	N/A	N/A	N/A	N/A
Kings Park	N/A	N/A	N/A	N/A
Kardinya	34.7	6.7	3.8	1.9
Henley	23.8	5.3	2.1	0.6
Pinjar	33.2	8.0	2.2	1.3
Wanneroo	31.0	6.8	2.1	1.2
Mariginiup	32.5	4.8	1.4	1.2
South Perth	34.7	3.4	1.9	0.9
Gage	21.8	4.4	1.8	0.8
Cattamarra Coal Measures	N/A	N/A	N/A	N/A

Table 4: Mean temperature at selected depths with associated standard deviation for wells AM42, AM45A, AM52, AM52Y, AM52Y 2010 and AM52Z

Depth	Mean temperature (ºC)	Temperature standard deviation (ºC)
30m	20.55	1.10
100m	22.53	1.29
200m	25.77	1.83
300m	28.44	1.69
350m	29.96	1.57
400m	31.02	2.17

3-2- Thermal conductivity from cores

Steady-state thermal conductivity measurements were collected by HDRPL (2008) for various representative samples of the Perth Basin, using

HDRPL's portable divided bar thermal conductivity apparatus. Using 36 representative core samples, thermal conductivities were measured ranging from 1.31 to 7.01 $W.m^{-1}.K^{-1}$ (Table 5). Note that HDRPL reported values in the shallow surficial sediments and Osborne Formation were derived from analogous sediments in the Carnarvon Basin of Western Australia. The Gage Formation samples were taken in shaly beds and may not accurately reflect the sandstone portions of this heterogeneous formation.

Table 5: Thermal conductivities mean and variability within units measured from HDPRL (2008) and CSIRO (Esteban et al., 2011).

Formations	Thermal conductivity mean (W m-1K-1)	Thermal conductivity standard deviation (W m-1K-1)	Nb samples
Yarragadee (HDRPL)	3.31	1.42	2
Yarragadee (CSIRO)	4.29	0.61	16
Cadda (HDRPL)	4.17	0.54	2
Cadda (CSIRO)	4.30	N/A	1
Cattamarra Coal Measures (HDRPL)	3.84	0.90	2
Cattamarra Coal Measures (CSIRO)	4.40	0.60	7

In 2011, a collection of 225 core plugs samples were collected by CSIRO from 4 deep wells in the Perth Metropolitan Area (Cockburn 1, Pinjarra 1, Gingin 1 and Gingin 2) to ensure a better statistical representation of the measured physical properties. Among this collection, 27 samples from the Cockburn 1 well were used to measure: porosity and permeability at 3 confining pressures (500, 1000 and 2000 psi) to re-create the *in-situ* conditions, acoustic ultrasonic P- and S- wave velocities Vp-Vs on dry and saturated conditions at room conditions pressure and temperature as well as thermal conductivity and thermal diffusivity using the Optical Thermal Scanner (OTS; Popov et al., 1999) from the University of Melbourne (Earth Science School).

Only 4 thermal conductivity (TC) data points from divided-bar apparatus are available from the literature in the same formation units (HDRPL, 2008; Table 5) and satisfactory match the new dataset of CSIRO values within the same range, excepted in Yarragadee unit with 1 $W.m^{-1}.K^{-1}$ difference (Table 5). The HDPRL data come from different wells from the Northern part of the Perth basin and may have undergone different diagenetic history from those in the central and southern part of the Basin.. The overall range of TC in Cockburn 1 samples (Fig. 2a) is around 2.5 $W.m^{-1}.K^{-1}$ and shift to around 4 $W.m^{-1}.K^{-1}$ when saturated. Interestingly if Cattamarra Coal measures and Yarragadee units present the same range of variability centred around 4.5 $W.m^{-1}.K^{-1}$ when water saturated (Fig. 2b), they record a distinct shift under dry condition from around 2.7 $W.m^{-1}.K^{-1}$ in Yarragadee to 3.5 $W.m^{-1}.K^{-1}$ in Cattamarra Coal Measures unit. This shift could be directly related to the porosity range with values < 15% in Cattamarra Coal Measures whereas it is > 15% in Yarragadee. But this porosity shift does not seem to affect the TC under wet conditions. This may be explained by differences in grain size distribution and number of contacts between grains between the two formations (Stutenbecker and Timms, 2011).

The variability of TC within each unit is much higher under saturated conditions with variability around the harmonic mean of ± 45% and 25% in Yarragadee and Cattamarra Coal Measures respectively, and ± 10-15 % in dry conditions in both formations.

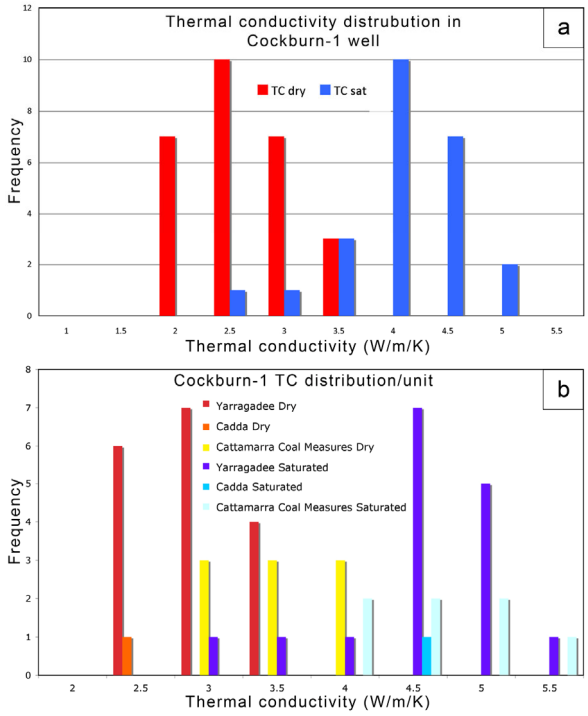

Figure 2: Thermal conductivity distribution from cores sampled in Cockburn 1 well: (a) full set in dry and water saturated conditions and (b) distribution per unit in dry and water saturated conditions.

Such variability underlines that cementation intensity in the sediments that acts as a first order control on the resulting TC. The small mismatch of TC between the techniques (OTS and divided-bar) rises from the problems of coupling between the rock and plattens in the divided-bar, the water re-hydration which could affect the reactive mineralogy (mostly clays) and the microstructural

differences after stress relaxation since the drilling period and sample preparation.

3-3- Thermal conductivity modelling

There is currently no reliable technique for estimating TC in situ due to a combination of factors such as: (i) the natural complexity of the geological settings of interest for geothermal applications in view of the available descriptive information; (ii) the inherent interactions between conductive and convective heat transport mechanisms taking place underground; and/or (iii) the effect of disturbances introduced by the observation borehole itself. In order to overcome these limitations, a new workflow for providing a first-order estimate of TC in-situ from widely-used seismic methods (borehole and/or surface seismic surveys) has been developed. This workflow is based on a combination of two robust models of effective TC and elastic wave velocities (EWV), relying on a generic rock microstructure. This microstructure involves simple parameters such as porosity and grain contact characteristics. Using available seismic data (elastic wave velocities in a given lithology), the microstructure of that particular lithology is quantified. The determined micro-structural parameters are then directly used to predict TC for that lithology (Pimienta et al., 2011). A typical outcome of this new workflow and associated micro-physics modelling is exemplified in Figure 3. Under well-constrained laboratory conditions, TC and EWV have been measured on rock cores recovered from Cockburn 1 well. Predictions of TC from EWV measurements using the new workflow (green squares) are compared to the direct measurements of TC (orange discs). A misfit of 15 to 20% between measured and predicted TC is observed in this figure. However, the over-all trends obtained by this predictive method are consistent with the direct TC measurements (Pimienta et al., 2011).

Apart from the inherent limitations associated with any modelling approach, the discrepancy between the predictions and the direct TC measurements could further be explained by experimental factors associated with the present study: (i) the non ideal preservation of the (dry) Cockburn 1 core plugs since underground recovery many years prior to the laboratory measurements of TC; (ii) the EWV were measured on these same plugs but after several cycles of water re-saturation and oven-drying at 65°C. Such cycles are known to irreversibly modify the rocks microstructure when even small amounts of clay are present, in particular in terms of grain contact characteristics. For instance, EWV are known to artificially decrease with an increasing number of re-saturation/drying cycles, which may lead to the observed under-estimation of the actual TC when such EWV are used for the prediction.

Therefore, the discrepancy between EWV-predicted and directly measured TC is likely to be reduced if a dedicated systematic experimental investigation is carried out. Note however that, as a first attempt for providing first-order estimates of TC, the current misfit is reasonable. Furthermore, if an optimal dataset is acquired in the laboratory, it is likely that the modelling side of the problem could also be improved to yield better predictions.

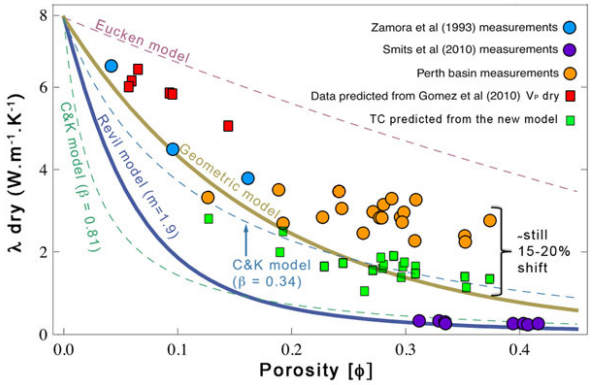

Figure 3: Comparison of EWV-predicted (squares) and directly measured (discs) TC for several rock aggregates: purple, orange, and blue discs denote the TC measurements for an unconsolidated sand, the Cockburn 1 sandstone, and the Fontainebleau sandstone, respectively; green and red squares denote the EWV-predicted TC for the Cockburn 1 and the Fontainebleau sandstones, respectively (Pimienta et al., 2011).

3-4- Thermal conductivity estimates from temperature logging measurement

Assuming an apparent vertical conduction heat transport, knowing an estimate of the vertical heat flow in Cockburn 1 of 76 $mW.m^{-2}$ (± 3.1 $mW.m^{-2}$, HDRPL, 2008) as well as the geothermal gradient by formation (Table 3), formation thermal conductivities could be estimated and compared to core measurements (Tables 5, 6). The shallow wireline temperature analysis can only be compared with formation thermal conductivities values available from HDRPL (2008). Significant differences are observed for the Rockingham, Kings Park, Kardinya, Henley, and Gage units. These differences could be explained by the non-validity of the vertical heat flow assumption and/or the uncertainty on the core thermal conductivity values. As core thermal conductivity values for these formations were derived from analogous sediments in the Carnarvon Basin of Western Australia, core measurements on samples from the Perth Basin will help to calibrate the thermal conductivity uncertainty for these formations. Once assessed, these values could be used for estimates of vertical heat flow variations on site.

3-5- Temperature predictions

Based on the modelled vertical heat flow, on the newly reassessed thermal conductivities values with associated uncertainties (including HDRPL 2008 and Esteban et al. 2011 data; Pimienta et al., 2011) and on lithology depths from Cockburn 1 and HDRPL (2008), temperature predictions at depth were estimated from Artesian Monitoring

wells AM42 (Fig. 4, Tables 7 and 8), AM45A, AM52, AM52Y and AM52Z. Only AM42 extrapolation is presented hereafter to save space.

Table 6: Formation thermal conductivities mean and variability within units estimated by HDPRL (2008) and by temperature interpretation of wells AM42, AM45A, AM52, AM52Y, AM52Y 2010 and AM52Z.

Formations	TC mean	TC std	HDRPL mean	HDRPL std
Rockingham	3.62	0.15	1.42	0.14
Kings Park	5.35	0.22	1.42	0.14
Kardinya	2.26	0.09	1.13	0.08
Henley	3.34	0.14	1.13	0.08
Pinjar	2.45	0.10	2.56	0.18
Wanneroo	2.53	0.10	2.56	0.18
Mariginiup	2.38	0.10	2.56	0.18
South Perth	2.21	0.09	1.71	0.14
Gage	3.59	0.15	1.93	0.04
Cattamarra Coal Measures	0.67	0.03	3.73	0.2

Table 7: Temperature estimates at well AM42.

Depth	Min T	Mean T	Max T
1000	43.76	46.37	49.82
2000	58.59	64.84	73.64
3000	72.80	82.80	97.21
4000	92.90	106.82	126.58

Table 8: Depths to 80, 100 and 110 ºC temperature at well AM42.

T	Min depth	Mean Depth	Max depth
80	2269	2844.10	3325
100	3094	3684.00	4000
110	3347	> 4000	> 4000

4 Discussion

In the Cockburn 1 area, the Leederville aquifer sees its temperature varying from 25 at the top of the Henley Sandstone member to 28.4 at the bottom of the Mariginiup Member (Table 9). For its part below the 28 ºC temperature, the Leederville aquifer represents an interesting heat rejection and Aquifer Thermal Energy Storage plays.

Considering deeper geothermal potential, temperature predictions at depth has a high level of uncertainty due to the uncertainties/variabilities in the formation thermal conductivities and therefore the heat flow estimates. Despite these uncertainties, direct-use geothermal applications within the Yarragadee aquifer have some potential.

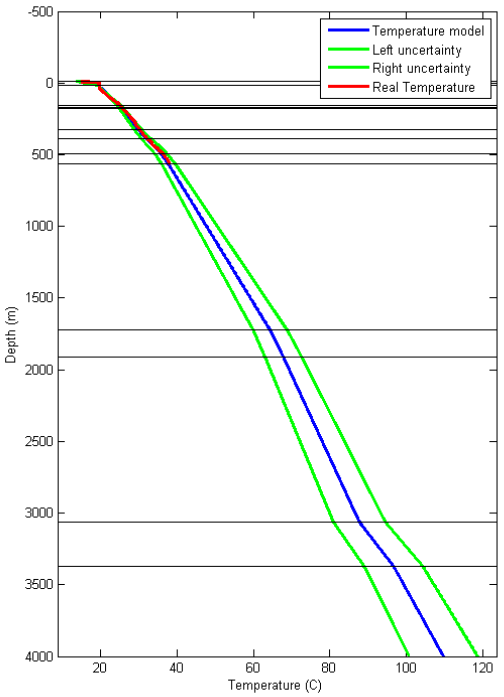

Figure 4: Temperature prediction for AM42 using modelled heat flow and thermal conductivities with associated uncertainties.

Table 9: Mean temperature at top of formation for wells AM42, AM45A, AM52, AM52Y, AM52Y 2010 and AM52Z (from Reid et al., 2011)

Formations	Temperature mean (ºC)	Temperature standard deviation (ºC)
Kardinya	21.2	1.6
Henley	25.0	0.3
Pinjar	24.2	3.0
Wanneroo	25.3	3.4
Mariginiup	26.9	2.8
South Perth	28.4	2.8
Gage	31.5	3.3

5 Conclusion

Locally to Cockburn 1, the overall temperature regime is apparently vertically conductive. New thermal conductivity measurements help to complete the poor dataset currently available while improving the evaluation of uncertainty and constraining the variability within units. Thermal conductivity measurement methods and conditions are compared for this well resulting on better understanding of the thermal conductivity measurement uncertainty. A comparison between thermal conductivity from core laboratory, wireline temperature logs, and predicted heat flow, delivers a consistent study capable of improving the estimation of formation thermal conductivities. This leads to the need of re-evaluating the thermal characterisation of several units of the shallow stratigraphic column of the Perth Basin for

a better heat rejection potential evaluation and vertical heat flow estimation. Finally, using the new values of thermal conductivities and associated uncertainties, temperature at greater depths can be predicted from nearby Wireline temperature measurements such as AM42.

Acknowledgments

The Western Australian Geothermal Centre of Excellence (WAGCOE) is funded by the Western Australian government. This work has benefited from the CSIRO-ESRE Petroleum Geoscience program Capability Development Fund. The authors would like to greatly thanks the University of Melbourne for access and help to the optical thermal scanner. This document is an output from the CSIRO Petroleum & Geothermal Portfolio.

References

Crostella A. and Backhouse J., 2000. Geology and petroleum exploration of the Central and Southern Perth Basin, Western Australia. Geological Survey of Western Australia Report 57, Perth.

Davidson W. A., 1995. Hydrogeology and groundwater resources of the Perth Region, Western Australia: Western Australia. Western Australia Geological Survey Bulletin 142.

Delle Piane C., Esteban L., Israni S., Pimienta L., Evans C., Harrison B. and McLarens, S., 2011. Physical properties of Cretaceous and Jurassic units of the Perth Basin, Western Australia. Implications for geothermal exploration. In preparation.

Esteban L., Evans C. and Pimienta L., 2011. Thermal conductivity and diffusivity characterization of Jurassic sandstones from the Perth Basin (WA). CSIRO report in preparation.

Hot Dry Rocks Pty Ltd, 2008. Geothermal energy potential in selected areas of Western Australia (Perth Basin): A report prepared for the Department of Industry and Resources, Western Australia. Hot Dry Rocks Pty Ltd, Report DOIR0060108.

Hot Dry Rocks Pty Ltd, 2011. Thermal conductivity of core specimens DMP001-DMP027. Geological Survey of Western Australia, Record 2011/19, 17 pp.

Giraud A., Gruescu C., Do D.P., Homand F. and Kondo D., 2007. Effective thermal conductivity of transversely isotropic media with arbitrary oriented ellipsoidal inhomogeneities, Int. J. Solids Struct., 44, 2627 - 2647.

Gomez C.T., Dvorkin J. and Vanorio T., 2010. Laboratory measurements of porosity, permeability, resistivity, and velocity on Fontainebleau sandstones, Geophys., 75, E191 - E204.

Israni S.R. and Delle Piane C., 2011. Rock physics and petrophysical characterization of units from the Perth Basin. CSIRO report, EP113342, 42 pp.

Pimienta L., Sarout J., Esteban L. and Delle Piane C., 2011. Prediction of rock thermal conductivity from mineral composition, elastic wave velocities and microstructure. 9th Euroconference on Rock Physics and Geomechanics, Trondheim, Norway, October 2011. Extended abstract.

Pimienta L., Sarout J., Esteban. L. and Delle Piane C., 2011. Thermal conductivity prediction from seismic velocities: A microstructurally-based approach using the effective medium theory. in preparation.

Popov Y., Pribnow D., Sass J., Williams C. and Burkhardt H., 1999. Characterization of rock thermal conductivity by high-resolution optical scanning. Geothermics, 28, 253-276.

Regenauer-Lieb K., Tong Chua H., Wang X., Horowitz F. G. and Wellmann J. F. (2009). Direct heat geothermal applications in the Perth Basin of Western Australia. Proceedings of the Thirty-Fourth Workshop on Geothermal Reservoir Engineering Stanford University, Stanford, California, February 9-11, 2009 SGP-TR-187.

Reid L. B., Bloomfield G., Botman C., Ricard L., and Wilkes P., 2011, Temperature regime in the Perth metropolitan area. Results of temperature and gamma logging and analysis, June/July 2010. CSIRO Report No: EP111422.

Ricard L. P. and Chanu J-B., 2011. GeoTemp 1.0: User Manual, WAGCOE/ CSIRO report in preparation.

Song T, and Cawood P.A. 2000. Structural styles in the Perth Basin associated with the Mesozoic break-up of Greater India and Australia. Tectonophysics, 317, 55-72.

Stutenbecker L., Timms N., and Trefry M., 2011. Petrography of samples of Cockburn-1 well. Perth Basin, Western Australia. WAGCOE report EP113151, 202 pp.

Zamora M., Vo-Thanh D., Bienfait G. and Poirier J.P., 1993. An empirical relationship between thermal conductivity and elastic wave velocities in sandstone, Geophys. Res. Lett., 20, 1679 - 1682.

Geological Study – Seasonal Storage of Air-Cooled Water for Arid Zone Geothermal Power Plants

Hugh Russell
h.russell@uq.edu.au
Queensland Geothermal Energy Centre of Excellence (QGECE), University of Queensland
QGECE, School of Mechanical and Mining Engineering, University of QLD 4072

In Australia, many regions of high geothermal potential are concentrated in arid areas, and these environments present a challenge for cooling. To achieve consistently low condenser temperatures evaporative cooling is ideal, but the requirement for an ongoing supply of water makes this unrealistic for large plants in such environments. Dry cooling by fan-forced methods is inefficient and can affect the plant's ability to consistently achieve low condenser temperatures, incurring a performance penalty during periods of high ambient temperatures. Collins [1] proposes a concept to use shallow aquifers for intermittent heat storage, with the aim of eliminating the need to carry out energy-intensive air cooling during periods of high ambient temperature. Despite the anticipated benefits of the scheme, a summary of the availability of suitable shallow aquifers was absent and it is this aspect that the current paper seeks to address.

Keywords: geothermal, cooling, aquifer, arid zone

System Summary

Collins presents a novel proposal whereby existing reserves of shallow groundwater could be used to provide direct cooling of a plant's condensers. The scheme focuses primarily on the substantial benefits of maintaining a consistently low condensing temperature by making use of assumed reserves of shallow groundwater with a temperature of around 23 °C. In doing so it uses three separate cooling systems (Figure 1):

- The first system is the production of cool water from the aquifer, which is circulated through the plant's condensers and introduced back into the aquifer via reinjection wells placed a substantial distance from the production wells.
- The second system intermittently cools the water from the condenser outlet using fan-forced air cooling when conditions for cooling are optimal.
- The third loop also operates intermittently to circulate and cool the groundwater via a secondary set of production/reinjection bores placed midway through the aquifer.

Collins suggests that a plant using fan-forced air cooling rated at 2 MW would produced a net power of only 1.2 MW on a hot day; by comparison, a scheme making use of groundwater would incur minimal parasitic losses in such a situation and would produce the rated 2 MW plus the 0.3 MW not required for air cooling [1].

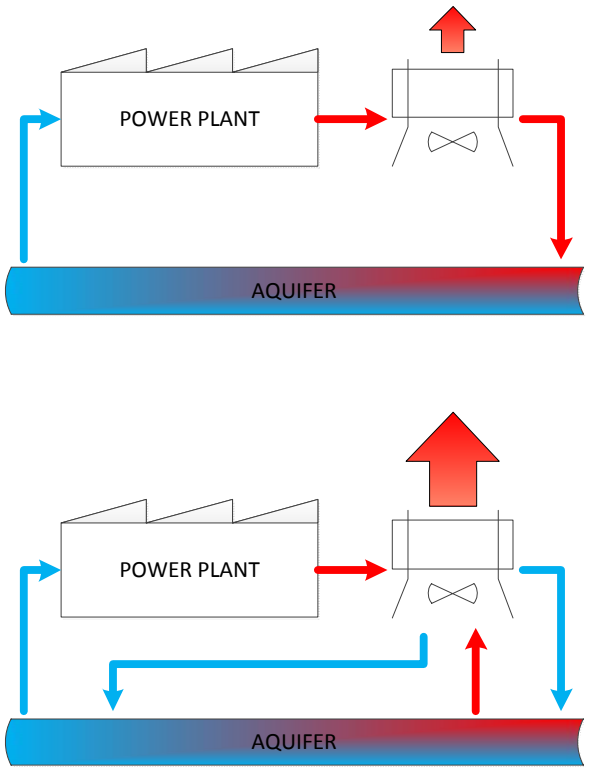

Figure 1: (a) operation with high ambient temperature, minimal heat rejection and (b) operation with low ambient temperature, maximum heat rejection to atmosphere

This scenario is countered by the times the plant is operating under the cooling regime, when heat is rejected to atmosphere by the second and third cooling systems. During these periods high parasitic losses would be incurred.

Region

There are two prominent geothermal sites situated in central Australia; the Birdsville Power Plant (Ergon Energy) and the Innamincka Deeps and Shallows ventures (Geodynamics). Both sites lie within the Eromanga Basin and the shallow geology of both sites is determined by the strata of this basin. Extensive research into the Eromanga has been undertaken as it makes up a very large proportion of the Great Artesian Basin. Aquifers within the Eromanga are tapped for potable water throughout central Australia.

The most important aquifers lie below 1000 m in the central Eromanga, and produce water at

temperatures above 80 °C. The target formations instead selected for initial examination are the two shallowest formations, the Winton formation (Cretaceous) and the overlying Cainozoic layers. Collins estimates that depths of around 40 m may be sufficient to obtain suitable volumes of water at a low temperature; to provide a limiting depth, a case was considered whereby cooling using water derived from an aquifer was compared directly with an established case for air cooling.

Parasitic Loss Comparison

A report commissioned by the Electric Power Research Institute [2] presents a case study of steam being condensed at 55 °C by air, with an ambient temperature of 37 °C. In the example scenario, a power equal to 1.3% of the total heat transfer is required to operate the fans.

By comparison, the simplest losses associated with drawing water from an aquifer for cooling come from pumping, as few artesian aquifers exist in the target formations. Assuming that water temperature remains approximately constant with depth at 23 °C, and that the maximum reinjection temperature is 40 °C, the required pumping power to draw sufficient water from the aquifer reaches the comparable 1.3% of heat rejected at a depth of around 90 m. In practice this is a maximum depth, as additional pumping losses are likely to be incurred and well production temperature will increase marginally with depth. Furthermore, losses from air cooling are rarely as excessive as described. It is an indicator, however, of the magnitude of the power requirements and the importance of locating extremely shallow groundwater.

Overview of Candidate Formations

In the region of interest, the Cainozoic layer is often less than 90 m thick, and the underlying Winton Formation is several hundred metres thick [3]. These formations are therefore the only candidates.

The Winton Formation is continuous through the Eromanga Basin, conformably overlying the relatively minor Mackunda Formation. Below these formations lie the major confining beds of the basin, composed of mudstone and shale [4]. The Winton is composed of interbedded layers of sandstone, mudstone, and coal, and it is noted as having some potential for water production as it contains some shallow, non-flowing bores.

A study [5] conducted to ascertain the likelihood of the Winton Formation acting as a continuous aquifer in the South Australian sector of the Eromanga Basin found that the aquifers within the formation were highly discontinuous. It was found that a poor depositional environment that created thin “shoestring” sands, rather than uniform sheets. Combined with the presence of extensive faulting in the area, this contributed to a conclusion that it is unlikely that the formation acts as an aquifer in the region studied. This overall perspective reinforces interpretations of bore lithology logs, such as at the Birdsville town bore [6], that indicate a number of thin interbedded layers of mudstone, shale and sandstone within the formation.

As the topmost layers of the Winton formation

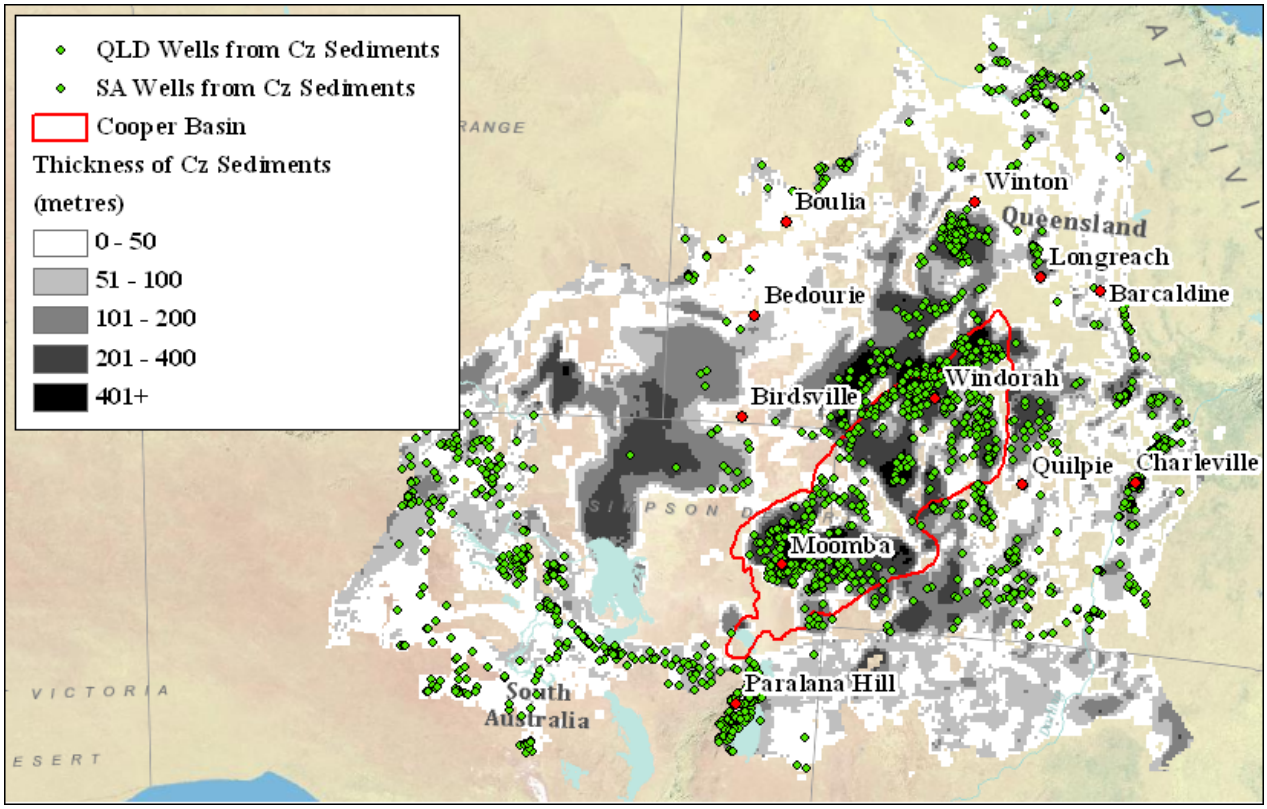

Figure 2: Map of Cainozoic sediment thickness, Eromanga Basin

form the upper confining beds in the Eromanga Basin, it is assumed that this layer will also form the hydrological base of the formations above. The Winton is often quite shallow and frequently outcrops over the area of the Eromanga Basin, but there are local regions where the Cainozoic layers above the Winton are substantial and may include 1-3 distinct stratigraphic units [3]. As their lithologies are dominated by sandstones, all units lying above the Winton are considered candidates. A map showing thickness of the Cainozoic layers was generated from combining elevation data of the Winton formation top [7] and a digital elevation model of the terrain [8]. The map (Figure 3) shows a distinct region of substantial depth in eastern South Australia, bordering on Innamincka and Birdsville. Significant depocentres are also located east of Innamincka in south-western Queensland. Further east, some scattered regions of deposition are more indicative of local ground elevation increases, where weather-resistant "duricrust" has created tablelands [9]. The most promising regions are the large depocentres mentioned.

Cainozoic Sediments of the Eromanga Basin

Several distinct layers exist within the Cainozoic sediments in the SA region of the Eromanga Basin. The first of these layers is the Lake Eyre formation, which extends over much of the region described and conformably overlies the Winton [10]. It is described as being composed predominantly of mature sandstones, with interbeds of clay, shale and coal. These interbeds are shown through type sections to be relatively minor. It is also noted that the basal sands in the Lake Eyre formation often carry brackish, sub-artesian water in synclinal regions and can produce significant quantities of water from sub-artesian bores, an indication of the possible suitability of such formations for a cooling scheme.

Towards the margins of the region shown in Figure 3 the Lake Eyre formation is found at the surface, up to a typical thickness of 30 m [10]. Other formations often overly the Lake Eyre formation in places where the Cainozoic layer thickness is greater, including the Namba and Etadunna formations, and Quaternary dunes [3]. Common deposition environments, predominantly lacustrine or fluvial, were responsible for the formation of the Lake Eyre and successive sediments. Similar lithologies are found in the deep artesian aquifers.

Availability of Groundwater in Cz Sediments

It is apparent from previous work that sandstones make up a large proportion of the near-surface geology in the SA sector of the Eromanga. Water borne in these layers may be affected by rainfall as there is no evidence for continuous impermeable layers above the Winton. For this reason it was of interest to examine the water levels measurements within the Cainozoic sediments. These measurements were obtained from PIRSA [11] and DERM. The data shows significant variability; possible sources of this variability include the effect of rainfall, local stratification with impermeable layers within the overall unit, leakage through fractures or other means from deeper formations, and may also be indicative of existing flow gradients. To indicate the availability of water in the Cainozoic sediments, a summary of the Standing Water Level (SWL) measurements from bores in both states is shown in Table 1. The average SWL values are comparable to the values assumed by Collins in the original proposal.

Table 1 Standing Water Level data for bores drawing from Cainozoic sediments in the Eromanga Basin

	Qld	SA
Readings (#)	2130	2088
Depth (min)	16m	15.2m
Depth (max)	99m	99.1m
SWL (max)	-81.5m	-82.3m
SWL (average)	-23.1m	-15.0m

Temperature of Groundwater in Cz Sediments

In the design of ground-source heat pumps, it is common to assume that between 15 and 100m depth the ground temperature remains constant [12].

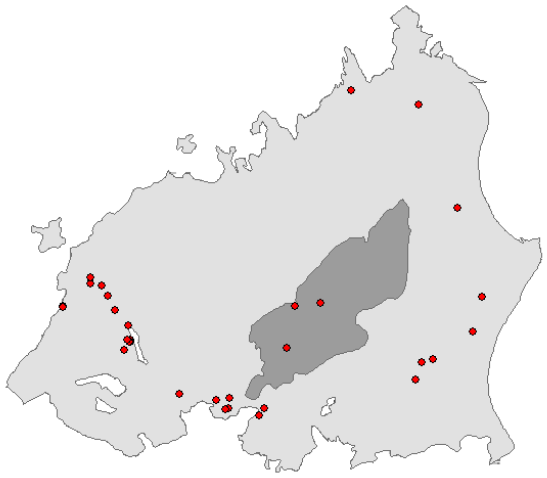

Figure 4 Location of production temperature data within Cooper (dark grey) and Eromanga (light grey) regions

Beardsmore [13], in estimating geothermal gradients in the Eromanga region, used a value of 25 °C for the ground temperature at the surface, similar to the 23 °C assumed by Collins. Despite a large number of bores in both Queensland and South Australia, there are few temperature measurements from wells specifically tapping the

Cainozoic-era sediments (see Figure 4). The available data has been summarized in Table 2.

Table 2 Summary of bore production temperature data (Eromanga Basin)

	Qld	SA
Wells (#)	9	28
Readings (#)	37	33
Depth (min)	15m	15.3m
Depth (max)	90m	74.6m
Readings ≤ 25°C	2/37	14/33
Temp (average)	41.7°C	28.1°C

It is not possible to draw definite conclusions from this data. It must not, however, be taken for granted that shallow groundwater in the region will be at a low temperature suitable for cooling. Some high production temperatures may be attributed to the transmission of warmer waters from deeper confined aquifers, such as exist in the lower part of the Winton formation. These bores are often found at the basin margins, where the thickness of the Winton formation is reduced (Figure 4).

Groundwater Yield from Cz Sediments

For a 2MW plant, Collins proposes in his original paper to supply cooling water at a rate of 159 L/s from 20 bores with a total load of 50kW, equivalent to 8 L/s per well with an individual power consumption of 2.5kW.

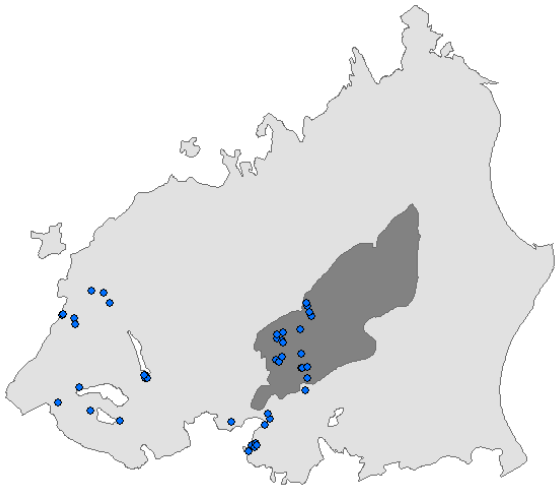

Figure 5 Location of bore yield data within Cooper (dark grey) and Eromanga (light grey) regions

Bore yield data is more commonly available than temperature data, and a considerable number of measurements have been recorded in regions of interest. Yield data from the South Australian sector of the Eromanga Basin was obtained for the locations shown in Figure 5. Only those measurements recorded from pumping were included. A summary of the available yield data is shown in Table 3.

Table 3 Summary of bore yield data in South Australian sector of the Eromanga Basin

	South Australia
Wells (#)	49
Readings (#)	52
Depth (min)	10.7m
Depth (max)	93.3m
Yield (max)	7.6 L/s
Yield (average)	1.5 L/s

If the bores with similar characteristics to those already in use in the region were implemented, withdrawing sufficient groundwater may present a challenge to the scheme. The average production value from these locations is just 20% of the flow rate requirement in the original proposal.

Conclusion

Following from the work of Collins in 2009, work was undertaken to determine if water reserves suitable for the scheme described are likely to be located in regions of interest to the geothermal industry. Suitable reserves refer to continuous, reliable aquifers located a short distance from the surface.

Evidence shows that water is to be found close to the surface, as was suggested by Collins. Existing studies suggest that the strata in this region are continuous over large areas and are of a type associated with productive aquifers. However, earlier assumptions regarding the production temperature and yield available from bores similar to those that would be required by the scheme may have been optimistic. While a lack of temperature data towards the centre of the basin may have an effect on conclusions in that regard, the relatively small yields obtained from bores located in promising areas are likely to exert a large influence on the effectiveness of the scheme. The effect of these factors will be evaluated in future work to determine if the resource can be used to improve cooling performance for arid-zone power generation.

References

[1] R. Collins, "Seasonal Storage of Air Cooled Water for Arid Zone Geothermal Power Plants," presented at the Australian Geothermal Energy Conference, 2009.

[2] K. Wilber, "Air-Cooled Condenser Design, Specification, and Operation Guidelines," Electric Power Research Institute (EPRI) 2005.

[3] J. J. Draper, Ed., *Geology of the Cooper and Eromanga Basins, QLD*. The State of

Queensland, Department of Natural Resources and Mines, 2002, p.^pp. Pages.

[4] A. Barron and R. Cox, "Great Artesian Basin Resource Study," Great Artesian Basin Consultative Council 1998.

[5] C. J. Brown, "The continuity of sands in the Winton Formation, South Australian sector, Eromanga Basin," Bachelor of Science, Petroleum Geology and Geophysics Honours Thesis, Australian School of Petroleum, The University of Adelaide, 2009.

[6] Unknown, "Bore Card Report - Birdsville Town Bore," DERM, Ed., ed, 2011.

[7] W. D. Welsh, "Great Artesian Basin transient groundwater model," Bureau of Rural Sciences 2006.

[8] M. F. Hutchinson*, et al.*, "GEODATA 9 Second DEM and D8: Digital Elevation Model Version 3 and Flow Direction Grid," G. Australia, Ed., ed, 2008.

[9] H. Wopfner and C. R. Twidale, "Geomorphological History of the Lake Eyre Basin," *Landform Studies from Australia and New Guinea,* vol. 1, pp. 119-143, 1967.

[10] H. Wopfner*, et al.*, "The lower tertiary Eyre Formation of the Southwestern Great Artesian Basin," *Australian Journal of Earth Sciences,* vol. 21, pp. 17-51, 1974.

[11] [Online]. Available: https://des.pir.sa.gov.au/page/desHome.html

[12] K. Ochsner, *Geothermal Heat Pumps: A guide for planning and installing*: Earthscan, 2008.

[13] G. Beardsmore, "The influence of basement on surface heat flow in the Cooper Basin," *Exploration Geophysics,* vol. 35, pp. 223-235, 2004.

Success Factors in Geothermal Heat Pump Development

Rybach, L.
rybach@geowatt.ch
Geowatt AG
Dohlenweg 28, CH-8050 Zurich, Switzerland

Geothermal heat pumps (GHP) are one of the fastest growing applications of renewable energy in the world and definitely the fastest growing segment in geothermal technology, in an increasing number of countries. Recent statistical data indicate rapid (exponential) growth, see Figure 1.

Although GHPs are increasingly installed, their advancing is highly different from country to country. The influence factors leading to market penetration and expansion are identified and discussed, current development trends and future expectations are presented.

Keywords: market penetration, financial incentives, environmental benefits

Technology brief

GHP represent a rather new but already well-established technology, utilizing the immense renewable storage capacity of the ground. GHPs use the relatively constant temperature of the ground to provide space heating, cooling and domestic hot water for homes, schools, factories, public and commercial buildings. The application size can vary from single-family homes with 1-2 borehole heat exchangers (BHE) to large-scale complexes with hundreds of BHEs. The decentralized systems can be tailor-made, taking into account the local conditions. It is essential to employ proper system design that takes into account meteorologic, ground property and thermal demand conditions. By these means, reliable long-term operation can be secured. Of the local conditions, the thermal conductivity of ground materials and the groundwater properties are of key importance. Three basic components make up a GHP system: 1) the heat extraction/storage part in the ground, 2) the central heat pump, 3) the heat distributor/collector in the building (e.g. floor panel). The key component is the heat pump. In essence, heat pumps are nothing more than refrigeration units that can be reversed. In the heating mode the efficiency is described by the coefficient of performance (COP) which is the heat output divided by the electrical energy input for the heat pump. Typically this value lies for GHPs between three and four (Rybach, 2005). Except for larger, singular applications where gas-driven heat pumps are used, most heat pumps use electricity for their compressors. Therefore GHPs are electricity consumers. The source of electricity varies from country to country; it would be elegant if the electricity to drive the GHP heat pumps would originate from renewable sources like solar, wind, or even geothermal!

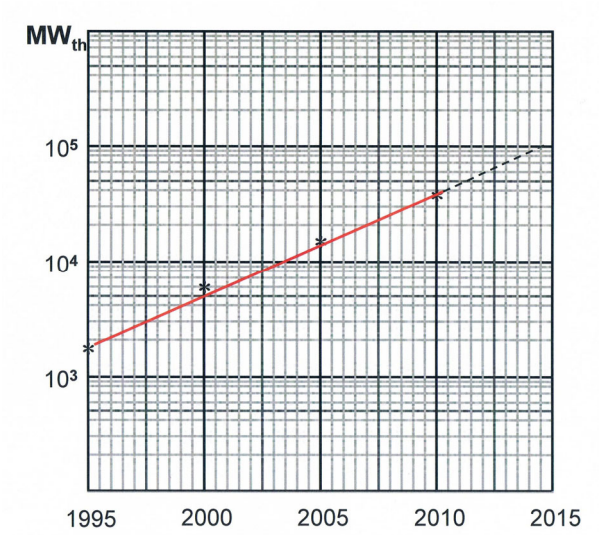

Figure 1: Global growth of installed GHP capacity 20 % per year (data from Lund et al. (2010) plotted).

Engineering design

The design of GHP systems aims at the appropriate sizing of the system components by taking into account a number of influence factors. The sizing must consider the demand characteristics of the object to be supplied (size, extension; heating alone, heating + domestic water, combined heating/cooling) as well as the local site conditions (climate, ground properties).

The proper design of GHP systems is a complex and demanding task, especially for large installations with several 10 or 100 BHEs. Correspondingly more sophisticated approaches and methods are needed and also available. Common in all design endeavors is that -starting with the heating and/or cooling needs of the objects in question- the number, depth and spacing of BHEs and their hydraulic connections are determined. Depth and number of the BHEs depend on the utilization purpose (heating alone, combined heating/cooling, ± domestic hot water), the object size, and not least on the local conditions. The BHE/HP design must take into account all these factors.
A key property is the thermal conductivity of the ground surrounding the BHE. The higher the rock thermal conductivity λ (W/m,K), the higher the specific heat extraction rate (W/m) and the energy yield (kWh/m,a) per unit BHE length (see Table 1).

Rock type	Thermal conductivity (W m^{-1} K^{-1})	Specific extraction rate (W per m)	Energy yield (kWh m^{-1} a^{-1})
Hard rock	3	max. 70	100 - 120
Unconsolidated rock, saturated	2	45 - 50	90
Unconsolidated rock, dry	1.5	max. 25	50

Table 1: Borehole heat exchanger performance (single BHE, depth ~ 150 m) in different rock types. From Rybach (2001).

Large system design (with several 100 BHEs) is a complex task (see Mégel et al. 2010). During the detailed planning of a large-scale BHE storage, measurements of ground thermal properties in test-BHEs are recommended in order to achieve the ground parameters for the dimensioning tools. However, the crucial planning parameters are predetermined by the location, the construction and the utilisation of a building, i.e. by the energy concept and the energy load profiles. Quality control during the installation of the BHE system and control of the operational behaviour by monitoring must be part of a modern geothermal engineering concept.

Success factors

When compared to other segments of geothermal technology the GHPs have definitely less requirements (number of success factors), see Table 2.

Factor	Flash plants	Binary plants	Direct use	GHP
Resource	xxx	xx	x	o
Ownership	xxx	xxx	xx	x
Permits	xxx	xxx	x	o
Environment	xxx	xx	x	o
Finances	x	xx	xxx	x
Risks	xxx	xx	x	o
Expertise	xxx	xxx	xx	x
Market	xxx	xxx	xxx	xx
Hero/Leader	xx	xx	xxx	x
Transmission	xxx	xx	x	o
Public acceptance	xxx	xx	x	o
xxx : major, xx : minor, o : none				

Table 2: Comparison of success factors ("conditions needed for success", Lund 2011)

Ownership does not really matter; the GHPs are installed in buildings with clear land ownership. Decisive is that the builder-owner is aware of the advantages and benefits (e.g. costs, environmental friendliness) of GHP technology.
Unlike with other forms of geothermal direct use (like district heating) a local hero –who is fully convinced in the geothermal solution and is ready to fight for it through all phases and instances– is not really needed for GHPs, only knowledgeable architects, designers, installers etc.
In the following, specific success factors are dealt with in more detail.

Production sustainability

Reliable long-term operation is a prerequisite of widespread acceptance of GHP systems. For GHPs the issue of sustainability concerns the various heat sources (horizontal and vertical het exchanger pipes, groundwater (Rybach and Mongillo 2006). Theoretical and experimental studies have been performed to establish a solid base of long-term reliability of GHP production characteristics (Rybach et al. 1992, Rybach and Eugster 1998, Eugster and Rybach 2000, Signorelli et al. 2005). Experience shows that properly designed GHP systems operate fully satisfactorily over decades (Rybach and Eugster 2010).

Finances

Finances of course are a key issue. Although GHPs need considerable initial investment (higher than for common fossil-fired systems), the overall performance is more favourable. The higher installation cost is due to the earth works (usually drilling and completion) and components (heat pump, connections, distributors). On the other hand, running costs are generally low (mainly only electricity for heat pumps and circulation pumps).
Prices/costs are certainly of paramount importance. Two factors are important in this respect for GHPs: 1) no need to burn fuel, 2) subsidies. This means that GHP operation costs are significantly lower and the environmental benefits entitle to subsidies in many countries. The economics of GHP systems can best be considered in comparison with other, conventional and fossil fired systems. For the comparison, a common single-family house in Central Europe with 150 m^2 living space, a heating system with 7.5 kW_{th} capacity), and an annual energy requirement of 65 GJ for a season of 2'400 heating hours per year is considered, in comparison with gas and oil heaters (Auer, 2010). Table 3 shows the comparison.
Of course the future price development of oil, gas and electricity is unknown; usually it is assumed that electricity prices will increase significantly slower than oil and gas prices. In the above comparisons the issues of CO_2 emission (i.e. a CO_2 taxation) are not considered. A CO_2 tax for space heating is already introduced in several European countries. It can be expected that this trend continues and thus the GHP systems will have increasing advantages. In addition, the above comparison is made only for heating. The great advantage of GHP systems is that the same equipment can be used for cooling in summer, a real benefit in times of global warming.

	GHP / BHE	Gas heater	GHP / BHE	Oil heater
Investment cost	18'000 €	8'800 €	18'000 €	12'500 €
Higher GHP investment	9'200 €		5'500 €	
O & M cost/year	680 €	1'720 €	680 €	2'000 €
GHP savings/year	1'040 €		1'320 €	
Amortisation period - without investment payment - at 6 % interest	 9 years 13 years			 just < 5 years just > 5 years

Table 3: Cost comparison of 1) BHE based GHP heater, 2) gas condensing heater, 3) oil heater (numbers from Auer, 2010)

Equally important is the subsidization of heat pump systems in some areas by the electric utilities (which are often owned by the municipalities); it is very common for direct grants in the investment phase and/or indirect funding breaks via reduced electricity rates for households and small and medium-sized businesses. Subsidization pays off for the electric utility on balance, since the pump systems use more electricity than oil heating, for instance.

Expertise

The proper design of GHP systems has already been discussed above. Equally important is the professional standard at installation. The consideration and optimization of the three main GHP circuits (heat source, heat pump, heating/cooling unit) belongs to the planning stage. While heat pumps and heating/cooling units (hydronic or fan-coil systems) can readily be purchased "off the shelf" the installation (=drilling and completion) of GHP boreholes is a demanding task, quality assurance is needed. In several countries (USA, Canada, EU countries) the professional standard of drillers and installers is documented by certificates; engineering norms like VDI 4640 in Germany or SIA 384/6 in Switzerland define the standards to be followed.

Easy licensing, environmental benefits

In general, GHP installation needs permits. In most countries the water protection agencies (local, regional, national) are providing permits. Regulation varies from country to country; is some cases even within the same country. Usually some standard forms need to be filled and submitted; usually the permitting procedure is easy and straightforward. However, it is common practice that in groundwater protection areas the installation of GHP systems is limited or forbidden.

GHPs operate with little or no greenhouse gas (GHG) emissions since no burning processes are involved. GHPs driven by fossil fuelled electricity reduce the CO_2 emission by at least 50% compared with fossil fuel fired boilers. If the electricity that drives the geothermal heat pumps is produced from a renewable energy source like hydropower or geothermal energy the emission savings are up to 100%.

Reducing current CO_2 emissions is the central option in all the efforts to mitigate global warming. Here a clear distinction must be made between actual emission reduction and merely avoidance of additional emission: by new GHPs only additional CO_2 emission can be avoided ("saving"), not a reduction of actual emissions. When GHPs are installed in refurbishment (to replace fossil-fueled systems) actual emission reduction can be achieved (Rybach 2009). Emission reduction is also evident when electric heater/cooler installations, driven by fossil-based electricity, are replaced by GHP systems.

Knowledge, outreach

The most important driving force of GHP development is simply knowledge and know-how. Besides, various applications and wide-scale realizations, high-level quality assurance and successful demonstration facilities are needed. Architects, engineers and building physicists are becoming nowadays increasingly knowledgeable about GHP system design and installation; drilling companies have the necessary special equipment to perform quick jobs. Heat pump promotion associations implement publicity campaigns to disseminate the good news about the benefits of the –in many countries still new– technology. All these factors led already to spectacular boosts of the GHP market in the last few years, especially in countries where only a couple of years before literally no installations existed.

Current trends, future prospects

Due to the rapidly growing GHP development, statistical data can provide only snapshots. Worldwide data on geothermal heat pump applications were presented at the World Geothermal Congress held in Nusa Dua/Bali, Indonesia, in 2010 (WGC2010). According to Lund et al. (2010) GHP's account for 69.7% of the worldwide geothermal direct use capacity and 49.0% of the energy use. The installed capacity is 35,236 MWth and the annual energy use is 214,782 TJ/yr, with a capacity factor of 0.19 in the heating mode. For the global growth see Figure 1.

Almost all of the installations occur in North American, Europe and China, increasing from 26 countries in 2000, to 33 countries in 2005, to the present 43 countries. The equivalent number of installed 12 kW units (typical of US and Western European homes) is approximately 2.94 million, over double the number of units report for 2005, and four times the number for 2000. The leaders in installed units are the United States, China, Sweden, Norway and Germany.

China is the most significant newcomer in the application of heat pumps for space heating. According to data Zheng et al. (2010) the total area of GHP engineering application was 7.67 million m^2 in 2004 but reached 20.35 million m^2 in 2006, and its annual increase was about 20 million m^2 in following years. Installed capacity grew from 383 MWth in 2004 to 5,210 MWth in 2009. It has increased by more than 10 times during the past 5 years. A batch of momentous GHP projects gained financial support from the Ministry of Construction and Ministry of Finance. The impressive numbers reflect the policy of the Chinese government to replace fossil fuels where possible with clean, renewable energy (Fridleifsson et al. 2008). The "Law of Renewable Energy of China" came into implementation in 2006.

Innovative technological solutions are emerging, like the HYY Single Well Groundwater Heat Pump System (Xu and Rybach 2010).

In Europe the GHP development is still progressing. For the future the Geothermal Heating and Cooling Action Plan (EGEC 2009) envisages steady growth, albeit at quite different growth rates in various countries (Figure 2).

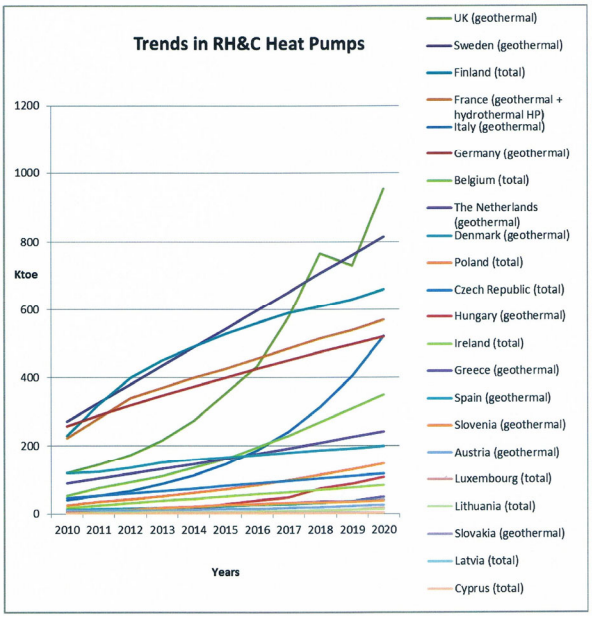

Figure 2: Projected GHP growth until 2020 (in kiloton oil equivalent units) in European countries (EGEC 2009).

Conclusions

Geothermal heat pump application will definitely grow, depending on the speed of information and know-how transfer, the latter especially in system design and installation. Other success factors are the demonstration of reliable and sustainable operation, technical expertise, quality assurance, financing helps like subsidies, easy licensing.
Besides GHP applications in new buildings the renovation market segment is highly promising. Significant CO_2 emission reduction can be achieved when fossil-fired systems are replaced by geothermal installations.

References

Auer, J., 2010, Geothermal energy – Construction industry a beneficiary of climate change and energy scarcity. Deutsche Bank Research, ISSN Print 1612-314X, 24 p.

EGEC, 2009, Geothermal Heating & Cooling Action Plan, European Geothermal Energy Concil, Brussells, 20 p.

Eugster, W.J., Rybach, L., 2000, Sustainable production from borehole heat exchange systems. In: Proc. World Geothermal Congress 2000, Kyushu-Tohoku, Japan, 825-830.

Fridleifsson, I.B., Bertani, R., Huenges, E., J. Lund, J.W., Ragnarsson, A., Rybach, L., 2008, The possible role and contribution of geothermal energy to the mitigation of climate change. In: O. Hohmeyer and T. Trittin (Eds.) IPCC Scoping Meeting on Renewable Energy Sources.

Proceedings, Luebeck, Germany, 20-25 January 2008, 59-80.

Lund, J.W., Freeston, D.H., Boyd, T.L., 2010, Direct Utilization of Geothermal Energy 2010 Worldwide Review. In: *Proceedings World Geothermal Congress 2010*, Bali, Indonesia, 25-30 April 2010. Available at: www.geothermal-energy.org/pdf/IGAstandard/WGC/2010/0007.pdf.

Lund, J.W., 2011, What works and what doesn't work in geothermal projects – The U.S.A. experiences. Presentation at West Australian Geothermal Conference, Perth, Slide nr. 7.

Mégel, T., Rohner, E., Wagner, R., Rybach, L.: The use of the underground as a geothermal storage for different heating and cooling needs. In: *Proceedings World Geothermal Congress 2010*, Bali, Indonesia, 25-30 April 2010. Available at: www.geothermal-energy.org/pdf/IGAstandard/WGC/2010/2956.pdf.

Rybach, L., 2001, Design and performance of borehole heat exchanger/heat pump systems. In: Proc. European Summer School on Geothermal Energy Applications, Oradea/Romania (CD-ROM).

Rybach, L., 2005, The advance of geothermal heat pumps world-wide. IEA Heat Pump Center Newsletter Vol. 23 No. 4, 13-18

Rybach, L., 2009, CO_2 emission mitigation by geothermal development – especially with geothermal heat pumps. GRC Transactions Vol. 43, p. 597-600

Rybach, L., Eugster, W., 1998, Reliable long term performance of BHE systems and market penetration - The Swiss success story. In: L. Stiles (ed.): Proc. 2nd Stockton International Geothermal Conference, 41-57.

Rybach, L., Mongillo, M., 2006, Geothermal Sustainability – A Review with Identified Research Needs. Geothermal Resources Council Transactions Vol. 30, p. 1083-1090.

Rybach, L., Eugster, W.J., 2010: Sustainability aspects of geothermal heat pump operation, with experience from Switzerland. Geothermics 39, 365-369

Rybach, L., Eugster, W.J., Hopkirk, R.J., Kaelin, B., 1992, Borehole heat exchangers: Long-term operational characteristics of a decentral geothermal heating system. Geothermics 22, 861-869.

Signorelli, S., Kohl, T., Rybach, L., 2005, Sustainability of production from borehole heat exchanger fields. In: Proc. 29th Workshop on Geothermal Reservoir Engineering, Stanford University, p. 356-361.

Xu, Sheng-heng, Rybach, L., 2010, Innovative groundwater heat pump system for space heating and cooling in USA and China. In: *Proceedings World Geothermal Congress 2010*, Bali, Indonesia, 25-30 April 2010.
Available at: www.geothermal-energy.org/pdf/IGAstandard/WGC/2010/2914.pdf.

Zheng, K., 2010, Growth of the Use of Geothermal Heat Pumps in China. In: *Proceedings World Geothermal Congress 2010*, Bali, Indonesia, 25-30 April 2010.
Available at: www.geothermal-energy.org/pdf/IGAstandard/WGC/2010/2937.pdf.

Queensland's Coastal Geothermal Energy Initiative: preliminary heat flow modelling results

Sargent, S.N.*, Maxwell, M., Talebi, B. and O'Connor, L.
Sarah.Sargent@deedi.qld.gov.au
Geological Survey of Queensland
PO Box 15216 City East QLD, 4002

Heat flow results modelled from the Coastal Geothermal Energy Initiative (CGEI) drilling program has highlighted geothermal potential within the Millungera and Maryborough Basins.

Preliminary heat Flow modelling for GSQ Dobbyn 2, GSQ Julia Creek 1 and GSQ Maryborough 16, have returned values of 107.4 ± 1.2 mW/m^2, 103.3 ± 4.2 mW/m^2 and 74.3 ± 2.5 mW/m^2 respectively.

Excellent insulating cover within the Maryborough Basin and high heat producing granitic heat source at depth present within the Millungera Basin suggest these elevated heat flow values could represent a broader geothermal potential across the both basins.

The viability of exploration projects within these two basins is favourable due to the close proximity to population and heavy industry centres. The Millungera Basin is located to the east of the Mount Isa mining area and infrastructure and the Maryborough Basin is proximal to the high population density (and power needs) of south east of Queensland.

This abstract gives preliminary heat flow modelling results for three sites drilled as part of the CGEI drilling program; GSQ Dobbyn 2, GSQ Julia Creek 1 and GSQ Maryborough 16.

Keywords: Queensland geothermal potential, thermal conductivity, heat flow modeling, down hole temperature data, Millungera Basin, Maryborough Basin.

Project Background

The CGEI is a Queensland Government project designed to investigate the potential for geothermal energy close to existing power networks and population or heavy industry centres. In Queensland petroleum exploration and water bore drilling has highlighted the south west portion of the state as highly prospective for geothermal energy. The CGEI aims to drill targets across other parts of the state where little temperature data is available (Figure 1 and 2). The drilling and collection of thermal data will occur through a more rigid scientific method than previously used and the resulting heat flow calculations will contribute to Queensland's heat flow data base. It will also provide a pre-competitive dataset to the state's growing number of geothermal explorers.

The CGEI program is a co-operative undertaking between the Office of Clean Energy and the Geological Survey of Queensland (GSQ).

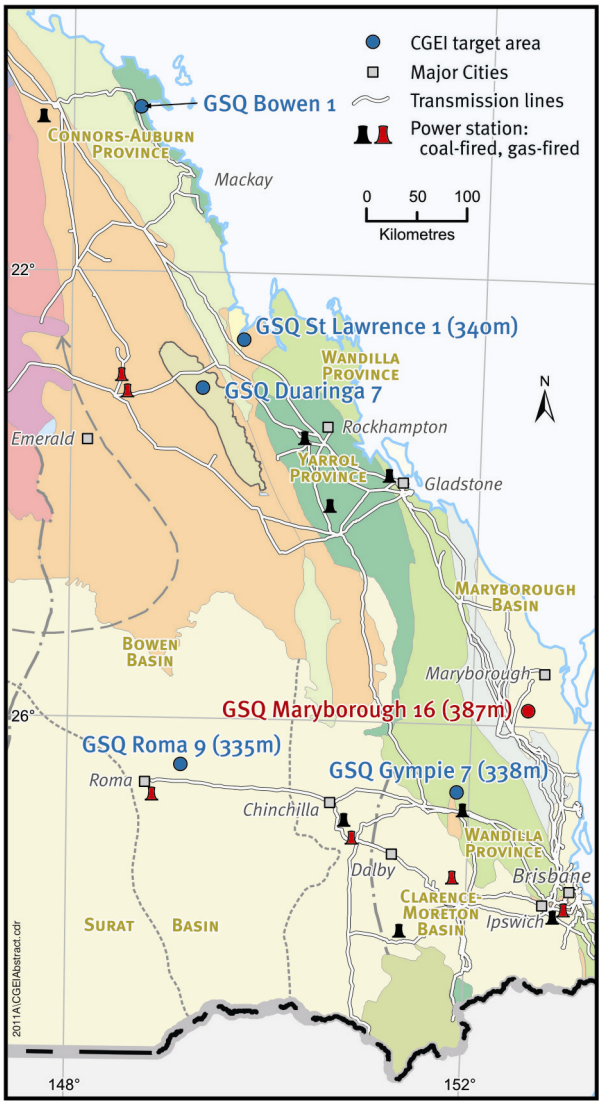

Figure 1: Southern Phase 1 drilling targets.

Status

Status of the program as of the 31st October 2011 is summarised in Table 1 with ten sites now drilled. GSQ Townsville 2 was abandoned in October after four attempts to reach consolidated ground within 150m. GSQ Bowen 1 and GSQ Duaringa 7 are to be drilled in the coming months.

Temperature logging conducted by both Geoscience Australia (GA) and Hot Dry Rocks (HDR) indicated thermal equilibrium had not been

reached for GSQ Gympie 7, GSQ Longreach 2, GSQ Roma 9 and GSQ St Lawrence 1. As a result, these sites will need to be cased and cemented again to ensure any permeable rock units are sealed. Consequently heat flow modelling for these sites has been delayed.

Table 1. Status of the CGEI program as of the 31st October. Green ticks indicate completed, TBC is to be completed and red crossed indicate unable to be completed due to abandoning the hole.

Site	Drilled	Temperature logging		Heat flow modelling
		GA	HDR	
MARYBOROUGH 16	387.4	✓	✓	✓
GYMPIE 7	338.6	✓	✓	TBC
LONGREACH 2	327.3	✓	✓	TBC
ROMA 9	335.9	✓	✓	TBC
ST LAWRENCE 1	340.0	✓	✓	TBC
JULIA CREEK 1	500.0	✓	TBC	✓
DOBBYN 2	500.0	✓	TBC	✓
GEORGETOWN 8	320.2	TBC	TBC	TBC
MOSSMAN 2	339.7	TBC	TBC	TBC
TOWNSVILLE 2	X	X	X	X
BOWEN 1	TBC	TBC	TBC	TBC
DUARINGA 7	TBC	TBC	TBC	TBC

Work program

The CGEI work program to date has involved four stages; site selection, drilling, thermal data collection and heat flow modelling.

Site selection

A total of 32 possible targets were initially selected and ranked on the following criteria (Fitzell et al, 2009 and Talebi et al, 2010):

- Insulating sediment cover greater than 3500 m
- Low thermal conductivity of overlying sediments < 3.0 W/mK
- Target heat source with heat production values > 5 μW/m^3
- Calculated geothermal gradients > 40 °C/km from temperature measurements
- Within 100 km of population centres or potential electricity markets

The estimated cost per hole following the receipt of the drilling tenders far exceeded the expected costs at the start of the project. As a result the program was split into three phases of drilling with phase 1 to drill 10-12 targets with the highest prospectivity (Figures 1 and 2). Phases 2 and 3 are to follow pending the approval of more funding.

The location of each drill site within Phase 1 was selected to ensure environmental disturbance was minimised, topographical influences on crustal heat flow were minimal, avoid underground infrastructure from other explorers and reasonable access was available.

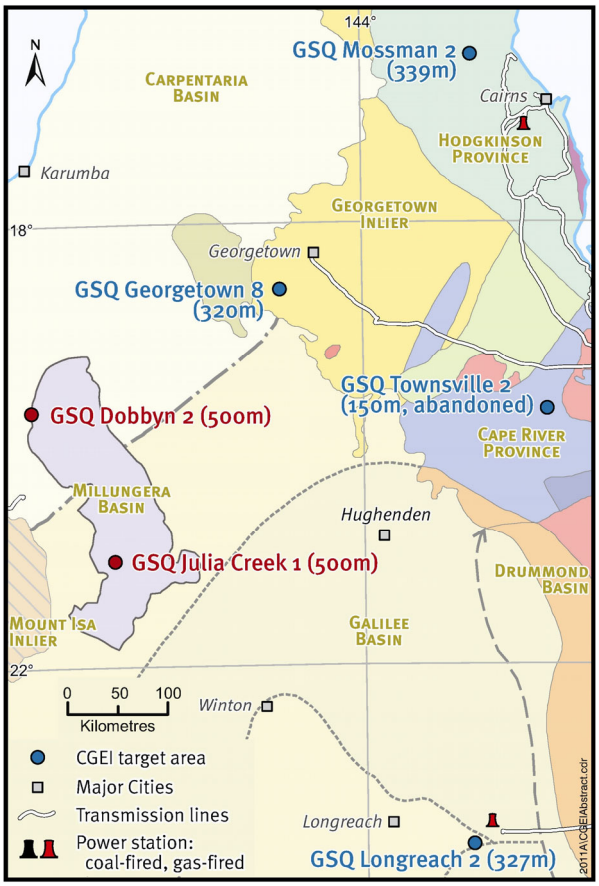

Figure 2: Northern Phase 1 drilling targets.

Drilling

Drilling of the Phase 1 targets required chipping to consolidated material with diamond coring to a total depth (TD) between 320-500 m. Each hole was cased with HWT steel casing to base of chipping, and Class 18 PVC to TD to ensure the hole remains open for the 6 to 8 week thermal stabilisation period required before temperature logging.

Thermal data collection

Requirements of the drilling at each target were to:

- Retrieve >200 m continuous HQ3 core
- Collect thermal conductivity samples 150 mm long every 20 meters
- After a period of thermal stabilisation, conduct temperature logging by HDR and GA and calculate the geothermal gradient down the hole

Heat flow modelling

Following receipt of thermal conductivity results and the collection of temperature data when the hole had reached thermal equilibrium, heat flow modelling was undertaken using customised in-house software called HF1D. The modelling is based on the following equation:

$$q = k.{dT}/{dz}$$

where q is the heat flow in milli Watts per metre squared (mW/m^2), k is the rock thermal conductivity in Watts per metre Kelvin (W/mK) for an interval of a particular lithological unit and dT/dz is the vertical geothermal gradient in Kelvin per metre (K/m) over the same interval.

Firstly, thermal boundaries for each hole were identified from the geothermal gradient, below casing. Thermal conductivity values for the dominant rock type present in each thermal unit as selected for heat flow modelling.

The heat flow was modelled using an inversion technique with theoretical temperature data being computed for a given magnitude of heat flow. This theoretical data was compared against the observed temperature log and the magnitude of the heat flow parameter in the model was adjusted until the computed temperature data best matched the logged temperatures. The vertical heat flow (q) was assumed to be a purely conductive regime and constant across all lithological units.

Once the heat flow was modelled, the values were compared to the average crustal heat flow value of 60 mW/m^2 (Cull, 1982) and the current heat flow map of Australia provided by Hot Dry Rocks (pers comms, 2011) to postulate the regional significance of the result.

Surrounding drill holes and regional geology are used to estimate the stratigraphy and rock units to 5 km depth. Thermal conductivity values were then assigned to the rock units in order to extrapolate the temperature to 5 km depth where values greater than 200 °C were considered highly prospective for Enhanced Geothermal Systems (EGS).

Heat flow modelling results

GSQ Dobbyn 2

The temperature profile for GSQ Dobbyn 2 shows a two stage increase with a bottom hole temperature of 61.1 °C at 500.0 m (Figure 3). A change in the temperature can be seen within the highly conductive sandstones in the Millungera Basin sequences.

The temperature gradient identified 4 thermal units suitable for heat flow modelling (Figure 3). Thermal units 1-3 consisted predominantly of mudstone and thermal conductivity values of 1.13, 1.11 and 1.1 W/mK respectively were assigned for modelling. The insulating capacity of the fourth thermal unit consisting of siliceous-haematitic sandstone (within the Millungera Sequence) is low, with a thermal conductivity value of 7.4 W/mK used for modelling.

Heat flow modelled over 90.5-500.0 m provided a value of 107.4 ± 1.2 mW/m^2.

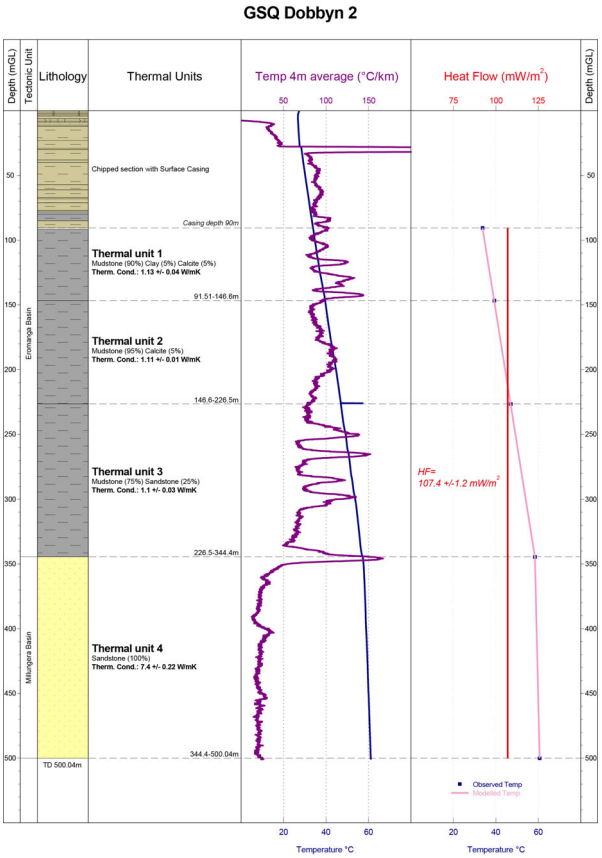

Figure 3: Thermal profile and modelled heat flow of GSQ Dobbyn 2, 107.4 ± 1.2 mW/m^2

GSQ Julia Creek 1

The temperature profile for GSQ Julia Creek 1 also showed two stage temperature profile, steepening towards the base of the Eromanga Basin then decreasing slightly within the quartzite and clays of the Millungera Basin. Near bottom temperature of 54.3 °C at 480.5 m was recorded (Figure 4).

Three thermal units were identified over the modelled section between 120.1 – 480.5 m. Thermal units 1 and 2 consisted predominantly of mudstone and the thermal conductivity values 1.2 and 1.64 W/mK respectively were assigned for modelling.

Siliceous-haematitic quartzite with thin bands of altered clay (Millungera Basin) was modelled as the third thermal unit. The thermal conductivity value increased sharply and a value of 6.4 W/mK was used to model this interval.

Heat flow modelling over 120.1 – 480.5m provided a value of 103.3 ± 4.2 mW/m^2.

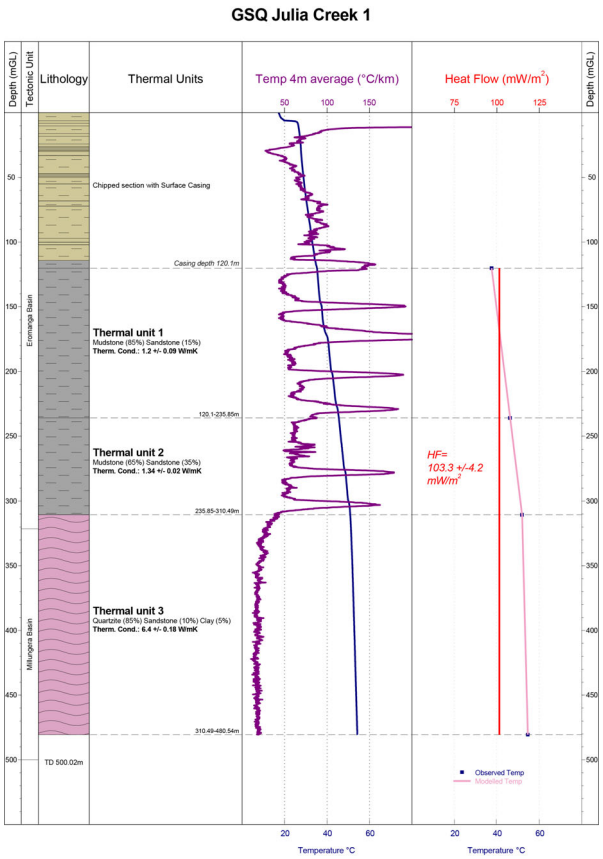

Figure 4: Thermal profile and modelled heat flow of GSQ Julia Creek 1, 103.3 ± 4.2 mW/m^2

GSQ Maryborough 16

The temperature profile for GSQ Maryborough 16 shows a steady increase with a near-bottom hole temperature of 34.86 °C at 380.5 m (Figure 5).

Five thermal units were identified for heat flow modelling within GSQ Maryborough 16. The temperature gradient is highly variable reflecting interbedded sandstone, mudstone and coal of the Tiaro Coal Measures. Thermal conductivity values of 2.49, 2.5, 2.5 and 2.39 W/mK were used to represent the mainly sandstone rock type within thermal units 1, 3, 4 and 5 respectively.

Thermal unit 2 contained a higher proportion of mudstone and was assigned a thermal conductivity value of 1.87 W/mK.

Heat flow modelling over 61.2 – 380.6 m returned a value of 74.3 ± 2.5 mW/m^2 (Figure 4).

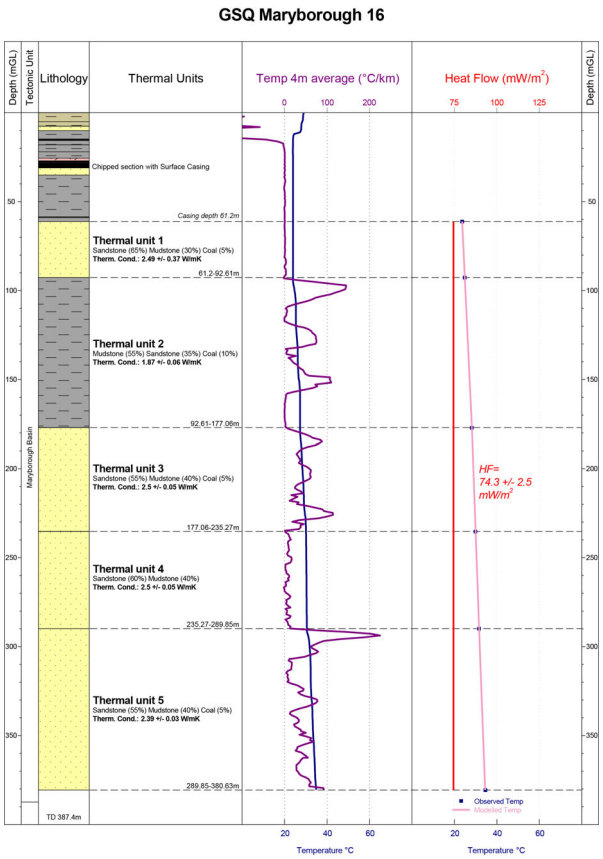

Figure 5: Thermal profile and modelled heat flow of GSQ Maryborough 16, 74.3 ± 2.5 mW/m^2

Regional implications

Millungera Basin

New heat flow values modelled for the Millungera Basin are much higher than 50-60 mW/m^2 previously estimated for the area (Figure 6). Temperature extrapolation to 5 km depth for GSQ Dobbyn 2 and GSQ Julia Creek 1 were 234 ± 15 °C and 223 ± 15 °C respectively.

There are several geological factors which suggest the two heat flow values modelled for GSQ Dobbyn 2 and GSQ Julia Creek 1 delineate a larger geothermal potential across the basin.

The insulating capacity of both overlying Eromanga Basin (overlying the Millungera Basin in the south) and the Carpentaria Basin (overlying the Millungera Basin in the north) is excellent with a median thermal conductivity value of 1.13 W/mK. In GSQ Dobbyn 2, Carpentaria Basin thickness was 345m whereas the thickness of the Eromanga Basin in GSQ Julia Creek 1 was 320 m.

Little information is known about the thermal properties of the entire Millungera Basin however the upper sequence intersected in the two GSQ drill holes consisted of quartzite and siliceous – haematitic altered sandstones. The insulating capacity is low with a median thermal conductivity value of 6.82 W/mK across both holes. The maximum thickness of the Millungera Basin has

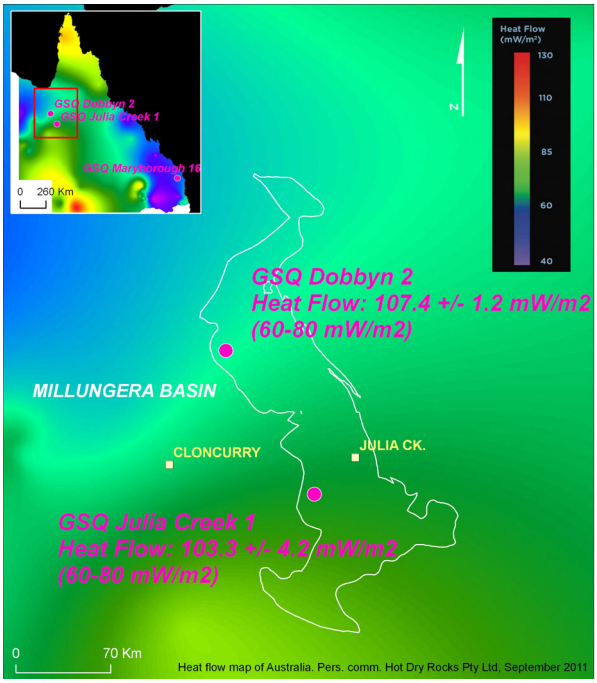

Figure 7: GSQ Dobbyn 2 and GSQ Julia Creek 1 heat flow compared to existing Millungera Basin heat flow estimates (courtesy of Hot Dry Rocks, 2011).

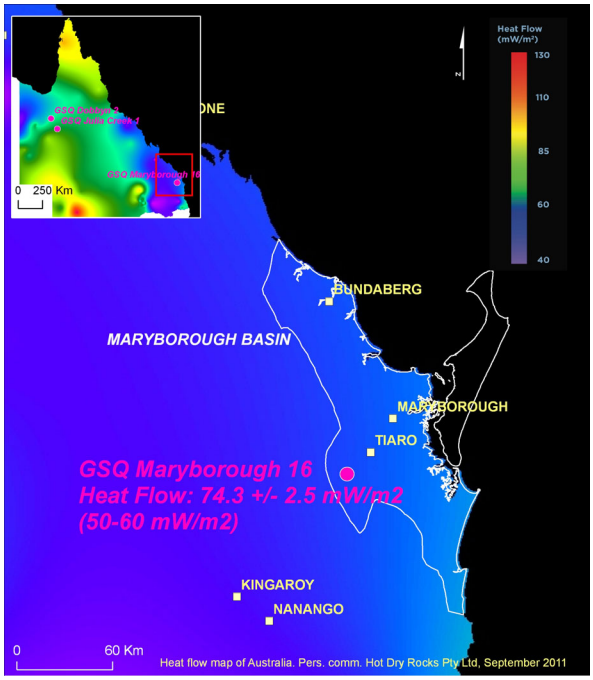

Figure 6: GSQ Maryborough 16 heat flow compared to existing Maryborough Basin heat flow estimates (courtesy of Hot Dry Rocks, 2011)

been estimated at up to 3,370 m towards the east (Korsch et al, 2011).

High heat producing Proterozoic granites which form basement to the Millungera Basin also outcrop to the west (Mount Isa Inlier) and east (Georgetown Inlier and Croydon Province) (Korsch et al, 2011). The heat production values of the Williams and Naraku Batholiths are greater than 5 µW/m3 and could form a considerable heat source at depth. Hot aquifers within the Eromanga and Carpentaria Basins such as the Hooray Sandstone (intersected in GSQ Julia Creek 1) and Gilbert River Formation (not intersected in Dobbyn 2) are also highly prospective with geothermal gradients in the area greater than 60 °C/km (Korsch et al, 2011).

Preliminary data collected by the CGEI program supports the existence of geothermal potential within the Millungera Basin. The proximity of the basin to Mount Isa mining communities improves the economic viability of any development in the future.

Maryborough Basin

Heat flow extrapolations based on previous datasets inferred the heat flow present in the southern Maryborough Basin was between 50-60 mW/m2 (Figure 6), which is considerably lower than 74.3 ± 2.5 mW/m2 modelled for GSQ Maryborough 16. From this heat flow result, a temperature of 202 ± 15 °C was estimated at 5 km.

The excellent insulating capacity of the southern Maryborough Basin is highlighted from the low thermal conductivity values measured from the interbedded sandstones, mudstones and coal units intersected in GSQ Maryborough 16.

Basin insulation capacity increases towards the north due a thickening of the stratigraphy from approximately 1400 m in the south to 7000 m in the north and secondly, the inclusion of additional coal measures up to 3000 m thick (Day et al, 1983).

The potential heat sources in the area are the Late Triassic and Late Jurassic – Early Cretaceous intrusives of the Gympie Block. There are no heat production values available for these intrusives, but recent seismicity could be indicative of a residual heat source remains in the area.

Heat flow modelling was undertaken by GA on a site 33 km north east of GSQ Maryborough 16 (Weber at al, 2011). The heat flow modelled over 204 to 310.7m was 68 +4/-10 mW/m^2. Expanding population and infrastructure demands on the south east corner of Queensland may enable these heat flow values to form the basis of viable geothermal exploration targets.

CGEI Deliverables

A detailed well completion report will be prepared for each CGEI drill hole after all the data for the hole has been received, assessed and interpreted. A final report will also be released, which aims to tie results gathered through the drilling program to a larger basin by basin preliminary prospectivity review.

Future work

Further funding for the program could result in;

- Completion of phase 2 and 3 drilling (20 sites approximately 320 m across Queensland).
- Deeper drilling (2km) within high heat flow areas delineated by Phase 1.
- Targeted geophysical surveying of areas with high geothermal potential.

Conclusions

Phase 1 of the CGEI drilling program is due for completion at the end of the year with further analysis and reporting to follow in 2012. Heat flow modelled for GSQ Dobbyn 2, GSQ Julia Creek 1 and GSQ Maryborough 16 are well above the global crustal heat flow of 60 mW/m2. and temperature extrapolations to 5 km depth for all three sites are above 200°C.

The preliminary heat flow results and temperature extrapolations gathered for this project don't consider complexities which arise with modelling geothermal systems at depth (such as the effect of stress regimes on delineating favourable horizons for reservoir creation and permeability enhancement at depth) but do highlight areas geothermal exploration opportunities closer to population and power consumption areas.

References

Beardsmore, G. R., and Cull, J. P., 2001, Crustal Heat Flow: A Guide to Measurement and Modelling, Cambridge University Press, 324pp.

Cull, J. P., 1982, An appraisal of Australian heat flow data, BMR Journal of Australian Geology and Geophysics 7, p. 11-21.

Day, R.W., Whitaker, W.G., Murray, C.G., Wilson, I.H., Grimes, K.G., 1983, Queensland Geology. A companion volume to the 1:2 500 000 scale geological map (1975). Geological Survey of Queensland. Publication 383.

Fitzell, M., Hamilton, S., Beeston, J., Cranfield, L., Nelson, K., Xavier, C. and Green P., 2009, Approaches for identifying geothermal energy resources in coastal Queensland, in: Budd and Gurgenci (editors), Proceedings of the 2009 Australian Geothermal Energy Conference, Geoscience Australia, Record 2009/35.

Korsch R.J., Struckmeyer H.I.M., Kirkby A., Hutton L.J., Carr L.K., Hoffmann K.L., Chopping R., Roy I.G., Fitzell M., Totterdell J.M., Nicoll M.G. and Talebi B., 2011, Energy potential of the Millungera Basin: A newly discovered basin in north Queensland. APPEA Journal 2011, vol 51, pp 295-332.

Rybach, L., 1989, Heat flow techniques in geothermal exploration, First Break Vol. 7, No.1, p. 9-16.

Talebi, B. Maxwell, M., Sargent, S. and Bowden, S., 2010, Queensland Coastal Geothermal Energy Initiative – An Approach to a Regional Assessment, in: Gurgenci and Weber (editors), Proceedings of the 2010 Australian Geothermal Energy Conference, Geoscience Australia, Record 2010/35.

Weber, R.D., Kirkby, A.L., and Gerner, E.J., 2011, Heat flow determinations for the Australian continent: Release 3. Geoscience Australia Record 2011/30, 60p.

Convection or conduction? Interpreting temperature data from sedimentary basins

Sheldon, H.A.*[1,2], Reid, L.B.[1,2,3], Florio, B.[3] and Kirkby, A.L.[4]
Heather.Sheldon@csiro.au
[1] Western Australian Geothermal Centre of Excellence
[2] CSIRO, PO Box 1130, Bentley WA 6102, Australia
[3] University of Western Australia, 35 Stirling Highway, Crawley WA 6009, Australia
[4] Geoscience Australia, GPO Box 378, Canberra ACT 2601, Australia

Hot groundwater in sedimentary basins can provide geothermal energy for low-temperature direct heat use applications, such as heating swimming pools, heating/cooling of buildings, desalination and industrial pre-heating (Regenauer-Lieb and Horowitz, 2007). The economic viability of geothermal energy projects depends on the depth that must be drilled to reach the required temperature. Thus, a primary goal of geothermal exploration is to identify areas where the geothermal gradient is higher than normal, such that useful temperatures are attained at relatively shallow depth. Our knowledge of temperature in the subsurface comes primarily from temperature measurements in boreholes, which can be interpolated to create a 3D model of temperature distribution. Such models reveal spatial variations in the geothermal gradient, which have traditionally been interpreted in terms of variations in thermal conductivity and basal heat flow, assuming that conduction is the dominant mechanism of heat transport. However, heat transport in sedimentary basins is dominated by advection and/or convection in some areas. The combined effects of advection, convection and conduction cause the temperature gradient to vary laterally and with depth, such that temperature predictions based on extrapolation of shallow geothermal gradients to greater depths may be incorrect. In this study we use borehole temperature measurements in the Perth Basin (Western Australia) and the Cooper Basin (South Australia and Queensland) to reveal spatial variations in the geothermal gradient. We consider whether these patterns are consistent with convection or conduction and discuss the implications for geothermal energy in these basins.

Keywords: convection, conduction, geothermal

Causes of variations in temperature gradient

The vertical temperature gradient in the earth's crust varies laterally and with depth. These variations in temperature gradient are caused by several factors, including variations in mantle heat flow, thermal conductivity, and radiogenic heat production, and the effects of advection and convection.

Advection is transport of heat by fluids moving due to external forces such as topographic head or injection/extraction of groundwater, while convection is fluid flow and heat transport driven by buoyancy due to gradients in fluid density, which in turn are caused by gradients in temperature and salinity. Convection can only occur if the buoyancy force is sufficient to overcome viscous resistance to flow and dissipation of heat by conduction. The competing effects of buoyancy, viscous dissipation and conduction are indicated by a dimensionless parameter known as the Rayleigh number (Ra). For the case of thermal convection (i.e. ignoring salinity gradients) in a uniform horizontal layer of porous rock, Ra is defined as:

$$Ra = \frac{k\alpha\rho_0^2 c_f g H \Delta T}{\mu\lambda} \qquad (1)$$

where k is permeability (m^2), α is the volumetric thermal expansion coefficient of the pore fluid (1/°K), ρ_0 is fluid density (kg/m^3), c_f is the specific heat capacity of the pore fluid (J/kg/K), g is gravity (m/s^2), H is the thickness of the layer (m), ΔT is the temperature difference between top and bottom of the layer (K), μ is fluid viscosity (Pa s), and λ is the effective thermal conductivity of the fluid-saturated rock (W/m/K) (Horton and Rogers, 1945; Lapwood, 1948). Ra must exceed a critical value for convection to take place, with the critical value depending on the boundary conditions at the top and bottom of the layer (Nield and Bejan, 1992). Thus, convection is most likely to occur in thick, highly permeable units such as aquifers.

Figure 1A shows the effect of varying thermal conductivity on temperature gradient in the absence of convection. Layers of relatively low thermal conductivity (e.g. shale) have a steeper thermal gradient than layers of higher thermal conductivity (e.g. sandstone). In Figure 1A, the top and bottom layers could be shale and the middle layer could be sandstone. The dashed line in Figure 1A illustrates the effect of advective heat

transport due to horizontal flow in part of the middle layer, e.g. due to meteoric recharge or groundwater extraction from an aquifer.

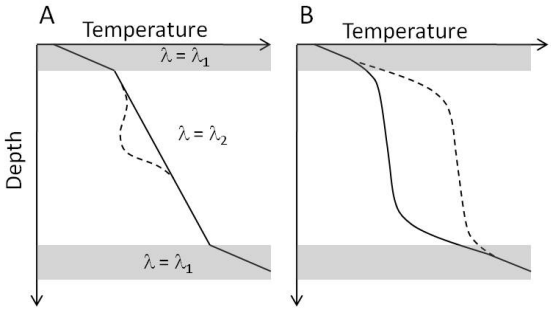

Figure 1: Temperature profiles associated with different modes of heat transport. (A) Conductive profile through three layers with two different values of thermal conductivity (λ). Dashed line shows influence of advective heat transport due to horizontal fluid flow in the middle layer. (B) Profiles through convective upwelling (dashed line) and downwelling (solid line), where convection is occurring in the middle layer.

Convection is characterised by a series of convection cells linking regions of hot, upwelling fluid with regions of cold, downwelling fluid (Fig. 2). In upwelling regions the temperature gradient changes from steep to shallow with increasing depth, whereas in downwelling regions the gradient changes from shallow to steep (Fig. 1B). Attempting to predict the temperature at the base of the aquifer in Figure 2 from the shallow temperature gradient at point A would result in an erroneously high value. Note also the different impact of drilling into an upwelling or a downwelling depending on the target temperature. If one was targeting a temperature of 60 °C the drilling cost would be considerably different at points A and B (Fig. 2). Conversely, there would be less difference in cost between these two locations if one was targeting 50 or 70 °C. Clearly it is important to understand the thermal regime in the subsurface in order to identify and assess the economic potential of geothermal resources.

Temperature gradient in the North Perth Basin

Bottom-hole temperatures (BHTs) from petroleum and water wells can be used to estimate the average geothermal gradient in each well, by applying appropriate corrections to the BHTs (e.g. Facer, 1991) and assuming some appropriate constant value of temperature at the ground surface. Mory and Iasky (1996) listed corrected BHTs and surface temperatures for 93 petroleum and 33 water wells in the North Perth Basin. We used these values to calculate an average geothermal gradient at each well and interpolated horizontally with an inverse distance algorithm with a radius of influence of 50 km to produce a map of average vertical temperature gradient (Fig. 3).

The calculated temperature gradient ranges from 15 to 50 °C/km, with a median value of 28.8 °C/km, a mean of 30.0 °C/km and a standard deviation of 7.6 °C/km. Accuracy and uncertainty of the calculated temperature gradients is limited by the accuracy and uncertainty of the corrected BHTs, which depends on many factors and is difficult to quantify (Facer, 1991). However, if the error is similar for all wells we can assume that the patterns that are observed in the calculated temperature gradient are qualitatively correct.

The map (Fig. 3) reveals patterning in the temperature gradient on several scales. Firstly, there is a general increase towards the northwest, where granitic basement is shallower. Superimposed on this trend are some smaller-scale variations, notably around Dongara, Eneabba, and between Cervantes and Green Head. The spacing between thermal highs and lows in these areas is ~10 to 30 km. For example, there is a thermal low at Jurien Bay (temperature gradient ~25 °C/km) with thermal highs located approximately 20 km to the east (temperature gradient ~35 °C/km) and to the north (temperature gradient ~45 °C/km).

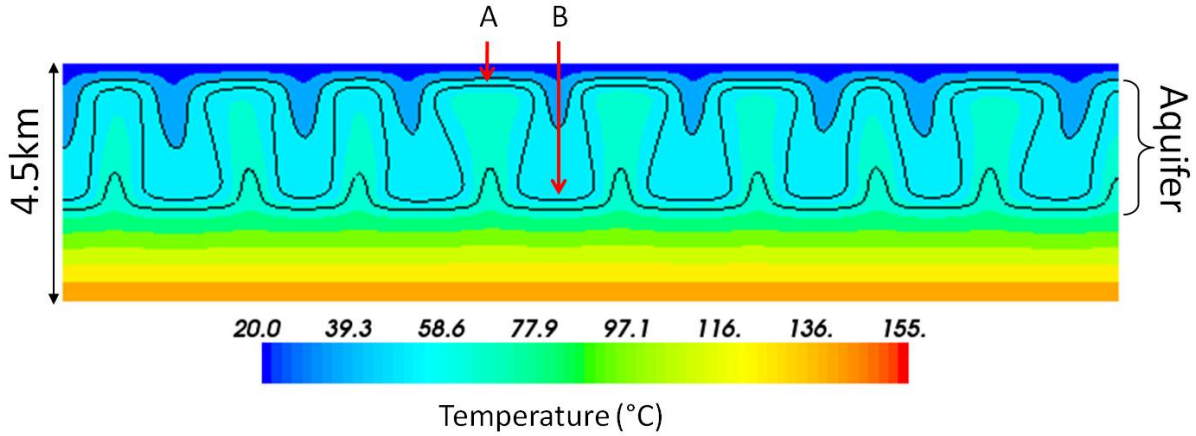

Figure 2: Hypothetical temperature distribution due to convection in a buried aquifer. The aquifer is bounded above and below by low-permeability units, representing shales or siltstones. Black lines highlight 50, 60 and 70°C isotherms. Note difference in depth, and therefore drilling cost, of 60°C isotherm in an upwelling (point A) and a downwelling (point B).

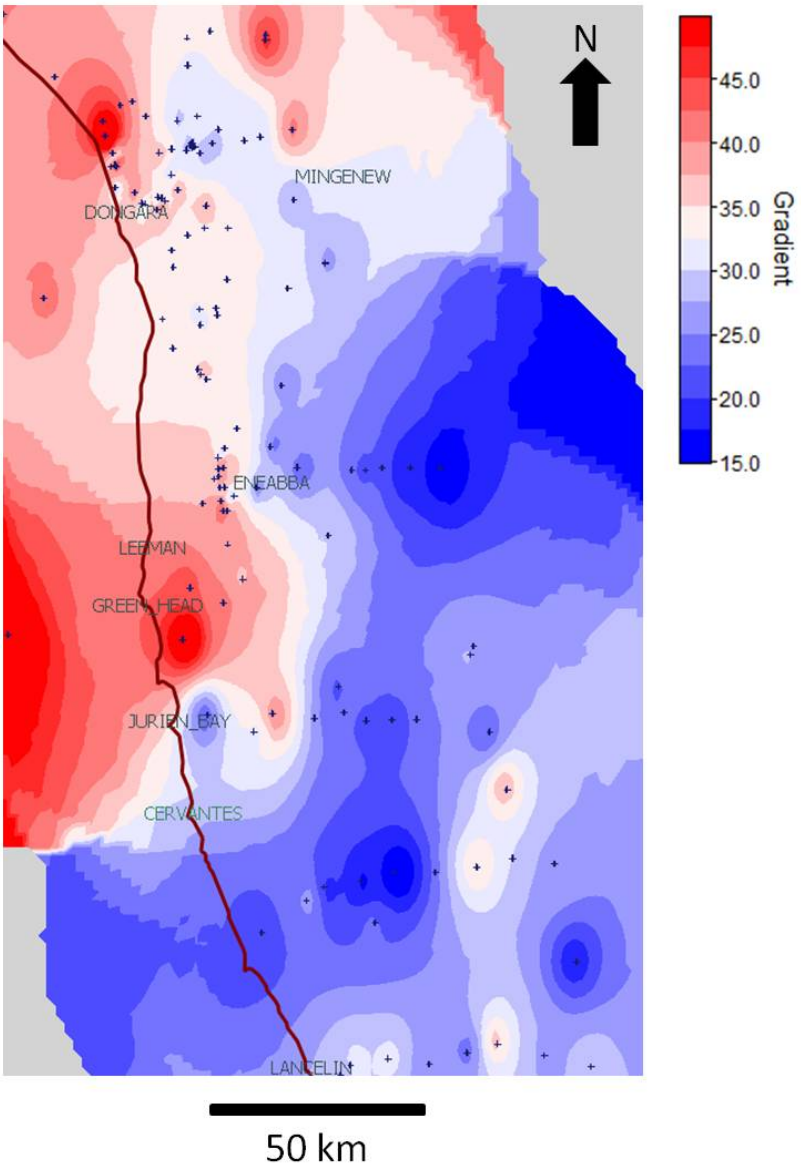

Figure 3: Average temperature gradient interpolated from wells in the North Perth Basin. Well locations indicated by crosses.

While some of the patterns in Figure 3 may be artefacts related to the contouring algorithm, sparsity of data and errors in corrected BHTs, some of the variations are likely to be real. In particular, we have confidence in the patterning observed in the Dongara region due to the high density of petroleum wells there. Variations in thermal conductivity and thickness of lithological units can account for some of the variation in calculated temperature gradients, but convection could be contributing to the thermal patterning in some areas. Variation of temperature gradient in the Dongara region was highlighted previously by Horowitz et al. (2008), who also suggested it could be due to convection.

We now use the theory of convection in porous media to assess whether the patterning shown in Figure 3 is consistent with convection in a permeable aquifer. In doing this we acknowledge that the convection theory applies to simple, homogeneous systems with uniform boundary conditions, which are not an accurate representation of the complexity in real sedimentary basins. This limitation is discussed further below.

According to Phillips (1991), the spacing of convection cells in a horizontal homogeneous layer with anisotropic permeability is:

$$W = H\left(k_H / k_V\right)^{0.25} \qquad (2)$$

where W is the width of convection cells (i.e. the distance between thermal highs and thermal lows), H is the thickness of the layer, and k_H and k_V are the horizontal and vertical permeabilities of the layer. The ratio k_H/k_V is described as the permeability anisotropy ratio. Sedimentary aquifers typically have $k_H/k_V >> 1$ due to the occurrence of sub-horizontal low-permeability layers within the aquifer (e.g. lenses of shale or siltstone); hence Equation 2 predicts W > H.

Figure 4 shows the expected convection cell width in a horizontal homogeneous aquifer as a function of k_H/k_V for aquifer thicknesses of 2 and 3 km. These thicknesses are representative for major aquifers in the Perth Basin (Davidson, 1995; Mory and Iasky, 1996). The permeability anisotropy ratio of an aquifer depends on the thickness, permeability and lateral continuity of layers within the aquifer. Accurate assessment of the anisotropy ratio of aquifers in the Perth Basin is beyond the scope of the present study. However, representative values can be obtained by assuming the aquifer comprises a series of continuous horizontal layers, each with uniform thickness and constant isotropic permeability. Then the average horizontal and vertical permeabilities of the aquifer are given by the arithmetic and harmonic means of the layer permeabilities, respectively (Renard and deMarsily, 1997). For example, an aquifer comprising alternating layers of sandstone and shale with thicknesses of 1 m and 0.1 m and permeabilities of 1000 mD and 0.01 mD, respectively, has an anisotropy ratio of 8265. This would result in a convection cell width of 19.0 km in a 2 km thick aquifer, and 28.6 km in a 3 km thick aquifer. Thus, the observed spacing between highs and lows in the temperature gradient map (~10-30 km; see Fig. 3) is consistent with expected convection cell widths in a homogeneous aquifer with anisotropic permeability.

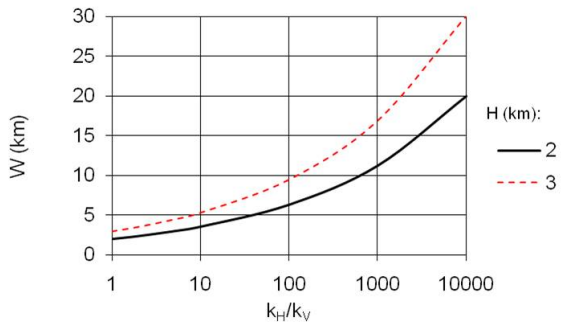

Figure 4: Width (W) of convection cells in a homogeneous horizontal aquifer as a function of aquifer thickness (H) and permeability anisotropy ratio (k_H/k_V).

Another aspect of the data that can be compared with convection theory is the range of values of the temperature gradient. For the case of convection in a horizontal homogeneous layer with fixed temperature and impermeable boundaries at the top and base, the vertical temperature gradient is given by:

$$\frac{\partial T}{\partial z} = \frac{\Delta T}{H}\left(4\pi\frac{\sqrt{Ra - Ra^*}}{Ra}\cos\left(\pi\frac{z}{H}\right)\cos\left(\pi\frac{x}{H}\right) - 1\right) \quad (3)$$

where ΔT is the temperature difference across the layer, z = 0 at the base of the layer, z = H at the top of the layer, x is horizontal distance along the layer, Ra is the Rayleigh number and $Ra^* = 4\pi^2$ is the critical Rayleigh number. Convection occurs when $Ra \geq Ra^*$.

Equation 3 has maxima and minima at $Ra = 2Ra^*$, with the minimum being 0 and the maximum being $2\Delta T/H$. In other words, the largest vertical temperature gradient that can be attained within a convecting layer is twice the temperature gradient across the whole layer. Thus, for an average temperature gradient of 30 °C/km we would expect gradients ranging from 0 to 60 °C/km within a convecting layer. This prediction is consistent with the range of values shown in Figure 3.

Discussion

It was noted previously that the theoretical analysis of convection that has been used in this study is based on a simple, homogeneous system, which is not a good representation of a real aquifer in a sedimentary basin. In particular, permeability typically varies over several orders of magnitude within aquifers, due to interbedding of fine-grained low-permeability rocks with coarser-grained, high-permeability rocks. The average or effective permeability of such layered systems can be calculated, but the relevance of using such average values to assess the potential for convection has been questioned (Simmons et al., 2001). Also, the size, shape and location of convection cells in a real aquifer would be influenced by geometric features of the basin, such as folds and faults. Nonetheless, the analysis presented here is useful as a first-pass attempt at assessing whether the temperature data are consistent with convection.

Conclusion

We have shown that the pattern of vertical temperature gradients inferred from borehole temperatures in the North Perth Basin is consistent with convection, at least in terms of the observed spacing of thermal highs and lows (interpreted as convective upwellings and downwellings) and the observed range of temperature gradients. To explain this pattern through conduction alone would require large variations in thermal conductivity within and between lithostratigraphic units. To assess whether such variations in thermal conductivity are reasonable is beyond the scope of the present study. For now we conclude that the observed temperature distribution is consistent with convection, and thus care must be taken in extrapolating shallow thermal gradients to predict temperatures beyond the limits of borehole data. In particular, if a geothermal target (i.e. an area of high geothermal gradient at the surface) represents a convective upwelling, there is little to be gained by drilling beyond the inflection point in the temperature-depth profile (see Fig. 1B).

We intend to conduct a similar analysis of temperature gradients in the Cooper Basin and will report our findings at the conference.

Acknowledgments

The Western Australian Geothermal Centre of Excellence (WAGCOE) is a collaboration between CSIRO, the University of Western Australia and Curtin University. WAGCOE is funded by the government of Western Australia.

References

Davidson, W.A., 1995, Hydrogeology and groundwater resources of the Perth region, Western Australia: Geological Survey of Western Australia Bulletin 142, 270p.

Facer, R.A., 1991, Temperature corrections for bore hole data as part of thermal state, source and maturation investigations of basins: Exploration Geophysics, v. 22, p. 567-574.

Horowitz, F.G., Regenauer-Lieb, K., Wellmann, J.F., Chua, H.T., Wang, X., and Poulet, T., 2008, Evidence for Hydrothermal Convection in the Perth Basin, Australia, in Gurgenci, H., and Budd, A.R., eds., Proceedings of the Sir Mark Oliphant International Frontiers of Science and Technology Australian Geothermal Energy Conference: Geoscience Australia Record 2008/18, p. 85-87.

Horton, C.W., and Rogers, F.T., 1945, Convection currents in a porous medium: Journal of Applied Physics, v. 16, p. 367-370.

Lapwood, E.R., 1948, Convection of a fluid in a porous medium: Proceedings of the Cambridge Philosophical Society, v. 44, p. 508-521.

Mory, A.J., and Iasky, R.P., 1996, Stratigraphy and structure of the onshore northern Perth Basin, Western Australia: Western Australia Geological Survey Report 46.

Nield, D.A., and Bejan, A., 1992, Convection in porous media: New York, Springer-Verlag, 408 p.

Phillips, O.M., 1991, Flow and reactions in permeable rocks: Cambridge, Cambridge University Press, 285 p.

Regenauer-Lieb, K., and Horowitz, F.G., 2007, The Perth Basin geothermal opportunity: Petroleum in Western Australia, Western Australia's Digest of Petroleum Exploration, Development and Production, September 2007, p. 42-44.

Renard, P., and deMarsily, G., 1997, Calculating equivalent permeability: A review: Advances in Water Resources, v. 20, p. 253-278.

Simmons, C.T., Fenstemaker, T.R., and Sharp, J.M., 2001, Variable-density groundwater flow and solute transport in heterogeneous porous media: approaches, resolutions and future challenges: Journal of Contaminant Hydrology, v. 52, p. 245-275.

A new database compilation of whole-rock chemical and geochronological data of igneous rocks in Queensland: A new resource for HDR geothermal resource exploration.

C.Siegel[1], S. Bryan[1], D. Purdy[2], D. Gust[1], C.Allen[3], T.Uysal[4], and D. Champion[5]
c.siegel@qut.edu.au
[1] Biogeoscience, Queensland University of Technology, GPO Box 2434 Brisbane QLD 4001
[2] Geological Survey of Queensland, PO Box 15261 City East QLD 4002
[3] Research School of Earth Sciences, Australian National University Canberra ACT 2601
[4] QGECE, The University of Queensland, St Lucia Brisbane QLD 4072
[5] Geoscience Australia, GPO Box 378 Canberra ACT 2601

The Geothermal industry in Australia and Queensland is in its infancy and for hot dry rock (HDR) geothermal energy, it is very much in the target identification and resource definition stages. As a key effort to assist the geothermal industry and exploration for HDR in Queensland, we are developing a comprehensive and new integrated geochemical and geochronological database on igneous rocks. To date, around 18,000 igneous rocks have been analysed across Queensland for chemical and/or age information. However, these data currently reside in a number of disparate datasets (e.g., Ozchron, Champion et al., 2007, Geological Survey of Queensland, journal publications, and unpublished university theses). The goal of this project is to collate and integrate these data on Queensland igneous rocks to improve our understanding of high heat producing granites in Queensland, in terms of their distribution (particularly in the subsurface), dimensions, ages, and controlling factors in their genesis.

Keywords: High heat producing granites (HHPG), Queensland, database compilation, whole-rock chemistry, geochronology, tectonic setting.

Introduction

The elevated crustal heat flows for significant parts of the Australian continent (e.g., McLaren et al., 2005; McLaren, 2008) reveal the potential for HDR. However, surface heat flow and crustal temperature maps (Chopra and Holgate, 2005), which underpin current approaches to define HDR resources, are poorly defined. It is widely acknowledged that heat flow data has limited spatial coverage, particularly over large regions of Queensland (Figure 1). Despite these lack of data, Queensland hosts enormous volumes of igneous rocks. Exposure at the surface exceeds 175,000 km^2, including a large proportion of granitic material, where heat flow data is nonexistent (Figure 1). Queensland also has widespread and thick sedimentary basin successions, providing significant potential for the thermal insulation of buried igneous rocks.

On a broader scale, geologic knowledge of the "heat engine" associated with geothermal energy systems is limited and an improved understanding is crucial to improve our ability to locate and define HDR resources for engineered geothermal systems (EGS). A compounding problem is that although high concentrations of radiogenic elements, and therefore high heat production, is exclusively found in igneous rocks with high silica contents (>70% SiO_2, Figure 2), not all high-silica igneous rocks are high heat producing. The observed extreme variation in calculated heat production for igneous rocks in Queensland (and globally), from ~0 to 25 $\mu W/m^3$ (Figure 2), thus raises the following questions: Why are some granites high heat producing and others not? Where are HHPG located in Queensland? Why are they located in those areas? When and how were they generated? And what has caused anomalous enrichments in heat producing elements?

Data sources

Over the last 50 years, many conventional studies of granitic rocks, generally focussing on their general mineralogical and compositional characteristics, have been undertaken to understand source rock compositions, igneous processes and associations with mineralisation. A renewed interest and new focus on granitic rocks in terms of their heat generating capacity has resulted from the development of EGS. Consequently, a substantial database exists on the mineralogy, chemistry and age of granitic rocks (in Queensland), that can be reassessed and utilised for HHPG identification and targeting. The main datasets (Table 1) include:

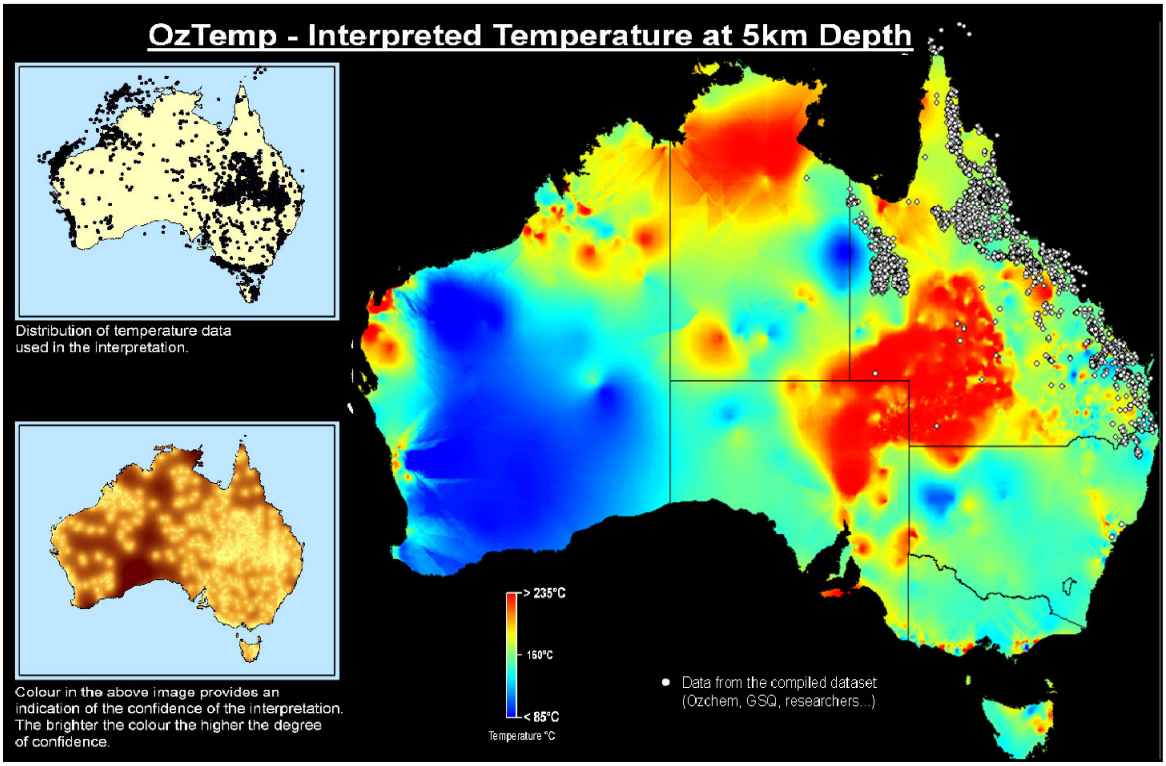

Figure 1. Interpreted temperature map at 5 km depth in Australia. Insert map shows locations of boreholes from which temperature measurements were made (from Geoscience Australia). Data points on main map are locations of whole-rock chemical data for igneous rocks in the compiled database for Queensland.

- Geoscience Australia: Ozchem (Champion et al., 2007) and an updated whole-rock chemical database for igneous rocks from North Queensland (due for public release in 2011), and Ozchron that contains geochronological information;
- Geological Survey of Queensland (GSQ): GSQ geochem and GSQ geochron and GA-GSQ-SHRIMP, a geochronology dataset based on collaborative projects between Geoscience Australia and the GSQ. These datasets are not publically available and access was made through collaboration with the GSQ.
- Published and unpublished datasets from several researchers
- A New England Fold Belt Age Database (unpublished) compiled by Associate Professor Rod Holcombe and co-workers from the University of Queensland
- A dataset of University of Queensland theses currently being compiled by Dr. Maria Mostert (School of Earth Sciences, UQ).
- New data generated by PhD projects currently underway within the QGECE.

Data type

The compiled dataset comprises two types of data: original data created by the collector or analyser and new data generated by the compiler from the original data. The generated data are significant and provide more relevant information for HHPG exploration (e.g. calculated heat production capacity).

Original data

The original data comprise 4 main groups of information:

- Sample description - Sample number(s), geological province, unit name, lithology, data source
- Location information - Coordinates, system, site description
- Chemistry (85 columns) - Major and trace elements, methods, laboratory
- Age information - radiometric, stratigraphic, methods, laboratory

Generated data

In the new database, major element geochemical data are normalised to 100% on an anhydrous basis. Additionally, several reference columns are added and all data are assigned an igneous event association number (Table 2). The igneous event association number relates igneous units to the main igneous events in Queensland (focussing on the Phanerozoic), which can then be related to tectonic setting. This igneous event association attribute is crucial to visualize and understand the different episodes of granite generation in Queensland. Heat production for all

Table 1: Major geochemical and geochronological datasets compiled in this study

Source	Number of igneous data	Location/Comments
Ozchem	~7250	Queensland
GSQchem	~8400	Queensland
North Queensland	~1780	Queensland
Dr. Bruce Chappell	~1270	New England Orogen (South QLD and North NSW)
Dr. Bruce Chappell	12	South-West QLD
GA-GSQ-Chem	~50	Queensland
Ozchron	~100	Queensland
GSQchron	~1000	Queensland
GA-GSQ-SHRIMP	~50	Queensland
Compiled dataset; Dr. Rod Holcombe	~560	East Queensland
Dr. Scott Bryan	~350	Whitsunday Islands, Campwyns and Yarrol
Dr. Charlotte Allen	~60	Bowen area
Prof. David Gust	~1000	Queensland
Compiled dataset;		
Dr. Maria Mostert	~2000	Queensland
Total	~23880	Includes many duplicates
Compiled dataset	~18000	Estimated <100 duplicates remain

igneous rocks is also calculated using the equation of Rybach (1988) and will supplement measurements of heat conduction on a subset of granitic rocks. Additional calculations to provide source and process-related information on the igneous rocks are also included in the new database (e.g., ASI, Fe number, Zr saturation temperature to distinguish "hot" and "cold" granites, Miller et al., 2003; Watson et al., 2006). Following database compilation and new data generation, a GIS study combining igneous event associations and heat production values of igneous rocks will be investigated to constrain the location, timing and setting of HHPG in Queensland.

Database issues encountered

A critical first-step has been to merge the different datasets (Table 1) into one single coherent database. Data integrity and consistency have been identified in this study as major issues; datasets commonly have vastly different contents and layouts (i.e. headers, unit of measurements, typography, etc), as well as some duplication. In this study, significant errors in the location information were revealed in the major national dataset: Ozchem (Champion et al., 2007). The locations are now corrected in Ozchem, Ozchron

Table 2. Summary of the main igneous events in Queensland that form the basis for grouping data in the compiled database and identifying tectonic associations

Igneous Event	Time Period (age range)	General Composition	Province Example
0	Proterozoic (>600 Ma)	Mafic to silicic	Mount Isa, Etheridge, Croydon
1	Neoproterozoic (~600-540 Ma)	Basaltic oceanic crust	Marlborough (central Queensland)
2	Cambrian-Ordovician (540-450 Ma)	?Mafic to silicic	North and western QLD
3	Silurian-Early Devonian (450-400 Ma)	Mafic to silicic	Lolworth Block, North QLD (Pama province), western QLD
4	Middle Devonian (400-380 Ma)	Silicic	Yarrol, Mt Morgan, Thompson/Drummond
5	early Late Devonian (380-365 Ma)	Mafic	Yarrol-Campwyn, Drummond
6	Late Devonian-Early Carboniferous (365-340 Ma)	Silicic	Yarrol-Campwyn, Drummond, North Queensland, Roma Shelf
7	Permo-Carboniferous (330-270 Ma)	Silicic to bimodal in Early Permian	Eastern Queensland (Kennedy-Connors-Auburn)
8	Permo-Triassic (260-230 Ma)	Mafic-intermediate	Eastern Queensland
9	Late Triassic (230-210 Ma)	Silicic to bimodal	Eastern Queensland
10	Jurassic (200-140 Ma)	Bimodal (rare)	Offshore and Eastern Queensland
11	Early Cretaceous (135-95 Ma)	Silicic to bimodal	Eastern Queensland (Whitsunday)
12	Late Cretaceous-Tertiary (80-0 Ma)	Mafic alkaline intraplate (weakly bimodal)	Eastern Queensland

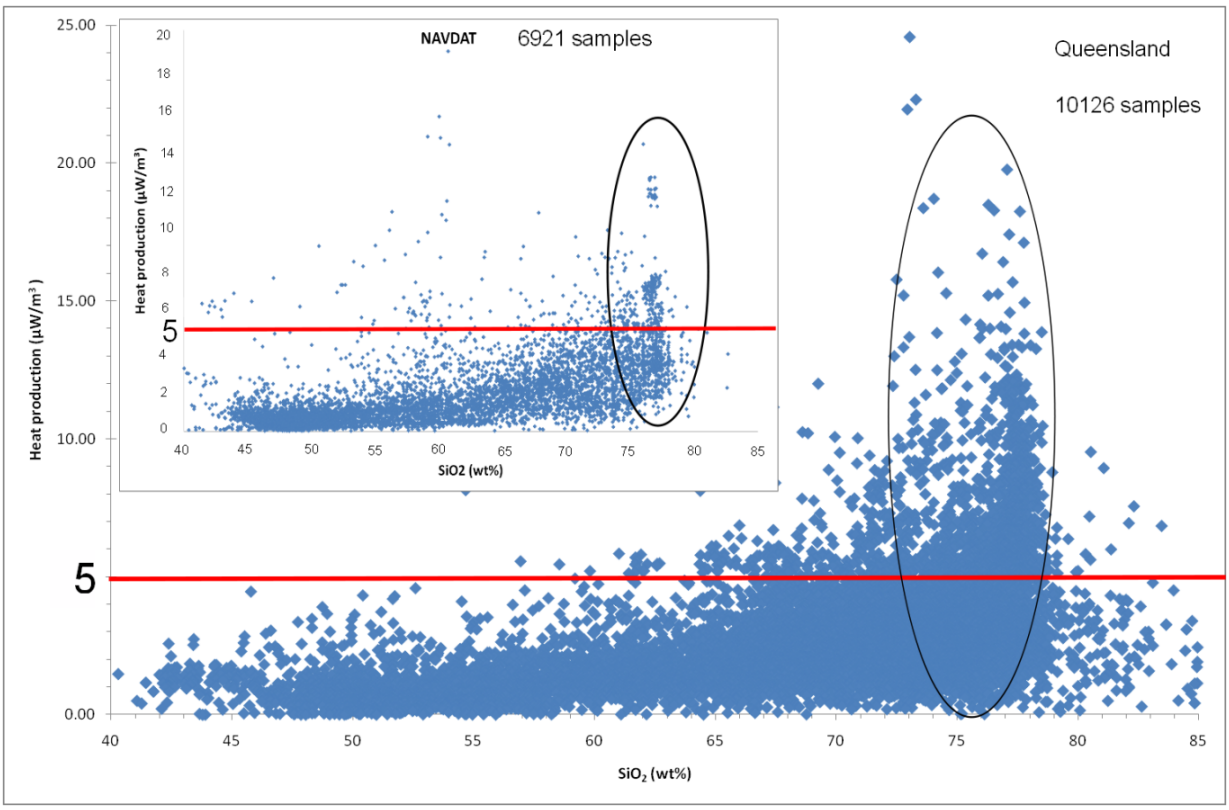

Figure 2: Heat production values versus SiO_2 content (anhydrous) for igneous rocks in Queensland. The inset graph illustrates the 6,921 Mesozoic to Cenozoic igneous rock data from western North America, extracted from the NAVDAT database (publically available online). The main graph displays 10,126 igneous rock data from the compiled database. The red line at a heat production value of 5 µW/m^3 is used to distinguish Low (below) and High Heat Producing Granites (above). The circled region shows the large spectrum of heat production values for igneous rocks with silica contents between ~73-78 wt %.

and the compiled dataset. Further errors were encountered in chemical data (e.g., incorrect Hf and Ta values and missing trace elements in the GSQ whole-rock chemical dataset). The compilation task, which was initially considered straightforward, has benefited from the duplication of data in different datasets to identify and correct errors. Collaboration with Geoscience Australia and the Geological Survey of Queensland has greatly assisted this correction effort.

Data quality

As the compiled dataset includes a large number of analysis (~18 000), it is expected that some data will contain errors and/or be of poor quality (e.g., altered samples, poor analytical precision, limited element analysis). These data will be flagged and retained in the compiled dataset. It is important to ensure integrity of the database and allow the different datasets to be meaningfully combined and compared. Steps to assess data quality include:

- Identification of anomalous chemistry (e.g., SiO2 values <40 wt% or >80 wt%; high Loss of ignition - LOI) via chemical plots. Sample description information can then be re-examined for anomalous data to assess degree of alteration or analytical issues.
  Samples without location coordinates have been removed from the compiled database.
- Location errors have been checked and corrected mostly through re-examination of the original data sources comparing duplicated data and visualisation using ArcGIS and other software (e.g., Google Earth).
- Collating information on the material dated (e.g., mineral, whole-rock) and technique (e.g., K/Ar, U/Pb, Ar/Ar) used to obtain radiometric age information so that potential resetting of emplacement ages can be assessed – this is a particular problem for eastern Queensland for example, where Cretaceous heating has resulted in the partial to complete resetting of the K/Ar system, yielding spurious ages (e.g., Allen et al., 1998).

Once the compiled dataset has been completed, the goal is to then interrogate it using GIS techniques (e.g., ArcGIS software) to examine spatial-temporal relationships of HHPG and granitic magmatism in QLD.

Discussion

High heat producing granites (i.e. granites with a heat production value greater than 5 µW/m3, Blevin, 2009; Hutton et al. 2010), will be an important contributor to producing the high thermal gradients required to make EGS viable. It

is widely recognised that these values characterise the high silica igneous rocks or granites (Blevin, 2009; Hutton et al., 2010; Huston et al., 2010). This is confirmed by an assessment of igneous rock compositions from Queensland compiled in the new dataset (Figure 2) that illustrates igneous rocks with high heat production values have silica (SiO_2) contents >70 wt% (Figure 2). Interestingly, in comparison, the North American Volcanic and Intrusive Rock database (NAVDAT) shows a similar trend (Figure 2) suggesting that this is likely a global pattern. Granites and HHPG in Queensland are therefore representative of other continental regions around the world and understanding their formation can have global applications to understanding the origin of HHPG.

A second significant feature of Figure 2 is that an extreme variation in heat producing capacity from ~0 to 25 μW/m^3 exists for the granitic rocks (SiO_2 >70 wt%) in Queensland. Consequently, a large percentage of granitic rocks are not HHPG. Only ~20% and ~5% of granitic rocks in Queensland have calculated heat production values greater than 5 μW/m^3 and 8 μW/m^3, respectively.

The compiled dataset has also allowed identification of some elevated heat producing granite suites. Figure 2 demonstrates at least one heat-producing element enriched granite suite with a peak at ~77 wt% SiO_2. This suite shows relatively higher U enrichment over Th, and ASI values of 1-1.1 implying a significant contribution from highly fractionated I-type granitic rocks, often with an A-type chemistry (e.g., O'Briens Creek). Highly enriched S-type granitic rocks from North Queensland also contribute to this range of high heat production values. A less distinct suite at 64-69 wt% SiO_2 with heat production values of 5 to <10 μW/m^3, moderate Th enrichment and no U enrichment corresponds to low-volume, fractionated, alkaline (A-type) Tertiary igneous rocks.

Further interrogation of the compiled dataset reveals that most HHPG in the database occur in the Mount Isa, Georgetown Inlier and Texas-Stanthorpe provinces. The Proterozoic HHPG from Mount Isa are characterised by high Th/U ratio (>5) whereas other suites (e.g., Permo-Carboniferous HHPG S-type of the Georgetown Inlier) have lower Th/U ratios (<1). HHPG in the Georgetown Inlier can be subdivided into two groups, the Proterozoic S-type HHPG from the Etheridge/Croydon provinces and the Permo-Carboniferous I- and S-types HHPG from the Kennedy province. HHPG from the Texas area are Permo-Triassic I-type and are mostly represented by the Stanthorpe Supersuite. Further studies will be undertaken in the next year to better understand the causes of HPE enrichment, as well as assessing the location, age, chemistry, tectonic setting and relationships of other potential but less well-studied HHPG suites (especially in the subsurface in SW QLD), in order to characterize their spatial-temporal distribution. The interrogation of the compiled database through graphs, calculations, and GIS will allow the characterisation of the granite suites existing in Queensland and in particular, the granite suites that are characterized by high U, Th and K_2O and thus high heat production and potential for EGS.

Additionally, new data on South-West QLD granites, that are co-incident with a major crustal heat flow anomaly (Fig. 1), indicate only moderate enrichments of U and Th and consequently, moderate heat production (~2-4 μW/m^3) values. These data suggest that thick and highly efficient thermal blanketing by sedimentary cover may be as or more important in generating the elevated temperatures in the subsurface for exploitation by EGS.

Conclusions

A new compilation dataset of igneous rocks in QLD is a crucial tool in exploring HDR geothermal resources. Its interrogation using GIS techniques will provide insight into the distribution, age and chemistry of HHPG in QLD. Globally, HHPG are characterised by high silica contents (70-85 wt%). Existing data indicate significant areas of HHPG in the Mount Isa, Georgetown Inlier and Texas-Stanthorpe regions. Some HHPG are indicated for the Cambrian-Silurian, Cretaceous and Cenozoic periods and further studies are required to assess their potential for EGS. The presence of moderate heat producing granites in South-West QLD associated with a thick sedimentary cover indicates that the elevated subsurface crustal temperatures in this region may owe its origin more to highly efficient thermal insulation rather than significant volumes of buried HHPG.

References

Allen, C. M., I. S. Williams, C. J. Stephens and C. R. Fielding (1998). "Granite genesis and basin formation in

an extensional setting: the magmatic history of the northernmost New England Orogen." Australian Journal of Earth Sciences 45(6): 875-888.

Blevin, P. (2009). Granites and mineral deposits in NSW, Sydney Mineral Exploration Discussion Group.

Champion, D. C., A. Budd and L. Wyborn (2007). OZCHEM National Whole-Rock Geochemistry Database., Geoscience Australia, http://www.ga.gov.au/meta/ANZCW0703011055.html.

Chopra, P. and F. Holgate (2005). "A GIS Analysis of Temperature in the Australian Crust." Proceedings World Geothermal Congress Antalya, Turkey, 24-29 April 2005.

Hutton, L., I. Withnall, T. Denaro, S. Sergent, J. Beeston, J. Tang (2010). Updating the North-West Queensland

Mineral and Energy Province Study Report. Digging Deeper 8 seminar. G. S. Q. Queensland. Brisbane. Queensland Geological Record 2010/04: 3-10.

McLaren, S. (2008). "Hot Southern Land." Australasian Science 29(7): 25.

McLaren, S., M. Sandiford and R. Powell (2005). "Contrasting styles of Proterozoic crustal evolution: A hot-plate tectonic model for Australian terranes." Geology 33(8): 673-676.

Miller, C. F., S. M. McDowell and R.W. Mapes (2003). "Hot and cold granites? Implications of zircon saturation temperatures and preservation of inheritance." Geology 31(6): 529-532.

Rybach, L. (1988). “Determination of heat production rate.” Handbook of Terrestrial Heat-Flow Density Determination. R. Haenel, L. Rybach and L. Stegena, Kluwer: 125-142.

Watson, E. B., D. A. Wark and J. B. Thomas (2006). "Crystallization thermometers for zircon and rutile." Contributions to Mineralogy and Petrology 151(4): 413-433.

Geothermal Energy Pile: Thermal cum Static Load Testing

Singh, R.M. [1]*, Bouazza, A.[1], Wang, B.[1],Barry-Macaulay, D.[1],Haberfield, C.[2], Baycan, S.[3] and Carden, Y.[4]
Rao.Singh@monash.edu
[1]Monash University, Department of Civil Engineering, Building 60, Clayton Campus, Vic. 3800
[2] Golder Associates Pty. Ltd., Botannica Corporate Park, Richmond, Vic. 3121
[3] Vibropile Pty. Ltd., Building 4, 540 Springvale Rd, Glen Waverley,Vic 3150
[4] Geoexchange Australia Pty.Ltd., 100 Walker Street, North Sydney, NSW 2060

This paper presents the first ever large scale field study undertaken in Australia on Geothermal Energy Pile. The Geomechanics Research Group at Monash University is currently leading the study in this specific research area in Australia. A fully instrumented large scale Geothermal Energy Pile has been installed and transient temperature, strain and stress measurements are continuously recorded via an automated data acquisition system. The main objective of this study is to explore the potential of pile foundation to extract heat from the ground during winter and to store it in the ground during summer. This research also looks into the effect of heating and cooling on load capacity of pile and soil-structure interaction. The fully instrumented pile is being subjected to thermal-mechanical loads. The thermal load is applied by a heat pump while a load cell also known as Osterberg cell is employed to apply the static mechanical load. Apart from the field scale study, a detailed experimental research is also being carried out to evaluate the thermal and mechanical properties of various Victorian soils using thermo-consolidation and thermo-triaxial testing. Cost-benefit analysis is being performed to compare the conventional heating/cooling system and the Geothermal Energy Pile system. This paper presents a summary of all the research activities on the Geothermal Energy Pile performed at Monash University and shares some important information observed to date.

Keywords: Geothermal Energy Pile, thermal load, static mechanical load, Load cell (Osterberg cell), thermo-consolidation, thermo-triaxial, heat pump.

Introduction

Earth contains enormous amount of heat energy also called Geothermal Energy which can be utilised not only for power generation but also for space heating and cooling. There are two types of geothermal energy viz. deep and shallow. The deep geothermal energy is found at few kilometres beneath the ground while the shallow geothermal energy is available just beneath the ground surface within top 50 m. The deep geothermal energy is generated due to radioactivity in the earth core. The shallow geothermal energy is the heat energy coming from the sun in the form of solar radiation which is absorbed by the ground every day. The deep geothermal energy is being harnessed for electricity/power generation while the benefits of shallow geothermal energy are less publicised especially in Australia. Shallow ground energy is stable throughout the year and can be used for heating and cooling built structures. Shallow ground energy is not unknown to mankind, thousands of years ago human started to use underground caves to avoid extreme outside temperatures during winter and summer. The ground temperature is constant irrespective of air temperature therefore the ground can be used as a heat source and heat sink during winter and summer respectively.

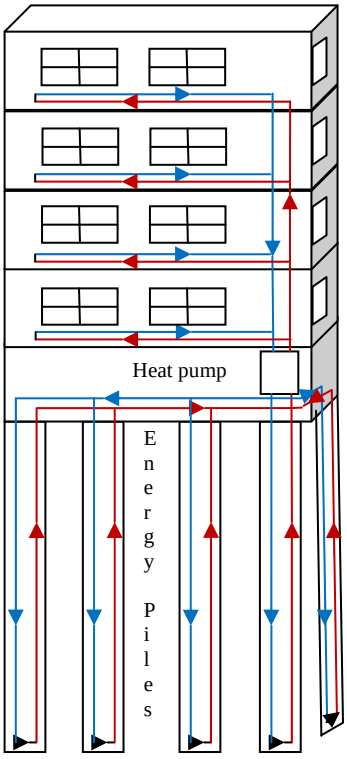

Figure 1: Geothermal Energy Pile

A geothermal energy pile is a pile foundation of a built structure (e.g. tall buildings, heavy structures, etc.) which extracts shallow ground energy via heat pump for heating the built structure during winter, the cycle can be reversed during summer and heat collected from the built structure can stored in the ground (Figure 1). The energy pile is

similar to vertical bore ground-source heat pump (GSHP) systems. The difference is pile foundation serves as an integral support part to the super-structure in addition to heating and cooling the built structure. This in turns saves the cost of installing vertical bores as well as the space required to drill the bore holes. Ground-source heat pump technology is very well established but its use via geostructures such as pile foundations is relatively a new concept. This concept is being extended beyond pile foundations and now heat exchanging pipes are being installed in diaphragm walls, barrettes, basement slab, basement wall and tunnel linings (Brandl, 2006).

Laloui et al. (2006) examined the combined thermodynamic and geotechnical performance of a geothermal energy pile. They have installed an instrumented test pile as part of a new structure at the Swiss Federal Institute of Technology, Lussane. Subsequently, Bourne-Webb et al. (2009) carried out a pile loading test that incorporated temperature cycles under an extended period of maintained loading to investigate the behaviour of an energy pile installed in London clay at Lambeth College, London. Very limited information is available regarding the impact of heating and cooling processes on the geotechnical performances of energy pile foundation incorporating pipe loops for ground-source heat pump apart from the findings reported by Laloui et al. (2006 and Bourne-Webb et al. (2009).

Presently, the geomechanics group at Monash University is performing a thermal cum static load testing on a field scale fully instrumented Geothermal Energy pile. As part of this study a detailed field and laboratory based research programme is being carried out to investigate uncertainties associated with the use of Geothermal Energy Pile. This paper presents the summary of the research programme and important information observed to date.

Uncertainties

When new technology is experimented, it raises many doubts and questions which bring uncertainties. Obvious questions associated with the use of Geothermal Energy Piles are: What does happen to the pile load carrying capacity if heat is transferred in and out of the pile foundation? Does the pile and surrounding soils expand and contract due to heating and cooling? Does the pile concrete crack due to cyclic heating and cooling? What is the amount of heat transfer and heat storage in the pile as well in surrounding soils? What does happen to the pile friction at the interface of pile surface and soil? Does excessive heating and cooling affect the heat balance of ground? How much does the Geothermal Energy Pile system cost? What is the energy saving of using it in comparison to conventional heating and cooling system?

Research at Monash University

With the aim of finding the answers to all the above mentioned uncertainties a very detailed research programme was put in place. This research programme has been divided into various components: Laboratory study, Field study, Numerical study and Cost-benefit analysis. The following sections discuss all these research components in detail.

Laboratory study

The laboratory study investigates the thermo-mechanical properties of various Victorian soils and concrete. Thermal properties such as thermal conductivity, thermal diffusivity and specific heat capacity have been measured experimentally using stead-state and transient-state approach. Consolidation and shear strength properties of soils are determined using modified conventional consolidation and triaxial testing equipment to incorporate thermal effects. A small laboratory scale model pile testing facility has been designed and constructed to investigate various types of pile subjected to thermal and mechanical load as shown in Figure 2. Main advantages of the laboratory scale model pile testing are various soil and pile combinations can be explored and soil can be compacted to varying degree of initial dry densities and moisture contents. The laboratory scale model pile is instrumented with deformation gauges and thermocouples to measure displacement of the pile and temperature in the soil.

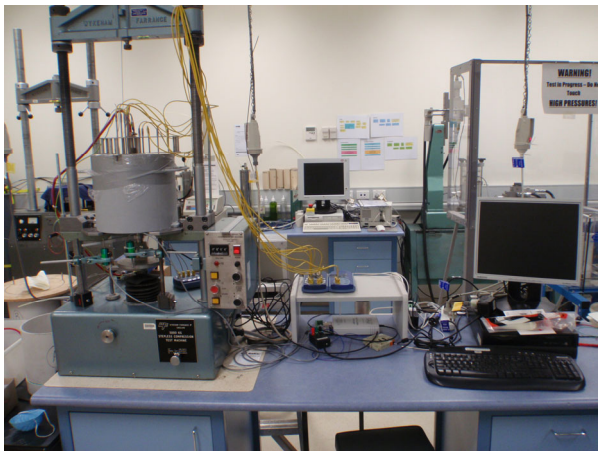

Figure 2: Laboratory scale model pile

Field study

Monash University Clayton Campus has been selected for the field study. A fully instrumented bored pile of 600 mm diameter and 18 m length has been assembled at the Vibropile Pty. Ltd. workshop, instrumented at Monash University and finally installed in December 2010. The pile is instrumented with vibrating wire strain gauges, thermocouples and linear variable displacement transducers (LVDT) at various depths within the

pile to measure transient strain, temperature and displacement. Three U-loops heat exchanger consisting of high density polyethylene (HDPE) pipes of 25 mm diameter are attached to the pile cage. These heat exchanging loops are connected to a heat pump. Thermal loading on the pile is applied and controlled by the heat pump. The pile is also subjected to static mechanical load via load cells also known as Osterberg Cell or O-cell. There are two bore holes adjacent to the pile for measuring temperature changes in the ground due to heat extraction and heat rejection from the energy pile to the ground. The schematic diagram of the field test set up is presented in Figure 3 and pile installation is shown in Figure 4. Temperature data gathered in one of the bore hole is presented in Figure 5. The ground temperature is around 16ºC after 2 m depth which remains same throughout the year. The ground surface temperature within 2 m is affected by daily air temperature.

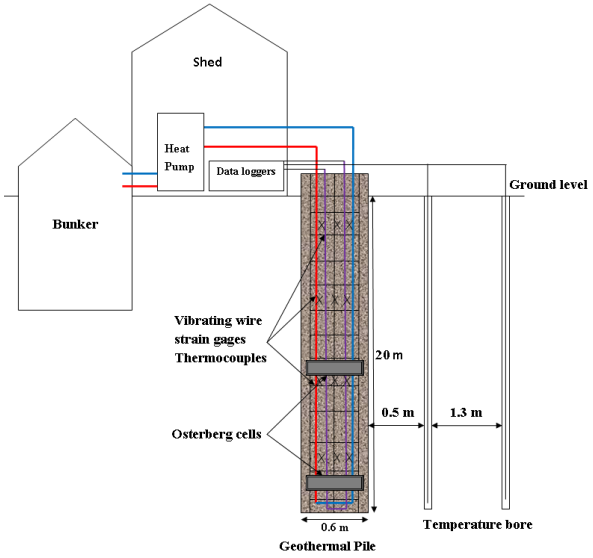

Figure 3: Schematic of Fully Instrumented Energy Pile

Numerical study

Experimental study has its own limitation in terms of time. It cannot be run for long period of time. Therefore, numerical study is required to predict the long term behaviour e.g. what will happen after continuous heating and cooling for 10, 20, 30 years or more? Numerical study will be carried out using a finite element model COMPASS (**Co**de for **M**odelling **Pa**rtially **S**aturated **S**oil) developed at Cardiff University. Thermo-hydraulic-mechanical (THM) analysis can be performed using the numerical model COMPASS. A numerical solution of the coupled heat and mass transfer equations is achieved via utilisation of the finite element method for spatial discretisation and the finite difference method for temporal discretisation, full details can be found in Thomas and King (1991), Thomas and He (1995) and Thomas and Sansom (1995).

Figure 4: Installation of Geothermal Energy Pile

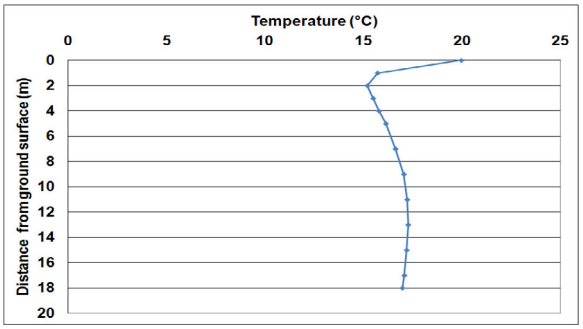

Figure 5: Ground temperature

Cost-benefit analysis

For any new technology, it is necessary to carry out a cost-benefit analysis to work out the cost and saving resulting from the implementation of a new technology. Similar approach has been adopted for the current Geothermal Energy Pile project. Genesis Now, one of the project partners, provided the electricity use and gas use for mechanical plant, chillers and boilers in a multi-storey office building in Victoria. The building uses the chillers for cooling and the boilers for heating and hot water. Figure 5 presents the daily energy use of the electric mechanical plant, the electric chillers and the gas boilers for the first 3 months

in year 2007 and the daily temperature which is shown by bars. If the building was built on Geothermal Energy Piles it will save $60,000 every year on its energy bills. In addition it will reduce 400 tonnes CO_2 (green house gas) emission annually which is equivalent to removing 130 cars off the road. The Ground Loop Design (GLD) software has been used for the cost-benefit analysis.

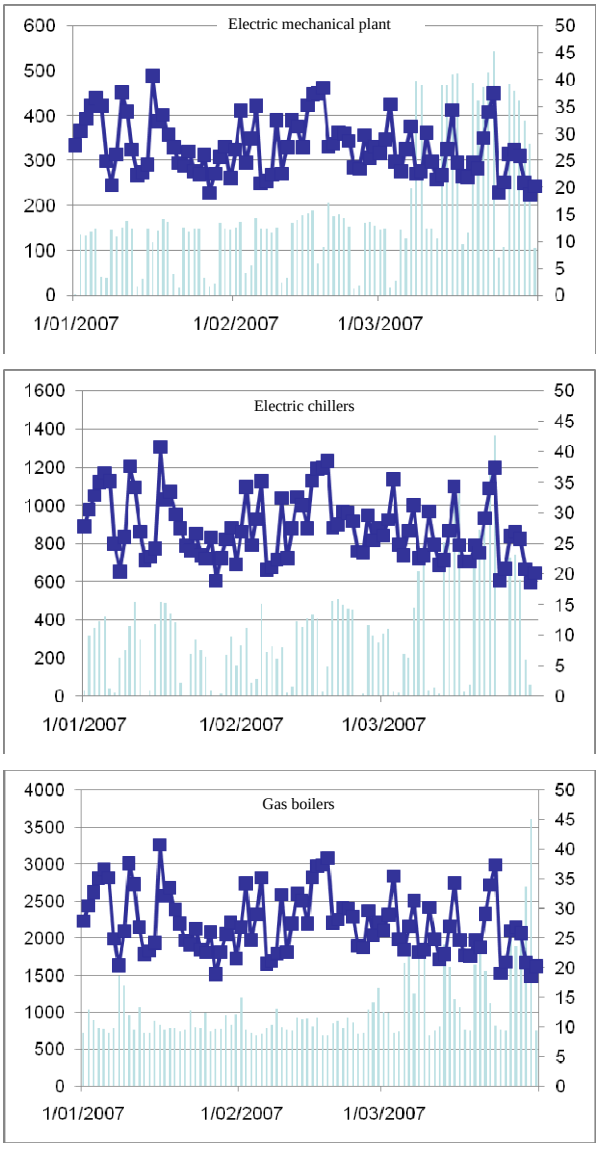

Figure 4: Daily energy use of an office building in Victoria

Conclusions

The paper presents the summary of research activities related to the Geothermal Energy Pile project currently carried out at Monash University. The paper highlights the uncertainties and challenges associated with the project. Laboratory scale and field scale study of Geothermal Energy Pile is discussed. Cost-benefit analysis of an office building in Victoria is also presented. This analysis shows the great benefits in terms of energy saving and reducing carbon footprint if the building was built on Geothermal Energy Piles.

Acknowledgement

This project is funded by the Victorian Government Sustainability Fund, Golders Associates Pty. Ltd., Vibropile Pty. Ltd., Geoexchange Australia Pty. Ltd. and Genesis Now. Their support is gratefully acknowledged.

References

Bourne-Webb, P.J., Amatya, B., Soga, K., Amis, T., Davidson. C. and Payne, P., 2009, Energy pile test at Lambeth College, London: geotechnical and thermodynamic aspects of pile response to heat cycles, Geotechnique, 59, No. 3, 237-248pp.

Brandl, H., 2006, Energy foundations and other thermo-active ground structures, Geotechnique, 56, No. 2, 81-122pp.

Thomas, H.R. and He, Y., 1995, Analysis of coupled heat, moisture and air transfer in a deformable unsaturated soil, Geotechnique, 45, No. 4, 677-689pp.

Thomas, H.R. and King, S.D., 1991, Coupled temperature/capillary potential variations in unsaturated soil, Journal of Engineering Mechanics, ASCE, 117, No. 11, 2475-2491pp.

Thomas, H.R. and Sansom, M.R., 1995, Fully coupled analysis of heat, moisture and air transfer in unsaturated soil, Journal of Engineering Mechanics, ASCE, 121, No. 3, 392-405pp.

Well Construction Technology Efficiencies - The research efforts of the United States Department of Energy, Geothermal Technologies

Greg Stillman[1] and Douglas Blankenship[2*]
dablank@sandia.gov
[1] U.S. Department of Energy
[2] Sandia National Laboratories

Reducing development costs associated with drilling and well completion are critical steps in achieving cost-competitive geothermal energy production, for both hydrothermal and Enhanced Geothermal Systems. This objective is being pursued through two broad areas of R&D activity being conducted by the U.S. Department of Energy's Geothermal Technology Program (the Program); reducing the cost of each well drilled and reducing the number of wells drilled for a given development project through improved exploration technologies. The former activity will be the focus of this discussion, but cost savings will be the most significant when done in concert with minimising the number of uneconomical wells drilled.

Investment decisions by the Program are informed by well cost analyses, techno-economic modelling of development scenarios, and technology gaps identified by road mapping. Resource temperature, which correlates to resource depth, has a significant effect on capital cost per power generation capacity. One such study was published by Sandia National Laboratory (SNL-2008) in which drilling and well construction costs are broken down into required tasks; time and costs for each task are identified through the use of a drilling script provided by Thermasource, Inc. This tool helped narrow the window of investment possibilities to those that are cost drivers for drilling and completing a well. Using this study, as well as other resources and analyses, Program activities have been adopted within each major cost driving category. The risk/reward profile of this R&D portfolio is clustered around near term activities at the component level that will generate step-wise improvements and long-term development of advance concepts that are high risk but have the possibility to be revolutionary in impact.

The discussion will highlight programmatic activities targeting cost drivers related to drilling technologies (including hole-opening), drilling efficiency, and unproductive time, with brief insights into cementing and casing activities. A description of a select group of Program sponsored projects, including advanced drilling concepts, component level R&D, and field activities will be presented along with the risk/reward trade-off and how this is managed.

Geothermal Resources of Russia and Their Complex Utilisation

Svalova, V.B.
inter@geoenv.ru
IEG RAS
Ulansky per., 13, PB 145, Moscow 101000, Russia

Geothermal energy use is the perspective way to clean sustainable development of the world. Russia has rich high and low temperature geothermal resources and makes good steps in their use.

The most perspective direction of usage of low temperature geothermal resources is the use of heat pumps. This way is optimal for many regions of Russia - in its European part, on Ural and others.

The electricity is generated by some geothermal power plants (GeoPP) only in the Kamchatka Peninsula and Kuril Islands.

There are two possible forms of utilisation of geothermal resources depending on structure and properties of thermal waters: heat/power and mineral extraction.

The mineral-extraction direction is basic for geothermal waters, containing valuable components in industrial quantities. The most significant deposits of thermal waters represent the brines containing from 35 up to 400 and more g/l of salts. They are mineral raw materials for many chemical elements.

Keywords: geothermal resources, mineral extraction, thermal waters, brines, rare elements, complex use

Introduction

Thermal waters are used for many purposes - for development of the electric power, for central heating and cooling, for hot water supply, in agriculture, animal industries, fish culture, in the food, chemical and oil-extracting industry, in balneology and spa, in the recreational purposes.

In Russia the geothermal resources are used predominantly for heat supply both heating of several cities and settlements on Northern Caucasus and Kamchatka. Besides in some regions of country the deep heat is used for greenhouses. Most active the hydrothermal resources are used in Krasnodar territory, Dagestan and on Kamchatka.

At the same time the problem of the most effective utilisation of a natural source of raw materials is put forward in the category of actual tasks, including thermomineral waters and brines. Involving of these waters in economic activities can promote the decision of some social - economic and environmental problems.

Geothermal energy use

In Russia the geothermal resources are used predominantly for heat supply both heating of several cities and settlements on Northern Caucasus and Kamchatka with a total number of the population 500000. Besides in some regions of country the deep heat is used for greenhouses of common area 465000 м2. Most active the hydrothermal resources are used in Krasnodar territory, Dagestan and on Kamchatka. (Gadzhiev et al. (1980), Kononov et al. (2000), Svalova (1998-2008)).

The approximately half of extracted resources is applied for heat supply of habitation and industrial puttings, third - to a heating of greenhouses, and about 13 % - for industrial processes. Besides the thermal waters are used approximately on 150 health resorts and 40 factories on bottling mineral water. Quantity of electrical energy developed by geothermal stations of Russia, per 1999 almost twice has increased as contrasted to by former level. Nevertheless, it remains extremely minor, making some 0,01 of percent from common development of the electric power in the country.

The Western Siberian plate is another promising region for direct use applications. The aquifers located down to 3 km in this region have a high hydrostatic pressure, temperatures of up to 75 °C, and are capable of producing about 180 m^3/s. These waters are used to heat dwellings in some small settlements and, on a small scale, assist in the recovery of oil, the extraction of iodine and bromide, and for fish farming. The region is rich in natural gas, which has limited geothermal development.

The most perspective direction of usage of low temperature geothermal resources is the use of heat pumps. This way is optimal for many regions of Russia - in its European part, on Ural and others.

Heat pumps are at an early stage of development in Russia. An experimental facility was set up in early 1999 in the Philippovo settlement of Yaroslavl district. The source supplies 5-6°C to eight heat pumps that heat the water to 60 °C for a 160-pupil school building. There are some buildings with supply of heated water, using heat pumps, in Moscow (Fig. 1,2).

Figure 1: Moscow, Anokhina Str.,50.House for pilot heat-pump installation.(Photo of Svalova V.)

Figure 2: Moscow, Anokhina Str., 62. House with heat-pump supply. (Photo of Svalova V.)

The electricity is generated by some geothermal power plants (GeoPP) only in the Kamchatka Peninsula and Kuril Islands. At present three stations work in Kamchatka: Pauzhetka GeoPP (11MW e installed capacity) and two Severo-Mutnovka GeoPP (12 and 50 MWe). Moreover, another GeoPP of 100 MVe is now under preparation in the same place. Two small GeoPP are in operation in Kuril's Kunashir Isl, and Iturup Isl, with installed capacity of 2.6 MWe and 6 MWe respectively.

Russia has considerable geothermal resources and the available capacity is far larger than the current application. This resource is far from adequately developed in the country. In the former Soviet Union, geological exploration was well supported for minerals and oil and gas. Such expansive activities did not aim to discover geothermal reservoirs even in a corollary manner; geothermal waters were not considered among energy resources. Still, the results of drilling thousands of "dry wells" (in oil industry parlance), bring a secondary benefit to geothermal research. These are the abandoned wells themselves, and the data on the subsurface geology, water-bearing horizons, temperature profiles, etc., that were collected during exploration. Not all currently operating companies are willing to disclose their well data, still, in face of the cost of maintaining shut-in wells, it is cheaper to turn them over to others for new purposes.

Development and implementation of geothermal power technology is facilitated by social, scientific, economical and environmental aspects.

Social aspects reflect public opinion and willingness to reject old, traditional power generating methods and implement new, non-traditional, environmentally friendly geothermal power technology.

Nowadays the scientific and technical level of geothermal technology is very high in Russia. Unique geothermal power equipment has been developed domestically and for the first time in the world two environmentally friendly power plants were constructed in Kamchatka, In 1999 the unique pilot Verkhne-Mutnovsky GeoPP (V-MGeoPP) of 12 (3x4) MW was constructed (Fig. 3, 4).

It has been operating in extremely severe climatic conditions on the site located near 1000 m above sea level. High level of environmental protection is provided due to isolating the geothermal fluid from the environment by using both air condensers and a system of full re-injection of the waste geothermal fluid back into reservoir. The major problem of protecting the GeoPP equipment from corrosion and salt depositions was solved by using a special technology of film-forming amine additives. Over the last years the V-MGeoPP has proved sustained reliability in generating reasonably priced electricity of about 1.5 cents/kWh (Nikolski, Parshin, and Bezotechestvo (2003)). The experience gained while constructing and operating the V-MGeoPP was used for construction of the 50 MW Mutnovsky GeoPP – a completely automated power plant with a satellite-based communication and control system (Fig. 5, 6, 7).

The economic impact from geothermal power plants is especially high in remote locations. As there is practically no detrimental gases emission,

modern GeoPPs can be considered as practically absolutely environmentally friendly (Tomarov, Bubon, and Martynova (2003)).

Figure 3: Verkhne-Mutnovsky GeoPP. First ecologically clean GeoPP(Photo of Svalova V.).

Figure 4: Verkhne-Mutnovsky GeoPP (Photo of Svalova V.)

Figure 5: Mutnovsky GeoPP(Photo of Svalova V.).

Thermal water complex utilisation

Thermal waters are used for many purposes - for development of the electric power, for central heating and cooling, for hot water supply, in agriculture, animal industries, fish culture, in the food, chemical and oil-extracting industry, in balneology and spa, in the recreational purposes.

Figure 7: Mutnovsky GeoPP. The main entrance(Photo of Svalova V.).

Thermal waters, it is especial chloride brines, contain in the structure a huge complex of metal and nonmetallic microcomponents. The saturation of brines microcomponents is in close dependence both on genetic essence of brines, and on lithological-structural and geothermal features of containing breeds.

Interest to geothermal waters and brines as mineral raw material is connected to a number of advantages of this kind of raw material in comparison with firm sources of rare elements, metals and mineral salts.

Industrial underground waters are characterised by wide regional distribution and big geological and exploitation stocks. They are polycomponental raw material and simultaneously can be used in balneology and power system. Extraction of this raw material demands realisation concerning small capital works and is carried out by boreholes methods, allowing to take hydro mineral raw material from the big depths.

Geothermal waters and brines are characterised by the big variety of mineralisation, a chemical compound, the contents of useful components and their quantitative ratio, and also gas structure and temperatures. The most widespread types of hydro mineral raw material are: thermal brines of intercontinental rift zones; thermal waters and brines of island arches and areas of Alpine folds; waters and brines of artesian pools; brines of modern evaporate pools of a sea or oceanic origin and continental lakes; sea waters (Table 1).

Profitability of industrial reception of those or other components from hydro mineral raw material is determined not only by their concentration, but also by depth of underground waters and operational chinks, filtration properties of rocks, flow rate of operational stocks etc. On economic parameters of operation the way of dump of the fulfilled waters that defines expenses for protection of the natural environment essentially influences.

Proceeding from the general conditions and laws of distribution of underground geothermal waters and the brines containing rare elements, and also in view of experience of use of such waters as hydro mineral raw material in Russia and abroad the following limits of concentration of elements at which waters represent industrial interest are established (mg / l): iodine - 10, lithium - 10, cesium - 0.5, germanium - 0.5, bromine - 200, rubidium - 3, strontium - 300. (Bondarenko (1999)).

Even before the Second World War abroad, in particular, in USA, the technology of extraction from hydro mineral raw material of one of its components - lithium was developed. In 70th years about 85 % of world extraction of this metal was carried out in such a way. (Kogan and Nazvanova (1974)).

In Japan from geothermal underground brines are commercially extracted I, Br, B, Li, As, Ge, W and a number of mineral salts. In Israel from brines of the Dead sea the carnallite, bromine, chlorides of magnesium and calcium, and also raw material for manufacture of medical products and perfumery are produced. In 80th years from hydro mineral raw material it was received 30 % of world extraction of lithium, 31 % - cesium, 8 % - a boron, 5 % - rubidium, and also in significant scales Ca, Mg, Na, K, S, Cl, U, Ra, Cu. (Bondarenko (1999)). (Table 2, 3).

Huge stocks of rare-metal raw material are in geothermal underground waters and brines on territories of Russia and the CIS. They contain over 55 % of the common stocks of lithium, 40 % of rubidium and 35 % of cesium. (Kremenetsky et al.(1999))

Thermal waters with a high mineralisation are located in the greater territory of Russia and the former USSR. They are known almost in all areas. Brines with mineralisation higher than 200 g/l are known in Perm and Kujbishev areas, Tatarstan, Moscow, Ryazan and other central areas. In Moscow, for example, on depth of 1650 m are met chloride brines with mineralisation of 274 g/l. In Western and Eastern Siberia there are large deposits of brines with high temperature. Some deposits have mineralisation of 400-600 g/l. There are many thermal brines in Central Asia, Kazakhstan, on Ukraine, Kamchatka, Kuriles, Sakhalin. (Shcherbakov (1985), Resources … (1985), Kurbanov(2001)).

There are chemical elements which are possible for taking only from underground waters. So iodine is extracted from brines since iodine is good dissoluble and in breeds iodine does not collect. Iodine concentrates in sea seaweed but to extract this seaweed as industrial raw material is effectively only at their big congestion. Bromine can be extracted from some salts and seaweed, but traditionally bromine also is extracted from superstrong chloride brines. (Antipov et al., (1998)). (Table 4).

The significant part of deposits of thermal waters represents the brines containing from 35 up to 400 and more g/l of salts. They are mineral raw material on many chemical elements. Many brines which are taking place on the big depth, can become deposits of the most valuable chemical elements: cesium, boron, strontium, tantalum, magnesium, calcium, tungsten etc. (Table 5,6,7).

Under the cheap technological circuit from natural solutions basically it is possible to take iodine, bromine, boron, chloride salts of ammonium, potassium, sodium, calcium, magnesium. Extraction of other chemical elements is complicated because of dearness of technology. A perspective method is use of ion-exchange pitches for selective extraction of the certain components from natural waters. In a basis of a method there is the principle of selective sorption of ions of useful elements or their complexes in solutions with special compounds.

Works of some scientific institutes in Russia allow to create the processes of chemical processing of hydromineral raw material and to expand spheres of its economic application. Many laboratory and natural tests on extraction of valuable components from thermal waters confirm the necessity and an opportunity of complex use of this nonconventional raw material.

It is planned to recover I, Br, KCl, CaCl, NaCl from brines in Yaroslavl area. New methods of mineral and valuable elements extraction from industrial solutions are developed on the basis of biosorbent use.

Conclusion

Depending on structure and properties of thermal waters it is possible to allocate two basic directions of use of geothermal resources: heat power and mineral-raw materials.

The heat power direction is the basic for fresh and low mineralised waters when valuable components in industrial concentration practically are absent, and the general mineralisation does not interfere with normal operation of system. When high potential waters are characterised by the raised mineralisation and propensity to

scaling, the recycling of mineral components should be considered as the passing process promoting the effective heat supply.

The mineral-raw direction is the basic for geothermal waters, containing valuable components in industrial quantities. Thus the substantiation of industrial concentration is caused by a level of technologies. For such waters the heat is a passing product which use can raise efficiency of process of reception of basic production and even to save fuel.

Designing such systems the process of allocation of valuable components should be dominant at. Calculations show, that complex use of thermal waters in a mineral-raw direction economically is more effective, than in heat power. The choice of a direction of complex use of thermal waters should be defined not only by their structure and properties, but also by the level of development of complex technological processes of extraction and processing of hydromineral raw material and by technology of heat power processes. But for all that the presence of consumers and needs for thermal water play the main role.

References

Antipov, M.A., Bondarenko, S.S., Strepetov, V.P., and Kasparov, S.M.: Mineral raw materials. Bromine and iodine, Reference book. “Geoinformmark”, M., 30 pp. (1998).

Bondarenko, S.S.: Mineral raw materials. Industrial waters, Reference book. “Geoinformmark”, M., 45 pp. (1999).

Gadzhiev, A.G., Kurbanov, M.K., and Suetnov V.V.: The problems of geothermal energy in Dagestan, Nedra, Moscow. (1980).

Kogan, B.I., and Nazvanova, V.A.:Industrial use of natural continental mineral waters abroad. Rare elements. Raw materials and economics. Ed. 10. Rare elements in natural mineral waters. Moscow, p. 4-117. (1974.)

Kononov, V.I., Polyak, B.G., and Kozlow,B.M.: Geothermal development in Russia: Country update report 1995-1999. Proceedings, the World Geothermal Congress 2000, Vol. 1, p. 201 – 206. (2000).

Kremenetsky, A.A., Linde, T.P., Yushko, N.A., Shaderman.: Mineral raw materials. Lithium, Reference book. “Geoinformmark”, M., 49 pp. (1999).

Kurbanov, M.K.: Geothermal and hydro mineral resources of Eastern Caucuses and Pre-Caucuses, Nauka, Moscow, 260 pp.,(2001).

Nikolski, A.I., and Parshin, B. Ye.: Verkhne-Mutnovsky geothermal power plant – the first environmentally friendly power plant, Energoprogress, Science Technology Newspaper, Moscow . (2003).

Resources of thermal waters of Dagestan and optimisation of schemes of their complex developing. Collection of articles, Editors: Kurbanov, M.K., Sardarov, S.S., Dejnega, G.I., et al., Ed. 4. Institute of geothermic problems, Dagestan branch of the USSR Academy of Sciences, Makhachkala, 156 pp.,(1985).

Shcherbakov, A.V.: Geochemical features of thermal waters as mineral resources for chemical industry, Geothermal investigations in Middle Asia and Kazakhstan. Nauka, Moscow, p.57-67, (1985).

Svalova, V.B.: The History of Geothermal Resources Use in the Former USSR. Proceedings, 1998 GRC Annual Meeting, San Diego, California, USA. (1998).

Svalova, V.B.: The history of geothermal resources use in Russia and the former USSR. Proceedings, World Geothermal Congress 2000, Japan. (2000).

Svalova, V. B.: Geothermal energy use in Russia and environmental parks. Proceedings, 2002 Beijing International Geothermal Symposium.(2002).

Svalova, V. B.: Geothermal Energy Use in Russia and Sustainable Development. Proceedings, International Geothermal Workshop, New Zealand (2002).

Svalova, V.B.: Geothermal energy use in Russia and environmental problems, Proceedings, World Geothermal Congress in Turkey, (2005).

Svalova, V.B.: Geothermal energy use in Russia: progress and future, Proceedings, First East African rift geothermal conference. Geothermal energy: an indigenous, environmentally benign and renewable energy resource, Addis Abeba, Ethiopia (2006).

Svalova, V.B.: Geothermal resources and thermal waters of Russia: complex use, Proceedings, Geothermal Resources Council 2006 Annual Meeting “Geothermal Resources Securing Our Energy Future”, San Diego, California (2006).

Svalova, V.B.: Mineral resources of geothermal waters and brines, Proceedings, International conference ”Mineral extraction from geothermal brines”, Tucson, Arizona, USA

Svalova, V.B.: Complex Use of Geothermal Resources. CD Proceedings, European Geothermal Congress 2007, Germany, N 233. (2007).

Svalova, V.B.: Problems and prospects of geothermal resources utilisation. Bulletin ”Use and protection of natural resources in Russia “, N5, pp. 3-10. (in Russian) (2008).

Tomarov, G.V., Bubon, S.V., and Martynova, M.V.: Investment and environmental attractiveness of geothermal power projects in

Kamchatka., Energoprogress, ScienceTechnology
Newspaper, Moscow (2003.

Table 1. The main types of hydromineral raw material

TYPE	VALUABLE ELEMENTS	EXAMPLES
Thermal brines of intercontinental rift zones	$CaCl_2$, CO_2, (NaCl, Zn, Pb, Cu, Fe, Ag, Li, Br)	Atlantis-II (Red Sea) Salton Sea (California, USA)
Thermal waters and brines of island arches and areas of Alpine folds	B, NH_4, CO_2, (Li, Cs, As, Ge, W)	Japan, Iceland, New Zealand, Toscana (Italy), Russia
Waters and brines of artesian pools	NaCl, KCl, CH_4, Mg, Br, I, Rb, CsO	San-Kristobal (Mexico), Danison-Trof (Australia), Michigan (USA), Niigata (Japan), Russia
Brines of modern evaporate pools	NaCl, Na_2CO_3, K, Li, Br, B, (W, Rb) NaCl, KCl, K_2SO_4, Na_2SO_4, Mg, Br, Li, B NaCl, $CaCl_2$, Mg, K, Li, (Sr, Rb)	Searles Lake, Great Salt Lake (USA), Kara-Bogas-Gol (Turkmenistan)
Sea waters	NaCl, $CaSO_4$, Mg, Br, K, (U, Li, B, D_2O)	USA, Japan, Germany
Man-caused waters: I-Br plants Oil-gas fields Heat-and-power engineering Salt-mines and K-plants Water-desalinating plants	 NaCl, Br, Sr Br, I $CaCl_2$, (NaCl, Zn, Pb, Fe, Ag, Li, B, As) NaCl, Br NaCl	 Russia USA (Oklahoma), Japan Salton Sea (USA), B. Pauzhetka (Russia) Germany, France, Russia, Japan Poland, Russia

Table 2. Extraction of rare elements and mineral salts from hydromineral raw material (during a year)

PRODUCTION	COMMON (thousand tons)	FROM HYDROMINERAL RAW MATERIAL/ % - part of common
NaCl	120000	36000/30
KCl	16000	1400/9
soda	35000	3500/10
Na_2SO_4	4600	1400/30
$CaCl_2$	2700	600/22
B_2O_3	1000	250/25
Br	350	320/90
Mg	200	50/25
Li	40	17/30
I	15	13/85

Table 3. The elements under development by industry for extraction from hydromineral raw material

	COMMON EXTRACTION (tons)	FROM HYDROMINERAL RAW MATERIAL
Fe	$4.1x10^8$	+
Cu	$6.0x10^6$	++
Zn	$5.0x10^6$	++
Pb	$2.3x10^6$	+
U	$3.8x10^4$	++
W	$4.3x10^4$	++
Sr	$5.8x10^4$	+
Ag	$1.0x10^4$	++
Hg	$4.3x10^3$	
Ge	$1.0x10^2$	
Cs	n x 10	
Rb	n x 10	
D_2O	-	

+ Technological testing, ++ Projects of extractions

Table 4. The limits of minimal industrial concentrations of i and br(mg/l)for mineral water deposits in Russia

TYPE	I	Br
I	16-44	-
Br	-	492-4700
I+Br	10-40	350-1650

Table 5. Concentrations of some rare elements in brines of Russian platform (mg/l)

WATER TYPE	MINERALISATION (g/l)	Cs	Rb	Sr	B
Cl-Ca-Na	35-75	0.1-0.4	0.1-0.5	50-150	5-30
	75-150	0.2-0.4	0.3-1.5	100-400	10-40
Cl-Na-Ca	150-340	0.2-1.0	1.0-3.0	100-300	5-30
	340-430	1.0-2.0	3.0-20.0	900-3000	90-100

Table 6. Middle concentrations of rare elements in water-bearing complexes of Azov-Kuban and Eastern Pre-Caucasus basins (mg/l)

Water-bearing complex	Rare metals	I	B	Br	Sr
Azov-Kuban Basin					
The Jura	19	19 (max 68)	29	122	158
Low Cretaceous	5	13	32	60	81
Eastern Pre-Caucasus Basin					
The Jura	43	12	5	54	500
Low Cretaceous	30	14	91	173	33

Table 7. Composition of valuable components in industrial waters of large artesian basins

Typical basins of underground industrial waters	Elements
Volga-Pre-Caucasus	I, Br, Sr, Cs, B, Rb
Volga-Kama	I, Br, Sr, B, Rb
Tungus	Br, Sr, B, Rb, Cs
Angara-Lena, Mangishlak-Ustyurt, Pechora, Dnepr-Donetzk	Br, Sr, B, Rb
Moscow	Br, Sr
Pre-Baltic	Br, Sr
Western-Turkmenistan, Kurinsko-Apsheronsky	I, Br, Sr
Western-Siberian, Sakhalin	I, Br

First results of monitoring fluid injection in EGS Reservoirs Using Magnetotellurics

Stephan Thiel[1]*, Jared Peacock[1], Graham Heinson[1], Peter Reid[2], Mathieu Messeiller[2]
*Corresponding author: stephan.thiel@adelaide.edu.au
[1] TRaX, School of Earth and Environmental Sciences, University of Adelaide, SA 5005
[2] Petratherm Ltd, Adelaide, Unley, SA 5061

Magnetotelluric (MT) data was recorded during a fluid fracture stimulation of an enhanced geothermal system (EGS), at Paralana, South Australia. MT is directly sensitive to the bulk electrical conductivity of the subsurface, specifically hot and electrically conductive, fluids. MT measurements before, during and after fluid injection are compared to estimate the lateral extent of the induced reservoir. 3D forward modelling studies show the residual MT response between a system with and without fluids to be small, of the order of a few degrees in MT phase. It is crucial to obtain accurate and precise noise-free MT responses throughout the surveys in order to produce a reliable model of the subsurface. Presented are MT responses and preliminary inversion models of base surveys in comparison with measurements throughout the fluid injection. After injection temporal and spatial changes of MT response function are visible and correlate with other monitoring data sets from seismic event analysis.

Keywords: Magnetotellurics, EGS, Monitoring

Introduction

EGS has the potential to supplement energy production as the world slowly shifts towards renewable energy. One important measurement of EGS is monitoring where the fluids go once injected into the thermally inclined lithology. Traditionally, reservoirs are monitored with micro earthquake arrays (MEQ), which measure seismic events generated by fractures (Phillips et al., 2002). Tomography can be applied to estimate location of the fracture (House, 1987), and shear-wave splitting can be used to estimate size and orientation of the fracture (Elkibbi and Rial, 2005). Unfortunately, these measurements do not provide information about fluid inclusion.

Magnetotellurics (MT)

MT is a passive volumetric measurement that exploits Faraday's law of magnetic induction by measuring orthogonal components of the Earth's natural magnetic field and the subsequent Earth's electric response. MT is a diffusive method,

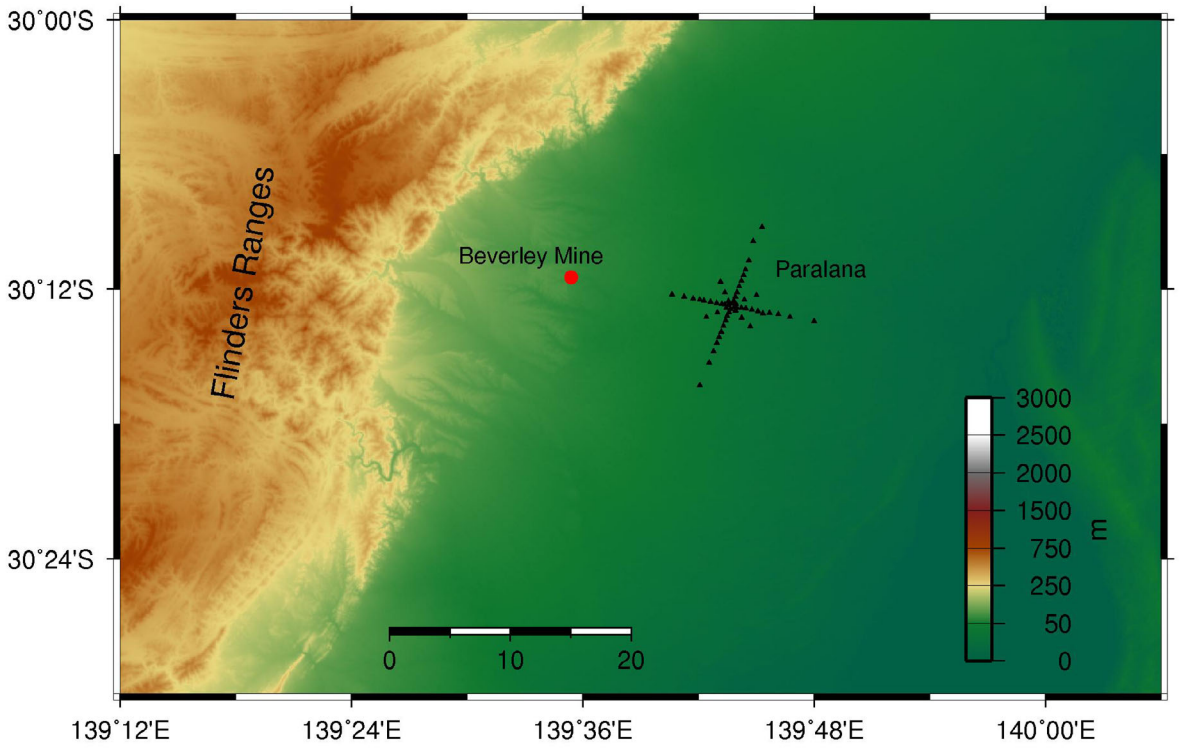

Figure 1: Survey design centred on Paralana 2 drill hole, overlaying elevation (m). Two orthogonal lines parallel to assumed principle stress directions and with existing roads provide dense 2D estimation with 22 stations each. Spacing varies from 200m near the centre to 1.5km near the extremities. Two off diagonal lines with variable spacing of 250m, 500m, 1km provide dimensionality constraints with 6 stations each. A total of 56 stations

which means resolution is proportional to period as defined by the skin depth. It is sensitive to variations in electrical conductivity of the subsurface, which makes it a prime technique to monitor changes as electrically conductive fluids are introduced. The fluids are assumed to be conductive due to thermal and dissolved ion enhancement and will provide a large contrast with resistive host rocks (Spichak, 2009).

Test site: Paralana, South Australia

The test site is in the northern part of South Australia, about 600 km due north of Adelaide, near the edge of the Flinders Ranges and Paralana hot springs. Here, the thermal activity is generated by an innately high density of radiogenic elements, where residual heat is a by-product of millions years of decay (Brugger, 2005). The aged crystalline lithology (1590 Ma) of the uplifted Flinders Ranges has heat production values up to 60 µW/m^3 (Neumann, 2000), compared to a typical heat production of basement rock of about 3 to 5 µW/m^3. To the East of the Flinders Ranges, the hot crystalline rocks are unconformably overlain by about 4000 m of Adelaidean sediments, which act as a lithologic blanket keeping heat from escaping. A heat flow of 112 µW/m^2 was measured at Paralana, making the area a prime location for EGS.

Petratherm and joint venture partners lease a 500 km^2 tenement where Paralana 2 has been drilled to a nominal depth of 4012 m and cased to 3725 m. The bottom hole temperature has been estimated at 190 °C and fluids were encountered at a depth of 3860 m. Note the stimulation is initiated within the sediment package above the basement and aims at enhancing and connecting to natural fractures within the sediments and at the boundary between the sediments and the underlying basement. It is proposed that improving natural fracture permeability in this sediment package and at the basement/basin interface via mechanical fracturing will be

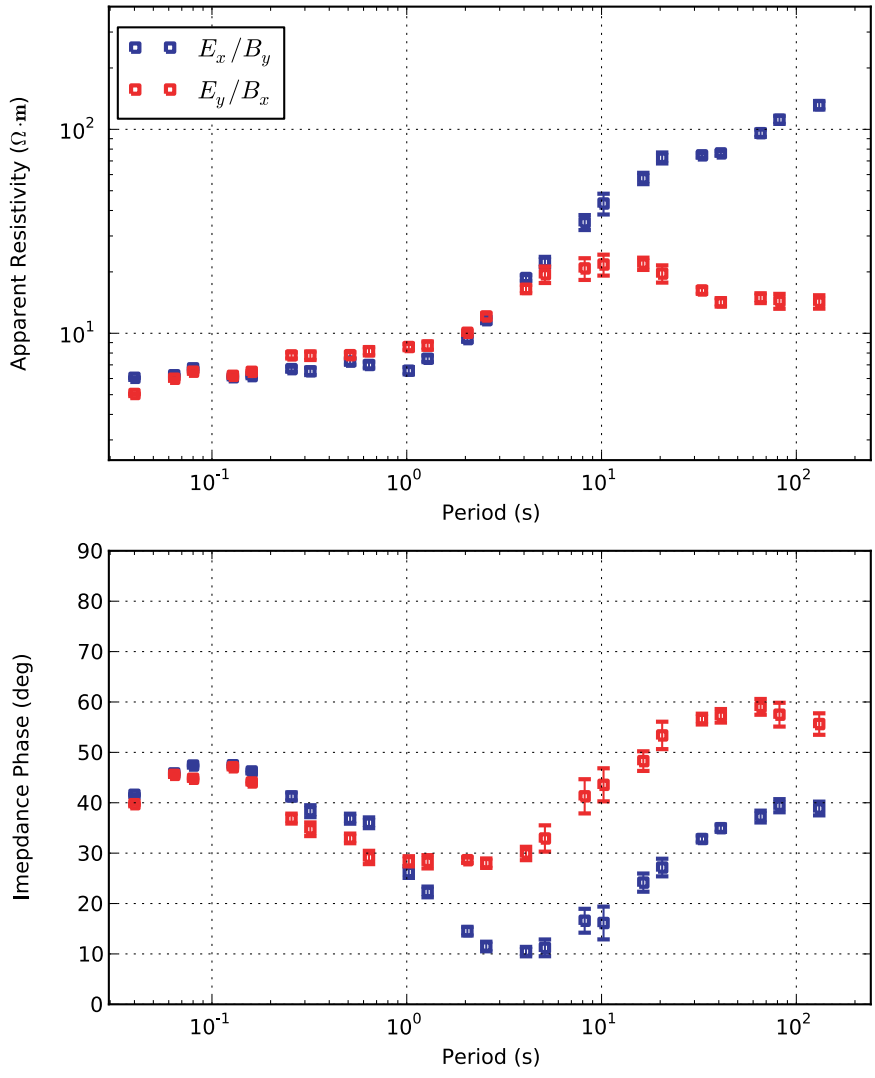

Figure 2: MT responses of TE and TM modes from station pb24 of base survey 1. Top: Log apparent resistivity (ohm-m) as a function of log period (s). Bottom: Impedance phase (deg) as a function of log period (s). Notice the larger error bars around 10 seconds, which is the range where changes with fluid inclusion are projected.

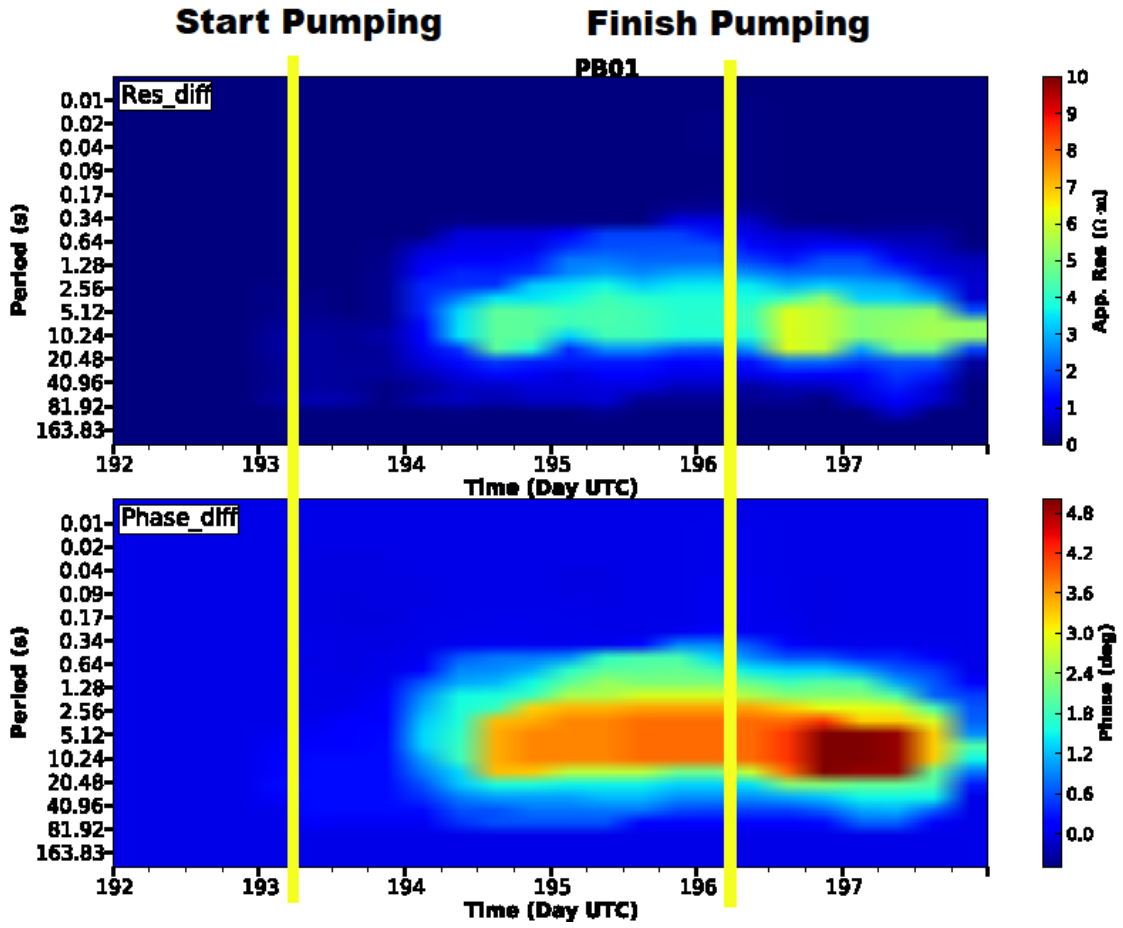

Figure 3: Temporal changes of apparent resistivity (top) and phase (bottom) throughout the fluid injection for a station 300m away from the borehole. MT transfer functions are computed every 6 hours and median filtered. The onset of transfer function changes is offset by about a day.

achieved more easily than developing a fracture network exclusively in a crystalline basement. The well was perforated in December 2010. A diagnostic fracture injection test was performed in January 2011, followed by a main hydraulic stimulation in July 2011.

Procedure

A preliminary survey will be collected to compare any changes in other surveys collected during and after the fracturing period. For all surveys, the basic layout, centred on Paralana 2, contains an orthogonal pair of NNE-SSW and WNW-ESE lines employing 22 stations each, Figure 1. The lines will have variable spacing of ~200 m near the centre increasing to 1.5 km near the extremities to get maximal coverage at depths of investigation. Two off diagonal lines containing 6 stations each, again centred on Paralana 2, with variable spacing of 250 m, 500 m, 1 km, will aid in spatial coverage of the injected fluid reservoir. Each survey will employ 56 stations in total plus 2 remote reference stations 60 km and 80 km south of Paralana. The survey design is based on forward modelling and logistics. The goal is to estimate reservoir extent as a function of time by measuring changes in the MT responses.

Base surveys

Three base surveys were collected between March, 2010 and April 2011 with AuScope instruments owned by the University of Adelaide. The sampling rate was 500 Hz, with 50 m dipole lengths, measuring B_x, B_y, E_x, E_y. Redundancy in the base survey deployment was necessary to overcome bad data quality due to gas pipeline noise, which resulted in unacceptably high error floors. A square wave signal is the most dominant effect visible from the gas pipeline and results in a near-field response of an electric dipole between periods of 1 and 10 seconds. Because this signal is distinctly periodic and regular, simple time series analysis can remove this from the data. By taking an average of a 12 second window the average wave form can be calculated. That wave form is convolved with a series of delta functions every 12 seconds. A linear trend calculated from the data is added to the filter time series to fit the data better.

The majority of the stations recorded for two days. MT responses were calculated using BIRRP (Chave, 2004) and an in house interface written in Python. Most data have low coherency and larger error bars around 1-10 seconds, Figure 2, which is the well known dead band. Remote-

referencing helps to overcome these issues and result in less biased responses. Also, the apparent resistivity and phase polarizations suggest a dominant 1D geoelectric structure to a period of about a few seconds, then a multidimensional structure after periods of a few seconds. The site is near a large working uranium mine, Beverly in Figure 1, which produces 50 Hz and harmonics EM signal. This is observed in the time-frequency spectrogram and in estimated apparent resistivities and phases below periods of 0.1 seconds, where the estimations are less smooth.

Repeat survey

Fluid injection took place in July 2011 and was accompanied by MT measurements. Instruments recorded during the entire injection for detection of temporal changes. A repeat survey followed with about 40 stations concentrated in the inner part of the grid to image spatial changes from the base survey.

MT transfer functions were computed for 6 hour blocks starting a day before the injection. About 24 hours after the injection the apparent resistivity and phase responses show changes in the period range of 1 to 10 seconds coincident with depths of the injected fluid. The apparent resistivity reduces with injection of fluids and remains lower after pumping finishes (Figure 3). A median filter has been applied to Figure 3 to avoid the influence local bad data points.

Subsequent repeat deployment of MT sites at locations identical to the base survey image the north-east extent of the zone of reduced resistivity. The result correlates well with seismic event location determined from micro earthquake arrays. However, an increase in resistivity is observed in the immediate vicinity of the injection hole.

Conclusions

The newly acquired MT data monitoring and imaging fluid injection at Paralana, South Australia, show both temporal and spatial changes in resistivity as a result of the fluid pumping. Changes are small as predicted by 3D forward modelling and are occurring at period ranges equivalent to skin depths of the fluid injection down hole. Future projects will focus on acquiring MT data during flow tests. The results indicate that MT is able to image fluid injection, with clearer results anticipated in areas of shallower injection or less electrically conductive cover.

References

Chave, A. D. & Thomson, D. J., Bounded influence magnetotelluric response function estimation, *Geophys. J. Int.,* 2004, 157, 988-1006

Brugger, J.; Long, N.; McPhail, D. C. & Plimer, I., An active amagmatic hydrothermal system: the Paralana hot springs, Northern Flinders Ranges, South Australia, *Chemical Geology,* 2005, 222, 35-64

Elkibbi, M. & Rial, J. A., The Geysers geothermal field: results from shear-wave splitting analysis in a fractured reservoir, *Geophys. J. Int.,* 2005, 162, 1024-1035

House, L. S., Locating microearthquakes induced by hydraulic fracturing in crystalline rock *Geophysical Research Letters,* 1987, 14, 919-92

Spichak, V. V., and Manzella, A, 2009, Electromagnetic Soundings of Geothermal Zones, Journal of Applied Geophysics, 68, pp459-478

Neumann, N.; Sandiford, M. & Foden, J. Regional geochemistry and continental heat flow: implications for the origin of the South Australian heat flow anomaly, *Earth and Planetary Science Letters,* 2000, 183, 107-120

Phillips, W. S.; Rutledge, J. T.; House, L. S. & Fehler, M. C., Induced microearthquake patterns in hydrocarbon and geothermal reservoirs: six case studies, *Pure and Applied Geophysics, Seismic Research Center, Los Alamos National Laboratory,* 2002, 159, 345-369

Opportunities for Shallow Heat Management via Subsurface Stirring

Trefry, M.G.[1,2,3], Lester, D.R.[4], Metcalfe, G.[5], Chua, H.-T.[6] and Regenauer-Lieb, K.[1,3]
Mike.Trefry@csiro.au
[1] Western Australian Geothermal Centre of Excellence. PO Box 1130, Bentley, WA 6102
[2] CSIRO Land and Water, Private Bag 5, Wembley, WA 6913
[3] School of Earth and Environment, University of Western Australia, Crawley, WA 6009
[4] CSIRO Mathematics, Informatics and Statistics, PO Box 312, Clayton South, VIC 3169
[5] CSIRO Materials Science and Engineering, PO Box 56, Highett, VIC 3190
[6] School of Mechanical Engineering, University of Western Australia, Crawley, WA 6009

In many sectors of urban and industrial activity waste heat is released to the atmosphere or hydrosphere. This energy release is wasteful both through the loss of potentially useable heat but also through the consumption of water during evaporation. Sustainable energy solutions will provide options to recycle heat and to minimise water consumption. Low-temperature geothermal reservoirs offer substantial capacity to accept and store waste heat.
Typical open-loop subsurface heat rejection or storage applications rely on arrangements of injection and extraction bores that pass heat-carrying fluid through the local porous medium, often in steady pumping modes. This abstract presents a new technology for enhancing heat transfer rates in the subsurface by using time-dependent pumping modes. Appropriate selection of pumping modes can induce useful flow characteristics, ranging from kinematic isolation of reservoir zones to chaotic mixing where thermal energy transfer is maximised. Theoretical aspects of the subsurface stirring approach are discussed, and comments on the transferability of this method to the geothermal context are made.

Keywords: heat rejection, thermal storage, pumping, chaos, subsurface stirring, geothermal

Subsurface Heat Management

In many sectors of urban and industrial activity waste heat is released to the atmosphere or hydrosphere. A large range of conventional engineering designs has been developed, including cooling towers, wastewater discharges etc. This engenders a net loss of low-grade energy and, through evaporative cooling, a potentially unsustainable consumption of water. In addition to these conventional sources, the growing direct heat use market ensures there will be continued pressure to develop efficient and economical means to reject or sequester surplus heat in groundwater systems. Low-temperature geothermal reservoirs offer substantial capacity to accept and store waste heat.

Typical open-loop subsurface heat rejection applications rely on arrangements of injection and extraction bores that pass heat-carrying fluid through the local porous medium, often in steady pumping modes. This abstract presents a new technology for managing heat in the subsurface by using time-dependent pumping modes. As will be demonstrated in the following sections, appropriate selection of pumping modes can induce useful flow and thermal energy characteristics, ranging from kinematic isolation of reservoir zones showing coherent orbit structure to chaotic mixing zones where fluid orbits lose coherence and where thermal energy transfer is maximised.

In the following sections we discuss briefly the fluid mechanical basis of subsurface stirring for idealised systems, and note the parallels with practical hydrogeological environments. We then discuss the robustness of the dynamical theory and then comment on the potential applications in the geothermal context.

Dynamics of Stirring

The motion of passive tracers advecting in a fluid velocity field can potentially display chaotic dynamics, even in the limit of small Reynolds number, e.g. laminar flows. Fluid mixing is promoted by chaotic dynamics, which can arise through repetitions of stretching and folding motions of the pathlines of transported fluid (Figure 1), even when no such stretching and folding motion exists in the streamlines of the velocity field. This stretching and folding process is referred to as stirring. If dispersive phenomena are also present, fluid mixing occurs.

Figure 1 Images of stretching and folding chaos in high Peclet number – low Reynolds number flows in a tube (after Metcalfe et al., 2006). Red, yellow and green fluids.

Rotated Potential Mixing

In hydrogeological systems, the chaotic dynamics of Darcian flow regimes are relevant. As shown by Lester et al. (2009), time-dependent Darcy flows can display chaotic characteristics. Metcalfe et al. (2010) applied the concept of rotated potential mixing (RPM) flow to Hele-Shaw cells, which are analogues of Darcian systems. In that work RPM flows were generated by programmed assemblies of dipole pumping pairs distributed around the perimeter of a unit disk. The conceptual layout is shown in Figure 2.

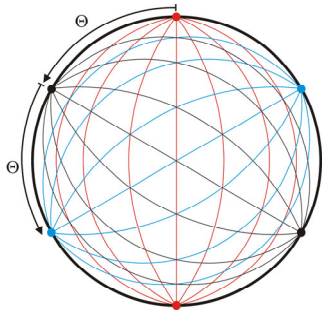

Figure 2 Schematic of RPM flow in a disk. Each dipole pair (red, black, blue) is activated in turn by sequential jumps of angle Θ (Trefry et al., 2011a).

Re-orientation of the flow is programmed by the jump angle Θ and the dipole activation time τ (see Trefry et al., 2011a for details). Figure 3 shows the effect of sequential dipole pumping on a dyetrace experiment.

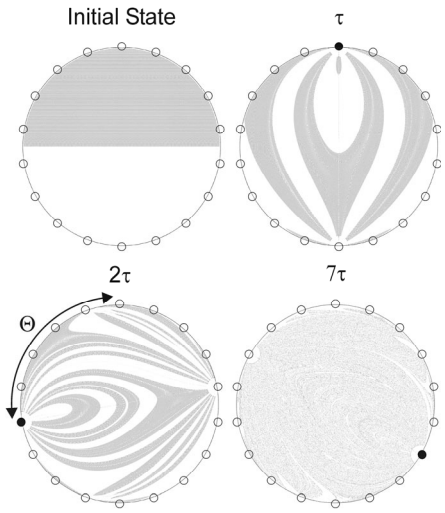

Figure 3 Stirring behaviour for an RPM flow with 9 dipoles and Θ = 100°. The initial tracer distribution is rapidly and efficiently homogenised after 7τ (after Trefry et al., 2011b).

For various combinations of Θ and τ, continued sequential dipole activations within the disk eventually lead to the three key regime types:

I. the establishment of periodic regimes with coherent and deterministic orbits

II. chaotic regimes with incoherent fluid trajectories

III. mixed regimes where both chaotic and coherent zones are present but are separated by kinematic boundaries

Figure 4 shows a Poincaré section for an RPM flow with both chaotic and coherent zones. Tuning the Θ and τ parameters can yield a large variety of RPM patterns which fall broadly into the three types listed above.

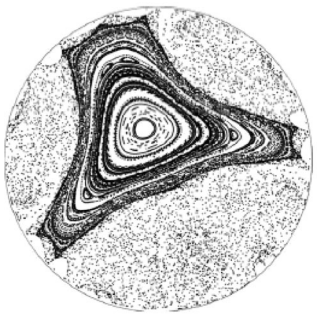

Figure 4 Poincaré section for an RPM flow displaying coherent orbits surrounded by an incoherent chaotic zone (after Trefry et al., 2011b).

Transport Dynamics and Engineering

Using a simplified theoretical approach involving potential theory, Lester et al. (2010) showed that the transport of scalar quantities (e.g. concentration and heat) is enhanced in the incoherent zones. That is, RPM flows may be engineered to induce enhanced dispersion within chaotic zones. As a corollary, the coherent zones yield conventional transport behaviour. Thus it is potentially feasible to consider designing RPM programmes to display the necessary coherent/incoherent structures that are required for any particular application.

Kinematic Confinement

Fluid present within the kinematic boundaries of an RPM flow, i.e. within the zone of coherent periodic orbits, will remain there for the duration of the RPM program. In the absence of hydrodynamic dispersion, this fluid will follow its coherent orbit in a periodic fashion, and will never leave this orbit. Thus, if a target zone can be engineered to lie within a kinematic boundary, its fluid can be sequestered within the kinematic boundary indefinitely, at least in theory.

Enhanced Mixing

Fluid lying in the chaotic zone will describe random trajectories, which is equivalent to strong stirring, but will never cross a kinematic boundary into the coherent zone. Again, simply by choosing an appropriate RPM programme, zones can be isolated and subjected to enhanced stirring.

Hydrogeological Considerations

The theoretical development raises many interesting possibilities for subsurface heat management in aquifers. However the theoretical

approach does not take into account the complexities of field settings which may provide significant perturbations to the simple potential flow models used above. Trefry et al. (2011a) discuss how several practical phenomena may impact upon the theoretical predictions. The most important of these are formation elasticity, physical heterogeneity within the aquifer permeability and porosity fields, and the presence of regional (advective) flow gradients which are almost always present in hydrogeological structures.

Formation Elasticity

Aquifer flow dynamics include elastic terms to account for the compressibility of the aquifer matrix. Such terms are not present in potential flow theories like RPM dynamics. Elasticity is manifested in the short-term response of fluid pressure to stresses, e.g. pumping or other loading, and is measured by the specific storage of the formation. In terms of an RPM-style system with sequential activation and de-activation of dipole pumping pairs, the elastic response of the aquifer is greatest at activation/deactivation time, and decays logarithmically thereafter. If the RPM duration τ is large with respect to the elastic decay time, which is a function of the specific storage, the potential flow theories provide reasonable approximations to the fluid behaviour within confined aquifer systems.

Heterogeneity

The main effect of heterogeneity on the RPM theories described above is to distort and eventually break down the kinematic barriers that separate coherent orbits from chaotic zones. For moderate to low permeability heterogeneity, this manifests as a gradual “leakage” of fluid over the kinematic boundary. In average terms, the leakage of heat originally inside the kinematic boundary describes an exponential decay law scaled by the log-permeability variance so that the higher the variance the higher the leakage rate with time. This heterogeneity-induced leakage limits the duration for which fluid can be sequestered within the kinematic boundary.

Regional Flows

Having a net pressure gradient across the RPM cell perturbs the flow regime. This can result in fluid trajectories being nudged out of the zone of influence of the RPM program, i.e. a net fluid exchange between external and internal zones. This again is equivalent to a leakage phenomenon and limits flexibility in engineering design. For regional flows that represent minor perturbations to the RPM flows, the answer is surprisingly simple. The dipoles, which are normally activated in balanced mode, can be run in slightly unbalanced mode to counteract the regional flow. This is achieved by weighting the dipoles by the cosine of the angle subtended by the dipole axis to the regional gradient, counterbalancing regional bias. This cosine weighting provides its own perturbation to the RPM regime, but the essential dynamics are robust to this kind of perturbation, as long as the regional flows are sufficiently small.

Applications of Subsurface Stirring to Waste Heat Management

In the previous sections we have established a conceptual basis for engineering fluid stirring/mixing processes in the subsurface. By conventional pumping it is easy to emplace heat in or extract heat from the subsurface, either by closed-loop or open-loop technologies. Once in situ, subsurface stirring techniques based on RPM approaches can be used to confine heat distributions within kinematic boundaries and hence limit dissipation, or to maximise dissipation in chaotic zones. Inherent in the following discussion are the following assumptions:

- the aquifer displays Darcian flow dynamics, i.e. can be well represented by a permeable continuum
- aquifer heterogeneity is moderate and regional flow gradients are not extreme
- the aquifer location is shallow enough to make multiple pumping wells economically feasible for heat management applications

Heat Rejection

Conventional heat rejection relies on arrays of pumping and extraction bores, usually run in steady duty cycles. The lifetime of such systems is set by the thermal breakthrough time, i.e. the time taken for the thermal plume to travel from an injection bore to the relevant extraction bore (which supplies cool water to the above-ground plant). If the extraction bore supplies water that is too hot for purpose, the system is no longer useful.

Subsurface stirring may be useful to heat rejection in that it may provide a means to capture injected heat within a kinematic boundary for long periods with minimal leakage (depending on aquifer heterogeneity properties). Alternatively, if the target extraction temperature permits, a purely chaotic RPM regime can be used to distribute the injected heat evenly over the RPM domain, thereby using the thermal capacity of the aquifer much more efficiently than conventional dipole operation can achieve. This may extend the operational life of a conventional heat rejection scheme significantly.

Heat Recycling

Heat is an energy resource that has value. Sustainable technologies will seek to recycle heat energies for benefit. Because of the significant heat capacity of sedimentary hydrogeological

systems they represent ideal storages for large amounts of heat. This may be useful for industrial processes, at large scale, and for seasonal heating/cooling applications in domestic markets. From on the work described earlier in this paper, it is feasible that resource managers may be able to engineer subsurface RPM regimes to preserve heat stores against local pumping perturbations, or to regulate temperatures via programmed dissipation. Given a suitable pumping system design, it should be possible to switch between types I, II and III above, as required.

Conclusions

Fluid mixing theories yield the tantalising prospect of engineering subsurface flow and transport regimes using simple programming of pumping duty cycles. These theories have been tested using Hele-Shaw cells and are now being compared with experiments using metre-scale rigs. If the theories are transferrable to field scale there is real prospect that they may be used for benefit in the management of heat in the shallow subsurface. This may potentially provide sustainable heat rejection technologies, reducing the need for evaporative water consumption. It may also stimulate interest in heat recycling applications, since the two key RPM characteristics of flow confinement and rapid mixing seem eminently suitable for advanced engineering purposes.

References

Lester, D. R., Metcalfe, G., Trefry, M. G., Ord, A., Hobbs, B. and Rudman, M., 2009, Lagrangian topology of a periodically reoriented potential flow: Symmetry, optimization and mixing. Physical Review E: Statistical, Nonlinear and Soft-Matter Physics 80(3), Article 036208.

Lester, D. R., Rudman, M., Metcalfe, G., Trefry, M. G., Ord, A. and Hobbs, B., 2010, Scalar dispersion in a periodically reoriented potential flow: acceleration via Lagrangian chaos. Physical Review E: Statistical, Nonlinear and Soft-Matter Physics 81(4), Article 046319.

Metcalfe, G., Rudman, M., Brydon, A., Graham, L. J. W. and Hamilton, R., 2006, Composing chaos: an experimental and numerical study of an open duct mixing flow. American Institute of Chemical Engineers Journal 52(1), 9-28.

Metcalfe, G., Lester, D. R., Ord, A., Kulkarni, P., Rudman, M., Trefry, M., Hobbs, B., Regenauer-Lieb, K. and Morris, J., 2010, An experimental and theoretical study of the mixing characteristics of a periodically reoriented irrotational flow. Philosophical Transactions of the Royal Society A: Mathematical, Physical and Engineering Sciences 368, 2147-2162.

Trefry, M. G., Lester, D. R., Metcalfe, G., Ord, A. and Regenauer-Lieb, K., 2011a, Toward enhanced subsurface intervention methods using chaotic advection. Journal of Contaminant Hydrology, in press.

Trefry, M. G., Metcalfe, G., Lester, D. R., Ord, A. and Regenauer-Lieb, K., 2011b, Toward enhanced remediation methods using chaotic advection, in M. Schirmer, E. Hoehn and T. Vogt (Eds) GQ10: Groundwater Management in a Rapidly Changing World, Proceedings of 7th IAHS Groundwater Quality Conference, ETH, Zurich, June 2010, IAHS Publication 342, p.217-220, (IAHS Press, Wallingford, UK), ISBN 978-1-907161-16-2, 2011.

Sustainable Geothermal Reservoir Management – A Modelling Suite

Pierre Ungemach, Miklos Antics, Pierre Lalos
pierre.ungemach@geoproduction.fr ; m.antics@geoproduction.fr
GPC IP, PARIS-NORD 2 – Immeuble Business Park – Bât. 4A
165, rue de la Belle Etoile – B.P. 55030, 95946 ROISSY CDG CEDEX, FRANCE

This paper presents the simulation strategy and modelling tools designated to encompass the wide usage spectrum, ranging from shallow to deep and ultra-deep seated, and from cold to tepid and hot water bearings, and their application to selected case studies discussed accordingly.

Keywords: Geothermal Energy, Paris Basin, reservoir modelling, sustainability

Introduction

Heat recovery, well deliverabilities, reservoir life and, last but not least, environmental impacts are key concerns when contemplating sustainable development of geothermal resources. These issues become particularly sensitive in low enthalpy sedimentary environments which address a variety of occasionally conflicting uses

STRATIGRAPHY			LITHOLOGY		RESERVOIRS	USCS	KEY ISSUES/PROBLEM AREAS
				Type			
TERTIARY			Symboles Litholigiques	Shallow Geoth.	Perivious limey/sandy/chalky facies	Shallow Geothermal Heating & Cooling GSHP & GWHP	Temperature maintenance Reservoir life Heat & Cold plumes (in shallow seated aquifers environments) water injection (sands) soil thermal integrity
CRETACEOUS	Senonian			Medium Depth Geoth.			
	Turonian						
	Cenomonian						
	Albian				Lower Albian & Necomian sands	Medium Depth H&C Geoth. GWHP	Reservoir life water injection Dual well completions
	Lower cretac.						
JURASSIC	MALM	Tithonian					
		Kimmeridgian					
		Oxfordian			Lusitanian limestones	Deep Geothermal GDH PH	Erratic permeability well architecture
	DOGGER	Callovian		Deep Geothermal			
		Bathonian			Oulitnic & barrier facies limestones	GDH&C PH oil prod.	Geomodelling reservoir structure Reservoir life cooling kinetics Optimum heat extraction well architecture (horizontal drilling) thermochemistry
		Bajocian					
		Aslenian					
	LIAS	Toarcian					
		Lower Lias			Sandstones	GDH&C PH + oil	
TRIAS		Rhetian					
		Keuper			Sandstones & canglomeratic	GDH&C PH	Reservoir performance well architecture and completion thermochemistry
		Bontsandstein		Ultra Deep Geoth.			
Permo-carbonifenos BASEMENT					EGS ?	CHP	EGS Problematic (temp. < 150°C)

Table 1: Summary of basin lithostratigraphic features and actual/potential geothermal usage. GSHP, GWHP: ground source/groundwater heat pumps (HPs). GDH: geothermal district heating. H&C: heating and cooling. CHP: combined heat and power. PH: process heat. PP: petroleum production.

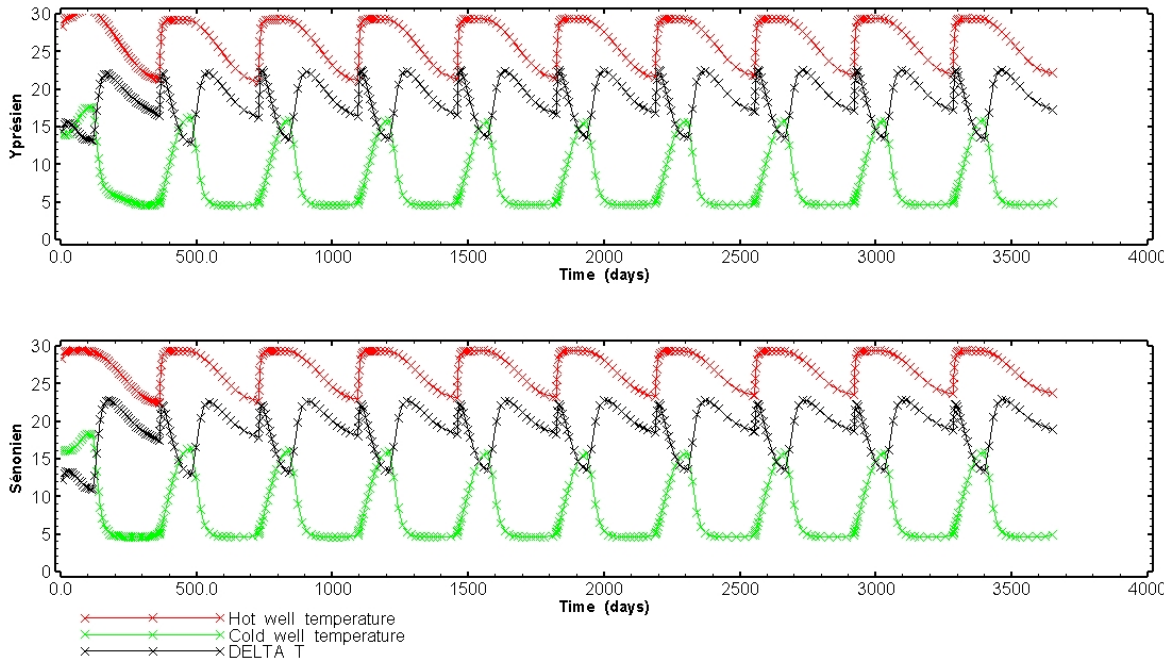

Figure 2: Cold and hot well temperatures and flow rate transients

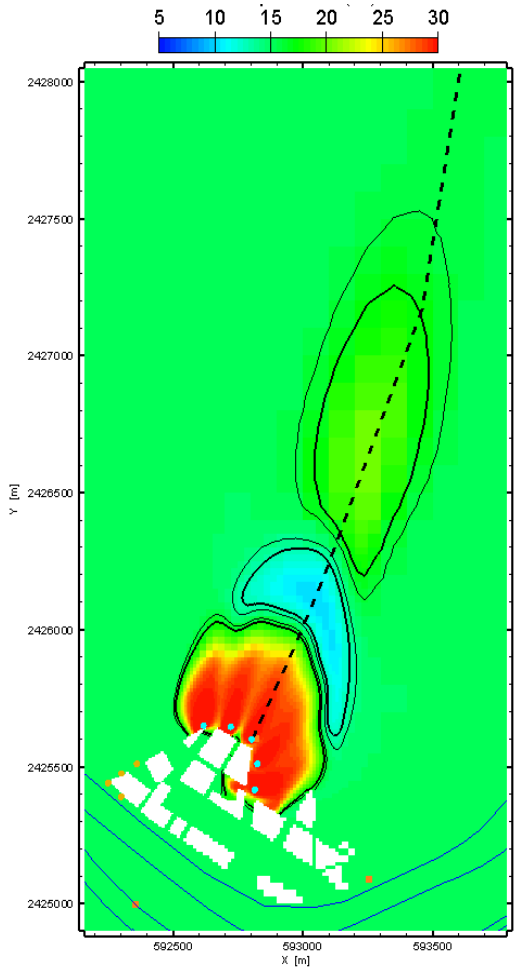

Figure 2: Extent of the thermal plume after 17.7 years of operation (red circled production wells, blue circled injection wells)

and related thermal, hydrodynamic and thermochemical implications requiring appropriate reservoir management policies. These problematic are exemplified in table 1 which displays a typical sedimentary sequence borrowed to the central part of the Paris basin, and the usage/key/issues/ problem areas vis-à-vis, chosen as a representative case study.

This paper presents the simulation strategy and modelling tools designated to encompass the wide usage spectrum, ranging from shallow to deep and ultra-deep seated, and from cold to tepid and hot water bearings, and their application to selected case studies discussed accordingly.

Simulation strategy and modelling tools

Meeting the aforementioned goals by quantifying/mitigating their impacts on reservoir behaviour has been the driving rationale in designing a relevant simulation strategy, thoroughly tested over the past decade (Antics, 2009).

The modelling suite consists of commercial – TOUGH2 V2 (Pruess et al, 1999), SHEMAT (Clauser 2003), TOUGHREACT (Xu et al 2004), MView (Intera) interfacing, GOCAD (Paradigm, 2009) and in-house – wellbore module, economic evaluation package – software. It covers almost the entire porous medium chain, from pore (water injection, plugging/bridging kinetics) to wellbore (well completion, near wellbore damage) and (local/regional) reservoir (optimisation of GDH, H&C, ATES systems, resource management) scales and shallow to deep reservoir settings.

Shallow geothermal

Simulation aims at (i) securing optimum heat (and cold) extraction in environmentally sensitive aquifer environments, and (ii) mitigating the

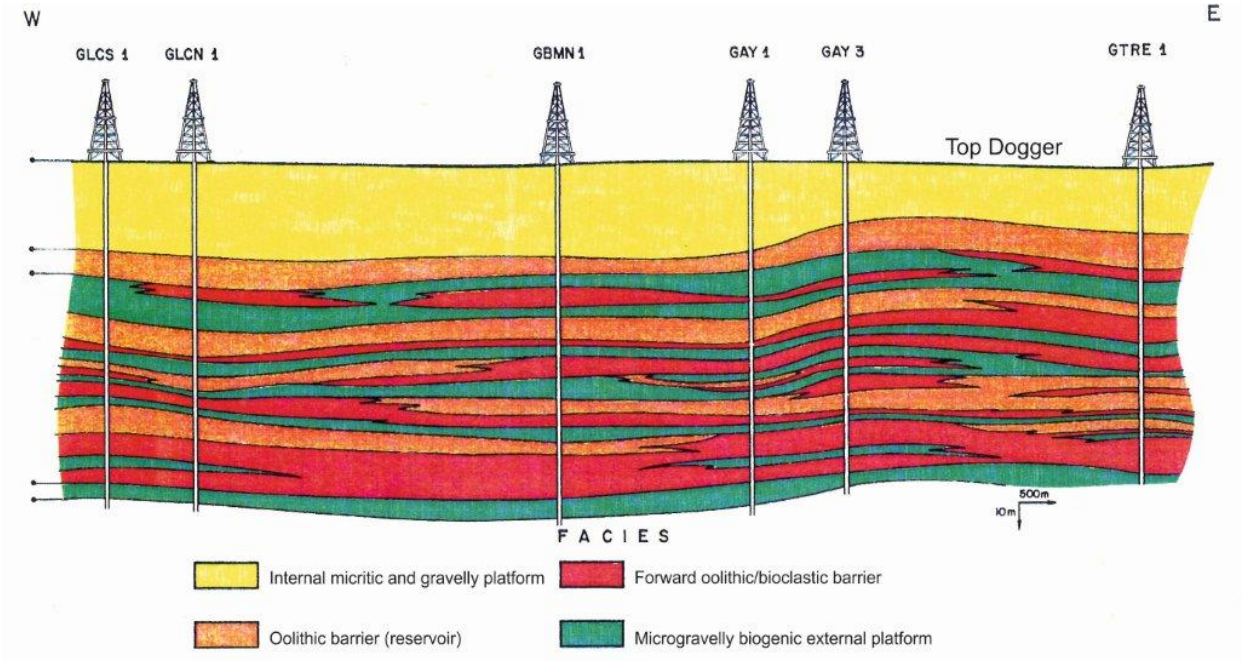

Figure 3: Tentative facies correlations. Northern area (Rojas *et al*, 1989)

thermo-hydraulic impacts on soil and aquifer conservation. Heat (cold) recovery is achieved via ground source (GSHP) and groundwater (GWHP) heat pump systems.

Borehole heat exchangers (GSHP) and water wells (GWHP) arrays are modelled with a view to keep thermal and hydraulic interferences within the limits of the claimed area and avoid the consequences of undue unbalanced heat and cold loads. Examples of GWHP modelling are shown in fig.1 (ATES) and 2 (simultaneous heat and cold production) (Lalos et al, 2010).

The ATES system exploits two aquifers hosted in chalky (lower) and sandy (upper) formations respectively for the heating and cooling of a residential/commercial building located downtown

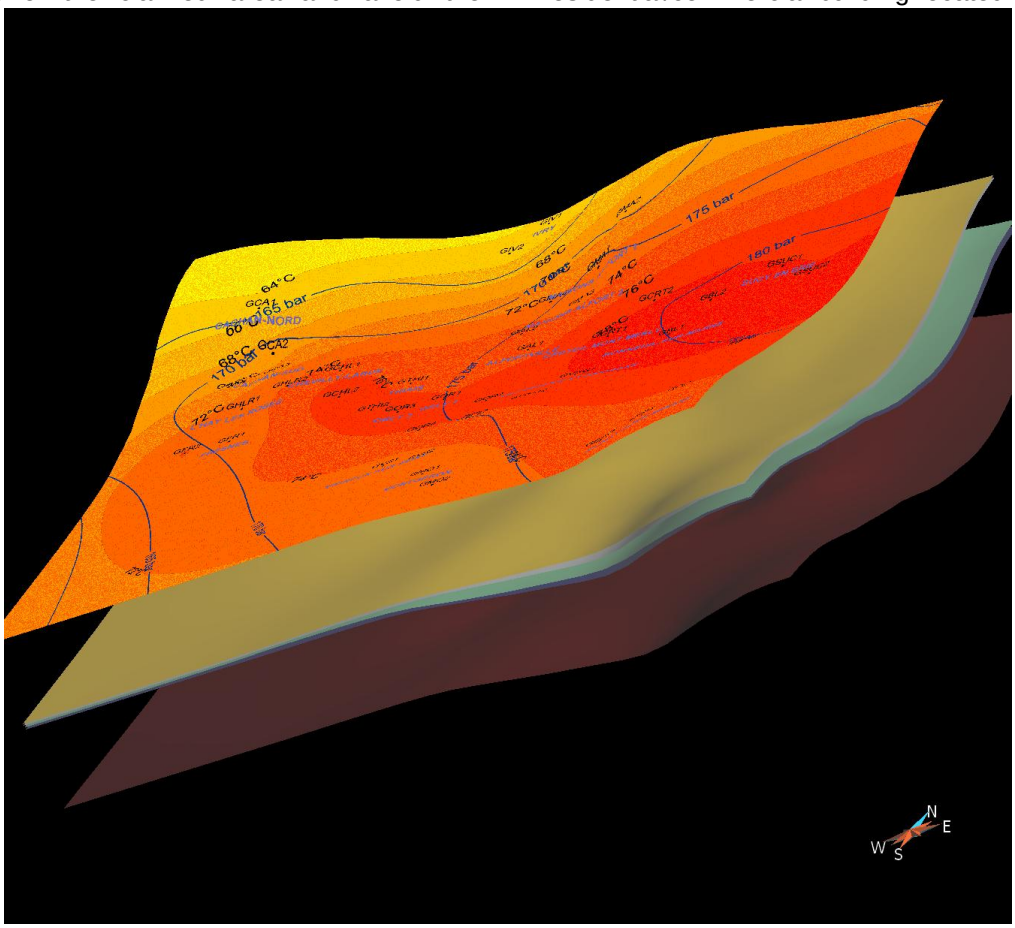

Figure 4: GOCAD 3D view of the sandwich reservoir.

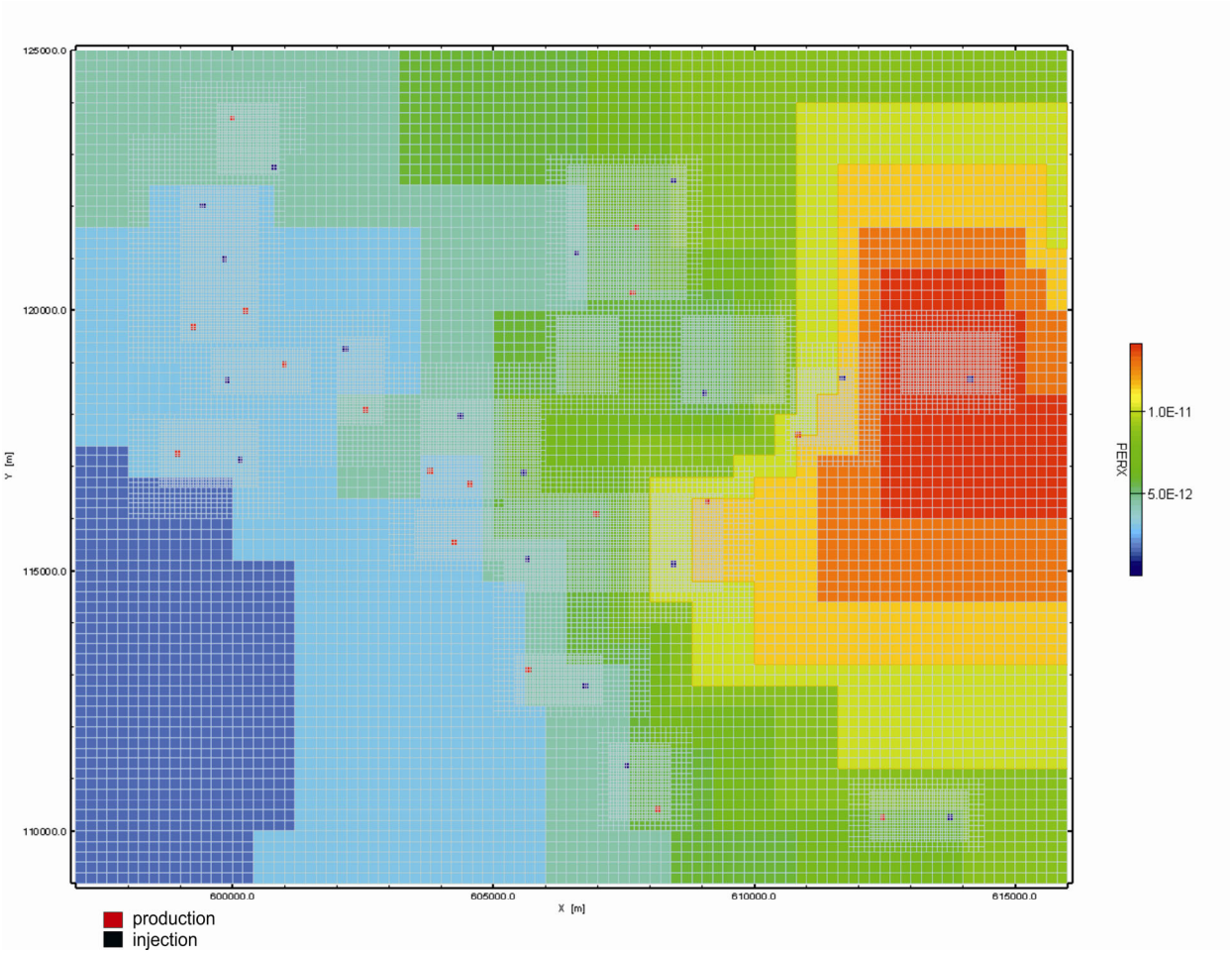

Figure 5: Model grid and discretised permeability field.

Paris. The system operates under thermally (heat vs cold) balanced conditions, with wells alternating seasonally production and injection modes. In fig.1 cold and hot well temperature transients show fast stabilisation following the first year provided the system operates at variable (vs temperature differentials) flow rates.

The H&C system includes a nine (4 producers, 5 injectors) well grid completed in a dependable if not prolific superficial (40 m deep) semi-confined aquifer. Here the system gets complicated by (i) the connection of the aquifer to an upward river stream, (ii) the presence of deep anchored car park walls acting as in-field impervious barriers, and (iii) severely unbalanced heat and (dominant) cold loads. The latter is only but partly counterbalanced by a thermal dilution favoured by a significant aquifer hydro-dynamism leading to the downstream diffusion of the hot plume (induced by the prevailing cold cycle) shown in fig.2. This result validated by the model calibration (history matching) on monitored observation wells led to the redesign of the initially planned H&C system.

Geomodelling of complex reservoir structures

The deep (ca 1800 m) multilayered interfingered structure (mid-Jurassic oolithic limestones) mentioned in table one and depicted in fig.3 has long been exploited for geothermal district heating (GDH) purposes (34 doublets operating to date). Previous reservoir simulations attempts failed in matching actual production well cooling kinetics induced by the (re)injection of the heat depleted brine. The reason was attributed to an oversimplified reservoir structure, assumed single layer (i.e. cumulating individual pervious thicknesses) equivalent (fig.3).

The aging of existing GDH grids added to new development expectations require an urgent commitment to reservoir management issues. This in turn implies a representative reservoir structure to be modelled in order to secure reliable thermo-hydrodynamic predictive simulations. The foregoing could be achieved thanks to an approach, suggested by fig 6 outputs, (i) applying a GOCAD geomodelling software (Paradigm, 2009) to a multidoublet heterogeneous “sandwich” (Antics et al, 2005, Ungemach et al, 2011) structure – stacking interbedded, hydraulically impervious but

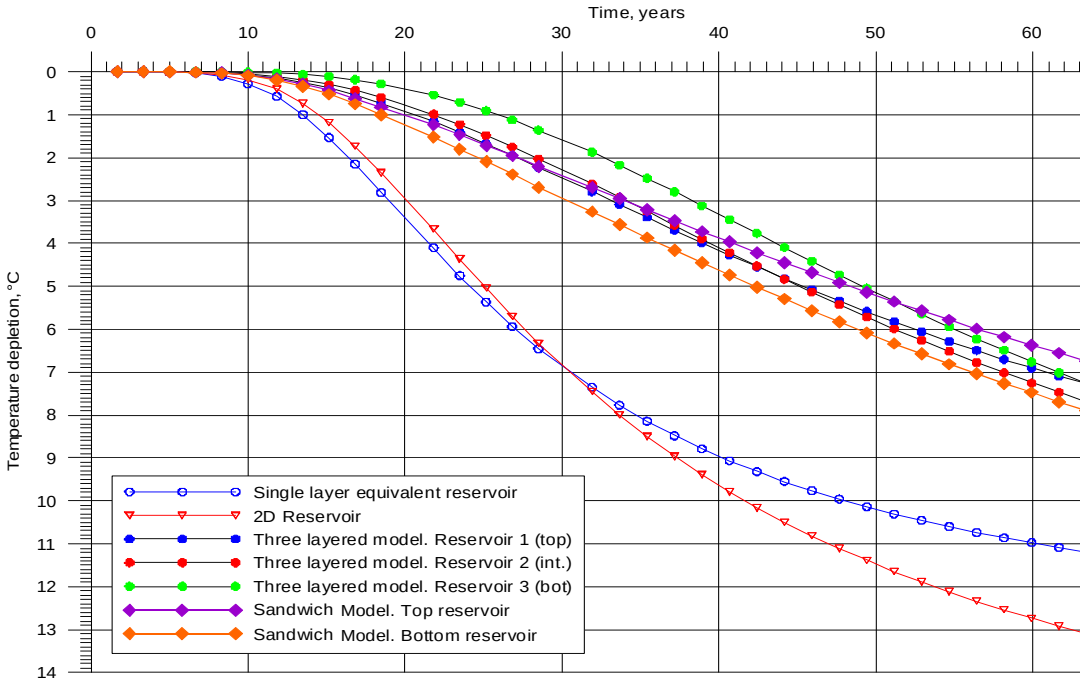

Figure 6: Cooling kinetics of three candidate (single layer, three layered, sandwich) equivalent structures.

thermally conductive, layers into one single heat storage/supply unit, squeezed between two symmetric reservoir layers, each sharing one half of the cumulative pervious bed (net pay) thicknesses, the overall three layered equivalent system overlain/underlain by cap and bed rocks respectively, (ii) exporting the GOCAD issued "sandwich" image, portrayed in fig.4, over the discretised domain (ca 300 km² in area) shown in fig.5, to a MVIEW interfaced TOUGH2 V2 (Pruess, 1991), and (iii) ultimately releasing feasible history matching sequences, never completed in past simulation runs (Ungemach et al, 2011, Foulquier et al, 2011). Work in progress address the interfacing of GOCAD with TOUGH2V2 input/output files.

Well architecture

- Dual completion wells. They aim at splitting in a simple well the production and injection flowrates in two aquifers according to fig.7a well profile. This design which responds to a need for reconciling high production ratings with lower injective capacities (case of loose sandy formations) leads to the temperature cross section imaged in fig.7b.
- Horizontal/sub-horizontal wells. Performances of horizontal, sub-horizontal and multilateral flow paths completed in either multilayered or thin layered reservoir structures shape quite attractive in consideration of upgraded well deliverabilities, reservoir longevities and heat recovery factors compared to conventional (vertical, slightly slanted) well designs (Ungemach *et al*, 2011, Promis *et al*, 2011). A simulation was exercised regarding the four well doublet trajectories, (i) two vertical wells, (ii) two slightly deviated wells (present status), (iii) two horizontal legs draining one preferential layer, and (iv) two sub-horizontal wells (slant angle nearing 85°) drains intersecting the whole pay-interval respectively, described in fig.8. Results which focused on production well cooling kinetics highlighted option (iv) as the best candidate, significantly delaying thermal breakthroughs.

A further simulation has investigated the multilayered reservoir/sub-horizontal well scheme reduced to its, stacked, three layered sandwich equivalent formalised by Antics et al, 2005, for assessing order to assess the sensitivity of thermal breakthrough to layer productivity distribution. This shortcut has been implemented in order to drastically reduce computer time without significantly distorting cooling kinetics (Antics et al, 2005).

Results listed in table 2 show that, depending upon the layer productivity pattern; thermal breakthroughs spread over a fourfold time span, indeed a rewarding outcome.

Table 2: Cooling kinetics. Multilayered reservoir. Sub-horizontal wells

LAYER PRODUCTIVITY % TOTAL FLOW		THERMAL BREAKTHROUGH
Q1	Q2	(YEARS)
0.75 X QTOT	0.25 X QTOT	21.5
0.25 X QTOT	0.75 X QTOT	77
0.65 X QTOT	0.35 X QTOT	29
0.35 X QTOT	0.65 X QTOT	71.5
0.50 X QTOT	0.50 X QTOT	49.5

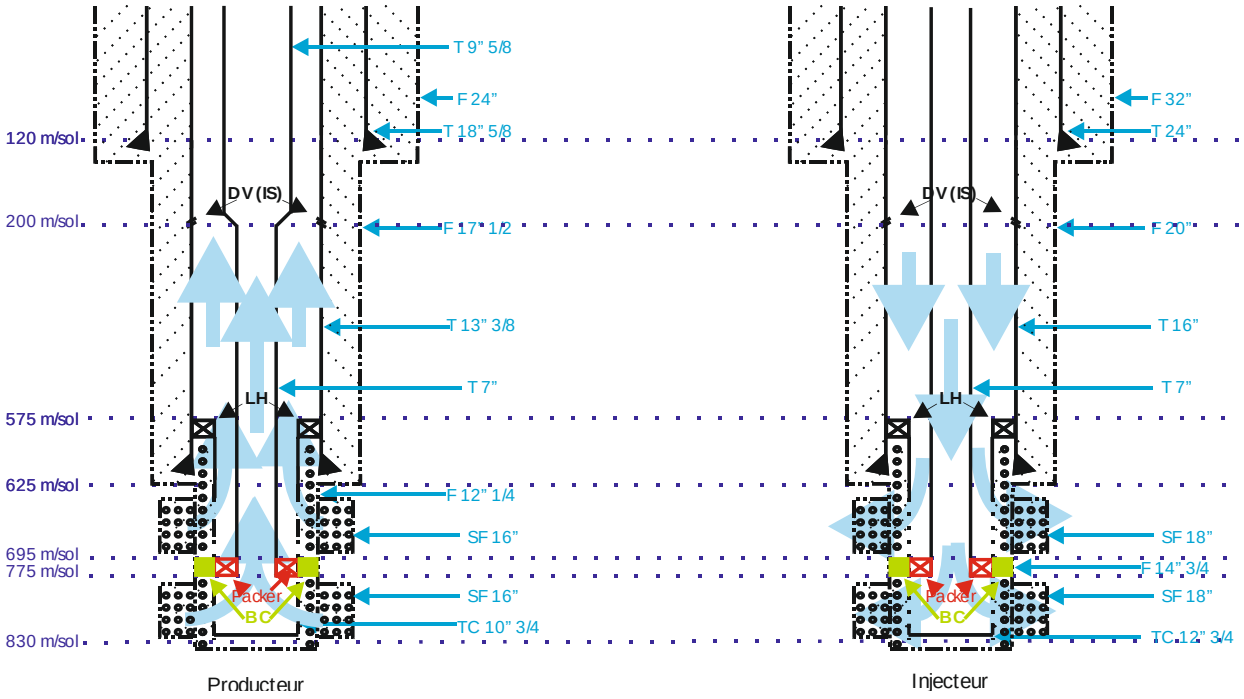

Figure 7a: Dual aquifer completion well profile

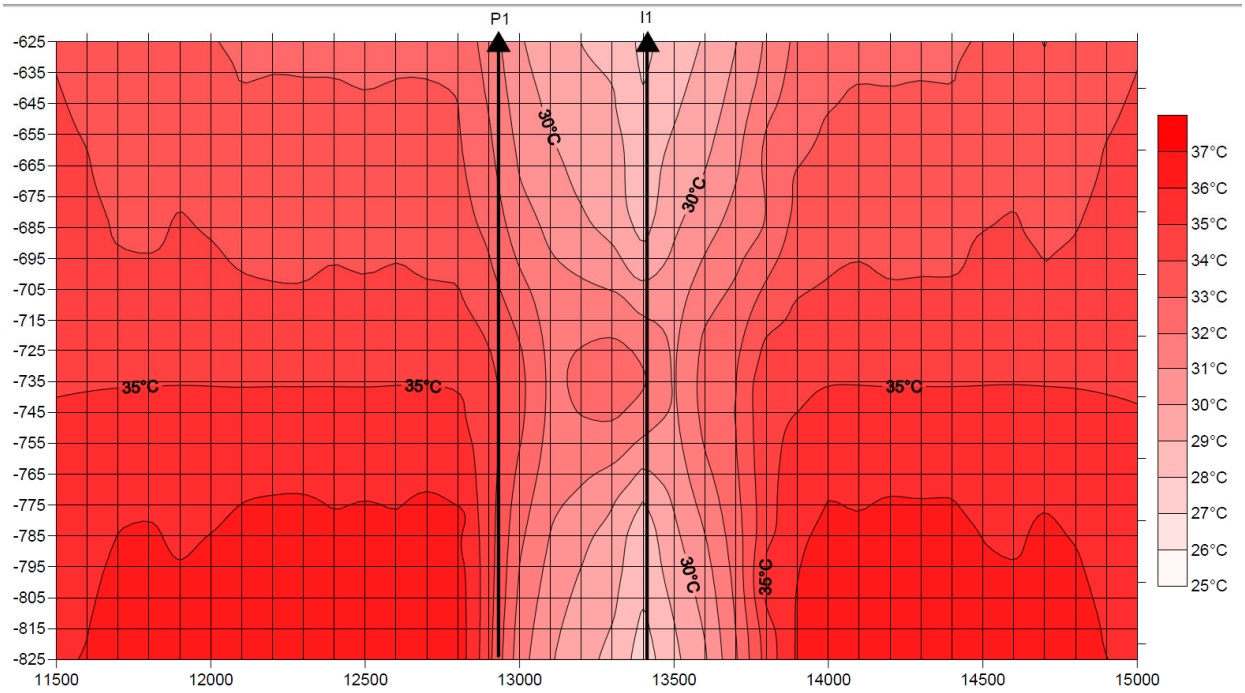

Figure 7b: Dual aquifer completion. Vertical temperature distribution

Thermochemistry, environmental impacts

Injection of cooled geothermal brine into the source reservoir is another concern as it may lead to severe, eventually irreparable, well/near well damage, a matter reviewed by Ungemach (2003) (11).

The consequence of cooler than usual (20 °C against 40 °C) injection practice into clastic and carbonate reservoirs have been investigated by Borozdina et al, 2011, from the rock-water interactive thermochemistry standpoint based on reactive transport modelling (Kühn and Schneider, 2003) using SHEMAT (Clauser, 2003) and TOUGHREACT (Xu et al, 2004).

Heat transfer and solute transport modelling indicate, for a sandstone matrix and a highly saline formation brine (ca 100 g/l), (i) fast silica oversaturation/precipitation kinetics stabilising after 48 hours at 6 m from well sandface, and (ii) a quartz concentration increase and porosity decrease. The resulting permeability near well pattern, displayed in fig.8, evidences a

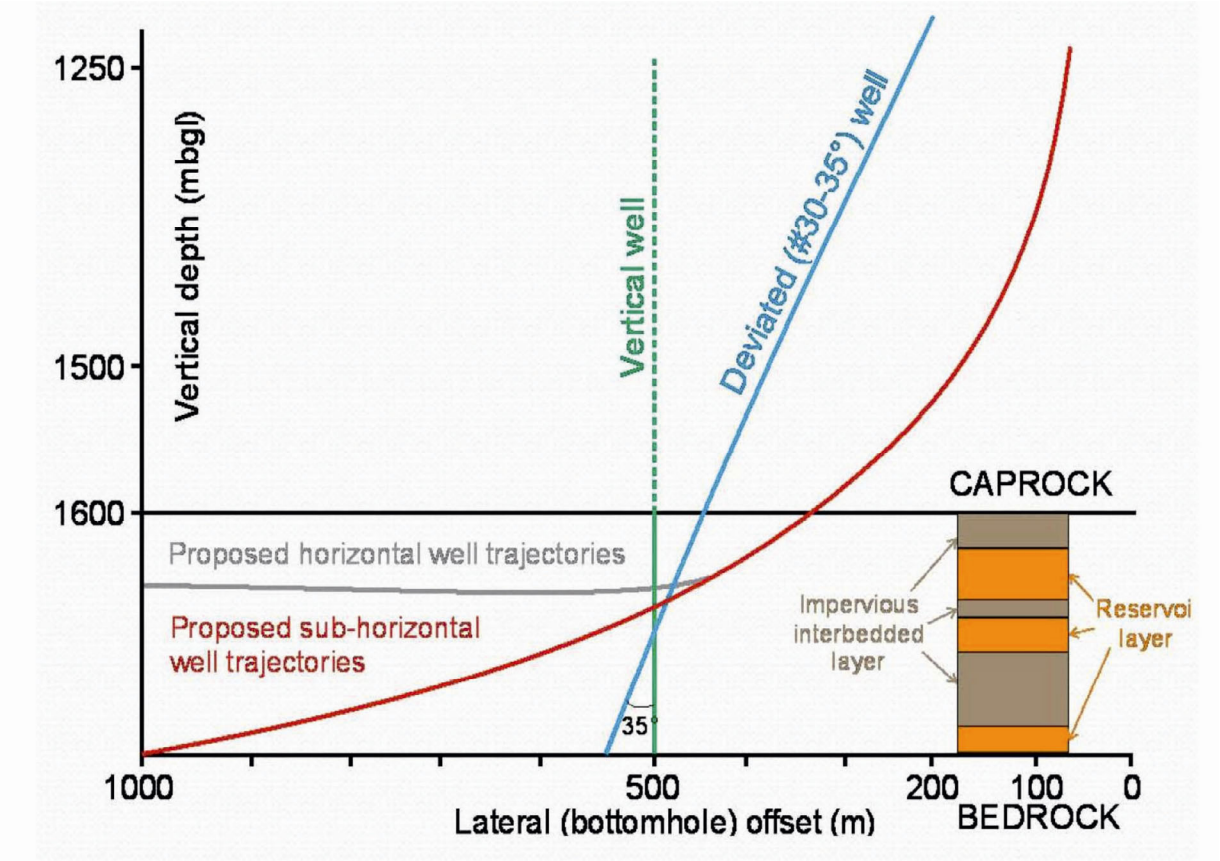

A. Candidate well trajectories. Multilayered reservoir. Conventional (vertical, deviated) and suggested (horizontal) well trajectories.

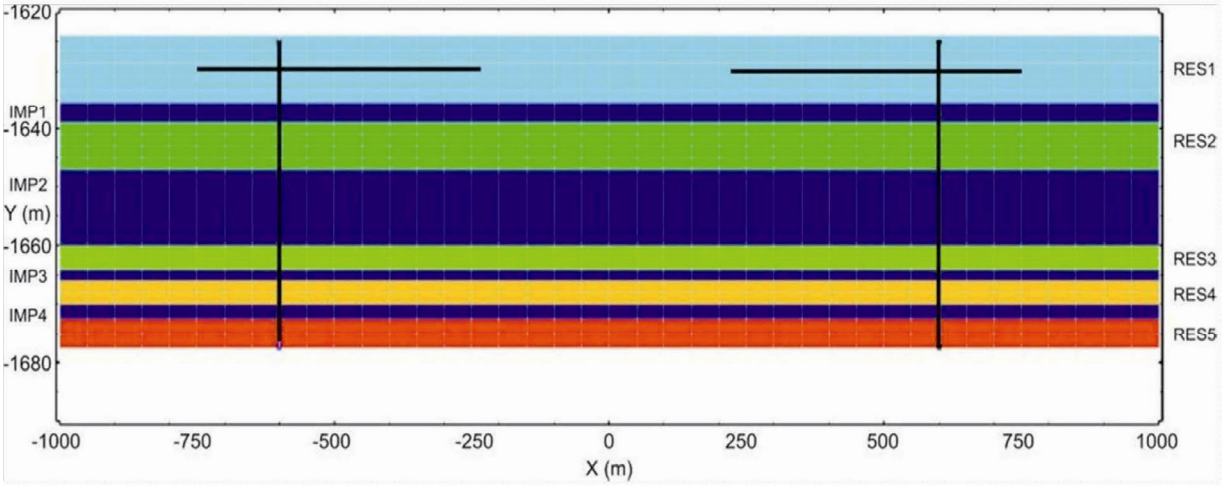

B. Well projections (vertical vs horiizontal) at reservoir depth.

Figure 8: A - Well Trajectories. B - Multilayered reservoir structure.

diminishing trend, whose magnitude is negligible – from 3% @ 30 °C (as a result of Silica deposition) to 3.15% @ 20 °C – is negligible from a practical engineering point of view.

Leaky well short comings are likely to occur owing to well aging as experienced on several GDH systems. The impact of a two level injector well casing piercing could be appraised in terms of thermal and chemical pollution of communicating aquifers, illustrated in fig.10, by means of a wellbore module coupled to a standard TOUGH2V2 simulator.

Conclusion

The applications of a modelling suite addressing the simulation of a wide range of contrasted uses,

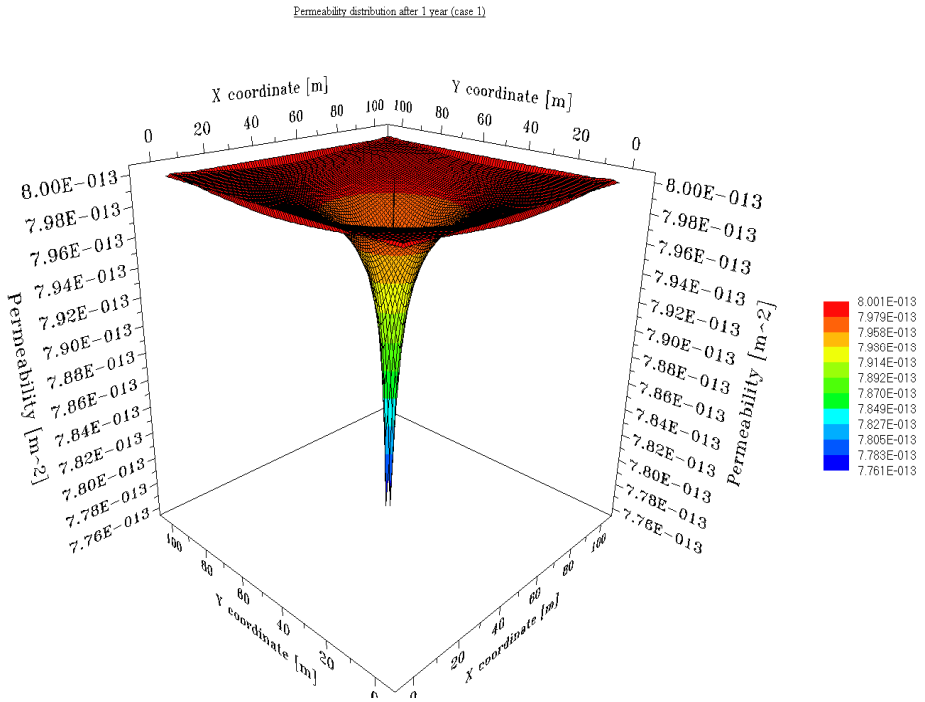

Figure 9: Permeability distribution as a function of x (m) and y (m) coordinates after one year of injection (injection temperature = 30°C)

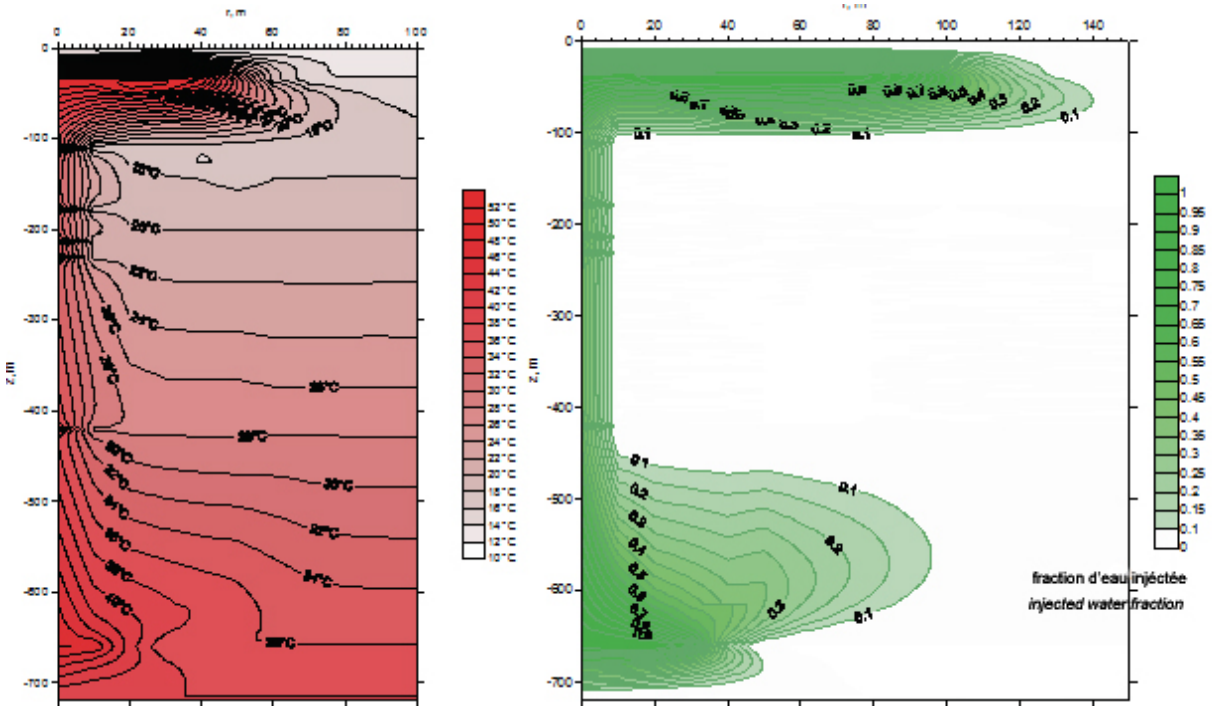

Figure 10: Extent of aquifer thermal and chemical invasion

reservoir settings and well configurations, inherent to the farming of low enthalpy sources have been presented.

Based on the aforementioned case studies this suite should be advocated as a tool box meeting the demands of concerned players-reservoir engineers, geothermal operators, control/ monitoring mining authorities and energy planners at large, committed to sustainable management of geothermal resources.

References

Antics, M. (2009). Insight Into Modern Geothermal Reservoir Engineering and Management Practice, Geothermal Energy and CO2 Storage: Synergy or Competition, GFZ Potsdam (2010)

Pruess, K., Oldenburg, C.M., Moridis, G.J. (1999). TOUGH2 User's Guide version 2.0. Lawrence Berkeley National Laboratory. Report LBNL-43134, Berkeley, CA, USA

Clauser, C. (Ed.) (2003). Numerical Simulation of Reactive Flow in Hot Aquifers. SHEMAT and Processing SHEMAT, Springer Publishers, Heidelberg, Germany

XU, H., Sonnenthal, E.L., Spycher, N., Pruess, K. (2004). TOGHREACT User's Guide : a Simulation Program for now. Isothermal Multiphase Reactive Geochemical Transport in Variably Saturated Geologic Media. Lawrence Berkeley National Laboratory Report LBNL-55460, 203p.

PARADIGM (2009). GOCAD 2009.1 User Guide

Lalos, P., Ungemach, P., Antics, M. (2010). Bali publ. Reservoir Management of Simultaneous Heat and Cold Production from Shallow Aquifers, WGC2010, Bali, Indonesia

Antics, M., Papachristou, M. Ungemach, P. (2005). Sustainable Heat Mining. A Reservoir Engineering Approach. Proceedings of the 30th Annual Workshop Geothermal Reservoir Engineering, Stanford, CA., USA, 2005

Ungemach, P. Antics, M. Lalos, P., Borozdina, O., Foulquier, L., Papachristou, M. (2011). Geomodelling and well Architecture Key issues to Sustainable Reservoir Development. Proceedings of the 36th Annual Workshop Geothermal Reservoir Engineering, Stanford, CA., USA, 2011

Foulquier, L., Antics, M., Ungemach, P. (2011). Geomodelling Input to the Simulation of Multilayered Geothermal Reservoirs. A Regional case study 1st Sustainable Earth Sciences Conference & Exhibition. Technologies for Sustainable Use of the Deep Sub-surface. 8-11 NOV. 2011, Valencia, Spain

Promis, M.P., Lalos, P., Ungemach, P., Antics, M. (2011). Geothermal Well Architecture, a Key Issue in Sustainable Reservoir Development. Valencia, Spain

Ungemach, P. (2003). Reinjection of Cooled Geothermal Brines into Sandstone reservoirs. Geothermics, 32, 743-761

Borozdina, O., Ungemach, P., Antics, M. (2011). Near Well Impact of Cooled Geothermal Brine Injection Application to Selected Sedimentary Reservoir Environments1st Sustainable Earth Sciences Conference & Exhibition. Technologies for Sustainable Use of the Deep Sub-surface. 8-11 NOV. 2011, Valencia, Spain

Kühn, M., Scheinder, W. (2003). Injection Well with Reaction Kinetics in Clauser, C. (2003), op.cit.

QGECE research on delineation of Australian geothermal resources

[1] I.Tonguç Uysal*, [2] Massimo Gasparon, and [3] Scott E. Bryan
t.uysal@uq.edu.au
[1] Queensland Geothermal Energy Centre of Excellence, The University of Queensland, St Lucia, QLD 4072
[2] School of Earth Sciences, The University of Queensland, St Lucia, QLD 4072
[3] Biogeoscience, Queensland University of Technology, GPO Box 2434, Brisbane, QLD 4001

The geology/reservoir program of the Queensland Geothermal Energy Centre of Excellence (QGECE) has the mission to improve the existing knowledge and develop new innovative scientific approaches for the identification of geothermal resources in Australia, with a particular focus on Queensland. Specifically, the QGECE geology/reservoir program is currently (1) producing a comprehensive geochemical dataset for high heat producing rocks, (2) conducting detailed mineralogical and geochronological studies of granites and hydrothermal alteration minerals, and (3) investigating the Cooper Basin representing a superb natural laboratory for understanding of radiogenic heat enrichment process and possible involvement of mantle heat flow. Seven research projects have been established, which are being conducted largely as PhD studies. In the preliminary studies, high quality and valuable results were obtained to address the research topics of understanding the causes and timing of heat producing element enrichment.

Keywords: Queensland, HHP granite, geochemistry, isotope, geochronology, hydrothermal alteration

Research topics of the QGECE geology/reservoir program

The current research projects of the QGECE geology/reservoir program include: (1) Petrological, geochemical and geochronological studies for characterisation and identification of high heat-producing granites (HHPG) in Queensland; (2) Generation of regional high crustal heat flow zones in relation to tectono-magmatic evolution of Queensland; (3) Geochemistry and geochronology of fluid flow events in high heat producing granitic rocks; (4) Origin and evolution of deep fluids and water-rock interactions in the Cooper Basin; (5) Evolution of the Cooper Basin and the origin of the geothermal energy; (6) CO_2 degassing in seismically active geothermal systems; (7) Trace element geochemistry of near-surface quartz deposits in the Drummond Basin as an exploration tool for geothermal systems.

Petrological, geochemical and geochronological studies for characterisation and identification of heat-producing granites in Queensland

The ongoing PhD studies of Vicki Marshall, Coralie Siegel and Jaco Van Zyl are obtaining new age data on HHP granites from Queensland, South Australia and Europe along with chemical information on the accessory U & Th-bearing zircons (e.g., Marshall et al. 2011). The preliminary observations indicate that strong U and Th enrichments in the granites examined so far may be derived through strong fractional crystallisation. While post-magmatic alteration may locally and variably redistribute U in some of the granites (e.g., Carnmenellis, UK), it is probably not responsible for the underlying enrichment in heat-producing elements. Thus it appears that magmatic differentiation must be called upon to produce the observed enrichments. The question that then arises is what factors lead to (and govern) this enrichment through fractional crystallisation. These studies will ultimately place important new constraints on the timing and spatial associations of accessory- and major-mineral precipitation and the influence this has on granite chemical evolution and ultimate HPE architecture. One important implication that emerges from preliminary analyses is that for S-type granites, the most fractionated (e.g., Rb-rich) do not necessarily represent those that are the most enriched in U and Th. This will have important consequences for the heat production through contrasting vertical and lateral distributions of HPE in zoned and composite plutons.

Understanding the spatial-temporal-compositional distribution of HHPG in Queensland

Queensland has >175,000 km^2 of exposed igneous rock; the potential for EGS is thus huge in the state. >15,000 analyses of granitic rocks that include geochemistry, age, lithology and distribution information have been compiled by Coralie Siegel from federal and state geological surveys with additional published and unpublished datasets. The data indicate the significant presence of HHPG in Queensland: approximately ~15% and ~22% of the analysed igneous rock and granitic rocks samples in the database have heat production values >5 $\mu W/m^3$, respectively.

However, there is a limited understanding of these HHPG in Queensland in terms of their distribution in the subsurface, dimensions, ages, and controlling factors in their genesis. Compounding this problem is that although high concentrations of radiogenic elements and therefore high heat production is exclusively found in igneous rocks with high silica contents (>70% SiO_2), not all high-silica igneous rocks are high heat producing; and show a spectrum of heat production values from 0 to 18 $\mu W/m^3$.The observed extreme variation in calculated heat production for igneous rocks in Queensland and globally, thus raises a number of questions that will be addressed by Coralie Siegel through her PhD study.

Geochemistry and geochronology of fluid flow events in high heat producing granitic rocks

Alex Middleton (PhD student) has presented preliminary results on the petrology and chemistry of secondary accessory minerals from the best-known European HHP granites and some examples from Queensland (Hodgkinson and Gallilee Basin target areas) (see Middleton et al., 2011). He showed that Th (generally considered as an immobile element) could be mobilised and stored in newly formed accessory minerals along with U and some rare earth elements. Electron microscopic studies combined with geochemistry of the Galilee Basin basement rocks (a possible source of HHP in this basin) show that pervasive hydrothermal alteration may have been responsible for secondary precipitation of monazite-cheralite as the predominant REY- and Th-bearing metastable phase. Vitrinite reflectance (VR) and recent temperature data from existing deep petroleum holes indicated that the Galilee Basin has geothermal potential in Queensland. Recent VR data of the Origin Energy show irregular distributions with depth indicating that hydrothermal fluid circulations may have affected the thermal history of the Galilee Basin (personal commun. with Richard Suttill, 2011).

Origin and evolution of deep fluids and water-rock interactions in the Cooper Basin: Geochemical investigation of a geothermal reservoir

Study of fluid-rock interaction in geothermal systems has become one of the major goals. This is mainly because fluids play an important role in heat transfer as well as mineral reactions and precipitations in the reservoir, geothermal loop, from the production casing to the surface tubing, the heat exchanger and the reinjection casing. Chemical and isotopic compositions of geothermal fluids in conventional hydrothermal systems have been studied extensively for reconstruction of the evolution of fluids in space and time, their migration pathways, and their sources (e.g., Pauwels et al., 1993). However, similar studies for understanding the fluid flow process and water-rock interaction process in Hot systems, particularly in the Cooper Basin are virtually missing. The QGECE geology/reservoir program is conducting a project to establish the viability of Sr-O-H isotope, trace and rare earth element geochemistry of deep waters in the granite and waters in the sediments of the Cooper/Eromanga Basin. The studies will provide understanding of mineral scaling in the geothermal system, and help determining the geothermal fluid pathways and evaluation of the potential of shallow waters as a geothermal exploration tool. Previously, we analysed trace element content of the granite of Big Lake Suite and reported that the most altered shallow granites have anomalously high U and Th concentrations (Uysal et al., 20110). We analysed recently trace element chemistry of deep geothermal fluids from the Habanero drill hole provided by Geodynamics. U content is low considering relatively high concentrations and mobility of this element in granitic environments. The low U indicates its extreme immobility and therefore strongly reducing conditions, which is consistent with positive Eu anomaly on the normalised REE diagram (Fig. 1). REE values are extremely low suggesting that fluid element composition comes from interaction with granite, but certainly not a high-heat producing granite. In other words, the chemistry of the deep reservoir water does not indicate interaction with HHPG. Our future research will include the investigation of more samples from Habanero holes as well as water samples from Cooper/Eromanga Basin sediments.

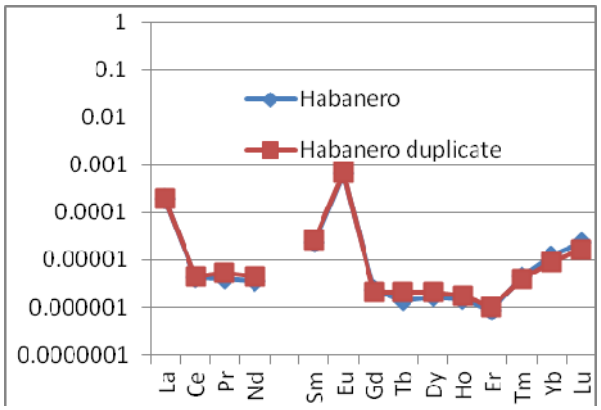

Figure 1. REE pattern of Habanero geothermal water

Evolution of the Cooper Basin and the origin of the heat production

We investigated trace element (analysed by ICP-MS) and stable isotope (Oxygen and hydrogen) geochemistry of whole rock granite samples and hydrothermal phyllosilicate alteration minerals separated from the granite and overlying sandstones and mudstones of the Cooper Basin. Granite core samples from shallow depths in the Moomba 1, Big Lake 1 and Mcleod 1 wells are strongly altered with pervasive sericite (illite) and

Table 1. Trace element data for Habanero geothermal water

Sample (ppb)	Habanero 03-1	Habanero 03-2
Li	68219	50856
Mg	116	94
Ca	6039	5487
As	607	416
Rb	6326	5749
Sr	1008	1030
Cs	11435	10357
Ba	847	959
La	0.0463	0.0464
Ce	0.0026	0.0028
Pr	0.0004	0.0005
Nd	0.0017	0.0020
Sm	0.0035	0.0040
Eu	0.0387	0.0399
Tb	5.02427E-05	7.91647E-05
Gd	0.000	0.000
Dy	0.000	0.001
Ho	8.25232E-05	9.75189E-05
Er	0.0001	0.0002
Tm	0.0001	0.0001
Yb	0.0020	0.0016
Lu	0.0006	0.0004
W	303	403
Pb	0.0011	0.0014
Th	0.0003	0.0004
U	0.0001	0.0001

quartz precipitation, associated with intense micro-fracturing and veining. The intensity of hydrothermal alteration is less in samples from Habanero 1, whereas no phyllosilicate mineral altyeration is observed in samples from Jolokia. Highly altered granites from former holes are substantially enriched in lithophile elements, particularly in Cs, Rb, Be, Th, U and rare earth elements (REE) relative to the upper continental crust (UCC). U and Th contents with concentrations of up to 30 and 144 ppm, respectively, are 10 and 13 times higher than those of the UCC. We propose that the enrichment of heat-producing elements was promoted by a regional hydrothermal event leading to the precipitation of U and Th- bearing minerals such as illite and thorite. Crystallinity index (illite crystallinity) of the sericite indicates hydrothermal temperatures ranging from 250 °C (in Moomba 1 and Big Lake 1) to 350 °C (in McLeod 1). In the overlying sedimentary rocks, crystallinity of authigenic illites translates to lower crystallisation temperatures (150 - 200 °C). Normalised REE patterns of the mostly altered granite samples show a strong negative Ce anomaly, signifying oxidation of trivalent Ce to less soluble tetravalent Ce. Geochemistry of whole rock and mineral samples suggest that, in contrast to the reducing environment in the current geothermal fluids in Habanero, fossil hydrothermal mineral deposition occurred under oxidising conditions. Oxygen and hydrogen isotope compositions of illites from the granites and sedimentary rocks are very similar, with $\delta^{18}O$ = -1.8‰ to +2.7‰; δD = -99‰ to -121‰ for granites and $\delta^{18}O$ = +2.3‰ to +9.7‰, δD = -78‰ to -119‰ for sedimentary rocks. The calculated oxygen and hydrogen isotope compositions of fluids in equilibrium with the illites are depleted in ^{18}O and deuterium, comparable to those of waters reported for most high-latitude sedimentary basins. Hence, stable isotope data of alteration minerals in the granite and the overlying sedimentary rocks suggest the operation of a hydrothermal system involving high latitude meteoric waters during extensional tectonism in the Cooper Basin region. Rb–Sr dating of hydrothermal illites have identified a hydrothermal event at ~95 Ma (Fig. 2) affected the Big Lake suite granite and the sediments from Warburton and Cooper Basins - this is possibly related to regional heating associated with a rifting events along the southern and eastern Australian margins at this time. Rb–Sr age data are consistent with the reported paleotemperatures that were highest at 90-100 Ma (Gallagher et al., 1994).

CO_2 degassing in seismically active geothermal systems

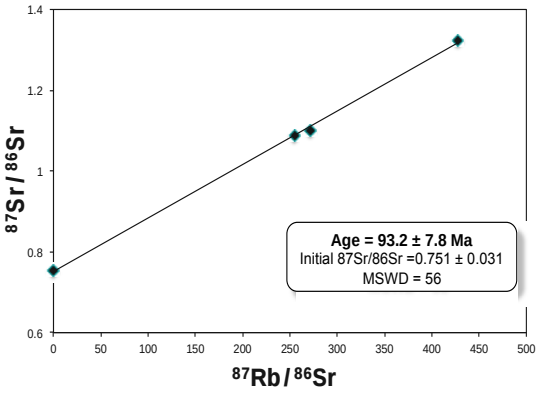

Figure. 2. Rb–Sr isochron diagram for hydrothermal illite from the Big Lake suite granite.

QGECE is pioneering a significant modification to the EGS technology called the supercritical CO2 thermosiphon (Gurgenci et al., 2008, Atrens et al 2009, Atrens et al. 2010). This expands on an earlier proposal of utilising CO_2 as heat transmission fluid (Brown, 2000; Pruess, 2006). In a CO_2 thermosiphon, CO_2 instead of brine is circulated through the hot dry rock reservoir to extract the heat and is directly expanded at the surface to produce electricity. This new approach may significantly enhance productivity, with thermal cycle efficiencies up to 50% higher than those for conventional geothermal binary power plants. An auxiliary benefit is the likely CO2 sequestration through its capture by the reservoir

(Pruess, 2006). The benefits of artificial CO2 injection into a predominantly water-filled HSA reservoir are deduced from past experience with naturally-sourced CO_2 injections into hydrothermal reservoirs. Intensive degassing of CO_2-saturated fluids in the hydrothermal systems has been known to give rise to a high fluid flux and the associated heat release (Chiodini et al., 2007). The presence of large amounts of CO_2 in the fluid makes convection much stronger (Straus and Schubert, 1979). The use of CO_2 injection to augment convection may substantially increase the commercial viability of HSA reservoirs.

Although the use of CO_2 in either context offers substantial promise, there are a number of geological, geochemical, and environmental uncertainties. It has to be demonstrated that: 1) the CO_2 injected will largely remain in the reservoir of the selected site without being degassed to the surface; 2) CO_2-bearing fluids will act as an optimal heat transmitter rather than a substance that damages the reservoir and the expander. In order to provide some understanding of the long-term fate of sub-surface CO_2 we are investigating existing conventional geothermal sites that have naturally elevated CO_2 concentrations. This project examines the periodic degassing of CO_2 from geothermal waters in Turkey leading to calcite vein and breccia deposition. Natural CO_2 discharges are abundant in Turkey as evident from ongoing deposition of recent terrace-mound travertines and emplacement of widespread carbonate vein and breccia deposits in fractured damage zones of active fault systems. Our field observations indicate that the calcite veins and breccias were initiated as hydro-fractures in basement rocks by CO_2-rich fluid overpressure and propagated to the surface (Uysal et al., 2009, 2011). As we demonstrated successfully in our recent studies, such unique fracture-filling carbonate deposits can be dated precisely by U-series dating technique (Uysal et al., 2007, 2009, 2011). Tectonism, climate and hydrology are considered to control the distribution and accumulation of CO_2 in spring or thermal waters in geothermal systems (Rihs et al., 2000; D'Alessandro et al., 2007). Previous studies have argued that travertine deposition in geothermal systems occurs preferentially during warm and humid periods in the late Quaternary probably due to increased availability of geothermal water of meteoric origin (Sturchio et al., 1993; Rihs et al., 2000). By contrast, a large number of carbonate veins we dated by the high-precision U-series technique coincides with times of cold/dry climate events (Uysal et al., 2009, 2011). We proposed that a significant reduction in surface discharge of CO_2 by spring or geothermal waters during dry climate periods may have promoted oversaturation of CO_2 in deep reservoirs. Host rock fracturing in response to seismic shaking and fluid overpressure results in rapid exsolution and expansion of the dissolved gas and consequently hydrothermal eruptions leading to massive and transient travertine vein deposition in the hydrothermal system (Uysal et al., 2009). In the non-hydrothermal but seismically active systems, CO_2 degassing occurs as a result of episodic seismic cycles, with the vein formation through repeated fracturing and sealing by new calcite precipitation (crack-seal mechanism) (Uysal et al., 2011).

Trace element geochemistry of near-surface quartz deposits in the Drummond Basin as an exploration tool for geothermal systems

Silica is the most abundant chemical compound in the Earth's upper crust; yet the trace element geochemistry of SiO_2 has not been utilised routinely in addressing not only exploration of mineral resources but also different geological problems. This is mainly due to the crystal structure of silica and the small size of the Si^{4+} ion, allowing only small amounts of trace elements to be incorporated into the crystal lattice. If some trace elements are present in quartz, they mostly occur either in micrometer-scale mineral inclusions, or more commonly in fluid inclusions (Götze et al., 2004). A number of studies used various minerals other than silica phases (e.g., carbonates and clays) for the geochemical tracing of hydrothermal fluid flow events in various tectonic settings (Bau and Dulski, 1995; Uysal and Golding, 2003; Uysal et al., 2009). However, only a few studies have reported trace element contents in quartz specifically to evaluate the petrogenetic and geochemical evolution of selected metamorphic, hydrothermal, and pegmatitic environments (Götze et al., 2004). Extensive Paleozoic sinter deposits occur at the surface associated with sub-surface quartz veining and epithermal Au mineralisation in the Drummond Basin, Australia. We investigated the trace element composition of the sinter deposits and quartz veins in an attempt to develop a new geochemical exploration guide for geological resources. We demonstrated in our recent study that rare earth elements and some other trace elements in siliceous materials may provide important information on the source of hydrothermal fluids, fluid chemistry, and physico-chemical environments of hydrothermal fluids (see Uysal et al., 2009, 2011 for more detail).

References

Atrens, A.D., Gurgenci, H., Rudolph, V. 2009. CO2 thermosiphon for competitive power generation. Energy & Fuels 23, 553-557.

Atrens, A.D., Gurgenci, H., Rudolph, V. 2010. Electricity generation using a carbon-dioxide thermosiphon. Geothermics 39, 161-169.

Bau, M. and Dulski, P., 1995. Comparative-study of yttrium and rare-earth element behaviors in

fluorine-rich hydrothermal fluids. Contributions to Mineralogy and Petrology, 119, 213-223.

Brown, D.W., 2000. A hot dry rock geothermal energy concept utilizing supercritical CO2 instead of water. Twenty-Fifth Workshop on Geothermal Reservoir Engineering, Stanford University, Stanford, California. pp.

Chiodini, G., A. Baldini, F. Barberi, M. L. Carapezza, C. Cardellini, F. Frondini, D. Granieri, and M. Ranaldi, 2007. Carbon dioxide degassing at Latera caldera (Italy): Evidence of geothermal reservoir and evaluation of its potential energy. Journal of Geophysical Reearch., 112, B12204, doi:10.1029/2006JB004896.

D'Alessandro, W., Glammanco, S., Bellomo, S. and Parello, F., 2007. Geochemistry and mineralogy of travertine deposits of the SW flank of Mt. Etna (Italy): Relationships with past volcanic and degassing activity. Journal of Volcanology and Geothermal Research, 165, 64-70.

Gallagher, K., Dumitru, T.A., and Gleadow, A. J. W., 1994, Constraints on the vertical motion of eastern Australia during the Mesozoic. Basin Research, 6, 77-94.

Götze, J., Plotze, M., Graupner, T., Hallbauer, D.K. and Bray, C.J., 2004. Trace element incorporation into quartz: A combined study by ICP-MS, electron spin resonance, cathodoluminescence, capillary ion analysis, and gas chromatography. Geochimica et Cosmochimica Acta, 68, 3741-3759

Gurgenci, H., Rudolph, V., Saha, T., Lu, M., 2008. Challenges for geothermal energy utilisation. Thirty-Third Workshop on Geothermal Reservoir Engineering, Stanford University, Stanford, California. pp.

Marshall, V., Knesel, K., and Bryan, S.E., 2011, Residence of accessory minerals in, and the geochemistry of, high heat-producing granites in Queensland and Europe. Australian Geothermal Energy Conference 2011.

Middleton, A., Uysal, I.T., Golding, S.D, and Forster, H.-J., 2011, Ca(La,Ce,Sm)(CO3)2(F,OH) (synchysite?) from the Soultz high-heat producing monzogranite, Soultz-sous-Forêts, France: Implications to titanite destabilisation and differential REE mobility in hydrothermal systems. Australian Geothermal Energy Conference 2011.

Pauwels, H., Fouillac, C., And Fouillac, A.-M., 1993, Chemistry and isotopes of deep geothermal saline fluids in the Upper Rhine Graben: Origin of compounds and water-rock interactions: Origin of compounds and water-rock interactions. Geochimica et Cosmochimica Acta, 51, 2737-2749.

Pruess, K. 2006. Enhanced geothermal systems (EGS) using CO2 as working fluid—A novel approach for generating renewable energy with simultaneous sequestration of carbon. Geothermics 35, 351–367.

Rihs, S., Condomines, M. and Poidevin, J.L., 2000. Long-term behaviour of continental hydrothermal systems: U-series study of hydrothermal carbonates from the French Massif Central (Allier Valley). Geochimica et Cosmochimica Acta, 64, 3189-3199.

Sturchio, N.C., Dunkley, P.N. and Smith, M., 1993. Climate-driven variations in geothermal activity in the Northern Kenya Rift-Valley. Nature, 362, 233-234.

Uysal, I.T. and Golding, S.D., 2003, Rare earth element fractionation in authigenic illite-smectite from Late Permian clastic rocks, Bowen Basin, Australia: implications for physico-chemical environments of fluids during illitization. Chemical Geology, 193, 167-179.

Uysal, I.T., Feng, Y, Zhao, J-X., Altunel, E., Weatherley, D., Karabacak, V., Cengiz, O., Golding, S.D, and Collerson, K.D., 2007, U-series dating and geochemical tracing of late Quaternary travertine in co-seismic fissures. Earth and Planetary Science Letters, 257, 450-462.

Uysal, I.T., Feng, Y, Zhao, Işik, V., Nuriel, P., Golding, S.D.,2009, Hydrothermal CO2 degassing in seismically active zones during the late Quaternary. Chemical Geology, 265, 442-454.

Uysal, I.T., Gasparon, M., van Zyl, J. and Wyborn, D., 2010. Alteration mineralogy and geochemistry as an exploration tool for detecting basement heat sources in sedimentary basins. European Geological Union Conference, Vienna, Austria, May 2010.

Uysal, I.T., Gasparon, M,, Bolhar, R., Zhao, J.-X., Feng, Y, and Jones, G., 2011, Trace element composition of near-surface silica deposits – a powerful tool for detecting hydrothermal mineral and energy resources. Chemical Geology, 280, 154-169.

Uysal, I.T., Feng, Y, Zhao, Bolhar, R., Işik, V., Baublys, K., Yago, A., and Golding, S.D., 2011, Seismic cycles recorded in late Quaternary crack-seal veins: Geochronological and microchemical evidence. Earth and Planetary Science Letters, 303, 84-96.

Using gravity and magnetic methods with geomorphology and geology for basement and structural studies to assist geothermal applications in the Perth Basin

Wilkes, P.G [1], Timms, N [2], Corbel, S[1] and Horowitz, F.G [3]
CSIRO [1], Curtin University [2], University of WA [3]
Paul.Wilkes@csiro.au
WA Geothermal Centre of Excellence, Perth, PO Box 1130, Bentley, WA 6102

This research is part of an ongoing investigation into the 'hot sedimentary aquifers' of the Perth Basin for geothermal applications by WA Geothermal Centre of Excellence (WAGCOE).

Keywords: hot sedimentary aquifer, basin analysis, isostatic residual gravity, gravity worms

Project description

Knowledge of the structural architecture and bedrock geology under Perth is a vital prerequisite for understanding subsurface fluid flow for targeting geothermal prospects and for aquifer management. This study has integrated new and existing geophysical data with Shuttle Radar Topographic data (SRTM), geomorphology and surface geology to provide a new interpretation of the subsurface geology of Perth and its setting within the Perth Basin. The onshore Perth Basin is a north-south trending series of troughs extending approximately 1000 km in extent from the Northampton Block in the north to the south coast of WA. (Song and Cawood, 2000). The eastern boundary with the Yilgarn Craton is the Darling Fault and the western margin is approximately 150 km offshore. Sediments were deposited from the Permian to Holocene and are associated with the separation of Greater India from Australia. The Basin has variable thickness of sediments, locally in excess of 10 km.

Data availability

Several generations of geological maps for the Perth Basin, Perth area and western part of the Yilgarn block have been used to provide a starting point for this study. Regional gravity and aeromagnetic data from Geoscience Australia (GA) are available for the onshore and offshore Perth Basin. Lockwood (2004) has produced an isostatic residual gravity dataset for the whole of WA and data have been extracted form this to encompass the Perth Basin that incorporate corrections for mantle-crust topography and seawater depth. The available aeromagnetic data over the Perth Basin is mainly from 1957, Gravity data for the offshore Perth Basin have been derived from satellite altimetry (Sandwell and Smith, 2009).

New ground gravity data have been acquired for the Perth metropolitan area by WAGCOE at a spacing of 1.5 x 1.5 km and some detailed traverses with 50 and 100 m station spacing. A new gravity image for Perth is shown in Figure 1. Shuttle radar topographic data at 90 x 90 m spacing have been used to create a digital elevation dataset for the Perth metropolitan area (Figure 2).

Data processing

The new gravity data for the Perth area have been processed with a wavelet technique – sometimes called 'worming' (Hornby et al, 1999) which involves multiscale edge detection on magnetic and gravity data to assist in definition of faults and other geological boundaries. Gravity gradient data have been most useful in this study. New images of geophysical data have been integrated with SRTM and geological data to provide a refined structural interpretation of the Perth Basin and a new structural interpretation of the Perth metropolitan area.

Key Results

Aeromagnetic and gravity data have been used to re-interpret the major fault network of the Perth Basin, yielding a preliminary statement of a new fault network. The main differences between the new fault network and previous interpretations are: identification of NW-SE trending fault systems that link faults in the Yilgarn craton with 'transfer zones' inferred by previous workers (these displace other fault sets in the Perth Basin); new faults identified in areas previously with sparse faults (e.g., from Cervantes to Bunbury); new faults identified as part of the Urella Fault system; key cross-cutting faults in the Bunbury Trough; new faults systems identified on the Yilgarn craton.

The new fault network in the Perth metropolitan area includes at least five differently oriented sets of faults (Fig. 3). Deep worms reveal the west-dipping Darling Fault, a blind northern strike extension of the Serpentine Fault, and a new onshore N-S fault that is sub-parallel to the coastline. Small displacement faults (approximate throws of tens of metres) identified by surface features are expressed as shallow worms and align with deflections in deeper worms, indicating that they exist to at least 2.5 km depth. Three main grabens have been generated by recent (at least post-Pleistocene) faults that control the

position and meanders of the Swan and Canning Rivers and the location of lakes and wetlands in the Perth metropolitan areas. In order of relative timing, these are the N-S trending Bibra graben, the NE-SW trending Kings Park graben, and the NW-SE trending Ardross graben. The newly recognised faults could be highly significant in controlling the paleo and modern day fluid flow in areas with geothermal potential.

References

Hornby, P., Boschetti, F., and Horowitz, F. G. (1999). Analysis of potential field data in the wavelet domain. Geophysical Journal Intl. 137(1), 175-196.

Lockwood, A.M., 2004 Western Australia Isostatic Residual gravity anomly and depth to basement model. GSWA Record 2004/14.

Sandwell, D. T., and Smith, W. H. F. (2009), Global marine gravity from retracked Geosat and ERS-1 altimetry: Ridge segmentation versus spreading rate, J. Geophys. Res., 114, B01411.

Song, T and Cawood, P.A., 2000 Structural styles in the Perth Basin associated with the Mesozoic break-up of Greater India and Australia, Tectonophysics, 317, 55-72.

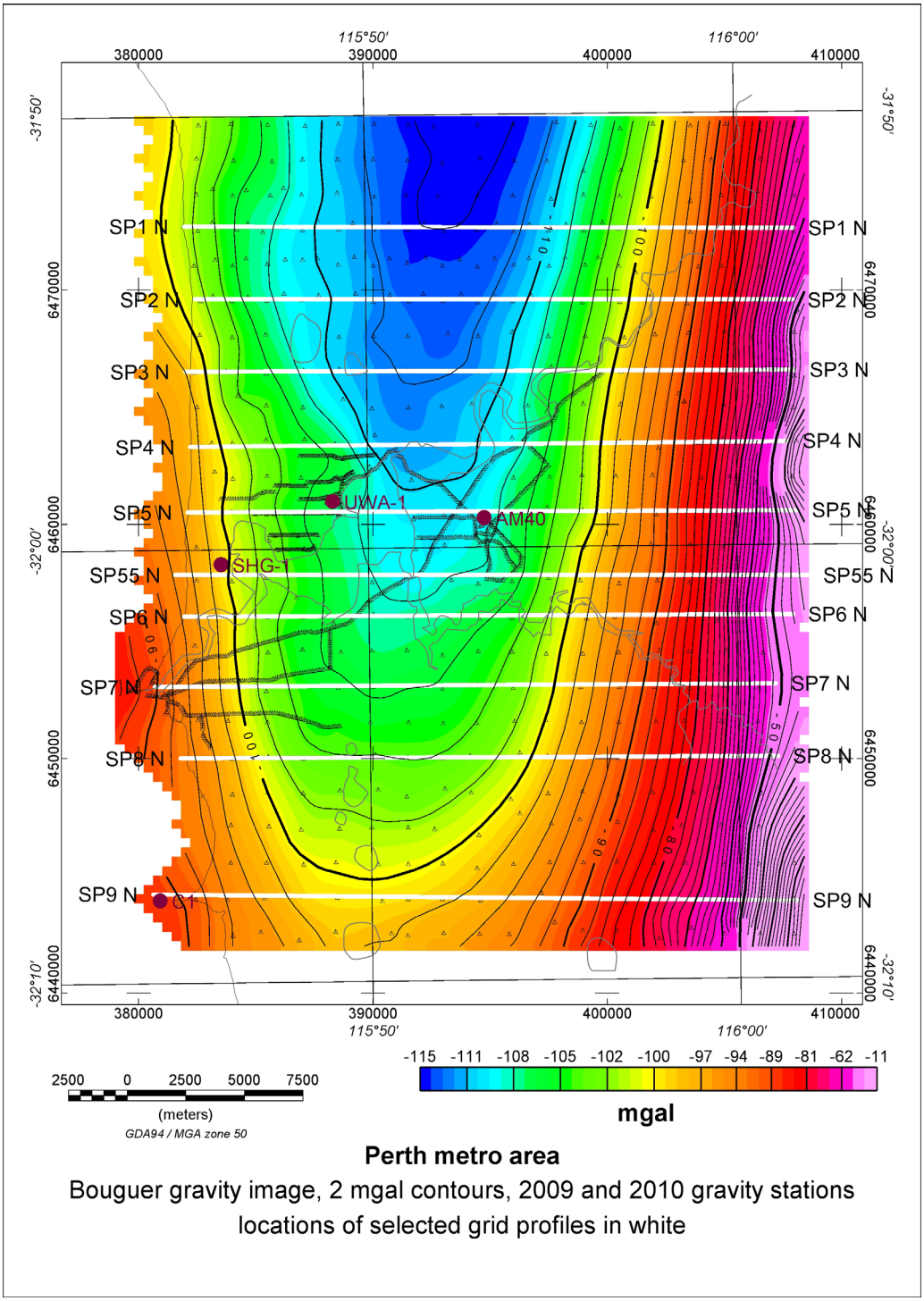

Figure 1: New gravity image for Perth area

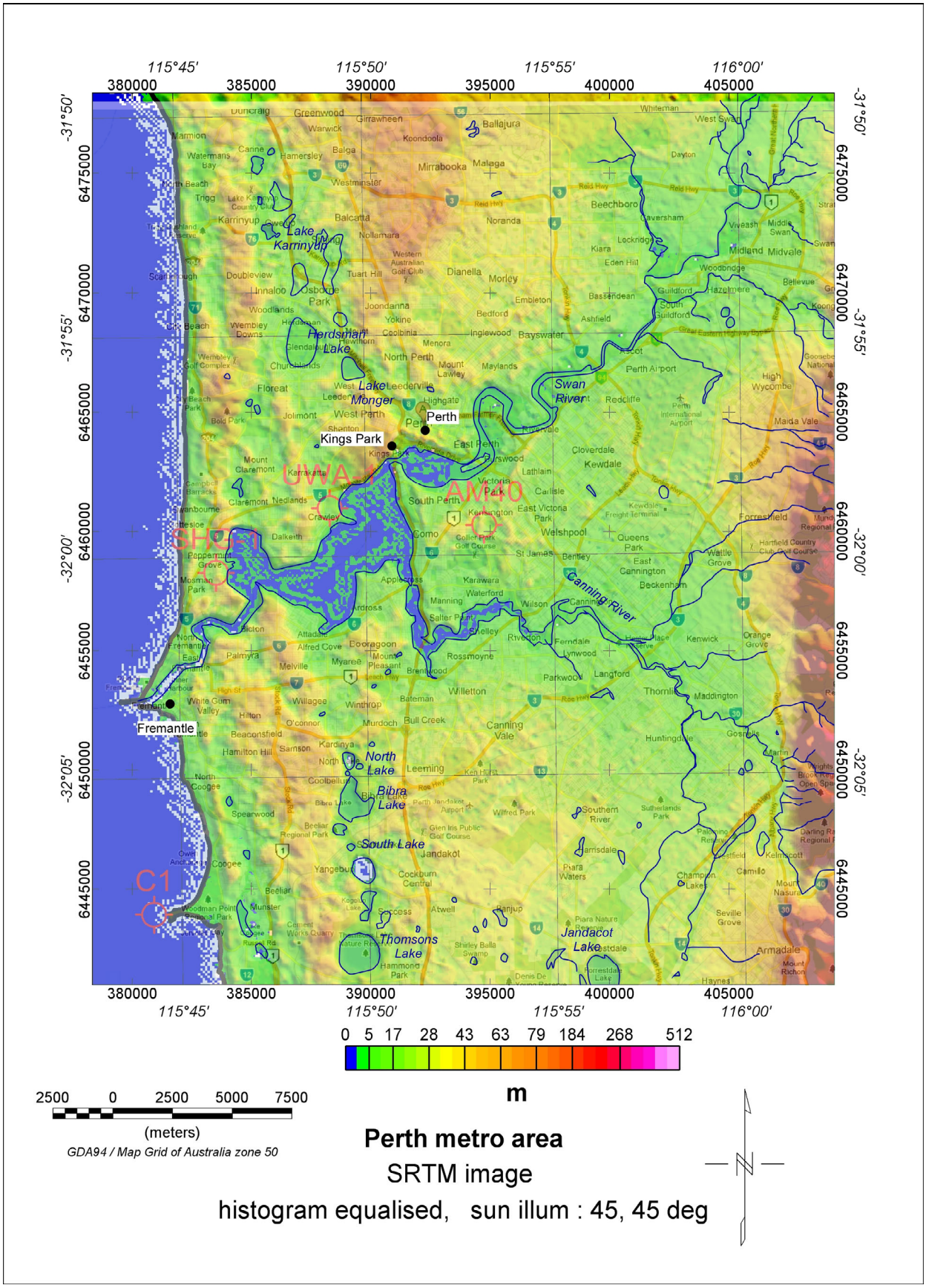

Figure 2: Perth area DEM from Shuttle Radar data

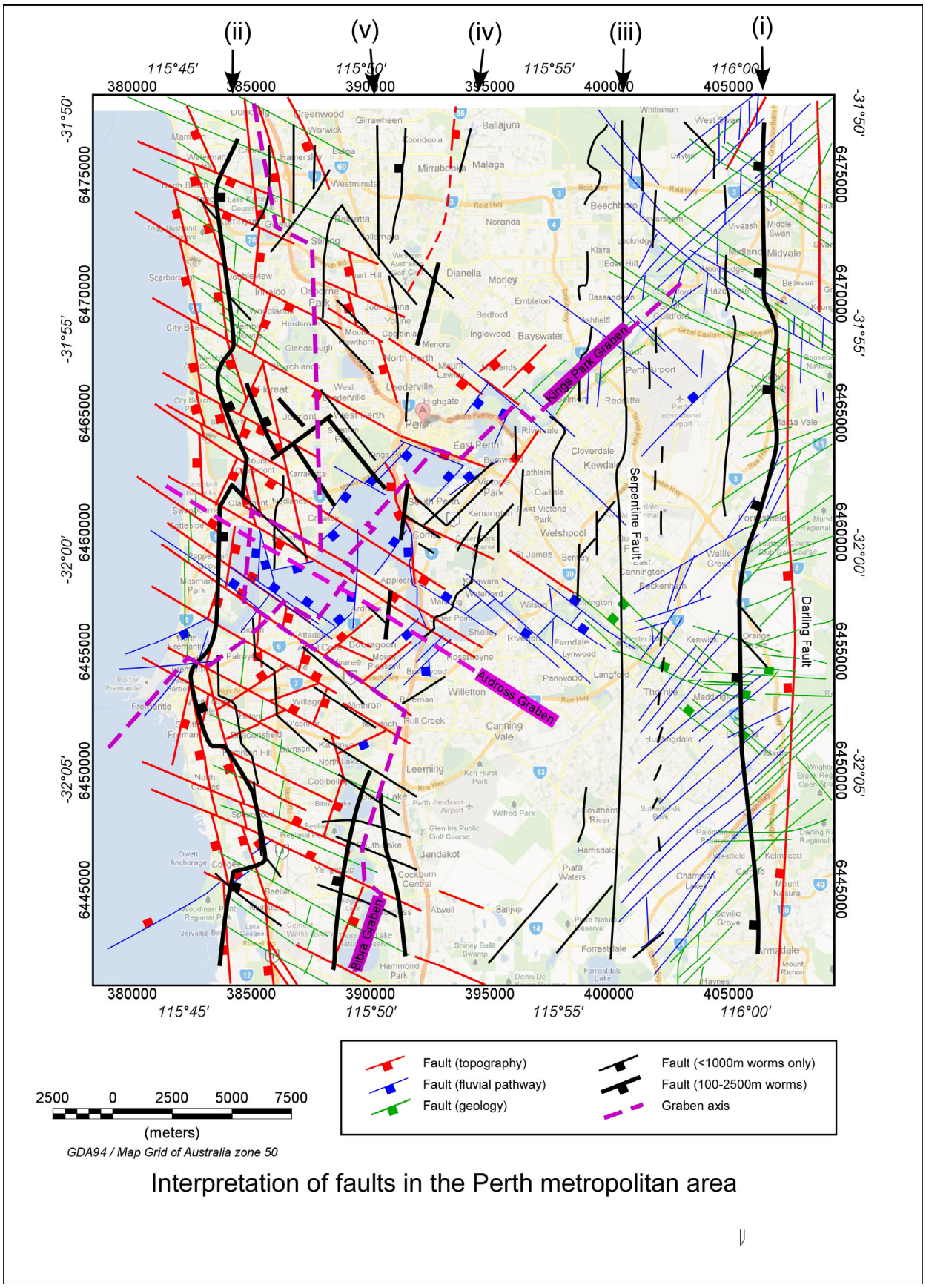

Figure 3: New preliminary fault interpretation for Perth area

Wellbore Temperature and Thermo-elastic Stress Analyses During Drilling or Stimulation

Bisheng Wu*, Bailin Wu, Xi Zhang and Rob Jeffrey
* Bisheng.wu@csiro.au
CSIRO Earth Science and Resource Engineering
Ian Wark Lab, Clayton, VIC 3168, Australia

In this paper, stress analyses around the bottom of a vertical wellbore during drilling were carried out using a fully coupled thermo-elastic wellbore model. To account for temperature evolution during drilling, a fluid circulation model was developed to track the fluid temperature in drill string and annulus. The combination of these two models provides the information required for wellbore stability analyses. In particular, numerical methods that were implemented in the models solving the respective problems are given. A special formula for the heat transfer coefficients between fluids and surrounding solid materials, which is dependent on the flow behaviour and material properties, is chosen. The predicted temperature change is incorporated into the wellbore stability model to calculate the stress changes. The results show that the drilling fluid circulation rates have a considerable effect on the borehole bottom-hole temperature; the choice of the model for calculating the heat transfer coefficient has a great effect on the prediction of the wellbore temperature. In addition, the thermal effect on the near-wellbore stresses is important. The cooling effect can not only reduce the compressive radial and hoop stresses, but also the vertical stresses. This stress reduction can have an impact on hydraulic fracture initiation in the rock formation.

Keywords: Wellbore temperature prediction, fluid circulation, analytical solutions, stress change, drilling

Introduction

Nowadays it is common to drill high temperature and high pressure wells deep into the earth's crust, for instance, to develop enhanced geothermal systems (EGS). As the depth of the wellbore increases, it becomes increasingly difficult to maintain the stability of the well due to the high in-situ stresses encountered at depth. In addition to variation of drilling fluid pressure along the well, the wellbore temperature can change due to the circulation of the drilling mud and the heat exchange with the host rock. These changes in pressure and temperature will affect significantly the thermo-elastic stress distributions around the wellbore. Under certain circumstances, rock failure can take place surrounding the wellbore, which can lead to wellbore collapse. It is therefore of great importance to accurately evaluate the bottom-hole temperature and the coupled thermo-elastic effect on wellbore stability during drilling.

A great deal of research on the temperature distribution due to drilling fluid circulation in a well has been carried out over the last several decades (Raymond 1969; Holmes & Swift 1970; Sump and Williams 1973 and Fomin et al. 2005). For example, Raymond (1969) used an explicit finite difference method to numerically solve this problem, but he did not provide a stability and convergence analysis of the proposed numerical method. Fomin et al. (2005) studied the borehole temperature during drilling in a fractured rock formation, but gave only the steady state solutions to the formulated problem. In our recent work (Wu et al. 2010), the problem similar to the cases studied in these two papers is re-visited with an objective of obtaining the fully-coupled transient solution. In particular, the plane-strain condition is used to simplify the problem as most models do. The analytical solutions are obtained in Laplace space and then the Stehfest inverse Laplace transformation is applied, which has been shown to give accurate results as a function of time.

This paper describes a solution method to incorporate the temperature prediction model for circulating fluid inside the well with the stress prediction model for thermo-elastic solids. A cold fluid (or drilling fluid) is circulated into a tubing string and back up the annulus between the tubing and the borehole wall. The heat exchange between fluids and solids will generate a time-dependent temperature profile along the well. The corresponding temperature change and rock deformation will be calculated by the proposed model.

Problem formulation

In Fig.1, a system for circulating fluids in the wellbore is illustrated. At the beginning (t=0), the fluid and rock temperatures are in equilibrium with the linearly varying temperature profile with depth shown on the right of Fig. 1. We refer to this temperature distribution as static. At t>0, the fluid with a given surface temperature T_{in}^*, is pumped into the drill string at an average fluid mass rate G_d, The corresponding volumetric flux is equal to G_d/ρ_l in which ρ_l is the liquid density. When the fluid mass reaches the bottom of the tubing string, it will return to the surface along the annulus. Although the fluid mass rate can, in general, be variable along the annulus, it is assumed to be

constant for this analysis. The return mass flow rate is denoted as G_a, which can be less than the mass injection rate after considering fluid loss. The tubing wall thickness is denoted as δ_0, which cannot be zero because, otherwise, the fluid temperature in the tube and in the annulus will be equal at all times.

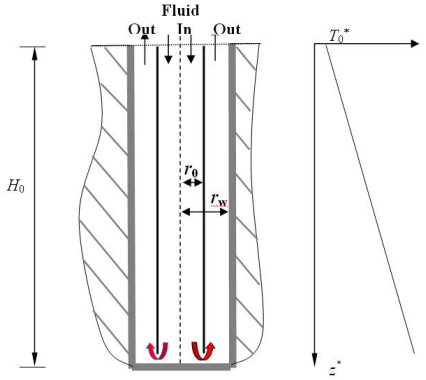

Figure 1 Injection system considered by the model.

The heat transfer along the well is a complicated process, which includes the heat advection in the tubing string, the heat exchange between the fluid and the interior or outside surfaces of the tubing string, and the heat exchange with the formation rock. Here the temperatures of the fluid inside the annulus, the tubing and the rock are denoted as T_a^*, T_d^* and T_r^*, with the first two of these independent of the radial position, r^*. The temperature on the borehole wall is denoted as T_w^*. The initial static temperature distribution for the rock is assumed to be linear with depth as shown in Fig. 1.

Note that the z^* position coordinate is pointing down so that z^* is zero at the surface and is positive and increases with depth in the model.

On the other hand, the fluid pressure at the bottom of the borehole can be assessed by the fluid density and the height as $\rho_l g H$ in which g is the gravitational acceleration. For the current version of the model, we ignore the details of viscous friction in the drill string and annulus.

We have provided a plane-strain model for stress analysis on the cross-section of a vertical wellbore (Wu et al. 2010). Basically the model provides the fully coupled solution to the stress, pore pressure and temperature in the thermo-elastic rock around the wellbore. A linear thermo-poro-elastic constitutive law is used. When the pressure and temperature are prescribed on the well wall and the initial conditions are stationary, the solutions can be obtained analytically in Laplace space. The reader is referred to our previous papers (Wu et al. 2010) for more details. In the present paper, we only use the thermo-elastic results.

In next section, we will provide the governing equations and initial and boundary conditions for the fluid circulation part only.

Governing equations and boundary conditions for fluid circulation model

The temperature of the fluid in the tubing is determined by the rate of heat convection down along the tubing and the rate of heat exchange between the tubing and the annulus. The temperature of the fluid in the annulus is determined by the rate of heat convection up along the annulus, the rate of heat exchange between the tubing and the annulus, and the rate of heat exchange between the fluid and the surrounding rock. According to Raymond (1969), the convective heat transfer equations for fluids inside the tubing string and the annulus are as follows

$$\rho_l c_l A_d v_d \frac{\partial T_d^*}{\partial z^*} + 2\pi r_0 h^{ad}(T_d^* - T_a^*) = -\rho_l A_d c_l \frac{\partial T_d^*}{\partial t^*},$$
$$\rho_l c_l A_a v_a \frac{\partial T_a^*}{\partial z^*} + 2\pi r_0 h^{ad}(T_d^* - T_a^*) + 2\pi r_w h_i^w (T_w^* - T_a^*) = \rho_l A_a c_l \frac{\partial T_a^*}{\partial t^*}, \quad (1)$$

The physical parameters in the above equations are assumed to be independent of temperature and pressure. The parameters' definition and typical values for drilling fluid and granite are listed in Table 1.

For the surrounding rock formation, because the temperature gradient in the radial direction is much greater than that in the vertical direction in the near wellbore region, the derivative of the formation temperature with respect to z^* can be ignored (Raymond 1969). Then the governing equation for heat transfer follows the classical 2D heat conduction equation

$$\frac{\partial T_r^*}{\partial t^*} = \frac{k_r}{\rho_r c_r} \frac{1}{r^*} \frac{\partial}{\partial r^*}\left(r^* \frac{\partial T_r}{\partial r^*} \right). \quad (2)$$

At the borehole wall, the heat flux from the rock formation into the annulus satisfies Fourier's law. That is, the heat exchange between the rock formation and the annulus fluid is expressed as

$$2\pi r_w h_r (T_r^* - T_a^*) = 2\pi r_w k_r \frac{\partial T_r^*}{\partial r^*} \quad \text{at } r = r_w, \quad (3)$$

On the other hand, heat transfer between the fluids in the tubing and in the annulus, has been considered in Eq. (1).In this equation we use the combined heat transfer coefficient h^{ad} to include the effect of the tubing thickness.

To solve the present problem, the boundary conditions are needed at the surface and the well bottom. These boundary conditions are given as

$$\begin{aligned} T_d^*(z^*, t^*) &= T_{in}^*, \quad \text{when } z^* = 0, \\ T_d^*(z^*, t^*) &= T_a^*(z^*, t^*), \quad \text{when } z^* = H^*, \end{aligned} \quad (4)$$

and the initial condition which is that at t=0, the formation temperature is given as

$$T_r^*(z^*, r^*, 0) = T_0^* = A_0 z^* + B_0, \quad (5)$$

where A_0 and B_0 are the constants which determine the initial static formation temperature as a function of depth.

In summary, the physical parameters defined above are given below

$$\frac{1}{h^{ad}} = \frac{1}{h_a} + \frac{1}{h_d} + \frac{\delta_0}{k_d},$$

$$h_a = 0.021(\mathrm{Re}_a)^{0.8}(\mathrm{Pr}_l)^{0.43}(\mathrm{Pr}_l/\mathrm{Pr}_d)^{0.25}k_l/(2(r_w - r_0) - \delta_0),$$

$$h_d = 0.021(\mathrm{Re}_d)^{0.8}(\mathrm{Pr}_l)^{0.43}(\mathrm{Pr}_l/\mathrm{Pr}_d)^{0.25}k_l/(2r_0 - \delta_0),$$

$$h_w = 0.021(\mathrm{Re}_a)^{0.8}(\mathrm{Pr}_l)^{0.43}(\mathrm{Pr}_l/\mathrm{Pr}_w)^{0.25}k_l/(2(r_w - r_0) - \delta_0),$$

$$\mathrm{Re}_a = \frac{\rho_l v_a 2(r_w - r_0)}{\mu}, \quad \mathrm{Re}_d = \frac{\rho_l v_d 2r_0}{\mu},$$

$$\mathrm{Pr}_d = \frac{\mu}{\rho_d d_d}, \quad \mathrm{Pr}_l = \frac{\mu}{\rho_l d_l}, \quad \mathrm{Pr}_w = \frac{\mu}{\rho_r d_r},$$

$$d_l = \frac{k_l}{\rho_l c_l}, \quad d_d = \frac{k_d}{\rho_d c_d}, \quad d_r = \frac{k_r}{\rho_r c_r},$$

$$v_a = \frac{G_a}{A_a \rho_l}, \quad v_d = \frac{G_d}{A_d \rho_l}, \quad A_a = \pi(r_w^2 - r_0^2), \quad A_d = \pi r_0^2.$$

It is clear from the above definition that the heat transfer between fluids and the surrounding solids is dependent on the Reynolds number and the Prandtl number, in addition to the well and drill string radii (Fomin et al., 2005). However, these empirical correlations are only valid when the Reynolds number is larger than 10,000. In the model, for Reynolds number less than 10,000, we use an approximation method. If Reynolds number is less than 2000, the fluid flow is laminar and the heat transfer coefficient is 3.66 W/(m^{2}K) and the borehole wall heat flux tends to become stable soon after circulation begins. If Reynolds number is within the range 2000 to 10,000, the heat transfer coefficient can be obtained by an interpolation method.

Methods for solution

Here we only provide the solution method for temperature changes along the well. The reader is referred to our previous work (Wu et al. 2010) for the solution method for stress analysis of the wellbore. The main approach for solving the fluid circulation problem is to use Laplace transformation to convert the partial differential equations (PDEs) into ordinary differential equations (ODEs). Then the analytical solutions are obtained by solving the ODEs based on the transformed boundary and initial conditions. The numerical values are calculated by using the Stehfest inverse Laplace transformation. The details for numerical inversion can be found in (Wu et al. 2011).

To validate the numerical inversion method, the results from the present numerical model have been compared to the experimental measurements and to simple cases such as no drill string present and an infinitely long wellbore. A good agreement is found.

Table 1 Parameters for the calculation

Parameter	Value
Pipe internal radius r_0 (m)	0.0462
Pipe thickness δ_0 (m)	0.01
Wellbore radius r_w (m)	0.1
Wellbore length H_0 (m)	4132
Injection rate G_d (Kg/s)	13
Pump out rate G_a (Kg/s)	13
Injection temperature T_{in}^* ($^\circ$C)	27
Temperature gradient A_0 ($^\circ$C/m)	0.0467
Surface temperature B_0 ($^\circ$C)	27
Initial temperature T_0^* ($^\circ$C)	$A_0 z^* + B_0$
Fluid specific heat c_l (J/(kg·K))	4200
Rock specific heat c_r (J/(kg·K))	790
Pipe specific heat c_d (J/(kg·K))	460
Fluid thermal conductivity k_l (W/(m·K))	0.68
Rock ther. conductivity k_r (W/(m·K))	2.2
Pipe ther. conductivity k_d (W/(m·K))	50
Fluid mass density ρ_l (Kg/m^3)	900
Rock mass density ρ_r (Kg/m^3)	2700
Pipe mass density ρ_d (Kg/m^3)	7800
Fluid viscosity μ (Pa·s)	0.0004

Numerical results

Bottom-hole and outlet temperature

First of all, let us consider the temperature changes along the well. Figs. 2 and 3 display the time dependent response of bottom-hole and surface outlet temperatures, respectively for several mass flow injection rates and fluid mass densities. Based on the given parameters, the rock temperature at the wellbore wall and annulus fluid temperature are identical along the well for these cases. It is clear from these figures that with increasing the injection flow rate, the bottom-hole temperature will drop more quickly to a lower level. The temperature continues to decrease after 1000 hours, but at an ever slower rate. Therefore, a significant portion of the cooling occurs in the first 100 hours or less and higher rates are required to produce significant cooling effect on wellbore temperature.

The outlet temperature can be easily measured in the field. Such a measurement would provide useful data for model verification presented here. It is found that after about 2 hours, the outlet temperature is nearly stable. Increasing the injection rate results in an increase in the outlet temperature at the annulus. This is largely due to more heat is carried away from the deep portion of the wellbore.

In addition, changing the fluid densities does not have a great effect on the bottom-hole and outlet temperatures as shown Fig. 2(b) and Fig. 3(b). It should be noted that the mass injection rate is used in the model.

Tubing and annulus temperature

Figure 4 shows the temperature distribution along the well at a specific time when G_d= G_a =13 kg/s. The temperature continuity between the tube and annulus fluid temperature at the bottom of the well is satisfied as expected. The red line is the reference line, giving the initial rock static formation temperature. The two curves for the annulus fluid temperature and borehole wall temperature are identical. This means the heat loss from the formation to the annulus is extremely small. On the other hand, the heat loss across the steel pipe is clear although the difference is not significant after 150 hrs injection.

Figures 5 and 6 show the temperature distributions in the tubing and in the annulus at different times. The drop of bottom-hole temperature with time elapsed is clear. Of course, the trends for two temperature curves are the same. Significant temperature drop occurs at larger depth. After 200hrs circulation, the bottom-hole temperature can be reduced by 50 degrees. The cooling will definitely change the local stress distribution due to formation shrinkage.

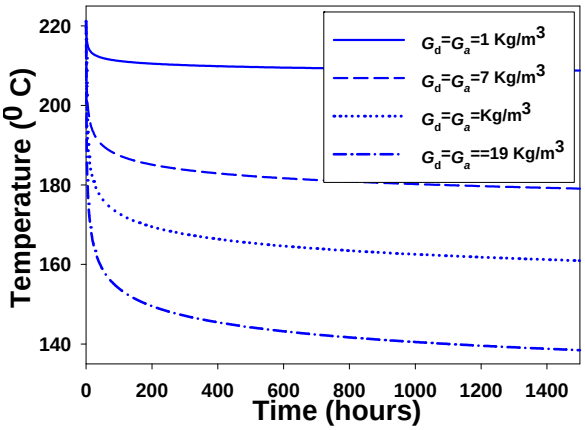

(a)

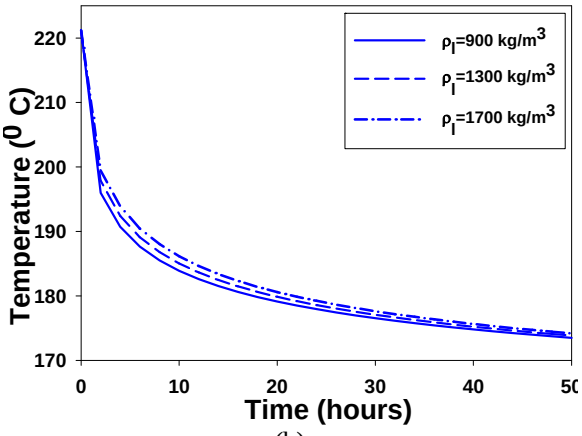

(b)

Figure 2 Bottom-hole temperature responses when T_{in}^*=B_0=27 °C. (a) Varying only the injection rates with the fluid density ρ_l=900 kg/m^3, (b) varying only the fluid densities with the injection rate G_d=G_a=13 kg/s.

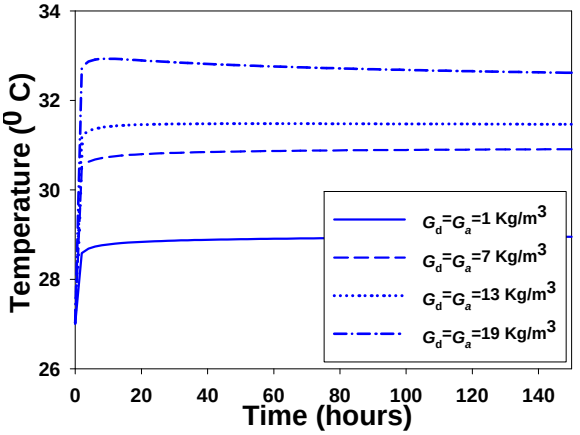

(a)

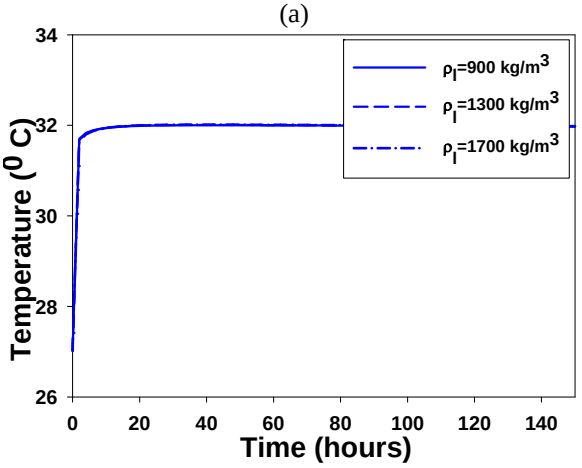

(b)

Figure 3 Outlet temperature responses when T_{in}^*=B_0=27 °C. (a) Varying only the injection rates with the fluid density ρ_l=900 kg/m^3, (b) varying only the fluid densities with the injection rate G_d=G_a=13 kg/s.

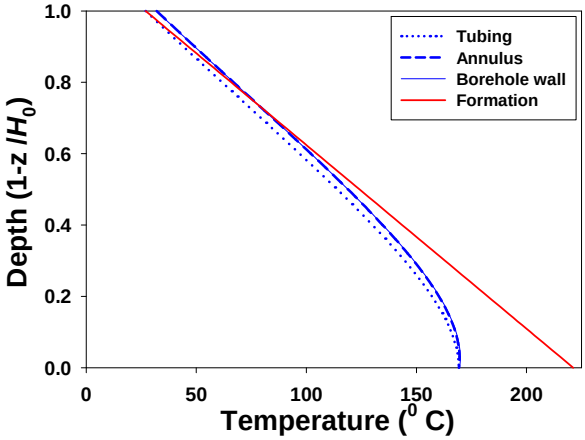

Figure 4 Temperature profiles in the drill string, annulus and borehole wall after 150 hours of circulation time when T_{in}^*=B_0=27 °C and G_d= G_a=13 kg/s.

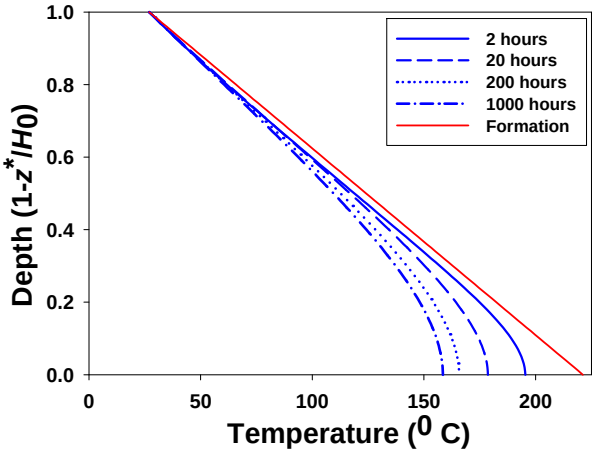

Figure 5 Temperature in the drill string as a function of time when $T_{in}^*=B_0$=27 °C and G_d= G_a=13 kg/s.

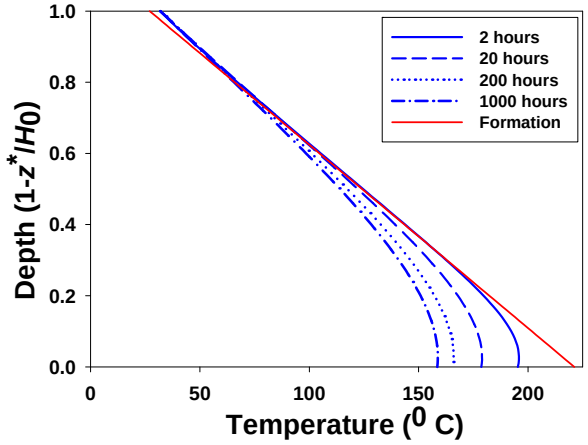

Figure 6 Temperature in the annulus as a function of time when $T_{in}^*=B_0$=27 °C and G_d= G_a=13 kg/s.

Temperature in the rock

Figure 7 shows the temperature contour around the circular well. It can be seen that the near-well region at the bottom of the well is greatly impacted by the circulation. The low temperature area near the bottom of the well can extend into the formation to a depth of one wellbore radius after 150 hrs. This cooled zone will induce thermo-elastic stresses that may be useful in helping initiate fractures and to enhance the permeability of certain natural fracture sets during stimulation.

Thermal effects on the stress changes

The temperature changes from the fluid circulation model are introduced in the stress analysis model as a boundary condition. A typical example is demonstrated here to show the thermal effect on the stress change. For values of the parameters for the thermo-elastic rock mass, see Wu et al. (2010).

In the case where the wellbore bottom hole temperature is reduced to 140 ºC, the radial and hoop stresses along the σ_{max} directions (θ=0) are displayed in Fig. 8 for different elapsed times. In the real cases, the temperature drop at the bottom is reduced progressively, and then the stress drop

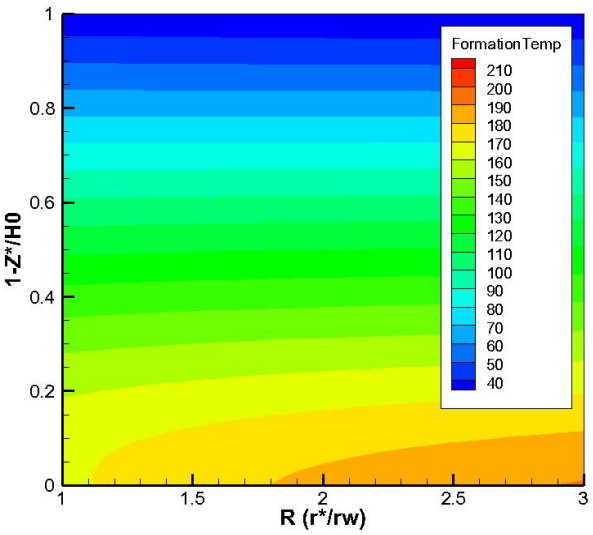

Figure 7 Temperature contours in the surrounding rock at t=150 hours when $T_{in}^*=B_0$=27 °C and G_d= G_a==13 kg/s.

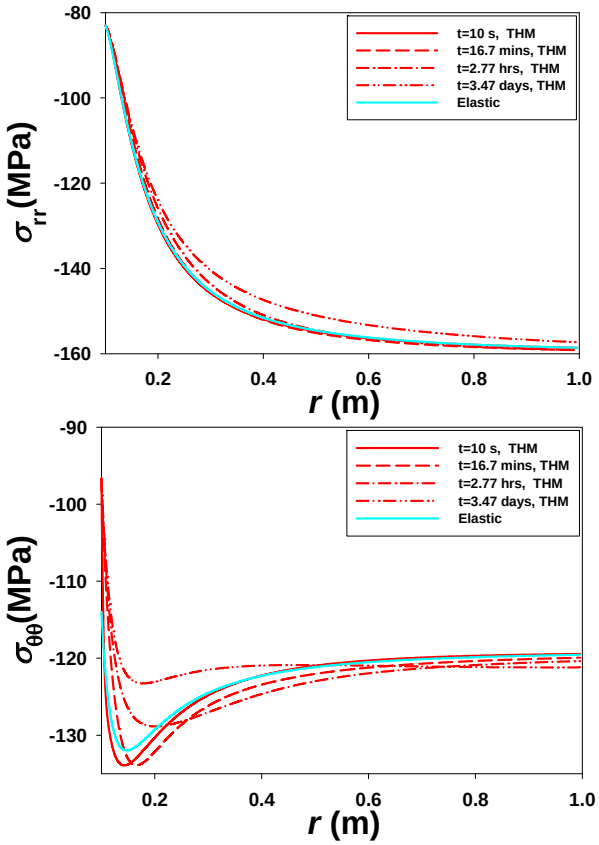

Figure 8 Radial and hoop stresses in the σ_{max} direction (θ=0) for T_w^*=140 ºC (negative stress is taken as compression) (a top, b bottom).

caused by accumulated heat exchange would be larger than the predictions given here. Therefore, the stress drop provided here is conservative.

In particular, from Fig. 8, the radial stress can be reduced up to 5 MPa and the hoop stress to 8 MPa at the location of twice the wellbore radius from the wellbore centre. This stress drop would provide another boundary condition for hydraulic fracture growth from the wellbore wall. The near-well fracture growth can be investigated accordingly.

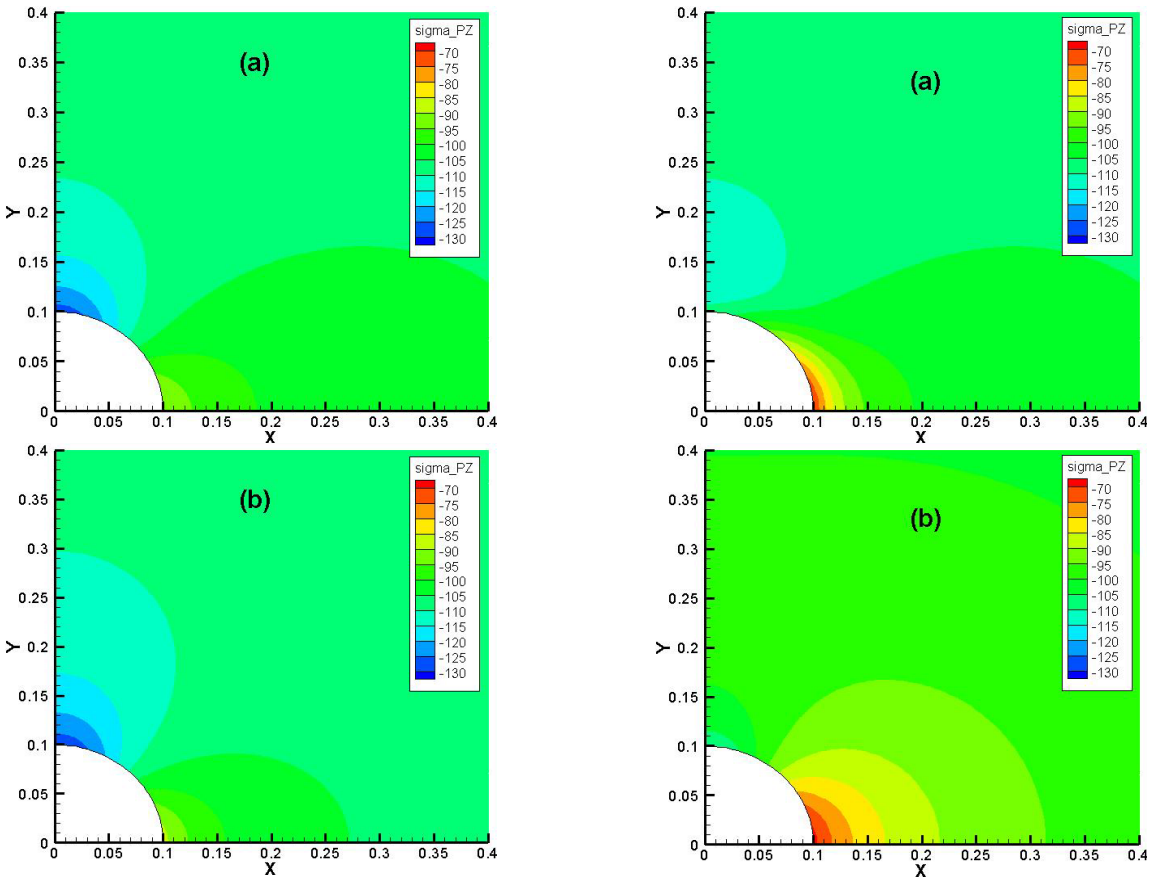

Figure 9 Vertical stress contours at different wellbore temperatures. Left T_w*=220 ºC at (a) 3 seconds and (b) 3.47 days. Right T_w*=140 ºC at (a) 3 seconds and (b) 3.47 days.

In addition, the thermal effects have a considerable effect on the vertical stress as shown in Fig.9. The stress reduction in the region adjacent to the wellbore wall along the σ_{max} direction can reach a maximum of 20 MPa (less compressive) when the wellbore temperature is reduced to 140 ºC. The lower the vertical stress, the more likely the creation of horizontal tensile fractures.

Conclusions

In this paper, the solutions for the wellbore temperature changes during fluid circulation are obtained and are introduced as a boundary condition for near-well stress analyses. Then the stress changes due to the cooling effects are investigated so that the wellbore stability caused by temperature variations during drilling or stimulation can be considered. Some conclusions are drawn as follows:

1. The borehole bottom temperature change is sensitive to the injection rate used, especially at the early time. Higher rates can produce significantly more cooling effect.
2. The surface outlet temperature will reach a steady state after several hours. The outlet temperature can be easily measured in the field and such data would allow an inversion method to be used to obtain heat transfer coefficients.
3. More importantly, the cooling can cause significant change in thermo-elastic stresses around the wellbore. The reduction in near-well stresses can facilitate hydraulic fracturing.

References

Raymond, L.R., 1969, Temperature distribution in a circulating drilling fluid, SPE-AIME.

Fomin, S., Hashida, T., Chugunov V. and Kuznetsov, A.V., 2005, A borehole temperature during drilling in a fractured rock formation, International Journal of Heat and Mass Transfer 48, 385–394.

Sump, G.D. and Williams, B.B., 1973, Prediction of wellbore temperature during mud circulation and cementing operations, Journal of Engineering for Industry, 1083-1092.

Holmes, C.S. and Swift, S.C., 1970, Calculation of circulating mud temperatures, Journal of Petroleum Technology, 670-674.

Wu, B., Zhang, X. and Jeffrey, R. G., 2010. A Thermo-poro-elastic analysis of stress fields around a borehole. Paper ARMA 10-442 presented at *the 44th US Rock Mechanics Symposium and 5th US-Canada Rock Mechanics Symposium* held in Salt Lake City, UT June 27-30, 2010.

PANDAS and its New Applications in Geothermal Modelling

Xing, H. L.*, Zhang, J., Gao, J., and Liu, Y.
h.xing@uq.edu.au
Earth Systems Science Computational Centre (ESSCC), School of Earth Sciences
The University of Queensland, St. Lucia, QLD 4072

PANDAS - Parallel Adaptive static/dynamic Nonlinear Deformation Analysis System - a novel supercomputer simulation tool has been developing for simulating the highly non-linear coupled geomechanical-fluid flow-thermal systems involving heterogeneously fractured geomaterials at different spatial and temporal scales. This abstract briefly introduces the software system, and then focuses on our recent research outcomes in high performance simulation of enhanced geothermal reservoir system.

Keywords: Integrated reservoir simulation, High performance computing, Finite element method, Lattice Boltzmann method, Mesh generation, Permeability, Enhanced geothermal reservoirs

1. An Integrated Geothermal Reservoir Simulator

Australia has a unique Hot Fractured Rock geothermal resource that could potentially provide enough Green energy to meet all its energy needs. A novel finite element and/or Lattice Boltzmann method based supercomputer simulation tool has been developing for simulating the highly coupled geomechanical-fluid flow-thermal systems involving heterogeneously fractured geomaterials to address the key scientific and technological challenge in developing EGS energy. Currently, it includes the following six key components: Pandas/Pre, ESyS_Crustal, Pandas/Thermo, Pandas/Fluid, Pandas/LBM and Pandas/Post as detailed in the following (Xing and Makinouchi, 2002; Xing et al 2006a, 2006b, 2007, 2008 and 2010):

- Pandas/Pre is developed to (1) visualise the microseismicity events recorded during the hydraulic stimulation process and to further evaluate the fracture location and evolution, geological setting, volume of fractured domain and the relevant material parameters (i.e. permeability) of a certain reservoir (Xing et al 2010); (2) generate the FEM based 2D/3D mesh by using microseismicity data (Xing et al 2010), 2D triangular and quadrilateral mesh by digital imaged structures and complicated fault system, and 3D tetrahedral mesh by using geometric models for 3D geological objects as detailed in section 3.4; (3) link with other commercial graphics software (such as Patran) for complicated cases such as hexahedron mesh generation of a 3D reservoir.
- ESyS_Crustal is a finite element method based module developed for the interacting fault system simulation. It employs the adaptive static/dynamic algorithm to simulate the dynamics and evolution of interacting fault systems and processes, in which several dynamic phenomena related with stick-slip instability along the faults need to be taken into account, i.e. (a). slow quasi-static stress accumulation, (b) rapid dynamic rupture, (c) wave propagation and (d) corresponding stress redistribution due to the energy release along the multiple fault boundaries. All these are needed to better describe ruputure/ microseimicity/earthquake related phenomena with applications in earthquake forecasting, reservoir engineering, hazard quantification, exploration, and environmental problems. It has been verified and applied in different cases (e.g. see Xing 2007 and references thereafter).
- Pandas/Thermo is a finite element method based module for the thermal analysis of the metals and the fractured porous media; the temperature distribution is calculated from the heat transfer induced by the thermal boundary conditions without/with the coupled fluid flow effects in the fractured porous media and the geomechanical energy conversion for the individual/coupled thermal analysis.
- Pandas/Fluid is a finite element method based module for simulating the Darcy and/or non-Darcy fluid flow in the fractured porous media by solving the conservation equations of macroscopic properties numerically. Here the fluid flow velocity and pressure are calculated from energy equilibrium equations without/with the coupling effects of the thermal and solid rock deformation for the individual/coupled fluid flow analysis.
- Pandas/LBM is a Lattice Boltzmann method (LBM) based module newly developed for explicitly simulating the 2D/3D complicated fluid flow in the complicated fractures involving the detailed fracture size and geometry. Instead of solving the conventional Navier–Stokes equations or its simplified form with macroscopic properties, the discrete Boltzmann equation is solved here to simulate the fluid flow with collision models such as Bhatnagar-Gross-Krook (BGK). LBM models the fluid consisting of fictive particles, and such parti-

cles perform consecutive propagation and collision processes over a discrete lattice mesh. By simulating streaming and collision processes across a limited number of particles, the intrinsic particle interactions evince a microcosm of viscous flow behaviour applicable across the greater mass (e.g. Sukop and Thorne, 2007). Due to its particulate nature and local dynamics, LBM has several advantages over other conventional CFD methods, especially in dealing with complex boundaries such as multiphase fluid flow in complicated fractures/porous media with detailed microstructures, incorporating microscopic interactions, and parallelization of the algorithm.

- Pandas/Post is to visualise the simulation results through the integration of VTK and/or Patran.

All the above modules can be used independently or together to simulate individual or coupled phenomena (such as interacting fault system dynamics, heat flow and fluid flow) without or with coupling effects.

3. Application Examples

PANDAS has been applied to various cases including those in geothermal reservoir and mining systems (Bringemeier et al 2010; Xing et al 2010; Zhang and Xing 2010). Four of new applications are listed as below.

3.1 Well drawdown pressure test

The drawdown pressure test is a well-test which is performed to obtain permeability data for the reservoir formation. For a drawdown test, a well, initially at equilibrium conditions, is produced at a constant flow rate while the bottom hole pressure history is recorded. Non-Darcy flow behaviour has been recognized as an important factor in fluid flow through porous and fractured rock, especially for the near-well region during high flow rate injection/production in a reservoir formation. The non-Darcy effect is mostly reported as existing in gas/oil fields as the high flow rate of a gaseous fluid, but it has been increasingly suggested that a liquid fluid reservoir such as a geothermal field also has a significant influence caused by the non-Darcy effect. In this study non-Darcy well flow behaviour is described using the Forchheimer equation and implemented in finite element code PANDAS to simulate the near-well performance in a geothermal reservoir (Fig.1). Calculation results show that by considering the Forchheimer flow in the near-well region, both the fluid velocity and wellbore pressure are highly different from the Darcy flow simulation, while the production well pressure is sensitive to the non-Darcy flow coefficient. A series of pressure drawdown tests are simulated on a round geothermal reservoir with liquid water, vapour and supercritical CO_2 as working fluids. Different equations of state (EOS) for water and CO_2 are considered in the simulation for calculating the pressure/temperature-dependent fluid properties. The simulation results suggest that the ratio of fluid density to viscosity has significant impact on non-Darcy flow behaviour in reservoir performance (Figs 2 and 3). For more details, please refer to (Zhang and Xing 2011).

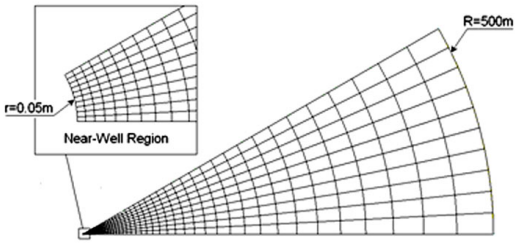

Fig. 1 Well drawdown test model and finite element grid

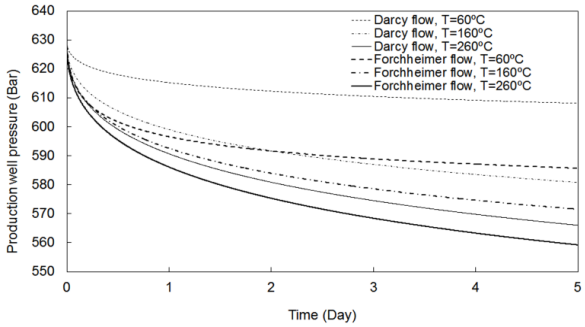

Fig. 2 Simulated pressure at the production well in water drawdown test under different reservoir temperatures with Darcy and non-Darcy models.

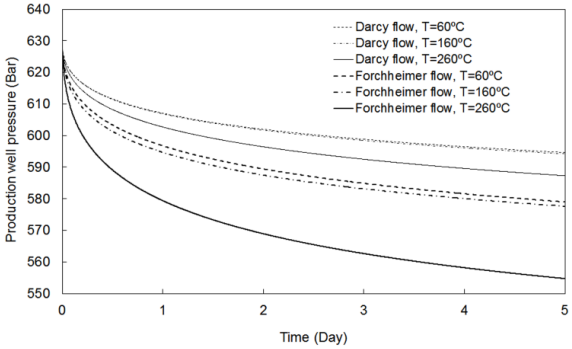

Fig. 3 Simulated pressure at the production well in CO_2 drawdown test under different reservoir temperatures with Darcy and non-Darcy models.

3.2 Fluid flow in fractured porous media

Pandas/LBM is applied here to simulate the fluid flow in fractured media. Fig. 4 shows the fractured rock image with fractures illustrated in black colour. Its range with the length of 315 and the width of 295 pixels (Fig. 4) is firstly converted and discretised to 93536 grid points and further modelled by the D2Q9 scheme for this 2D case. Each lattice node is connected to its neighbours by 9 lattice velocities. There can be either 0 or 1 particle

at a lattice node moving in a lattice direction. Assume that fluid flows in from the bottom side at the velocity of 0.1 pixels/s with the closed boundary along the left and right sides (i.e. zero velocity boundary condition are applied for the left and right sides). Fig. 5 shows the snapshots of velocity distribution at the different stages. This demonstrates its capability to simulate the fluid flow in complicated factures considering the fracture size and geometry.

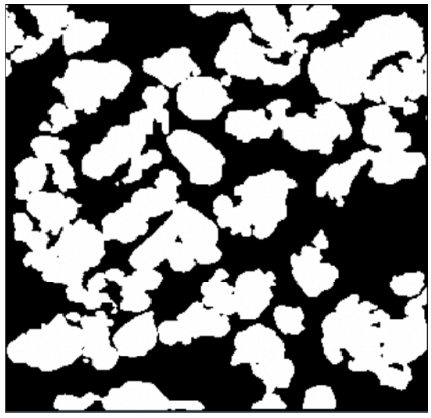

Fig 4: A fractured porous media with a length of 315 and width of 295 pixels to be analysed (pores in black colour and matrix in white colour)

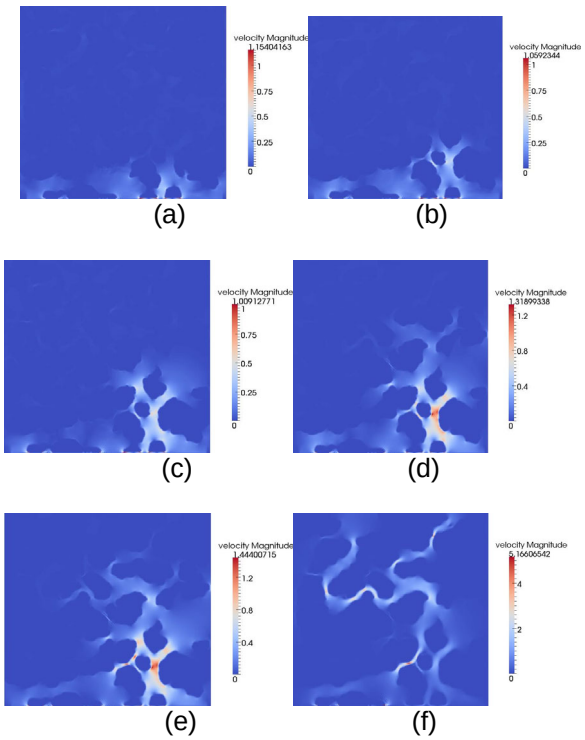

Fig. 5: Fluid flow velocity (unit: pixels/s) at different calculation time (s): (a) 600, (b) 1000, (c) 1600, (d) 2000 (e) 2600 and (f) 3200.

3.3 Hydraulic stimulation

PANDAS is applied here to simulate the hydraulic stimulation process which is widely applied to construct the HDR/HFR geothermal reservoir system. A 3-dimensional finite element based module for modeling nonlinear frictional contact behaviours between multiple deformable bodies with the arbitrarily-shaped contact element strategy has been developed, which provides a means to simulate interacting fault systems including crustal boundary conditions and various nonlinearities. It has been successfully applied in a wide range of fields and is extended here to simulate the hydraulic stimulation process.

We constructed a 3D fault geometry model within a block with dimensions of about 4000 x 4000 x 2500 m^3 and discretised the whole block to 132984 nodes and 112000 8-node hexahedron elements (Fig. 6). The preliminary simulation results are shown in Fig. 7 with the following conditions:

(1) The simulation of hydraulic stimulation process was carried out in the following two steps:

(a) loading by self weight, i.e. the gravity force;

(b) sustaining the above load, and hydraulically loaded through a wellbore

(2) Boundary conditions: The bottom surface is fixed in the x, y and z directions; the rate dependent weakening frictional law is applied along all the faults (Xing et al 2007). Fig 7 shows the preliminary simulation results at the 2nd loading stage of the hydraulic stimulation process which demonstrates the stability and potential usefulness of this ongoing research for analysing hot fractured geothermal reservoir construction processes.

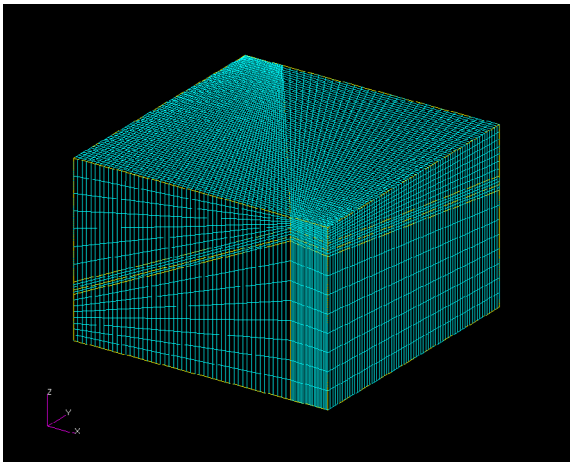

Fig. 6. The 3D model to be simulated for hydraulic stimulation process.

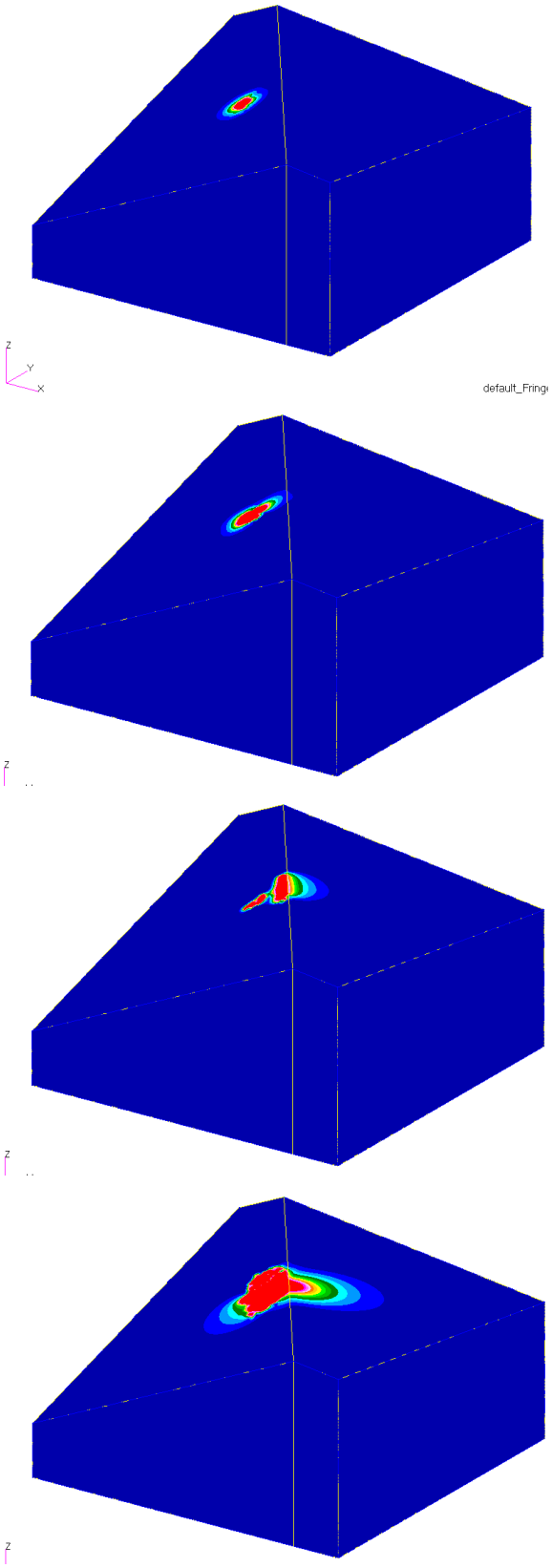

Fig. 7. The simulation results of geothermal reservoir construction processes at the different stages by using hydraulic stimulation.

3.4 Automatic meshing and model construction

PANDAS/Pre is developed and applied here for automatic meshing and model construction across the different scales of a geothermal reservoir system, which focuses on transforming geometric models and/or digital imaged structures into an FEM mesh.

3.4.1 Automated mesh generation for digital image structures

A cross-section image of rock (Fig. 8 (a), material properties represented by 8 different colours) is utilized here to illustrate the capability of PANDAS/Pre for automated mesh generation for digital image structures. Firstly, the noises are removed from the original data as illustrated in Fig. 8(b); secondly, boundaries of different colours/materials are extracted, smoothed and discretised into edges, and then the smoothed boundaries are treated as constrained lines to generate a corresponding triangular mesh (Fig. 8 (c)); finally, based on this triangular mesh, a reasonable quadrilateral mesh with both boundaries and colours of the original image is generated through combined operations of triangular composing, advancing front technology and mesh optimisation (Fig. 8(d)). For more details, refer to Liu and Xing (2011).

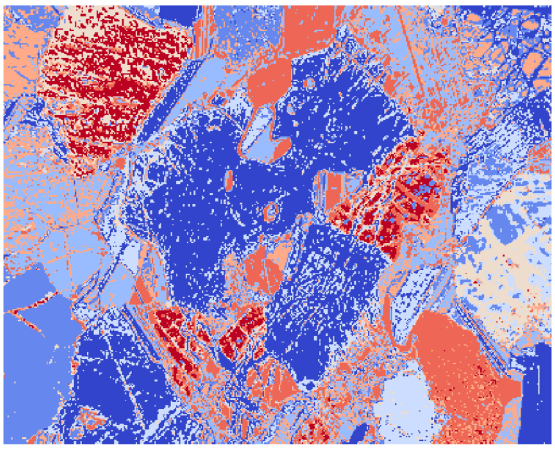

(a)

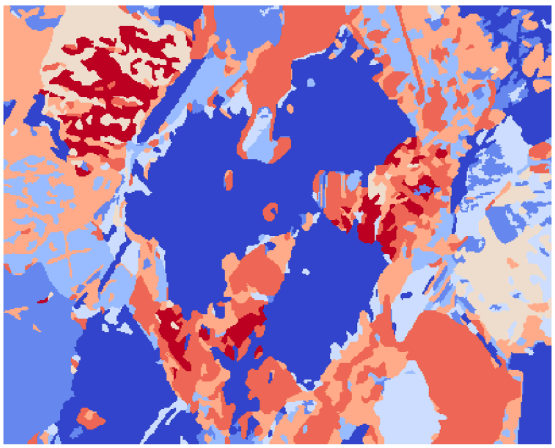

(b)

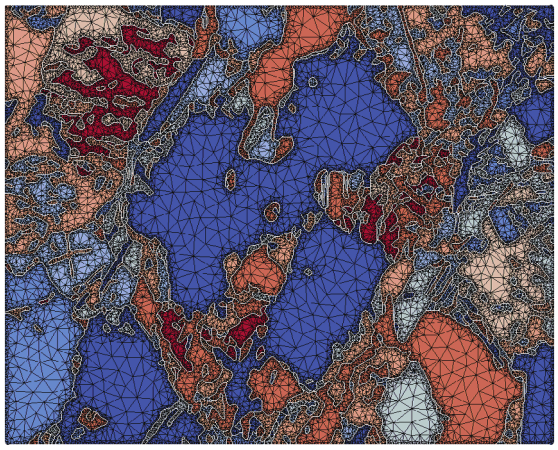

(c)

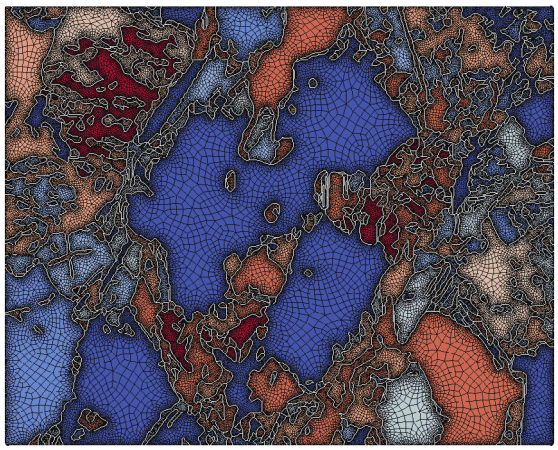

(d)

Fig. 8 Automatic mesh generation with constraints of a rock image: (a) original rock image; (b) image after removing noises; (c) triangular mesh; (d) optimised quadrilateral mesh. White lines in (c) and (d) are multi-colour boundaries inside this image.

3.4.2 Automated quadrilateral mesh generation for arbitrary fault system

A new approach to the automatic generation of an adaptive quadrilateral mesh with arbitrary fault constraints is proposed and developed. It is an indirect all-quad mesh generation including following steps: (1) discretising the constrained lines (fault geometries) within the domain; (2) converting the above domain to an adaptive triangular mesh together with the line constraints; (3) transforming the generated triangular mesh with line constraints to an all-quad mesh through performing an advancing front algorithm from the line constraints, which enables the construction of quadrilaterals layer by layer, and roughly keeps the adaptive feature of the initial triangular mesh; (4) optimizing the topology of the quadrilateral mesh to reduce the number of irregular nodes; (5) smoothing the generated mesh towards high-quality all-quad mesh generation. An application example of Chuan-Dian fault system is given to illustrate the meshing process and demonstrate the reliability and usefulness of the proposed algorithm (Fig 9). For more details, please refer to (Liu et al 2011).

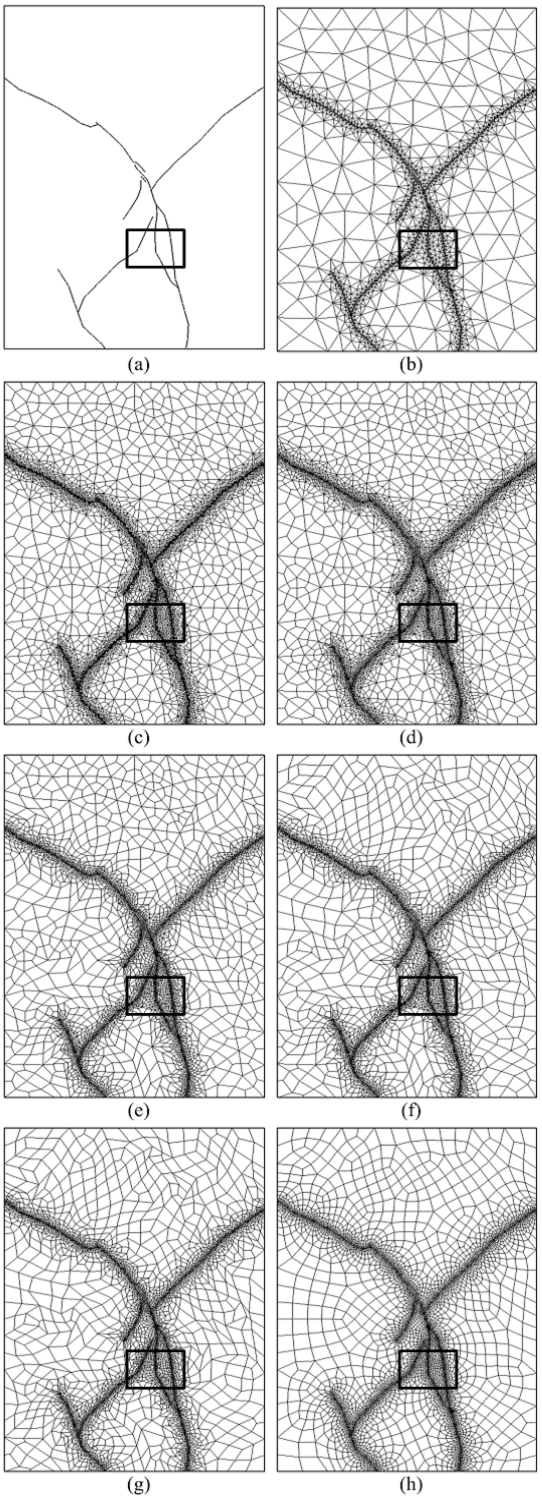

Fig. 9: All-quad mesh generation with Chuan-Dian fault system constraints: (a) fault data; (b) triangular mesh with fault constraints; (c) initial all-quad mesh generation; (d) quadrilateral mesh with one layer of new quadrilateral elements; (e) quadrilateral mesh with four lays of new quadrilateral elements; (f) new quadrilateral mesh after generating layer by layer; (g) mesh after optimizing; (h) high quality mesh after smoothing.

3.4.3 Automatic Meshing and Construction of a 3D Reservoir System

The development of digital 3D geological modelling tools and applications (such as GeoModeller and GoCad) makes it possible to establish geometric models for 3D geological objects, where the geometric features could be illustrated by a set of triangles. PANDAS/Pre is developed to focus on constructing a reservoir system which transforms geometric models used in 3D geological visualization into FEM models. A 3D Geological model for visualization is used as input here, and the transformation processes are implemented following: (1). generating a tetrahedral mesh by 3D Delaunay triangulation methods; (2) abstracting and refining the boundaries of different geological objects; (3) tetrahedral mesh generation with the constraints of the refined boundaries; (4) revising the meshed model locally according to users' requirements, such as setting up well models by tetrahedral mesh refinement. Our approach presents a way of using geological data for visualization to construct an FEM mesh for geothermal simulation, which demonstrated by a practical geothermal reservoir system model construction using the practical data provided by Geomodeller (Liu and Xing 2010).

Conclusions

Our research in an integrated geothermal reservoir simulator PANDAS for high performance simulation of enhanced geothermal reservoirs is introduced and then tested by the relevant cases to address the key issues in simulating and deep understanding an enhanced HDR/HFR/HWR geothermal reservoir system. Application examples demonstrated its accuracy, stability and potential usefulness in simulating and evaluating the enhanced geothermal reservoir systems.

Acknowledgements

Support is gratefully acknowledged by the Australian Research Council and Geodynamics Limited through the ARC Linkage project LP0560932, ARC Discovery project DP066620, and ARC Linkage International LX0989423. The authors are grateful to Drs Doone Wyborn, Hehua Xu, Wenhui Yu, Enlong Liu and Professor Hans Muhlhaus, for their discussion and collaboration in the relevant research.

References

Bringemeier D., Wang, X, Xing, H. L. and Zhang, J, 2010. Modelling of Multiphase Fluid Flow for an Open Pit Development within a Geothermal Active Caldera, Proceedings of the 11th IAEG Congress (IAEG-International Association for Engineering Geology and the Environment), 9 pages, Auckland, New Zealand.

Liu, Y. and Xing, H., 2010. Automatic Meshing and Construction of a 3D Reservoir System: From Visualization towards Simulation. In: Gurgenci, H. and Weber, R. D., Proceedings of the 2010 Australian Geothermal Energy Conference, Adelaide, Nov 17~19 (6 pages).

Liu, Y, H. L. Xing and Z Guan, 2011. An indirect approach for automatic generation of quadrilateral meshes with arbitrary line constraints. Int J Num Methods Engng, DOI: 10.1002/nme.3145

Liu, Y and H. L. Xing, 2011. An automatic quadrilateral mesh generation algorithm for multi-colour imaged structures, technical report of ESSCC, The University of Queensalnd.

Sukop, M. C. and Thorne, D. T.: *Lattice Boltzmann Modeling:* An Introduction for Geoscientists and Engineers, Springer, (2007).

Xing, H.L., and Makinouchi, A.: Three Dimensional Finite Element Modelling of Thermomechanical Frictional Contact Between Finite Deformation Bodies Using R-minimum Strategy, Computer Methods in Applied Mechanics and Engineering, **191**, (2002), 4193-4214

Xing, H. L., Mora, P. and Makinouchi, A. 2006a: A Unified Frictional Description and It's Application to the Simulation of Frictional Instability Using the Finite Element Method, Philosophical Magazine, **86**, (21-22), 3453-3475.

Xing, H. L., Mora, P. 2006b: Construction of an Intraplate Fault System Model of South Australia, and Simulation Tool for the iSERVO Institute Seed Project. Pure and Applied Geophysics. **163**, 2297-2316. DOI 10.1007/s00024-006-0127-x

Xing, H. L., Makinouchi, A. and Mora, P. 2007: Finite Element Modelling of Interacting Fault System, Physics of the Earth and Planetary Interiors, **163**, 106-121.

Xing, H. L.: Progress Report: Supercomputer Simulation of Hot Fractured Rock Geothermal Reservoir Systems, ESSCC/ACcESS Technical Report, The University of Queensland, pp1-48, (2008).

Xing, H.L., J. Gao, J., Zhang, J. & Liu, Y. 2010. Towards An Integrated Simulator For Enhanced Geothermal Reservoirs. Proceedings World Geothermal Congress 2010. Paper 3224 (11 pages). Bali, Indonesia, 25-29 April 2010.

Zhang J., Xing H.L., 2010. Numerical simulation of geothermal reservoir systems with multiphase fluids. In: Gurgenci, H. and Weber, R. D., Proceedings of the 2010 Australian Geothermal Energy Conference, Adelaide, Nov 17~19

Zhang, J and H.L. Xing. 2011, Numerical Modeling of Non-Darcy Flow in Near-well Region of a Geothermal Reservoir, Technical report of ESSCC, submitted to Geothermics.

Comparison of Habanero fracture models derived from seismic signal analysis and a Bayesian framework

Chaoshui Xu[1*], Peter .A. Dowd[2] and Doone Wyborn[3]
cxu@civeng.adelaide.edu.au
[1] School of Civil, Environmental and Mining Engineering, University of Adelaide.
[2] Faculty of Engineering, Computer and Mathematical Sciences, University of Adelaide.
[3] Geodynamics Ltd

A model of fractures and fracture networks is a fundamental input to reservoir modelling and characterisation for enhanced geothermal systems (EGS). The characterisation of rock fracture networks is a very difficult problem not least because accurate field measurement of a single fracture is difficult and measurement of all fractures is impossible. Thus, in practice, the whole fracture system is not observable on any meaningful scale and the only realistic approach is via a stochastic model conditioned by sparse core data and by seismic events monitored during fracture stimulation.

This paper describes two ways of model conditioning: one is based on the similarity analysis of seismic signal characteristics and the other is based on a more recently proposed approach using a Bayesian framework in the form of Markov Chain Monte Carlo (MCMC) simulation. Both methods are applied to Geodynamics' Habanero reservoir in the Cooper Basin and their performances are assessed and compared and recommendations are given.

Keywords: rock fracture network model, seismic events, Markov chain Monte Carlo simulation

Hydrochemical and isotopic properties of geothermal fluids in a tectonically active (Bingol-Erzurum) Province, Eastern Anatolia, Turkey

[1] Yuce, G* and [2] Taskiran, L
e-mail: galipyuce@gmail.com
[1]Queensland Geothermal Energy Centre of Excellence, QLD, 4072, Australia.
[2]General Directorate of Mineral Research and Exploration, Geothermal Survey Division, Ankara, Turkey.

More than 1000 thermal and mineral water manifestations are distributed in Turkey (Mertoglu et al, 2003; Dagistan et al, 2010). Hence, Turkey has been considered as the seventh richest country in the world regarding geothermal potential (Balat, 2006). While the Western Turkey has been widely investigated regarding the geothermal potential, East of Turkey has partly or insufficiently examined for the same purpose. In this respect, it has a value for being a pilot research in the area. The target of the study was to find out the hydrochemical characteristics of thermal waters discharging to the province between Bingol and Erzurum. Moreover, evaluation of geo-thermometers to estimate reservoir temperature was also performed. For this purpose, Thermal and cold water samples collected from the study area were analyzed to understand their hydrogeochemical properties. The physical and chemical parameters were measured on-site. Major and minor elements, deuterium, oxygen-18 and tritium analyses of water samples were determined by suitable laboratory techniques. All analysis results were plotted on several diagrams and examined.

North and East Anatolian Fault Zones are located in the southwest of the studied area (Fig. 1). Thus, thermal waters appear to the surface along the extensional fractures that formed by above-mentioned fault zones. Fractured rocks in the area are the reservoir rock, while Miocene volcanic is the cap rocks. The magma chamber, where the Bingol Mt volcanic lavas were originated, is deduced as the possible heat source. Two different water types were determined: NaCl and Ca-Mg-HCO_3. Isotopic analyses show that the cold groundwaters and some thermal waters have shallow circulation, whereas the rest of geothermal samples have deep circulation. The discharge temperatures of thermal waters range from 29 to 57 ^{0}C. The reservoir temperatures were calculated between 100 ^{0}C and-170 ^{0}C. It is obviously seen from silica-enthalpy diagram (Fig. 2) that cold waters mixed with Cerme and Ilipinar springs and thus the waters get cool during ascending to the surface. Geothermometers are also used for the estimation the temperature of fluids in the aquifers. Since the formation of silica molecules is not affected from the escape of volatiles (Fournier, 1977), only silica solubility is used as geothermometers.

By the evaluation of the current study, an utilizable amount of geothermal fluid at the reasonable temperature was acquired from the exploration well (in 550m depth) that was drilled in the close vicinity of the study area. The temperature and yield of the fluid in the exploration well were 71 ^{o}C and 33 l/s, respectively. Thus, the projected presence of the cap and reservoir rocks in the study was verified from the well cuttings (sediments of the aquifers). It is inferred from the evaluation of obtained results; some thermal waters are sourced from the high enthalpy geothermal reservoir where the enthalpy increases from NE to SW in the area.

Keywords: thermal water, hydrochemistry, environmental isotopes, geothermometers.

References

Balat, M., 2006, Current geothermal energy potential in Turkey and use of geothermal energy sources, Part B: Economics, planning and policy, 1:1, p. 55-65.

Dagistan, H., Dogu, N., Karadaglar, M. 2010, Geothermal explorations and investigations by MTA in Turkey, Poceedings World Geothermal Congress 2010, Bali, Indonesia, 25-29 April 2010, p. 1-5

Fournier, R.,O. 1977, A Review of Chemical and Isotopic Geothermometers for Geothermal Systems In: Proceeding of the Symposium on Geothermal Energy, Cento Scientific Program, p.133-143

Mertoglu, O., Bakir, N., Kaya,T. 2003,Geothermal applications in Turkey. Geothermics 32, p. 419–428.

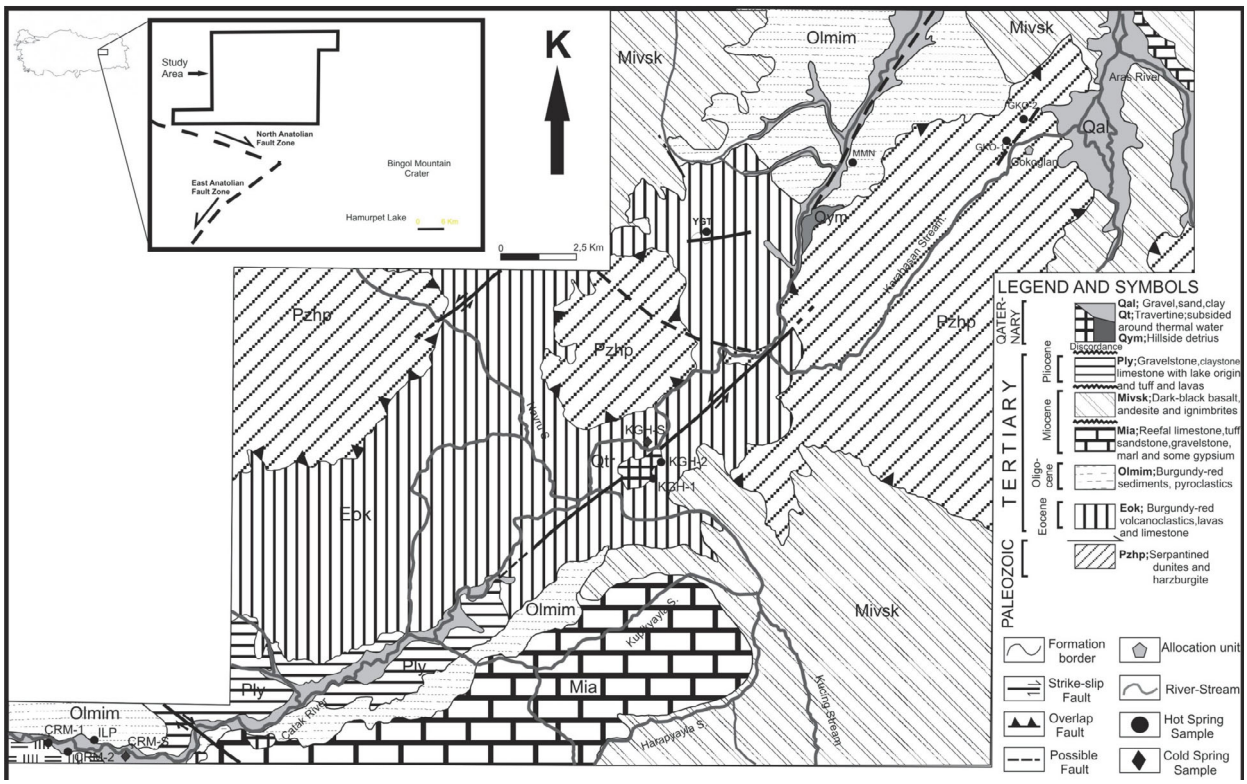

Figure 1. Geological map of the study area and the sample locations.

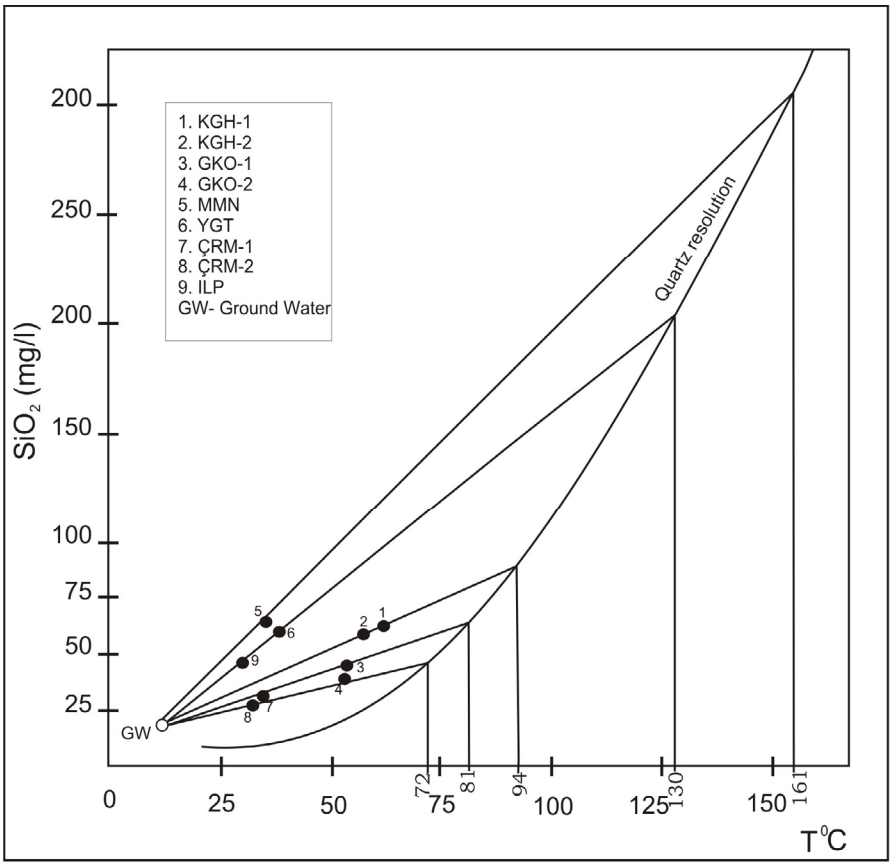

Sample No	1	2	3	4	5	6	7	8	9
Cold water mixing rate (%)	15	19	44	62.5	12.5	25	65	67.5	69

Figure 2. Enthalpy-silica diagram of the study area with mixing ratios of thermal and cold waters

Can Reservoir Conductivity be Enhanced by Shear Fractures Alone?

Xi Zhang and Rob Jeffrey*
Xi.Zhang@csiro.au and Rob.Jeffrey@csiro.au
CSIRO Earth Science and Resource Engineering
Ian Wark Lab, Bayview Ave. Clayton, VIC 3168, Australia

In fractured or faulted geothermal reservoirs, the opening of some fractures may occur in response to the sliding patterns of shearing on other fractures. This is due to the interchange of slip and opening between intersected fractures. However, the issue still exists as to how a pressure, less than the minimum stress level, can extend initially unconnected fractures to coalescence as they slip in shear, producing the desired connected fracture network and permeability enhancement. In this paper, we consider fractures arranged in such a way that sliding displacement along each fracture can be larger than its opening, which means that the transfer of the slip to the opening of the intersected fracture is significant. In the numerical simulations, we use a high in situ stress difference to promote shear deformation. Results demonstrate that shearing may act to assist opening or act to restrict opening of a connected fracture, but the injection pressure must be increased above the minimum principal stress for either case to occur. The combined opening and slip suggests that the natural fractures must be interconnected before stimulation if the stimulation is carried out at a pressure below the minimum stress magnitude. To bridge unconnected fractures, the stimulation must then use pressure sufficient to propagate tensile hydraulic fractures in addition to shearing.

Keywords: hydraulic fracturing, fracture conductivity, shear or tensile fracture, numerical modelling

Introduction

Enhanced geothermal systems are created mainly through stimulation of lower permeability target formations using hydraulic fracturing to create or improve the conductivity and volume of the reservoir. In these naturally fractured reservoirs, the coexistence of pre-existing and newly created fractures complicates the process of modelling the development of flow paths and conductivity. The natural fractures must already be or become inter-connected to form a network that can transport the injected fluids. The opening of a fracture can be induced by the slip along the connected fracture, as dictated by kinematics. One opinion prevails that the reservoir permeability can best be enhanced through the shearing movement of closed fractures in the absence of tensile fractures, since fracture shear is taken as the primary mechanism of stimulation for enhanced geothermal systems (Pine and Batchelor, 1984; Tezuka and Niisuma, 2000; Evans et al., 2005; among others). In this way, the fluid pressure used during stimulation can be lower than the minimum principal stress and still result in enhanced conductivity. However, the conditions under which this hypothesis is valid need to be investigated. In this paper, we will use several numerical examples to explore the mechanism associated with slip-dominated fracture growth and fluid flow.

A research hydraulic fracturing model capable of addressing growth of multiple fractures was developed by Zhang et al. (2007, 2009), and this model is suitable to simulate the deformation and flow in a set of discrete fractures in hard rock. The model has been used in other work to study and simulate the mechanisms of fracture intersection and crossing, flow diversion and frictional slip, and fracture growth. The model has been compared to existing analytical solutions and to other numerical results and has been shown to be adequate for the fracture geometries studied when applied to coupled fluid-mechanical fracture problems.

The reservoir connectivity is always an issue. In this paper, we will first provide the fundamental formulation of the model and then will give numerical results for four example problems that are used to study the interaction among fractures in affecting reservoir conductivity and fracture connectivity.

Governing equations

Fracture surface friction

In a closed fracture, the two sides of the fracture are in contact. The model allows for contact stresses to develop across fracture such surfaces and uses a cohesionless Coulomb friction criterion for slip on surfaces in contact

$$|\tau| \le \lambda(\sigma_n - p_f) \qquad (1)$$

where τ is the shear stress along the closed fractures, σ_n is the normal stress acting across the fractures, p_f is the fluid pressure and λ is the coefficient of friction.

Elasticity

In addition to the tangential displacement discontinuity (DD), v, associated with shear displacements or slip along the closed fracture segments, there exists opening displacement w

along any opened fractures, which contributes to fracture conductivity. These elastic displacements give rise to changes in the rock stress or changes in the tractions acting along the fracture surfaces. The governing equations for stresses, fluid pressure and displacements are given in Zhang et al. (2007, 2009), in terms of Green's functions. We employ the displacement discontinuity method (DDM) for the simulation of rock deformation in a 2D homogeneous and isotropic elastic material, on which a uniform stress is applied at infinity.

Fluid flow

The governing equations for fluid flow in the fracture channel are given by Zhang et al. (2009). There are two type of fluid movement along fractures. The fluid not only can diffuse along the closed fractures without any mechanical opening of the fracture, but also can flow through an open channel as a result of opening mode hydraulic fracturing processes. In the latter case, the fluid pressure is balanced by the compressive stress caused by rock elastic deformation, which is expressed as $\sigma_n = p_f$. We use Reynolds' equation to describe fluid movement inside the opened hydraulic fractures:

$$\frac{\partial(w+\varpi)}{\partial t} = \frac{\partial}{\partial s}[\frac{(w+\varpi)^3}{\mu'}\frac{\partial p_f}{\partial s}] \qquad (2)$$

where w vanishes for the closed segments, ϖ is the hydraulic aperture arising from surface roughness and microstructures and $\mu' = 12\mu$.

However, we note that effective stress changes in the fluid-infiltrated and pressurised fracture portion can produce changes of the hydraulic aperture without fully opening a fracture. This dilatation can slightly affect the internal pressure distributions since the resulting fluid conductivity varies in location and time. The hydraulic aperture at the beginning is assigned an initial value w_0 for each closed fracture segment. The evolution of ϖ obeys a nonlinear spring model in response to any increments of the internal pressure. In particular, an equation governing the hydraulic aperture change associated with pressure change is given as follows,

$$d\varpi / dP_f = \chi\varpi \qquad (3)$$

where χ is a small constant with a value of 10^{-8} per MPa in the model. A pressure diffusion equation is applied to calculate fluid flow inside a closed natural fracture (Zhang et al., 2009)

$$\frac{\partial p_f}{\partial t} - c\frac{\partial}{\partial s}(\varpi^2\frac{\partial p_f}{\partial s}) = 0 \qquad (4)$$

where $c = 1/(12\chi\mu)$. This calculation applies to all closed portions of fractures, whether they are undergoing or have undergone slip or not. It should be mentioned that non-linear terms such as shear-induced dilation have not been included in Eq. (4).

Boundary and initial conditions

To complete the problem formulation, we need boundary and initial conditions for the above governing equations. Initially, all fracture segments are assumed to be evacuated and the rock mass is stationary. Rock failure criterion will be given below, as well as the method used for handling fracture intersection and associated flux redistribution. For the fractures connected to the borehole, the sum of the fluid flux entering them is equal to the injection rate, that is,

$$\sum_{i=1}^{N} q_i(0,t) = Q_{in} \qquad (5)$$

where N is the number of fractures and q_i the fluid volumetric flux into fracture *i.*

At the fracture tip, the opening and shearing DDs are zero, that is,

$$w(l) = v(l) = 0 \qquad (6)$$

and the fracture opening profile near the crack tip possesses a square root shape with distance from the tip as predicted by Linear Elastic Fracture Mechanics (LEFM) theory.

When the stress intensity factor at the fracture tip reaches the fracture toughness of the rock, fracture growth occurs. In general, the fracture propagation direction may change as dictated by the near-tip stress field characterised by the Stress Intensity Factors (SIFs). In particular, a mixed-mode fracture criterion is used for determining fracture growth unless a shear mode toughness is reached earlier in the calculation. The propagation direction is not changed if the fracture propagates in the pure shear mode.

Numerical method

The coupled fluid flow (to obtain pressure) and rock deformation (to obtain fracture opening) problem is solved in an implicit manner by incorporating the elasticity equation into the Reynolds equation. The responses obtained are history dependent because of the nonlinear and path dependent fluid flow and frictional sliding processes. Additionally, there are three moving fronts inherent in the problem, namely the slip front, the fluid front and the fracture opening (crack tip) front. The reader is referred to Zhang et al. (2007, 2009) for a detailed description of the numerical solution methods applied in modelling these processes. Through Eq. (5), the injection rate into each fracture is found using the iteration method described in our previous work applied to fracture junctions (Zhang et al., 2007). In the calculation, the convergence of the solution is

very sensitive to the time step and the convergence error tolerance. To rapidly find a converged wellbore pressure, a relaxation factor is used in updating the injection rate and pressure level for fractures connected at junctions. A tolerance ($<10^{-4}$) is set for the relative error between the injection rates. Therefore, in the program, an iteration loop is introduced for obtaining converged injection rates and pressure solutions at junctions.

The numerical method has been verified, in our previous papers, by comparison to published solutions to a range of problems; see Zhang et al. (2009).

Numerical results

Table 1. Material constants for granite, as used in the numerical calculations

Material Properties	Values
E (GPa)	65
ν	0.25
K_{Ic} (MPa m$^{1/2}$)	1.35
K_{IIc} (MPa m$^{1/2}$)	3.05 or 0.5
λ	0.5 (to promote slippage)
Q_0 (m^2/s)	0.0004
μ (Pa·s)	0.0004

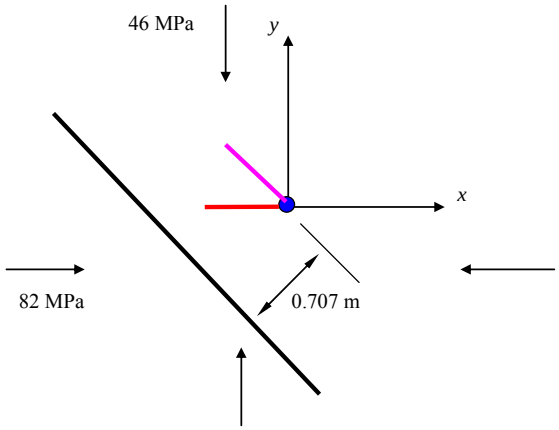

Figure 1 Fracture configuration. The hydraulic fracture starts to grow along one of the short natural fractures with two different fracture propagation directions (pink and red fractures) considered as separate cases. The hydraulic fracture then intersects the long natural fracture (black line). One short natural fracture lies horizontally and the other parallel to the black line. The in situ effective stresses are shown.

Hydraulic fracture orientation and conductivity

We denote the fracture initially connected to the wellbore as a hydraulic fracture and the pre-existing fracture which is later intersected by the hydraulic fracture as a natural fracture. For example, the black line in Fig. 1 is the natural fracture. It is supposed that there exist two natural fracture sets with one set lying perpendicular to the minimum principal stress and the other along the maximum shear stress direction. Therefore, two different starting hydraulic fracture geometries are considered as shown in Fig. 1, each along one pre-existing natural fracture orientation, and the purple slanted fracture is assigned a different initial conductivity. The hydraulic fracture is assigned an initial length extending from the wellbore to simulate the natural fracture (the red and purple lines in Fig. 1). This part of the fracture can be thought of as representing a natural fracture that has intercepted the wellbore, and acts as a site for initiation of the hydraulic fracture. The crack propagation in the opposite direction is prohibited in our simulation to simplify the problem and the computational effort required.

A borehole is located at the origin of the coordinate system as shown in Fig.1. The details of the fracture geometry are as follows. The natural fracture which is of 3.2 m long is oriented at 135 degrees with respect to the x-axis. The distance from the injection borehole to the natural fracture is 0.707 m. The hydraulic fractures are oriented at 135 degrees (slant) and 180 degrees (straight), and both have an initial length of 0.48 m. For the slant hydraulic fracture, two initial conductivities, 0.01 mm and 0.05 mm, are used to represent a less and more conductive initial fracture.

The far-field stress magnitudes shown in Fig.1 are based on the effective stress because we need to consider if frictional sliding occurs on the black natural fracture.

The coefficient of friction along the fracture is taken as equal to 0.5 (relatively small, but we wish to ensure that sliding will be induced). The authors recognized the variability of the coefficient of friction for a specific rock. Sensitivity to variation of the coefficient of friction has not been considered in this paper.

Upon starting fluid injection, the fluid will first fill and eventually extend the existing hydraulic fracture. The effective normal stress on the fracture is thus reduced by the internal pressure, which reduces the frictional strength of the fracture and promotes shearing. In the case of the slant fracture, the fracture may then kink out of the initial plane of the fracture because of the large mode II stress intensity factor generated. The kink angle would in theory be 70.5 degrees for an isolated non-opening fracture when the fracture kinks to propagate in an opening, but this reorientation is modified by the local in situ stresses arising from the presence of the other natural fracture. In general, the fracture therefore reorients as it extends, producing the configuration in Fig. 2.

In Fig. 2, the opening profile along fracture segments is shown. The blue bars, which are perpendicular to the fracture plane, are proportional in length to the magnitude of the

opening. It is clear that near the kinking point, the fracture opening is strongly restricted. The narrow opening restricts the fracture conductivity at that point and results in elevated pressure on the upstream side as fluid is forced through that point into the fracture on the downstream side.

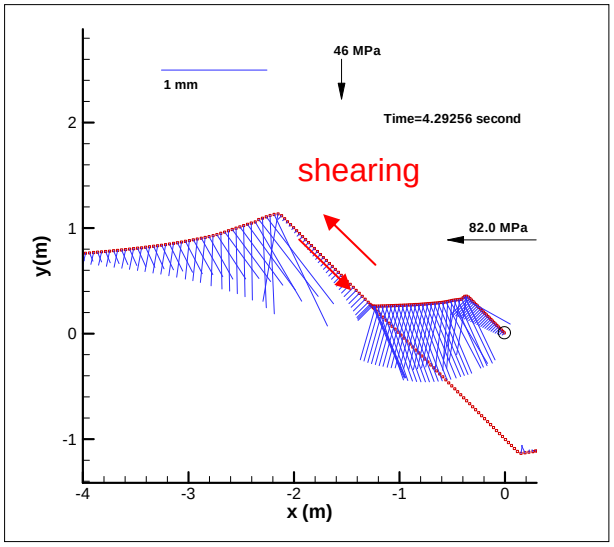

Figure 2 Fracture trajectory and opening profiles

Moreover, the fracture is found to eventually re-initiate at the end of the longer natural fracture. The growth will then continue with fluid eventually filling the entire fracture path. However, the restricted opening at the end of the natural fracture will also increase the fluid pressure on the upstream side back to the wellbore. The red arrows in Fig. 2 indicate the sliding direction along the natural fracture. The slip in this direction acts to help open the newly-created fracture at the tip of the natural fracture. Indeed, the crack opening arising from this shear deformation can be quite large. Figure 3 shows the variation of injection pressure in time for different cases. For the straight growing fracture (the red one in Fig. 1), the injection pressure is lowest at the beginning because this fracture opens against the minimum stress which is lower in magnitude than the normal stress acting across the inclined fracture Assigning more conductivity to the inclined (purple in Fig. 1) hydraulic fracture will also reduce the injection pressure. There is a jump in injection pressure for these curves, corresponding to the crack initiation at the end of the sheared natural fracture.

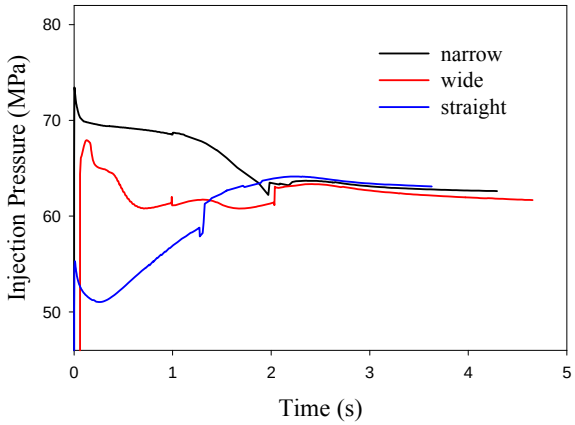

Figure 3 Injection pressure responses

The crack opening and trajectory at the moment that the new fracture forms at the tip of the natural fracture, for the narrow width/ low conductivity case, are displayed in Fig. 4. Note that a small fracture initiates at the lower end of the natural fracture as a result of the shear displacement along the natural fracture. This small fracture does not extend far because fluid pressure does not enter that part of the natural fracture. After the new fracture initiation, all three curves follow each other more or less, as shown in Fig. 3. Therefore, the local fluctuation arising from different initial crack geometries becomes less important at large time.

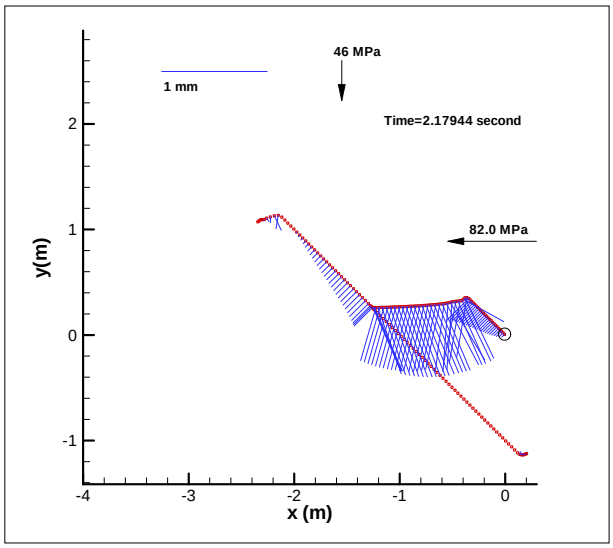

Figure 4 Fracture trajectory and opening profile at an early time for the same case shown in Fig. 2.

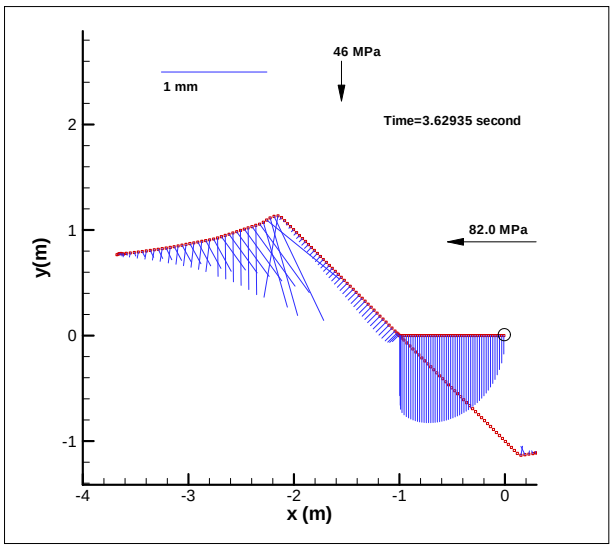

Figure 5 Fracture trajectory and opening profile for the initially-straight-growing fracture.

Moreover, for the straight growing crack case (red), the confinement across the fracture is lowest before it intersects the natural fracture and this is reflected in the lower injection pressure. However, the fluid penetration along the natural fracture is associated with an increase in injection pressure because the confining stress is increased. The corresponding opening at large time is displayed in Fig. 5.

Fracture distance to the injection point

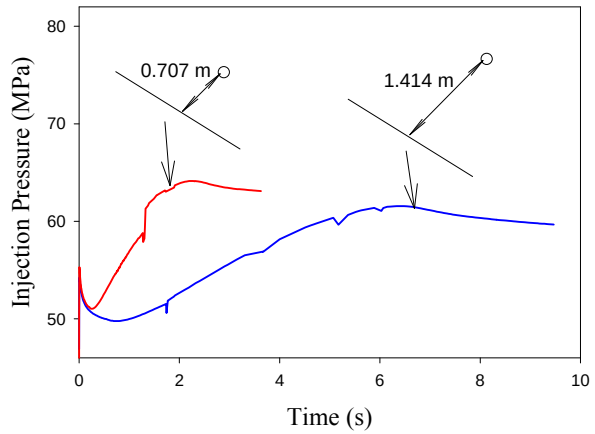

Figure 6 Injection pressure responses for two crack distances

If the distance between the borehole and the natural fracture is doubled, the extent of the hydraulic fracture that forms prior to intersection becomes larger. The resulting longer initial fracture contributes to the compliance of the overall stepped fracture system allowing more shear and opening to occur along it which in turn results in a somewhat lower peak pressure. Therefore, the longer the hydraulic fracture, the easier it is for the fracture to open and the lower the pressure level. The wider overall fracture also results in more fracture volume which is reflected in the slower growth rate. This behaviour can be seen in Fig. 6 when the fracture propagates straight towards the natural fracture.

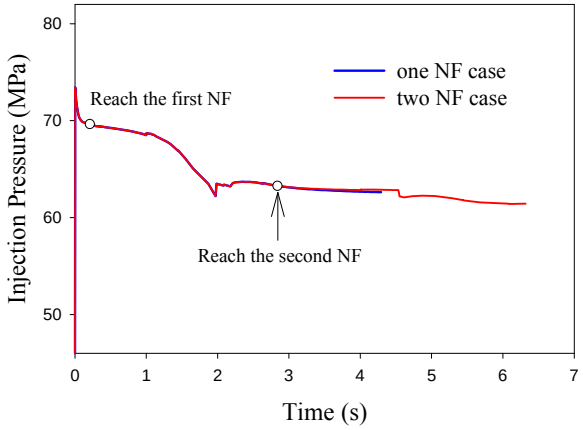

Figure 7 Injection pressure curves for the cases crossing one and two natural fracture.

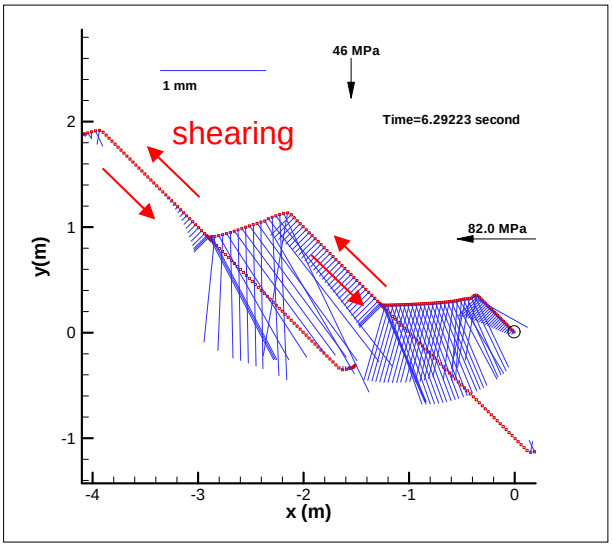

Figure 8 Fracture trajectory and opening profile for the case crossing two natural fractures.

Growth through two natural fractures

When the hydraulic fracture passes one natural fracture and then encounters a second natural fracture, the injection pressure is only very slightly affected as shown in Fig. 7. Although the fracture growth direction is changed again, the injection pressure does not vary much. A slight increase in fluid pressure can maintain fluid flow along both natural fractures. The onset of new crack opening at the tip of the second natural fracture is seen to induce a sudden drop as shown in Fig. 7.

The crack opening and fracture trajectory that correspond with the pressures in Fig. 7 are displayed in Fig. 8. The new fracture has already been initiated at the end of the second natural

fracture and a part of the second NF is opened. Assisted by the shear slip, the opening along the first natural fracture changes from linear to more uniform with time. Also, the slip induced opening can further increase the fracture conductivity and thus reduce the pressure level.

Shear-mode crack growth

For this case, the mode II toughness must be greatly reduced (0.5 MPa $m^{1/2}$) and must be less than the mode I toughness so that straight shear-mode fracture growth becomes possible. The hydraulic and natural fractures that undergo shearing are both oriented at 45 degrees to the principal stress so that the maximum shearing stress acts along the fracture plane, as shown in Fig. 9. We have introduced a second natural fracture at a position on the main natural fracture as shown. The second natural fracture will serve as a site for growth of a new shear mode hydraulic fracture, rather than extension of the hydraulic fracture from the ends of the natural fracture.

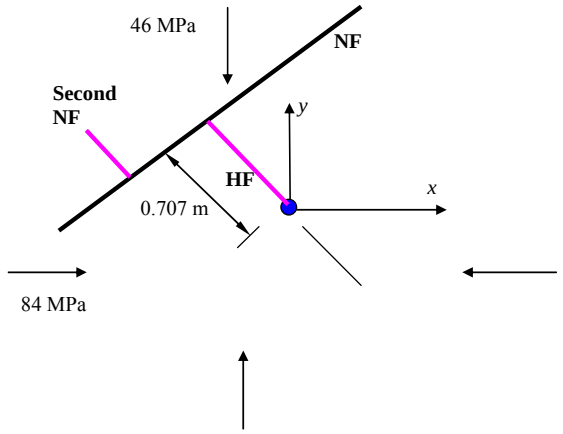

Figure 9 The abbreviations are HF for hydraulic fracture, NF for natural fracture, and Second NF for the secondary natural fracture

After fracture connection, the fluid will flow along the natural fracture and the second fracture will inflate and slide, as shown in Fig. 10. The relatively large crack opening along the segment lying along the natural fracture and between the hydraulic fracture and the second natural fracture is increased by the slip of the two fracture segments that intersect the natural fracture. The shearing directions are indicated in Fig. 10. In addition, the shear slippage along the out-of-natural-fracture –plane segments acts to close the NF portions outside the natural fracture portion between these two segments. In the end, a volume of fluid is contained along the fracture segment between the two out-of-NF-plane segments along the natural fracture plane.

Figure 11 shows the evolution of injection pressure. A higher injection pressure than the minimum stress (which is 46 MPa) is also required in this case largely because the opening along the hydraulic fracture is confined partially due to the slip along the natural fracture. The slip direction along the NF is also shown in Fig. 10.

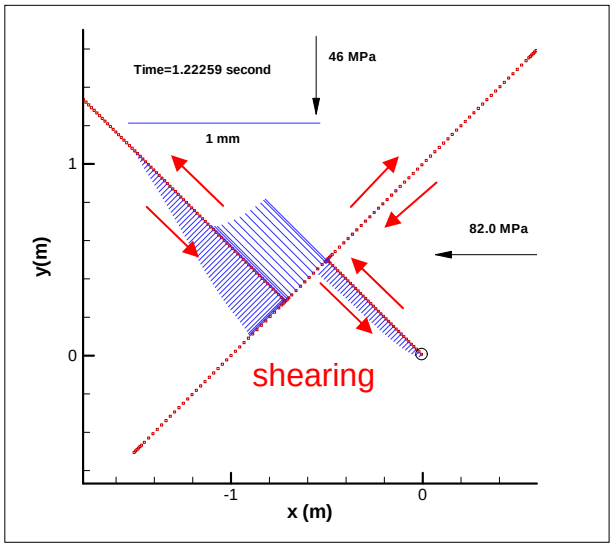

Figure 10 Fracture trajectory and opening profile for pure shear-mode fractures

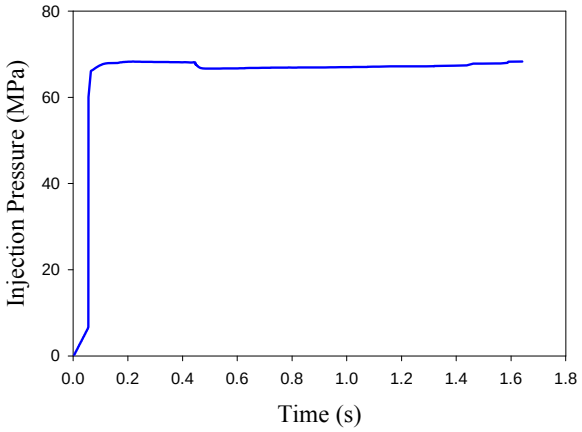

Figure 11 Variations of injection pressure in time

Conclusions

Results from numerical simulation of four different fracture geometries have been presented. The existing natural fracture is arranged so that the shear stress acting on it is optimal. The fracture surface shear slip plays an important role in modifying the fracture opening on the fractures connected to the sheared fracture. Shearing may act to assist opening or act to restrict opening of a connected fracture. In the calculation, a strong in-situ stress difference is generated by assigning far-field stress conditions with a large difference between the maximum and minimum principal effective stresses. However, it is found for these cases, which use a constant injection rate, that the injection pressure must be increased above the minimum principal stress (46 MPa) before fracture growth occurs. This result holds for both opening and shearing mode fracture growth starting with different directions and for different

geometric fracture settings near the wellbore. When the mode II toughness is larger than the mode I toughness, tensile fractures are created as part of the fracture process. Only by lowering the mode II toughness to be less than the mode I toughness, which is not supported by laboratory toughness measurements, can a mode II fracture be made to extend along an unfractured path. We therefore conclude that stimulation of reservoirs without opening mode fracturing is only possible if the natural fractures sets present form a well connected network before the stimulation begins. Pressurisation of such a network will allow shearing to occur, resulting in shear induced dilation and permeability enhancement. On the other hand, the results presented here are based on quasi-static fracture growth and it may be that seismic events recorded during hydraulic stimulation of geothermal reservoirs, which reflect dynamic shear events, will produce new shear fracture growth and form new connections between existing natural fractures.

Acknowledgements

The authors thank Mark Tingay of The University of Adelaide for his valuable comments and suggestions.

References

Evans, K., Moriya, H., Niitsuma, H., Jones, R., Phillips, W., Genter, A., Sausse, J., Jung, R., and Baria, R., 2005, Microseismicity and Permeability Enhancement of Hydrogeologic Structures during Massive Fluid Injections into Granite at 3 km Depth at the Soultz HDR site, Geophysical Journal International. 160: 388-412

Pine, R. J., and Batchelor. A. S., 1984, Downward Migration of Shearing in Jointed Rock During Hydraulic Injections, International Journal of Rock Mechanics and Mining Sciences & Geomechanical Abstracts. 21: 249-263.

Tezuka, K., and Niisuma H., 2000, Stress Estimated using Microseismic Clusters and its Relationship to the Fracture System of the Hijiori Hot Dry Rock Reservoir, Engineering Geology. 56: 47-62,

Zhang, X. Jeffrey, R. G. and Thiercelin, M., 2007, Deflection of fluid-driven fractures at bedding interfaces: A numerical investigation, J. Structural Geology 29, p. 396-410.

Zhang, X. Jeffrey, R. G. and Thiercelin, M., 2009, Mechanics of fluid-driven fracture growth in naturally fractured reservoirs with simple network geometries, J. Geophysical Research -Solid Earth, 114, B12406.